U.PORTO

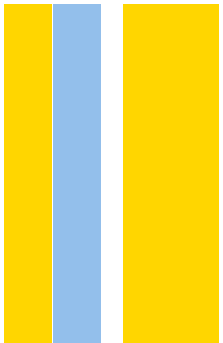
PROGRAMA DOUTORAL EM PATOLOGIA E GENÉTICA MOLECULAR

Drug Repurposing as a Strategy to Overcome Ovarian Cancer Chemoresistance

Mariana Oliveira Nunes

D

2024



MARIANA OLIVEIRA NUNES

DRUG REPURPOSING AS A STRATEGY TO OVERCOME OVARIAN CANCER CHEMORESISTANCE

Tese de Candidatura ao grau de Doutora em Patologia e Genética Molecular
Programa Doutoral da Universidade do Porto (Instituto de Ciências Biomédicas de Abel Salazar e Faculdade de Medicina da Universidade do Porto)

Professora Doutora Sara Alexandra Vinhas Ricardo
Professora Auxiliar no Instituto Universitário de Ciências da Saúde (IUCS) e Investigadora na Unidade de Biociências Moleculares Aplicadas (UCIBIO) e Instituto de Saúde e Bioeconomia (i4HB)

Professora Doutora Raquel Maria da Silva Graça Almeida
Professor Auxiliar Convidada na Faculdade de Ciências da Universidade do Porto (FCUP) e Investigadora Principal no Instituto de Investigação e Inovação em Saúde da Universidade do Porto (i3S)

This Doctoral Thesis is made public under the condition that anyone consulting it must recognize that its copyright belongs to the author. No quotation from the thesis or information derived from it may be published without proper acknowledgment.

This Doctoral Thesis received financial support from the *Fundação para a Ciência e a Tecnologia (FCT, Portugal), Ministério da Ciência, Tecnologia e Inovação (MCTES),* and *União Europeia (UE)* through a doctoral fellowship granted to Mariana Oliveira Nunes (2020.04720.BD and doi:10.54499/2020.04720.BD), co-sponsored by the *Fundo Social Europeu (FSE)* through the *Programa Operacional Regional Norte (Norte 2020).*

The experimental work conducted under this Doctoral Project was financially supported by the *Fundo Europeu de Desenvolvimento Regional (FEDER)* through the *COMPETE 2020 – Programa Operacional para Competitividade e Internacionalização (POCI), Portugal 2020*, and *FCT/MCTES* under the project POCI01-0145-FEDER-029503 (PTDC/MEC-ONC/29503/2017); the *Gabinete para a Investigação e a Inovação (GI2),* through the financial program GI2-*Cooperativa de Ensino Superior Politécnico e Universitário (CESPU)* under the projects "ComeTarget_CESPU_2017", "OVCARTEST_GI2-CESPU_2022", and "ImmunoT4OC_GI2-CESPU-2023"; and HOPE: Improving Ovarian Cancer Patients´ Survival – Donation from an Ovarian Cancer Patient.

The experimental work presented in this Doctoral Thesis was developed at the Differentiation and Cancer Group at the Institute for Health Research and Innovation (i3S) of the University of Porto, Portugal, an Associate Laboratory of the *Ministério da Ciência, Tecnologia e Inovação (MCTES)*, partially supported by the *Fundação para a Ciência e a Tecnologia (FCT).*



Declaro que a presente tese é de minha autoria e não foi utilizada previamente noutro curso ou unidade curricular, desta ou de outra instituição. As referências a outros autores (afirmações, ideias, pensamentos) respeitam escrupulosamente as regras da atribuição, e encontram-se devidamente indicadas no texto e nas referências bibliográficas, de acordo com as normas de referenciação. Tenho consciência de que a prática de plágio e auto-plágio constitui um ilícito académico.



Mariana Oliveira Nunes

I declare that I am the sole author and organizer of this thesis. I confirm that this work has not been previously submitted, in whole or in part, to obtain another academic degree. I also confirm that I completed the described work alongside the other authors. My contribution is explicitly indicated below for joint publications in Chapters I, III, IV, and V:

I wrote the initial draft of the review and the book chapter in Chapter I, integrating feedback from the other co-authors afterward.

The research in Chapter III results from a collaboration between Diana Luisa Almeida-Nunes and me. I handled the experimental work and formal analysis of the malignant ascites samples collected post-treatment. Meanwhile, Diana Luisa Almeida-Nunes worked on the experimental tasks and formal analysis of the samples obtained pre-treatment, with input from the other co-authors. While we were both engaged in the experimental work, I was responsible for drafting the initial version of the paper and later integrating suggestions from Diana and the other co-authors. This publication will be submitted soon and will solely be part of my PhD thesis, as Diana will focus on different research areas.

All the experimental work and formal analysis presented in Chapter IV were conceived by me under the supervision of Sara Ricardo, except in the manuscript "Generation of Two Paclitaxel-Resistant High-Grade Serous Carcinoma Cell Lines With Increased Expression of P-Glycoprotein." Here, the electronic microscopy analysis was performed by Carla Pinto and Albina Resende. The time-lapse microscopy, image acquisition and processing, wound healing assay, RNA isolation and quantitative real-time PCR, cell extracts and western blotting, rhodamine 123 accumulation assay, and SRB assay were performed by Patrícia M. A. Silva. I wrote the first draft of the chapter and all the papers and later incorporated suggestions from the other co-authors.

The experimental work and formal analysis presented in Chapter V were conceived by me under the supervision of Sara Ricardo. For the research presented here, Miguel Abal Posada and Andrea Estrella Arias-Diaz contributed to the implementation of the malignant ascites-derived cultures.

Mariana Oliveira Nunes

Mariana Oliveira Nunes

“Somewhere, something incredible is waiting to be discovered.”

– Carl Sagan –

ACKNOWLEDGMENTS

Ao meu marido Diogo, expresso a minha eterna gratidão pela paciência e compreensão que demonstraste diariamente, especialmente nos últimos meses. O teu apoio incondicional foi fundamental, e agradeço-te por nunca deixares que eu desanimasse. Estiveste sempre ao meu lado, especialmente nos momentos em que me senti perdida. Obrigada por acreditares em mim, mesmo quando eu duvidei das minhas capacidades. Sem ti, este percurso não teria sido possível.

Aos meus pais, Lucília e José, sou profundamente grata pelo apoio inabalável que sempre me proporcionaram. Obrigada pela vossa paciência, amor e por acreditarem nos meus sonhos, ajudando-me a acreditar neles também.

Ao meu irmão Francisco, agradeço-te por estares sempre ao meu lado e por me incentivares a seguir as minhas ambições. O teu simples "Força mana, vais conseguir" será sempre um dos meus maiores amuletos.

À minha família e amigos, agradeço pelo carinho e apoio constantes. Um agradecimento especial às minhas meninas *Não te conto;* a vossa presença e apoio, mesmo à distância, foram fundamentais ao longo deste percurso.

Às minhas orientadoras, Sara Ricardo e Raquel Almeida, agradeço por terem aceite fazer parte deste projeto. A vossa confiança em mim e no meu trabalho foi crucial. Sou grata pelos ensinamentos que me proporcionaram, pela vossa constante disponibilidade e dedicação.

À Diana Luísa Almeida-Nunes, obrigada por me motivares e por partilhares momentos bons e desafiantes ao longo destes três anos. A tua presença foi uma âncora, especialmente nos dias em que parecia impossível continuar. Obrigada por todos os áudios, mensagens e chamadas sempre acompanhados de “está quase” e “vais conseguir”!

A todos os membros do *Differentiation and Cancer Group,* agradeço pelas colaborações e discussões científicas que enriqueceram a minha experiência ao longo dos últimos seis anos. Um agradecimento especial à Ana Rita Silva, à Vanessa Machado e à Catarina Oliveira pela amizade e companheirismo, pelos risos, mas também pelas lágrimas que partilhamos ao longo dos últimos anos.

A todos aqueles que, de alguma forma, contribuíram para o sucesso deste projeto, em especial à Diana Duarte, ao Nuno Vale, à Patrícia M. A. Silva, ao Miguel Abal Posada e à Andrea Estrella Arias-Diaz, agradeço pela partilha de conhecimentos, pela paciência e dedicação que sempre tiveram.

À equipa clínica e patológica do Instituto Português de Oncologia do Porto (IPOP), especialmente à Doutora Carla Bartosch e ao Doutor Miguel Abreu, obrigada por todas as amostras de ascites malignas que fizeram chegar até nós. Este trabalho não teria sido possível sem a vossa colaboração.

Finalmente, a todas as guerreiras que enfrentam diariamente a luta contra o cancro do ovário, a minha profunda gratidão. Nunca desistam de lutar! "Carregar um cancro dentro de nós é como guardar um inimigo dentro de casa", mas nunca deixem morrer a esperança, um dia vencerão esta batalha.

TABLE OF CONTENTS

ABBREVIATIONS……..XXIII
LIST OF FIGURES……XXXI
LIST OF TABLES……..XXXV
LIST OF SUPPLEMENTARY FIGURES……XXXVII
LIST OF SUPPLEMENTARY TABLES……XXXIX
PUBLICATIONS…….....XLI
ABSTRACT…….....XLV
RESUMO…….....XLIX
GRAPHICAL ABSTRACT……LIII

CHAPTER I | General Introduction……...1
1. Ovarian Cancer……..3
1.1. Epidemiology……3
1.2. Histopathological Subtypes…..…….…… 6
1.3. Treatment Strategies……..……..6
1.4. Malignant Ascites……..……10
1.4.1. Transcoelomic Dissemination……..11
1.4.2. The Microenvironment of Malignant Ascites……..12
1.4.3. The Management of Malignant Ascites and Chemoresistance……...13
1.4.4. Malignant Ascites as an Opportunity for Translation Research……..16
1.4.5. A Personalized Medicine Approach on Ovarian Cancer using Malignant Ascites……17
1.5. Chemoresistance ……..……19
1.5.1. Mechanisms of Platinum Resistance in Ovarian Cancer…….....21
1.5.1.1. Pre-Target Resistance Mechanisms…….....23
1.5.1.1.1. Drug Influx and Efflux…….....23
1.5.1.1.2. Detoxification Systems…….....24
1.5.1.2. On-Target Resistance Mechanisms…….....24
1.5.1.2.1. DNA Damage Repair…….....24
1.5.1.3. Post-Target Resistance Mechanisms…….....26
1.5.1.3.1. Apoptosis and Cell Cycle Regulation……...26
1.5.1.4. Off-Target Resistance Mechanisms…….....26

1.5.1.4.1. Tumor Microenvironment and Cancer Stem Cells…….26
1.5.1.4.2. Epigenetic Modifications…….....27
1.5.2. Mechanisms of Paclitaxel Resistance in Ovarian Cancer…….....29
1.5.2.1. Intracellular Drug Concentration……..…....31
1.5.2.1.1. Solubility Absorption, Distribution, Metabolism, and Elimination…….....31
1.5.2.1.2. Drug Efflux…….....31
1.5.2.1.3. Metabolizing Enzymes……..….....31
1.5.2.2. Microtubule Regulatory Proteins and Tubulin Isotypes…….....32
1.5.2.3. Apoptosis and Cell Cycle Regulation……..….....34
1.5.2.4. Signal Transduction Pathways…….....35
1.5.2.5. Oxidative Stress…….....35
1.5.2.6. Cellular Homeostasis and Glucose Metabolism…….....36
1.5.2.7. MicroRNAs and LncRNAs…….……..….....36
1.5.2.8. Tumor Microenvironment…….....37
1.5.2.9. Extracellular Vesicle-Dependent Intercellular Communications….37
1.5.2.10. Multi-Micronucleus and Laminin A/C Expression…….....37
1.5.2.11. Polyploid Giant Cancer Cells…….....38
1.5.3. Mechanisms of Resistance to PARP Inhibitors in Ovarian Cancer…….....38
1.5.3.1. PARPi Resistance Mechanisms Associated with Restoration of Homologous Recombination……..…....40
1.5.3.1.1. Homologous Recombination…….....40
1.5.3.1.2. PARP Functions…….....41
1.5.3.2. PARPi Resistance Mechanisms Not Associated with Homologous Recombination…….....41
1.5.3.2.1. Replication Fork…….....41
1.5.3.2.2. Drug Efflux Pumps…….....42
1.5.3.2.3. Cell Cycle Regulation…….....42
1.5.3.2.4. Polyploid Giant Cancer Cells…….....43
1.5.4. Mechanisms of Resistance to Bevacizumab in Ovarian Cancer…….....43
1.5.4.1. VEGF-Independent Revascularization……..….....45
1.5.4.2. Neovasculature……..….....46
1.5.4.3. Hypoxia……..….....46
1.5.4.4. Tumor Microenvironment……..….....47

1.5.4.5. Tumor Invasiveness and Metastasis……..…....47

CHAPTER II | Thesis Motivation, Hypothesis, and Aims……..49
1. Thesis Motivation……..51
2. Hypotheses……51
3. Aims……..……52

CHAPTER III | Evaluation of the Expression of Specific Biomarkers to Identify Chemoresistance Profiles in Patient-Derived Samples……...……..55
Expression of ALDH1A1, SOX2, CD44v6, and P-gp as a Chemotherapy Footprint in Malignant Ascites Samples…….....57
1. Abstract.…...57
2. Introduction ……..57
3. Materials and Methods……59
3.1. Patient Samples……..59
3.2. Malignant Ascites Processing and Storage……59
3.3. Histogel™ Cell Processing……..……....60
3.4. Immunocytochemistry……60
3.5. Statistical Analysis……..61
4. Results……..61
4.1. Characterization of Patient Cohort and Full-Volume Centrifugation of Malignant Ascites.……61
4.2. Expression of ALDHA1, SOX2, CD44v6, and P-gp is Associated with Chemotherapy……..……..……64
4.3. Expression of ALDH1A1, SOX2, CD44v6, and P-gp is Associated with Platinum-resistance.……...69
5. Discussion……73
6. Conclusion……...78
7. Acknowledgments and Funding……78
8. Supplementary Material……80

CHAPTER IV | Establishment and Characterization of Chemoresistant OC Cell Line Models Followed by the Sensitization Step using Drug Repurposing…..……85
a. Generation and Characterization of Chemoresistant Ovarian Cancer Cell Lines….87

Generation of Two Paclitaxel-Resistant High-Grade Serous Carcinoma Cell Lines with Increased Expression of P-Glycoprotein……89
1. Abstract…….. 89
2. Introduction……...89
3. Materials and Methods……..90
3.1. Cell Line and Drugs……90
3.2. Generation of OVCAR8 PTX R Cell Lines……..91
3.3. Cell Viability Assay……91
3.4. Proliferation Assay……92
3.5. Viability Test……92
3.6. Cell Microarray Construction and Immunocytochemistry Expression Analysis…92
3.7. Electronic Microscopy Analysis……93
3.8. Apoptosis and Cell Cycle Analysis……...94
3.9. Time-lapse Microscopy, Image Acquisition, and Processing……...94
3.10. Anoikis Resistance Assay……..95
3.11. Colony Formation Assay……95
3.12. Wound Healing Assay……95
3.13. RNA Isolation and Real-time Quantitative Reverse Transcription Polymerase Chain Reaction……96
3.14. Cell Extracts and Western Blotting……96
3.15. Rhodamine 123 Accumulation Assay……...96
3.16. Sulforhodamine B Assay……97
3.17. Statistical Analysis……..97
4. Results……97
4.1. OVCAR8 PTX R Variants Demonstrate High Resistance to Paclitaxel……..97
4.2. OVCAR8 PTX R Variants Overcome Paclitaxel-Induced G_2/M Arrest and Apoptosis……100
4.3. OVCAR8 PTX R Variants Retain OVCAR8 Features: High Anoikis Resistance, Colony Formation, and Migration Capacity……102
4.4. OVCAR8 PTX R Variants Acquire a New Phenotype with P-glycoprotein Overexpression……104
5. Discussion……106
6. Acknowledgments and Funding……108
7. Supplementary Material……..110

b. Targeting Chemoresistant Ovarian Cancer Cells using Drug Repurposing……113

i. Pitavastatin and Ivermectin Enhance the Efficacy of Paclitaxel in Chemoresistant High-Grade Serous Carcinoma……115

1. Abstract……115

2. Introduction ……115

3. Materials and Methods……118

3.1. Cell Lines and Culture Conditions……118

3.2. Drugs……118

3.3. Cell Viability Assays……118

3.4. Drug Treatment……119

3.5. Drug Interactions Analysis……119

3.6. Microscopic Evaluation……120

3.7. Statistical Analysis……120

4. Results……120

4.1. Repurposed Drugs Show High Effectiveness in Reducing Cellular Viability of Chemoresistant High-Grade Serous Carcinoma Cells……120

4.2. Repurposed Drugs Increase the Efficacy of Paclitaxel in Reducing Cellular Viability of Chemoresistant High-Grade Serous Carcinoma Cells……123

4.3. Combining Paclitaxel with Repurposed Drugs Has a Synergistic Effect on Chemoresistant High-Grade Serous Carcinoma Cells……127

5. Discussion……137

6. Conclusion……142

7. Acknowledgements and Funding……143

8. Supplementary Material……144

ii. The Antineoplastic Effect of Carboplatin is Potentiated by Combining it with Pitavastatin or Metformin in a Chemoresistant High-Grade Serous Carcinoma Cell Line……151

1. Abstract……151

2. Introduction ……151

3. Materials and Methods……154

3.1. Cell Lines and Culture Conditions……154

3.2. Drugs…… 154

3.3. Cell Viability Assays……154

3.4. Drug Treatment and Interactions Analysis…….....154
3.5. Microscopic Evaluation…….....155
3.6. Statistical Analysis…….....155
4. Results…….....155
4.1. Repurposing Drugs Increase the Efficacy of Carboplatin in Reducing OVCAR8 and OVCAR8 PTX R P Cellular Viability……155
4.2. Combining Repurposed Drugs with Carboplatin Has a Synergistic Effect on OVCAR8 and OVCAR8 PTX R P Cells……..159
5. Discussion……...170
6. Conclusion……..176
7. Acknowledgments and Funding……..……176
8. Supplementary Material……..…...178

iii. Ivermectin Boosts Paclitaxel Effectiveness in High-Grade Serous Carcinoma in 3D Cell Cultures…….181
1. Abstract……181
2. Introduction ……182
3. Materials and Methods……...183
3.1. Cell Lines and Culture Conditions……183
3.2. Drugs……..……184
3.3. Cell Viability Assays……..……184
3.4. Drug Treatment and Interactions Analysis…….....184
3.5. Microscopic Evaluation…….....185
3.6. Statistical Analysis…….....185
4. Results……185
4.1. Combining Carboplatin with Pitavastatin or Ivermectin Has an Additive Effect on OVCAR8 and OVCAR8 PTX R C Cells…….....185
4.2. Combining Paclitaxel with Pitavastatin or Ivermectin Has an Additive Effect on OVCAR8 and OVCAR8 PTX R C Cells……..189
4.3. Morphological Assessment Reveals Drug Efficacy in Combined Treatments……..191
5. Discussion…….....194
6. Conclusion…….....197
7. Acknowledgements and Funding……197

8. Supplementary Material…….198

CHAPTER V | Establishment of Malignant Ascites-Derived Cultures to Perform *Ex Vivo* Drug Efficacy Tests……..……...211

Development of Patient-Derived Cultures from Ovarian Cancer Malignant Ascites for *Ex Vivo* Drug Testing …….213

1. Abstract……..213

2. Introduction……...213

3. Materials and Methods……..……..215

3.1. Patient Samples……..215

3.2. Malignant Ascites Processing and Storage……...…..215

3.3. Establishment and Characterization of Malignant Ascites-derived Cultures...……...215

3.3.1. Cultrex Reduced Growth Factor Basement Membrane Extract Cultures.……215

3.3.2. PolyHEMA Coating Cultures……...……216

3.4. Histogel™ Cell Processing……...……217

3.5. Immunocytochemistry……...……217

3.6. CellTiter-Glo® 2.0 Luminescent Cell Viability Assay…….....217

3.7. Alamar Blue™ Assay……...…….....218

4. Results and Discussion……...219

4.1. SOM is the Best Medium for Malignant Ascites-Derived Cultures…….220

4.2. Medium Supplementation with Autologous Supernatant is an Advantage to the Growth of Malignant Ascites-Derived Cultures……222

4.3. PolyHEMA Coating is the Most Appropriate Cell Culture Setup to More Rapidly Produce Malignant Ascites-Derived Cultures……..225

4.4. Maintaining Cell Aggregates is Beneficial in the Early Steps of Malignant Ascites-Derived Cultures Establishment.……227

4.5. Layered Techniques are More Effective in Maintaining Malignant Ascites-Derived Cultures...……..234

4.6. Immunocytochemistry is a Reproducible Technique to Characterize Malignant Ascites-derived Cultures Phenotype..…….....……..234

4.7. Drug Tests in Malignant Ascites-Derived Cultures – A Proof of Concept for Future Works……..…....236

5. Conclusion……..…....239

6. Supplementary Material……..……....240

CHAPTER VI | General Discussion, Main the Conclusions and Future Perspectives……241
1. General Discussion……243
2. Main Conclusions……...245
3. Future Perspectives……...246

REFERENCES……..249

ABBREVIATIONS

ABC – ATP-binding cassette

ADME – Absorption, distribution, metabolism, and elimination

AI – Artificial intelligence

Akt – V-akt murine thymoma viral oncogene homolog 1

ALDH1 – Aldehyde dehydrogenase 1

ANGPT – Angiopoietins

ANXA3/JNK – Annexin A3/c-jun N-terminal kinase

APC/c – Anaphase-promoting complex/cyclosome

ATM – Ataxia–telangiectasia-mutated

ATP7A/7B – ATPase copper transporting 7 alpha/7 beta

ATR – Rad3-related

ATRX – Alpha-thalassemia retardation x-linked

BAD – Bcl-2 associated agonist of cell death

BAK – Bcl-2 antagonist/killer

BAX – Bcl-2-like protein 4

Bcl-2/X_L/W – B-cell lymphoma 2/extra-large/W

BER – Base excision repair

BID – BH3 interacting domain death agonist

BIK – Bcl-2 interacting killer

BIM – Bcl-2-like 11

BMDC – Bone marrow-derived cell

BMF – Bcl-2 modifying factor

BOK – Bcl-2 related ovarian killer

BRCA1/2 – Breast cancer 1/2

BRCP – Breast cancer resistance protein

BrdU – Bromodeoxyuridine

BRIP1 – BRCA1 interacting helicase 1

BUB1B – Mitotic checkpoint serine/threonine kinase B

BUBR1 – BUB1-related kinase 1

C – Continuous

C-Jun – Protooncogene jun

CAAs – Cancer-associated adipocytes

CAFs – Cancer-associated fibroblasts

CCC – Clear cell carcinoma

CCNA1 – Cyclin A1

CCNB1 – Cyclin B1

CCNE1 – Cyclin E1

CDK2 – Cyclin-dependent kinase

cfDNA – Circulating free desoxyribonucleic acid

CHD4 – Chromodomain helicase DNA-binding protein 4

CHK1/2 – Cell cycle checkpoint kinases 1/2

CI – Combination index

CMA – Cell microarray

CO_2 – Carbon dioxide

CR – Complete response

CREB – cAMP-responsive element binding protein

CSC – Cancer stem cell

CTR1/2 – Cooper transporter 1/2

CXCL12 – C-X-C motif chemokine 12

CXCR4 – Chemokine receptor 4

CYP – Cytochrome P450

DAB – Diaminobenzidine

DAPI – 4',6-diamidino-2-phenylindole

DDR – Deoxyribonucleic acid damage response

DIC – Differential interference contrast

DMSO – Dimethyl sulfoxide

DNA – Desoxyribonucleic acid

DSB – Double-strand break

EC – Endometrioid carcinoma

ECM – Extracellular matrix

EDTA – Ethylenediaminetetraacetic acid

EGF – Epithelial growth factor

EGFR – Epidermal growth factor receptor

EMA – European Medicines Agency

EMT – Epithelial-mesenchymal transition

EOC – Epithelial ovarian cancer

EpA1/2 – Ephrins

ERCC – Excision repair cross-complementing

ERCC6L2 – Excision repair cross-complementing repair 6 like 2

ESGO – European society of gynecological oncology

ESMO – European society for medical oncology

EVs – Extracellular vesicles

Fa – Effect level

FANCD2 – Fanconi anemia complementation group D2

FBS – Fetal bovine serum

FER1L4 – Fer-1-like protein 4

FGF – Fibroblast growth factor

FIGO – International Federation of gynecology and obstetrics

FITC-A – Fluorescein isothiocyanate A

FZD1/10 – Frizzled class receptor 1/10

G-CSF – Granulocyte colony-stimulating factor

GM-CSF – Granulocyte-macrophage colony-stimulating factor

GSH – Glutathione

GSK3B – Glycogen synthase kinase 3 beta

HDAC1/10 – Histone deacetylase 1/10

HDI – Human Development Index

HGF – Hepatocyte growth factor

HGSC – High-grade serous carcinoma

HIF1-α – Hypoxia-induced factor 1-α

HIPEC – Hyperthermic intraperitoneal chemotherapy

HMGCR – 3-hydroxy-3-methylglutaryl-coenzyme A reductase

HR – Homologous repair

Hrk – Harakiri, Bcl-2 interacting protein

HRP – Horseradish peroxidase

HSA – Highest single agent

HSP90 – Heat-shock protein 90

IAP – Inhibitor of apoptosis protein

IC_{50} – Half-maximal inhibitory concentration

ICC – Immunocytochemistry

IGF1 – Insulin-like growth factor 1

IL-11/11R/17 – Interleukin 11/11R/17

IP – Intraperitoneal

JAK2 – Janus kinase

JNK – JUN N-terminal kinase

LAMA3 – Laminin alpha 3

LGSC – Low-grade serous carcinoma

LINC01118 – Long intergenic non-protein coding RNA 1118

lncRNAs – Long non-coding ribonucleic acid

Ls – Lysosomes

m/v – Mass/volume

MA – Malignant ascites

MAD2 – Mitotic arrest deficiency protein 2

MAP – Microtubule-associated protein

MC – Mucinous carcinoma

Mcl-1 – Myeloid cell leukemia-1

MDR – Multidrug resistance

MDSCs – Myeloid-derived suppressor cells

MFAP5 – Microfibrillar-associated protein 5

MFI – Mean fluorescence intensity

Mi – Mitochondria

miRNAs – Microribonucleic acid

MLL3/4 – Mixed-lineage leukemia protein 3/4

MMP – Metalloproteinase

MMR – Mismatch repair

MRE11 – Meiotic recombination 11

mRNA – Messenger ribonucleic acid

MRP1/2/4 – Multidrug resistance-associated protein 1/2/4

MRPS11 – Mitochondrial ribosomal protein S11

MS/LH1/2 – MUTL protein homolog 1/2

MSX1 – Msh homeobox 1

MT – Metallothionein

mTOR – Mammalian target of rapamycin

mTORC1 – Mammalian targets of rapamycin complex 1

MTT – 3-(4.5-Dimethylthiazol-2-yl)-2,5-diphenyltetrazolium

NACT – Neo-adjuvant chemotherapy

NCALD – DNA hypermethylation of neurocalcin delta

NEAT1 – Nuclear enriched abundant transcript 1

NER – Nucleotide excision repair

NF1 – Neurofibromatosis type 1

NFkB – Factor nuclear kappa B

NHEJ – Non-homologous end joining

NOXA – Phorbol-12-myristate-13-acetate-induced protein 1

Nrf2 – Nuclear factor erythroid 2-related factor 2

ºC – Celsius

OC – Ovarian cancer

OCT4 – Octamer-binding transcription factor 4

OE – Overexpression

OS – Overall survival

P – Pulse

P-gp – P-glycoprotein

PALB2 – Partner and localizer of BRCA2

PARG – Poly(ADP-ribose) glycohydrolase

PARP1 – Poly(ADP-ribose) polymerase 1

PARPis – Poly(ADP-ribose) polymerase inhibitors

PARylation – Poly(ADP) ribosylation

PB – Presto Blue

PBS – Phosphate-buffered saline

PDGF – Platelet-derived growth factor

PFI – Platinum-free interval

PFS – Progression-free survival

PGCCs – Polyploid giant cancer cells

PGF – Placenta growth factor

PI – Propidium iodide

PI3K/Akt – Phosphoinositide 3-kinase/protein kinase B

PLK1 – Polo-like kinase 1

POLH – DNA polymerase eta

PolyHEMA – Poly(2-hydroxyethyl methacrylate)

PR – Partial response

PTEN – Phosphatase and tensin homolog

PTIP – Pax transactivation domain-interacting protein

PTX R – Paclitaxel-resistant

PUMA – p53 upregulated modulator of apoptosis

qRT-PCR – Real-time quantitative reverse transcription polymerase chain reaction

R0 – Microscopic or no residual disease

RAD51C/D – RAD51 recombinase C/D

RB1 – Retinoblastoma protein 1

RER – Rough endoplasmic reticulum

RH-123 – Rhodamine 123

ROS – Reactive oxygen species

Rpm – Rotation per minute

RT – Room temperature

SAC – Spindle assembly checkpoint

SD – Standard deviation

SIRT5 – Sirtuin 5

SLFN11 – Schlafen 11

SOX2/9 – Sex-determining region Y-box transcription factor 2/9

SRB – Sulforhodamine B

STAT3 – Signal transducer and activator of transcription 3

STR – Short tandem repeat

SYK – Spleen tyrosine kinase

TAMs – Tumor-associated macrophages

TANs – Tumor-associated neutrophils

TCGA – The cancer genome atlas

TDP1 – Tyrosyl-DNA phosphodiesterase 1

TFI – Treatment-free interval

TGF-β – Transforming growth factor beta

TILs – Tumor-infiltrating lymphocytes

TME – Tumor microenvironment

TNF – Tumor necrosis factor

TWIST – Twist-related protein 1

v/v – Volume/volume

VEGF – Vascular endothelial growth factor

VEGFR – Vascular endothelial growth factor receptor

WHO – World Health Organization

Wnt – Wingless/Integrated

XIAPs – X-linked inhibitors of apoptosis proteins

XPA/C/DG – Xeroderma pigmentosum complementation group A/C/D/G

ZIC1 – Zic family member 1

LIST OF FIGURES

Graphical abstract. Schematic representation of the experimental work performed in this project.....LIV

CHAPTER I

Figure 1. Estimated new cases (A) and deaths (B) of gynecologic cancers.....4

Figure 2. Estimated incidence and mortality of OC.....5

Figure 3. Illustrative diagram depicting the natural history of ovarian cancer, its main treatments, and the challenges of chemoresistance.....10

Figure 4. The accumulation of MA in OC.....12

Figure 5. A personalized medicine approach in OC using MA.....19

Figure 6. Schematic representation of the main molecular mechanisms contributing to Carboplatin resistance in OC.....22

Figure 7. Schematic representation of the main molecular mechanisms contributing to Paclitaxel resistance in OC.....30

Figure 8. Schematic representation of the main molecular mechanisms contributing to PARPi resistance in OC.....40

Figure 9. Schematic representation of the main molecular mechanisms contributing to Bevacizumab resistance in OC.....45

CHAPTER III

Figure 10. Representative scheme of the clinical evolution of ovarian cancer through the analysis of malignant ascites during the disease's time course.....59

Figure 11. Expression of ALDH1A1, SOX2, CD44v6, and P-gp is Associated with chemotherapy.....65

Figure 12. Expression of ALDH1A1, SOX2, CD44v6, and P-gp is increased in MA samples obtained after chemotherapy.....68

CHAPTER IV

Figure 13. OVCAR8 PTX R variants demonstrate high resistance to Paclitaxel.....99

Figure 14. OVCAR8 PTX R variants overcome Paclitaxel-induced G_2/M arrest and apoptosis.....101

Figure 15. OVCAR8 PTX R variants demonstrate high anoikis resistance, colony formation, and migration capacity.……103
Figure 16. OVCAR8 PTX R variants shown p-gp overexpression.……105
Figure 17. Repurposed drugs have shown high efficacy in reducing the cellular viability of chemoresistant HGSC cells.……122
Figure 18. Repurposed drugs have been found to enhance the effectiveness of Paclitaxel in reducing the cellular viability of chemoresistant HGSC cells……...125
Figure 19. Representative microscopy images of (A) OVCAR8 and (B) OVCAR8 PTX R P cells after exposure to the following treatment at their respective IC_{50} concentrations for 48 hours.……...……...126
Figure 20. Combining Paclitaxel with repurposed drugs has a synergistic effect on chemoresistant HGSC cells……...……..129
Figure 21. Combining Paclitaxel with repurposed drugs demonstrates a synergistic effect on OVCAR8 cells.……...……..133
Figure 22. Combining Paclitaxel with repurposed drugs demonstrates a synergistic effect on OVCAR8 PTX R P cells.……...……..135
Figure 23. Combining Paclitaxel with repurposed drugs demonstrates an antagonistic effect on HOSE6.3 cells.……...…….....137
Figure 24. Repurposed drugs increase the efficacy of Carboplatin in reducing the cellular viability of chemoresistant HGSC cells…..……...…….....156
Figure 25. Repurposed drugs improved the cytotoxic effect of Carboplatin on chemoresistant HGSC cells.……...…….157
Figure 26. Combining Carboplatin with repurposed drugs has a synergistic effect on chemoresistant HGSC cells.……...…….161
Figure 27. Combining Carboplatin with Metformin has a synergistic effect on OVCAR8 cells...…..……...…….163
Figure 28. Combining Carboplatin with Pitavastatin and Metformin has a synergistic effect on OVCAR8 PTX R P cells…..……..166
Figure 29. Combining Carboplatin with repurposed drugs has an antagonistic effect on HOSE6.3 cells.……...……...168
Figure 30. The combination of Carboplatin with repurposed drugs has an antagonistic effect on HOSE6.3 cells…….....……...……..170
Figure 31. Combining Carboplatin with Pitavastatin has an additive effect on OVCAR8 and OVCAR8 PTX R C cells according to the Loewe synergy model. …….....……187

Figure 32. Combining Carboplatin with Ivermectin has an additive effect on OVCAR8 and OVCAR8 PTX R C cells according to the Loewe synergy model…….....……...188
Figure 33. Combining Paclitaxel with Pitavastatin has an additive effect on OVCAR8 and OVCAR8 PTX R C cells according to the Loewe synergy model…….....……...190
Figure 34. Combining Paclitaxel with Ivermectin has an additive effect on OVCAR8 and OVCAR8 PTX R C cells according to the Loewe synergy model…….....……...191
Figure 35. Pitavastatin and Ivermectin improved the cytotoxic effect of Carboplatin and Paclitaxel on OVCAR8 cells..…….....…….....……192
Figure 36. Pitavastatin and Ivermectin improved the cytotoxic effect of Carboplatin and Paclitaxel on OVCAR8 PTX R C cells..…….....…….....193

CHAPTER V

Figure 37. Illustrative figure showing the various methods, techniques, and conditions tested during the development of the patient-derived cultures..…….....……...220
Figure 38. Representative images of MA-derived culture (HGS#55) after 31 days in culture demonstrate the impact of different culture conditions…….……223
Figure 39. Representative images of MA-derived culture (HGS#56) after 30 days in culture demonstrate the impact of different culture conditions…….……224
Figure 40. Representative images of MA-derived culture (HGSC#55) over 31 days in culture illustrate the effects of different culture procedures…….……229
Figure 41. Representative images of MA-derived culture (HGSC#56) over 30 days in culture illustrate the effects of different culture procedures...…….……..231
Figure 42. Representative images of MA-derived culture (HGSC#56) over 36 days in culture highlight the differences after passages and medium changes to reduce the number of fibroblasts and increase Ma-derived culture yield…….…….....233
Figure 43. Representative MA-derived culture model over 30 days in culture, demonstrating the retention of key morphological and immunophenotypic characteristics from the original MA sample.…….…….…….…….……238
Figure 44. Establishment of patient-derived cultures from the malignant ascites of a platinum-resistant HGSC patient..…….…….....……238

LIST OF TABLES

CHAPTER III

Table 1. Characterization of MA samples collected from HGCS patients both before (n=19) and after (n=18) Chemotherapy……..……..62

Table 2. Association of ALDH1A1/SOX2/CD44v6/P-gp expression in HGSC MA samples collected from patients before (n=19) and after chemotherapy (n=18) cycles.……67

Table 3. Association of ALDH1A1/SOX2/CD44v6/P-gp expression in HGSC MA samples collected from patients' platinum-sensitive before (n=14) and after chemotherapy (n=10)...69

Table 4. Association of ALDH1A1/SOX2/CD44v6/P-gp expression in HGSC MA samples collected from patients' platinum-refractory/platinum-resistant before (n=2) and after chemotherapy (n=8)……71

Table 5. Association of ALDH1A1/SOX2/CD44v6/P-gp expression in HGSC MA samples collected from patients' platinum-sensitive (n=10) and platinum-refractory/resistant (n=8) after chemotherapy…….72

CHAPTER IV

Table 6. Fa values and the corresponding CI values to determine the synergistic effects of drugs on OVCAR8 and OVCAR8 PTX R P cells……129

LIST OF SUPPLEMENTARY FIGURES

CHAPTER IV

Figure S1. Expression of ALDH1A1, SOX2, CD44v6, and P-gp is not associated with platinum response in MA obtained before chemotherapy……..83

Figure S2. IC_{50} and fold-resistance for Paclitaxel in OVCAR8 and OVCAR8 PTX R cell lines…….110

Figure S3. Proportion of sub-G1 and polyploid (>4C) populations in OVCAR8 and OVCAR8 PTX R cell lines……..110

Figure S4. Repurposed drugs demonstrate low efficacy in reducing the cellular viability of HOSE6.3 cells……..……144

Figure S5. Representative microscopy images of HOSE6.3 cells…….145

Figure S6. Combining Paclitaxel with repurposed drugs has an antagonistic effect on HOSE6.3 cells……147

Figure S7. Pitavastatin and Ivermectin increase the efficacy of Carboplatin in reducing the cellular viability of chemoresistant HGSC cells…….....198

Figure S8. Combining Carboplatin with Pitavastatin has an antagonistic effect on OVCAR8 and OVCAR8 PTX R C cells for HSA, Bliss Independence, and ZIP synergy models…….200

Figure S9. Combining Carboplatin with Ivermectin has an antagonistic effect on OVCAR8 and OVCAR8 PTX R C cells for HSA, Bliss Independence, and ZIP synergy models…….202

Figure S10. Pitavastatin and Ivermectin increase the efficacy of Paclitaxel in reducing the cellular viability of chemoresistant HGSC cells..…….....204

Figure S11. Combining Paclitaxel with Pitavastatin has an antagonistic effect on OVCAR8 and OVCAR8 PTX R C cells for HSA, Bliss Independence, and ZIP synergy models…….206

Figure S12. Combining Paclitaxel with Ivermectin has an antagonistic effect on OVCAR8 and OVCAR8 PTX R C cells for HSA, Bliss Independence, and ZIP synergy models…….208

LIST OF SUPPLEMENTARY TABLES

CHAPTER III

Table S1. Clinical characteristics of malignant ascites samples before and after chemotherapy.....80

Table S2. Association of ALDH1A1/SOX2/CD44v6/P-gp expression in HGSC MA samples collected from patients' platinum-sensitive (n=14) and platinum-refractory/resistant (n=2) before chemotherapy.....84

CHAPTER IV

Table S3. List of antibodies used for ICC and western blotting studies….....111

Table S4. The cellular viability (%) of OVCAR8 and OVCAR8 PTX R P cells after treating with Paclitaxel and repurposing drugs…….....145

Table S5. Fa values and the corresponding CI values to determine the synergistic effects of drugs on HOSE6.3 cells…….....147

Table S6. The cellular viability (%) of HOSE6.3 cells after treating with Paclitaxel and repurposing drugs…….....148

Table S7. The cellular viability (%) of OVCAR8 and OVCAR8 PTX R P cells after treating with Carboplatin and repurposing drugs...…….....178

Table S8. The cellular viability (%) of HOSE6.3 cells after treating with Carboplatin and repurposing drugs...…….....179

CHAPTER V

Table S9. Table displaying the composition of the SOM, outlining the specific components, concentrations, and conditions used to establish MA-derived cultures.....…….....240

PUBLICATIONS

This section presents all the original research and review papers, book chapters, and poster communications within the scope of this Doctoral Thesis.

A) ORIGINAL RESEARCH PAPERS PUBLISHED IN NATIONAL AND INTERNATIONAL PEER-REVIEWED JOURNALS

1. **Nunes M**, Almeida-Nunes DL, Abreu M, Bartosch C, & Ricardo S. (2024). *Que outra utilidade clínica poderão ter as ascites no carcinoma do ovário? Revista Portuguesa De Oncologia,* 7(1-2), 25–30. https://rponcologia.com/index.php/rpo/article/view/65.
2. **Nunes M**, Duarte D, Vale N, Ricardo S. (2022). The Antineoplastic Effect of Carboplatin Is Potentiated by Combination with Pitavastatin or Metformin in a Chemoresistant High-Grade Serous Carcinoma Cell Line. Int J Mol Sci. 2022 Dec 21;24(1):97. doi: 10.3390/ijms24010097.
3. **Nunes M**, Duarte D, Vale N, Ricardo S. Pitavastatin and Ivermectin Enhance the Efficacy of Paclitaxel in Chemoresistant High-Grade Serous Carcinoma. Cancers (Basel). 2022 Sep 7;14(18):4357. doi: 10.3390/cancers14184357.
4. **Nunes M**, Pacheco F, Coelho R, Leitão D, Ricardo S, David L. Mesothelin Expression Is Not Associated with the Presence of Cancer Stem Cell Markers SOX2 and ALDH1 in Ovarian Cancer. Int J Mol Sci. 2022 Jan 18;23(3):1016. doi: 10.3390/ijms23031016.
5. **Nunes M**, Silva PMA, Coelho R, Pinto C, Resende A, Bousbaa H, Almeida GM, Ricardo S. Generation of Two Paclitaxel-Resistant High-Grade Serous Carcinoma Cell Lines with Increased Expression of P-Glycoprotein. Front Oncol. 2021 Oct 21;11:752127. doi: 10.3389/fonc.2021.752127.

B) REVIEW PAPERS PUBLISHED IN INTERNATIONAL PEER-REVIEWED JOURNALS

1. **Nunes M**, Bartosch C, Abreu MH, Richardson A, Almeida R, Ricardo S. Deciphering the Molecular Mechanisms behind Drug Resistance in Ovarian Cancer to Unlock Efficient Treatment Options. Cells. 2024 May 4;13(9):786. doi: 10.3390/cells13090786.

C) BOOK CHAPTERS PUBLISHED IN INTERNATIONAL PEER-REVIEWED PUBLICATIONS

1. **Nunes M**, Ricardo S. Chemoresistance in Ovarian Cancer: The Role of Malignant Ascites. In: Lele S, editor. Ovarian Cancer [Internet]. Brisbane (AU): Exon Publications; 2022 Sep 8. Chapter 2. PMID: 36343141.

D) ORAL COMMUNICATIONS IN NATIONAL AND INTERNATIONAL CONGRESSES

1. **Nunes M**, Ricardo S. (2024). Ivermectin: an ally to reverse P-glycoprotein-associated multidrug resistance in ovarian cancer. III 1H-TOXRUN International Congress 2024: No Boundaries for Toxicology: One Health, One Society, One Planet, The Big Challenges for the 21st Century, organized by TOXRUN/IUCS-CESPU and realized in Hotel Cristal, Porto, Portugal.

E) POSTER COMMUNICATIONS IN NATIONAL AND INTERNATIONAL CONGRESSES

1. **Nunes M**, Ricardo S. (2024). Repurposing Ivermectin to Enhance Chemotherapy's Effectiveness in High-Grade Serous Carcinoma**,** EACR 2024 Congress: Innovative Cancer Science, organized by European Association for Cancer Research, and realized in Rotterdam Ahoy, Rotterdam, Netherlands.
2. **Nunes M**, Almeida-Nunes DL, Costa A, Ricardo S. (2023). Cell Microarray as a Powerful Tool to Accelerate Cancer Research: Focus on Drug Screening, II TOXRUN International Congress 2023: No Boundaries for Toxicology: One Health, One Society, One Planet, organized by TOXRUN/IUCS-CESPU and realized in Hotel Cristal, Porto, Portugal.
3. **Nunes M**, Duarte D, Vale N, Ricardo S. (2022). Synergism Between Carboplatin and Repurposed Drugs in Chemoresistant High-Grade Serous Carcinoma. EACR Conference 2022: The invisible phase of metastasis: Impact of dormancy, cancer cell plasticity and evolution of the niche during metastatic progression, virtual event, worldwide. – ***Travel Grant – EACR Conference.***
4. **Nunes M**, Nunes D, Abreu M, Bartosch C, Ricardo S. (2022). Recycling the Discarded Ovarian Cancer Ascites to Monitor Therapy Resistance, 23rd European Congress on Gynaecological Oncology, organized by ESGO and realized in Berlin, Germany.
5. **Nunes M**, Duarte D, Vale N, Ricardo S. (2022). Combining Repurposing Drugs with Paclitaxel Has a Synergic Effect in Chemoresistant High-Grade Serous Carcinoma. 5th ASPIC International Congress, organized by *Associação Portuguesa de Investigação em Cancro,* Porto, Portugal.

6. **Nunes M**, Brandão C, Ricardo S. (2022). Combining Paclitaxel with Repurposing Drugs Improve Ovarian Cancer Management. *I Congresso Internacional da TOXRUN/V Congresso da Associação Portuguesa de Ciências Forenses/XIV Jornadas Científicas de Ciências do Instituto Universitário de Ciências da Saúde,* Porto, Portugal. – ***Best Poster Award offered by APCF Portuguese Association of Forensic Sciences.***
7. Ferreira, S, **Nunes M**, Almeida-Nunes DL, Ricardo S. (2022). Phenotypic Evaluation of the Ovarian Tumor Cells Presents in Malignant Ascites. *I Congresso Internacional da TOXRUN/V Congresso da Associação Portuguesa de Ciências Forenses/XIV Jornadas Científicas de Ciências do Instituto Universitário de Ciências da Saúde,* Porto, Portugal.
8. **Nunes M**, Ricardo S. (2021). Pitavastatin Partially Restore Paclitaxel Sensitivity in High-Grade Serous Carcinoma Cell Lines. EACR Conference 2021: Goodbye Flat Biology: Next Generation Cancer Models, virtual event, worldwide.

ABSTRACT

Ovarian cancer survival rates have remained relatively the same over recent decades. Patients typically undergo cytoreductive surgery to minimize residual disease, followed by systemic chemotherapy with Carboplatin and Paclitaxel. Adding Bevacizumab and PARP inhibitors has improved disease-free survival before progression. Various drugs, used alone or in combination, are being explored for recurrent cases to improve survival and quality of life. However, about 70% to 80% of advanced ovarian cancer patients experience recurrence and develop therapy resistance within five years.

Drug repurposing identifies new uses for existing drugs. This approach is faster and more cost-effective than developing new drugs since established ones have known toxicological and pharmacokinetic profiles. Additionally, repurposed drugs often progress to clinical trials due to their tolerability and availability as generics, making them more accessible and affordable than newly patented compounds.

Drug repurposing, which involves using two or more agents, can enhance traditional chemotherapy. This approach improves treatment effectiveness, potentially reducing chemotherapy doses and side effects while maintaining therapeutic benefits and decreasing chemoresistance. It is particularly effective when drugs target different pathways, promoting a synergistic effect that allows for lower concentrations.

Malignant ascites in ovarian cancer often contain tumor cells that can be isolated and cultured to create patient-derived cultures. This fluid includes components from the tumor microenvironment, such as cytokines and extracellular matrix proteins, which can influence the growth of these cultures. Such models are valuable for assessing drug effectiveness and identifying personalized treatment options for patients.

We hypothesize that drug repurposing can influence chemoresistant ovarian cancer cells, leading to new therapies that improve patient outcomes.

This PhD project aimed to characterize patient-derived samples by assessing biomarkers for chemoresistance profiles using immunocytochemistry. Two chemotherapy-resistant ovarian cancer cell lines were developed and treated with standard chemotherapy alongside drug-repurposing strategies involving Pitavastatin, Metformin, Ivermectin, Itraconazole, and Alendronate. Finally, patient-derived cultures from malignant ascites were created to test the effectiveness of both approved ovarian cancer treatments and repurposed drugs.

To evaluate biomarkers to identify chemoresistance in patient-derived samples, malignant ascites samples were obtained from high-grade serous carcinoma patients pre-

and post-chemotherapy. We assessed the immunoexpression of four biomarkers linked to cancer stem cells and drug resistance – ALDH1A1, SOX2, CD44v6, and P-gp – in 37 samples (19 before and 18 after chemotherapy). The results highlight the need to centrifuge the entire volume of malignant ascites to evaluate low-expression biomarkers. Furthermore, the ALDH1A1/CD44v6/SOX2/P-gp profile was more frequently observed in post-chemotherapy samples ($p=0.003$), suggesting that chemotherapy impacts these markers and correlates with platinum-resistance ($p=0.068$). These findings indicate that chemotherapy induces molecular changes in malignant cells, reflecting tumor progression dynamics. Our goal is to develop a lab test to measure platinum-based chemotherapy resistance accurately, thereby improving upon the current clinical methods.

Two high-grade serous carcinoma cell lines, OVCAR8 PTX R C and OVCAR8 PTX R P, were developed to study chemoresistance. These cell lines are inherently resistant to Carboplatin and have developed resistance to Paclitaxel. Notably demonstrating stable Paclitaxel-resistance over long-term culture and freeze/thaw cycles. The primary mechanism for this resistance is increased P-glycoprotein levels, as shown by the restoration of sensitivity to Paclitaxel when Verapamil inhibits the efflux pump. These cell lines represent a significant portion of ovarian cancer recurrence phenotypes, serving as a reliable resource for preliminary drug testing and the development of new therapeutic strategies.

This project developed innovative combination models for ovarian cancer treatment. Initial drug tests identified repurposing potential for ovarian cancer therapy. We assessed the therapeutic benefits of combining Carboplatin or Paclitaxel with repurposed drugs like Pitavastatin (antilipidemic), Metformin (antidiabetic), Ivermectin (antiparasitic), Itraconazole (antifungal), and Alendronate (antiosteoporosis). The effects on chemoresistant and non-tumoral (HOSE6.3) cell lines were measured for cellular viability using the Pesto Blue™ (2D cellular models) and CellTiter-Glo® Luminescent Cell Viability (3D cellular models) assays. To evaluate the synergistic effects of combining chemotherapy with repurposed drugs, we quantified the synergism using models like Chou-Talalay, Highest Single Agent, Bliss independence, and Loewe, with CompuSyn and SynergyFinder software.

Our findings indicate that Pitavastatin and Ivermectin are promising for repurposing ovarian cancer alongside frontline chemotherapeutics. Combining Paclitaxel with Pitavastatin or Ivermectin produces significant synergistic and cytotoxic effects on both chemoresistant cell lines. Combining Carboplatin with Pitavastatin or Metformin also shows enhanced effects compared to Carboplatin alone. These combinations exhibit a favorable

pharmacological profile in non-tumoral cells, suggesting potential for safe clinical use. Consequently, the therapeutic potential of Pitavastatin and Ivermectin in this context merits further investigation.

Ivermectin inhibits P-glycoprotein in specific cancer cell lines, potentially overcoming drug resistance by increasing the intracellular concentration of chemotherapy. It may also reduce P-glycoprotein expression, improving drug sensitivity. The effects of Pitavastatin on P-glycoprotein are complex; it might induce expression in some cases while modulating activity in others. Its capacity to influence P-glycoprotein suggests utility in treating chemoresistant cancers, where P-glycoprotein contributes significantly to chemoresistance. More research is needed to clarify their combined effects and clinical use.

Ultimately, a series of experiments was carried out to establish patient-derived cultures from malignant ascites of high-grade serous carcinoma patients. The study compared the control medium with autologous supernatant to evaluate how the tumor microenvironment affects growth and viability. Both static and agitated culture conditions were explored to understand mechanical influences on culture development. Various matrices, including Poly(methyl methacrylate) and Cultrex Reduced Growth Factor Basement Membrane Extract type 2, along with different culture media, were tested for their effects on patient-derived culture maintenance. Carboplatin treatment was assessed for its impact on culture viability. Finally, several assays, including the CellTiter-Glo® Luminescent Cell Viability Assay and the Alamar Blue™ assay, were conducted to evaluate cellular responses to culture conditions and treatments.

The optimal culture conditions used standard organoid medium (SOM) without agitation, supplemented with autologous supernatant from malignant ascites. The cost-effective viability assay employed was Alamar Blue™. This method enables the development of a personalized assay to assess drug efficacy according to each patient's needs. The test can be performed within a clinically relevant timeframe, facilitating the selection of the most effective treatment options for each case. Consequently, therapeutic choices can be optimized, leading to more targeted and effective treatments based on individual responses to drugs.

KEYWORDS

Ovarian Cancer, Chemoresistance, Drug Repurposing, Patient-Derived Cultures, Malignant Ascites-Derived Cultures, Personalized Medicine.

RESUMO

A taxa de sobrevivência no cancro do ovário tem permanecido relativamente constante nas últimas décadas. As pacientes realizam uma cirurgia de citoredução para obter uma doença residual mínima ou inexistente, seguida de quimioterapia sistémica com Carboplatina e Paclitaxel. A introdução do Benvacizumab e dos inibidores da PARP melhorou a sobrevivência livre de doença antes da progressão. Diversos fármacos, isolados ou em combinação, estão a ser investigados para casos recorrentes, com o objetivo de melhorar a sobrevivência e a qualidade de vida das pacientes. No entanto, cerca de 70% a 80% das pacientes com cancro do ovário avançado têm uma recorrência e desenvolvem resistência à terapia em menos de 5 anos.

O reaproveitamento de fármacos identifica novos usos terapêuticos para drogas já existentes. Esta estratégia é mais rápida e económica do que o desenvolvimento de novos fármacos, uma vez que os que já estão estabelecidos têm perfis toxicológicos e farmacocinéticos bem conhecidos. Além disso, o reaproveitamento de fármacos apresenta uma maior probabilidade de avançar para ensaios clínicos, dado que são mais tolerados e estão disponíveis como genéricos, tornando-os mais acessíveis e económicos do que compostos recém-patenteados.

O reaproveitamento de fármacos pode melhorar a quimioterapia tradicional através do uso de dois ou mais compostos. Este método melhora a eficácia do tratamento, potencialmente reduzindo as doses dos quimioterápicos e os efeitos secundários, enquanto mantem os benefícios terapêuticos e diminui a quimiorresistência. Particularmente quando os fármacos atuam em diferentes vias, o que pode promover um efeito sinérgico que permite utilizar concentrações mais baixas.

As ascites malignas no cancro do ovário frequentemente contêm células tumorais que podem ser isoladas e utlizadas em culturas derivadas de pacientes. Este fluido inclui elementos do microambiente tumoral, como citocinas e proteínas da matriz extracelular, que podem influenciar o crescimento destas culturas. Estes modelos são úteis para avaliar a eficácia de diferentes fármacos e identificar opções de tratamento personalizadas para cada paciente.

Hipotetizamos que o reaproveitamento de fármacos pode afetar as células de cancro do ovário quimioresistentes, facilitando o desenvolvimento de novas opções terapêuticas para melhorar o tratamento das pacientes.

Este projeto de doutoramento teve como objetivo caracterizar amostras derivadas de pacientes, avaliando biomarcadores para determinar perfis de quimiorresistência através

de imunocitoquímica. Duas linhas celulares de cancro do ovário resistentes à quimioterapia foram desenvolvidas e tratadas com Carboplatina ou Paclitaxel e combinadas com estratégias de reaproveitamento de fármacos, utilizando Pitavastatina, Metformina, Ivermectina, Itraconazole e Alendronato. Finalmente, foram desenvolvidas culturas derivados de pacientes a partir de ascites malignas para testar a eficácia tanto dos tratamentos aprovados para o cancro do ovário como de fármacos reaproveitados.

Para avaliar a expressão de biomarcadores e identificar perfis de quimiorresistência nas amostras derivadas de pacientes, foram utilizadas ascites malignas obtidas de pacientes com carcinoma seroso de alto grau antes e após o tratamento com quimioterapia. A imunoexpressão de quatro biomarcadores associados às *cancer stem cells* e resistência a fármacos — ALDH1A1, SOX2, CD44v6 e P-gp — foi avaliada em 37 amostras recolhidas antes (n=19) e após (n=18) quimioterapia. Os resultados destacam a necessidade de centrifugar o volume total das ascites malignas para avaliar biomarcadores com baixa expressão. Além disso, o perfil ALDH1A1/CD44v6/SOX2/P-gp foi mais frequentemente observado nas amostras pós-quimioterapia (p=0,003), sugerindo que a quimioterapia impacta esses marcadores e está relacionado com a platino-resistência (p=0,068). Estes resultados indicam que a quimioterapia induz alterações moleculares nas células malignas, refletindo a dinâmica da progressão tumoral. O nosso objetivo é desenvolver um teste laboratorial para medir com precisão a resistência à quimioterapia à base de platina, para melhorar os métodos clínicos atuais.

Duas linhas celulares de carcinoma seroso de alto grau, OVCAR8 PTX R C e OVCAR8 PTX R P foram desenvolvidas para estudar a quimiorresistência. Estas linhas são intrinsecamente resistentes à Carboplatina e desenvolveram resistência ao Paclitaxel. Notavelmente, essa resistência permaneceu estável mesmo durante culturas a longo prazo e após processos de congelação/descongelação. O mecanismo primário para a resistência ao Paclitaxel foi identificado como o aumento nos níveis da P-glicoproteína, evidenciado através da restauração da sensibilidade ao Paclitaxel quando é adicionado Verapamil que inibe a bomba de efluxo. Estas linhas celulares representam a maioria do fenótipo de recidivas de cancro do ovário, tornando-as num recurso essencial para testes preliminares de fármacos com vista ao desenvolvimento de novas estratégias terapêuticas.

Este projeto também teve como objetivo desenvolver modelos inovadores de combinação para o tratamento do cancro do ovário. Testes de drogas foram realizados inicialmente para identificar classes de medicamentos com potencial de reaproveitamento para a terapia do cancro do ovário. Foram explorados os benefícios terapêuticos de

combinar Carboplatina ou Paclitaxel com os fármacos reaproveitados, tais como: Pitavastatina (antilipémico), Metformina (antidiabético), Ivermectina (antiparasitário), Itraconazole (antifúngico) e Alendronato (antiosteoporótico). Os efeitos destas combinações nas linhas celulares quimioresistentes e não tumoral (HOSE6.3) foram avaliados, através de ensaios de viabilidade celular, nomeadamente pelo *Pesto Blue*™ (nos modelos celulares 2D) e *CellTiter-Glo® Luminescent Cell Viability* (nos modelos celulares 3D). Para avaliar os efeitos sinérgicos da combinação de quimioterapia com os fármacos reutilizados, quantificámos a sinergia através dos modelos: *Chou-Talalay, Highest Single Agent, Bliss independence* e *Loewe*, com os softwares *CompuSyn* e *SynergyFinder*.

Os nossos resultados demostraram que a Pitavastatina e a Ivermectina são os fármacos mais promissores para reaproveitamento no tratamento de cancro do ovário em combinação com os quimioterápicos utilizados na terapia de primeira linha. A combinação de Paclitaxel com Pitavastatina ou Ivermectina produziu efeitos sinérgicos e citotóxicos significativos em ambas as linhas celulares quimioresistentes. A combinação de Carboplatina com Pitavastatina ou Metformina também apresentou efeitos citotóxicos pronunciados em comparação com a Carboplatina. Estas combinações apresentaram um perfil farmacológico favorável em células não tumorais, indicando o seu potencial para uma aplicação clínica segura. Consequentemente, o potencial terapêutico da Pitavastatina e da Ivermectina neste contexto de doença devem ser explorados como opções terapêuticas.

A Ivermectina inibe a atividade da P-glicoproteína em linhas celulares de cancro, potencialmente ultrapassando a quimiorresistência ao aumentar a concentração intracelular dos quimioterápicos. Pode também reduzir a expressão da P-glicoproteína, aumentando a sensibilidade ao tratamento. Os efeitos da Pitavastatina sobre a P-glicoproteína são complexos, podendo induzir a expressão da P-glicoproteína em alguns casos, enquanto modula a sua atividade em outros. A sua capacidade para influenciar a P-glicoproteína sugere utilidade no tratamento de cancros quimioresistentes, onde a P-glicoproteína contribui significativamente para a quimiorresistência. Mais dados são necessários para esclarecer os seus efeitos combinados e o uso clínico.

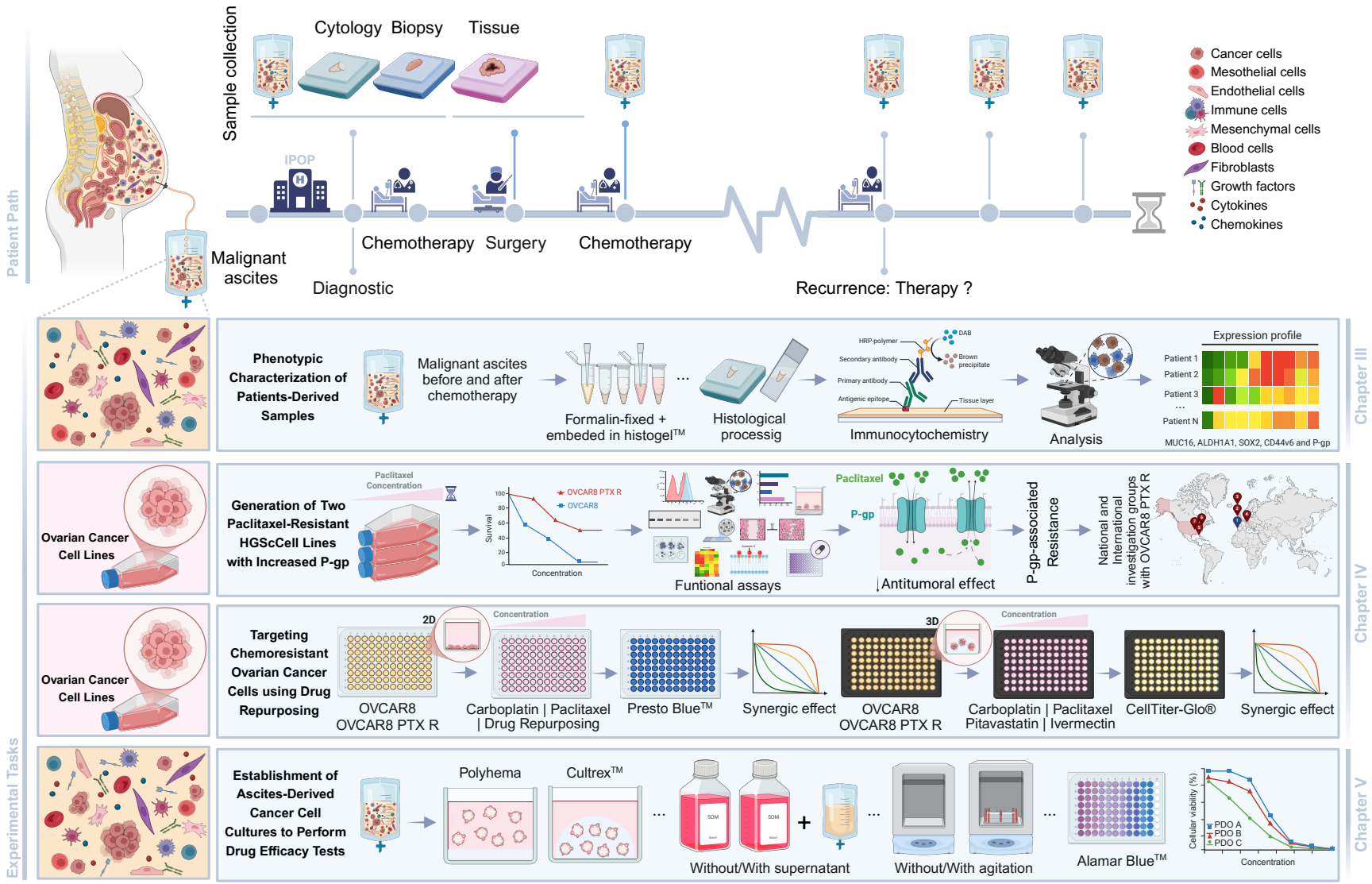
Finalmente, foram realizadas uma série de experiências para estabelecer culturas derivados de pacientes a partir de ascites malignas proveniente de pacientes com carcinoma seroso de alto grau. Este estudo comparou o meio de cultura controlo com meio suplementado com sobrenadantes de ascites malignas autólogas para avaliar como o microambiente tumoral influência o crescimento e a viabilidade. Também foram exploradas condições de cultura estáticas e com agitação para compreender os efeitos dos fatores

mecânicos no desenvolvimento das culturas. Varias matrizes, incluindo *Poly(methyl methacrylate)* e *Cultrex Reduced Growth Factor Basement Membrane Extract type 2* bem como várias formulas de meios de cultura, foram testadas para avaliar a sua influência na formação e manutenção das culturas derivados de pacientes. O tratamento com Carboplatina foi avaliado pelo seu impacto na viabilidade das culturas. Finalmente, vários ensaios, incluindo o *CellTiter-Glo® Luminescent Cell Viability Assay* e *Alamar Blue™,* foram realizados para avaliar as respostas celulares às condições de cultura e tratamentos.

As condições ótimas de cultura envolveram a utilização do meio de cultura *standard organoid medium* (SOM), sem agitação e suplementado com o sobrenadante autólogo das ascites malignas. O ensaio de viabilidade utilizado para testar diferentes tratamentos que demonstrou ser mais rentável foi o Alamar Blue™. Este método permite o desenvolvimento de um ensaio personalizado para avaliar a eficácia dos medicamentos de acordo com as necessidades de cada paciente. O teste pode ser realizado dentro de um prazo clínico relevante, facilitando a seleção da opção de tratamento mais eficaz para cada paciente. Consequentemente, as escolhas terapêuticas podem ser otimizadas, levando a um tratamento mais direcionado e eficaz com base nas respostas individuais aos fármacos.

PALAVRAS-CHAVE

Cancro do Ovário, Quimiorresistência, Reaproveitamento de Fármacos, Culturas Derivadas de Pacientes, Culturas Derivadas de Ascites Malignas, Medicina Personalizada.


Patient Path
Sample collection
Cytology
Biopsy
Tissue
IPOP
Malignant ascites
Chemotherapy
Surgery
Chemotherapy
Diagnostic
Recurrence: Therapy ?
Cancer cells
Mesothelial cells
Endothelial cells
Immune cells
Mesenchymal cells
Blood cells
Fibroblasts
Growth factors
Cytokines
Chemokines
Experimental Tasks
Phenotypic Characterization of Patients-Derived Samples
Malignant ascites before and after chemotherapy
Formalin-fixed + embeded in histogel™
Histological processig
Immunocytochemistry
Analysis
Expression profile
Patient 1
Patient 2
Patient 3
Patient N
MUC16, ALDH1A1, SOX2, CD44v6 and P-gp
Chapter III
Ovarian Cancer Cell Lines
Generation of Two Paclitaxel-Resistant HGScCell Lines with Increased P-gp
Paclitaxel Concentration
OVCAR8 PTX R
OVCAR8
Survival
Concentration
Funtional assays
Paclitaxel
P-gp
Antitumoral effect
P-gp-associated Resistance
National and International investigation groups with OVCAR8 PTX R
Chapter IV
Ovarian Cancer Cell Lines
Targeting Chemoresistant Ovarian Cancer Cells using Drug Repurposing
2D
OVCAR8
OVCAR8 PTX R
Concentration
Carboplatin | Paclitaxel | Drug Repurposing
Presto Blue™
Synergic effect
3D
OVCAR8
OVCAR8 PTX R
Concentration
Carboplatin | Paclitaxel
Pitavastatin | Ivermectin
CellTiter-Glo®
Synergic effect
Establishment of Ascites-Derived Cancer Cell Cultures to Perform Drug Efficacy Tests
Polyhema
Cultrex™
Without/With supernatant
Without/With agitation
Alamar Blue™
Cellular viability (%)
PDO A
PDO B
PDO C
Concentration
Chapter V

Graphical abstract. Schematic representation of the experimental work performed in this project. The clinical pathway for an ovarian cancer patient consists of initial diagnosis, chemotherapy, malignant ascites development, surgical intervention, and the emergence of chemoresistance. This journey underscores the difficulties in managing the disease and the intricate treatment options during advanced stages. Chapter III focuses on evaluating biomarkers associated with chemoresistance in malignant ascites samples from HGSC patients, both before and after chemotherapy. Key biomarkers analyzed include differentiation markers (MUC16), cancer stem cell markers (SOX2, ALDH1A1, CD44v6), and drug resistance markers (P-gp). In Chapter IV, two chemoresistant OC cell lines (OVCAR8 PTX R C and OVCAR8 PTX R P) were developed by exposing OVCAR8 cells to increasing concentrations of Paclitaxel. These cell lines were tested for the stability of drug resistance and analyzed for biological behaviors such as proliferation, migration, apoptosis, and cell-cycle distribution. In recent years, several national (3) and international (5) investigation groups have solicited our chemoresistant cell lines. Chemoresistant cells were treated with Pitavastatin, Metformin, Ivermectin, Itraconazole, and Alendronate, which were used as promising candidates for combination with Carboplatin or Paclitaxel in 2D and 3D culture models. Cellular viability was evaluated through Presto Blue™ and CellTiter-Glo® Luminescent Cell Viability assays, respectively. Drug interactions were assessed for synergism using multiple reference models and software tools, and the most promising combinations were selected for further studies. Chapter V describes the optimization of protocols to establish malignant ascites-derived cultures for *ex vivo* drug efficacy testing. The effectiveness of Carboplatin was evaluated in these models using the Alamar Blue™ assay. Successful patient-derived cultures were established, and the potential for drug repurposing to enhance chemotherapy response will be explored in future projects. Figure created with Biorender.com. HGSC, high-grade serous carcinoma; MUC16, mucin 16; OC, ovarian cancer; P-gp, P-glycoprotein.

CHAPTER I

General Introduction

The information presented in this chapter is partially based on the following publications:

Nunes M, Ricardo S. Chemoresistance in Ovarian Cancer: The Role of Malignant Ascites. In: Lele S, editor. Ovarian Cancer [Internet]. Brisbane (AU): Exon Publications; 2022 Sep 8. Chapter 2. PMID: 36343141. – **1.4. Malignant Ascites**

Nunes M, Bartosch C, Abreu MH, Richardson A, Almeida R, Ricardo S. Deciphering the Molecular Mechanisms behind Drug Resistance in Ovarian Cancer to Unlock Efficient Treatment Options. Cells. 2024 May 4;13(9):786. doi: 10.3390/cells13090786. – **1.5. Chemoresistance**

1. Ovarian Cancer

1.1. Epidemiology

Cancer remains the leading cause of death globally, presenting significant challenges to life expectancy across many countries (1). Gynecological cancers, including ovary, corpus uteri, cervix uteri, vulva, and vagina, have a notable impact on women's health, with substantial disparities in early detection and management projected by 2050, particularly in regions with low Human Development Index (HDI) (2-5). In lower-HDI counties, the anticipated average risk of developing gynecological cancers could soar to a concerning 150%, compared to around 19.60% in nations with very high HDI (2-4) (**Figure 1A**). Additionally, in these low HDI nations, the projected average risk of mortality from gynecological cancers might rise to a staggering 154.60%, in contrast to roughly 35.50% in countries with very high HDI (2-4) (**Figure 1B**). This difference highlights the widening gap in mortality risks associated with gynecological cancers across different economic environments. Cervical cancer continues to be the leading cause of cancer-related deaths in low HDI nations, while ovarian and endometrial cancers dominate mortality rates in very high HDI countries (2-6). Ovarian cancer (OC), which includes ovarian, primary peritoneal, or fallopian tube cancers, is a significant global health concern (7). It represents the seventh most common cancer among women and the sixth leading cause of cancer-related mortality worldwide, contributing substantially to the burden of female cancers (3).

According to Globocan data, the estimated number of OC cases worldwide is currently about 324,600. Projections indicate that this number will increase to 476,900 by 2050, marking a rise of approximately 46.92% (2-4) (**Figure 2**). Similarly, the estimated number of deaths is expected to surge from 207,000 to 336,600 during the same period, reflecting an increase of roughly 62.61% (2-4) (**Figure 2**). OC is associated with one of the worst prognoses among gynecological malignancies, with a mortality rate significantly higher than that of breast cancer – despite its lower prevalence (8, 9). This high mortality rate can largely be attributed to the asymptomatic nature of tumor growth, delayed onset of symptoms, and the lack of effective screening methods, often resulting in diagnoses at advanced stages (10).

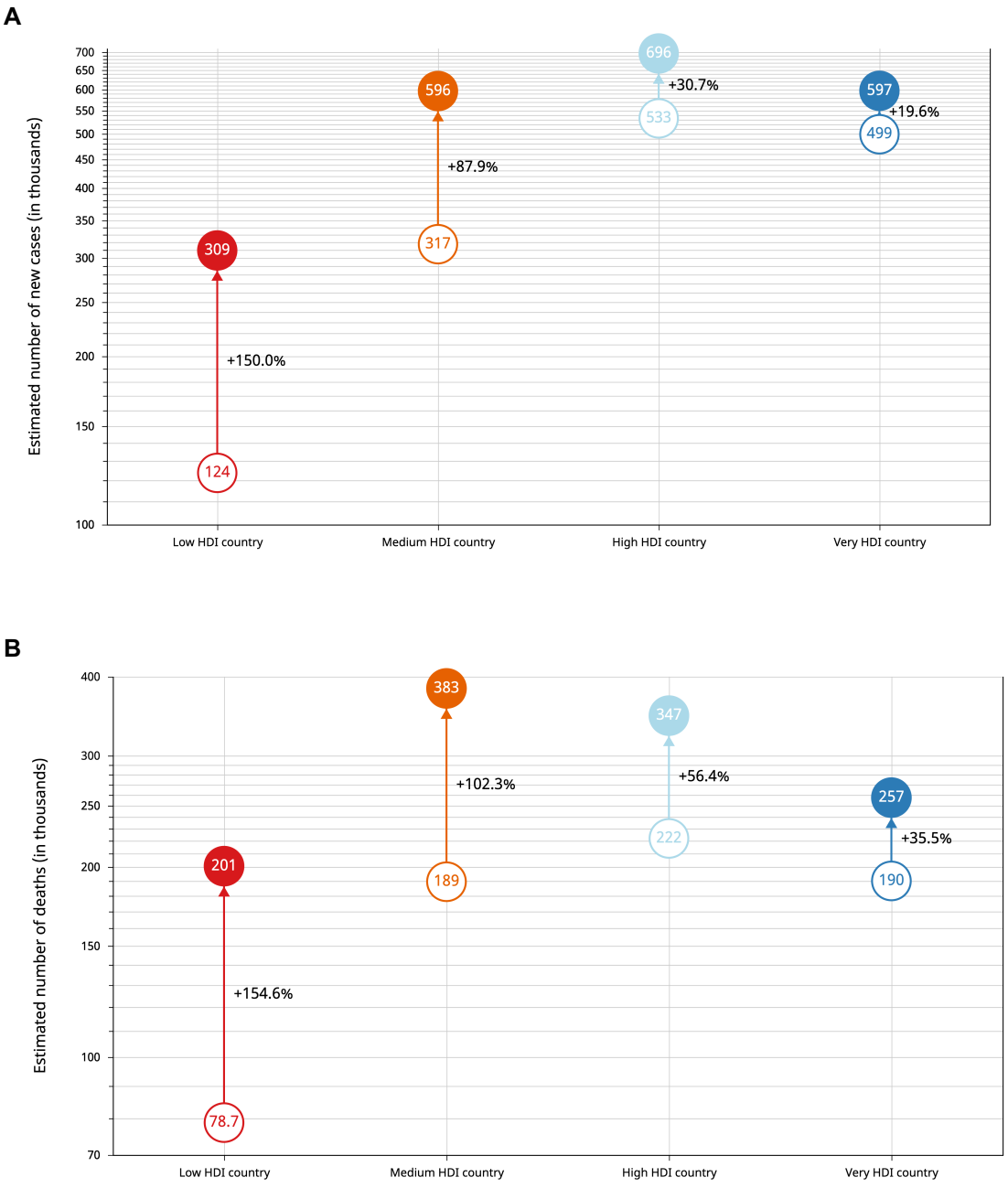


Figure 1. Estimated new cases (A) and deaths (B) of gynecologic cancers. This includes ovarian, uterine corpus, cervical, vulvar, and vaginal cancers among females aged 0 to 85+ from 2022 to 2050. Data obtained from Globocan 2022 (version 1.1) – 08.02.2024 (4). HDI, Human Development Index.

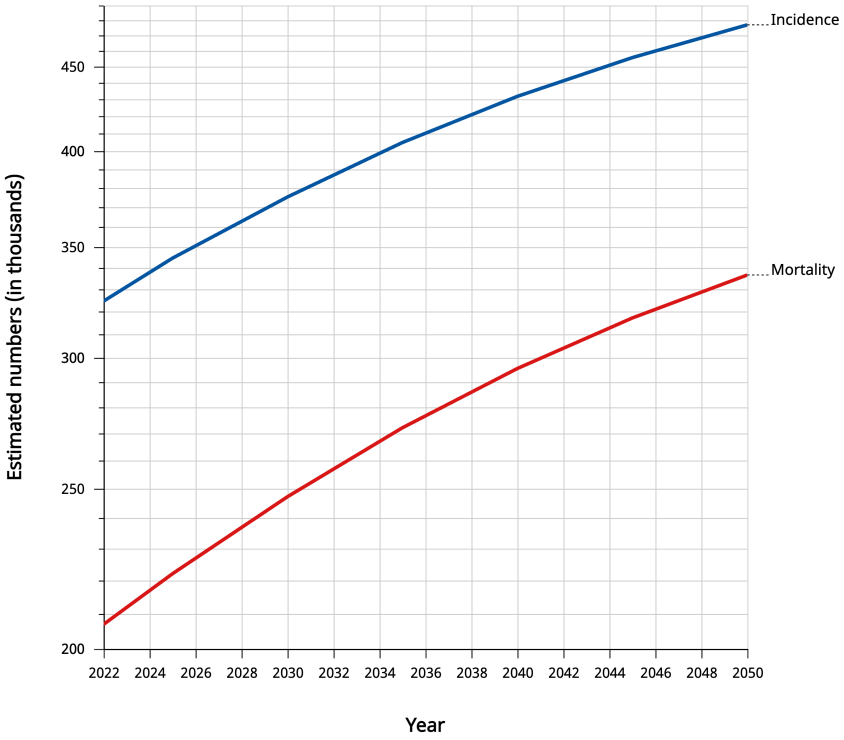


Figure 2. Estimated incidence and mortality of OC. This includes OC among females aged 0 to 85+ from 2022 to 2045. Data obtained from Globocan 2022 (version 1.1) – 08.02.2024 (4). OC, Ovarian cancer.

The majority of OC diagnoses occur in women over 60, emphasizing the importance of awareness and screenings for postmenopausal women (1). Major risk factors include age and inherited genetic mutations, particularly in the breast cancer genes (BRCA1 and BRCA2) (11). Additionally, a family history of ovarian or breast cancer, nulliparity, and hormone replacement therapy further elevate the risk (12).

OC incidence is higher in North America and Europe than in Asia and Africa. Some high-income countries show a slight decline in incidence, possibly due to better reproductive health and oral contraceptive use (13). Disparities in detection and treatment lead to worse outcomes in low- and middle-income countries (1), reflecting differences in genetics, healthcare access, and screening (1, 5). Due to the global non-uniformity of these trends, ongoing surveillance and research are crucial.

Prognosis varies by stage; the five-year survival rate for localized OC exceeds 90%, dropping to around 30% for advanced stages. Many women are diagnosed late due to a lack of early symptoms (1). Early detection remains a critical challenge, as many women present with advanced disease due to the lack of early symptoms.

In conclusion, the epidemiology of OC is complex and multifaceted, shaped by various biological, socio-economic, and healthcare factors. Continued research is essential to address the disparities in incidence and outcomes. Enhanced awareness, education, and effective screening strategies are critical to improving the prognosis and survival rates for women diagnosed with this challenging disease.

1.2. Histopathological Subtypes

OC is a heterogeneous disease encompassing several types with distinct precursor lesions, pathogenesis, dissemination, risk factors, molecular profiles, chemotherapy response, clinical course, and outcomes (14). According to the 5th edition of the World Health Organization (WHO) classification of female genital tract tumors, OC is subdivided into at least five main types: high-grade serous carcinoma (HGSC, 70%), endometrioid carcinoma (EC, 10%), clear cell carcinoma (CCC, 6–10%), low-grade serous carcinoma (LGSC, 5%), mucinous carcinoma (MC, 3–4%), along with rare histotypes (15). Epithelial ovarian cancer (EOC), which includes HGSC and LGSC, can be categorized into type I and II tumors (16). Type I tumors primarily originate from the ovary and are linked to continuous ovulation cycles, endometriosis, or inflammation; they are often diagnosed at an early stage, resulting in lower mortality and better clinical outcomes (16). This group includes low-grade EC, CCC, LGSC, MC, and borderline serous carcinomas (7). Conversely, type II tumors, predominantly HGSC (6), typically arise in the distal fallopian tube and are associated with genetic mutations in BRCA1/2, tumor protein 53 (p53), and other tumor-suppresser genes (16). HGSC is the most common histological subtype, and while it is highly sensitive to initial platinum-based therapy, nearly 90% of patients with advanced stages (FIGO stage III and IV) experience recurrence within five years, developing chemotherapy resistance and exhibiting shorter progression-free survival (PFS) (17, 18).

1.3. Treatment Strategies

The standard treatment for advanced OC involves primary debulking surgery followed by a combination of Carboplatin and Paclitaxel (19-21) (**Figure 3**). In patients with advanced stages, the amount of remaining disease after surgery is a crucial factor in predicting outcomes (7). The main aim of the surgical treatment is to achieve complete resection with clear margins, and the classification of residual tumors as R0 or R1 indicates better survival rates (22).

Calvert *et al.* demonstrated through a pharmacokinetic study that Paclitaxel and platinum compounds could be safely administrated with little pharmacodynamic interactions (23). The GOG111 trial showed that combining Paclitaxel with Cisplatin was superior to Cyclophosphamide with Cisplatin presenting a complete response (CR) rate of 51% compared to 36%, respectively (24). Additionally, there was a significant improvement in PFS from 13 to 18 months and overall survival (OS) from 24 to 38 months when Cisplatin and Paclitaxel were combined (24). Bookman *et al.* showed that combining Carboplatin with Paclitaxel demonstrated equivalent improved response rates, albeit with a more favorable toxicity profile (i.e., reduced risk of emesis, neuropathy, nephropathy, and hearing loss) compared to Cisplatin plus Paclitaxel (25). Moreover, du Bois *et al.* showed that Carboplatin could replace Cisplatin with comparable efficacy, better tolerance, and improved quality of life (26). The OV10 trial demonstrated that Paclitaxel, when compared to cyclophosphamide, improved overall response (OR 59% vs. 45%), CR (41% vs. 27%), PFS (15.5 months vs. 11.5 months), and OS (35.6 months vs. 25.8 months) (27). Although the effectiveness of Paclitaxel as a first-line single chemotherapeutic agent for OC was questioned, based on ICON3, GOG111, OV10, and GOG158 trials, the combination of Carboplatin and Paclitaxel continues to be the preferred first-line treatment for OC patients (21, 24, 27, 28).

For patients with aggressive tumor spread (i.e., bulky and extensive disease) or those who are not eligible for surgery, such as patients with cytologically stage IIIC and IV disease, an alternative treatment approach involves receiving 3–4 cycles of neo-adjuvant chemotherapy (NACT) followed by interval debulking surgery and additional chemotherapy (29-31). NACT, followed by interval debulking surgery, can be particularly useful in patients with poor performance status, significant medical comorbidities, visceral metastases, and those who have large pleural effusions and gross, malignant ascites (MA) (32, 33).

In OC, second-line chemotherapy involves administering systemic therapy after the initial treatment. This may consist of multiple subsequent treatment regimens (34). Various combinations of chemotherapeutic drugs have been studied to overcome chemoresistance following the initial Paclitaxel plus platinum treatment. However, clinical responses have been brief and have resulted in only minor improvements in survival (35). In clinical practice, three different platinum doublets have been utilized: Carboplatin and Paclitaxel, Carboplatin and Gemcitabine, and Carboplatin and Pegylated Liposomal Doxorubicin (26-28). These combinations are more effective than using a single platinum agent (17, 36).

Bevacizumab is an anti-angiogenic inhibitor that is currently approved by the Food and Drug Administration (FDA) as a component of primary therapy (in combination with

Carboplatin/Paclitaxel) for OC. It is also approved as a second-line treatment for platinum-sensitive or platinum-resistant disease (37-39). The results of the GOG0218 and ICON7 trials showed that after six cycles of chemotherapy plus Bevacizumab, continuing Bevacizumab as a single maintenance agent for about an additional year of treatment led to a superior PFS when compared to chemotherapy alone in the first-line setting and as maintenance therapy (38, 39). In oncology, maintenance therapy is used after achieving an initial response to anti-cancer drugs with the goal of "maintaining" the response with an acceptable toxicity profile (34). The rationale for maintenance therapy is to delay disease progression or relapse for as long as possible after first-line treatment, regardless of the amount of residual disease (34).

According to the AURELIA phase III trial, the addition of Bevacizumab to Paclitaxel, Topotecan, or Pegylated Liposomal Doxorubicin significantly improved PFS in patients with platinum-resistant OC (40). The OCEANS and GOG0213 phase III trials investigated the effectiveness of adding Bevacizumab to Carboplatin plus Paclitaxel or Carboplatin plus Gemcitabine in recurrent platinum-sensitive OC. These trials revealed superior PFS outcomes associated with the addition of Bevacizumab (41, 42). In 2018, based on the GOG0218 phase III clinical study, the FDA approved Bevacizumab as a component of primary OC therapy in combination with Carboplatin plus Paclitaxel, followed by a single-agent Bevacizumab as a maintenance option for the treatment of patients with advanced (stage III or IV) OC after initial surgery (38).

PARP inhibitors (PARPi) such as Olaparib, Niraparib, and Rucaparib have been approved by the FDA and the European Medicines Agency (EMA) as maintenance therapy for patients who have achieved a CR or partial response (PR) to their most recent platinum treatment (40, 43-47). According to the SOLO1 phase III trial, using Olaparib as a maintenance therapy provided a substantial benefit within PFS in women with newly diagnosed advanced OC and a BRCA1/2 mutation, reducing the risk of disease progression or death by about 70% (48). Additionally, Olaparib has been found to have a higher clinical benefit rate in women with platinum-sensitive tumors compared to those with platinum-resistant cancers (49). Other trials, including Study19, SOLO2, NOVA, and ARIEL3, have also demonstrated PFS benefits with PARPi (Olaparib, Niraparib, and Rucaparib) maintenance therapy in platinum-sensitive recurrent OC (19, 40, 43-45, 50).

Furthermore, Olaparib has been approved in combination with Bevacizumab by the FDA for the first-line maintenance treatment of patients with HRD-positive advanced EOC, fallopian tube or primary peritoneal cancer who are in CR or PR to first-line platinum-based

therapy (43, 46, 47). The FDA has approved Niraparib for the first-line maintenance treatment of patients with recurrent EOC, fallopian tube, or primary peritoneal cancer who are in CR or PR to platinum-based chemotherapy, regardless of their BRCA or HRD status (44). The ARIEL3 trial supports that Rucaparib has been approved by the FDA and EMA for use in the setting of recurrent disease, either as a single-agent treatment for BRCA-mutated patients who have been treated with two or more prior lines of platinum-based chemotherapy and are unable to tolerate further platinum-based chemotherapy or as a maintenance treatment after a CR or PR to platinum-based chemotherapy, independent of the BRCA status (45, 51). The role of PARPi as maintenance therapy has also been evaluated in a frontline setting in four phase III trials: SOLO1 (48), PRIMA (52), PAOLA1 (53), and VELIA (54). However, it is important to note that the development of resistance to PARPi ultimately occurs in most patients (55).

Recent studies have suggested that using PARPi in combination with immune checkpoint blockade could benefit patients with BRCA mutation (47, 56). For example, a clinical trial (NCT02657889) found that combining Niraparib with Pembrolizumab showed promising antitumor activity in patients with OC (57). Additionally, a randomized phase II trial by Zamarin *et al*. demonstrated that combining Nivolumab and Ipilimumab in platinum-resistant EOC resulted in better response and longer PFS (58). There are also ongoing clinical trials evaluating immune checkpoint inhibitors in combination with anti-angiogenic agents in EOC patients, which may be beneficial (59). Another study showed the efficacy of Prexasertib, a cell cycle checkpoint kinase 1 and 2 (CHK1/2) inhibitor, for patients with BRCA wild-type and recurrent HGSC (60).

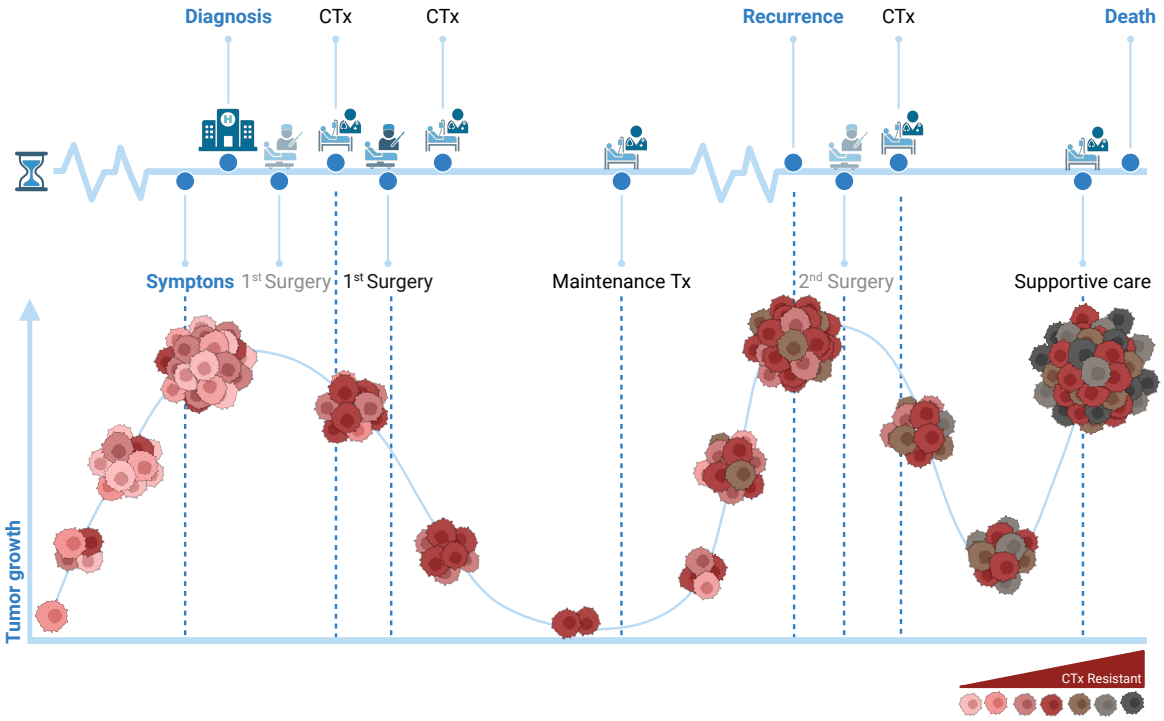


Figure 3. Illustrative diagram depicting the natural history of ovarian cancer, its main treatments, and the challenges of chemoresistance. This diagram covers the progression of the disease from its often-silent onset to advanced stages, highlighting key treatment modalities, including surgery and chemotherapy. Figure created with biorender.com. Chemotherapy, chemotherapy; Tx, therapy.

1.4. Malignant Ascites

The information presented in 1.4. Malignant Ascites is based on the publication **Nunes M**, Ricardo S. Chemoresistance in Ovarian Cancer: The Role of Malignant Ascites. In: Lele S, editor. Ovarian Cancer [Internet]. Brisbane (AU): Exon Publications; 2022 Sep 8. Chapter 2. PMID: 36343141.

Ascites can occur in different diseases, including cirrhosis, pancreatitis, nephritis, heart failure, and cancer (61, 62). MA is a pathological accumulation of fluid in the peritoneal cavity and is present in several types of neoplasms, such as ovarian, endometrial, pancreatic, gastric, colorectal, liver, and peritoneal cancers (61, 63-65). It can also, at a lower frequency, develop in extra-abdominal tumors such as lung and breast cancers (63, 64). This inflammatory condition occurs due to a disruption in the balance of fluid production and reabsorption (64, 66) driven by different pathophysiologic mechanisms, including increased vascular permeability [largely driven by upregulation of vascular endothelial

growth factor (VEGF)], peritoneal lymphatic obstruction, and high levels of fluid production (63, 64, 67, 68). The presence of MA is often indicative of tumor cells in the peritoneal cavity or peritoneal carcinomatosis (67). It can cause several comorbidities, such as dyspnea, abdominal tenderness and pain, nausea, anorexia, fatigue, early satiety, weight change, and compromised movements (63, 69).

MA is a hallmark of advanced OC, as more than one-third of patients develop this condition (66, 69, 70). MA occurs in all epithelial OC subtypes, including serous (i.e., LGSC and HGSC), CCC, MC, and EC (70, 71). Some studies compare serous subtypes and show a significant difference in MA accumulation in both grades. It is higher in HGSC, the most aggressive subtype (70, 72).

MA provides a nurturing environment facilitating cancer progression by containing various cellular and acellular components strictly associated with poor prognosis, facilitating the metastatic process, and contributing to chemoresistance and recurrence (**Figure 4A**) (63-66, 73). Additionally, MA comprises immunological constituents that create an inflammatory environment by secreting pro-inflammatory cytokines and chemokines, accelerating disease progression (66, 73). While chemotherapeutic agents can prevent MA accumulation, they often lead to a chemoresistant or recurrent disease, resulting in intractable MA and a worse prognosis (64, 66). As a result, patients may require repeated paracentesis for palliation, which can lead to clinical complications such as catheter-associated infections (63, 66, 73). Nevertheless, this regular sampling of cellular and acellular components from MA during tumoral progression provides a unique opportunity for translational research (65, 74).

1.4.1. Transcoelomic Dissemination

The most common route OC spreads is through transcoelomic dissemination, spreading across the peritoneal cavity (75, 76). Less commonly, it can also spread through the lymphatic and hematogenous routes (66, 75). Transcoelomic dissemination leads to peritoneal carcinomatosis, a more diffuse and widespread metastatic form of metastasis that has a significant negative impact on surgical resectability (77). This route is a more efficient process for cancer spread, as tumor cells follow the dynamics of peritoneal fluid until they implant in cell aggregates at the mesothelial lining (68). Metastatic implants are dispersed in areas with extensive and constant contact with peritoneal fluid, especially the omentum, Pouch of Douglas, and right subphrenic region (78, 79). In OC, peritoneal metastasis involves shedding cells from the primary tumor, dissemination in the abdominal cavity,

attachment and invasion of the mesothelial lining, and colonization of intra-peritoneal organs (**Figure 4B**) (76, 80). MA is described as a requirement for transcoelomic metastasis, facilitating the dissemination of tumor cells and creating a growth-promoting environment (80, 81). MA is also reported as a promotor of lymphatic and hematogenous dissemination (82).

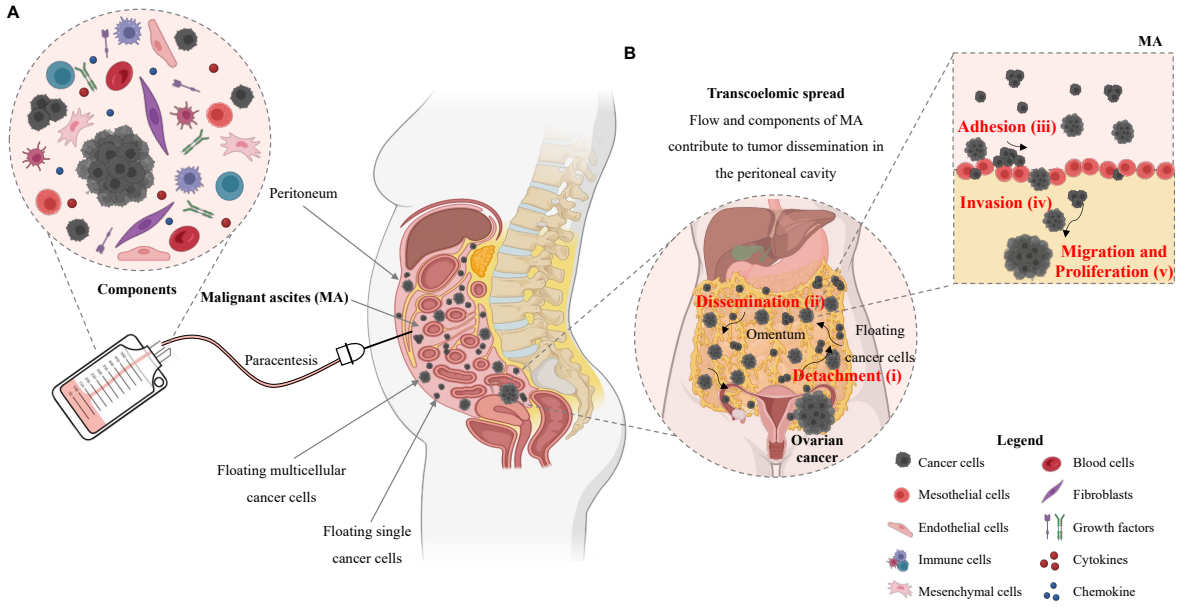


Figure 4. The accumulation of MA in OC. (**A**) MA comprises cancer and non-cancer cells (such as fibroblasts, mesothelial, endothelial, immune, mesenchymal, and blood cells) as well as acellular components (such as growth factors, cytokines, and chemokines). (**B**) MA contributes to transcoelomic dissemination: OC cells detach from the primary tumor in single or multicellular spheroids (**i**) and travel to other peritoneal sites (**ii**). The cells adhere and implant on the peritoneum and peritoneal organs surface (e.g., omentum), where they clear the mesothelial lining (**iii**), invade the submesothelial extracellular matrix (**iv**), migrate, and proliferate, creating secondary lesions (**v**). ECM, extracellular matrix; MA, malignant ascites; OC, ovarian cancer.

1.4.2. The Microenvironment of Malignant Ascites

MA is made up of tumor cells as well as non-tumor cells such as fibroblasts, adipocytes, mesothelial, endothelial, and immunological cells (66, 83). Additionally, there is a liquid acellular fraction that contributes to tumor progression, metastasis, and chemoresistance (67, 84). MA often contains cell aggregates, including both cancer and non-cancer cells, which form spheroids with a higher potential for metastasis (85, 86). Several *in vitro* multicellular spheroids systems exhibit resistance to anoikis (87), limited penetration of cytotoxic drugs (85, 88), and increased resistance to chemotherapy due to slow cycling and quiescent states (89, 90). Lafiti *et al.* found that approximately 95% of

chemoresistant patients had a higher proportion of spheroids in their MA than chemo-naïve patients, who had only approximately 25% (86). Furthermore, the liquid fraction of MA contains tumor-derived circulating free desoxyribonucleic acid (cfDNA), which allows tracking of changes in the mutation profile related to chemoresistance and relapse (65).

The non-cellular components of MA contain a dynamic mix of factors that can either promote or inhibit tumor growth. These factors include cytokines (91-95), chemokines, growth factors (96), integrins (97, 98), and metabolites that contribute to cancer spread and resistance to therapy (65, 83, 88). In OC, the cytokine profiles of MA show high levels of pro-tumorigenic (such as interleukin IL-6, IL-8, IL-10, and IL-15) and reduced levels of anti-tumorigenic (such as IL-2, IL-5, IL-7, and IL-17) factors, contributing to a pro-inflammatory and immunosuppressive tumor microenvironment (TME) (64, 83, 94, 99). Both IL-6 and IL-10 are linked to poor prognosis and reduced response to therapy (92, 100). High levels of IL-6 promote MA accumulation, OC progression (100), and dissemination (101, 102). Moreover, higher IL-6 levels are associated with shorter PFS (100, 103), poor OS, reduced response to initial therapy, and the development of chemoresistance (95).

In OC, VEGF levels correlate with MA accumulation (96, 104) and poor prognosis (105). Zhan *et al.* showed that MA presents high levels of VEGF compared to benign ascites and is associated with poor survival rates (96). Also, VEGF is commonly related to advanced-stage disease, high tumor grade, and increased metastatic potential (67). High expression of epidermal growth factor receptor (EGFR) in OC tissues is often associated with aggressive, invasive, and metastatic disease (106, 107), as well as decreased OS and disease-free survival (108). Extracellular vesicles (EVs), abundant in MA, play an important role in facilitating communication between cancer cells and their TME (109, 110). These vesicles containing glycolytic pathway-related proteins have been found to contribute to chemoresistance and disease progression in OC (111). Proteomic profiling of MA has identified potential therapeutic options to overcome OC chemoresistance (112-115). High-resolution mass spectrometry analysis has revealed specific diminished or enriched proteins, namely 178 and 175 proteins, respectively, in chemoresistant OC patients compared to chemonaïve patients (112). Both cellular and acellular components play crucial roles in regulating proliferation, metastasis, and chemoresistance in OC. Exploring MA cell populations and the signaling molecules that they produce during disease progression, particularly throughout therapy, will be crucial in improving patient outcomes (65).

1.4.3. The Management of Malignant Ascites and Chemoresistance

Over the last decades, the standard care for advanced OC patients has predominantly involved platinum-based (e.g., Carboplatin) and taxane-based (e.g., Paclitaxel) chemotherapy after cytoreductive surgery (116, 117). In some instances, NACT is utilized as an alternative to the standard treatment options (30, 31). The management of MA can involve aspiration during debulking surgery, specific chemotherapeutic treatments, or a paracentesis procedure, which entails removing MA by inserting a wide-bore needle percutaneously through the abdominal wall (65, 67). Paracentesis, although providing immediate relief of symptoms, requires repeated procedures and can lead to severe complications such as continuous draining site leakage or bowel perforation (64, 118, 119). Many chemoresistant patients develop intractable MA and undergo repeated paracentesis throughout their clinical management (64, 67).

The use of a drainage catheter placed subcutaneously in the peritoneal cavity is an alternative intervention for managing MA. It is easy for patients to self-drain, which increases their independence and reduces the necessity for frequent paracentesis at the hospital (120). Studies have shown that intraperitoneal (IP) catheter drainage is a successful procedure with low complication rates, supporting its use as a first-line approach for refractory MA (121). Recently, Fotopoulou *et al.* demonstrated that in patients with hepatic and ovarian malignancies implanted subcutaneously with Sequana Medical Alfapump System, which continuously drains MA via the urinary bladder, the need for paracentesis decreased from 4 to 1 (122, 123). However, further studies are necessary to establish catheter drainage as a routine procedure in oncological practices.

IP chemotherapy involves administering high concentrations of chemotherapy directly into the peritoneal cavity, providing direct exposure of peritoneal organs to drugs. This method offers advantages over intravenous administration by avoiding systemic chemotherapy toxicity (63, 64). A study on OC patients at stage III who underwent optimal debulking surgery showed that IP administration as first-line treatment resulted in a 16-month survival benefit (124). However, less than half of the women completed all chemotherapy cycles and those who didn’t have higher complications and toxicity rates (124). Early-phase trials suggest that IP delivery is more effective in controlling MA (64).

Hyperthermic intraperitoneal chemotherapy (HIPEC), which combines cytoreductive surgery with heated IP chemotherapy, has shown promise in reducing MA (125). Cytoreductive surgery removes macroscopic tumor implants, while IP chemotherapy acts directly in the peritoneal cavity, improving drug absorption and targeting the remaining microscopic tumor implants (126, 127). In advanced OC with extensive peritoneal

metastasis, HIPEC has been effective in improving patient survival (128, 129). A study by Van Driel *et al.* demonstrated that combining cytoreductive surgery with HIPEC resulted in longer OS and PFS compared to surgery alone (130). Nevertheless, it is challenging to establish HIPEC as a standard treatment. This is due to significant variations in patient outcomes across different studies, which use varying chemotherapeutic drugs, concentrations, temperatures, and procedure durations, leading to heterogenous and incomparable studies (128, 131). Thus, it requires more well-designed trials to obtain a more specific conclusion regarding the utilization of IP and HIPEC as an essential OC armamentarium.

Studies on pharmacological therapy for managing MA are limited and include antiangiogenic and metalloproteinase (MMP) inhibitors, as well as immunological modulators (64, 132-135). Bevacizumab, which targets VEGF and delays recurrent disease while alleviating symptoms associated with MA accumulation, has shown promising results (37, 64, 136). For instance, Numnum *et al.* reported that Bevacizumab treatment reduced the levels of MA, allowing the discontinuation of repeated paracentesis (136). Several phase III trials in OC, such as GOG18 (NCT00262847) and ICON7 (NCT00483782), have added Bevacizumab to standard treatments and reported improved PFS and OS in patients with advanced-stage disease (38, 39). Furthermore, randomized clinical trials OCEANS (NCT00434642) and AURELIA (NCT00976911) indicate that Bevacizumab can provide benefits by delaying the recurrences in platinum-sensitive and platinum-resistant OC patients (40, 41). Although Bevacizumab was not initially intended to affect MA specifically, it was found to be very effective in reducing its formation (137, 138). Recently, a study demonstrated that IP administration of Bevacizumab presents an acceptable safety profile and reduces the formation or delay of MA accumulation in chemoresistant patients (139). A pilot study using Aflibercept (a VEGF inhibitor) demonstrated an extension in the time between paracentesis procedures (140).

Additionally, preclinical models showed that Aflibercept prevents the accumulation of MA and inhibits tumor proliferation by blocking VEGF. However, there was an increased risk of morbidity associated with bowel perforation (133, 138). Batimastat (an MMP inhibitor) has been studied in animal models and was shown to decrease tumor growth, metastasis, and the volume of MA (141, 142). However, a Phase I study that administered Batimastat intraperitoneally in OC patients found that the reduction in the volume of MA was limited to a small number of patients (143, 144). Using an OC mouse model, Zhao *et al.* demonstrated that Losartan (an antihypertensive therapy targeting the renin-angiotensin system), as a

matrix-depleting strategy, enhances the efficacy of Paclitaxel and reduces MA (145). Octreotide (a Somatostatin analog) is particularly helpful for chylous ascites, a rare form containing high levels of triglycerides, by reducing splanchnic blood flow and contributing to decreased lymph flow and obstructive bowel symptoms (67). Jatoi *et al.* found that a monthly intramuscular injection of long-acting Octreotide delayed the need for paracentesis from 14 to 28 days (146). The efficacy of Batimastat, Losartan, and Octreotide is still under investigation, and further studies are needed to clarify their impact on managing MA.

Multiple studies have suggested using immunological approaches to improve the management of MA in OC patients. These include the use of IP triamcinolone (134), IP interferon α and β (147), tumor necrosis factor (TNF) (148), and non-pathogenic infectious agents (149, 150). Recently, prospective randomized phase II/III trials were conducted using Catumaxomab, a trifunctional IgG2 antibody (anti-CD3, anti-EpCAM, and anti-Fc receptors), which showed promising results in generating a strong immune reaction response against tumor cells when administrated IP (64, 119, 135). Heiss *et al.* demonstrate that IP administration of Catumaxomab leads to longer paracentesis-free survival, fewer ascites-related symptoms, and improved palliation (135). In 2009, Catumaxomab became the first therapeutic agent approved for managing MA in Europe (64, 135).

Despite these advances, current treatment options have shown limited success in managing MA in OC patients. Therefore, it is essential to explore more effective drugs and develop improved methods for drug delivery to prevent MA accumulation during the clinical course of OC patients.

1.4.4. Malignant Ascites as an Opportunity for Translation Research

The presence of MA is a valuable resource for research due to easy accessibility, the ability for repeated collection, and its capacity to reflect both the primary tumor and metastatic implants, along with their TME. MA provides a continuous sampling of the milieu in which OC spreads, making it an ideal resource for translational studies. This includes predicting drug response and monitoring drug efficacy (64, 65, 151). The accumulation of MA is more frequently observed in cases where patients have tumor recurrences and are absent in cases when patients respond to therapy (65). Understanding the mechanisms involved in the accumulation of MA and metastatic spread of OC will help to identify potential drug targets that could be used in a disease stage associated with chemoresistance. The pathways responsible for driving epithelial-mesenchymal transition (EMT) phenotypic changes are also accountable for spheroids' tumorigenicity and can potentially target (65,

152). Saine *et al.* reported that high expression levels of signal transducer and activator of transcription 3 (STAT3) in MA-derived OC cells promote invasion and metastasis (153). STAT3 inhibitors reduce chemoresistance and spheroid tumorigenicity in mouse models (153, 154).

Additionally, transforming growth factor β (TGF-β) present in MA cells is a major driver in metastatic spread (152, 155). The acellular components of MA provide a microenvironment that sustains cancer cells' survival and can potentially lead to the discovery of new treatment strategies based on disrupting this TME (156). Analyzing malignant effusions from OC patients has shown high expression levels of V-akt murine thymoma viral oncogene homolog 1 (Akt), cAMP-responsive element binding protein (CREB), and JUN N-terminal kinase (JNK) compared to benign effusions (157). Furthermore, high levels of p8, an increase in the ratio of phosphorylated EGFR, and phosphorylated JNK were associated with worse outcomes (157). Therefore, all mentioned proteins and respective pathways are potential therapeutical targets contributing to overcoming chemoresistance and abrogation of peritoneal dissemination of OC.

1.4.5. A Personalized Medicine Approach on Ovarian Cancer Using Malignant Ascites

The occurrence of MA at the initial presentation and subsequent relapse in OC provides a readily accessible source of biological material to monitor the sensitivity or resistance of tumor cells. This is important because it encompasses various populations that make up the TME (64, 65). By comparing sequential samples, such as those taken before and after chemotherapy, can be identified molecular changes that might predict how well a patient respond to treatment (156-158).

Conventional treatment strategies only offer a "one-size-fits-all" approach based on a limited panel of drugs, which excludes alternative options (159). Using patient-derived tumor cells allows for associating specific tumor characteristics with personalized treatment (159). Patient-derived cultures have recently emerged as a powerful modeling approach in cancer research (160-163). Many studies in different cancer models established patient-derived cultures that recapitulate the features of the original lesions (164-169). Velletri *et al.* recently used OC clinical samples from primary tumors and metastatic sites to demonstrate that patient-derived cultures retain key subpopulations and recapitulate features of the original samples, acting as 'patient-matched avatars' that can be used in a precision oncology platform (170, 171).

Furthermore, other groups have demonstrated the ability to grow tumor cells from MA *in vitro* for drug sensitivity testing (159, 172) and to predict clinical responses to therapy by assessing several biomarkers in MA tumor cells (92, 173, 174). A study by Bi *et al.* demonstrated that patient-derived cultures could be established in a high percentage of cases, used to perform drug tests promptly, and had the potential to identify more effective treatment regimens (159). Additionally, they demonstrated a specific case in which the patient-derived culture revealed patient resistance to standard therapy (159). Another study indicated that exposing MA-derived spheroids to a panel of drugs reflects the patients' therapy responses and identifies the best viable candidate (175). Many co-clinical trials, which involve conducting preclinical studies and clinical trials in parallel, are currently underway in various types of tumors, including OC. These trials compare therapy responses in patient-derived cultures to corresponding patient outcomes, as outlined in NCT04555473 and NCT05175326. This new strategy allows for real-time data integration, which helps accurately stratify and customize treatment for patients (176). Additionally, other clinical trials aim to evaluate therapeutical responses in patient-derived cultures, predict the clinical efficacy of drugs, and select the best treatment regimen for each patient to guide clinical decisions, as seen in NCT04279509 and NCT04768270.

Establishing patient-derived cultures from MA provides a valuable preclinical platform. MA contains natural cellular aggregates floating in a liquid environment, which makes it easy to obtain efficiently in a short period (177). These systems can be used to test drug efficacy with a variety of approved and novel compounds, either alone or in combination, within an acceptable time frame specific to each case. This approach can help predict therapy responses and guide clinical decisions (**Figure 5**) (159, 178-181).

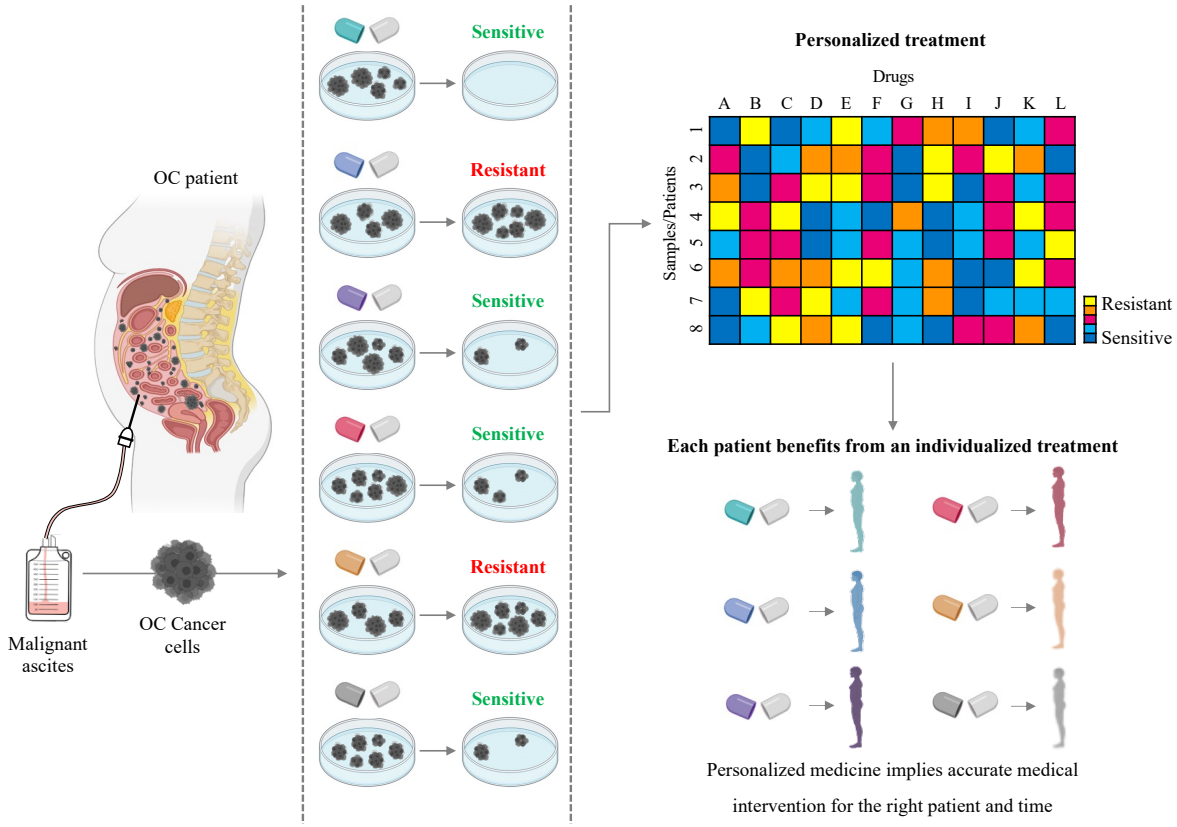


Figure 5. A personalized medicine approach in OC using MA. MA obtained from OC patients by paracentesis will be used to create patient-derived culture models. These will be exposed to a panel of drugs to predict patients' responses. The most promising drugs will be selected for administration to the corresponding patient. MA, malignant ascites; OC, ovarian cancer.

Acknowledgments and Funding

This work was developed at *Instituto de Investigação e Inovação em Saúde (i3S)*, an Associate Laboratory of the *Ministério da Ciência, Tecnologia e Inovação (MCTES),* and it was partially supported by *Fundação para a Ciência e a Tecnologia (FCT).* MN acknowledges *FCT, MCTES*, and *União Europeia (UE)* for financial support through a PhD fellowship (2020.04720.BD) that was co-sponsored by *Fundo Social Europeu (FSE)* through *Programa Operacional Regional Norte (Norte 2020).*

1.5. Chemoresistance

The information presented in 1.5. Chemoresistance is based on the publication **Nunes M**, Bartosch C, Abreu MH, Richardson A, Almeida R, Ricardo S. Deciphering the Molecular Mechanisms behind Drug Resistance in Ovarian Cancer to Unlock Efficient Treatment Options. Cells. 2024 May 4;13(9):786. doi: 10.3390/cells13090786.

Drug resistance in tumor cells develops through a stepwise molecular evolution, giving them a survival advantage, and can be categorized as intrinsic and acquired (182, 183). Intrinsic resistance refers to the natural ability of cancer cells to withstand and tolerate the initial exposure to treatment. Acquired resistance, conversely, refers to the capacity of neoplastic cells to adapt after drug exposure, enabling them to continue growing despite the treatment (182, 183). The amplification of cyclin E1 (CCNE1) is described as an early event (intrinsic) in the development of HGSC being mutually exclusively in BRCA1/2 dysfunctional and frequently identified in patients with platinum-resistant and refractory disease (184, 185). Instead, genetic aberrations in inactivating tumor suppressor genes, such as retinoblastoma protein 1 (RB1), neurofibromatosis type 1 (NF1), RAD51 recombinase B (RAD51B), and phosphatase and tensin homolog (PTEN) are more associated with acquired resistance (186).

Intrinsic resistance mechanisms include drug degradation by metabolic enzymes (187), modifications of drug transporters and drug targets (188), poor vascularization leading to decreased intracellular drug concentration (189), extracellular matrix (ECM) interactions, and cellular metabolic processes that can promote resistance mediated by the TME (190). Acquired resistance is characterized by an increase in the mutational burden and other molecular alterations that affect drug efficacy and can be attributed to an increased drug efflux, activation of anti-apoptotic signaling pathways, and inactivation of DNA damage response (DDR) mechanisms to evade cell death (191, 192). In addition, cancer cells can develop changes to drug targets through multiple mechanisms or bypass them through alternative pathways (193, 194). Still, it is challenging to distinguish between intrinsic and acquired mechanisms that can contribute to both categories of resistance.

One of the challenges in oncological treatment is the development of multidrug resistance (MDR), which occurs when tumor cells become resistant to structurally and mechanistically unrelated types of antineoplastic drugs, which compromises the effectiveness of therapy (195). A decreased drug uptake, an increased expression of drug-metabolizing enzymes, altered cell cycle checkpoint progression, changes in apoptosis or survival pathways, and deregulation of signal transduction pathways characterize the MDR phenotype (187, 188, 196). Efflux pumps, such as ATP-binding cassette (ABC) protein families, including P-glycoprotein (P-gp), multidrug resistance-associated protein 1 (MRP1), and breast cancer resistance protein (BCRP), are often overexpressed and are described as the significant contributors to MDR phenotype in many types of tumors (197). The co-administration of anticancer drugs with MDR inhibitors can enhance therapeutic response

by inhibiting drug efflux. Nevertheless, the clinical translation of drug efflux pump modulators failed due to pharmacokinetic interactions and adverse effects (195, 198, 199).

1.5.1. Mechanisms of Platinum Resistance in Ovarian Cancer

Platinum compounds are a type of antineoplastic agent that can prevent tumor growth by inhibiting DNA synthesis (200). Platinum can enter cells through passive diffusion or the copper transporter 1 (CTR1); it binds to DNA and creates intra-strand and inter-strand crosslinks that cause DNA damage, leading to cell death (201, 202).

The platinum-free interval (PFI; defined as the time between the last dose of platinum-based therapy and the documented relapse) has been used for the past three decades as the primary factor to determine the likelihood of patient response if they are rechallenged with platinum (51). OC patients are categorized into three groups based on their response to platinum-based chemotherapy. “Platinum-refractory” refers to patients who experience disease recurrence during or within four weeks after discontinuing platinum-based treatment. “Platinum-resistant” includes patients who do not respond to platinum-based therapy or experience a recurrence within six months following the conclusion of the first treatment cycle. “Platinum-sensitive” indicates patients who respond well to platinum-based chemotherapy and do not experience a recurrence within six months of finishing treatment (36, 51). However, the occurrence of platinum resistance is a continuous process, and the PFI-based cut-off to define sensitivity can be quite arbitrary as it does not consider other essential factors (51), such as maintenance therapy with targeted agents (203). Therefore, in the 5th OC Consensus Conference and 2019 ESMO–ESGO guidelines, the PFI-based paradigm was revisited and partially replaced with the concept of the treatment-free interval (TFI) that subdivides patients into two categories: those eligible for platinum rechallenge and those for whom platinum is not considered an option (36, 204). A platinum rechallenge is not regarded as feasible if a progression is observed during a platinum-based treatment or early after its completion. Non-platinum compounds like Topotecan, Gemcitabine, Anthracyclines, and Paclitaxel can be alternatives. These chemotherapeutic drugs show significant activity and lower toxicity compared to combinatorial schemes (51, 205-208). TFI considers data from histopathology, BRCA1/2 mutation status, number/type of previous therapies, the outcome of prior surgery, and reported symptoms (36).

Platinum resistance is a complex process that involves various factors that can hinder the effectiveness of platinum-based therapy. These factors can operate before or after platinum binds to its target. For example, reduced drug uptake or increased efflux can

decrease the concentration of platinum inside the cell, known as pre-target resistance. Similarly, enhanced DNA repair mechanisms can overcome platinum–DNA binding, leading to on-target resistance. Moreover, mutations or changes in downstream signaling pathways that affect the cell's ability to undergo apoptosis can cause post-target resistance. Additionally, alterations in cellular pathways that are not directly related to platinum's biochemical activity, such as EMT and epigenetic changes, can cause off-target resistance (**Figure 6**) (209).

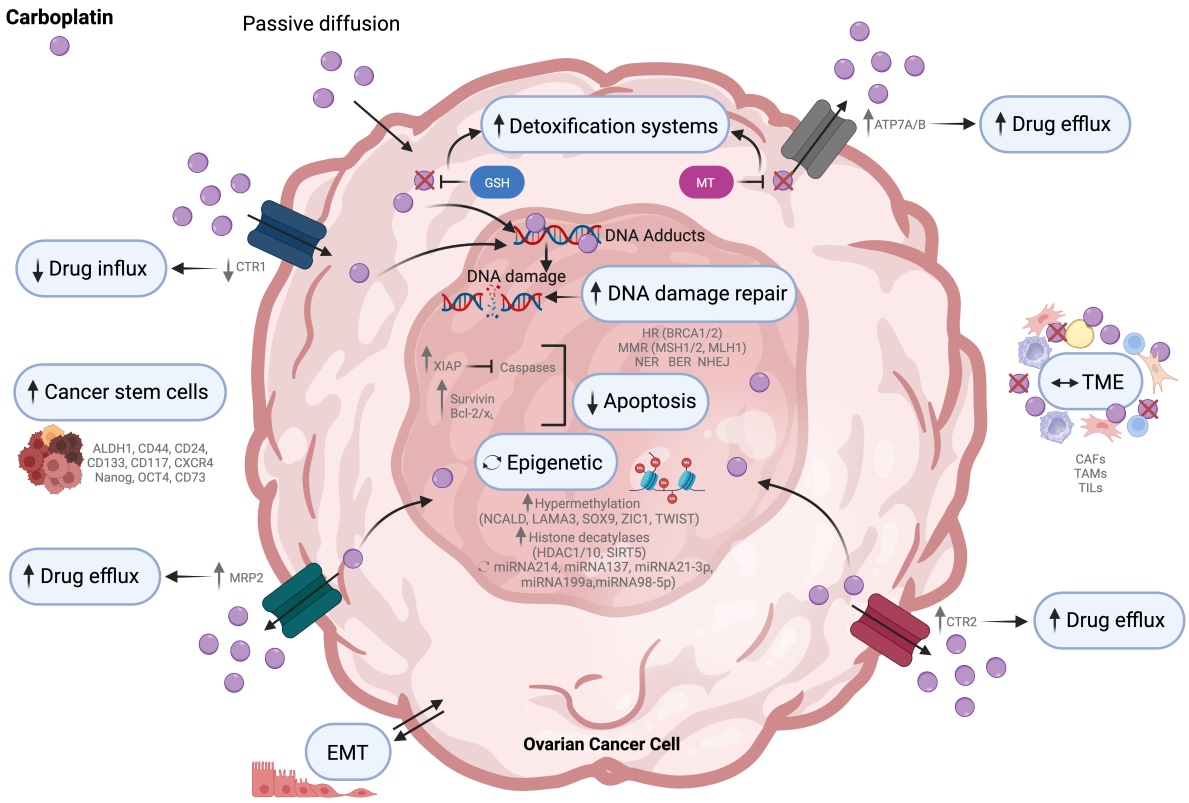


Figure 6. Schematic representation of the main molecular mechanisms contributing to Carboplatin resistance in OC. Increased drug efflux by overexpression of MRP2/4 and ATP7A/B and decreased drug influx by CTR1/2 upregulation and detoxification systems; for example, GSH and MT can reduce the concentration of platinum inside the cells. Enhanced DNA repair mechanisms, such as alterations in BRCA1/2 and MMR genes, can overcome platinum–DNA binding. Mutations or changes in downstream signaling pathways that affect the cell's ability to undergo apoptosis, such as increased Bcl-2/XL, XIAP, and survivin, and decreased caspases, can also cause Carboplatin resistance. Additionally, alterations in cellular pathways that are not directly related to platinum's biochemical activity, such as EMTs, TME, and epigenetic changes, can cause Carboplatin resistance. Figure created with BioRender.com. ALDH, aldehyde dehydrogenase; ATP7A/B, ATPase copper-transporting alpha/beta; Bcl2/X_L, B-cell lymphoma 2/extra-large; BER, base excision repair; BRCA1/2, breast cancer 1/2; CAFs, cancer-associated fibroblasts; CTR1/2, cooper transporter 1/2; CXCR4, chemokine receptor

4; DNA, desoxyribonucleic acid; EMT, epithelial–mesenchymal transition; GSH, glutathione; HDAC1/10, histone deacetylase 1/10; HR, homologous repair; LAMA3, laminin alpha 3 expression; miRNAs, microribonucleic acid; ML/SH1/2, MUTL protein homolog 1/2; MMR, mismatch repair; MRP2/4, multidrug resistance-associated protein 2/4; MT, metallothionine; NCALD, DNA hypermethylation of neurocalcin delta; NER, nucleotide excision repair; NHEJ, non-homologous end joining; OC, ovarian cancer; OCT4, octamer transcription factor 4; SIRT5, sirtuin 5; SOX9, Sex-determining region Y-box transcription factor 9; TAMs, tumor-associated macrophages; TILs, tumor-infiltrating lymphocytes; TME, tumor microenvironment; TWIST, twist-related protein 1; XIAP, x-linked inhibitor of apoptosis protein; ZIC1, zic family member 1.

1.5.1.1. Pre-Target Resistance Mechanisms

1.5.1.1.1. Drug Influx and Efflux

When they accumulate inside cells, platinum agents cause cytotoxicity. One main reason for resistance to these agents is the dysregulation of drug influx and efflux pumps/transporters, which reduces the quantity of drugs that accumulate inside cells (210). Platinum-based compounds can enter cancer cells by passive diffusion or CTR1-mediated import (211) and can be exported by ATPase copper-transporting 7 alpha/7beta (ATP7A/7B) and MRP2/4 (212, 213).

CTR is a transmembrane influx transporter involved in copper homeostasis. It also plays an essential role in the intracellular uptake of platinum salts by facilitating the entry of drugs inside the cells. Consequently, its downregulation reduces treatment efficacy (214). Studies have shown that deleting CTR1 can reduce the intracellular accumulation of Cisplatin, leading to chemoresistance (215), while overexpression (OE) of CTR1 can increase sensitivity to platinum compounds (216, 217). It has been shown that Cisplatin-sensitive A2780 cells express higher levels of CTR1 compared to Cisplatin-resistant A2780CP cells (218). Ishida *et al.* found that HGSC patients with platinum-sensitive disease at stage III or IV expressed significantly higher levels of CTR1 messenger ribonucleic acid (mRNA) than those with platinum-resistant or platinum-refractory disease (214). On the other hand, copper transporter 2 (CTR2) is involved in regulating platinum levels inside the cells, acting as a platinum efflux transporter, and high levels are associated with platinum resistance in OC cells (219).

ATP7A sequesters platinum derivates to prevent their nucleus access, while ATP7B facilitates drug efflux (220, 221). Chisholm *et al.* showed that cells expressing high levels of ATP7A present low intracellular platinum concentration and exclude the drug from the nucleus (222). ATP7A/B genes were expressed at higher levels in platinum-resistant cells compared with platinum-sensitive cells (221). According to a study by Mangala *et al.,* when ATP7B is silenced, it reduces Cisplatin half-maximal inhibitory concentration (IC_{50}) by 2.5

times and increases DNA adduct formation in Cisplatin-resistant cells (221). Patients with low ATP7B mRNA expression levels in colorectal cancer have better PFS and optimal curative effects from Oxaliplatin plus 5-Fluorouracil treatment compared to those with high ATP7B mRNA expression (223).

Many studies in OC have shown that high MRP2 expression is linked to platinum resistance and adverse outcomes (213, 224, 225).

1.5.1.1.2. Detoxification Systems

Neoplastic cells have a higher level of intracellular reactive oxygen species (ROS) than normal cells, which plays a significant role in pathogenesis (226). Excess ROS production is caused by ionizing radiation and chemotherapeutic compounds, activating apoptosis pathways (227). Cancer cells upregulate antioxidant enzymes like glutathione (GSH) and metallothionein (MT) to counteract the effect of ROS, which provides them with a survival benefit (228, 229). Several cancers, including OC, show high levels of GSH expression that is linked with increased activity of GSH-related enzymes and exporter proteins, such as γ-glutamyl-cysteine ligase, γ-glutamyl-transpeptidase, and GSH-transporting export pumps (230, 231). These enzymes have been associated with platinum resistance (230-232). GSH has a high affinity toward platinum compounds, forming platinum-thiol conjugates, reducing platinum-induced oxidative stress levels, and decreasing the cytotoxicity of reactive platinum (233). The ability of GSH transferase and MT to sequester and inactivate platinum compounds has been linked to platinum resistance by reducing their availability (228, 234).

On the other hand, Criscuolo *et al.* found that Cisplatin-resistant cells display lower levels of reduced GSH and reduced expression of enzymes involved in GSH biosynthesis and recycling. This is due to Cisplatin binding, which hinders GSH oxidation and accumulates ROS (235). Interestingly, only platinum-sensitive cells showed a significant increase in ROS levels following Cisplatin treatment, making them more susceptible to oxidative stress-induced cell death (235).

1.5.1.2. On-Target Resistance Mechanisms

1.5.1.2.1. DNA Damage Repair

The first step towards the cytotoxicity of platinum-based agents is the formation of DNA adducts. Therefore, cell sensitivity is modulated by their capacity to recognize and repair drug-induced DNA damage (201, 236). This process is known as DDR. It can activate

one or more DNA repair pathways, including mismatch repair (MMR), base excision repair (BER), nucleotide excision repair (NER), homologous repair (HR), and non-homologous end joining (NHEJ) (236, 237). In many tumors, abnormal activity in one of these pathways is frequently observed, leading to increased capacity to repair or tolerate platinum-induced DNA damage, resulting in platinum resistance (201). Moreover, the upregulation of DNA repair proteins may lead to removing platinum adducts and increased capacity to repair DNA damage (201). Indeed, most platinum-resistant tumors display upregulation of DNA damage repair proteins, including MMR repair proteins [MUTL protein homolog 1/2 (MSH1/2 and MLH1)], excision repair cross-complementing (ERCC) proteins, and Fanconi anemia complementation group D2 (FANCD2), and also secondary mutations in BRCA1/2 genes (201, 238-241).

The proteins encoded by BRCA1/2 are essential for DNA double-strand break (DSB) repair by the HR pathway (242). Around 25% of OC patients have BRCA1/2 mutations, increasing their sensitivity to DNA-damaging agents, such as platinum and PARPi (243, 244). Some studies suggest that prolonged exposure to platinum may create selective pressure, leading to reversion mutations or intragenic deletions in BRCA1/2-mutated genes. This could restore the BRCA1/2 reading frame, produce a functional protein, and re-acquire HR proficiency as a possible mechanism of platinum resistance (241, 245, 246). BRCA1/2 is also implicated in the response to replication stress. Pax transactivation domain-interacting protein (PTIP) is part of the histone methyltransferase complex protecting stressed replication forks. Loss of PTIP, poly(ADP-ribose) polymerase 1 (PARP1), and chromodomain helicase DNA-binding protein 4 (CHD4) in a BRCA2-deficient background is associated with Cisplatin resistance due to an increased protection of replication forks (247). According to The Cancer Genome Atlas (TCGA) database, OC patients who had BRCA1/2 mutations and were treated with a platinum agent with a high level of PTIP had longer PFS, presumably reflecting the increased sensitivity of their cancer cells to chemotherapy (247). Moreover, some studies suggest that Cisplatin-resistant OC cells exhibit an enhanced NER pathway (248, 249). The expression levels of several NER proteins [e.g., xeroderma pigmentosum complementation group A/C/G (XPA/C/G), excision repair cross-complementation group 1–xeroderma pigmentosum complementation group F (ERCC1-XPF)] and somatic mutations in XPD significantly affect cellular sensitivity to Cisplatin (250, 251). Indeed, the OE of XPC in several types of cancer cells (e.g., colorectal and gastric cancers) leads to elevated Cisplatin resistance (250, 251).

1.5.1.3. Post-Target Resistance Mechanisms

1.5.1.3.1. Apoptosis and Cell Cycle Regulation

Most anticancer agents trigger cell death through processes such as apoptosis; however, cancer cells can develop mechanisms to avoid this process. Key apoptotic regulators and signaling pathways mediate cellular cytotoxic response to platinum agents, and consequently, deficiencies within the pathways contribute to chemoresistance (252). Platinum compounds can trigger apoptosis by extrinsic and intrinsic pathways (253-255). Proapoptotic signaling activation leads to mitochondrial outer-membrane permeabilization and release of cytochrome C that triggers the activation of the caspase cascade (256). Platinum-resistant tumors can express high levels of anti-apoptotic proteins or have defects in mitochondrial signaling (200). In OC, the B-cell lymphoma 2 (Bcl-2) family of apoptosis inhibitors, including Bcl-2 and B-cell lymphoma/extra-large (Bcl-X_L), can be upregulated, preventing activation of apoptosis and allowing time for DNA repair (257-260).

X-linked inhibitors of apoptosis proteins (XIAPs) are the most potent among human anti-apoptotic proteins (IAPs). They can block apoptosis pathways by selectively binding and inhibiting caspase-3/7/9, decreasing chemotherapy-induced apoptosis (261). In OC, several studies showed that XIAPs and survivin are overexpressed and contribute to platinum resistance (262, 263).

1.5.1.4. Off-Target Resistance Mechanisms

1.5.1.4.1. Tumor Microenvironment and Cancer Stem Cells

OC cells can survive in MA, which acts as a liquid TME where neoplastic cells disseminate throughout the abdominal cavity (67). TME is a complex ecosystem comprising normal cells such as stromal cells, immune cells, endothelial cells, adipocytes, bone marrow-derived cells (BMDC), and lymphocytes, as well as ECM components that contribute to tumor cell growth, differentiation, and invasiveness (264).

Non-tumor cells in the TME may contribute to the platinum resistance of OC cells. Indeed, the ECM signaling is dysregulated through the activation of cancer-associated fibroblasts (CAFs) and tumor-associated macrophages (TAMs), which lead to excessive ECM remodeling, promoting tumor progression and activating multiple signaling pathways that cause platinum resistance (265). Two studies have found that cancer cells can stimulate mesothelial cells by releasing TGF-β. This stimulation causes the mesothelial cells to secrete either osteopontin (266) or fibronectin (267), which reciprocally stimulate survival signaling in the cancer cells. Additionally, collagen types I, V, and XI, presumably originating

from fibroblasts, have been shown to contribute to the platinum resistance of OC cells (268, 269). CAF-induced resistance can also result from the secretion of specific cytokines, proteins, or exosomal microribonucleic acid (miRNAs) to activate anti-apoptosis-related signaling pathways, such as phosphoinositide 3-kinase/protein kinase B (PI3K/Akt), annexin A3/c-JNK (ANXA3/JNK), and interleukin-11/interleukin 11R (IL-11/IL-11R)/STAT3 (270-273). IL8 derived from OC cells or CAFs induces OC stemness, platinum (274), and taxane resistance (275). C-X-C motif chemokine 12 (CXCL12) derived from CAFs can induce EMT and Cisplatin resistance (276). CAFs can also release cysteine and GSH, limiting intracellular platinum concentration (277, 278). Another player contributing to drug resistance is the cancer-associated adipocytes (CAAs) responsible for arachidonic acid secretion. This chemoprotective lipid mediator acts directly on OC cells and inhibits Cisplatin-induced apoptosis through Akt pathway activation (279).

Some studies have indicated that platinum resistance might be caused by the interaction between ECM and cell adhesion molecules, such as CD44, CD117, CD133, and β-integrins, providing a survival advantage to tumor cells when exposed to cytostatic drugs (280). Additionally, tumor-infiltrating lymphocytes (TILs), including regulatory T cells and TAMs, can promote platinum resistance. TAMs can cause platinum resistance by inducing EMT and ECM remodeling (265, 281). It has been observed that stromal cells can influence the sensitivity of cancer cells to chemotherapy, and spatial transcriptomics has shown the uneven intratumoral distribution of CAFs (282). Therefore, the heterogeneous response of tumor cells to chemotherapy results from cancer cell-intrinsic factors and the spatial heterogeneity of stromal cells, which directly affect patient survival (282).

OE of cancer stem cell (CSC) biomarkers is also associated with enhanced EMT features and chemoresistance (283). These CSC markers include aldehyde dehydrogenase (ALDH), CD44, CD24, CD133, CD117, and chemokine receptor 4 (CXCR4), which are more prevalent in platinum-resistant OC cells compared to platinum-sensitive ones (284, 285). Additionally, in OC, an enhanced expression of stemness-maintaining proteins, including Nanog, octamer-binding transcription factor 4 (OCT4), and CD73, are reported to be expressed in platinum-resistant cells (286-288).

1.5.1.4.2. Epigenetic Modifications

Epigenetic modifications are associated with acquiring a platinum-resistant phenotype through multiple mechanisms. Studies have extensively considered the role of DNA methylation in OC chemoresistance, and it has been observed that platinum-resistant

samples have a higher frequency of hypermethylation as compared to platinum-sensitive (289, 290). Cardenas *et al.* have shown that EMT may be driven by aberrant methylation, resulting in the development of a platinum-resistant phenotype (289). DNA hypermethylation of neurocalcin delta (NCALD) and reduced laminin alpha 3 (LAMA3) expression is also associated with EMT in HGSC, which is correlated with chemoresistance and poor outcomes (291). Furthermore, hypermethylation of genes such as sex-determining region Y-box transcription factor 9 (SOX9), zic family member 1 (ZIC1), and twist-related protein 1 (TWIST), which are involved in EMT, is also associated with Carboplatin-resistant OC (292). The genes frizzled class receptor 1/10 (FZD1/10) and glycogen synthase kinase 3 beta (GSK3B) involved in the wingless/integrated (Wnt) signaling pathway have been found to have different levels of methylation in both platinum-resistant and platinum-sensitive samples (293). Another study demonstrated that most differentially methylated sites were hypomethylated in the Cisplatin-resistant cell lines compared to the sensitive ones (294). Indeed, Bonito *et al.* showed that msh homeobox 1 (MSX1) transcription factor can influence EMT in OC and that DNA hypomethylation leads to decreased MSX1 expression, which is associated with Cisplatin resistance. At the same time, MSX1 OE sensitizes cells to Cisplatin (295).

The OE of some histone deacetylases, including histone deacetylase 1/10 (HDAC1/10) and sirtuin 5 (SIRT5), has also been reported in OC platinum resistance (296-299). Moreover, dysregulation of miRNAs miR-214, miR-137, miR-21-3p, miR-199a, and miR-98-5p has also been linked to platinum resistance in OC (300-304). Xiao *et al.* showed an inverse correlation between miR-139 and ATP7A/B expression, demonstrating that high expression levels of miR-139 sensitize OC cells to Cisplatin-based chemotherapy through ATP7A/B regulation (305). Moreover, Dwivedi *et al.* also showed that miR-15a and miR-16 restored Cisplatin sensitivity by inhibiting ATP7B expression (306). Similarly, the upregulation of miR-490-3p and downregulation of miR-411 were associated with increased Cisplatin sensitivity via the inhibition of MRP2 (307, 308). MiR-514 also increases Cisplatin chemosensitivity by targeting ABC family members ABCA1/10 and ABCF2 (309). Furthermore, miRNAs can influence pathways involved in DNA repair, inducing platinum resistance. MiR-211 facilitated platinum-induced DNA damage by targeting DDR effector genes [i.e., DNA polymerase eta (POLH), tyrosyl-DNA phosphodiesterase 1 (TDP1), alpha-thalassemia retardation x-linked (ATRX), mitochondrial ribosomal protein S11 (MRPS11), and germline ERCC repair 6 like 2 (ERCC6L2)], enhancing platinum sensitivity in OC cells (310). MiR-30a-3p and miR-770-5p target ERCC1/2, essential effectors of the NER pathway

(311, 312), and its upregulation restores Cisplatin sensitivity (311, 312). Finally, miR-152 can increase platinum sensitivity by targeting RAD51 and suppressing HR (304).

1.5.2. Mechanisms of Paclitaxel Resistance in Ovarian Cancer

Paclitaxel belongs to the taxane family of compounds and is the first example of a microtubule-stabilizing class of antimitotic drugs successfully used to treat multiple neoplasms (313, 314). Microtubules are a dynamic network of α and β tubulin that play a critical role in the formation of mitotic spindle fiber, which is essential for chromosomal separation during M-phase (315). Additionally, they are necessary for maintaining cell structure, motility, and cytoplasmic trafficking (316).

Paclitaxel suppresses microtubule dynamics by binding to the β-subunit of the tubulin heterodimer (317, 318), which disrupts the assembly of mitotic spindles, induces mitotic arrest and aberrant mitosis, and subsequently leads to cell death (319, 320). It can also exert cytotoxic activity against cancer cells through non-mitotic mechanisms (321, 322), including inducing phosphorylation of apoptotic protein Bcl-2 (323), disruption of microtubule-mediated intracellular transport (324), or physical breaking of the nuclear envelope by forming rigid microtubule bundles (325). Moreover, Paclitaxel can stimulate an inflammatory response by inducing nuclear fragmentation (326), and it possesses antiangiogenic activity by increasing the dynamic instability of interphase microtubules in endothelial cells and inhibiting these cell migration (327).

Paclitaxel is commonly used alone or in combination with Carboplatin to manage OC and is considered the primary treatment option. However, the disease often returns and becomes resistant to this drug (328, 329). Furthermore, the treatment may cause severe side effects, such as peripheral neuropathy, which may require dose de-escalation or treatment cessation (330, 331). To improve the effectiveness of treatment and potentially reverse resistance to Paclitaxel, finding drug partners that can work together with Paclitaxel is recommended.

In OC, Paclitaxel-resistance mechanisms involve a decreased intracellular drug concentration (mediated by an increased drug export) (332), increased metabolism of taxanes [a consequence of upregulating cytochrome P450 (CYP) enzymes], and changes associated with microtubules' structure, stability, and expression, including mutations in β-tubulin or altered isotype expression. Changes in microtubule-binding proteins may underlie reduced drug-binding affinity (35). In addition, hypoxic conditions (35), the alteration of the drug target, deranged nuclear-cytoplasmic shuttling, and increased ability to counter drug-

induced damage or apoptosis also contribute to taxane resistance (316). Modifications in the nuclear envelope, such as the reduction in/loss of lamin A/C proteins, were also found to be associated with Paclitaxel-induced nuclear envelope breakage and formation of micronuclei (333) that ultimately impact Paclitaxel resistance (**Figure 7**).

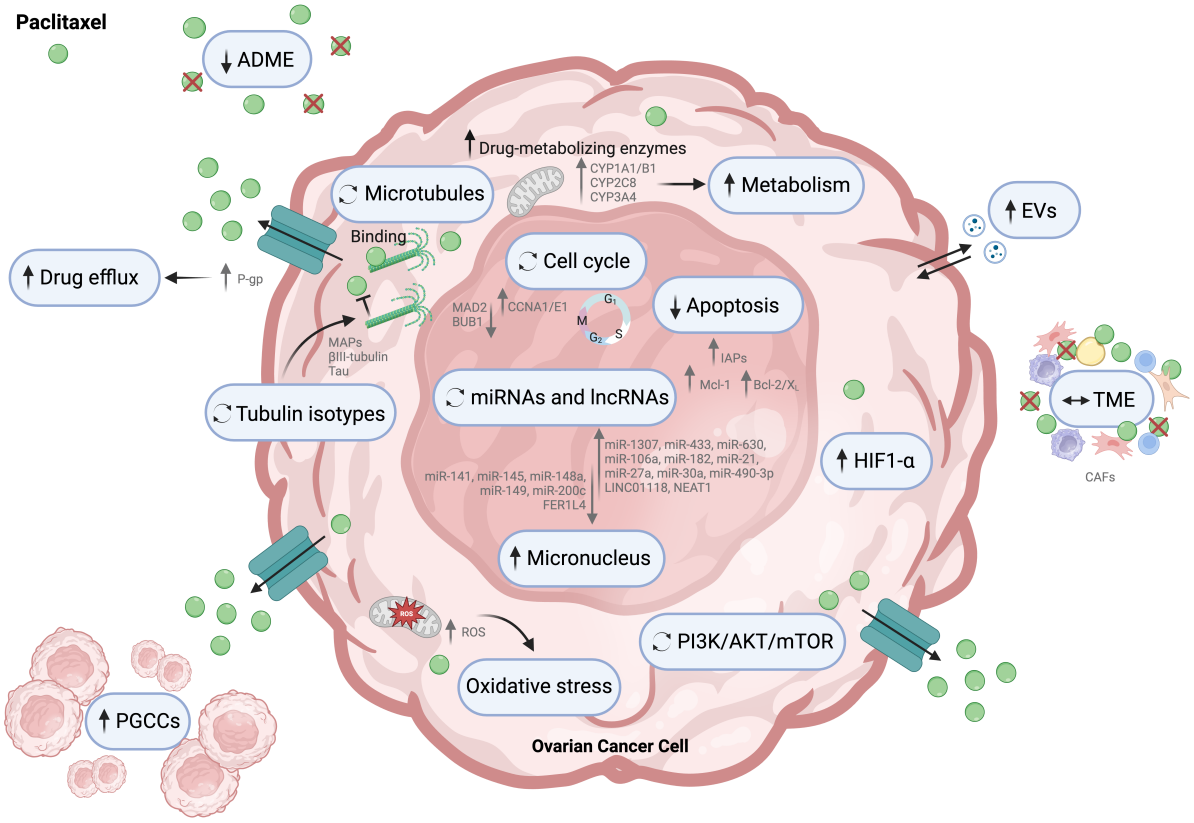


Figure 7. Schematic representation of the main molecular mechanisms contributing to Paclitaxel resistance in OC. Paclitaxel resistance mechanisms in OC involve a decreased cellular drug accumulation by decreased ADME, increased drug efflux pumps (such as P-gp), and metabolizing enzymes (such as upregulation of CYP enzymes). Moreover, Paclitaxel resistance can also be associated with microtubule structure, stability, and expression, including mutations in *β*-tubulin or altered isotype expression (such as increased MAPs). Changes in microtubule-binding proteins may underlie reduced drug-binding affinity. In addition, hypoxic conditions, the alteration of the drug target, deranged nuclear-cytoplasmic shuttling, and increased ability to counter drug-induced damage or apoptosis also contribute to taxane resistance. Cell cycle regulation by enhanced Bcl-2/X_L, Mcl-1, and IAPs, oxidative stress by enriched ROS, TME, EVs, and multi-micronucleus also impact Paclitaxel resistance. Modifications in the nuclear envelope, such as the reduction in/loss of lamin A/C proteins, were also found to be associated with Paclitaxel-induced nuclear envelope breakage and the formation of micronuclei. Figure created with BioRender.com. ADME, absorption, distribution, metabolism, and elimination; Bcl2/X_L, B-cell lymphoma 2/extra-large; BUB1, mitotic checkpoint serine/threonine kinase; CCNA1/E1, cyclin A1/E1; CYPs, cytochrome P450; EVs, extracellular vesicles; FER1L4, er-1-like protein 4; HIF1-α, hypoxia-induced factor 1-α; IAP, inhibitor of apoptosis protein; lncRNAs, long non-coding ribonucleic acid; MAD2, mitotic

arrest deficiency protein 2; MAPs, microtubule-associated proteins; Mcl-1, myeloid leukemia 1; miRNAs, microribonucleic acid; OC, ovarian cancer; PGCCs, polyploid giant cancer cells; P-gp, P-glycoprotein; PI3K/AKT/mTOR, phosphoinositol three kinases/protein kinase B/mammalian target of rapamycin; ROS, reactive oxygen species; TME, tumor microenvironment.

1.5.2.1. Intracellular Drug Concentration

Maintaining adequate intracellular levels of Paclitaxel is crucial for exerting its cytotoxic effects. Still, various mechanisms can influence the concentration of taxane in the cellular compartment, ultimately affecting tumor cytotoxicity (334).

1.5.2.1.1. Solubility Absorption, Distribution, Metabolism, and Elimination

Different types of taxanes have varying solubility, absorption, distribution, metabolism, and elimination properties. These differences result in distinct efficacy and drug effects that affect cell death (335). Moreover, taxanes are hydrophobic compounds with low solubility, preventing them from being orally administered (336). To overcome this limitation and optimize their effectiveness, formulations are being developed to improve their absorption and cellular uptake, reduce Paclitaxel resistance, and minimize collateral toxicity (336).

1.5.2.1.2. Drug Efflux

P-gp is a drug efflux pump whose OE increases the efflux of its substrates, reducing their intracellular concentration and making them less effective (337). These substrates include Paclitaxel, and undeniably, one of the most well-known causes of taxane resistance is P-gp OE (338-340). It has been negatively correlated with Paclitaxel response, including in OC (339, 340). Studies have shown that chemoresistant OC tumors have higher P-gp levels than their chemosensitive counterparts (316, 341).

To reverse Paclitaxel resistance in OC, P-gp inhibitors such as Verapamil and Elacridar are being tested preclinically (342, 343). Unfortunately, most inhibitors are unsuitable because of the difficulty of explicitly inhibiting the P-gp binding domain, the toxicity related to the high doses required, and compensation by other drug pumps (342, 343). There is also a risk that P-gp inhibitors may inhibit some CYP enzymes essential to detoxifying normal cells during chemotherapeutic treatment (183).

1.5.2.1.3. Metabolizing Enzymes

An alternative way taxane resistance can be developed is through increased drug metabolism. Paclitaxel is a substrate of the hepatic P450 enzymes CYP1A1/B1, CYP2C8, and CYP3A4 (344-346). CYP enzymes are present in both healthy and cancer tissues. However, increased expression and oxidizing activity in neoplastic cells led to an increase in the hydroxylation of metabolites of taxanes (196, 345). As a result, the metabolized drugs have low levels of cytotoxic antitumor activity (196). However, inhibiting CYP enzymes can cause other problems, such as different drugs not being properly metabolized, which can lead to unexpected or potentially dangerous drug-drug interactions (347).

CYP2C8 is the primary enzyme responsible for Paclitaxel metabolism, and it is overexpressed in OC (345). This enzyme could be an essential biomarker to predict Paclitaxel response (196). In addition, CYP3A is associated with taxane metabolism (348), and its inhibition by taxanes could lead to increased drug toxicity from other drugs, which are also CYP3A substrates (196).

A study using OC cell lines revealed an essential increase in CYP1A1 mRNA and protein expression compared to primary cultures or immortalized HOSE cell lines (349). Similarly, the authors also found that various types of OC patients' specimens showed a moderate-to-high cytoplasmic expression of CYP1A1 compared with benign epithelia (349). McFadyen *et al.* found that most OC specimens investigated (92%) had significantly higher levels of CYP1B1 expression. They demonstrated a strong correlation between CYP1B1 expression in primary and metastatic OC (346). Downie *et al.* also revealed that CYP1B1 was the only enzyme not detected in normal ovarian tissue, a finding consistent with previous studies showing the presence of CYP1B1 in OC cells without expression in normal tissue (350). Another study showed that Paclitaxel treatment induces CYP1B1 expression, and inhibiting CYP1B1 can reverse resistance to Paclitaxel (351). Preclinical studies have demonstrated that Resveratrol and its analog (DMU-212) inhibit CYP1A1/B1 transcription, protein expression, and enzymatic activity (352-354). However, further studies are needed to determine whether its biological effects are associated with reversing Paclitaxel resistance.

1.5.2.2. Microtubule Regulatory Proteins and Tubulin Isotypes

Considering that Paclitaxel exerts its cytotoxic activity through binding to β-tubulin, a reduction in intracellular tubulin concentrations, point mutations in the gene(s) encoding tubulin, selective alterations in the expression of tubulin isotypes, and changes in

microtubule-associated proteins (MAPs) are significant mechanisms of Paclitaxel resistance (355, 356).

The expression of different tubulin isoforms with other binding domains, for example, the upregulation of β3-tubulin, can influence drug resistance by altering the binding affinity of taxanes (196, 357). Usually, β3-tubulin is found only in neuronal tissues, but in epithelial tumor cells, it can be aberrantly expressed (358). In many neoplasms, including OC, high levels of β3-tubulin have been associated with poor PFS, higher histological grade, and increased taxane resistance (330, 356, 359). Therefore, high levels of β3-tubulin can inhibit the microtubule-stabilizing activity (360, 361). Conversely, when β3-tubulin is depleted, the sensitivity to Paclitaxel can be increased (360, 361).

Mutations in β-tubulin can reduce the affinity of Paclitaxel (330, 362); however, studies evaluating patient samples have not found frequent mutations, suggesting that this molecular alteration is not a general mechanism for Paclitaxel resistance (363). The post-translational modification of tubulin, such as phosphorylation, acetylation, and detyrosination, can affect the organization and dynamics of microtubules. However, this has also not been found to occur frequently in clinical samples (330).

MAP4 and Tau proteins can competitively bind to microtubules at the same site as Paclitaxel, making them potential modulators of resistance (364). Smoter *et al.* evaluated clinical data from patients treated with platinum plus taxane and found a correlation between Tau expression and Paclitaxel resistance. Tau may limit the access of Paclitaxel to microtubules (364). On the other hand, MAP4 facilitates microtubule assembly and stabilization by increasing the longitudinal interaction within filaments, preventing depolymerization of microtubules (365). Therefore, alterations in the expression of MAP4 isoforms can affect the sensitivity of cancer cells to microtubule-targeting agents (365). In the OC context, Poruchynsky *et al.* found a positive correlation between MAP4 phosphorylation and Paclitaxel resistance (366). Similarly, Yu *et al.* found that MAP kinase spleen tyrosine kinase (SYK) also mediated Paclitaxel resistance (367). The increase in taxane resistance results from the upregulation of SYK, leading to the phosphorylation of tubulin and MAP (367). Some studies indicate that SYK inhibitors offer an excellent alternative to target microtubules by preventing this phosphorylation and restoring Paclitaxel sensitivity (196, 368). Stathmin, a microtubule-sequestering protein, induces microtubule destabilization. Its expression is markedly increased in taxane-resistant breast and ovarian tumors and was associated with an increased Paclitaxel resistance and an unfavorable prognosis (369, 370).

1.5.2.3. Apoptosis and Cell Cycle Regulation

Alterations in specific protein expression within intrinsic and extrinsic apoptotic pathways can suppress apoptosis, which leads to increased DNA repair and high tolerance for genetic damage (371). The intrinsic apoptosis pathway is the most prominent cell death signaling cascade, and the Bcl-2 protein family mainly controls it. This can be divided into pro-survival/anti-apoptotic [Bcl-2, Bcl-X_L, myeloid cell leukemia-1 (Mcl-1), Bcl-W, BFL1], effectors [Bcl-2 Antagonist/Killer (BAK), Bcl-2-like protein 4 (BAX), Bcl-2 related ovarian killer (BOK)], BH3-only activator [Bcl-2-like 11 (BIM), BH3 interacting domain death agonist (BID), p53 upregulated modulator of apoptosis (PUMA)], and sensitizer [phorbol-12-myristate-13-acetate-induced protein 1 (NOXA), Bcl-2 associated agonist of cell death (BAD), Bcl-2 modifying factor (BMF), Bcl-2 interacting killer (BIK), Harakiri, Bcl-2 interacting protein (Hrk)] proteins (372). In OC, the OE of the pro-survival protein family members Bcl-X_L, Bcl-2, and Mcl-1 has been associated with a worse prognosis (373) and resistance to taxane-induced apoptosis (257, 374, 375).

Survivin, a member of the IAP family, is often overexpressed in various cancers, including HGSC (376, 377). However, targeting survivin remains problematic due to its physiologic roles in mitosis, motility, and several other cellular pathways (378).

CCNE1 complexes with cyclin-dependent kinase 2 (CDK2) to regulate the transition from G_1 to S phase, which marks the beginning of DNA replication and cell cycle initiation (379). Increased CCNE1 leads to increased DNA synthesis and uncontrolled replication, enhancing the probability of chromosomal errors and genetic instability (196, 380). Moreover, cyclin A1 (CCNA1) expression increase is widely observed in Paclitaxel-resistant OC patients, particularly those with HGSC (196, 381, 382). Targeting CCNE1 is complex, and a more promising option proposes the indirect inhibition of CDK2 or polo-like kinase 1 (PLK1) (196). CDK2 inhibitors effectively suppressed pathway hyper-activation caused by CCNE1 (383). Moreover, PLK1 (a key regulator in mitosis) inhibitors combined with Paclitaxel showed an increased potential to induce apoptosis in HGSC cells with amplified CCNE1 (384).

Changes in spindle assembly checkpoint (SAC) proteins may also contribute to resistance to Paclitaxel. To target taxane-resistant mitotic cells, it may be most effective to focus on the mechanisms responsible for mitotic slippage and catastrophe (196). Mitotic checkpoint serine/threonine kinase B (BUB1B), BUB1-related kinase 1 (BUBR1), and mitotic arrest deficiency protein 2 (MAD2) are proteins that play an impactful role in active SAC/mitotic arrest response (385). Downregulation of these proteins (386) prevents

Paclitaxel-induced activation of the SAC and reduces subsequent apoptosis, thereby increasing resistance (387, 388). The relaxation of the SAC signal and degradation of CCNB1 regulates mitosis exit (385). OC cells bypass the Paclitaxel-induced mitotic arrest by weakening the SAC signal and effector proteins (196). In Paclitaxel-resistant OC cells, decreased CCNB1 and BUB1 expression disrupts SAC signal control during mitotic arrest (389). Likewise, manipulating the anaphase-promoting complex/cyclosome (APC/c) and proteins that regulate mitotic exit may provide another therapeutic opportunity to overcome taxane-mediated cell arrest (196). During Paclitaxel-induced mitotic arrest, the SAC is activated, which results in the inhibition of APC/c. Consequentially, CCNB1 is not degraded, sister chromatids do not separate, and microtubules attempt to reconnect with kinetochores (196, 390). However, Paclitaxel treatment causes microtubule stasis, and cells remain in this "non-mitotic mitosis limbo" until they die or enter senescence (391). To prevent cells from escaping mitotic arrest, some studies suggest that targeting PLK1 may be a better alternative (196, 392). Noack *et al.* and Raab *et al.* showed that combining Paclitaxel with an inhibitor for PLK1 can re-sensitize OC cells to taxane agents (384, 392). Alternatively, inhibiting the SAC may allow Paclitaxel-arrested cells to abort mitosis, resulting in polyploid cells. One way to indirectly achieve this is by stimulating branched-chain amino acid metabolism, leading to the inactivation of mammalian targets of rapamycin complex 1 (mTORC1) and aurora kinases (393).

1.5.2.4. Signal Transduction Pathways

The PI3K/AKT/mTOR pathway is widely known to be altered in most cancers, including OC. It can contribute to taxane resistance (265, 394) and suppress apoptosis, but some studies have shown that specific path inhibitors (e.g., AZD8835, AZD8186, and D-11688) can sensitize resistant cells to taxanes (395, 396).

1.5.2.5. Oxidative Stress

ROS-dependent resistance to taxanes can also occur by redox-responsive transcription factors [e.g., nuclear-factor kappa beta (NFκB), protooncogene jun (c-Jun), nuclear factor erythroid 2-related factor 2 (Nrf2), and hypoxia-inducible factor 1 subunit alpha (HIF-1α)], which activate the cellular antioxidant systems and increase the expression of survival proteins (397). Other ROS-dependent mechanisms, such as a switch from apoptosis to autophagy, EMT stimulation, and differentiation of CSCs by ROS, can also contribute to taxane resistance (398).

1.5.2.6. Cellular Homeostasis and Glucose Metabolism

Tumor cells have increased metabolic demands because they require a continuous supply of glucose and amino acids to support cell proliferation (334). The altered glucose metabolism is an essential source of metabolic plasticity that helps tumor cells undergo sustained growth and proliferation and acquire chemoresistance (399). Hypoxia, a prominent feature of solid tumors, is not *per se* a driver mechanism of taxane resistance; however, it affects several cellular pathways, activates multiple resistance mechanisms, and mediates reduced apoptosis following taxane treatment (196, 400). HIF1-α alters the expression of proteins, including cyclins, TGF-β, and c-JNK, that ultimately reduce taxane-induced G_2-M arrest and apoptosis (196, 400, 401). Moreover, tumor cells can inhibit apoptosis in adverse oxygen conditions by interacting with HIF1-α and members of the Bcl-2 family (402). Under hypoxic conditions, HIF1 is stabilized, translocates to the nucleus, and activates target gene expression that promotes resistance to anticancer therapy by regulating metabolism, survival, drug efflux, signaling, and DNA repair (401). Indeed, HIF1-α upregulation induces the expression of proteins associated with stemness, which increases resistance to taxane-induced apoptosis (401). It will be worthwhile to consider targeting pathways downstream of HIF1, which may not be involved in normal cell metabolism but are involved in cancer cell metabolism (196).

1.5.2.7. MicroRNAs and LncRNAs

Several studies in OC samples have shown that OE of miR-1307, miR-433, miR-630, miR-106a, miR-182, miR-21, miR-27a, miR-30a, and miR-490-3p, as well as the downregulation of miR-141, miR-145, miR-148a, miR-149, and miR-200c are associated with the development of taxane resistance (334, 403-405). On the other hand, the upregulation of miR-29b, miR-199a, miR- 200a, miR-200c, and miR-215, along with the downregulation of miRNA-146a and miR-194 are associated with increased sensitivity to taxanes (334, 405-407).

Regarding long non-coding ribonucleic acids (lncRNAs), the downregulation of fer-1-like protein 4 (FER1L4) and the OE of long intergenic non-protein coding RNA 1118 (LINC01118) and nuclear enriched abundant transcript 1 (NEAT1) lead to Paclitaxel resistance (408-410). Although many other studies have documented the relevance of miRNAs and lncRNAs in developing taxane resistance in OC, targeting more than one miRNA or lncRNA might be necessary to achieve a therapeutic response. Nevertheless, these miRNAs and lncRNAs can serve as biomarkers to predict taxane response (196).

1.5.2.8. Tumor Microenvironment

The TME can also contribute to chemoresistance to multiple antineoplastic drugs, including Paclitaxel (411). These effects are achieved by diverse signaling interactions, possibly via direct cell-to-cell contact or the release of soluble factors that promote cancer dissemination and MDR (412). Zhang *et al.* demonstrated that adipose stromal cells derived from the omental tissue of patients with OC promoted Paclitaxel and Carboplatin resistance when co-cultured with various OC cell lines (413). CAFs, one of the most critical immunosuppressive cells within TME, can secrete IL-6 and promote TGF-β-mediated EMT in OC via the janus kinase (JAK2)/STAT3 pathway. This leads to the inhibition of apoptosis and subsequent Paclitaxel resistance (414). Leung *et al.* showed that the CAF-derived factor, microfibrillar-associated protein 5 (MFAP5), increases the expression of lipoma-preferred partner in microvascular endothelial cells, leading to alterations in endothelial cell permeability and compromised Paclitaxel delivery to tumor cells (415).

1.5.2.9. Extracellular Vesicle-Dependent Intercellular Communications

EVs are small structures secreted by cells and can contain bioactive molecules, proteins, RNA, and DNA. Other cells can take them up and play an essential role in intercellular signaling (416). Cancer cells can secrete high amounts of EVs, and some studies showed that their molecular content mediates resistance to many chemotherapeutic drugs (417, 418). Indeed, Docetaxel resistance can be transferred via the horizontal transfer of EVs containing miRNAs, including miR-9-5p, miR-195-5p, and miR-203a-3p (419, 420). Lv *et al.* showed in breast cancer that EVs can sequester chemotherapeutic drugs, transport proteins, such as P-gp, and transfer taxane chemoresistance from cell to cell (421).

1.5.2.10. Multi-Micronucleus and Laminin A/C Expression

Recent evidence suggests that Paclitaxel can also operate as an anticancer therapy through a non-mitotic that forms multi-micronucleated cells (325), impacting interphase cells (422). Micronuclei result from the physical breaking of nuclei and are unstable and readily ruptured to release enclosed DNA (423). Paclitaxel-induced aberrant mitosis generates multiple nuclear lobules and micronuclei that trigger apoptosis (325). Indeed, cancer cells often have a defective and flexible nuclear envelope that presents a deformed nuclear morphology and the tendency to undergo transient rupture (424). Lamin A/C proteins are crucial in maintaining a sturdy nuclear envelope structure (425) and are usually lost, reduced, or heterogeneously expressed in OC (426). Recently, Smith *et al.* showed that

Paclitaxel caused multi-micronucleation in malignant OC cells but not in normal cells, as well as susceptibility to undergo nuclear fragmentation and cell death correlated with a reduction in the nuclear lamina protein lamin A/C (427). In lamin A/C-deleted mice, cells lose physical strength, become easily deformed, are susceptible to Paclitaxel, and undergo nuclear breakage (427). On the other hand, lamin A/C OE reinforces nuclear envelope structure and increases the resistance to Paclitaxel-induced nuclear breakage in cancer cells (427). Indeed, Paclitaxel induces nuclear breakage in cancer cells with a malleable nucleus but not in normal cells with a stiffer nuclear envelope (427).

1.5.2.11. Polyploid Giant Cancer Cells

Polyploid giant cancer cells (PGCCs) are observed in HGSC samples after chemotherapy and are associated with Paclitaxel resistance (428-430). Previously, they were thought to be nonviable cells due to their senescent nature and inability to execute mitosis (431). However, PGCCs are viable cells and can grow progressively by amitotic budding, splitting, and bursts of proliferation from mononucleated or multinucleated giant cells (428). To further study the role of PGCCs in OC cells treated with Paclitaxel, Niu *et al.* analyzed the mRNA expression profile of PGCCs. They found that IL-6 activation dominated the senescence-associated phenotype (432). The study confirmed the relevance of these findings by blocking IL-6 and showing that it prevented PGCC formation and inhibited tumor growth in a patient-derived xenograft HGSC model (432).

1.5.3. Mechanisms of Resistance to PARP Inhibitors in Ovarian Cancer

PARP is an enzyme partly responsible for the correct repair of DNA damage. However, in cells with defective HR repair systems, DSBs are repaired by NHEJ, which is an error-prone process that can result in cell death (433).

PARPi has two main effects. First, it inhibits PARP1's catalytic activity, which prevents the formation of PAR chains [poly(ADP) ribosylation (PARylation)] that recruit more DNA repair proteins. Second, it traps PARP1 by stopping its release from damaged DNA, thus halting the progression of replication forks (434).

Around 50% of HGSC tumors have defective HR. PARPi are now available to patients with first-line and recurrent platinum-sensitive disease (435). HR-deficient phenotype can result from germline or somatic mutation in BRCA1/2 (20% of the HGSC patients), non-mutational changes (such as BRCA1 promoter methylation), and mutations in other repair-associated genes [e.g., BRCA1 interacting helicase 1 (BRIP1) and RAD51C,

which collectively account for 2% of the HGSC cases] (436, 437). The use of PARPi has significantly improved outcomes in many HGSC patients in recent years. However, the benefits are most evident in patients with germline or somatic BRCA1/2 mutations and patients with non-BRCA-related HR deficiency (44). Despite the remarkable clinical benefit of PARPi in patient OS (438), acquired PARPi resistance has emerged as a critical challenge in improving treatment success in most patients with advanced HGSC (439, 440). In platinum-sensitive recurrent HGSC, the response rate to PARPi monotherapy was about 30–45% in BRCA1/2 mutation patients (441). Patients with HR-proficient tumors present minimal benefits to PARPi as they present an innate resistance to them (439).

PARPi resistance mechanisms in OC can be categorized into two main groups: those associated with HR and those not. Additionally, OC cells can develop PARPi resistance through various mechanisms, including the restoration of HR repair activity; replication stress mitigation, whereby the cancer cell slows the cell cycle and stabilizes replication forks; and mechanisms not currently assigned to a single DNA repair pathway-related process but still alter the response to PARPi, such as mutations in PARP itself, genomic events that change PARylation, PARP trapping, upregulation of drug efflux pumps and activation of alternate pathways (**Figure 8**) (442).

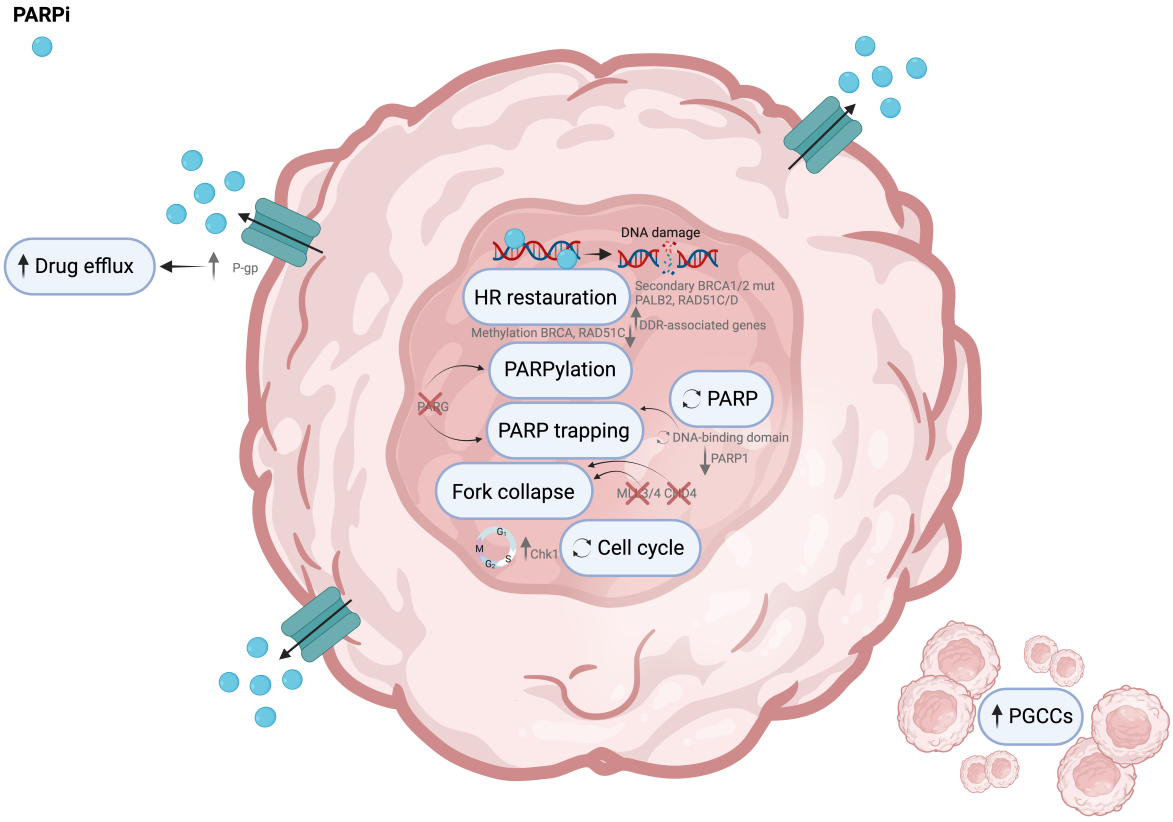


Figure 8. Schematic representation of the main molecular mechanisms contributing to PARPi resistance in OC. OC cells can develop PARPi resistance through various mechanisms, including the restoration of HR repair activity (alterations in BRCA1 and MMR genes) and replication stress mitigation, whereby the cancer cell slows the cell cycle and stabilizes replication forks. Moreover, mutations in PARP itself, genomic events that change protein poly(ADP) ribosylation (PARylation), PARP trapping, upregulation of drug efflux pumps (P-gp OE), and activation of alternate pathways can also alter PARPi response, leading to PARPi resistance. Figure created with BioRender.com. BRCA1/2, breast cancer 1/2; CHD4, chromodomain helicase DNA-binding protein4; CHK1, cell cycle checkpoint kinase 1; DDR, deoxyribonucleic acid damage response; DNA, deoxyribonucleic acid; HR, homologous recombination; MMR, mismatch repair; OC, ovarian cancer; OE, overexpression; PALB2, partner and localizer of BRCA2; PARG, poly(ADP-ribose) glycohydrolase; PARP1, poly(ADP-ribose) polymerase 1; PARPi, poly(ADP-ribose) polymerase inhibitor; PGCCs, polyploid giant cancer cells; P-gp, P-glycoprotein; RAD51C/D, RAD51 recombinase C/D.

1.5.3.1. PARPi Resistance Mechanisms Associated with Restoration of Homologous Recombination

1.5.3.1.1. Homologous Recombination

Platinum-resistant tumors have a higher capacity for DNA repair. Patients previously exposed to platinum agents may also show PARPi cross-resistance (443). Platinum sensitivity, as defined by PFI, is one of the best response indicators to PARPi. However, even among BRCA-mutated tumors with a PFI longer than six months, around 30% of patients may still show intrinsic resistance to PARPi (49, 444). On the other hand, for platinum-resistant BRCA-mutated tumors, the overall response rate to PARPi is around 30–40% (49). PARPi undermines SSB damage repair, either by trapping PARP proteins on the DNA site of the lesion or by blocking PARP catalytic domain (445). Unrepaired SSBs lead to DSBs and genomic instability, which triggers cell death (440). Synthetic lethality due to the accumulation of DSB occurs in cells exposed to PARPi and has impaired HR repair machinery (446-448). Restoring HR in HR-deficient tumors represents the most common acquired resistance mechanism to PARPi (186, 449). The restoration of HR activity can be achieved by directly affecting the HR machinery through genomic, epigenetic, and post-translational alterations or indirectly by growth factor receptor-mediated signaling pathways that increase the expression or activity of HR machinery (450). The direct restoration of HR includes secondary mutations such as germline or somatic insertion or deletion mutations in BRCA1/2 that restore the open reading frame of the BRCA gene, remove the original deleterious mutation, and restore the expression of a functional protein (451, 452). Indeed, reversion mutations are one of the most prevalent and well-known causes of PARPi resistance (453, 454). Somatic reversions have also been observed in other HR pathway

genes, such as partner and localizer of BRCA2 (PALB2), RAD51C, and RAD51D, and are associated with poor prognosis (451, 455).

Epigenetic regulation involving the reduced promoter methylation of BRCA1 and RAD51C restores their functional expression and leads to PARPi resistance in HGSC (456). Oncogenic signaling pathways, including the vascular endothelial growth factor receptor (VEGFR), PI3K, and heat-shock protein 90 (HSP90), can also promote HR proficiency indirectly by increasing the expression of DDR-associated genes (450).

1.5.3.1.2. PARP Functions

PARP inhibition impairs DNA replication by generating PARP-DNA adducts; however, downregulation of PARP1 or alterations in its DNA-binding domains renders inhibitors of the PARP enzyme ineffective for inducing PARP trapping (457). Furthermore, PARP1 binds to damaged DNA through its zinc finger DNA-binding domain, which can be modified by the allosteric effects of PARPi joining at the catalytic site (458). Moreover, mutations or post-translational modifications in PARP1 were linked to a diminished PARP1 trapping activity on DNA and have also been uncovered as a mechanism of resistance (457, 458).

The poly(ADP-ribose) glycohydrolase (PARG) enzyme also regulates PARP1 trapping by counterbalancing the activity of PARP1. PARG catabolizes PAR chains, the product of PARP activity (459). PARylation is crucial for DNA repair by the HR and is reversed by PARG. Therefore, the loss of PARG can restore PARylation and PARP trapping and consequentially cause PARPi resistance (459).

1.5.3.2. PARPi Resistance Mechanisms Not Associated with Homologous Recombination

1.5.3.2.1. Replication Fork

Replication fork degradation is an essential contributor to the synthetic lethality mechanism underlying the activity of PARPi; in contrast, the stabilization of stalled replication forks confers PARPi resistance (460). The protection of stalled replication forks is a function usually performed by BRCA1/2 and PARP1. When BRCA1 and BRCA2 are lost, the loss of replication fork protection allows cells to proceed unchecked into G_2 and mitosis when, ultimately, replication forks collapse and cause cell death (439). Therefore, when PARPi traps PARP on SSBs and replication forks stall, cells must rely on BRCA1/2 for survival (439). Studies in BRCA-deficient cell lines showed loss of the mixed-lineage leukemia protein 3/4 (MLL3/4) complex protein PTIP or nucleosome remodeling factor CHD4, which

leads to fork collapse (247). Both these proteins are involved in recruiting the meiotic recombination 11 (MRE11) nuclease to the site of a stalled replication fork; in the absence of MRE11, newly synthesized DNA single strands are protected from degradation; cells with stalled replication forks do not enter mitosis and become resistant to PARPi (247, 461).

Schlafen 11 (SLFN11) is another important mediator of PARPi resistance. It acts at the G_1/S checkpoint by binding to a stressed replication fork and eventually causes irreversible cell cycle arrest and death (462). In cells with a BRCA1/2 mutation, SLFN11 depletion allows the fork to progress through G_1/S, diminishing the efficacy of PARPi (462, 463).

1.5.3.2.2. Drug Efflux Pumps

Increased drug efflux is a well-described mechanism of PARPi resistance (449). Mutations in OE of ABCB1 that result in increased transcription of the drug efflux pump P-gp were found in tissue samples from PARPi-treated breast and ovarian cancers (464). In Paclitaxel-resistant OC cells, P-gp expression and gene copy numbers increased (465). Indeed, PARPi, such as Olaparib and Rucaparib, are P-gp substrates, and prior treatment with Paclitaxel may induce P-gp upregulation and indirectly induce PARPi resistance (465). These findings hold immense clinical significance, highlighting the need for careful analysis when prescribing specific PARPi to OC patients. Administering these drugs as a second-line or maintenance treatment may not be effective in some patients due to the Paclitaxel-resistance and the consequent active efflux of both drugs from cells, compromising the clinical response. Therefore, evaluating P-gp expression in patients who have failed Paclitaxel therapy before administering a PARPi that is also a P-gp substrate (342) would be prudent.

1.5.3.2.3. Cell Cycle Regulation

For proper execution of DNA repair, cell cycle regulation is critical (466). Upon recognition of DNA damage, the checkpoint ataxia–telangiectasia-mutated (ATM) and Rad3-related (ATR) kinases control downstream signaling pathways to determine whether the cell cycle progresses or is interrupted to allow for DNA repair (467). The cell cycle arrest induced by genotoxic stress is mediated by CHK1, which is activated in response to both short-term and chronic replication stress (439). Considering that approximately 95% of HGSC patients harbor a p53 mutation (184), causing a dysfunctional G_1/S checkpoint, cancer cells depend on CHK1-mediated G_2/M cell cycle arrest for DNA repair (468). ATR mediates the G_2/M cell

cycle arrest and allows HR to repair DSBs in the presence of a collapsed replication fork (439). CHK1 also phosphorylates BRCA2 and RAD51 recombinase to DSBs to facilitate HR. Therefore, inhibition of CHK1 impairs G_2 arrest, preventing DNA repair via HR and leading to apoptosis (469, 470).

1.5.3.2.4. Polyploid Giant Cancer Cells

A newly described PARPi resistance mechanism relies on activating the giant cell life cycle, leading to whole genome reprogramming in response to catastrophic stress, known as PGCCs. Zhang X. *et al.* developed an experimental work to understand the mechanism of acquired resistance associated with PARPi in HGSC-derived organoids and patient-derived xenografts (471). They showed that PGCCs exhibit features of senescent cells but, after Olaparib withdrawal, can escape via the restitution of multipolar endomitosis and other noncanonical modes of cell division to generate mitotically competent resistant daughter cells (471). The authors also found that Mifepristone (an antiprogestin contraceptive drug) synergistically acts with Olaparib to promote apoptosis of cells that are undergoing endoreplication, resulting in the inability to form PGCCs. This mechanism suggests that Mifepristone may be more effective in killing newly formed PGCCs induced by therapeutic stress than preexisting PGCCs in patient tumors (471). These authors presented a proof concept on how targeting PGCCs may represent a promising approach to overcome PARPi-induced resistance. Importantly, the authors looked for an association between p53 and BRCA mutational status and its association with PGCCs associated with Olaparib resistance. Although mutation or loss of p53 can sensitize cancer cells to polyploidization due to defective cell checkpoints, the authors demonstrated the formation of PGCCs in all cell lines regardless of p53 mutations (471). Additionally, using patient-derived xenograft models with acquired Olaparib resistance from both BRCA1 mutation and BRCA1 wild-type (WT) HGSC patient tumors, they found that PGCCs were more common in the Olaparib-treated patient-derived xenografts. This suggests that PGCCs, not BRCA status, are associated with acquired resistance to Olaparib in patients with relapsed OC (471). These results are consistent with the previous work reporting an increased ploidy in PARPi-resistant OC samples (472).

1.5.4. Mechanisms of Resistance to Bevacizumab in Ovarian Cancer

Tumorigenesis is a proliferative process highly dependent on developing a new vascular supply (473). Angiogenesis refers to the stimulation of the growth of endothelial

cells, which gives rise to more blood vessels. It is a crucial factor in the progression of solid tumors and metastases because it supplies nutrients and oxygen and removes metabolic wastes (473). Particularly in OC, angiogenesis induces MA formation and the spread of metastases, which leads to poor prognosis (474). Therefore, angiogenesis has been an essential focus for the targeted treatment of OC.

The VEGF-VEGFR pathway is a crucial regulator of angiogenesis, including in OC (474). Cancer cells produce VEGF to drive blood vessel growth and deliver oxygen and nutrients directly to tumors (475). VEGF signaling is highly activated and closely associated with widespread IP carcinoma and the formation of large volumes of MA in OC (474, 476). VEGF gene expression has been found in OC tissue, omental metastases, MA, and the sera of patients with OC (104).

Bevacizumab is a humanized anti-VEGF monoclonal antibody that inhibits angiogenesis. It was the first angiogenesis inhibitor used in oncology clinical practice and the first approved for OC patients (477). The FDA has approved Bevacizumab as a first-line combination therapy with Carboplatin/Paclitaxel and a second-line strategy in platinum-sensitive or platinum-resistant OC (37-39). Bevacizumab prevents the interaction between circulating VEGF and VEGFR, destroying existing vessels, disturbing neovascularization, releasing intratumor pressure, and consequently inhibiting angiogenesis (475). Although several clinical studies have shown improvements in PFS in a subset of patients with advanced OC (39), the improvement in OS was not obvious, the duration of activity was relatively short (only 3–8 months in monotherapy), and the individual discrepancies and widespread resistance greatly limited the effectiveness of this antiangiogenic (478, 479).

Bevacizumab-resistant mechanisms have been studied in different types of neoplasms. These include pharmacodynamic tolerance, tachyphylaxis (an acute decrease in response to a drug after repeated administration), alteration of the neovascular architecture, redundant angiogenic factors inducing hypoxia, increased tumor invasiveness, and metastatic behavior (449, 480, 481). Additionally, alterations in the ratio between VEGF-dependent and VEGF-independent vascular subtypes during antiangiogenic therapy led to Bevacizumab resistance (**Figure 9**) (482).

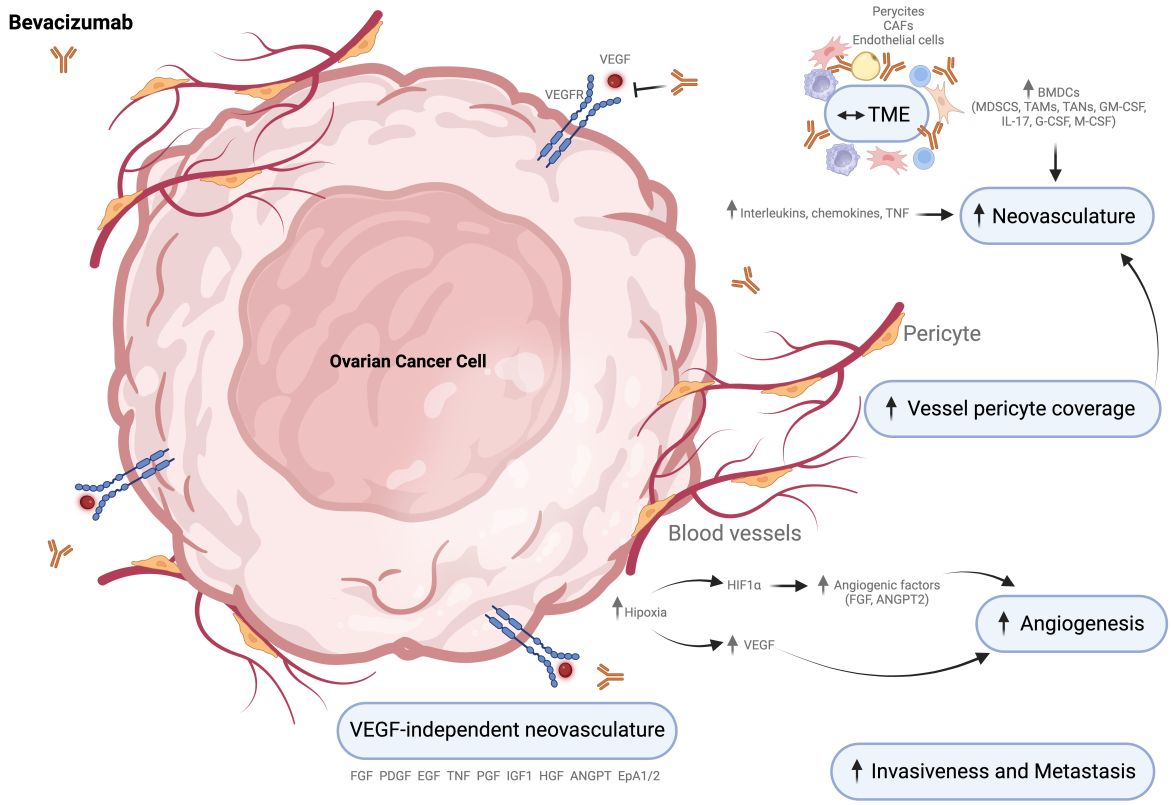


Figure 9. Schematic representation of the main molecular mechanisms contributing to Bevacizumab resistance in OC. Bevacizumab resistance includes pharmacodynamic tolerance, tachyphylaxis, alteration of the neovascular architecture, redundant angiogenic factors, induction of hypoxia, increased tumor invasiveness, and metastatic behavior. Additionally, alterations in the ratio between VEGF-dependent and VEGF-independent vascular subtypes during antiangiogenic therapy led to Bevacizumab resistance. Figure created with BioRender.com. ANGPTs, angiopoietins; CAFs, cancer-associated fibroblasts; EGF, epithelial growth factor; EpA1/2, ephrins; FGF, fibroblast growth factor; G-CSF, granulocyte colony-stimulating factor; GM-CSF, granulocyte-macrophage colony-stimulating factor; HGF, hepatocyte growth factor; HIF1-α, hypoxia-induced factor 1-α; IGF1, insulin-like growth factor 1; IL-17, interleukin 17; M-CSF, macrophage colony-stimulating; MDSCs, myeloid-derived suppressor cells; OC, ovarian cancer; PDGF, platelet-derived growth factor; PGF, placenta growth factor; TAMs, tumor-associated macrophages; TANs, tumor-associated neutrophils; TGF, transforming growth factor; TME, tumor microenvironment; TNF, tumor necrosis factor; VEGF, vascular endothelial growth factor; VEGFR, vascular endothelial growth factor receptor.

1.5.4.1. VEGF-Independent Revascularization

Resistance to Bevacizumab can occur through the reactivation of tumor revascularization by “VEGF-independent pathways.” Antiangiogenic inhibitors can increase hypoxia, which then upregulates the production of other proangiogenic factors (483) such as fibroblast growth factor (FGF), platelet-derived growth factor (PDGF), epithelial growth

factor (EGF), TGF, TNF, placenta growth factor (PGF), insulin-like growth factor 1 (IGF1), hepatocyte growth factor (HGF), angiopoietins (ANGPT), and ephrins (EpA1/2), among others (484). PGF has been identified as a potential contributor to anti-VEGF resistance because its upregulation has been observed in patients receiving anti-VEGF (485). Therefore, targeting only the VEGF pathway may not be enough to prevent angiogenesis, as other angiogenic factors or pathways can compensate to stimulate angiogenesis, ultimately leading to resistance.

1.5.4.2. Neovasculature

HGSC patients exhibiting an immunoreactive profile trigger an immune response, which results in the recruitment of pro-angiogenic monocytes from the bone marrow, increased intratumoral hypoxia, upregulated HIF1-α, and a high pericyte coverage of the tumor vascular system. This results in an inefficient response to antiangiogenic drugs (486, 487).

In solid tumors, angiogenesis leads to a defective vasculature with increased vascular and tumor permeability, consequently changing the TME and affecting intra-tumoral drug delivery (488). Long-term antiangiogenic therapy significantly alters the expression of angiogenic factors, causing an extensive morphological change in the vessels, and this remodeled neovascular architecture leads to treatment failure (484). Recently, Arjaans *et al.* demonstrated in OC xenograft that Bevacizumab decreased tumor uptake of antiangiogenic drugs while increasing the number of vessel pericytes (488, 489). Increased pericyte coverage in the tumor vasculature is a consequence of antiangiogenic treatment but is also a mysterious mechanism (490).

1.5.4.3. Hypoxia

Antiangiogenic therapies result in vascular regression and can increase intra-tumoral hypoxia levels, leading to an abnormal upregulation of HIF1-α that can stimulate tumor and stromal cells to secrete large amounts of angiogenic factors, such as FGF and ANGPT2 (491). This exacerbates vascular disorders and accelerates non-productive angiogenesis in an endless cycle of self-enhancement. As a result, therapy resistance increases, and the risk of disease progression becomes higher (491). Additionally, antiangiogenic therapy can cause genetic alterations and hypoxia in the TME, which can lead to VEGF upregulation and the rebound of tumor angiogenesis. Other factors related to inflammation, immunosuppression, and bone BMDC recruitment, such as interleukins, chemokines, and

TNF, have also been shown to be upregulated in patients treated with antiangiogenic therapy. These factors contribute to the evasion of antiangiogenic therapy by promoting neovascularization and enhancing aggressive malignant behaviors in tumor cells (490).

1.5.4.4. Tumor Microenvironment

In TME, apart from tumor cells, the increased infiltration of BMDCs, such as myeloid-derived suppressor cells (MDSCs), TAMs, and tumor-associated neutrophils (TANs), mediated by various attractants, such as granulocyte-macrophage colony-stimulating factor (GM-CSF), IL-17, granulocyte colony-stimulating factor (G-CSF), and macrophage colony-stimulating (M-CSF), lead to neovascularization and immunosuppression induction and allow tumor cells to escape antiangiogenic therapy (490). Local stromal cells, including pericytes, CAFs, and endothelial cells, are also involved in tumor escape (490). Endothelial cells are the central components of blood vessel walls and can be activated by various proangiogenic factors to initiate angiogenesis. Moreover, they can become refractory to antiangiogenic therapy by altering biological functions, cellular phenotypes, and secretory protein expression (490).

1.5.4.5. Tumor Invasiveness and Metastasis

Antiangiogenic inhibitors block tumor growth. However, they also have been linked with increased local invasiveness and distant metastasis in different neoplasms (481, 492, 493). For instance, in renal cell carcinoma and glioblastoma, tumor cells showed increased proliferation and became more invasive after being treated with Bevacizumab (492, 493).

Acknowledgments and Funding

This work was developed at *Instituto de Investigação e Inovação em Saúde (i3S)*, an Associate Laboratory of the *Ministério da Ciência, Tecnologia e Inovação (MCTES),* and it was partially supported by *Fundação para a Ciência e a Tecnologia (FCT).* MN acknowledges *FCT, MCTES*, and *União Europeia (UE)* for financial support through a PhD fellowship (2020.04720.BD and DOI:10.54499/2020.04720.BD) that was co-sponsored by *Fundo Social Europeu (FSE)* through *Programa Operacional Regional Norte (Norte 2020).*

CHAPTER II

Thesis Motivation, Hypotheses, and Aims

1. Thesis Motivation

OC is a deeply challenging journey for women. It often goes undetected until advanced stages and is frequently noted for its high rates of chemoresistance, leading to treatment failure and poor outcomes. This resistance is usually exacerbated by the metastatic niche of MA that forms in the advanced stages of the disease. MA not only supports tumor cell proliferation but also creates a unique TME that can foster resistance mechanisms. Given the urgent need for effective therapies, drug repurposing emerges as a strategic solution.

This thesis is motivated by a desire to make a meaningful difference in the lives of those affected by OC. Many women, after enduring the rigors of chemotherapy, confront the harsh reality of treatment resistance. This inspired us to explore the potential of drug repurposing as a beacon of hope. Exploring existing drugs with well-known safety profiles for new uses can potentially identify effective treatments that bypass the lengthy timelines typically associated with novel agents. This is crucial for timely intervention, which can significantly improve survival rates.

Incorporating patient-derived cultures into this drug research strategy offers a cutting-edge methodology for investigating drug responses that reflect individual tumor characteristics. Patient-derived cultures from MA can more accurately mimic tumor behavior than traditional cell lines, providing insights into the unique resistance mechanisms in each patient's cancer.

This project aims to harness the synergy of drug repurposing, chemotherapy, and patient-derived culture technology to overcome chemoresistance and tailor therapies to individual patients. By focusing on drugs that can effectively target the specific pathways exploited by tumor cells in the MA environment, this research seeks to enhance treatment efficacy and improve clinical outcomes for OC patients.

2. Hypotheses

Based on the outlined objectives of this PhD project, four hypotheses have been formulated:

- **Hypothesis 1 –** Specific biomarkers associated with differentiation in cancer, CSC, and drug resistance can be used to identify chemoresistant OC cell populations in patient-derived samples.

- **Hypothesis 2 –** Chemoresistant OC cell line models exhibit resistance profiles similar to those in patients and can be used to assess drug sensitivity assays.

- **Hypothesis 3 –** Combining drug repurposing with conventional chemotherapy enhances the cytotoxic effects against chemoresistant OC cell populations compared to conventional treatments alone.

- **Hypothesis 4 –** Optimizing culture conditions for MA-derived cell cultures significantly improves their viability *ex vivo,* which can be used to perform drug efficacy tests.

3. Aims

The primary objective of this PhD project is to identify and characterize chemoresistant OC cell populations using MA-derived samples and MA-derived cultures. The project aims to identify novel therapeutic strategies to overcome chemoresistance by combining drug repurposing with conventional chemotherapy. To achieve this goal, the following four specific objectives were established and are presented in three dedicated results chapters:

Chapter III – Evaluate the expression of specific biomarkers to identify chemoresistance profiles in patient-derived samples. Chapter III focused on assessing differentiation (MUC16), CSCs [sex-determining region Y-box transcription factor 2 (SOX2), ALDH1A1, and CD44v6], and resistant (P-gp) markers. To achieve this, a phenotypic evaluation was conducted using MA samples obtained from HGSC patients before and after chemotherapy.

Chapter IV – Establish and characterize chemoresistant OC cell line models, followed by the sensitization step using drug repurposing. In Chapter IV, two chemoresistant OC cell lines (OVCAR8 PTX R C and OVCAR8 PTX R P) were developed from the OVCAR8 parental cell line by exposing them to increasing concentrations of Paclitaxel through continuous or short-term exposure. Drug sensitivity assays were conducted to confirm the stability of the resistance profile, and various biological behaviors such as proliferation, migration, apoptosis, and cell-cycle distribution were evaluated. Additionally, the expression of relevant biomarkers was assessed through immunocytochemistry (ICC) and western blot.

A drug test involving multiple drugs was performed to evaluate their potential for drug repurposing in OC. The cytotoxic effects of Pitavastatin, Metformin, Ivermectin, Itraconazole, and Alendronate were studied in OVCAR8 and OVCAR8 PTX R C/R P cell lines. Each repurposed drug's IC_{50} was calculated and combined with Carboplatin or Paclitaxel. Furthermore, the safety of these drug combinations was assessed using a non-tumoral cell line (HOSE6.3). Lastly, the drug interactions were evaluated on previously tested drug combinations to determine potential synergistic interactions. The analysis of drug interactions was conducted using different reference models, including Chou-Talalay, Zero Interaction Potency (ZIP), Highest Single Agent (HSA), Bliss independence, and Loewe, employing CompuSyn and SynergyFinder software.

Chapter V – Establish malignant ascites-derived cultures to perform *ex vivo* drug efficacy tests and make them more effective than conventional chemotherapy through drug repurposing. Chapter V presents different optimization protocols to establish MA-derived cell cultures. During several months, multiple media and culture conditions were tested to obtain maximum efficiency regarding tumor cell growth and organoid formation *ex vivo.* We successfully established several MA-derived organoid cultures from our cohort of HGSC samples. Then, the effectiveness of Carboplatin in the established *ex vivo* models was tested. Drug response profiles were evaluated using the Alamar Blue™ assay.

CHAPTER III

Evaluation of the Expression of Specific Biomarkers to Identify Chemoresistance Profiles in Patient-Derived Samples

Expression of ALDH1A1, SOX2, CD44v6, and P-gp as a Chemotherapy Footprint in Malignant Ascites Samples

1. Abstract

MA are commonly observed in advanced stages of HGSC and during disease recurrence. The molecular analysis of cells found in MA provides a unique opportunity to track tumor cell kinetics during the progression of OC. This study evaluated the immunoexpression of four biomarkers associated with a CSC profile and drug resistance: ALDH1A1, SOX2, CD44v6, and P-gp, in HGSC. ICC was performed on 37 MA samples collected from patients before (n=19) and after (n=18) chemotherapy. This study highlights the importance of centrifuging the entire volume of MA drained during paracentesis for biomarker searches using ICC. It is a procedure commonly performed for symptomatic relief that yields a sample rich in tumor cells, thus enhancing its utility for molecular pathology studies. We observed that the expression of the ALDH1A1/CD44v6/SOX2/P-gp profile was more frequently found in MA samples drained from patients after chemotherapy cycles ($p = 0.003$), suggesting that chemotherapy is associated with the expression of these CSC and drug-resistance biomarkers. Additionally, this profile was associated with platinum resistance ($p = 0.068$). These findings support the idea that chemotherapy-induced molecular alterations in MA cells reflect the dynamic kinetics of tumor progression. The ALDH1A1/SOX2/CD44v6/P-gp profile could serve as promising predictive biomarkers for chemoresistance in HGSC. This study underscores the potential of using MA as a non-invasive tool to monitor molecular alterations in HGSC, which can have an important impact on therapy decisions.

Keywords

Malignant Ascites, Ovarian Carcinoma, Chemoresistance, Immunocytochemistry, Predictive Biomarkers.

2. Introduction

OC is a highly aggressive malignancy that primarily affects the female reproductive system. It is the eighth most commonly occurring cancer and the seventh leading cause of cancer-related deaths in women worldwide (494). Among the various subtypes of OC, HGSC is the most aggressive and lethal, primarily due to the challenges in detecting it at early stages and the tendency for it to be diagnosed only once it has spread extensively within the peritoneal cavity (495). Although HGSC initially responds to chemotherapy with a partial or CR in

approximately 50-80% of patients receiving platinum-taxane treatment, many patients, unfortunately, experience relapse and disease recurrence due to the development of chemoresistance (496-498).

A major complication of advanced OC is ascites, which refers to the abnormal accumulation of fluid in the peritoneal cavity (499). Ascites can arise from a variety of pathologies, including cirrhosis, pancreatitis, nephritis, heart failure, and malignancies like OC (62). More than one-third of OC patients present MA at the time of diagnosis, especially in the later stages of the disease (66, 69, 70). Cytological analysis of MA at diagnosis is crucial for determining the disease stage and assessing tumor cell presence. However, once drained, this fluid is often discarded, which means its full potential for ongoing study is not fully exploited (64, 67). MA is a complex biological fluid comprising both cellular (e.g., cancer cells, immune cells, stromal cells, and mesothelial cells) and acellular components (such as cytokines, chemokines, and metabolites) (499). These components play a key role in promoting cancer cell dissemination within the peritoneal cavity and can contribute to distant metastasis, which is linked to a poor prognosis (499). Despite its complexity, MA represents an underutilized resource for deeper molecular studies due to its large volume, widespread occurrence, and ease of accessibility. When analyzed, MA can provide critical insights into disease progression and tumor biology and offer valuable molecular data to inform treatment decisions and personalize patient care (500).

To answer the question, “What are the other clinical applications of OC MA?" an immunocytochemical evaluation of MA samples obtained from HGSC patients before chemotherapy (at diagnosis) and after chemotherapy (during or after chemotherapy cycles) was conducted. We focused on the expression of aldehyde dehydrogenase 1 (ALDH1A1), SOX2, CD44v6, and P-gp—biomarkers commonly associated with CSC characteristics and drug resistance. The goal was to identify any predictive "footprint" of chemotherapy in the MA and to understand better the molecular alterations that may be involved in the progression of the disease (**Figure 10**). This study aims to uncover novel ways in which the analysis of MA can contribute to a better understanding of tumor behavior and treatment response and potentially aid in identifying biomarkers for chemoresistance.

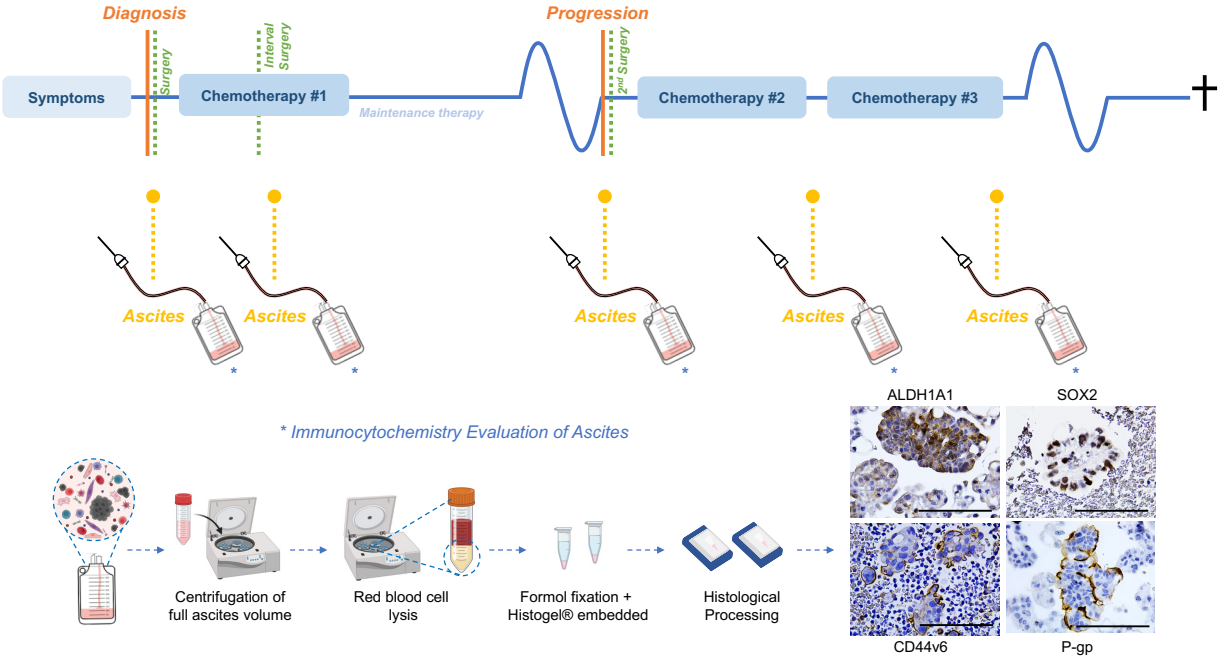


Figure 10. Representative scheme of the clinical evolution of ovarian cancer through the analysis of malignant ascites during the disease's time course. Figure created with Bionrender.com.

3. Materials and Methods

3.1. Patient Samples

Instituto Português de Oncologia do Porto FG, EPE (IPOP)-MA is a retrospective series of 37 samples from 33 HGSC patients diagnosed between 2018 and 2024. Nineteen and eighteen samples were collected before and after the chemotherapy, respectively. Four patients, HGSC#2, HGSC#5, HGSC#11, and HGSC#26, had paired MA samples collected before (HGSC#2.1, HGSC#5.1, HGSC#11.1, and HGSC#26.1) and after (HGSC#2.2, HGSC#5.2, HGSC#11.2, and HGSC#26.2) chemotherapy.

All samples were obtained from the IPOP Pathology Department Biobank, following the Declaration of Helsinki and ethical guidelines set by the IPOP Ethical Committee (REF CES.092R1/019). **Table S1** shows the clinicopathological characteristics of the IPOP-MA series.

3.2. Malignant Ascites Processing and Storage

In recent years, the protocol for processing samples from OC patients for MA has seen enhancements, and other researchers have adopted a similar method (501). An optimized procedure has been developed for the reception, storage, and processing (including separation

and cryopreservation) to guarantee the quality of biological samples for multi-assessment. MA must remain on ice throughout the processing, which should occur in a sterile laminar flow biosafety cabinet. Briefly, MA samples were repeatedly mixed to resuspend any cells that had settled. Then, it was aliquoted into 50 ml conical tubes and centrifuged (400 g, 10 minutes, at 4 ºC) to separate the cell pellet from the supernatant. The acellular fraction (supernatant) was collected for 1.5 ml (x10), 5 ml (x10), and 50 ml tubes and stored immediately at -80 °C. These samples were used later for cytokines and growth factors studies and to supplement patient-derived culture models. The cell pellet was combined into a unique conic tube and treated with 5 ml red blood cell lysis solution (Miltenyi Biotec, Bergisch Gladbach, Germany) for 10 minutes at RT. Then, the reaction was stopped, centrifuged (400 g, 5 minutes, at 4 ºC), and the supernatant was discarded. The majority of MA samples ranged from $1x10^9$ to $1x10^{10}$ nucleated cells/litter of cellular fractions. Subsequently, the cellular fraction was divided and used for different purposes: a) fixed with 10% (*v/v*) neutral-buffered formalin (PanReac AppliChem, Darmstadt, Germany) and re-suspended in liquefied HistoGel™ (Thermo Fisher Scientific, Waltham, MA, USA) (see next section). The cells underwent standard histological processing and paraffin embedding; b) resuspended in a freezing medium [90% fetal bovine serum (FBS) + 10% dimethyl sulfoxide (DMSO; AppliChem, Barcelona, Spain)], and stored at -80 ºC; and c) used to establish patient-derived cultures. Sometimes, MA has large tissue pieces that were fixed with 10% (*v/v*) neutral-buffered formalin (PanReac AppliChem, Darmstadt, Germany) and undergo standard histological processing and paraffin embedding.

3.3. Histogel™ Cell Processing

Cells derived from MA samples were resuspended in 10% (v/v) neutral-buffered formalin (PanReac AppliChem, Barcelona, Spain) and fixed for at least one hour at RT with gentle agitation. Following this, the cell pellet was centrifuged at 2800 rpm for 5 minutes at RT. The supernatant was discarded, and the cell pellet was resuspended in liquefied Histogel™ (650W, 50 sec; Thermo Fisher Scientific, Waltham, MA, USA) and quickly centrifuged at 4000 rpm for 1 minute at RT. The mixture was then allowed to solidify for 1 hour at 4 ºC. The Histogel™ encased cell pellet was transferred to a histological cassette, underwent standard histological processing, was embedded in paraffin, and finally sectioned for histological analysis.

3.4. Immunocytochemistry

The ICC procedure was conducted following the previously described method (502). In this study, we used the following antibodies: mucin 16 (MUC16; 1:60, M11, Agilent Dako, Santa

Clara, CA, USA), ALDH1A1 (1:200, D9Q8E, Cell Signaling Technology, MA, USA), SOX2 (1:25, SP76, Cell Marque, CA, USA), CD44v6 (1:100; MA54, Life Technologies, CA, USA) e P-gp (1:1200, EPR10364-57, Abcam, Cambridge, UK), for 1 hour at RT. To ensure the reliability of the results, an additional slide with previously tested positive tissues for each antibody was used as a positive control in every set of reactions. Slides were examined under a Brightfield Microscope Leica DM2000 LED (Leica Microsystems, Wetzlar, Germany). Three independent observers (S.R., M.N., and D.L.A-N) evaluated the slides and recorded the staining pattern (nuclear, cytoplasm, or membrane) and the percentage of cancer cells stained: Negative (0 – 10%) and Positive (11 – 100%).

3.5. Statistical Analysis

The statistical analyses were carried out using GraphPad Prism 10 (GraphPad Software Inc., San Diego, CA, USA) and SPSS Statistics 29 software (IBM SPSS Inc., Chicago, IL, USA). Fisher's Exact Test was performed to identify associations between ICC results. We set a significance level of 5% for all analyses, and a p-value of <0.05 was considered statistically significant.

4. Results

4.1. Characterization of Patient Cohort and Full-Volume Centrifugation of Malignant Ascites

The IPOP-MA retrospective series comprises 37 samples from 33 HGSC patients diagnosed between 2018 and 2024. Among them, 19 samples were collected before chemotherapy, and 18 samples were collected after chemotherapy.

The mean age was 70.7 ± 10.7 years before chemotherapy and 65.7 ± 11.0 years after chemotherapy, with no significant difference observed between the groups ($p = 0.165$) (**Table 1**). Before chemotherapy, 45.5% of the MA samples (5 out of 11) were classified as FIGO stage IIIB/IIIC, while 54.5% (6 out of 11) were at stage IV. Following chemotherapy, the distribution shifted, with 66.7% (4 out of 6) in stage IIIB/IIIC and 33.3% (2 out of 6) in stage IV. However, the distribution of FIGO stages did not show a significant difference between the groups ($p = 0.620$) (**Table 1**).

Before chemotherapy, 83.3% of patients did not have BRCA1/2 mutations, while 16.7% had mutations. After chemotherapy, all patients (100%) tested negative for BRCA1/2 mutations. The difference between groups was non-significant ($p = 0.078$) (**Table 1**).

Prior to chemotherapy, 61.1% of patients had not received surgery, whereas 38.9% had. Following chemotherapy, 70.6% of patients had not undergone surgery, compared to 29.4% who had. The difference between the two groups was not statistically significant (p = 0.725) (**Table 1**).

Regarding therapy response, MA samples collected prior to chemotherapy revealed a complete response (CR) in 2/16 samples (12.5%), stable disease or partial response (PR) in 10/16 samples (62.5%), progression in 2/16 samples (12.5%), and no treatment response in 2/16 samples (12.5%). In contrast, MA samples collected after chemotherapy showed that 13/15 samples (86.7%) had stable disease or PR, while 2/15 samples (13.3%) indicated progression (p=0.307) (**Table 1**).

The collected samples were clinically classified into 24 platinum-sensitive, 6 platinum-resistant, and 4 platinum-refractory cases. Both groups (before and after chemotherapy) include patients who are platinum-refractory to treatment, indicating ongoing chemoresistance. In detail, 14/16 (87.5%) of the MA samples taken prior to chemotherapy show a platinum-sensitive profile, while 2/16 (12.5%) exhibit a platinum-refractory profile. Furthermore, out of 18 MA samples obtained before chemotherapy, 10 (55.6%) were categorized as platinum-sensitive, 2 (11.1%) as platinum-refractory, and 6 (33.3%) as platinum-resistant. A significant difference was observed in the response to platinum between the groups (p = 0.025), with an increased resistance to platinum after chemotherapy (**Table 1**). As anticipated, the post-chemotherapy group contains platinum-resistant patients – those who did not adequately respond to earlier treatments. Typically, these patients have gone through multiple treatment lines with different agents and, in certain cases, targeted therapies (**Table S1**). Despite these treatment efforts, they have not achieved lasting remission or have quickly relapsed after treatment.

Table 1. **Characterization of MA samples collected from HGCS patients both before (n=19) and after (n=18) chemotherapy.** Statistical analysis was performed using Fisher's exact test for categorical variables, including FIGO stage, BRCA1/2 mutations, surgery, response to treatment, and platinum sensitivity. Age means were compared using a t-test. P-value < 0.05 was considered statistically significant. FIGO (n=20 missing cases); BRCA1/2 Mutations (n=2 missing cases); Surgery (n=2 missing cases); Response to treatment (n=6 missing cases); Response to Platinum (n=3 missing cases). CTx, chemotherapy; HGSC, high-grade serous carcinoma; MA, malignant ascites.

	Timing of HGSC MA samples collection		
	Before CTx (n=19)	**After CTx (n=18)**	**p-value**
Age (Years)			
Mean ± SD	70.7±10.7	65.7±11.0	0.165
FIGO, n (%)			
IIIB/IIIC	5 (45.5%)	4 (66.7%)	0.620
IV	6 (54.5%)	2 (33.3%)	
BRCA1/2 Mutations, n (%)			
No	15 (83.3%)	17 (100%)	0.078
Yes	3 (16.7%)	0 (0.0%)	
Surgery, n (%)			
No	11 (61.1%)	12 (70.6%)	0.725
Yes	7 (38.9%)	5 (29.4%)	
Response to treatment, n (%)			
Complete response	2 (12.5%)	0 (0%)	0.307
Stable disease/partial response	10 (62.5%)	13 (86.7%)	
Progression	2 (12.5%)	2 (13.3%)	
No treatment	2 (12.5%)	0 (0%)	
Response to Platinum, n (%)			
Sensitive	14 (87.5%)	10 (55.6%)	**0.025**
Refractory	2 (12.5%)	2 (11.1%)	
Resistant	0 (0%)	6 (33.3%)	

During the experimental assays, it became evident that centrifuging the entire volume of the MA was a critical step to maximize the number of cells available for analysis. This approach ensured that a larger pool of cells could be processed, which is essential for assessing a comprehensive panel of biomarkers with greater accuracy and sensitivity. The volume of MA received in the laboratory varied between approximately 1 and 4 liters per sample, reflecting the natural variability in the patient's clinical presentations. In practice, centrifuging the entire liquid volume rather than just a fraction of it was crucial to recovering a sufficient number of

nucleated cells. The cell yield typically ranged from $1x10^9$ to $1x10^{10}$ nucleated cells/litter of MA. This volume of cells produced a well-defined pellet that could be used for downstream applications, including immunophenotyping and other molecular analyses.

4.2. Expression of ALDH1A1, SOX2, CD44v6, and P-gp is Associated with Chemotherapy

Tumor cells in MA were arranged in papillary clusters and exhibited moderate to marked nuclear pleomorphism. In many MA samples, neoplastic cells were intermixed with varying numbers of reactive mesothelial and several subtypes of inflammatory cells (data not shown). In this cohort, all MA samples exhibited high expression levels of MUC16, with over 75% of cancer cells showing positive staining. A strong membranous staining pattern and high intensity characterized the expression. MUC16 is a well-known protein that is commonly overexpressed in HGSC, and this expression remained consistent when comparing MA samples both before and after chemotherapy, indicating no significant change in its expression following treatment. This persistent OE of MUC16 suggests its potential role as a stable biomarker for HGSC, regardless of chemotherapy exposure (data not shown).

When analyzing the semi-quantitative expression of ALDH1A1, SOX2, CD44v6, and P-gp, we observed notable differences in the samples before and after chemotherapy (**Figure 11A and Table 2**). To assess this, a profile based on the expression of these four markers (ALDH1A1/SOX2/CD44v6/P-gp) was created. A sample was considered positive if at least one of the markers showed >10% of cancer cells positive upon microscopic analysis. A significant shift in the expression of the combined biomarker panel was observed in samples collected after chemotherapy. Before chemotherapy, 15/19 (78.9%) of MA samples were negative for this panel, while 4/19 (21.1%) were positive. In samples after chemotherapy, this trend reversed, with 13/18 (72.2%) of MA samples showing positivity and only 5/18 (27.8%) being negative. These differences were statistically significant ($p=0.003$), highlighting a clear shift in these markers' expression following chemotherapy (**Figure 11A and Table 2**). This may reflect changes in tumor biology, or the activation of specific cancer-related pathways post or during chemotherapy.

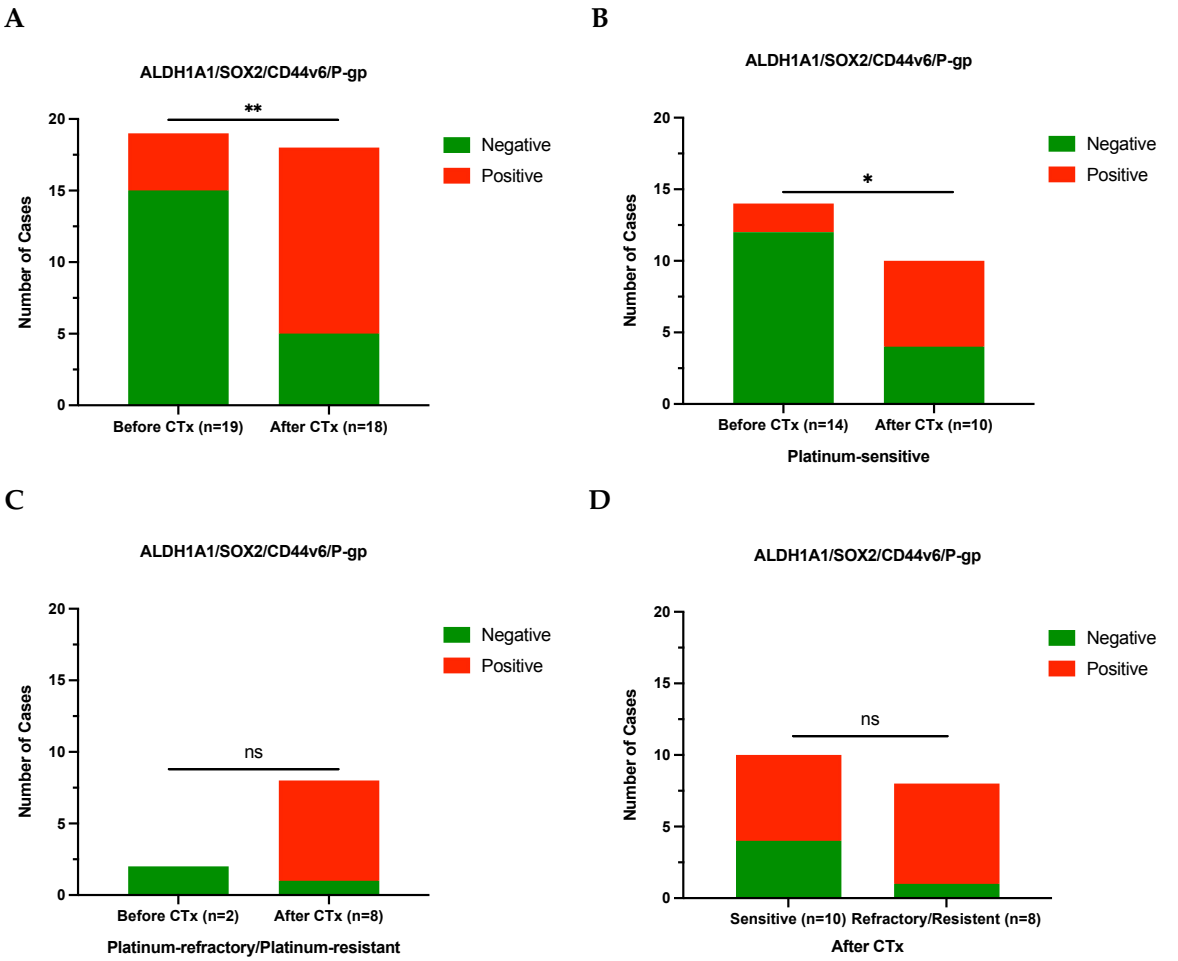


Figure 11. Expression of ALDH1A1, SOX2, CD44v6, and P-gp is associated with chemotherapy (**A**) Bar plot showing the number of MA samples obtained before (n=19) and after (n=18) chemotherapy with at least one cancer stem cell and resistant markers (ALDH1A1, SOX2, CD44v6, and P-gp) positives. (**B**) Bar plot showing the number of MA samples obtained before (n=14) and after (n=10) chemotherapy for platinum-sensitive patients with at least one cancer stem cell and resistant markers (ALDH1A1, SOX2, CD44v6, and P-gp) positives. (**C**) Bar plot showing the number of MA samples obtained before (n=2) and after (n=8) chemotherapy for platinum-refractory/platinum-resistant patients with at least one cancer stem cell and resistant markers (ALDH1A1, SOX2, CD44v6, and P-gp) positives. (**D**) Bar plot showing the number of MA samples obtained after chemotherapy for platinum-sensitive (n=10) and platinum-refractory/platinum-resistant (n=8) with at least one cancer stem cell and resistant markers (ALDH1A1, SOX2, CD44v6, and P-gp) positives. The data are expressed as the number of cases with at least one cancer stem cell and resistant markers (ALDH1A1, SOX2, CD44v6, and P-gp) positives and plotted using GraphPad Prism Software Inc. v6 (GraphPad Software Inc., Boston, CA, USA). Statistical analysis was performed using Fisher's exact test, with * $p < 0.05$ and ** $p < 0.001$ considered statistically significant. CTx – chemotherapy; HGSC, high-grade serous carcinoma; ns, not significant.

Regarding the positivity of each biomarker, no significant change was observed in the expression of ALDH1A1 between the pre- and post-chemotherapy samples. Before

chemotherapy, 84.2% of patients were negative for ALDH1A1, and 15.8% were positive. After chemotherapy, 72.2% of patients remained negative, while 27.8% became positive (p = 0.447) (**Table 2**). The staining for ALDH1A1 was predominantly cytoplasmic, with medium to high intensity observed in the positive cancer cells. A significant increase in the expression of SOX2 was noted after chemotherapy. Initially, 100% of MA samples were negative for SOX2, while after chemotherapy, 72.2% of MA samples were negative, and 27.8% were positive (p = 0.020) (**Table 2**). The staining for SOX2 was nuclear, with medium to high staining intensity observed in the positive cancer cells. A significant increase in positivity for CD44v6 was also observed after chemotherapy. Before chemotherapy, 94.7% of MA samples were negative for CD44v6, and only 5.3% were positive. After chemotherapy, 66.7% of MA samples were negative, while 33.3% were positive (p = 0.042) (**Table 2**). The staining for CD44v6 was cytoplasmic, with medium to high staining intensity in the tumor cells. There was no significant change in the expression of P-gp between the pre- and post-chemotherapy samples. All MA samples were negative for P-gp before chemotherapy, while after chemotherapy, 88.9% of MA remained negative, and 11.1% presented positive membrane expression (p = 0.230) (**Table 2**).

In **Figure 12**, representative ICC images show the positive expression of MUC16, ALDH1A1, SOX2, CD44v6, and P-gp in samples obtained before (HGSC#3.1 and HGSC#5.1) and after (HGSC#9.1 and HGSC#11.2) chemotherapy. These samples also depict platinum-sensitivity vs platinum-refractory/platinum-resistant profiles that we will address in the next section. Specifically, HGSC #5.1 and HGSC#11.2 were obtained from a patient labeled as platinum-sensitive, while HGSC#3.1 and HGSC#9.1 were obtained from platinum-refractory/platinum-resistant patients.

In HGSC#3.1 and HGSC#5.1 samples, obtained both before chemotherapy, no positive expression for ALDH1A1, SOX2, CD44v6, and P-gp was observed (**Figure 12**). This suggests a relatively low expression of CSC markers and drug-resistance-associated proteins prior to chemotherapy. For HGSC#9.1, an MA sample obtained from a patient after chemotherapy, a positive cytoplasmatic and membrane expression was observed for ALDH1A1 (<25% of tumor cells positive) and P-gp (<25% of tumor cells positive), respectively. However, SOX2 and CD44v6 were negative (**Figure 12**). This pattern indicates the presence of markers associated with chemotherapy resistance (ALDH1A1 and P-gp) without the activation of SOX2, a key marker of stemness and drug resistance. For the HGCS#11.2 sample, also obtained after chemotherapy, a positive expression for SOX2 (<50% of tumor cells positive) was observed but was negative for ALDH1A1, CD44v6, and P-gp (**Figure 12**). This profile suggests that SOX2 may be linked to CSC-like properties and chemotherapy. In contrast, the absence of P-gp

suggests a different mechanism of resistance, possibly involving cellular pathways independent of drug efflux mechanisms. The expression profiles of CSC and resistant biomarkers are varied, but when integrated, a profile reveals a tendency towards an increased expression in patients after chemotherapy.

Table 2. Association of ALDH1A1/SOX2/CD44v6/P-gp expression in HGSC MA samples collected from patients before (n=19) and after chemotherapy (n=18) cycles. P-values were obtained by the Fisher's exact test. CTx, chemotherapy; HGSC, high-grade serous carcinoma; MA, malignant ascites.

	Before CTx (n=19) (%)	**After CTx (n=18) (%)**	**p-value**
ALDH1A1/SOX2/CD44v6/P-gp			
Negative (n=20)	15 (78.9%)	5 (27.8%)	**0.003**
Positive (n=17)	4 (21.1%)	13 (72.2%)	
ALDH1A1			
Negative (n=29)	16 (84.2%)	13 (72.2%)	0.447
Positive (n=8)	3 (15.8%)	5 (27.8%)	
SOX2			
Negative (n=32)	19 (100%)	13 (72.2%)	**0.020**
Positive (n=5)	0 (0.0%)	5 (27.8%)	
CD44V6			
Negative (n=30)	18 (94.7%)	12 (66.7%)	**0.042**
Positive (n=7)	1 (5.3%)	6 (33.3%)	
P-gp			
Negative (n=35)	19 (100.0%)	16 (88.9%)	0.230
Positive (n=2)	0 (0.0%)	2 (11.1%)	

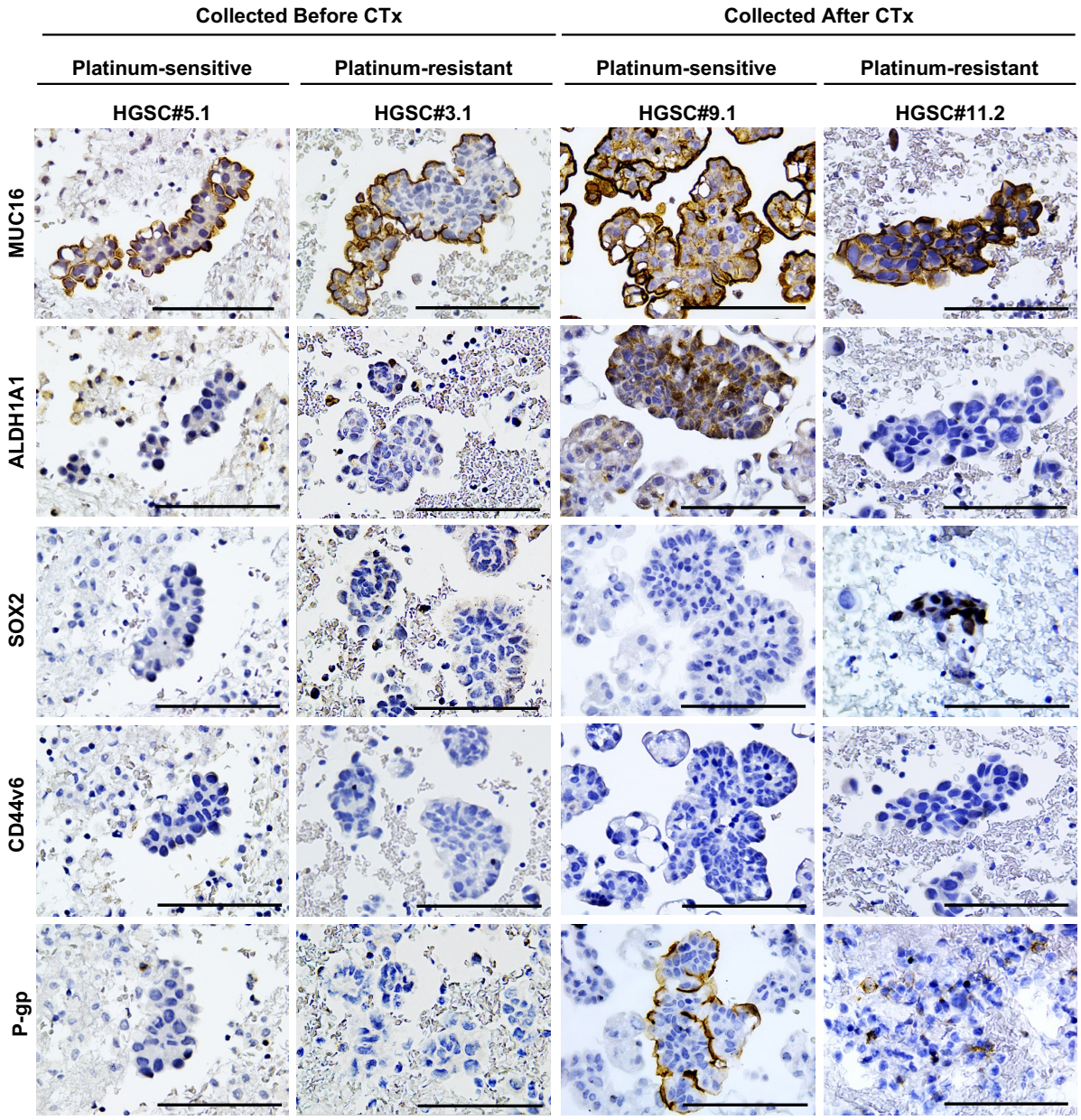


Figure 12. Expression of ALDH1A1, SOX2, CD44v6 and P-gp is increased in MA samples obtained after chemotherapy. Representative microscopical figures of MUC16, ALDH1A1, SOX2, CD44v6, and P-gp protein immunostaining shown by DAB staining (brown) in two patients before (HGSc#3.1 and HGSC#5.1) and two patients after (HGSC#9.1and HGSc#11.2) Chemotherapy. All images were taken with a Brightfield Microscope Leica DM2000 LED (Leica Microsystems, Wetzlar, Germany). The figures are taken at 400x magnification, and the scale bar represents 100 µm. DAB, diaminobenzidine; CTx, chemotherapy; MA, malignant ascites.

4.3. Expression of ALDH1A1, SOX2, CD44v6, and P-gp is Associated with Platinum-resistance

For platinum-sensitive samples obtained before chemotherapy, the ALDH1A1/SOX2/CD44v6/P-gp profile showed 12 (85.7%) negative and 2 (14.3%) positive results (**Figure 11B and Table 3**). For samples obtained after chemotherapy, 4 (40%) were negative, and 6 (60%) were positive. The results indicate a significant increase in the combined expression of ALDH1A1, SOX2, CD44v6, and the P-gp profile in platinum-sensitive MA samples after chemotherapy (p = 0.032) (**Figure 11B and Table 3**).

Table 3. Association of ALDH1A1/SOX2/CD44v6/P-gp expression in HGSC MA samples collected from patients' platinum-sensitive before (n=14) and after chemotherapy (n=10). P-values were obtained by the Fisher's exact test. CTx, chemotherapy; HGSC, high-grade serous carcinoma; MA, malignant ascites; NA, not available.

	Platinum-sensitive		
	Before CTx (n=14) (%)	**After CTx (n=10) (%)**	**p-value**
ALDH1A1/SOX2/CD44v6/P-gp			
Negative	12 (85.7%)	4 (40%)	**0.032**
Positive	2 (14.3%)	6 (60%)	
ALDH1A1			
Negative	13 (92.9%)	8 (80%)	0.550
Positive	1 (7.1%)	2 (20%)	
SOX2			
Negative	14 (100%)	7 (70%)	0.059
Positive	0 (0.0%)	3 (30%)	
CD44V6			
Negative	13 (92.9%)	7 (70%)	0.272
Positive	1 (7.1%)	3 (30%)	
P-gp			
Negative	14 (100.0%)	10 (100%)	NA
Positive	0 (0.0%)	0 (0%)	

Individual markers such as ALDH1A1, SOX2, and CD44v6 showed trends toward increased expression for platinum-sensitive samples obtained after chemotherapy (**Table 3**). For platinum-sensitive samples obtained before chemotherapy, 13 (92.9%) MA samples tested negative, while 1 (7.1%) MA sample tested positive for ALDH1A1 (**Table 3**). Following chemotherapy, 8 (80%) MA samples were negative, and 2 (20%) MA samples tested positive for ALDH1A1 (p=0.550) (**Table 3**). Before chemotherapy, 13 (92.9%) MA samples were negative, and 1 (7.1%) was positive for CD44v6. After chemotherapy, 7 (70%) MA samples were negative and 3 (30%) positive (p = 0.272), showing no significant change in CD44v6 expression post-chemotherapy (**Table 3**). Interestingly, P-gp expression remained negative in all samples, both before and after chemotherapy (**Table 3**). Before chemotherapy, all 14 (100%) MA samples were SOX2 negative. After chemotherapy, 7 (70%) MA samples were negative, while 3 (30%) MA samples were positive (p=0.059), indicating a trend towards increased SOX2 expression after chemotherapy but lacking statistical significance.

These findings suggest that chemotherapy may induce a phenotypic shift in platinum-sensitive tumors, increasing the expression of biomarkers typically associated with stemness and drug resistance. However, further studies with larger cohorts are needed to confirm these trends and explore the mechanisms driving these changes in each marker expression. This highlights the potential for body fluid-based liquid biopsy approaches to monitor dynamic changes in tumor biology during treatment and provides insights into possible strategies for overcoming chemotherapy-induced resistance.

The analysis of platinum-refractory/platinum-resistant patients showed no significant differences in the expression of ALDH1A1, SOX2, CD44v6, or P-gp before and after chemotherapy. While there was a trend towards increased expression of the combined panel of markers (ALDH1A1/SOX2/CD44v6/P-gp) after chemotherapy (p = 0.067), this did not reach statistical significance (**Table 4**). Similarly, expression levels of the individual biomarkers (ALDH1A1, SOX2, and CD44v6) did not change significantly (p=1.00) following chemotherapy in this evaluation (**Figure 11C and Table 4**).

These results suggest that platinum-refractory/platinum-resistant tumors in this cohort may not show substantial changes in the expression of the tested markers in response to chemotherapy. While there is a trend toward increased expression of resistance-associated biomarkers after chemotherapy, further studies with a larger cohort are needed to confirm these findings and explore the potential role of each marker in the development of chemotherapy resistance.

Table 4. Association of ALDH1A1/SOX2/CD44v6/P-gp expression in HGSC MA samples collected from patients' platinum-refractory/platinum-resistant before (n=2) and after chemotherapy (n=8). P-values were obtained by the Fisher's exact test. CTx, chemotherapy; HGSC, high-grade serous carcinoma; MA, malignant ascites; NA, not available.

	Platinum-refractory/Platinum-resistant		
	Before CTx (n=2) (%)	**After CTx (n=8) (%)**	**p-value**
ALDH1A1/SOX2/CD44v6/P-gp			
Negative (n=20)	2 (100%)	1 (12.5%)	0.067
Positive (n=17)	0 (0%)	7 (87.5%)	
ALDH1A1			
Negative (n=29)	2 (100%)	5 (62.5%)	NA
Positive (n=8)	0 (0%)	3 (37.5%)	
SOX2			
Negative (n=32)	2 (100%)	6 (75%)	NA
Positive (n=5)	0 (0%)	2 (25%)	
CD44V6			
Negative (n=30)	2 (100%)	5 (62.5%)	NA
Positive (n=7)	0 (0%)	3 (37.5%)	
P-gp			
Negative (n=35)	2 (100%)	6 (75%)	NA
Positive (n=2)	0 (0%)	2 (25%)	

The analysis of MA samples collected before chemotherapy did not reveal significant differences in the expression of ALDH1A1, SOX2, CD44v6, and P-gp between platinum-sensitive and platinum-refractory/platinum-resistant samples. In both groups, the majority of samples tested negative for these markers, and there was no significant association between marker expression and platinum sensitivity or resistance (**Figure S1 and Table S2**). Specifically, ALDH1A1, SOX2, CD44v6, and P-gp were predominantly negative in both the platinum-sensitive group (ranging from 85.7% to 100% negative) and the platinum-refractory/platinum-resistant group (100% negative for all markers) (**Table S2**). This result may indicate that these markers may not be reliable predictors of platinum resistance at this early

time point, and their roles in resistance may become more evident after chemotherapy or as part of a dynamic response throughout treatment.

Higher positivity rates were noted for platinum-refractory/resistant compared to platinum-sensitive samples in post-chemotherapy samples. Still, differences were not statistically significant for most markers, including the panel of ALDH1A1/SOX2/CD44v6/P-gp ($p = 0.314$), ALDH1A1 ($p = 0.608$), SOX2 ($p = 1.00$), and CD44v6 ($p = 1.00$) (**Table 5**). The exception was for P-gp expression, showing higher positivity rates (25% platinum-resistant vs. 0% platinum-sensitive) but without a statistically significant value ($p = 0.183$) (**Figure 11D and Table 5**).

The relatively high expression of ALDH1A1, SOX2, and CD44v6 in both platinum-sensitive and platinum-refractory/platinum-resistant samples obtained after chemotherapy indicates that these biomarkers might be induced by chemotherapy itself rather than specifically being associated with platinum resistance. Given the observed trend towards higher expression in platinum-resistant cases, the role of P-gp in chemoresistance needs further investigation as it can be associated with therapies that are P-gp substrates. These results highlight the complexity of resistance mechanisms in HGSC and the potential for chemotherapy to modulate CSC markers.

Table 5. Association of ALDH1A1/SOX2/CD44v6/P-gp expression in HGSC MA samples collected from patients' platinum-sensitive (n=10) and platinum-refractory/resistant (n=8) after chemotherapy. P-values were obtained by the Fisher's exact test. CTx, chemotherapy; HGSC, high-grade serous carcinoma; MA, malignant ascites; NA, not available.

	After CTx		
	Platinum-sensitive (n=10) (%)	**Platinum-refractory/ Platinum-resistant (n=8) (%)**	**p-value**
ALDH1A1/SOX2/CD44v6/P-gp			
Negative	4 (40%)	1 (12.5%)	0.314
Positive	6 (60%)	7 (87.5%)	
ALDH1A1			
Negative	8 (80%)	5 (62.5%)	0.608
Positive	2 (20%)	3 (37.5%)	
SOX2			
Negative	7 (70%)	6 (75%)	NA
Positive	3 (30%)	2 (25%)	
CD44V6			
Negative	7 (70%)	5 (62.5%)	NA
Positive	3 (30%)	3 (37.5%)	
P-gp			
Negative	10 (100.0%)	6 (75%)	0.183
Positive	0 (0.0%)	2 (25%)	

5. Discussion

In this study, we aimed to highlight the clinical significance of MA in OC, particularly the value collected before or after chemotherapy that is typically discarded. This approach challenges the current clinical practices, where the collection and use of MA samples after diagnosis are not utilized for further molecular analysis. Here, we suggest that MA, before or after chemotherapy, holds a critical prognostic potential to be useful in improving patient management and treatment outcomes. Therefore, we propose that the current analytical circuit of these body fluids in the context of OC needs to be reconsidered. Currently, when OC patients develop MA after diagnosis, this liquid is not used for a comprehensive analysis, missing the opportunity to capture valuable information about tumor dynamics and therapy response. As chemotherapy becomes a cornerstone of OC management, performing molecular studies on

this biological material is vital. This body fluid is a non-invasive source of tumor-derived cells in a context where second surgeries or biopsies are rare.

The low cellularity of tumor populations present in MA has been described as the main disadvantage of the studies (503). Regarding serous effusions for diagnosis, it is accepted that a volume between 50 and 75 ml is sufficient to conduct morphological and molecular analyses with an acceptable rate of false-negative cases (504). However, it is important to reconsider this procedure and assess the significance of centrifuging the total volume of drained liquid to maximize the number of cells available for comprehensive molecular studies. Indeed, MA can be placed into a formalin-fixed cell block and paraffin-embedded for histology-based techniques, such as ICC stainings and molecular analysis (503, 505). Recently, Uehara *et al.* showed that performing an MA cell block in conjunction with or as an alternative to tumor biopsies is a reliable diagnostic tool for OC (506). While this initial centrifuge protocol is important to improve diagnosis, it is equally essential in MA drained during the disease time course where patients present MS that require repeated paracentesis. We can pinpoint an important weakness in MA analysis: the frequency of drainage during each patient's clinical course, as this can vary from patient to patient. This also requires good articulation between the clinical team at the hospital and the pathology lab where cytological samples are received. The changes in the MA circuits require a new routine that can be challenging for hospital organizations with a heavy workload. Despite these drawbacks, the analysis of MA during disease progression can be very useful, as this biological material allows us to assess valuable information for oncologists.

Centrifuging the full volume of MA is key to analyzing low-expression biomarkers and maximizing cell availability, especially from small populations. This is vital to optimizing tumor cell recovery when investigating low-expression biomarkers like ALDH1A1, SOX2, CD44v6, and other chemoresistance markers, such as P-gp. Complete centrifugation increases the harvest of nucleated cells (tumor, endothelial, and immune cells), which is vital for biomarker analysis and an accurate evaluation. If only part of the fluid is processed, the cell count may be insufficient for low-expression markers detection. Centrifuging the entire volume concentrates cells, enhancing the sensitivity of ICC and flow cytometry, enabling the detection of rare pulls of tumor cells with low expression-level biomarkers such as CSC-like or drug-resistant associated proteins.

The morphological examination of the MA samples revealed high cellularity and three-dimensional papillary clusters, with nuclei showing moderate to marked pleomorphism in most MA samples, consistent with findings from other studies (507). The expression of the well-

known OC biomarker MUC16 showed that most of the MA samples tested had very high membrane expression, regardless of the timing of collection, which agrees with other published evidence (76, 508).

HGSC's aggressive nature partially arises from CSC populations, a small group of undifferentiated cells with self-renewal, proliferation, differentiation, and multipotency abilities (509). These cells are linked to peritoneal dissemination, chemoresistance, and disease recurrence (510, 511). However, there are inconsistencies in the literature regarding the markers for CSC due to variations in methodologies and the definition of CSC populations, which can limit the interpretation of results and their relevance and accuracy (512) . The role of CSC markers in OC requires further confirmation (502, 513). This study focuses on ALDH1A1, SOX2, and CD44v6 as CSC markers based on their consistent detection by ICC using available antibodies despite the presence of other potential markers described in the literature (514, 515).

ALDH1A1 plays a key role in detoxifying and reducing oxidative stress (516) by converting aldehydes into carboxylic acids (515). Additionally, cells exhibiting high ALDH1A1 activity demonstrated enhanced self-renewal abilities and greater resistance to stress (510, 517). SOX2, a transcription factor regulating embryonic development and stem cell maintenance (518, 519), has been implicated in cancer studies regarding tumor initiation, maintenance, and targeted therapy (520, 521), with detection rates of 10–60.5% in OC and association with poor outcomes (518, 522, 523). The expressions of ALDH1A1 and SOX2 indicate stemness, aiding the detection of cancer cell proliferation, migration, invasion, and metastasis (524, 525). OE of SOX2 and ALDH1A1 has been observed in cancer cells, especially in HGSC, where it is associated with increased tumorigenicity and invasive capabilities (526, 527). Their expression levels correlate with chemoresistance and an unfavorable prognosis (527, 528). CD44v6 is widely recognized as a CSC marker in solid tumors, and in OC, it has also been shown to be present in a metastasis-initiating population (529).

Our results showed that the positivity of the combined biomarker panel ALDH1A1/SOX2/CD44v6/P-gp showed a significant increase ($p = 0.003$) in post-chemotherapy samples, indicating a possible change in cellular characteristics post-chemotherapy. SOX2 and CD44v6 showed significant upregulation after chemotherapy ($p = 0.020$ and $p = 0.042$, respectively), demonstrating changes in their expression profiles as a response to treatment. The expression of ALDH1A1 and P-gp did not show significant differences before and after chemotherapy ($p = 0.447$ and $p = 0.230$, respectively), suggesting these markers may be less

sensitive to chemotherapy-induced changes in the studied series. Expanding the patient cohort and increasing the statistical power will be crucial to validating these findings. A larger sample size may help to clarify whether the trends observed for ALDH1A1 and P-gp become statistically significant and could provide a more comprehensive understanding of the molecular changes occurring in tumor cells following chemotherapy. This expansion will also enable a deeper exploration of the role of these biomarkers in chemotherapy response and resistance, potentially guiding more effective therapeutic strategies in the future.

The majority of our MA sample express low levels (10 – 25% of cancer cells positive) of CSC and drug-resistant markers, suggesting that while ALDH1A1, SOX, and CD44v6 may be present in some cancer cells, their expression is not widespread across the entire tumor population. This means that only a subset of cells express these markers at detectable levels, which could be associated with their ability to survive chemotherapy. In our series, cancer cells showed low membrane expression levels of P-gp. This relatively low expression suggests that P-gp, known for its role in drug efflux and chemotherapy resistance, identifies only a pull of tumor cells with more drug-resistant phenotypes. Given P-gp's association with multidrug resistance, its restricted expression in less than 25% of the cancer cells could imply that these cells are more capable of effluxing chemotherapeutic drugs, contributing to chemoresistance. The low expression might indicate tumor heterogeneity, with only specific subpopulations of cells expressing P-gp at levels high enough to confer drug resistance.

The varying expression profiles highlight the complexity and heterogeneity of CSC and chemoresistance biomarkers. Although the profiles differ between patients, a combined profile increases the probability of identifying rare tumor populations with molecular profiles associated with chemoresistance. Our results suggest that chemotherapy may induce upregulation of the markers related to CSC and drug resistance, potentially contributing to chemotherapy failure.

Our results also demonstrated that chemotherapy itself could induce these markers' expression, even in platinum-sensitive patients. Chemotherapy triggers a biological response in all tumor cells, regardless of their platinum sensitivity. The chemotherapy activates cellular mechanisms that promote survival, such as CSC pathways or the upregulation of resistance proteins like P-gp and ALDH1A1. Even in initially platinum-sensitive tumors, chemotherapy fosters an environment that selects resistant cells, possibly contributing to eventual resistance to other drugs. Furthermore, the link between biomarker expression and chemotherapy seems stronger than its connection to platinum resistance, indicating chemotherapy (Carboplatin, Paclitaxel, Bevacizumab and PARPi, among others) significantly influences biomarker modulation, regardless of initial treatment response. These changes may involve phenotypic

and molecular reprogramming of tumor cells post-chemotherapy, leading to traits linked to stemness or drug resistance. This phenomenon calls for dynamic monitoring during therapy, as marker changes could indicate patients who, despite early platinum sensitivity, may develop resistance over time, offering new targets to counteract tumor adaptation and preserve treatment efficacy.

Some patients received other drugs besides platinum-based chemotherapy, complicating the interpretation of the results. The effects of multidrug regimens on tumor biology, particularly regarding CSC markers, may differ from platinum alone. Additional drugs might influence these markers by inducing resistance mechanisms, such as P-gp OE, which is common in Paclitaxel resistance. Thus, other drugs (Gemcitabine, Bevacizumab, and Olaparib, among others) could explain the upregulation of certain biomarkers, regardless of platinum treatment sensitivity. Therefore, while platinum-based chemotherapy appears to induce the expression of resistance markers significantly, the additional drugs could further influence the overall expression profiles and complicate the understanding of the specific mechanisms involved in resistance. This adds another layer of complexity to how we interpret the biomarker profiles in the MA samples and highlights the need for careful consideration of all treatment regimens when analyzing post-treatment tumor characteristics.

Whether intrinsic or acquired chemoresistance is a significant barrier to chemotherapy effectiveness (530). One of the primary mechanisms associated with Paclitaxel resistance is the increased ability of tumor cells to expel drugs, reducing their accumulation inside the cells (531, 532). ABC transporters, such as P-gp, facilitate this process (531, 532). P-gp is one of the main transmembrane proteins responsible for actively pumping drugs out of the cells, which decreases intracellular drug concentrations, promotes cancer cell survival, and is found in high levels in many tumors, including OC (533). This has been linked to the development of MDR (533) and worse prognosis (534). Our research indicates that P-gp is more commonly expressed in OC samples obtained after chemotherapy than those collected before chemotherapy. Some MA samples express these markers associated with chemotherapy resistance at diagnosis. These different phenotypes before chemotherapy reveal tumor heterogeneity, which, in these cases, may be related to intrinsic resistance (535).

Several studies in OC have shown that comparing paired primary tumors and metastatic samples can reveal discrepancies in their phenotypic profile due to tumor evolution. This evolution can have important clinical implications, such as affecting prognosis or changing treatment schemes (536-538). This study found that the combined evaluation of the ALDH1A1, CD44v6, SOX2, and P-gp expression is more frequently found in MA samples drained from

patients after chemotherapy cycles (p=0.003). Phenotypic differences between MA samples obtained before and after chemotherapy reveal the emergence of a CSC population and the increase of chemotherapy-resistant associated biomarkers protein levels, indicating tumor kinetics linked to tumor progression and chemotherapy (535). Hence, examining these samples can yield further insights into the evolution of tumor phenotype and generate data that may support treatment adjustments.

6. Conclusion

The findings of this study indicate that centrifuging the total volume of MA samples may enhance the quantity of in-depth analyses performed on HGSC cytologic specimens, particularly when testing low-expression biomarkers. Further extensive cohort studies are needed to validate these conclusions. The findings indicate that ALDH1A1, SOX2, CD44v6, and P-gp expressions act as markers in MA samples collected post-chemotherapy. This phenotype is frequently found among platinum-resistant patients, indicating a possible connection between these biomarkers and chemoresistance. The upregulation of these markers, typically linked to CSC and drug resistance, reflects the tumor's adaptation to chemotherapy-induced selective pressure, possibly leading to tumor recurrence or persistence despite treatment.

These results highlight the significance of MA samples as a non-invasive body-fluid liquid biopsy tool for monitoring the molecular characteristics of HGSC, particularly regarding the platinum resistance scenario. This approach is especially beneficial for patients who cannot undergo conventional tissue biopsies due to disease progression, anatomical constraints, or other patient-related issues, which is the case for HGSC patients.

By analyzing MA, clinicians and researchers can obtain real-time insights into the tumor's molecular dynamics, identifying changes in biomarker expression that could guide treatment decisions. This may ultimately pave the way for more personalized management strategies for HGSC, enhancing our ability to predict treatment outcomes, monitor minimal residual disease, and modify therapies in response to changing tumor characteristics.

7. Acknowledgement and Funding

This work was developed at *Instituto de Investigação e Inovação em Saúde (i3S)*, an Associate Laboratory of the *Ministério da Ciência, Tecnologia e Inovação (MCTES),* and it was partially supported by *Fundação para a Ciência e a Tecnologia (FCT).* This project was supported by the project "HOPE – Improving Ovarian Cancer Patients Survival," a donation

from an ovarian cancer patient to the Instituto de *Patologia e Imunologia Molecular da Universidade do Porto (IPATIMUP)* and by *Fundo Europeu de Desenvolvimento Regional (FEDER)* through the *COMPETE 2020 – Programa Operacional Competitividade e Internacionalização (POCI), Portugal 2020* and *FCT/MCTES*, under the project POCI 01-0145-FEDER-029503 (PTDC/MEC-ONC/29503/2017). M.N. and D.L.A-N acknowledge *FCT/MCTES* and *UE* for financial support through a PhD fellowship (2020.04720.BD/DOI: 10.54499/2020.04720.BD and 2021.05081.BD, respectively) that was co-sponsored by *Fundo Social Europeu (FSE)* through *Programa Operacional Regional Norte (Norte 2020).*

8. Supplementary Material

Table S1. Clinical characteristics of malignant ascites samples before and after Chemotherapy. AwD – Alive with Disease; AwoD – Alive without Disease; CTx – Chemotherapy; DOD – Died of Disease; DS – Debulking Surgery; Dx – Diagnostic; FIGO – International Federation of Gynecology and Obstetrics; HGSC – High-Grade Serous Carcinoma; IDS – Interval Debulking Surgery; NA – Not available; NR – No Respond; OS – Overall Survival; R – Respond; S – surgery; SD/PR – Stable Disease/Partial Response; woCTx – without Chemotherapy. *[1]Carboplatin + Paclitaxel + Bevacizumab (1st line), Carboplatin + Gemcitabine + Letrozole (2nd line), Carboplatin + Gemcitabine + Niraparib (3rd line); *[2]Carboplatin + Paclitaxel (1st line), Pegylated liposomal doxorubicin + Bevacizumab (2nd line), Carboplatin + Gemcitabine (3rd line), Paclitaxel (4thline); *[3]Carboplatin + Paclitaxel (1st line), Carboplatin + Gemcitabine (2nd line), Paclitaxel + Bevacizumab (3rd line), PLD (4th line), Topotecan (5th line); *[4]Carboplatin + Paclitaxel (1st line); *[5]Carboplatin + Paclitaxel (1st line); *[6]Carboplatin + Paclitaxel (1st line), Carboplatin + Gemcitabine + Niraparib (2nd line).

Patients	Age at Dx	OS (months)	Status	FIGO	Surgery	Samples	Collecting timing	Clinical Response	Platinum Response	CTx
HGSC#2	73	32	DOD	IIIC	-	HGSC#2.1	Before CTx	NA	Sensitive	-
						HGSC#2.2	After CTx	SD/PR	Sensitive	Carboplatin + Paclitaxel (1st line, 1st cycle)
HGSC#3	70	5	DOD	IV	-	HGSC#3.1	Before CTx	NR	Refractory	-
HGSC#4	72	7	DOD	NA	-	HGSC#4	After CTx	SD/PR	Sensitive	Carboplatin + Paclitaxel (1st line, 3rd cycle)
HGSC#5	71	13	DOD	IV	IDS	HGSC#5.1	Before CTx	NA	Sensitive	-
						HGSC#5.2	After CTx	SD/PR	Sensitive	Carboplatin + Paclitaxel (1st line, 5th cycle)
HGSC#6	50	80	DOD	NA	-	HGSC#6.1	After CTx	NR	Resistant	Carboplatin + Gemcitabine (4th line, 5th cycle) *[1]
HGSC#7	65	3	DOD	IV	-	HGSC#7	Before CTx	NR	Refractory	-
HGSC#9	60	47	DOD	NA	-	HGSC#9.1	After CTx	SD/PR	Resistant	Topotecan (5th line, 1st cycle) *[2]
HGSC#10	89	1	DOD	IV	-	HGSC#10	Before CTx	WoCTx	NA	-

HGSC#11	67	12	DOD	IIIC	-	HGSC#11.1	Before CTx	SD/PR	Sensitive	-
						HGSC#11.2	After CTx	SD/PR	Sensitive	Carboplatin + Paclitaxel (1st line, 1st cycle)
HGSC#12	64	26	DOD	NA	IDS	HGSC#12	After CTx	NA	Resistant	Carboplatin + Paclitaxel (Palliative, 1st cycle)
HGSC#14	56	48	DOD	NA	-	HGSC#14.1	After CTx	NR	Refractory	Carboplatin + Gemcitabine (6th line, 1st cycle) *3
HGSC#18	80	2	DOD	IIIC	-	HGSC#18	Before CTx	woCTx	NA	-
HGSC#19	68	27	AwD	IIIC	-	HGSC#19	Before CTx	SD/PR	Sensitive	-
HGSC#20	62	14	DOD	NA	-	HGSC#20.1	After CTx	NA	Resistant	Paclitaxel + Bevacizumab (2nd line, 1st cycle) *4
HGSC#21	84	21	DOD	NA	-	HGSC#21.1	After CTx	SD/PR	Resistant	Carboplatin + Paclitaxel (1st line, 1st cycle)
HGSC#23	70	19	AwoD	IV	IDS	HGSC#23	Before CTx	R	Sensitive	-
HGSC#24	73	22	DOD	IIIC	DS	HGSC#24	After CTx	NA	Sensitive	Carboplatin + Paclitaxel (1st line, 2nd cycle)
HGSC#26	84	17	AwD	IV	-	HGSC#26.1	Before CTx	SD/PR	Sensitive	-
						HGSC#26.2	After CTx	SD/PR	Sensitive	Carboplatin (1st line, 1st cycle)
HGSC#28	53	13	AwoD	IIIB	IDS	HGSC#28.2	After CTx	SD/RP	Sensitive	Carboplatin + Paclitaxel (1st line, 1st cycle)
HGSC#30	70	15	DOD	NA	-	HGSC#30	After CTx	SD/PR	Refractory	Carboplatin + Paclitaxel (1st line, 5th cycle)
HGSC#31	80	14	AwD	IIIC	IDS	HGSC#31.1	Before CTx	SD/PR	Sensitive	-
HGSC#32	43	27	AwD	NA	-	HGSC#32	After CTx	SD/PR	Resistant	Carboplatin + Gemcitabine + Niraparib (2nd line, 1st cycle) *5
HGSC#33	61	75	AwD	NA	DS	HGSC#33	After CTx	SD/PR	Sensitive	Carboplatin + Gemcitabine (3rd line, 1st cycle) *6
HGSC#37	66	12	AwD	NA	-	HGSC#37	Before CTx	SD/PR	Sensitive	-

HGSC#38	76	27	DOD	NA	-	HGSC#38	After CTx	SD/PR	Sensitive	NA
HGSC#39	73	10	AwD	NA	S	HGSC#39	Before CTX	SD/PR	Sensitive	-
HGSC#40	86	1	DOD	NA	-	HGSC#40	Before CTx	NA	NA	-
HGSC#45	70	9	AwD	NA	NA	HGSC#45	Before CTx	SD/PR	Sensitive	-
HGSC#46	74	6	AwD	NA	S	HGSC#46	Before CTx	R	Sensitive	-
HGSC#47	59	9	AwD	NA	S	HGSC#47.1	Before CTx	SD/PR	Sensitive	-
HGSC#48	47	7	AwD	NA	-	HGSC#48	Before CTx	SD/PR	Sensitive	-
HGSC#50	52	6	AwD	NA	S	HGSC#50	Before CTx	SD/PR	Sensitive	-
HGSC#52	63	4	AwD	NA	NA	HGSC#52	After CTx	SD/PR	Sensitive	Carboplatin + Paclitaxel (1^{st} line, 1^{st} cycle)

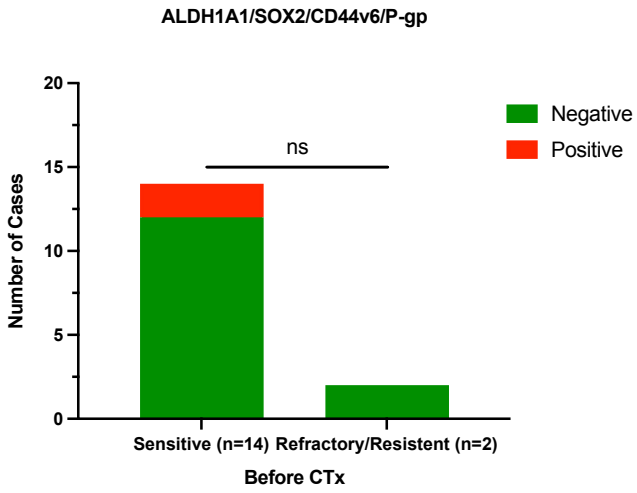


Figure S1. Expression of ALDH1A1, SOX2, CD44v, and P-gp is not associated with platinum response in MA obtained before chemotherapy. Bar plot showing the number of MA samples obtained before chemotherapy for platinum-sensitive (n=14) and platinum-refractory/platinum-resistant (n=2) patients with at least one cancer stem cell and resistant markers (ALDH1A1, SOX2, CD44v6, and P-gp) positives. The data are expressed as the number of cases with at least one cancer stem cell and resistant markers (ALDH1A1, SOX2, CD44v6, and P-gp) positives and plotted using GraphPad Prism Software Inc. v6 (GraphPad Software Inc. Boston, CA, USA). Statistical analysis was performed using Fisher's exact test. CTx – chemotherapy; HGSC, high-grade serous carcinoma; ns, not significant.

Table S2. Association of ALDH1A1/SOX2/CD44v6/P-gp expression in HGSC MA samples collected from patients' platinum-sensitive (n=14) and platinum-refractory/resistant (n=2) before chemotherapy. P-values were obtained by the Fisher's exact test. Response to Platinum (n=3 missing cases). CTx, chemotherapy; HGSC, high-grade serous carcinoma; MA, malignant ascites; NA, not available.

	Before CTx		
	Platinum-sensitive (n=14) (%)	**Platinum-refractory or Platinum-resistant (n=2) (%)**	**p-value**
ALDH1A1/SOX2/CD44v6/P-gp			
Negative	12 (85.7%)	2 (100%)	NA
Positive	2 (14.3%)	0 (0%)	
ALDH1A1			
Negative	13 (92.9%)	2 (100%)	NA
Positive	1 (7.1%)	0 (0%)	
SOX2			
Negative	14 (100)	2 (100%)	NA
Positive	0 (0%)	0 (0%)	
CD44V6			
Negative	13 (92.9%)	2 (100%)	NA
Positive	1 (7.1%)	0 (0%)	
P-gp			
Negative	14 (100.0%)	2 (100%)	NA
Positive	0 (0.0%)	0 (0%)	

CHAPTER IV

Establishment and Characterization of Chemoresistant OC Cell Line Models Followed by the Sensitization Step using Drug Repurposing

a. Generation and Characterization of Chemoresistant Ovarian Cancer Cell Lines

The information presented in this chapter is partially based on the following publications:

Nunes M, Silva PMA, Coelho R, Pinto C, Resende A, Bousbaa H, Almeida GM, Ricardo S. Generation of Two Paclitaxel-Resistant High-Grade Serous Carcinoma Cell Lines with Increased Expression of P-Glycoprotein. Front Oncol. 2021 Oct 21;11:752127. doi: 10.3389/fonc.2021.752127.

Generation of Two Paclitaxel-Resistant High-Grade Serous Carcinoma Cell Lines with Increased Expression of P-Glycoprotein

1. Abstract

Debulking surgery followed by chemotherapy remains the standard treatment for HGSC. Despite an initial favorable treatment response, most patients eventually relapse with chemotherapy-resistant disease, leading to poor OS. Treatments for HGSC typically combine traditional chemotherapeutic agents, such as Carboplatin and Paclitaxel. Understanding the mechanisms of chemoresistance and discovering new drugs are essential to improving patient outcomes. Effective cellular models that closely mimic chemoresistant disease are fundamental for investigating these mechanisms and testing potential drugs.

In this study, was established two HGSC cell lines, OVCAR8 PTX R C and OVCAR8 PTX R P, which show inherent resistance to Carboplatin and induced resistance to Paclitaxel derived from the OVCAR8 cell line. This resistance remained stable during long-term culture and after freeze/thaw cycles. These variants exhibited increased resistance to Paclitaxel-induced cell death by enhancing drug efflux capacity. The key mechanism behind Paclitaxel resistance was a significant increase in P-gp levels. When Verapamil inhibited the drug efflux pump, the cells recaptured sensitivity to Paclitaxel.

We developed two HGSC cell lines with dual resistance to Carboplatin and Paclitaxel, reflecting most OC recurrences. This reliable tool is ideal for preliminary drug testing to develop new therapeutic strategies to overcome chemoresistance.

Keywords

Chemoresistance, High-Grade Serous Carcinoma, Ovarian Cancer, Paclitaxel, P-glycoprotein.

2. Introduction

The high mortality rate of HGSC patients is mainly due to late diagnosis and resistance to treatment (80, 539). Improvements are needed in these areas to extend patients' survival. Successful debulking surgery (R0) is currently the best prognostic factor for HGSC patients (540). After surgery, a combination of classical chemotherapy drugs, such as Carboplatin and Paclitaxel, is the standard of care (80, 541-543), although

treatments with Bevacizumab and PARP inhibitors have shown improvements in survival (38, 39, 43, 44, 49, 544).

Platinum-taxane-based chemotherapy is commonly used in cancer therapy to induce tumor cell death by disrupting different cellular mechanisms involved in the regulation of the cell cycle (545, 546). However, many HGSC patients experience disease relapse within six months after first-line therapy, with a median OS of approximately 12 months in this setting (547). Resistance mechanisms to platinum-based drugs include decreased drug uptake (mediated by CTR1/2 and OCT), increased drug efflux [mediated by ATPase copper transporting 7 alpha/beta (ATP7A/7B), and MRP2], drug inactivation (mediated by GSH and MT), and alterations in DNA damage repair system (ERCC1/4 and BRCA1/BRCA2) (548). Paclitaxel resistance mechanisms involve alterations in α- and β-tubulins, increased expression and activity of MDR efflux transporters, OE of anti-apoptotic proteins, inhibition of apoptotic and tumor-suppressor proteins, and modulation of several cytokines, chemokines, and transcription factor pathways (334, 382, 549-555).

In established chemoresistant cell lines, Cisplatin is commonly used for the induction of resistance (556). In contrast, Paclitaxel-resistance induction is less common and has been established in certain cancer models such as gastric adenocarcinoma (OCUM-2M/Paclitaxel), breast cancer (MCF7/TAX), and prostate cancer (DU145-TxR, PC-3-TxR) models (557-559). In the context of OC, most established chemoresistant cell lines are patient-derived and have intrinsic resistance (560, 561). Also, A2780 and IGROV1 Paclitaxel-induced variants are available, but these cell lines correspond to the EC subtype (562-566).

To address the high mortality rate of double-resistant tumors, two HGSC cell line models combining intrinsic resistance to Carboplatin and acquired Paclitaxel chemoresistance have been created. These models, derived from the OVCAR8 cell line, feature stable acquired Paclitaxel resistance induced by P-gp OE. These cell lines serve as a key tool for the discovery of therapeutic alternatives to improve patients' outcomes.

3. Materials and Methods

3.1. Cell Line and Drugs

The OVCAR8 was selected as a model for HGSC because it is known to be resistant to Carboplatin. This particular cell line was obtained from an HGSC patient who had undergone high-dose Carboplatin (567). The OVCAR8 was kindly provided by Doctor Francis Jacob, Gynecological Cancer Center and Ovarian Cancer Research, Department of

Biomedicine, University Hospital Basel and University of Basel, Basel, Switzerland. The cells were grown in complete media; specifically, RPMI-1640 medium (Thermo Fisher Scientific, Waltham, MA, USA), supplemented with 10% (*v/v*) inactivated and FBS (Biowest, Nuaillé, France) and 1% (*v/v*) penicillin/streptomycin (Thermo Fisher Scientific, Waltham, MA, USA) and maintained at 37 ° C and 5% CO_2. The OVCAR8 was authenticated using short tandem repeat (STR) profiling and regularly tested for the absence of mycoplasma.

Carboplatin and Paclitaxel were purchased from Selleckchem (Houston, Texas, USA), dissolved in distilled water and DMSO (AppliChem, Barcelona, Spain), respectively, and stored at -80 ° C, according to the manufacturer's instructions. Immediately prior to use, an aliquot was diluted to the required concentrations.

3.2. Generation of OVCAR8 PTX R Cell Lines

Two OVCAR8 PTX R variants were established from OVCAR8 cells. This was done by exposing the OVCAR8 cells to increasing concentrations of Paclitaxel (2 to 74.9 nM), continuous (C), and pulse (P) schemes over three months (details are shown in **Figure 13A**). The starting Paclitaxel concentration used for creating the resistant variants was determined based on the IC_{10} value obtained from dose-response curves after exposing the OVCAR8 cells to Paclitaxel (1.56 to 200 nM) for 48 hours (**Figure S2A**).

Initially, each OVCAR8 PTX R variant was continuously exposed to Paclitaxel. After one month, and during more than two months, was adopted two different approaches: one group of cells was constantly exposed to Paclitaxel (continuous-selection strategy), while the other group was exposed to Paclitaxel for four days and then allowed to recover in drug-free media for four days (pulse-selection strategy) for two months. Next, it was tested if the Paclitaxel-resistant phenotype was stable in culture without the drug. After two months of freezing cycles, the cells were cultured without Paclitaxel (**Figure 13B**).

We used the Preston Blue (PB) assay to evaluate cell viability in response to Paclitaxel at different time points and confirm the maintenance of IC_{50} values after freezing cycles and persistent cultures.

3.3. Cell Viability Assay

To assess cell viability in response to Paclitaxel, was conducted a resazurin-based assay – PB – according to the manufacturer's instructions. Here, seeded $2x10^3$ cells/well into a 96-well plate in complete media and incubated at 37 ° C and 5% CO_2. After 48 hours, the cells were exposed to increasing concentrations of Paclitaxel (1.56 to 200 nM) and were

further incubated under the same conditions. Following an additional 48 hours was added 50 µl of Presto Blue™ Cell Viability Reagent 1x (Thermo Fisher Scientific, Waltham, MA, USA) to each well and allowed to incubate for 45 minutes at 37 ° C and 5% CO_2, protected from light. Then was measured the fluorescence (560 nm excitation/590 nm emission) using a Bio Tek Synergy™ 2 multi-mode microplate reader (BioTek, Winooski, VT, USA). Treated cells were compared with control cells (considered 100% viable) containing 1% (*v/v*) of the vehicle (DMSO). The IC_{50} for OVCAR8 and OVCAR8 PTX R variants were used to determine fold resistance according to the following formula (568, 569):

$$Fold\ Resistance = \frac{Resistant\ Cell\ Line\ IC50}{Parental\ Cell\ Line\ IC50}$$

3.4. Proliferation Assay

To evaluate cell proliferation, the 3-(4.5-Dimethylthiazol-2-yl)-2,5-diphenyltetrazolium (MTT) assay was performed as previously described (570). Briefly, was seeded $1x10^3$ cells/well into a 96-well plate in complete media and incubated at 37 ° C and 5% CO_2 for up to 6 days. At each time point, was added 500 µg/ml of MTT dye reagent (Sigma-Aldrich, St. Louis, MO, USA) and incubated at 37 ºC and 5% CO_2 for 3 hours. Then, the formazan crystals were in 100 µl of DMSO. Absorbance was measured (570 nm wavelength) using a Bio Tek Synergy™ 2 multi-mode microplate reader.

3.5. Viability Test

A trypan blue assay was performed to distinguish viable and non-viable cells. Cells at 80% confluence were diluted and mixed with a 0.4% trypan blue solution (Thermo Fisher Scientific, Waltham, MA, USA). The mixture was then placed in a Neubauer chamber and counted in five counting grid squares under a Leica DMi1 inverted phase contrast microscope (Leica Microsystems, Wetzlar, Germany) at 50x magnification.

3.6. Cell Microarray Construction and Immunocytochemistry Expression Analysis

All the conditions were arranged in a cell microarray (CMA) block, which was designed and constructed as previously described (571, 572). In brief, $2x10^5$ cells/well were seeded into 6-well plates and incubated at 37 ° C and 5% CO_2. After 48 hours, the cells were treated with 10 nM Paclitaxel and incubated under the same conditions. After another 48 hours, the cells were scraped from culture dishes, fixed with 10% (*v/v*) neutral-buffered formalin (PanReac AppliChem, Darmstadt, Germany), and re-suspended in liquefied

HistoGel™ (Thermo Fisher Scientific, Waltham, MA, USA) according to the manufacturer's instructions. The cells underwent standard histological processing and paraffin embedding. Finally, CMA blocks were constructed and sectioned with a microtome (573).

For ICC, slides were deparaffinized and hydrated. Next, heat-induced (98 ºC) antigen retrieval was performed with citrate buffer solution (1:100 at pH 6.0; Thermo Fisher Scientific, Waltham, MA, USA) or ethylenediamine tetraacetic (EDTA, 1:100; Thermo Fisher Scientific, Waltham, MA, USA) for 40 minutes. Endogenous peroxidase activity was blocked with hydrogen peroxide solution 3% (*v/v*) (Thermo Fisher Scientific, Waltham, MA, USA) for 10 minutes. Slides were incubated with a specific primary antibody (conditions described in **Table S3**) and detected using a secondary antibody with Horseradish peroxidase (HRP) labeled polymer (Dako REAL™ EnVision™ Detection System Peroxidase/DAB+, Rabbit/Mouse, Agilent, Santa Clara, CA, USA) for 30 minutes. The reaction was visualized using DAB according to the manufacturer's instructions. Finally, nuclear staining with hematoxylin was performed, and the slides were dehydrated, clarified, and covered using a permanent mounting medium for optical microscope analysis.

Two independent observers (MN and SR) evaluated the ICC results. They recorded the staining pattern (nuclear, cytoplasm, or membrane) and the percentage of cells stained (0%, 1 – 10%, 11 – 25%, 26 – 50%, 51 – 75%, and 76 – 100%).

3.7. Electronic Microscopy Analysis

The cell ultrastructure was qualitatively assessed using electron microscopy. To perform transmission electron microscopy and semithin section analysis, cultured cells were grown until they reached 80% confluence. There, cells were washed three times with PBS (Thermo Fisher Scientific, Waltham, MA, USA), gently scraped from culture dishes, and fixed overnight in glutaraldehyde (2,5%), paraformaldehyde (2%), and 0.1M sodium cacodylate buffer (1:1) solution, at 4 ºC. After fixation, cells were pelleted by centrifugation and washed three times in 0.1 M sodium cacodylate buffer for 5 minutes each. Subsequently, a post-fixation step was performed in 0.1 M sodium cacodylate buffered 2% osmium tetroxide for 2 hours at RT. The cells were then washed three times in distilled water for 5 minutes each. The samples were incubated with 1% uranyl acetate for 30 minutes at RT, followed by three washes in distilled water for 5 minutes each. Finally, the cell pellet was embedded in Histogel™, dehydrated in ethanol, and embedded in an epoxy resin. Ultrathin sections were stained and observed in a JEOL 100CXII transmission electron microscope (JEOL, Tokyo,

Japan) operated at 80 kV, and images were digitally recorded using a CCD digital camera Orius 1100W (JEOL).

3.8. Apoptosis and Cell Cycle Analysis

To evaluate cell apoptosis and cell cycle distributions, the Annexin V-FITC apoptosis detection kit (Thermo Fisher Scientific, Waltham, MA, USA) and propidium iodide (PI) staining, respectively, were used, following the manufacturer's instructions. Initially, $2x10^5$ cells/well were seeded into 6-well plates and incubated at 37 ° C and 5% CO_2. After 48 hours, the cells were treated with 10 nM Paclitaxel and incubated under the same conditions.

For apoptosis analysis, after 48 hours, both floating and adherent cells were collected using a cell dissociation buffer enzyme-free in PBS. These cells were pelleted by centrifugation (800 g, 5 minutes), filtrated through a 70 µm filter to obtain single-cell suspensions, and finally suspended in 195 µl binding buffer. Subsequentially, 5 µl of Annexin V-FITC was added, and the cells were incubated for 10 minutes, protected from light. The cells were then washed and resuspended in 190 µl binding buffer, followed by the addition of 10 µl of PI (20 µg/ml), incubated for 1 minute, protected from light.

For the cell cycle, after 24 hours, both floating and adherent cells were collected, pelleted by centrifugation, and resuspended in PBS. The cells were then fixed with 70% (*v/v*) cold ethanol and incubated at 4 ºC for 30 minutes. Subsequently, they were pelleted by centrifugation, resuspended in PBS containing PI (250 µg/ml) and RNase A (100 µg/ml), and incubated at 4 ºC for 15 minutes, protected from light.

Fluorescence from both assays was evaluated using a BD FACS Canto™ II flow cytometer, and the data were analyzed by FlowJo software v10.0.7 (Ashland, Oregon, USA).

3.9. Time-lapse Microscopy, Image Acquisition, and Processing

Live-cell imaging experiments were performed as previously described (574). Briefly, $1.2x10^5$ cells were seeded into LabTek II chambered cover glass (Nunc, New York, NY, USA) with 1 ml of culture medium and then incubated at 37 ° C with 5% CO_2. After 24 hours, the cells were treated with 20 nM Paclitaxel in RPMI without phenol red and supplemented with 5% FBS. Images were taken at 5-minute intervals up to 72 hours under differential interference contrast (DIC) optics, with a 63x objective under an Axio Observer Z.1 SD inverted microscope equipped with an incubation chamber at 37 ° C and 5% CO_2. Movies were created from time-lapse images using ImageJ 1.4v software (Rasband, W.S., ImageJ, U. S. National Institutes of Health, Bethesda, MD, USA). The duration of mitosis and the

number of cells arrested at mitosis, dead by apoptosis, or bypassing cytokinesis were scored.

3.10. Anoikis Resistance Assay

An aggregate formation assay was performed to evaluate anoikis resistance, following the method described (570). Briefly, $1x10^6$ cells/well were seeded into polyHEMA (Poly2-hydroxyethyl methacrylate; Sigma-Aldrich, St. Louis, MO, USA) coated plates and then incubated at 37 ° C and 5% CO_2 for up to 15 days. At each time point (5, 10, and 15 days), floating cells were collected, dissociated using trypsin, pelleted by centrifugation, and resuspended in PBS. The cell suspensions were then incubated with 4',6-diamidino-2-phenylindole (DAPI;1 µg/ml) for 2 minutes. Fluorescence was assessed by BD FACS Canto™ II flow cytometer, and the data was analyzed by FlowJo software v10.0.7.

3.11. Colony Formation Assay

To assess clonogenic capacity, $1x10^3$ cells/well were seeded into 6-well plates and then incubated at 37 ° C and 5% CO_2. After 24 hours, the cells were treated with 10 nM Paclitaxel and incubated under the same conditions. After 48 hours, the media was replaced, and the cells were allowed to recover for eight days. The surviving colonies were then fixed and stained as previously described (575). The percentage of cell survival was determined using the following formula:

$$Cell\ Survival\ (\%) = \frac{\text{Colonies Number in Control x } 100\%}{\text{Colonies Number in Treatment}}$$

3.12. Wound Healing Assay

To assess migration capacity, cell monolayers were grown to confluence in 6-well plates, then serum-starved overnight and placed in an incubator at 37 ° C and 5% CO_2. The monolayers were washed twice with PBS and scratched in half using a sterile 200 µl pipette tip. Cell migration was monitored by capturing phase contrast microscopy images at 0, 24, and 48 hours. The remaining unmigrated area was measured using ImageJ 1.4v software to quantify wound closure.

3.13. RNA Isolation and Real-time Quantitative Reverse Transcription Polymerase Chain Reaction

The total RNA was extracted from cells with PureZOL™ RNA Isolation Reagent (Bio-Rad Laboratories, Hercules, CA, USA), following the manufacturer's instructions. The cDNA synthesis was performed with iScript™ cDNA Synthesis Kit (Bio-Rad Laboratories, Hercules, CA, USA) using total cell RNA as a template, following the supplier's instructions. For real-time PCR, cDNA was amplified using iQ™ SYBR Green Supermix Kit (Bio-Rad Laboratories, Hercules, CA, USA). The following primers were used for amplification: P-gp: forward: 5'-GCCAAAGCCAAAATATCAGC -3' and reverse: 5'-TTCCAATGTGTTCGGCATTA-3'; GAPDH: forward: 5'-ACAGTCCAGCCGCATCTTC-3' and reverse: 5'-GCCCAATACGACCAAATCC-3'; and β-Actin (used as housekeeping gene): forward: 5'-AAT CTG GCA CCA CAC CTT CTA-3' and reverse 5'-ATA GCA CAG CCT GGA TAG CAA-3'. The data were acquired with CFX Manager™ Software v1.0 (Bio-Rad Laboratories, Hercules, CA, USA), and results were analyzed according to ΔCT.

3.14. Cell Extracts and Western Blotting

The total cell protein extracts were prepared, and Western blotting was performed, as previously described (576). The membrane was first exposed to primary antibodies (**Table S3**) and then to secondary antibodies: anti-rabbit HRP from Vector Laboratories, Newark, CA, USA) and anti-mouse HRP (Sigma-Aldrich, St. Louis, MO, USA), diluted at 1:1000 or 1:4000, respectively. The protein signal intensity was quantified using ImageJ 1.4v software and normalized against the expression levels of α-tubulin.

3.15. Rhodamine 123 Accumulation Assay

To evaluate the functional activity of P-gp, 1×10^5 cells were seeded into 6-well plates and then incubated at 37 ° C and 5% CO_2. After 24 hours, 1 μM of the fluorescent P-gp substrate Rhodamine 123 (RH-123; Sigma-Aldrich, St. Louis, MO, USA) was added. This was done both in the presence or absence of 20 μM Verapamil (Sigma-Aldrich, St. Louis, MO, USA), which is a P-gp inhibitor. The cells were then incubated under the same conditions. After 1 hour, the cells were harvested and washed twice with ice-cold PBS. The cell pellet was gently re-suspended in ice-cold PBS for analysis. The mean fluorescence intensity (MFI) was assessed using a BD Accuri C6™ II flow cytometer (BD Biosciences, Milpitas, CA, USA), and data was analyzed by BD Accuri C6 Plus Software, version 1.0.27.1 (BD Biosciences).

3.16. Sulforhodamine B Assay

To determine cell viability in response to Paclitaxel after Verapamil incubation, a Sulforhodamine B (SRB) assay was conducted. Briefly, $5x10^6$ cells/well were seeded in 96-well plates and then incubated at 37 ° C and 5% CO_2. After 24 hours, was treated the cells with ten-fold serial dilutions of Paclitaxel, both in the presence and absence of 10 μM Verapamil, under the same conditions. In parallel, cells were treated with an equivalent amount of vehicle (DMSO) up to 0.25% concentration. Subsequently, the cells were fixed with 50% (*m/v*) trichloroacetic acid (Merck Millipore, Darmstadt, Germany) for 1 hour, washed with distilled water, and stained with 0.1% (*m/v*) SRB in acetic acid (Sigma-Aldrich, St. Louis, MO, USA) for 30 minutes at RT. After washing with 1% (*v/v*) acetic acid aquae solution (Merck Millipore, Darmstadt, Germany), the plates were left to dry at RT. The SRB complex was then solubilized with 10 mM Tris-Base buffer (Sigma-Aldrich, St. Louis, MO, USA) for 30 minutes. Finally, it was measured the absorbance at 515 nm wavelength using a Bio Tek Synergy™ 2 multi-mode microplate reader. The IC_{50} of Paclitaxel, in the presence or absence of Verapamil, was determined as described above in section 3.3.

3.17. Statistical Analysis

All assays were done in triplicate with at least three independent experiments. The data were expressed as mean ± standard deviation (SD). Statistical analysis was carried out using GraphPad Prism Software Inc. v6, employing ordinary one-way or two-way ANOVA, followed by Turkey's or Šídák's multiple comparison test. Statistically significant values were denoted as *<0.05; **<0.001; ***<0.0005; ****<0.0001.

4. Results

4.1. OVCAR8 PTX R Variants Demonstrate High Resistance to Paclitaxel

The OVCAR8 and OVCAR8 PTX R variants were exposed to increasing concentrations of Paclitaxel, and their cell viability was assessed by PB assay. The cell viability of the OVCAR8 when exposed to 10 nM Paclitaxel was 51.52 ± 7.69%, while for the OVCAR8 PTX R C and OVCAR8 PTX R P, it was 89.16 ± 6.62% and 86.79% ± 4.25%, respectively (**Figure 13B**). A significant increase in the IC_{50} Paclitaxel was observed for OVCAR8 PTX R C (128.97 ± 6.48 nM, $p<0.001$) and OVCAR8 PTX R P (152.80 ± 6.51 nM, $p<0.001$) compared to the OVCAR8 (10.51 ± 1.99 nM), indicating a 12.27-fold and 14.54-fold increase in resistance, respectively (**Figure S2B**).

We assessed the stability of acquired resistance in both OVCAR8 PTX R variants by evaluating their sensitivity to Paclitaxel after two continuous months in culture and after cryopreservation cycles without Paclitaxel medium supplementation. The results indicate that OVCAR8 PTX R variants remain stable in the long term without drug supplementation and maintain their resistant phenotype following freeze/thawing cycles (**Figures 13B and S1B**).

We also examined whether the OVCAR8 PTX R variants developed increased resistance to Carboplatin, as the OVCAR8 was described as being resistant to this drug. The results indicate that there were no significant differences in the IC_{50} for Carboplatin concentrations in OVCAR8 PTX R C (125.74 $\pm$ 3.60 nM) and OVCAR8 PTX R P (151.26 $\pm$ 10.17 nM) when compared to OVCAR8 (127.49 $\pm$ 4.76 nM) (**Figure 13C**).

To further investigate the Paclitaxel-resistant phenotype, was performed cell proliferation, apoptosis, and viability tests. According to the MTT assay, was not observed a significant increase in proliferation in the OVCAR8 PTX R variants compared to OVCAR8 at 120 hours in culture (**Figure 13D**). Additionally, ICC showed no significant differences in proliferation (75 – 100% of Ki67 staining) and apoptosis (1 – 10% of cleaved-PARP staining) for the OVCAR8 PTX R variants compared to OVCAR8 after 48 hours in culture (**Figure 13E**). The trypan blue exclusion assay, used to assess viability, indicated no significant differences between the OVCAR8 PTX R variants (both 97.50% viable) and the OVCAR8 (97.50% viable) (**Figure 13F).**

We qualitatively analyzed transmission electron microscopy images to evaluate ultrastructural changes in OVCAR8 PTX R variants. The observations did not reveal any significant differences in ultrastructure between OVCAR8 and OVCAR8 PTX R variants. Both cell lines exhibited similar ultrastructural features, including numerous dense mitochondria, a well-developed Golgi apparatus, a rough endoplasmic reticulum, and multiple lysosomes (**Figure 13G**).

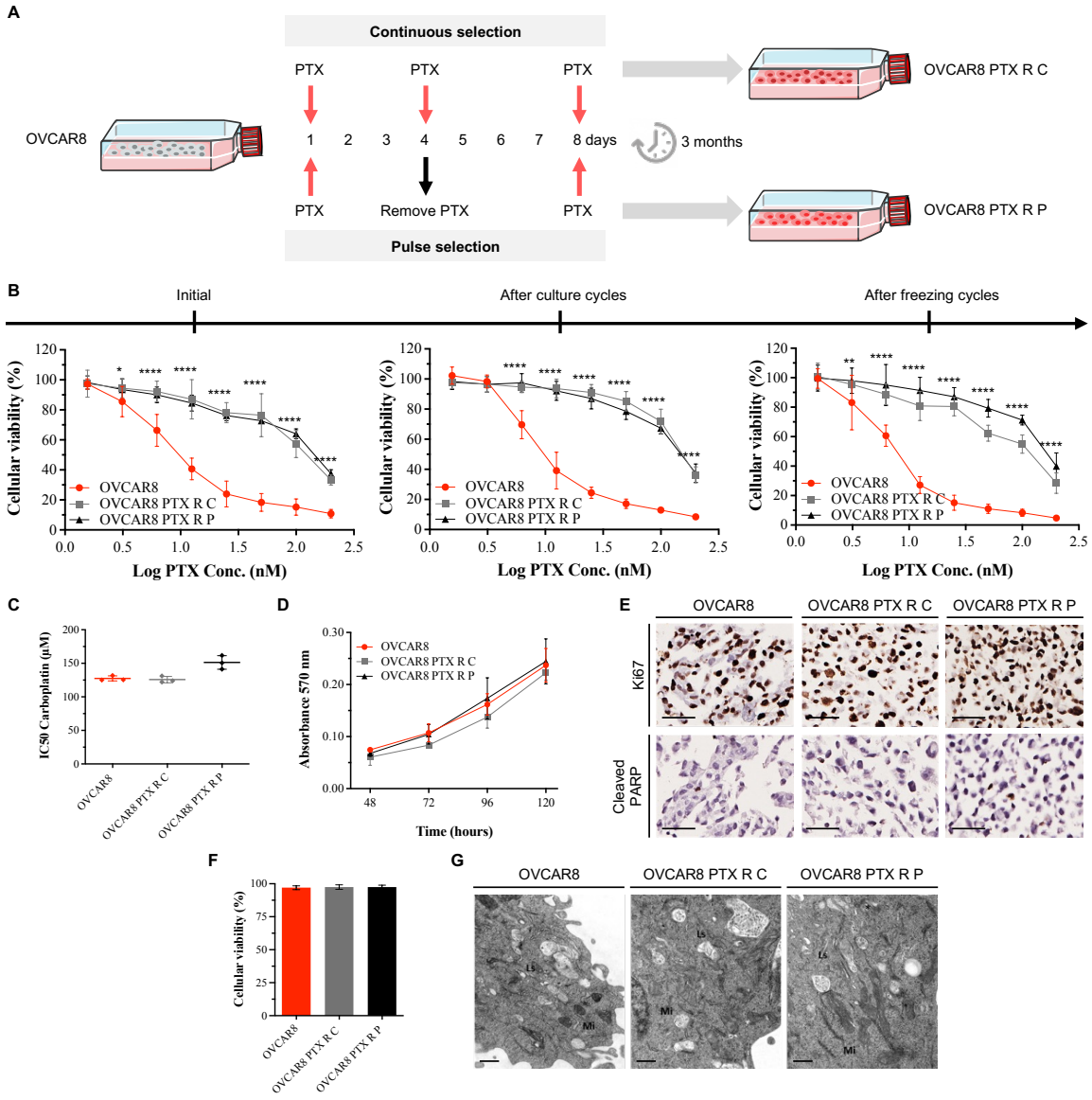


Figure 13. OVCAR8 PTX R Variants Demonstrate High Resistance to Paclitaxel. (**A**) The experimental design used to generate two OVCAR8 PTX R variants by means of two different treatment approaches: C and P selection. (**B**) Line chart showing cell viability for OVCAR8 and OVCAR8 PTX R variants obtained by PB assay after exposure to Paclitaxel (1.56 to 200 nM) for 48 hours. (**C**) Dot plot showing IC_{50} for Carboplatin in OVCAR8 and OVCAR8 PTX R variants obtained by PB assay after exposure to Carboplatin (3.12 to 400 µM) for 48 hours. (**D**) Line chart showing cell proliferation of OVCAR8 and OVCAR8 PTX R variants obtained by MTT assay for 120 hours. (**E**) Representative ICC images for Ki67 and cleaved-PARP of OVCAR8 and OVCAR8 PTX R variants after 96 hours in culture. (**F**) Bar chart showing cell viability of OVCAR8 and OVCAR8 PTX R variants determined by trypan blue exclusion assay after 48 hours in culture. (**G**) Ultrathin sections of OVCAR8 and OVCAR8 PTX R variants show the ultrastructure of Mi, Ls, Golgi complex (asterisk), and RER (arrows). All assays were done in triplicate in at least three independent experiments. Data is expressed as mean ± SD and plotted using GraphPad Prism Software Inc. v6. Statistical analysis was performed using ordinary two-way ANOVA followed by Turkey's multiple comparison test (**B** and **D**) and ordinary one-way ANOVA followed by Turkey's multiple comparison test

(**C** and **F**) and values of *<0.05; **<0.001; ***<0.0005; ****<0.0001 as considered statistically significant. Scale bar 50 μm (**E**) and 0.5 μm (**G**) for ICC images. C, continuous; ICC, immunocytochemistry; Ls, lysosomes; Mi, mitochondria; MTT, 3-(4.5-Dimethylthiazol-2-yl)-2,5-diphenyltetrazolium; P, pulse; PARP, poly (ADP-ribose) polymerase; PB, presto blue; PTX R, Paclitaxel-resistant; RER, rough endoplasmic reticulum; SD, standard deviation.

4.2. OVCAR8 PTX R Variants Overcome Paclitaxel-Induced G_2/M Arrest and Apoptosis

The levels of Paclitaxel-induced apoptosis were measured using the Annexin V-FITC apoptosis detection kit™ by flow cytometry. After 48 hours of exposure to 10 nM Paclitaxel, there was a significant ($p<0.0001$) increase in Paclitaxel-induced apoptosis observed in the OVCAR8 (37.01 ± 1.63%) compared to the nontreated control (7.40 ± 2.48%) (**Figure 14A**). In contrast, following exposure to 10 nM Paclitaxel exposure, the findings revealed a significant decrease ($p<0.0001$) in Paclitaxel-induced apoptosis in OVCAR8 PTX R C and P (11.74 ± 4.58% and 13.38 ± 2.33%, respectively) compared to OVCAR8 (37.01 ± 1.63%) (**Figure 14A**).

After exposure to 10 nM Paclitaxel, OVCAR8 showed a significant decrease ($p<0.0001$) in the percentage of cells in the G_1 phase (54.61 ± 3.32% vs. 27.84 ± 2.89%) and an increase in accumulation of cells in the G_2/M phase (18.77 ± 0.56% vs. 44.18 ± 4.75%) compared to the control (**Figure 14B**). However, the OVCAR8 PTX R variants did not exhibit significant changes in G_1, S, and G_2/M subpopulations after the same Paclitaxel exposure (**Figure 14B**). Furthermore, there was a significant difference ($p<0.0001$) in the G_1 phase for OVCAR8 PTX R C and P (48.92 ± 0.84% and 46.41 ± 2.62%, respectively, compared to OVCAR8 (27.84 ± 2.89%) (**Figure 14B**). A significant difference ($p<0.0001$) was also observed in the G_2/M population for OVCAR8 PTX R C and P (19.57 ± 1.94% and 20.82 ± 2.45%, respectively) compared to OVCAR8 (44.18 ± 4.75%) (**Figure 14B**). Additionally, there was a significant increase ($p<0.001$) in the sub-G_1 fraction (debris and apoptotic cells) for both OVCAR8 (3.11 ± 0.91% vs 7.60 ± 1.16%) and OVCAR8 PTX R C and P (2.41 ± 0.79% and 7.15 ± 0.76%, respectively) when compared to controls (**Figure S3A**) after exposure to 10 nM of Paclitaxel. Both OVCAR8 and OVCAR8 PTX R variants showed a similar proportion of polyploid (>4C) population (**Figures S3A and S3B**).

To further study the behavior of OVCAR8 and OVCAR8 PTX R C, was used live-cell imaging with time-lapse DIC microscopy to analyze mitosis duration and cell fate. Here, it was found that the OVCAR8 PTX R C spent 55.33 ± 7.66 minutes in mitosis, from nuclear envelope breakdown to anaphase onset, which was similar to the 39.35 ± 16.70 minutes

observed in OVCAR8 (**Figure 14C**). When exposed to 20 nM Paclitaxel, the OVCAR8 PTX R C showed a mitosis duration similar to untreated cells (33.00 ± 15.18 minutes). In contrast, the OVCAR8 exhibited a significant increase ($p<0.001$) in mitosis duration (331.29 ± 106.82 minutes) after the same exposure (**Figure 14C**). Additionally, after 20 nM Paclitaxel exposure, 37.5% of OVCAR8 cells died in mitosis after mitotic arrest, while 62.5% underwent normal cycling (**Figure 14C**). In contrast, the OVCAR8 PTX R C variant underwent normal and multiple mitosis (**Figure 14C**).

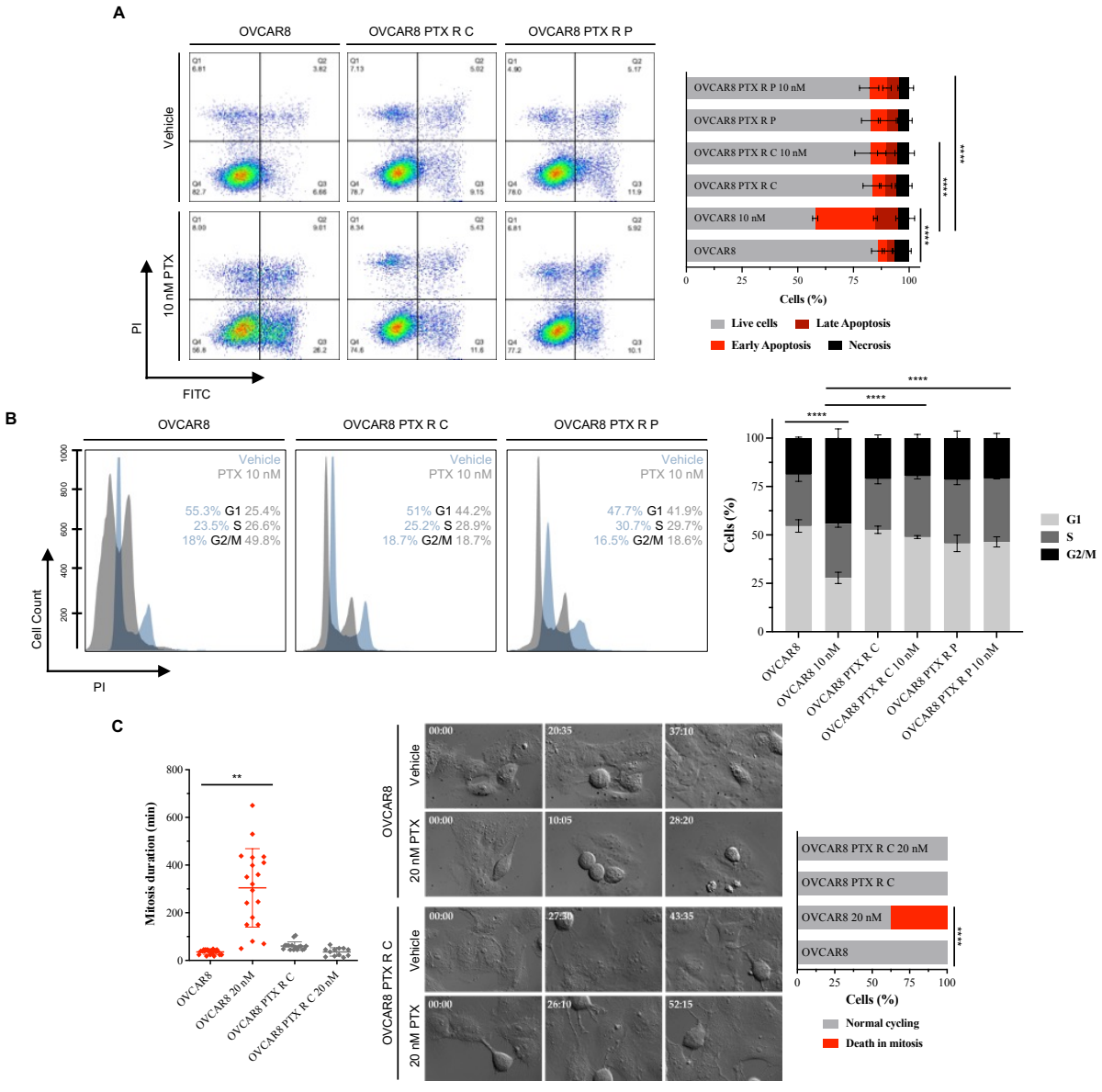


Figure 14. OVCAR8 PTX R Variants Overcome Paclitaxel-Induced G_2/M Arrest and Apoptosis (**A**) Representative flow cytometry dot plots and bar chart showing the percentage of cell populations – necrosis (Q1), late apoptosis (Q2), early apoptosis (Q3) and live cells (Q4) – of OVCAR8 and OVCAR8 PTX R variants using Annexin V/PI staining after being exposed to 10 nM Paclitaxel for 48 hours. (**B**) Representative flow

cytometry histogram and bar chart for cell cycle distribution (G_1, S, and G_2/M) of OVCAR8 and OVCAR8 PTX R variants using PI staining after exposure to 10 nM Paclitaxel for 24 hours. (**C**) Representative time-lapse images and corresponding dot plot for mitosis duration and bar chart for quantification of cell fate (normal cycling or death in mitosis) in OVCAR8 and OVCAR8 PTX R variants after exposure to 20 nM Paclitaxel for 72 hours. All assays were done in triplicate in at least three independent experiments. Flow cytometry was performed using BD FACS Canto™ II (BD Biosciences) flow cytometer, and data were analyzed by FlowJo software v10.0.7. Data is expressed as mean ± SD and plotted using GraphPad Prism Software Inc. v6. Statistical analysis was performed using ordinary one-way ANOVA followed by Turkey's multiple comparison test (**A**, **B,** and **C**) and two-way ANOVA followed by Turkey's multiple comparison test (**C**) and values of *<0.05; **<0.001; ***<0.0005; ****<0.0001 as considered statistically significant. Scale bar 100 µm for microscopic images. PTX R, Paclitaxel-resistant; PI, propidium iodide; SD, standard deviation.

4.3. OVCAR8 PTX R Variants Retain OVCAR8 Features: High Anoikis Resistance, Colony Formation, and Migration Capacity

To assess resistance to anoikis (cell detachment-induced apoptosis), was performed an aggregate formation assay and evaluated the results using flow cytometry. The findings show that there are no significant differences in cell viability (DAPI negative cells) between OVCAR8 PTX R C (87.88 ± 3.29% and 78.20 ± 3.73%) and OVCAR8 PTX R P (89.96 ± 1.74% and 84.03 ± 4.97%) compared to OVCAR8 (94.32 ± 1.15% and 86.47 ± 1.66%) after 5 and 10 days of culture, respectively (**Figure 15A**). Furthermore, there were no significant differences observed in the percentage of positive cells for Ki67 (76 – 99%), Bromodeoxyuridine (BrdU; 11 – 25%), cleaved caspase 3 (1 – 10%), and cleaved PARP (1 – 10%) for OVCAR8 PTX R variants compared to OVCAR8 (**Figure 15B**). Additionally, it was found that the aggregation capacity was partially affected as OVCAR8 PTX R cells formed different and irregular aggregates compared to OVCAR8 (**Figure 15C**).

To assess clonogenic capacity, a colony-forming assay was performed. The results indicate that exposure to 10 nM Paclitaxel resulted in a significant decrease ($p<0.0005$) in the number of colonies in OVCAR8 compared to the untreated control (274.78 ± 49.27 vs 10.56 ± 8.59) (**Figure 15D**). Conversely, after exposure to 10 nM Paclitaxel, no significant differences in colony formation capacity were observed in OVCAR8 PTX R C (294.22 ± 57.45 vs 254.00 ± 58.68) and OVCAR8 PTX R P (241.44 ± 24.44 vs 182.11 ± 44.29) compared to untreated control (**Figure 15D**). In fact, the percentage of cell survival was significantly higher ($p<0.0005$) in OVCAR8 PTX R C (85.80 ± 4.80%) and OVCAR8 PTX R P (74.92 ± 7.72%) compared to OVCAR8 (3.98 ± 2.08%) (**Figure 15D**).

A wound-healing assay was conducted to evaluate migration capacity. The results show no significant differences in migration behavior for OVCAR8 PTX R C (32.48 ± 4.79%)

and OVCAR8 PTX R P (25.27 ± 3.55%) at 48 hours compared to the OVCAR8 (27.63 ± 0.81%) (**Figure 15E**).

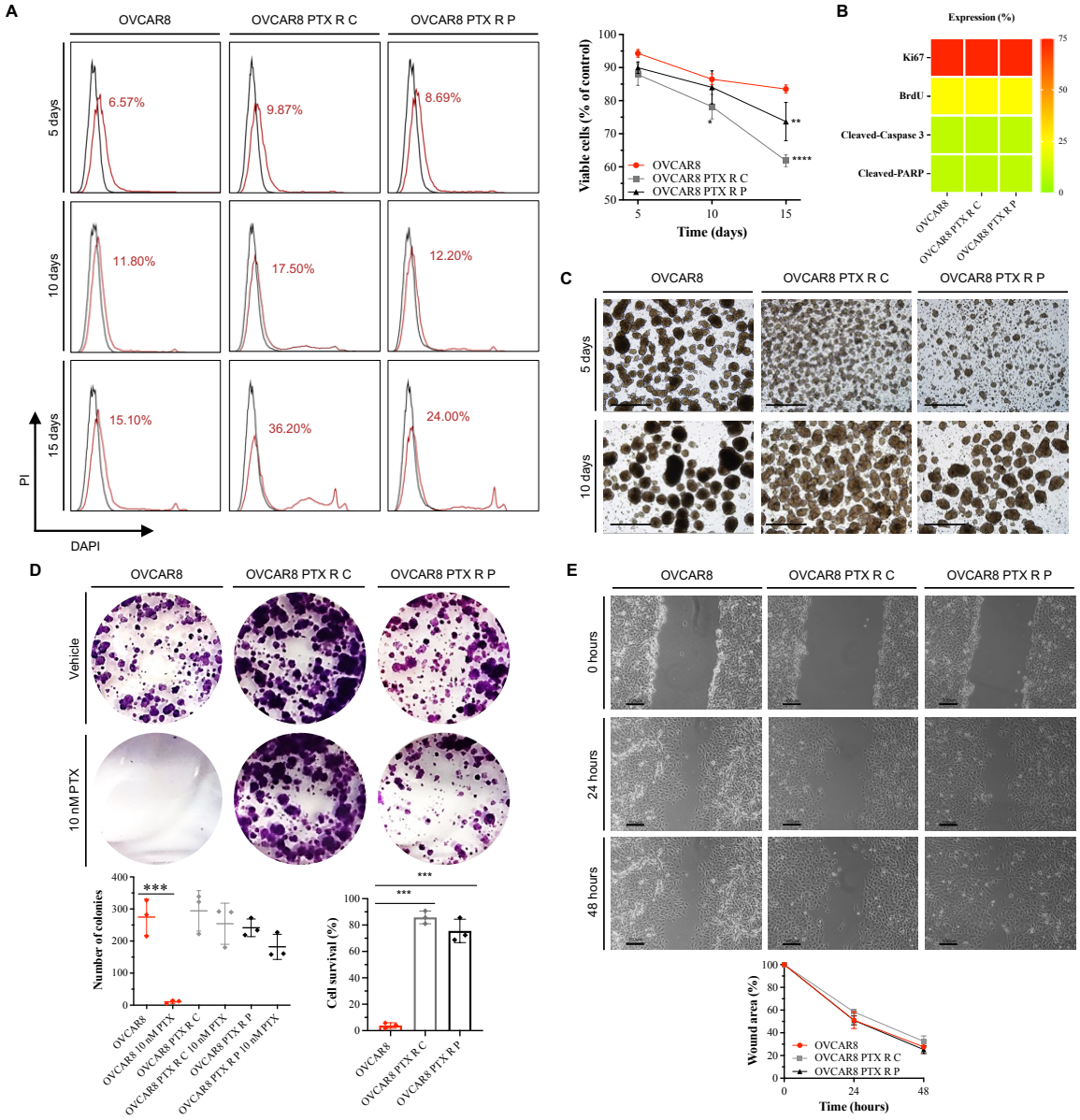


Figure 15. OVCAR8 PTX R Variants Demonstrate High Anoikis Resistance, Colony Formation, and Migration Capacity. (**A**) Representative flow cytometry histograms for cell-detachment-induced apoptosis (anoikis) and a line chart showing the percentage of viable cells (DAPI negative cells) for OVCAR8 and OVCAR8 PTX R variants for 5, 10, and 15 days. Unstained (black) and percentage of DAPI stained cells (dead cells, red). DAPI positivity percentage is indicated in each histogram. (**B**) Proliferation (Ki67 and BrdU) and apoptosis (cleaved-PARP and cleaved-caspase 3) expression for OVCAR8 and OVCAR8 PTX R variants by ICC after 15 days cultured in low adhesion culture conditions. (**C**) Representative images of OVCAR8 and OVCAR8 PTX R variants after 5 and 10 days cultured in low adhesion culture conditions. (**D**) Representative wells from colony forming assay and dot plot showing quantification of number of cell colonies (n = 9 wells) and percentage of cell survival for OVCAR8 and OVCAR8 PTX R variants after eight days in culture. (**E**) Representative phase-contrast

microscopy images for wound healing assay and a line chart showing wound area quantification for OVCAR8 and OVCAR8 PTX R variants at 0, 24, and 48 hours. All assays were done in triplicate in at least three independent experiments. Data is expressed as mean ± SD and plotted using GraphPad Prism Software Inc. v6. Statistical analysis was performed using two-way ANOVA followed by Turkey's multiple comparison test (**A** and **E**) and ordinary one-way ANOVA followed by Turkey's multiple comparison test (**D**). The values of *<0.05; **<0.001; ***<0.0005; ****<0.0001 as considered statistically significant. Scale bar 20 µm (**C**) and 100 µm (**E**) for microscopic images. BrdU, bromodeoxyuridine; DAPI, 4',6-diamidino-2-phenylindole; PARP, poly(ADP-ribose) polymerase; PB, presto blue; PTX R, Paclitaxel-resistant; SD, standard deviation.

4.4. OVCAR8 PTX R Variants Acquire a New Phenotype with P-glycoprotein Overexpression

P-gp, which MDR1 encodes, is abundantly expressed in the cellular membrane and acts as a pump that expels a wide variety of different substances, including Paclitaxel (343). OE of P-gp is the primary mechanism of resistance to chemotherapeutics, as it causes the drugs to be pumped out of the cells, leading to low drug concentrations within the cancer cells and allowing them to survive (577, 578). P-gp expression was evaluated at both mRNA and protein levels using real-time quantitative reverse transcription polymerase chain reaction (qRT-PCR), western blot, and ICC. The qRT-PCR analysis showed an increase in P-gp expression in OVCAR8 PTX R C (12.60 ± 2.90-fold increase) and OVCAR8 PTX R P (8.08 ± 4.00-fold increase) compared to OVCAR8 (**Figure 16A**). This finding was confirmed at the protein level using western blot and ICC, which revealed a high percentage of P-gp-positive cells in OVCAR8 PTX R variants (76 – 100% positive cells) when compared to OVCAR8 (negative/residual expression) (**Figure 16A**).

To confirm whether P-gp upregulation is the mechanism of chemoresistance in OVCAR8 PTX R variants was assessed the IC_{50} of Paclitaxel in the presence and absence of Verapamil, a well-known P-gp inhibitor. Here, was observed a significant decrease in the IC_{50} of Paclitaxel in OVCAR8 PTX R C (40-fold) and OVCAR8 PTX R P (33-fold) when Verapamil was added (**Figure 16B**). Additionally, flow cytometry was used to evaluate P-gp activity by measuring the MFI of cells exposed to RH-123, a known P-gp fluorescent substrate. The percentage of MFI is indicative of intracellular uptake and extracellular efflux of RH-123. Here, it was found that intracellular accumulation of RH-123 was notably low for OVCAR8 PTX R C and OVCAR8 PTX R P (16.57 ± 8.46% and 6.99 ± 3.91%, respectively) compared to OVCAR8 (considered 100%). Furthermore, in the presence of Verapamil, the relative MFI significantly increased ($p<0.0005$) for OVCAR8 PTX R C (89.73 ± 3.22%) and OVCAR8 PTX R P (83.14 ± 3.30%) compared to control, indicating an accumulation of RH-123 due to P-gp pump inhibition (**Figure 16C**).

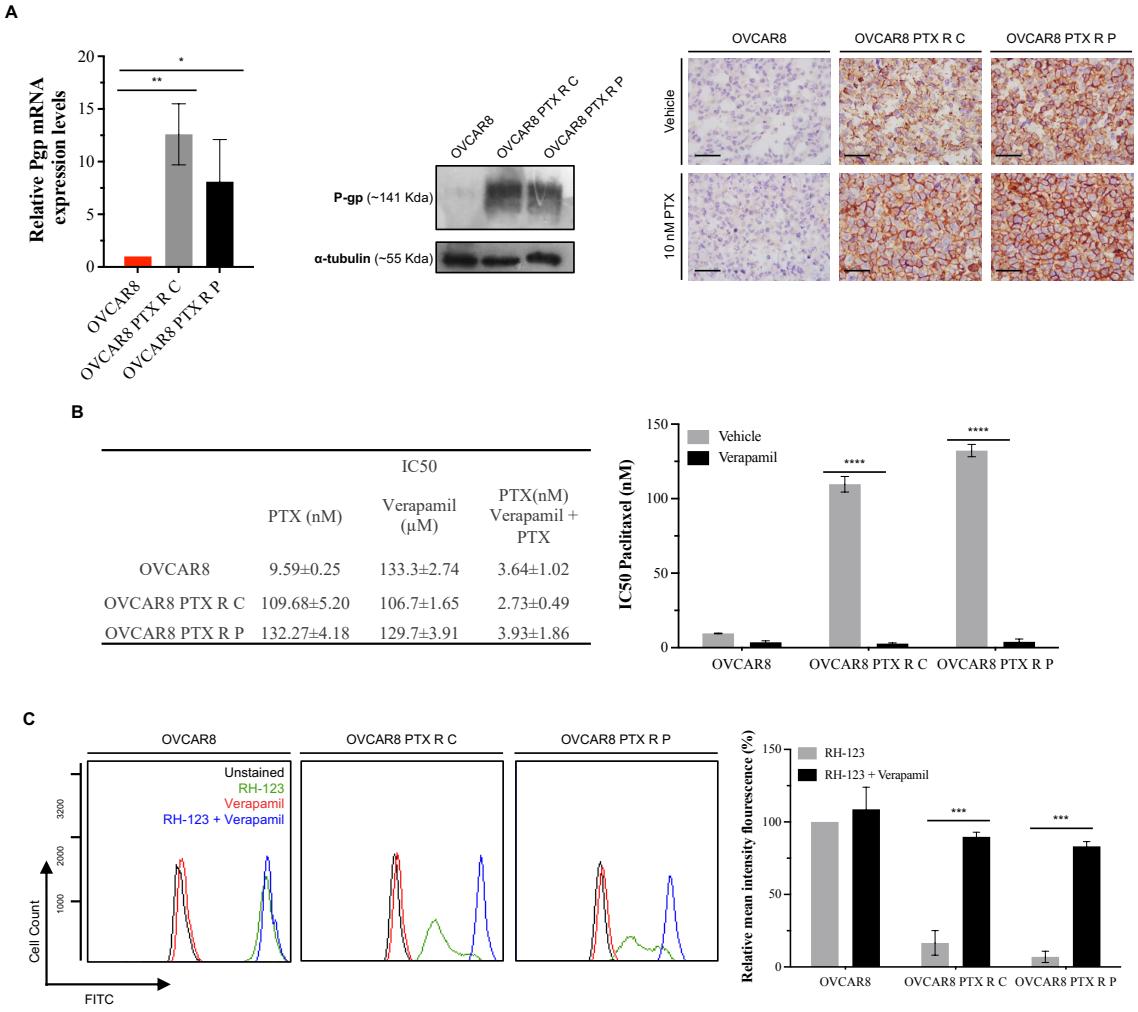


Figure 16. OVCAR8 PTX R Variants Shown P-gp Overexpression. (**A**) Bar charts display relative P-gp mRNA expression levels in OVCAR8 and OVCAR8 PTX R variants determined by qRT-PCR with β-Actin used as a housekeeping gene. Representative western blot showing P-gp expression in OVCAR8 and OVCAR8 PTX R variants using α-tubulin as a loading control. Representative ICC images for P-gp expression in OVCAR8 and OVCAR8 PTX R variants lines after exposure to 10 nM Paclitaxel for 48 hours. (**B**) Table and Bar chart showing IC_{50} Paclitaxel for OVCAR8 and OVCAR8 PTX R variants, obtained by SRB assay after exposure to 10-fold serial dilutions of Paclitaxel, in the presence or absence of 10 μM of Verapamil for 48 hours. (**C**) Representative flow cytometry histogram and respective bar chart showing RH-123 accumulation using FITC-A intensity in untreated (unstained, black) and RH-123-treated (stained, green) cells in the presence (blue) or absence (red) of P-gp inhibitor (Verapamil) for OVCAR8 and OVCAR8 PTX R variants. All assays were done in triplicate in at least three independent experiments. Data is expressed as mean ± SD and plotted using GraphPad Prism Software Inc. v6. Statistical analysis was performed using ordinary two-way ANOVA followed by Turkey's multiple comparison test (**A**) or Šídák's multiple comparison test (**B** and **C**). The values of *<0.05; **<0.001; ***<0.0005; ****<0.0001 as considered statistically significant. Scale bar 500 μm for immunocytochemistry images. FITC-A, fluorescein isothiocyanate A; mRNA, messenger ribonucleic acid; P-gp, P-glycoprotein; PTX R, Paclitaxel-resistant; qRT-PCR, real-time quantitative reverse transcription polymerase chain reaction; RH-123, Rhodamine 123; SD, standard deviation; SRB, sulforhodamine B.

5. Discussion

Surgery and chemotherapy are the two major pillars of oncology treatments. Unfortunately, tumor recurrences and multidrug-resistant phenotypes are common phenomena in the context of HGSC. Since a second surgery is not a valid option for most patients, finding alternatives to first-line chemotherapy is crucial in the treatment of OC. This research aimed to establish two double-resistant HGSC cell lines. Here, a cell line with intrinsic resistance to Carboplatin – OVCAR8 – and induced Paclitaxel resistance by pulse and continuous drug exposure (569). Both methods resulted in the generation of two Paclitaxel-resistant cell lines showing over 12-fold-resistance when compared to OVCAR8 (12.3 and 14.5-fold resistance for OVCAR8 PTX R C and OVCAR8 PTX R P, respectively).

Interestingly, when the clonogenic assay was used to examine long-term survival, these values were even higher, with the Paclitaxel-resistant cells being over 18-fold more resistant to Paclitaxel than their parental cells, which is particularly relevant in the biological tumor context. Additionally, in these models, the Paclitaxel-resistance phenotype remained stable in long-term cultures without Paclitaxel medium supplementation and following freeze/thaw cycles. This stability of acquired resistance ensures the reliability of these *in vitro* tools commonly used to study chemoresistance mechanisms and drug discovery (569, 579).

The use of combination therapies with independent mechanisms of action, such as platinum and taxane drugs, is common in oncology to reduce the development of drug resistance. Some studies suggest that Cisplatin-resistant cells are also shown to be cross-resistant to anti-microtubule drugs such as Paclitaxel (580-582). Recently, Patel *et al.* generated two Cisplatin-resistant cell lines and found that the less Cisplatin-resistant cell line (OVCAR8-CP1) maintained its resistance to Paclitaxel. In contrast, the more Cisplatin-resistant cell line (OVCAR8-CP5) showed significantly higher resistance to Paclitaxel (583). This resistance was linked to increased levels of pro-survival TNF/factor nuclear kappa B (TNFkB) signaling (583). However, other studies did not observe cross-resistance between drugs with different mechanisms of action (339). These conflicting findings show the need for further research to understand the mechanism behind cross-resistance. The results show that OVCAR8 PTX R variants, which were obtained from a patient treated with high-dose Carboplatin, maintained high resistance to Carboplatin without showing cross-resistance. Similar results were reported by Vaidyanathan *et al.,* who established a Paclitaxel-resistant OC cell line model (A2780pacR) without affecting Carboplatin resistance (465). Additionally, a systematic review by Stordal *et al*. found a positive interaction between taxanes and

platinum with residual cross-resistance (546). Also concluded that the relationship between platinum and taxane resistance observed in cell models is reflected in the clinical response to these agents in OC (546), indicating that resistant cellular models could be useful for predicting response to salvage chemotherapy and identifying new therapeutic targets.

To better understand the characteristics of these new Paclitaxel-resistant variants, was performed a series of functional assays. The findings indicate that OVCAR8 PTX R variants exhibit similar levels of proliferation and cell viability in culture compared to the OVCAR8 cells. Also maintains apoptotic levels, resistance to cell death when detached from a surface (anoikis resistance), and the ability to migrate. OVCAR8 is a Carboplatin-resistant cell line and has a naturally high rate of cell proliferation, as well as resistance to anoikis and the ability to form colonies and migrate (567, 570). These results demonstrate that the main features of the OVCAR8 were preserved, and the induced resistance to Paclitaxel did not enhance these original cellular characteristics. These findings contradict some studies that have observed an increased migratory capacity in chemoresistant variants (584). It has been reported that Paclitaxel-resistant cells often show morphological alterations in their mitochondria at the ultrastructural level due to the accumulation of ROS (585). A thorough examination of cellular structures revealed that OVCAR8 and OVCAR8 PTX R variants exhibit similar mitochondrial morphology. Therefore, the induced resistance to Paclitaxel did not alter the biological behavior or the original cell line's morphology.

Paclitaxel is an antimitotic agent by binds to β-tubulin and affects microtubule dynamics. This causes Paclitaxel-treated cells to be stuck in the G_2/M phase of the cell cycle, leading to apoptosis (586-588). The research demonstrated that Paclitaxel-resistant OVCAR8 cells survive by developing a new ability to remove the drug from their cells, preventing them from being affected and avoiding cell cycle arrest. This ability to escape cell death is commonly observed in Paclitaxel-resistant cell lines (589). The main reason for resistance to Paclitaxel is the overproduction of drug transporters from the ABC family promoting cellular drug efflux (578, 590). One of these transporters is P-gp, which is found in a variety of normal tissues, such as the brain, liver, kidney, placenta, and intestine (591), and has a protective action against xenobiotic substances and toxic compounds (590). In the cancer setting, P-gp is highly expressed in the ovary, colon, kidney, adrenocortical, and hepatocellular tumors (533, 592-594) and is correlated with the MDR phenotype (533). In breast and ovarian carcinomas, high P-gp expression levels are associated with the lack of chemotherapy response and poor prognosis (534, 590, 595). The study found that OVCAR8 cells have low levels of P-gp, while the Paclitaxel-resistant variants have significantly

increased, with more than 75% of cells showing strong staining for P-gp. This change in P-gp levels is also seen in other OC cell lines after exposure to Paclitaxel (465). The increase in P-gp levels is due to the OE of the gene responsible for producing P-gp (546).

Verapamil is a P-gp inhibitor that has been shown to enhance the effectiveness of Paclitaxel in several cancer cell lines *in vitro* (596, 597). It is well established that inhibiting P-gp and reducing its expression can reverse Paclitaxel resistance (551). These findings indicate a significant increase in the accumulation of RH-123 in OVCAR8 PTX R variants when Verapamil is present. Also, these results suggest that after P-gp inhibition, cells retain Paclitaxel, leading to reduced cell viability and induction of apoptosis. Although there are conflicting data (465), previous studies have demonstrated that Paclitaxel-resistant cell lines maintained high levels of P-gp expression following their inhibition, suggesting that the inhibitory effects result from direct inhibition of the efflux pump rather than changes in protein expression levels (590). Consistent with these results, it was observed that OVCAR8 PTX R variants maintained high levels of P-gp expression following treatment with the inhibitory molecule (data not shown).

The inhibition of P-gp is a therapeutic strategy for re-sensitizing tumor cells to chemotherapeutic drugs like Paclitaxel. This strategy is important, as evidenced by the development of many P-gp inhibitors (598), some of which have entered clinical trials (NCT00001302, NCT00001383, and NCT00001944) but have certain limitations in effectiveness. Here, two HGSC cell lines that are resistant to Paclitaxel and have increased P-gp expression can be used to test new and more effective P-gp inhibitors. Additionally, since OVCAR8 cells have inherent resistance to Carboplatin, the two OVCAR8 PTX R models can also be used to assess the effectiveness of drugs in reversing resistance to platinum and taxanes. It is crucial to develop powerful tools to study chemoresistance in an HGSC setting to find effective drugs for treating double-resistant tumors. The future goal is to use these double chemoresistant cell models to evaluate the ability of non-oncology medicines to make cells sensitive again to first-line chemotherapy drugs.

6. Acknowledgments and Funding

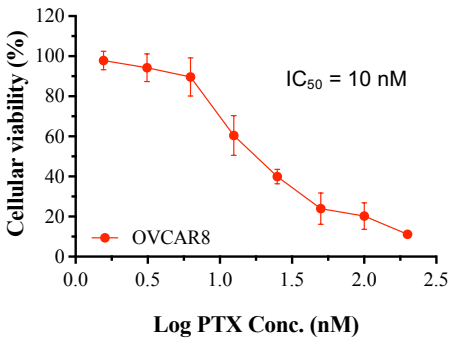
This work was developed at *Instituto de Investigação e Inovação em Saúde (i3S)*, an Associate Laboratory of the *Ministério da Ciência, Tecnologia e Inovação (MCTES),* and it was partially supported by *Fundação para a Ciência e a Tecnologia (FCT).* This research was supported by *Fundo Europeu de Desenvolvimento Regional (FEDER)* through the *COMPETE 2020 – Programa Operacional Competitividade e Internacionalização (POCI),*

Portugal 2020 and *FCT/MCTES*, under the project POCI 01-0145-FEDER-029503 (PTDC/MEC-ONC/29503/2017) and *Cooperativa de Ensino Superior Politécnico e Universitário (CESPU)* under the project ComeTarget_CESPU_2017 (to HB). M.N. acknowledge FCT/MCTES and UE for financial support through a PhD fellowship (2020.04720.BD) that was co-sponsored by *Fundo Social Europeu (FSE)* through Programa Operacional Regional Norte (Norte 2020).

The authors acknowledge the support of the i3S Scientific Platform HEMS, a member of the national infrastructure PPBI – Portuguese Platform of Bioimaging (PPBI-POCI-01-0145-FEDER-022122). The authors also acknowledge the support of the Translational Cytometry Unit (TraCy) i3S Scientific Platform.

7. Supplementary Material

A



B

Fold resistance	Initial	Persistent culture	Freeze/thawing cycles
OVCAR8 PTX R C	12.271	14.878	14.587
OVCAR8 PTX R P	14.537	14.676	20.810

Figure S2. IC_{50} and Fold-Resistance for Paclitaxel in OVCAR8 and OVCAR8 PTX R cell lines. (**A**) Line chart showing cell viability and IC_{50} for Paclitaxel in OVCAR8 cells obtained by PB assay after exposure to PTX (1.56 to 200 nM) for 48 hours. (**B**) Table showing Paclitaxel fold-resistance for OVCAR8 PTX R cell lines. All assays were done in triplicate in at least three independent experiments. Data is expressed as mean ± SD and plotted using GraphPad Prism Software Inc. v6. PB, presto blue; PTX, Paclitaxel; SD, standard deviation.

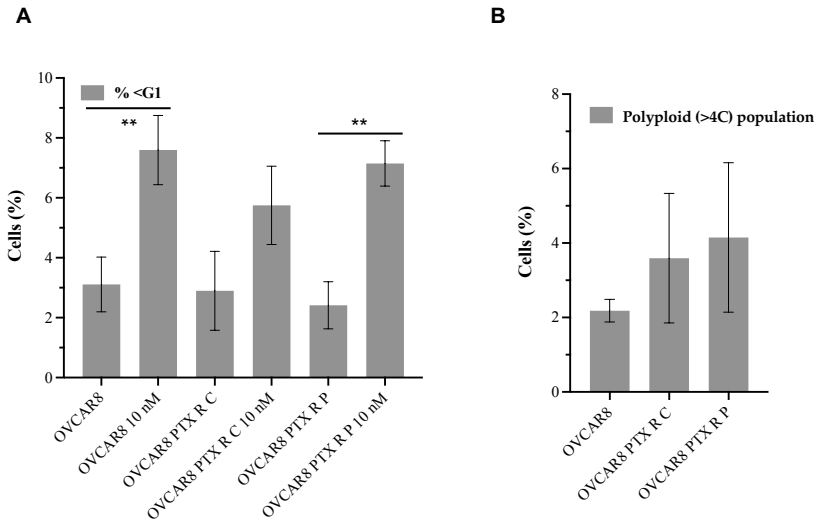


Figure S3. Proportion of Sub-G_1 and polyploid (>4C) populations in OVCAR8 and OVCAR8 PTX R cell lines. (**A**) Bar chart for cell debris and apoptotic cells (%<G_1) of OVCAR8 and OVCAR8 PTX R cell lines using PI

staining after exposure to 10 nM PTX for 24 hours. (**B**) Bar chart showing the percentage of polyploid (>4C) populations of OVCAR8 and OVCAR8 PTX R cell lines using PI staining. Flow cytometry was performed using BD FACS Canto™ II (BD Biosciences) flow cytometer, and data was analyzed by FlowJo software v10.0.7. The assay was done in triplicate in at least three independent experiments. Data is expressed as mean ± SD and plotted using GraphPad Prism Software Inc. v6. Statistical analysis was performed using ordinary one-way ANOVA followed by two-way ANOVA followed by Turkey's multiple comparison tests (**A** and **B**) and values of *<0.05; **<0.001; ***<0.0005; ****<0.0001 as considered statistically significant. PI, propidium iodide, PTX, Paclitaxel; SD, standard deviation.

Table S3. List of antibodies used for ICC and western blotting studies. EDTA, ethylenediamine tetraacetic acid; ICC, immunocytochemistry; mAb, monoclonal antibody; RT, room temperature.

Antigen	Clone	Reference	Origin	Animal origin	Immunohistochemistry				Western Blot		
					Antigen retrieval buffer	Dilution	Incubation conditions	Localization	Molecular weight (kDa)	Dilution	Incubation conditions
α-tubulin	**B-5-1-2**	t568	Sigma-Aldrich	Mouse mAb	-	-	-	-	50	1:5000	Overnight
Bromodeoxyuridine (BrdU)	**Bu20a**	M0744	Dako	Mouse mAb	Citrate at pH 6	1:100	60´RT	Nuclear	-	-	-
Cleaved-PARP	**D175 5A1E**	9664	Cell Signalling Technology	Rabbit mAb	Citrate at pH 6	1:100		Nuclear	-	-	-
Cleaved-Caspase 3	**Asp214 D64E10**	5625	Cell Signalling Technology	Rabbit mAb	Citrate at pH 6	1:50		Nuclear	-	-	-
Ki67	**SP6**	MA5-14520	ThermoFisher Scientific	Rabbit mAb	Citrate at pH 6	1:100		Nuclear	-	-	-
P-Glycoprotein	**EPR10364-57**	ab170904	Abcam	Rabbit mAb	EDTA	1:1200		Membrane	141	1:1000	Overnight

b. Targeting Chemoresistant Ovarian Cancer Cells Using Drug Repurposing

The information presented in this chapter is partially based on the following publications:

Nunes M, Duarte D, Vale N, Ricardo S. Pitavastatin and Ivermectin Enhance the Efficacy of Paclitaxel in Chemoresistant High-Grade Serous Carcinoma. Cancers (Basel). 2022 Sep 7;14(18):4357. doi: 10.3390/cancers14184357.

Nunes M, Duarte D, Vale N, Ricardo S. (2022). The Antineoplastic Effect of Carboplatin Is Potentiated by Combination with Pitavastatin or Metformin in a Chemoresistant High-Grade Serous Carcinoma Cell Line. Int J Mol Sci. 2022 Dec 21;24(1):97. doi: 10.3390/ijms24010097.

Nunes M, Ricardo S. (2024). Ivermectin Boosts Paclitaxel Effectiveness in High-Grade Serous Carcinoma in 3D Cell Cultures. Pharmaceuticals. ***Under review.***

i. Pitavastatin and Ivermectin Enhance the Efficacy of Paclitaxel in Chemoresistant High-Grade Serous Carcinoma

1. Abstract

Chemotherapy is a hallmark of managing HGSC. However, it often leads to chemoresistance and side effects, which can interrupt treatment. Combining repurposing drugs with chemotherapy has the potential to enhance the effectiveness of antineoplastic therapies, as these drugs may have independent mechanisms of action and can suppress different pathways simultaneously.

This study aimed to investigate whether combining Paclitaxel with repurposed drugs could provide therapeutic benefits. Here, was evaluated the cytotoxic effects of Paclitaxel alone and in combination with several repurposed drugs (Pitavastatin, Metformin, Ivermectin, Itraconazole, and Alendronate) in two tumor chemoresistant cell lines (OVCAR8 and OVCAR8 PTX R P) and a non-tumoral cell line (HOSE6.3). To assess cellular viability, was used the PB assay, and evaluated synergistic interactions using Chou–Talalay, Bliss Independence, and HSA reference models.

The combination of Paclitaxel with Pitavastatin or Ivermectin showed the highest cytotoxic effect and the strongest synergism among all combinations for both chemoresistant cell lines. This resulted in a superior chemotherapeutic effect compared to using either drug alone. Additionally, almost all the repurposed drugs, when combined with Paclitaxel, demonstrated a safe pharmacological profile in non-tumoral cells.

Overall, proposes that Pitavastatin and Ivermectin may be used in combination with Paclitaxel, showing promise as a two-drug therapy for managing HGSC.

Keywords

Chemoresistance, Drug Repurposing, Paclitaxel, High-Grade Serous Carcinoma, Combinatory Regiment, Synergy.

2. Introduction

Cytoreductive surgery and chemotherapy remain the most common therapeutical options for HGSC. However, many patients experience recurrence, which is evident through the presence of MA. This recurrence is characterized by intratumoral heterogeneity and resistance to conventional antineoplastic agents (65, 67, 599). Paclitaxel is a mitotic inhibitor used to treat many types of cancers, including advanced HGSC (541, 542). It targets β-

tubulin, a protein that supports the stability of microtubule polymers, thereby blocking cells in phases G_0/G_1 and G_2/M and leading to tumor cell death (600). However, Paclitaxel treatment is limited by acquired chemoresistance and severe side effects such as peripheral neuropathy, which can lead to interruption of treatment (601, 602). Several molecular factors may contribute to acquired chemoresistance in HGSC, including modification of drug targets, decreased cellular drug accumulation, increased expression of drug pumps and detoxification systems, improved DNA repair process, reduced sensitivity to apoptosis, and enhanced proliferation (193, 200, 603).

Current strategies to delay chemoresistance and achieve a significant therapeutic outcome include developing new synthetic analogs of existing drugs, targeted therapy, immunotherapy, sequential strategies, and combinatory regiments (193, 604). However, some of these therapeutic strategies, such as developing new drugs, involve a time-consuming and cost-consuming process, which is accompanied by a low approval rate and occasionally severe side effects (605). Therefore, it is crucial to explore more advantageous pharmacological strategies to improve therapeutic regimens.

Drug repurposing involves finding new uses for existing drugs that are already approved for treating other diseases (606-608). This approach relies on the idea that different diseases may have overlapping therapeutic targets and molecular features, as well as the concept of pleiotropic drug effects, where a drug can have effects beyond those for which it was originally developed (609). Drug repurposing offers a more accessible alternative because all the necessary information regarding their development, including pharmacokinetics, pharmacodynamics, safety and toxicological profiles, dosage, drug interactions, mechanisms of action, molecular targets, and clinical experience, is already well-known (610-612). This familiarity streamlines the regulatory processes for drug approval. It increases the likelihood of successful clinical applicability, especially in addressing the therapeutic challenges of malignant diseases and the economic impact on health systems (613). Nevertheless, repurposing drugs still requires conducting clinical trials to assess their effectiveness and determine the maximum tolerated dose to avoid potentially harmful side effects, such as unacceptable toxicities (610).

Continuous treatment with a single agent can cause tumor cells to develop resistance to the drug by seeking out alternative pathways (614). This can be addressed by using a combination of two or more drugs that target different pathways, which can improve treatment efficacy and reduce the risk of acquired chemoresistance and toxicity (614-618). Additionally, combining drugs can help overcome intratumoral and intertumoral

heterogeneity (619). Given the heterogeneous nature of HGSC, it is important to identify and combine multitargeting drugs to create personalized therapies that can target all cancer populations. Synergistic interactions, where the combined effect of the drugs is greater than the sum of their individual effects, are the most desirable in pharmacology. Additive interactions result in the combined effect being equal to the sum of the individual effects of each drug. In contrast, antagonistic interactions lead to a combined effect that is weaker than the sum of the individual effects of each drug (620). Therefore, when two drugs act synergistically, it is possible to achieve the desired outcome using lower doses of each drug. This can reduce systemic toxicity and minimize adverse side effects (615, 621, 622).

Several studies suggest that combining antineoplastic agents with repurposed drugs can effectively improve antitumoral activity. These drugs have acceptable toxicological profiles and can simultaneously enhance the activity of the referenced drug while reducing therapeutical doses (623-627). In a previous review, based on experimental and observational studies, it was proposed that Pitavastatin, Metformin, Ivermectin, Itraconazole, and Alendronate exhibit anti-tumoral effects across various tumoral contexts and have the potential to be used in the treatment of OC (607). Here, it was hypothesized that these five repurposed drugs could synergistically act with Paclitaxel in two chemoresistant HGSC cell lines, OVCAR8 and OVCAR8 PTX R P. The OVCAR8 PTX R P is a Carboplatin and Paclitaxel-resistant cell line previously established from parental OVCAR8, which is an acquired Carboplatin-resistant cell line, by pulse exposure to a stepwise increasing paclitaxel concentrations (628). Additionally, was tested these conditions in a non-tumoral cell line (HOSE6.3) to ensure a safe pharmacological profile.

We have shown that Pitavastatin and Ivermectin have anticancer activity and are the most promising repurposed drugs when used alone. Also presented the lowest IC_{50} value for chemoresistant HGSC cell lines. When Paclitaxel is combined with Pitavastatin or Ivermectin, it results in the highest cytotoxic effect and the strongest synergism for both HGSC chemoresistant cell lines, providing a chemotherapeutic effect superior to using either drug alone.

Furthermore, the results for OVCAR8 PTX R P (Carboplatin and Paclitaxel-resistant) cells were even more promising than those for OVCAR8 (Carboplatin-resistant), with a higher number of synergistic pairs for all the combinations considered. Importantly, almost all the repurposed drugs tested alone and in combination with Paclitaxel presented a safe pharmacological profile and did not significantly reduce the cellular viability of HOSE6.3, a

non-tumoral cell line. These promising results may lead to new therapeutic strategies for managing HGSC.

3. Materials and Methods

3.1. Cell Lines and Culture Conditions

The OVCAR8 and OVCAR8 PTX R P cells were chosen as models for HGSC, particularly since they are described as Carboplatin-resistant (567) and Carboplatin and Paclitaxel-resistant (628) cell lines, respectively. Doctor Francis Jacob kindly provided the OVCAR8 cell line from the Gynecological Cancer Center and Ovarian Cancer Research, Department of Biomedicine, University Hospital Basel, and University of Basel, Basel, Switzerland. The OVCAR8 PTX R P cell line was previously established from parental OVCAR8 through pulse exposure (628).

The OVCAR8 PTX R P cell line was uninterruptedly exposed to Paclitaxel for one month and then subjected to a pulse-selection strategy of four days of Paclitaxel exposure followed by four days of recovery in drug-free media over two months (628). Additional experiments were conducted using a non-tumoral cell line (HOSE6.3), which is a human ovarian epithelial cell line derived from a normal ovary removed from patients with non-malignant disease (629). All cell lines were cultured in complete media, i.e., RPMI-1640 medium, GlutaMAX^{TM} Supplement, HEPES (Thermo Fisher Scientific, Waltham, MA, USA), supplemented with 10% (v/v) inactivated and filtered FBS (Biowest, Nuaillé, France) and 1% (v/v) penicillin/streptomycin (Thermo Fisher Scientific, Waltham, MA, USA), and maintained at 37 °C and 5% CO_2. Cells were authenticated using STR profiling and regularly tested to ensure the absence of mycoplasma.

3.2. Drugs

All drugs (Paclitaxel, Pitavastatin, Metformin, Ivermectin, Itraconazole, and Alendronate) were purchased from Selleckchem (Houston, TX, USA). Drugs were dissolved in DMSO (AppliChem, Barcelona, Spain) or distilled water and then stored at −80 ºC, following the manufacturer's instructions. Immediately prior to use, an aliquot was diluted to the required concentrations.

3.3. Cell Viability Assays

To assess the impact of single and combined drug treatments on the viability of cell lines, was conducted a PB assay, which is based on the use of resazurin. In brief, $5x10^3$

cells/well were seeded into a 96-well plate containing complete media and then incubated at 37 °C and 5% CO_2. The cells were allowed to adhere overnight before exposure to drugs. After 24 hours, the cells were treated with increasing drug concentrations and then further incubated under the same conditions. Following a 48-hour incubation period, the culture medium was removed, and 50 µL/well of PrestoBlue™ Cell Viability Reagent 1× (Thermo Fisher Scientific, Waltham, MA, USA) was added to each well. The cells were then incubated for 45 minutes in the absence of light at 37 °C and 5% CO_2. Fluorescence was measured using a Bio Tek Synergy™ 2 multi-mode microplate reader (BioTek, Winooski, VT, USA) with an excitation wavelength of 560 nm and an emission wavelength of 590 nm.

3.4. Drug Treatment

The IC_{50} values were initially determined for each drug alone for OVCAR8, OVCAR8 PTX R P, and HOSE6.3 cell lines. The IC_{50} for all drugs was calculated by comparing treated cells with control cells (considered 100% viable) containing 1% (v/v) of the vehicle (DMSO or distilled water). No differences were observed between control cells with or without a vehicle in all experiments. For single-drug treatment, cells were treated with Pitavastatin (0.04 to 5 µM) (630), Metformin (0.08 to 10 mM) (631), Ivermectin (0.39 to 50 µM) (632), Itraconazole (0.39 to 50 µM) (633), and Alendronate (7.81 to 1000 µM) for 48 hours (634). Combination studies were carried out using increasing concentrations of both drugs in a fixed ratio, as suggested by Chou–Talalay (623, 635). First, Paclitaxel (Drug 1) was combined simultaneously with different repurposed drugs (Drug 2) in a fixed-dose ratio corresponding to 0.25, 0.5, 1, 2, and 4 times the individual IC_{50} values for 48 hours.

3.5. Drug Interactions Analysis

In order to measure the interaction between Paclitaxel (Drug 1) and repurposed drugs (Drug 2), was used the Chou–Talalay method with CompuSyn Software (ComboSyn, Inc., New York, NY, USA) to calculate the Combination Index (CI) (636). This method assumes that drugs act through enterally different mechanisms (637). Here, was combined Drug 1 and Drug 2 in a fixed ratio of doses corresponding to 0.25, 0.5, 1, 2, and 4 times the individual IC_{50} values. The CI represents the pharmacological interactions (i.e., CI < 1, synergism; = 1, additive; and >1, antagonism), plotted on the y-axis as a function of effect level (Fa) on the x-axis to assess drug synergism between drug combinations. Also, was evaluated the expected drug combination responses based on the Bliss independence and HSA reference models using SynergyFinder 2.0 Software (Netphar, Faculty of Medicine,

University of Helsinki, Helsinki, Finland) (638). In the synergy score values, >10 and <-10 denote synergy and antagonism, respectively. Additionally, the cNMF algorithm implemented in SynergyFinder 2.0 was used to estimate outlier measurements (639).

3.6. Microscopic Evaluation

All microscopic figures were obtained under a Leica DMi1 inverted phase contrast microscope (Leica Microsystems, Wetzlar, Germany) at 50× magnification.

3.7. Statistical Analysis

All assays were performed in triplicate with at least three independent experiments. The data were expressed as mean ± SD. Statistical analysis was carried out in GraphPad Prism 8 (GraphPad Software Inc., Boston, CA, USA), using either ordinary one-way or two-way ANOVA followed by Šıdák's multiple comparison test.

4. Results

4.1. Repurposed Drugs Show High Effectiveness in Reducing Cellular Viability of Chemoresistant High-Grade Serous Carcinoma Cells

We initially assessed the potential anti-tumoral effects of each repurposed drug as a single agent on OVCAR8 and OVCAR8 PTX R P cells using increasing concentrations of each drug and evaluating cellular viability after 48 hours of treatment. The analysis yielded a dose-response curve and allowed for the calculation of IC_{50} values, which were subsequently used in combination studies. The findings revealed that all repurposed drugs exhibit anti-tumor activity in both chemoresistant HGSC cell lines. Pitavastatin demonstrated the strongest anti-cancer effect among drugs tested alone, with the lowest IC_{50} values of 0.801 ± 0.061 and 0.850 ± 0.142 μM for OVCAR8 and OVCAR8 PTX R P cells, respectively (**Figure 17A**). Metformin displayed a cytotoxic effect at high concentrations, with IC_{50} values of 1.495 ± 0.169 and 1.458 ± 0.193 mM for OVCAR8 and OVCAR8 PTX R P cells, respectively (**Figure 17B**). Ivermectin exposure resulted in a strong cytotoxic effect, with IC_{50} values of 15.960 ± 2.909 and 15.522 ± 1.859 μM for OVCAR8 and OVCAR PTX R P cells, respectively (**Figure 17C**). The cytotoxic effect of Itraconazole was observed at high concentrations, with IC_{50} values of 39.118 ± 3.376 and 35.571 ± 0.480 μM for OVCAR8 and OVCAR PTX R P cells, respectively (**Figure 17D**). Alendronate treatment showed a cytotoxic effect with IC_{50} values of 219.068 ± 13.555 and 196.325 ± 20.234 μM for OVCAR8 and OVCAR8 PTX R P cells, respectively (**Figure 17E**).

We also tested the effects of repurposing drugs on normal-like cells by using increasing concentrations of each drug on HOSE 6.3, which is obtained from a normal ovary removed from a patient with non-malignant disease (629). The results showed that the tested drugs had little to no efficacy in reducing the cellular viability of HOSE6.3, unlike their effects on tumor cells (**Figure S4**). Specifically, the drugs Pitavastatin, Metformin, and Alendronate showed no efficacy in reducing the cellular viability of HOSE6.3 cells within the considered concentration ranges (**Figure S4**). On the other hand, Ivermectin and Itraconazole demonstrated a cytotoxic effect on HOSE6.3 cells at higher concentrations, with IC_{50} values of 12.635 ± 2.185 and 38.574 ± 5.112 μM, respectively (**Figure S4**). Moreover, was observed subtle morphological differences for all the repurposed drugs at the highest concentration tested compared to the vehicle, confirming an acceptable safety profile of these drugs in normal HOSE 6.3 cells (**Figure S5**). This suggests that these drugs could be good candidates for testing in combination with Paclitaxel as they demonstrate significant anticancer efficacy in chemoresistant tumor cells.

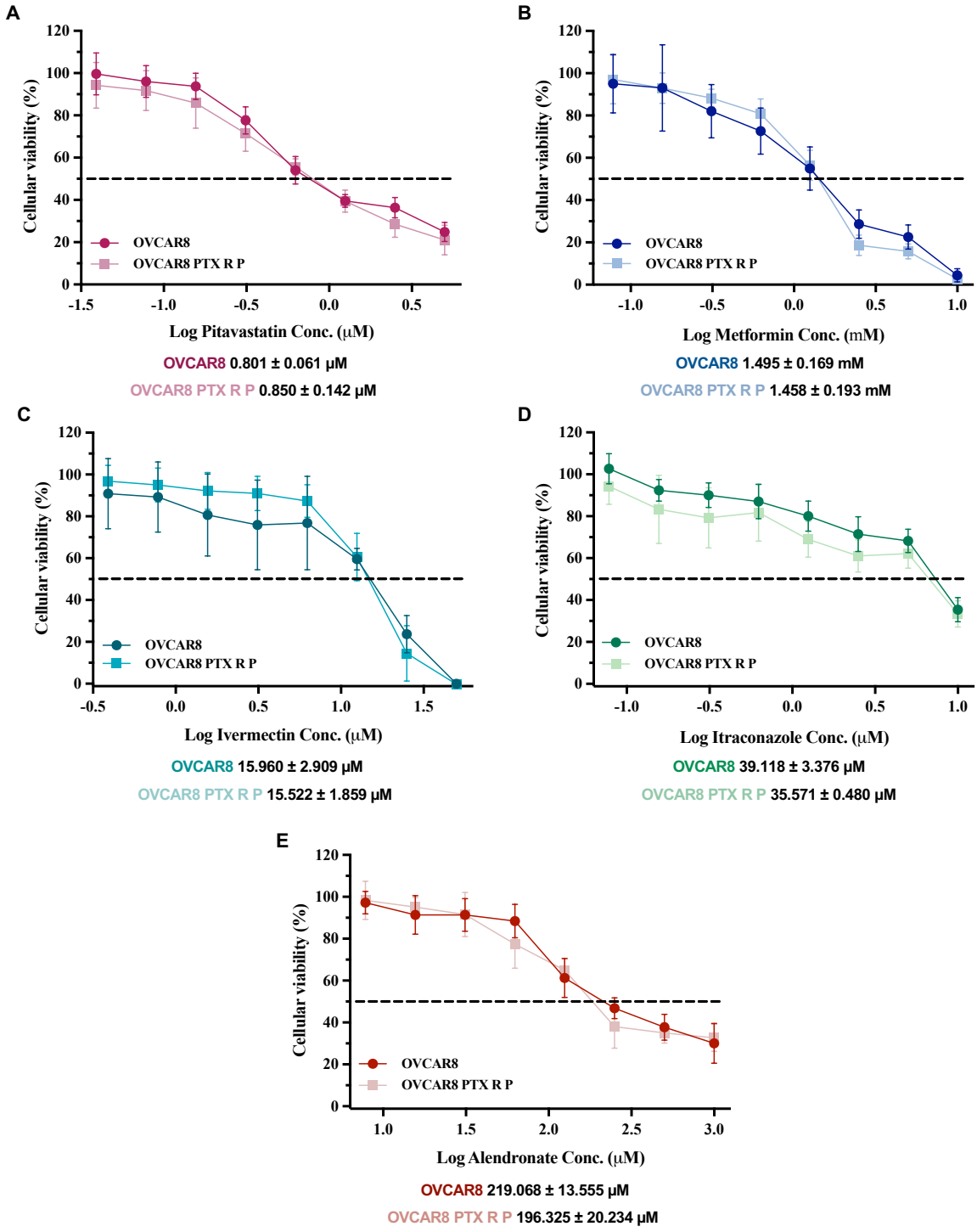


Figure 17. Repurposed drugs have shown high efficacy in reducing the cellular viability of chemoresistant HGSC cells. (**A**–**E**) Dose-response curves for OVCAR8 and OVCAR8 PTX R P cells were obtained by PB assay after exposure to increasing concentrations of the following drugs for 48 hours: (**A**) Pitavastatin (0.04 to 5 μM), (**B**) Metformin (0.08 to 10 mM), (**C**) Ivermectin (0.39 to 50 μM), (**D**) Itraconazole (0.39 to 50 μM) and (**E**) Alendronate (7.81 to 1000 μM). A dotted line in each dose-response curve represents the IC_{50} values. All assays were performed in triplicate in at least three independent experiments. Data are expressed as

mean ± SD and plotted using GraphPad Prism Software Inc. v8 (GraphPad Software Inc., Boston, CA, USA). Statistical analysis was performed using ordinary two-way ANOVA followed by Šidák multiple comparison test (**A**–**E**). HGCS, high-grade serous carcinoma, PB, presto blue, SD, standard deviation.

4.2. Repurposed Drugs Increase the Efficacy of Paclitaxel in Reducing Cellular Viability of Chemoresistant High-Grade Serous Carcinoma Cells

After obtaining the IC_{50} values for all the drugs, was assessed the combination of Paclitaxel with each repurposed drug using the previously described combination model (624). In brief, OVCAR8 and OVCAR8 PTX R P cells were exposed to two drugs (Drug 1 and Drug 2) alone and in combination at fixed ratios corresponding to concentrations 0.25, 0.5, 1, 2, and 4 times the individual IC_{50} values of each drug (**Figure 18 and Table S4**). Additionally, was conducted a morphological evaluation for each treatment condition (**Figure 19**).

For OVCAR8 cells, combining Paclitaxel with Pitavastatin led to a significant increase in the anti-cancer effect of concentrations 0.25 ($p < 0.005$), 0.5, and 1 ($p < 0.0001$) times the IC_{50} values compared to Paclitaxel alone (**Figure 18A and Table S4**). Similarly, for OVCAR8 PTX R P cells, this combination resulted in a significant reduction in cellular viability ($p < 0.0001$) for all the concentrations compared to Paclitaxel as a single agent (**Figure 18B and Table S4**).

For OVCAR8 cells, the combination of Paclitaxel with Metformin caused a significant reduction in cellular viability at concentrations 0.25 ($p < 0.001$), 0.5, and 1 ($p < 0.0001$), and 2 ($p < 0.05$) times the IC_{50} values compared to Paclitaxel alone (**Figure 18C and Table S4**). Moreover, for OVCAR8 PTX R P cells, this combination demonstrated a significant increase in anti-tumor effect for all the concentrations tested (i.e., $p < 0.001$ for 0.25 and $p < 0.0001$ for 0.5, 1, 2, and 4 times the IC_{50} values) compared to Paclitaxel as a single agent (**Figure 18D and Table S4**).

In OVCAR8 cells, a combination of Paclitaxel and Ivermectin resulted in a significant increase in anti-cancer effect for all the tested concentrations. Specifically, the combination showed a $p < 0.05$ for concentrations 0.25 and 4 and $p < 0.0001$ for concentrations 0.5, 1, and 2 times the IC_{50} values when compared to Paclitaxel alone (**Figure 18E and Table S4**). Furthermore, for OVCAR8 PTX R P cells, the combination also led to a significant increase in anti-tumor effect ($p < 0.0001$) for concentrations 0.5, 1, 2, and 4 times the IC_{50} values compared to Paclitaxel alone (**Figure 18F and Table S4).**

On the other hand, the combination of Paclitaxel with Itraconazole in OVCAR8 did not result in a significant reduction in cellular viability compared to Paclitaxel alone (**Figure**

18G and Table S4). However, it demonstrated a substantial increase in anti-cancer effect compared to Itraconazole when used as a single agent, for concentrations 0.5 ($p < 0.005$), 1, 2, and 4 ($p < 0.0001$) times the IC_{50} values (**Figure 18G and Table S4**). In OVCAR8 PTX R P cells, this combination resulted in a significant reduction in cellular viability ($p < 0.0001$) for concentrations 1, 2, and 4 times the IC_{50} values compared to Paclitaxel alone (**Figure 18H and Table S4**).

For OVCAR8 cells, there was a significant decrease in cellular viability ($p < 0.0001$) when comparing Paclitaxel with Alendronate to Paclitaxel alone at the concentrations of 1 time the IC_{50} values (**Figure 18I and Table S4**). Additionally, for OVCAR8 PTX R P cells, the results indicate a significant increase in anti-cancer effect for concentrations 0.5 ($p < 0.005$) and 1, 2, and 4 ($p < 0.0001$) times the IC_{50} values when compared to Paclitaxel alone (**Figure 18J and Table S4**).

In line with the previously mentioned results, morphological differences were observed for all the single and combined treatments compared to the vehicle in both OVCAR8 and OVCAR8 PTX R P cells. The combinatory treatments induced a more aggressive phenotype, showing a decrease in cell number, reduced aggregate formation, and smaller and rounded cells, which are indicative of cell death compared to single treatments (**Figures 19A and 19B**).

These results demonstrate the anti-cancer effect of all the repurposed drugs and support the combinations tested in this study. Additionally, for all the drug pairs tested, certain concentrations significantly increased the anti-cancer effect compared to both drugs alone. Here, better drug combination pairs were identified for OVCAR8 PTX R P cells characterized by a double resistance profile (Carboplatin and Paclitaxel).

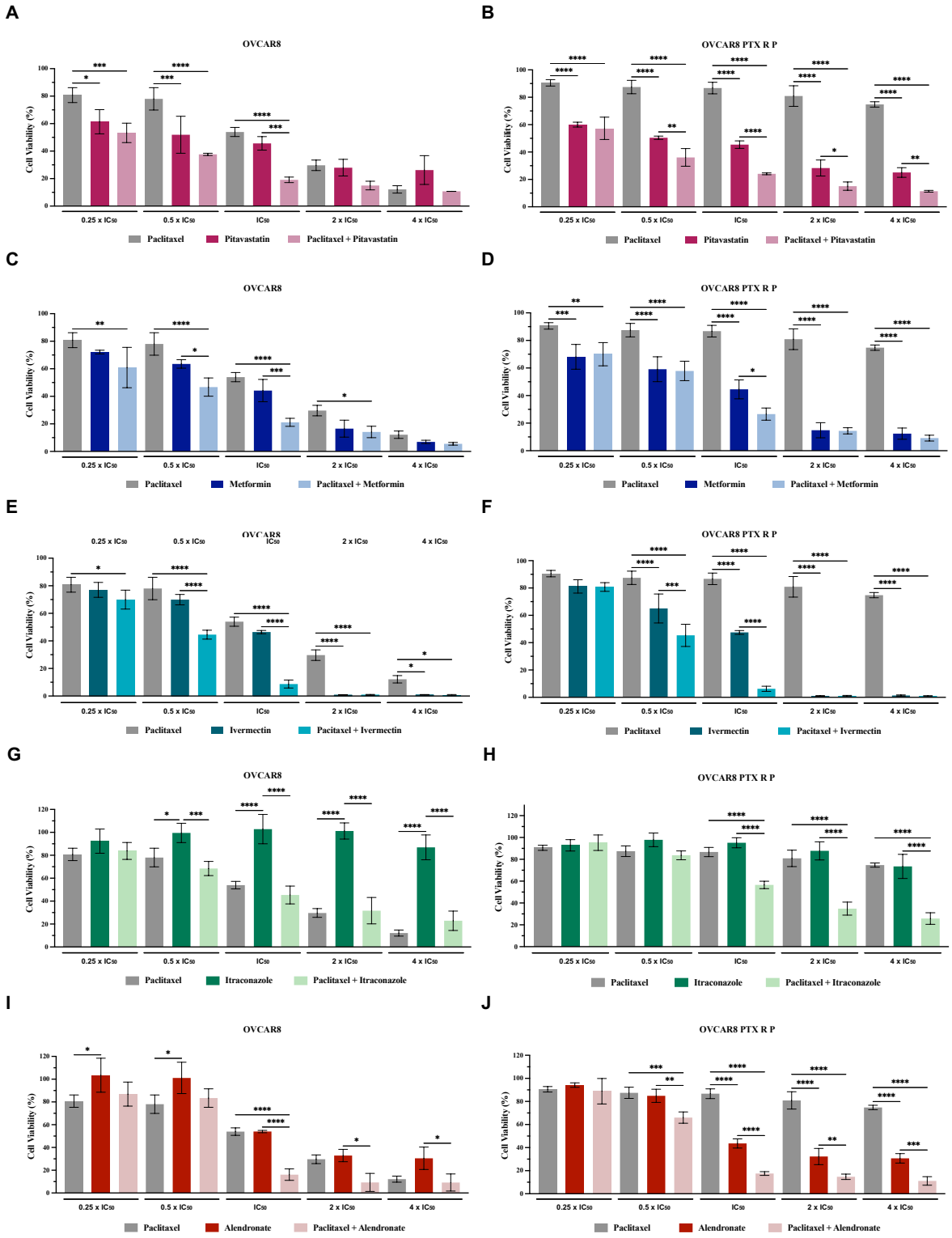


Figure 18. Repurposed drugs have been found to enhance the effectiveness of Paclitaxel in reducing the cellular viability of chemoresistant HGSC cells. (A–J) Bar charts showing cell viability of OVCAR8 and OVCAR8 PTX R P cells obtained by PB assay after exposure to a fixed-dose ratio that corresponds to 0.25, 0.5, 1, 2, and 4 times the individual IC_{50} values of each following drugs for 48 hours: Paclitaxel combined with (**A** and

B) Pitavastatin, (**C** and **D**) Metformin, (**E** and **F**) Ivermectin, (**G** and **H**) Itraconazole and (**I** and **J**) Alendronate. The combined treatment was co-administered at the same time. All assays were performed in triplicate in at least three independent experiments. Data are expressed as mean ± SD. They are plotted using GraphPad Prism Software Inc. v6. Statistical analysis was performed using ordinary one-way ANOVA followed by Šıdák's multiple comparison test (**A**–**J**), and values of *< 0.05; **< 0.001; *** <0.005; ****< 0.0001 were considered statistically significant. HGCS, high-grade serous carcinoma, PB, presto blue, SD, standard deviation.

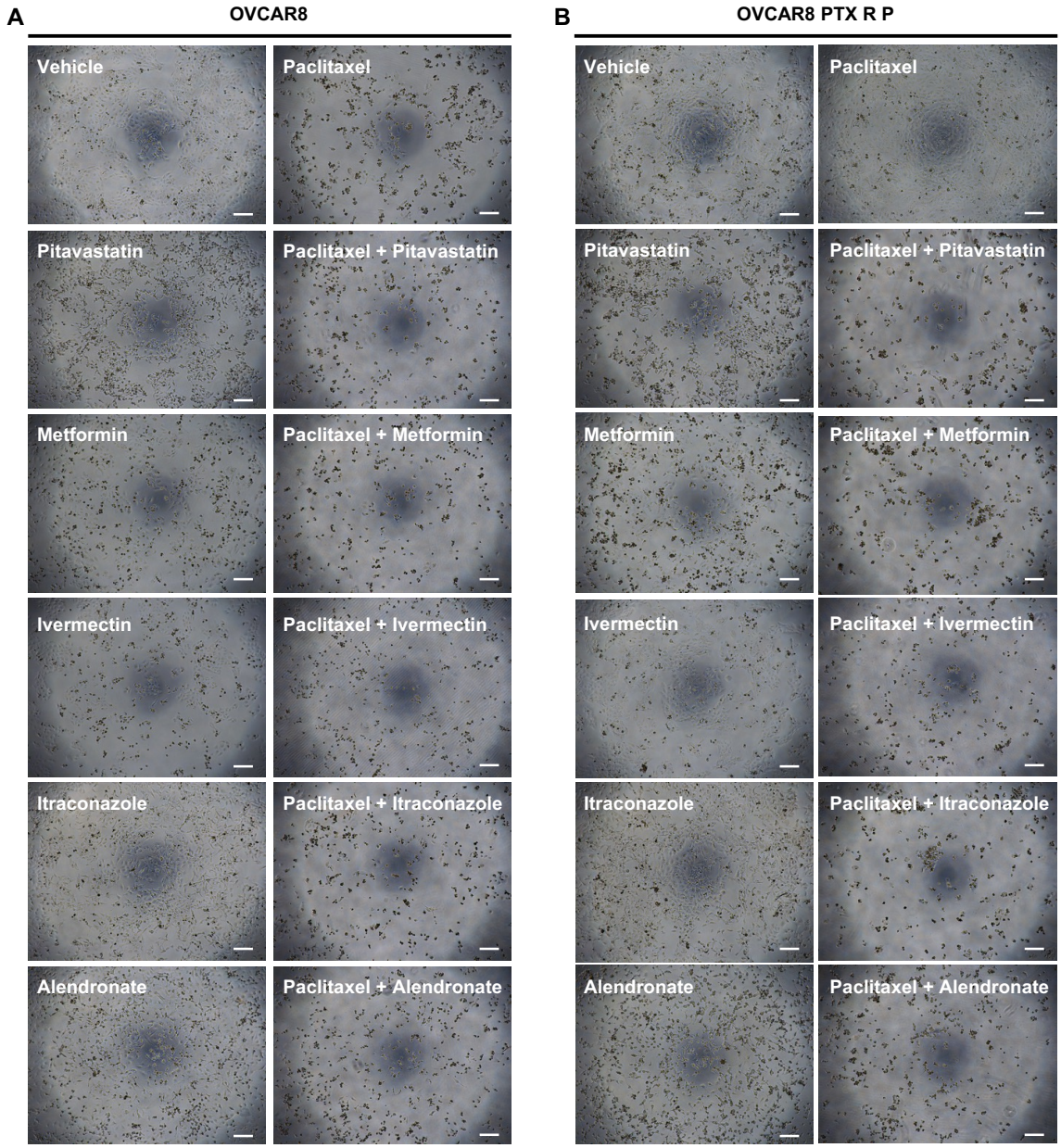


Figure 19. Representative microscopy images of (A) OVCAR8 and (B) OVCAR8 PTX R P cells after exposure to the following treatment at their respective IC_{50} concentrations for 48 hours: vehicle, Paclitaxel, Pitavastatin, Paclitaxel + Pitavastatin, Metformin, Paclitaxel + Metformin, Ivermectin, Paclitaxel +

Ivermectin, Itraconazole, Paclitaxel + Itraconazole, Alendronate, and Paclitaxel + Alendronate. All assays were performed in triplicate in at least three independent experiments. Scale bar, 200 μm.

4.3. Combining Paclitaxel with Repurposed Drugs Has a Synergistic Effect on Chemoresistant High-Grade Serous Carcinoma Cells

The combination of drugs aims to achieve a therapeutic effect by taking advantage of the synergy between two drugs. This approach helps in reducing therapeutic doses, minimizing associated side effects, and overcoming MDR. Nevertheless, a review by Goldin and Mantel (640) described seven different definitions of synergism, while another review from Greco *et al.* (641) mentioned 13 different methods for assessing drug synergism. This shows that the evaluation of synergism may yield different outcomes based on the author.

Currently, the Chou–Talalay method is one of the most widely used in biological studies for determining drug synergism due to its simplicity, flexibility, quantitative definition, efficiency, and economy. This method is based on a unified theory that incorporates major biochemical and biophysical equations (Henderson–Hasselbach, Hill, Michaelis–Menten, and Scatchard equations) to derive the median-effect equation used to determine the CI. Supported by computer software, it has gained popularity due to its user-friendly interface. It does not require extensive knowledge of the mechanisms of action of each drug, making it mechanism-independent (636). This is beneficial as many drugs have various mechanisms that are not well understood. In contrast, others have several mechanisms of action, making it difficult to determine the contribution of each mechanism to the synergy (636).

To study how Paclitaxel interacts with previously repurposed drugs, the CI was calculated using the Chou–Talalay method. The CI values were then plotted on the y-axis as a function of Fa on the x-axis to assess drug synergism. The CI indicates synergism (<1), additivity (=1), or antagonism (>1). Fa is a parameter between 0 and 1, where 0 indicates the drug does not affect cellular viability, and 1 means the drug fully decreases cellular viability (636, 642).

When Paclitaxel was combined with Pitavastatin, it showed promising synergism, with all five pairs being synergic (CI < 1) for both chemoresistant HGSC cell lines (**Figure 20 and Table 6**). For OVCAR8 cells, the Fa values were 0.467, 0.623, 0.809, 0.850, and 0.893 for concentrations 0.25, 0.5, 1, 2, and 4 times the IC_{50} values, respectively (**Figure 20A and Table 6**). Similarly, OVCAR8 PTX R P cells showed Fa values of 0.427, 0.639,

0.759, 0.849, and 0.886 for concentrations 0.25, 0.5, 1, 2, and 4 times the IC_{50} values, respectively (**Figure 20B and Table 6**).

Combining Paclitaxel with Metformin demonstrated synergism for two pairs in OVCAR8 cells, particularly for Fa values of 0.391 and 0.789 at concentrations 0.25 and 1 times the IC_{50} values, respectively (**Figure 20A and Table 6**). Additionally, for OVCAR8 PTX R P cells, this combination revealed synergism for four synergic pairs, with Fa values of 0.300, 0.734, 0.855, and 0.908 at concentrations for 0.25, 1, 2, and 4 times the IC_{50} values, respectively (**Figure 20B and Table 6**).

When Paclitaxel was combined with Ivermectin, it showed significant synergism with two pairs for OVCAR8 cells, producing Fa values of 0.913 and 0.992 for concentrations 1 and 2 times the IC_{50} values, respectively (**Figure 20A and Table 6**). Additionally, this combination demonstrated synergism for OVCAR8 PTX R P cells, with Fa values of 0.193, 0.546, 0.938, and 0.990 for concentrations 0.25, 0.5, 1, and 2 times the IC_{50} values, respectively (**Figure 20B and Table 6**).

In contrast, the combination of Paclitaxel with Itraconazole did not result in any synergism for OVCAR8 cells, presenting a CI > 1 for all the pairs tested (**Figure 20A and Table 6**). However, for OVCAR8 PTX R P cells, this combination demonstrated synergism for four pairs with Fa values of 0.163, 0.434, 0.652, and 0.742 for concentrations 0.5, 1, 2, and 4 times the IC_{50} values, respectively (**Figure 20B and Table 6**).

The combination of Paclitaxel with Alendronate showed two synergic pairs for OVCAR8 cells, with Fa values of 0.839 and 0.907 for concentrations 1 and 2 times the IC_{50} values, respectively (**Figure 20A and Table 6**). Likewise, for OVCAR8 PTX R P cells, this combination revealed four synergic pairs with Fa values of 0.340, 0.825, 0.853, and 0.889 for concentrations 0.5, 1, 2, and 4 times the IC_{50} values, respectively (**Figure 20B and Table 6**).

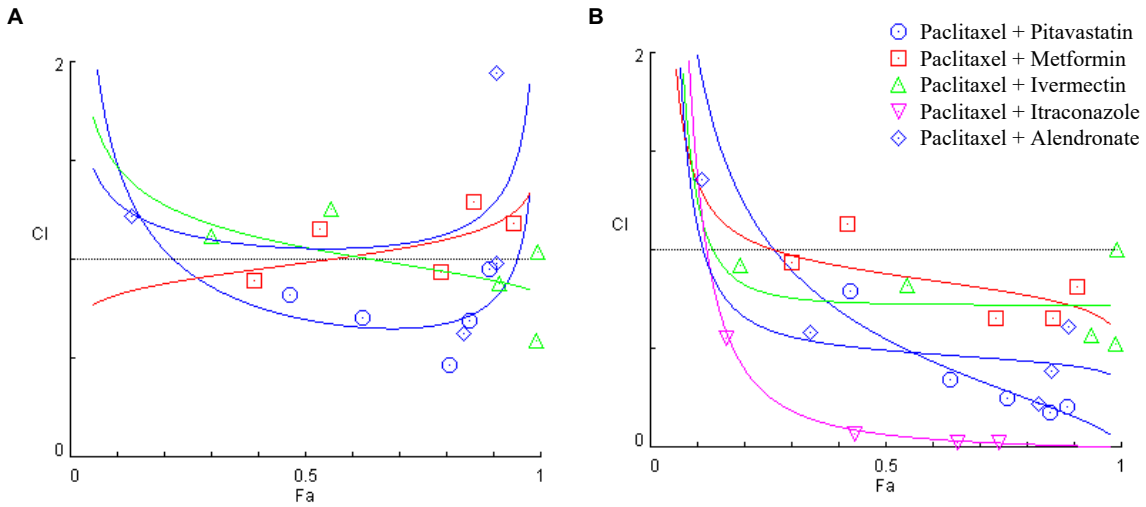


Figure 20. Combining Paclitaxel with repurposed drugs has a synergistic effect on chemoresistant HGSC cells. (**A** and **B**) The Chou–Talalay method Fa-CI plot shows drug synergism of (**A**) OVCAR8 and (**B**) OVCAR8 PTX R P cells after exposure to a fixed-dose ratio corresponding to 0.25, 0.5, 1, 2 and 4 times the individual IC_{50} values each following drug for 48 hours: Paclitaxel combined with Pitavastatin, Metformin, Ivermectin, Itraconazole and Alendronate. The combined treatment was administered simultaneously. All assays were performed in triplicate in at least three independent experiments. The CI was plotted on the y-axis as a function of Fa on the x-axis to evaluate drug synergism, where CI <1 (synergism), CI =1 (additivity), and CI >1 (antagonism).CI, combinatory index; Fa, effect level. HGCS, high-grade serous carcinoma.

Table 6. Fa values and the corresponding CI values to determine the synergistic effects of drugs on OVCAR8 and OVCAR8 PTX R P cells. Cellular viability was measured after exposure to a fixed dose-ratio equivalent to 0.25, 0.5, 1, 2, and 4 times the individual IC_{50} values of each drug for 48 hours. The combined treatment was administered simultaneously. All assays were performed in triplicates in at least three independent experiments. All assays were performed in triplicate in at least three independent experiments. CI > 1 (antagonism), CI = 1 (additivity), and CI < 1 (synergism, bold). CI, combinatory index; Fa, effect level.

				OVCAR8		OVCAR8 PTX R P	
Combination (Drug 1 + Drug 2)	**Total Dose** (Drug 1 + Drug 2)	**Dose** (Drug 1)	**Dose** (Drug 2)	**Fa**	**CI Value**	**Fa**	**CI Value**
Paclitaxel (nM) + Pitavastatin (µM)	2.7	2.5	0.2	**0.467**	**0.82421**	**0.427**	**0.79315**
	5.4	5	0.4	**0.623**	**0.70479**	**0.639**	**0.34518**
	10.8	10	0.8	**0.809**	**0.47060**	**0.759**	**0.25029**
	21.6	20	1.6	**0.850**	**0.69536**	**0.849**	**0.18051**
	43.2	40	3.2	**0.893**	**0.95039**	**0.886**	**0.20425**
Paclitaxel (nM) + Metformin (mM)	2.875	2.5	0.375	**0.391**	**0.89201**	**0.300**	**0.94013**
	5.75	5	0.750	0.533	1.15336	0.421	1.13628
	11.5	10	1.5	**0.789**	**0.93824**	**0.734**	**0.65835**
	23	20	3	0.859	1.29623	**0.855**	**0.65412**
	46	40	6	0.945	1.18166	**0.908**	**0.81439**
Paclitaxel (nM) + Ivermectin (µM)	6.25	2.5	3.75	0.300	1.12000	**0.193**	**0.92626**
	12.5	5	7.5	0.555	1.25771	**0.546**	**0.82499**
	25	10	15	**0.913**	**0.88150**	**0.938**	**0.57172**
	50	20	30	**0.992**	**0.58873**	**0.990**	**0.52306**
	100	40	60	0.994	1.04089	0.991	1.00081
Paclitaxel (nM) + Itraconazole (µM)	6.25	2.5	3.75	0.162	21.2198	0.048	6.07196
	12.5	5	7.5	0.315	62.8931	**0.163**	**0.55679**
	25	10	15	0.547	199.149	**0.434**	**0.06910**
	50	20	30	0.683	526.726	**0.652**	**0.02842**
	100	40	60	0.771	1307.81	**0.742**	**0.02802**
Paclitaxel (nM) + Alendronate (µM)	40	2.5	37.5	0.131	1.22326	0.111	1.35589
	80	5	75	0.166	2.01748	**0.340**	**0.58361**
	160	10	150	**0.839**	**0.62588**	**0.825**	**0.22371**
	320	20	300	**0.907**	**0.97858**	**0.853**	**0.38535**
	640	40	600	0.908	1.94872	**0.889**	**0.61148**

Different methods for predicting synergism can lead to different outcomes. In addition to evaluating drug interactions using the Chou-Talalay methodology, was also utilized the Bliss independence and HSA methods have different mathematical frameworks and therefore can produce slight different results (**Figures 21 and 22**) (643). The Bliss independence model assumes a stochastic method in which two drugs produce their effects independently, and the expected combined effect can be assessed based on the probability of these independent events occurring (638). The HSA method is the simplest synergy model that assumes the expected combined effect is equal to the maximum of the single-drug responses at corresponding concentrations (638). To conduct these studies, the SynergyFinder 2.0 Software allows for interactive analysis and visualization of multi-drug

combination profiling data by two different synergism evaluation methods (644). The synergy score for a drug combination is averaged over all the dose combination measurements, giving a positive (synergism) or negative (antagonism) value that can be observed in 2D and 3D synergy maps dose regions, i.e., synergistic (red) and antagonistic (green) (623).

According to the Bliss independence model, combining Paclitaxel with Pitavastatin resulted in positive synergy scores of 9.210 and 20.025 for OVCAR8 and OVCAR8 PTX R P cells, respectively, indicating additivity and synergism for each cell line (**Figures 21A and 22A**). Additionally, according to the Chou–Talalay method, the HSA model revealed that combining Paclitaxel with Pitavastatin demonstrated stronger and positive synergy scores of 16.946 and 14.399, indicating synergism for OVCAR8 and OVCAR8 PTX R P cells, respectively (**Figures 21B and 22B**).

Furthermore, combining Paclitaxel with Metformin, as per the Bliss independence model, showed positive synergy scores of 5.378 and 10.141, demonstrating additivity and synergism for OVCAR8 and OVCAR8 PTX R P cells, respectively (**Figures 21C and 22C**). Additionally, the HSA model indicated that this combination results in synergy scores of 12.861 and 7.010, suggesting synergism and additivity for OVCAR8 and OVCAR8 PTX R P cells, respectively (**Figures 21D and 22D**).

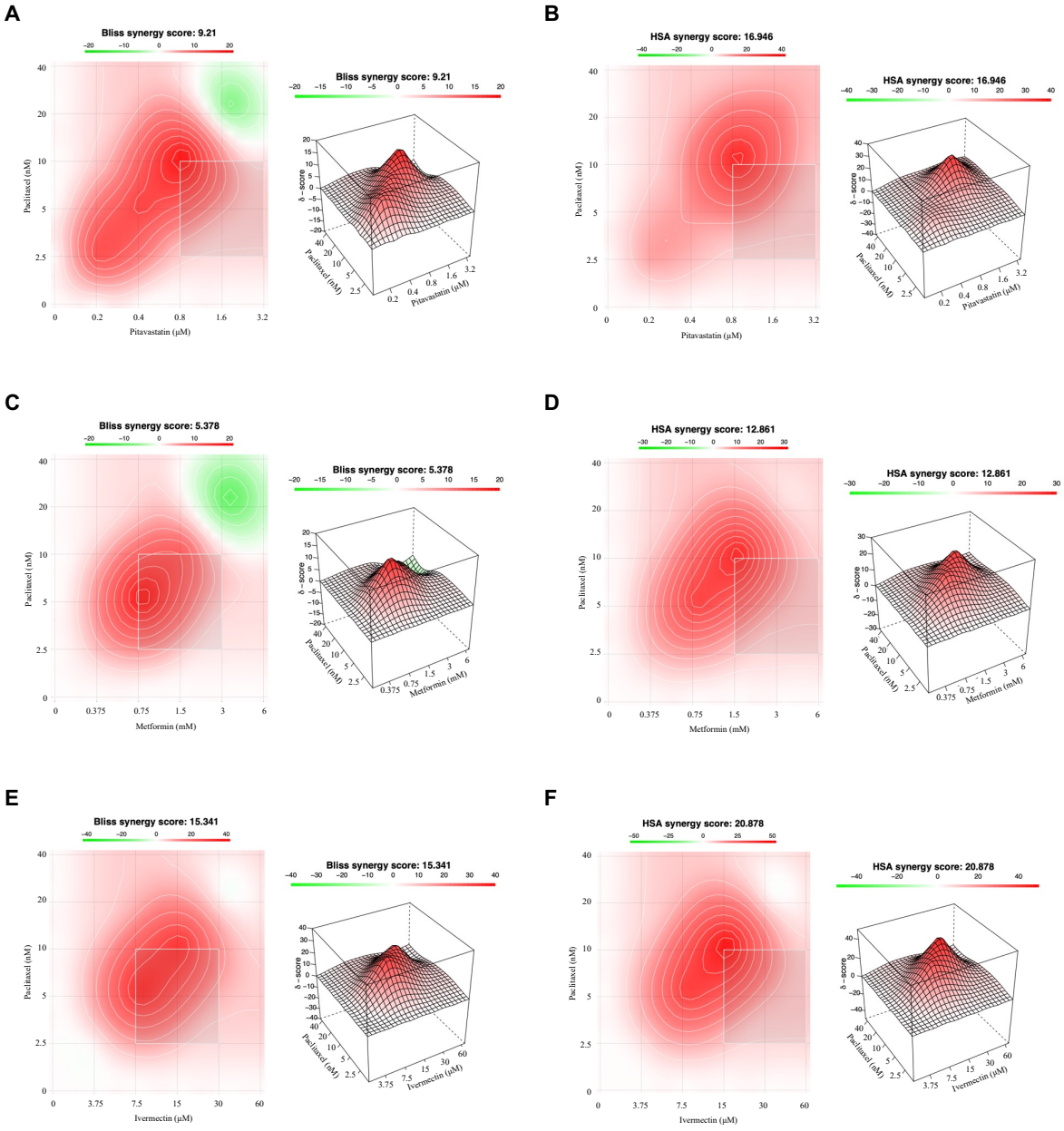
According to the Chou–Talalay method, the combination of Paclitaxel and Ivermectin resulted in strong synergism, with positive synergy scores of 15.341 and 21.791 for the Bliss independence model and 20.878 and 19.650 for the HSA model for OVCAR8 and OVCAR8 PTX R P cells, respectively (**Figures 21E, 21F, 22E, and 22F**).

When evaluated using Bliss independence and HSA models, the combination of Paclitaxel and Itraconazole demonstrated synergism, with positive scores of 11.367 and 20.982 for OVCAR7 and 5.889 and 18.762 for OVCAR8 PTX R P cells (**Figures 21G, 21H, 22G, and 22H**).

Additionally, the Bliss independent model showed that the combination of Paclitaxel and Alendronate resulted in positive synergy scores of 4.865 and 13.108 for OVCAR8 and OVCAR8 PTX R P cells, respectively, suggesting additivity and synergy (**Figures 21I and 22I).** The HSA model revealed positive synergy scores of 12.377 and 16.121 for OVCAR8 and OVCAR8 PTX R P cells, respectively, indicating synergism for this combination (**Figures 21J and 22J**).

Our results indicate that different synergy evaluation models can produce differing results. However, for all the drug combinations tested, the three methods demonstrated at least one pair of concentrations with synergic behavior. As such, the findings indicate that

combining Paclitaxel with Pitavastatin or Ivermectin represents the most promising drug pair combinations for chemoresistant HGSC cell lines.



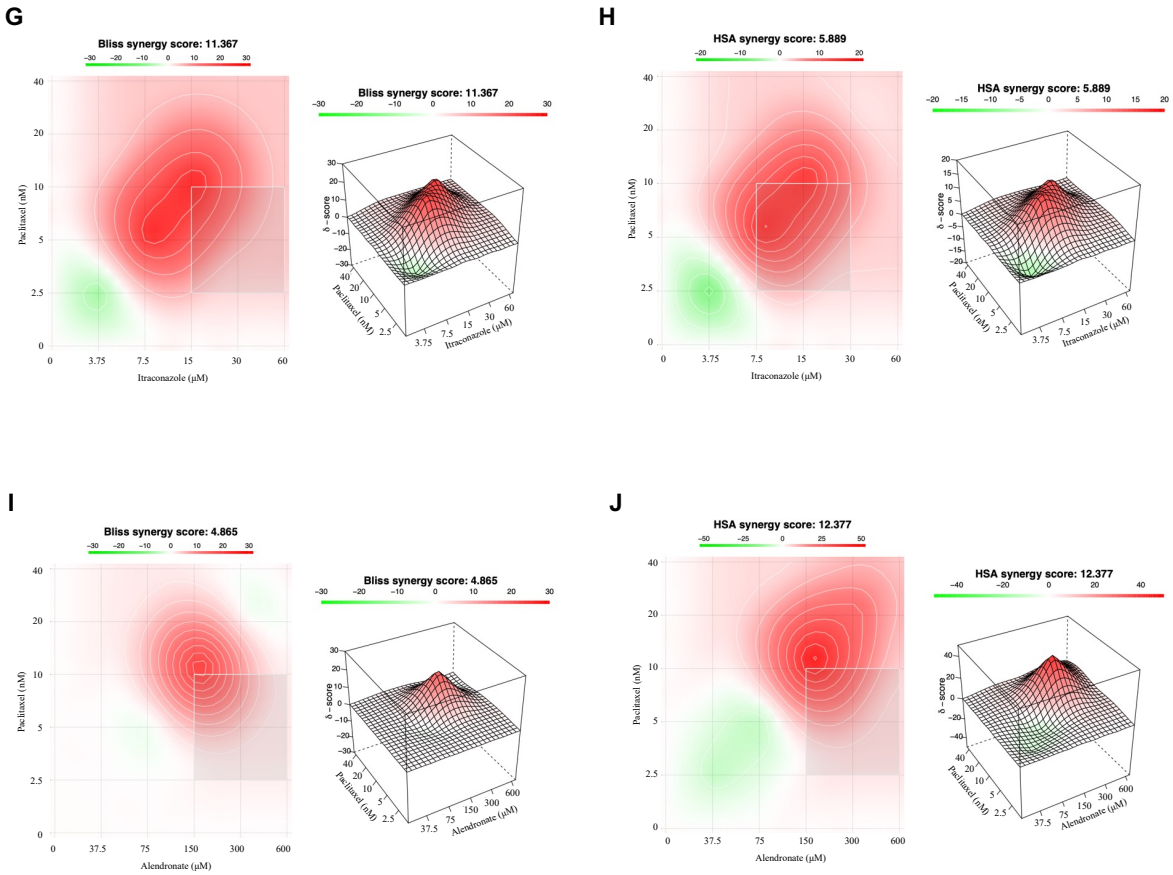
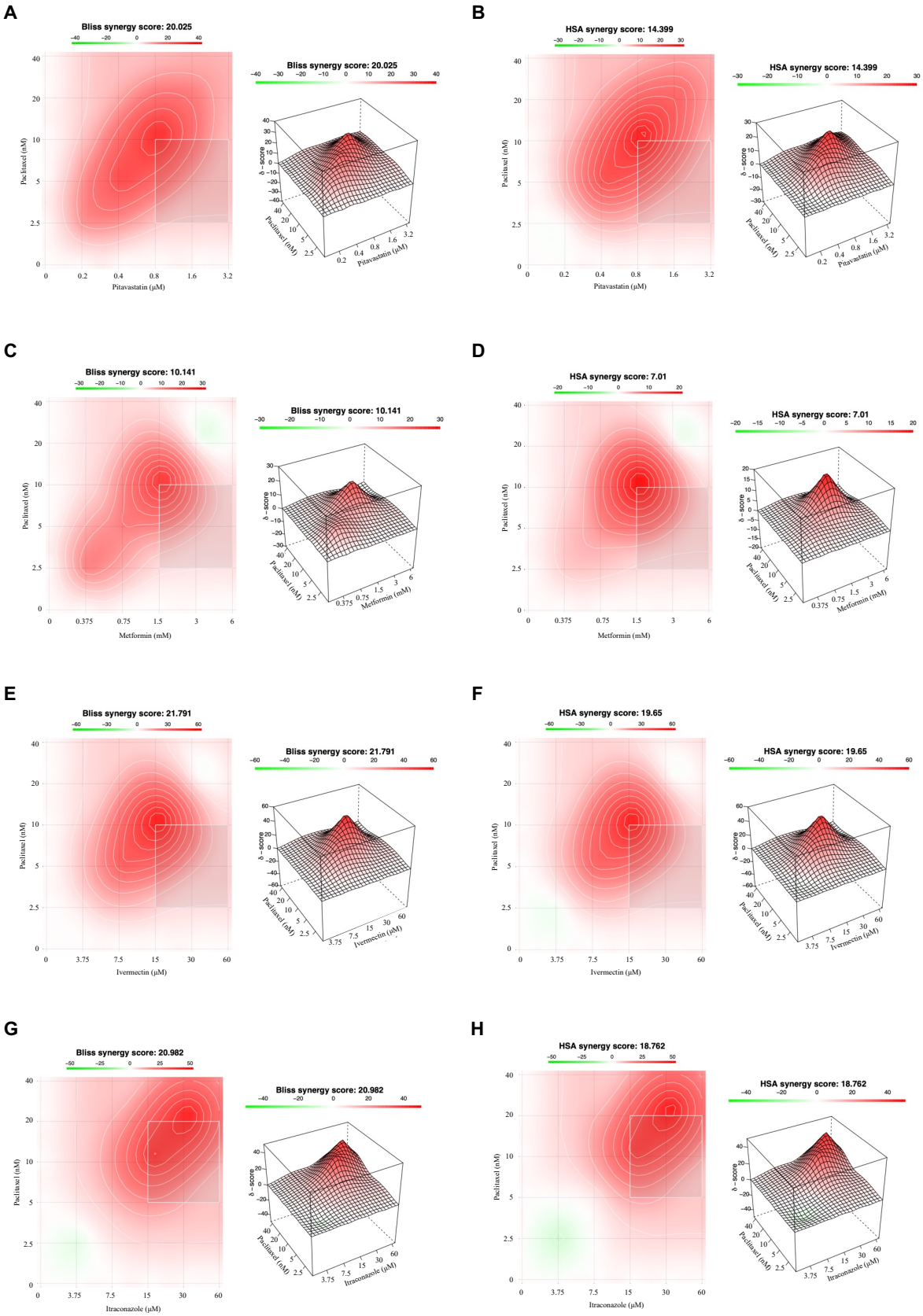


Figure 21. Combining Paclitaxel with repurposed drugs demonstrates a synergistic effect on OVCAR8 cells. (**A**–**J**) The drug synergism of OVCAR8 cells was observed through 2D and 3D plots representing Bliss independence and HSA synergy after exposure to a fixed-dose ratio equivalent to 0.25, 0.5, 1, 2, and 4 times the individual IC_{50} values for each following drug for 48 hours: Paclitaxel combined with (**A** and **B**) Pitavastatin, (**C** and **D**) Metformin, (**E** and **F**) Ivermectin, (**G** and **H**) Itraconazole and (**I** and **J**) Alendronate. The combined treatment was administered stimulatingly. All assays were performed in triplicate in at least three independent experiments. The synergy scores were categorized as follows: <−10 (antagonism, green), −10 to 10 (additivity, white), and >10 (synergism, red). HSA, high single agent.


A
Bliss synergy score: 20.025
Paclitaxel (nM)
Pitavastatin (μM)
δ – score
B
HSA synergy score: 14.399
C
Bliss synergy score: 10.141
Metformin (mM)
D
HSA synergy score: 7.01
E
Bliss synergy score: 21.791
Ivermectin (μM)
F
HSA synergy score: 19.65
G
Bliss synergy score: 20.982
Itraconazole (μM)
H
HSA synergy score: 18.762

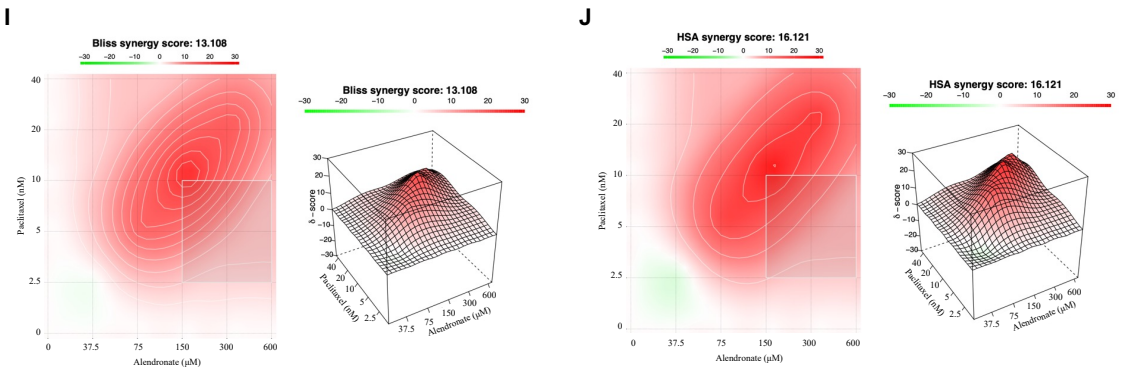


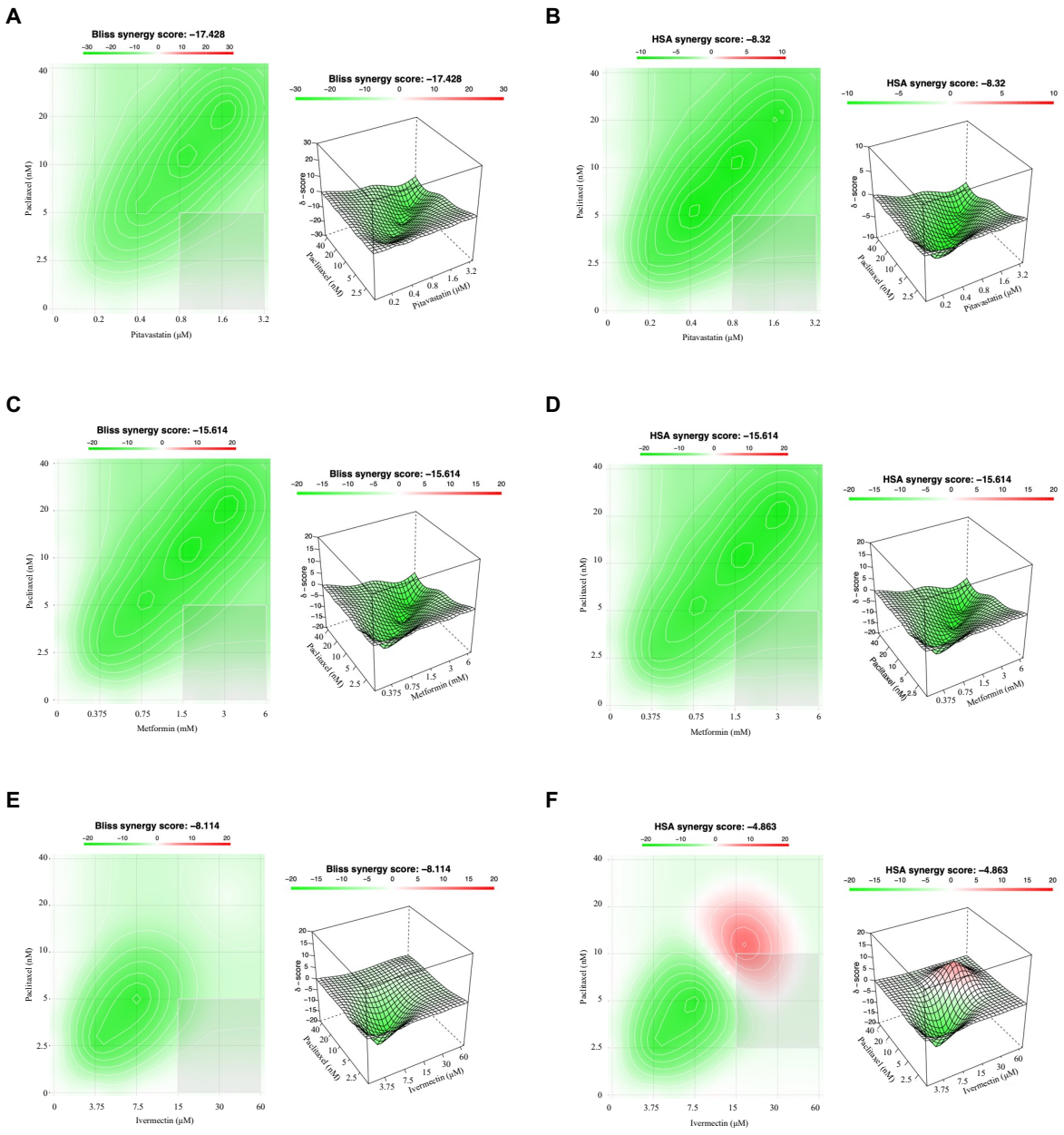
Figure 22. Combining Paclitaxel with repurposed drugs demonstrates a synergistic effect on OVCAR8 PTX R P cells. (**A**–**J**) The drug synergism of OVCAR8 cells was observed through 2D and 3D plots representing Bliss independence and HSA synergy after exposure to a fixed-dose ratio equivalent to 0.25, 0.5, 1, 2, and 4 times the individual IC_{50} values for each following drug for 48 hours: Paclitaxel combined with (**A** and **B**) Pitavastatin, (**C** and **D**) Metformin, (**E** and **F**) Ivermectin, (**G** and **H**) Itraconazole and (**I** and **J**) Alendronate. The combined treatment was administered stimulatingly. All assays were performed in triplicate in at least three independent experiments. The synergy scores were categorized as follows: <−10 (antagonism, green), −10 to 10 (additivity, white), and >10 (synergism, red). HSA, high single agent.

This study also assessed the interaction between Paclitaxel and repurposed drugs in HOSE6.3 (a non-tumoral cell line) using the Chou–Talalay, Bliss independence, and HSA models. The findings using the Chou–Talalay model indicated antagonism (CI > 1) for all the five combinations of Paclitaxel with Pitavastatin, Metformin, Ivermectin, Itraconazole, and Alendronate in HOSE6.3 cells (**Figure S6, Tables S5 and S6**). Additionally, according to the Chou–Talalay method, the Bliss independence and HSA models also showed a stronger and negative synergy score, suggesting antagonism for HOSE6.3 cells (**Figure 23**).

These results indicate an acceptable safety profile for the tested combination regiments in non-tumoral HOSE6.3 cells and support the potential use of the tested repurposed drugs in combination with Paclitaxel in HGSC patients.

We found that the results obtained by the Bliss independence and HSA reference models were similar to those obtained by the Chou–Talalay method for OVCAR8, OVCAR8 PTX R P, and HOSE6.3 cell lines demonstrating that these reference models yield comparable outcomes. However, these reference models have limitations (643), including the requirement for ideal dose-effect curves for single drugs, the need for a large amount of data for precise synergy analysis, and difficulties in evaluating synergism in clinical trials due to practical and ethical constraints. Furthermore, determining the optimal dose ratio for

synergy and the inadequacy of some reference models for drug combinations of more than two drugs are also challenges to be addressed.



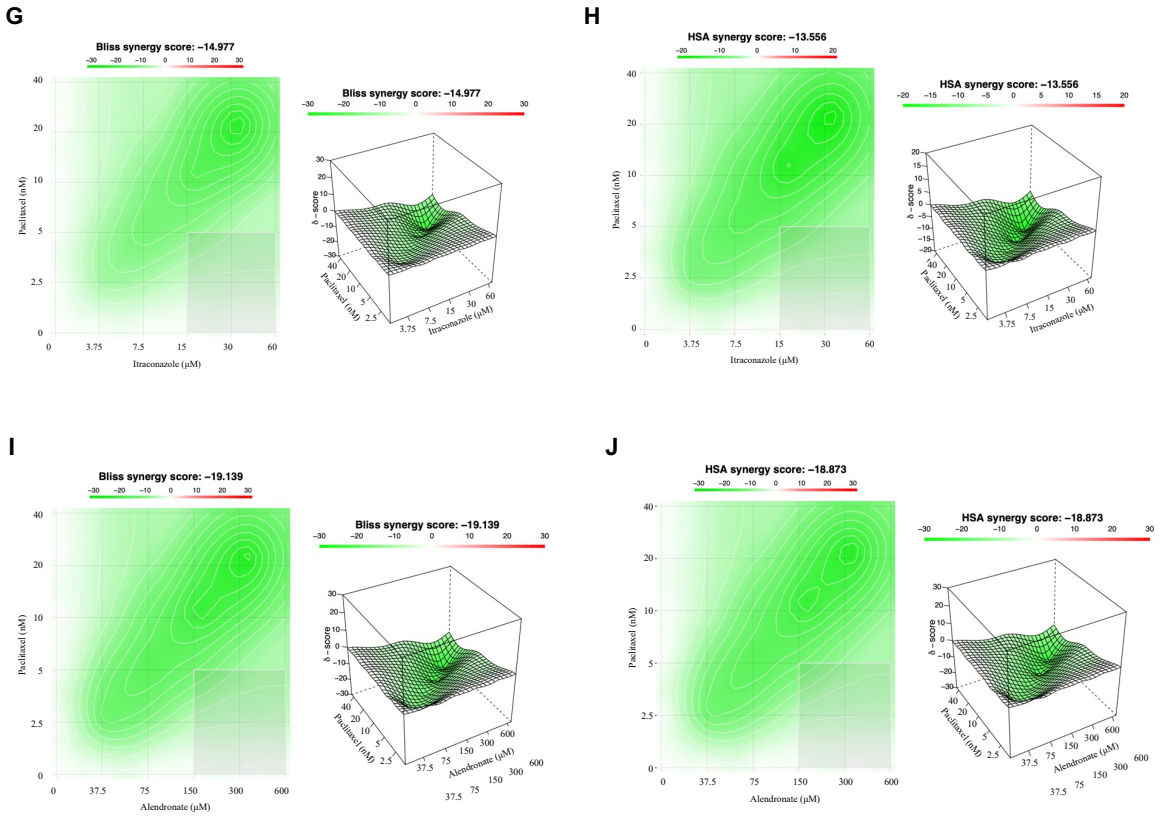


Figure 23. Combining Paclitaxel with repurposed drugs demonstrates an antagonistic effect on HOSE6.3 cells. (**A**–**J**) The drug synergism of HOSE6.3 cells was observed through 2D and 3D plots representing Bliss independence and HSA synergy after exposure to a fixed-dose ratio equivalent to 0.25, 0.5, 1, 2, and 4 times the individual IC_{50} values for each following drug for 48 hours: Paclitaxel combined with (**A** and **B**) Pitavastatin, (**C** and **D**) Metformin, (**E** and **F**) Ivermectin, (**G** and **H**) Itraconazole and (**I** and **J**) Alendronate. The combined treatment was administered stimulatingly. All assays were performed in triplicate in at least three independent experiments. The synergy scores were categorized as follows: <−10 (antagonism, green), −10 to 10 (additivity, white), and >10 (synergism, red). HSA, high single agent.

5. Discussion

Monotherapy systems are not enough for treating chemoresistant HGSC patients. Combining two or more antineoplastic drugs is a more suitable strategy, as it has shown improved treatment efficacy (614, 645) and a synergistic effect in inhibiting tumor growth (646). The goal of combining drugs is to maximize effectiveness using lower drug concentrations to minimize the lowest amount of toxicity and side effects for normal cells (647). Combinatory regiments usually involve a sensitizing agent and another drug that takes advantage of the vulnerable state, increasing its cytotoxic effect (614, 644). In advanced HGSC, combinatory regimens often include the simultaneous administration of Carboplatin and Paclitaxel as the first-line treatment (21, 648, 649). These drugs have

different mechanisms of action, which enhance their cytotoxic effect when combined (650). Carboplatin binds to DNA, causing DNA cross-linking and inhibiting DNA synthesis, protein synthesis, and cell proliferation (651, 652). Paclitaxel targets β-tubulin, blocking cells in phases G_0/G_1 and G_2/M, resulting in tumor cell death (600). However, the therapeutical response rate is still low when these drugs are combined, leading to severe side effects and chemoresistance (653, 654). Therefore, new models of drug combinations are urgently needed to decrease the chemotherapeutic dosage and exposure time to overcome chemoresistance. Combining antineoplastic agents with repurposing drugs could be a promising approach, as it increases therapeutic efficacy by targeting multiple signaling pathways in a synergistic or additive manner (614, 644, 655, 656).

Paclitaxel is a well-recognized antineoplastic agent used in the management of OC. In a previous study, the anti-tumor activity of this antimitotic agent in OVCAR8 and OVCAR8 PTX R P cell lines was analyzed (628). Many studies have been conducted in search of new drugs that can work together with antineoplastic drugs. Still, few reports have been done using repurposing drugs with Paclitaxel for HGSC (657). In a recent study, Hirst *et al.* demonstrated that Licofelone, an analgesic and anti-inflammatory agent, enhances the effectiveness of Paclitaxel in OC by reversing chemoresistance and tumor stem-like properties (657). Another study indicated that CEP-1347 and AS602801, which target survivin expression, make OC cells more responsive to Carboplatin and Paclitaxel treatment (658, 659). In other tumoral contexts, there have been reports of combining Paclitaxel with different repurposing agents. For example, Duarte *et al.* found that antimalarial drugs, such as Chloroquine, Artesunate, and Mefloquine, can act synergistically with Paclitaxel in breast cancer therapy (623, 624). More recently, Branco *et al.* demonstrated that Pirfenidone, an antifibrotic drug, can enhance the sensitivity of non-small cell lung cancer cells to Paclitaxel (660).

Pre-clinical and retrospective studies suggest that statins, which are inhibitors of 3-hydroxy-3-methylglutaryl-coenzyme A reductase (HMGCR) used to treat cardiovascular diseases, may have anti-cancer activity in various types of tumors, including OC (661-664). De Wolf *et al.* showed that Pitavastatin, a long half-life lipophilic statin, inhibits the growth of OC cell lines with a Carboplatin-resistant profile. This suggests great potential for treating chemoresistant tumors (630). In OC, experimental evidence indicates that Metformin, widely used in the treatment of type 2 diabetes due to its ability to induce anti-hyperglycemia, enhances the effectivity of chemotherapeutic agents such as platinum and taxane compounds and reverses chemoresistance states (631, 665-669). Ivermectin, a broad-

spectrum antiparasitic agent, has been shown to improve the anti-cancer effects of chemotherapeutic drugs and, in some cases, can reverse chemoresistance (670-672). Experimental and clinical data suggest that combining Itraconazole, a broad-spectrum antifungal agent, with other chemotherapeutic drugs can be effective in treating various types of cancers, increasing drug efficacy (613, 673-675), and reversing Paclitaxel chemoresistance (633, 676-678). Studies also suggest that bisphosphonates such as Alendronate and Zoledronic Acid, which are potent inhibitors of bone resorption used for the treatment and prevention of osteoporosis, exhibit antineoplastic properties and can delay cancer recurrences when combined with neoplastic agents (679-681). Previous research indicates the anti-cancer potential of these drugs for cancer management.

To the best of our knowledge, this is a unique study that explores the potential synergic effect of combining Paclitaxel with Pitavastatin, Metformin, Ivermectin, Itraconazole, and Alendronate in chemoresistant HGSC. Here, was aimed to investigate the potential anti-cancer effects of these five repurposed drugs on two chemoresistant HGSC cell lines: OVCAR8 (Carboplatin-resistant) and OVCAR8 PTX R P (Carboplatin and Paclitaxel-resistant). Also, it was aimed to assess any possible synergistic effects when these drugs are combined with Paclitaxel. All the drugs were tested at various concentrations to determine their IC_{50} values and evaluate their potential as repurposed drugs in HGSC management. The results demonstrate that all repurposed drugs used as single agents showed some antitumor activity by decreasing cellular viability in a concentration-dependent manner in both chemoresistant HGSC cell lines. All five drugs were selected for combination with Paclitaxel, and cells were treated with different concentrations of 0.25, 0.5, 1, 2, and 4 times the IC_{50} of each drug, alone and in combination with Paclitaxel, using a combination model previously described by Duarte and Vale (624). Here, was compared the anti-tumor effect of combining Paclitaxel with Pitavastatin, Metformin, Ivermectin, Itraconazole, or Alendronate to Paclitaxel alone for OVCAR8 and OVCAR8 PTX R P cells. In this study, it was found that Pitavastatin and Ivermectin were the most promising candidates to enhance the effectiveness of Paclitaxel in both chemoresistant HGSC cell lines. Additionally, the cell morphology was analyzed after each treatment, and the observer cell phenotype aligned with PB assays. Furthermore, it was assessed synergism using three different methods: Chou–Talalay, Bliss independence, and HSA models. The Chou–Talalay method is based on the median-effect equation, which is derived from the mass-action law principle. It encompasses the Michaelis–Menten, Hill, Henderson–Hasselbach, and Scatchard equations in biochemistry and biophysics. In drug combinations,

this method provides a quantitative definition of additive (CI = 1), synergic (CI < 1), and antagonistic (CI > 1) effects (636, 642). According to the Bliss independence method, when two drugs produce independent effects, the expected combination effect can be calculated based on the probability of independent events (623, 638, 682). Furthermore, the HSA model states that the predicted combination effect is the highest effect achieved by one of the two drugs (i.e., the more effective drug) (623, 682).

Our analysis showed that all tested repurposed drugs can synergistically decrease cellular viability when combined with Paclitaxel. Pitavastatin and Ivermectin show the most promise at lower concentrations for OVCAR8 and OVCAR8 PTX R P cells. Here, it was found that there are more synergistic combinations for OVCAR8 PTX R P compared to OVCAR8 cells, with almost all combinations resulting in synergistic pairs at the lowest concentrations. Despite this, the results of single-drug treatments with repurposed drugs in OVCAR8 (which is only Carboplatin-resistant) are encouraging and suggest the potential effectiveness of these drugs in a platinum-resistant scenario.

Pitavastatin was found to be the most effective repurposed drug, displaying the lowest IC_{50} values. When combined with Paclitaxel for OVCAR8 and OVCAR8 PTX R P cells, it resulted in four and five synergistic pairs, respectively. The results indicate that the dominant behavior of drug combination comes from Pitavastatin, and the mechanism of these combinations may be related to this class of drug.

As an anticancer agent, Statins inhibit HMGCR, thereby blocking cholesterol biosynthetic pathways (662, 664, 683). Martirosyan *et al.* demonstrated that Lovastatin triggers apoptosis of OC cells as a single agent by blocking HMGCR activity and sensitizing chemoresistant cells to Doxorubicin by blocking drug efflux pumps (661). Furthermore, results from the literature indicate that Pitavastatin is not a substrate of P-gp, unlike other statins such as Simvastatin, Lovastatin, and Atorvastatin (684). We hypothesize that the synergic effect of combining Pitavastatin with Paclitaxel occurs through a similar mechanism; however, further studies are required to elucidate the mechanism behind the observed results.

In terms of pharmacotherapy, the ideal drug selectively kills neoplastic cells while minimizing adverse effects on normal cells. Here, the collateral effects of these drugs were tested in a normal-like cell line. Pitavastatin showed no efficacy in reducing the cellular viability of HOSE6.3, indicating that it is non-toxic to normal cells.

Many mechanisms of Metformin's anti-cancer activity have been proposed, including its ability to modulate immunological and anti-inflammatory responses, inhibit mTOR, and

block insulin signals and glucose synthesis through respiratory-chain complex I blockade (683, 685-688). The findings align with Lengyel *et al.* demonstrated that Metformin inhibits OC growth and increases sensitivity to Paclitaxel (665). However, the experiments indicate that a higher concentration of Metformin (mM) is required to achieve an effect, which may pose challenges in translating these results to clinical applications.

Ivermectin's anti-cancer activity can be explained through various mechanisms, including the inhibition of MDR, modulation of Akt/mTOR, and Wnt/TCF signaling pathways, as well as the inactivation of PAK-1 expression (632, 689-694). The results obtained with Ivermectin are in accordance with the ones obtained by Kodama *et al.,* which showed that Ivermectin has an anti-tumoral effect on its own and in combination with Paclitaxel, producing a synergistic effect versus each drug alone in OC (670). Additionally, Ivermectin enhances the inhibitory effect of Cisplatin by suppressing the phosphorylation of key molecules in the Akt/mTOR signaling pathway (671). Furthermore, Ivermectin has been reported to reverse chemoresistance in colorectal, breast, and chronic myeloid leukemia cancer cells by inhibiting the EGFR/ERK/Akt/NF-κB pathway (672). The combination of Paclitaxel and Ivermectin exhibited a significant anti-neoplastic effect even when treated with a half IC_{50} dose of each drug in two chemoresistant cell lines.

Itraconazole targets different oncobiology mechanisms, including reversing chemoresistance mediated by P-gp, inhibiting Hedgehog, mTOR, and Wnt/β-catenin signaling pathways, and reducing angiogenesis and lymphangiogenesis (673, 695-699). Choi *et al.* demonstrated a synergistic effect when combining Itraconazole with Paclitaxel, thereby enhancing efficacy in xenograft and patient-derived xenograft models derived from OC chemoresistant patients (633). Both preclinical and clinical trial data suggest that Itraconazole is capable of reversing Paclitaxel chemoresistance (676, 700, 701). However, in this study, was did not obtain a stable IC_{50} value for Itraconazole, making it invaluable for drawing feasible conclusions for its use in combination studies.

Bisphosphonates block farnesyl pyrophosphate synthase, which is located downstream of HMGCR. This leads to the impairment of cholesterol biosynthesis (702). When combined with chemotherapeutic agents to inhibit tumor proliferation and dissemination, bisphosphonates exhibit anti-metastatic and anti-tumoral properties (680, 681, 703). Experimental evidence suggests that Alendronate reduces stromal invasion, tumor burden, and MA, indicating an anti-tumoral effect in OC (634). The findings align with those of Knight *et al.,* who demonstrated the direct activity of bisphosphonates (Alendronate, Clodronate, and Zoledronic Acid) in five OC cell lines and tumor-derived cells. However, when combined

with cytotoxic agents such as Cisplatin and Paclitaxel, they do not substantially increase the activity of the chemotherapeutic agents (704).

P-gp, also known as MDR, acts as a transmembrane efflux pump, preventing the uptake of various compounds, including certain chemotherapy drugs (705). OE of P-gp is a major factor in developing resistance to chemotherapeutic agents like Paclitaxel (577, 578). In a previous study, it was demonstrated that OVCAR8 PTX R P cells had high levels of P-gp, leading to the efflux of Paclitaxel from the cells (628). According to existing literature, drugs like Metformin, Ivermectin, and Itraconazole may reverse chemoresistance caused by P-gp OE (706-711). These drugs are able to inhibit P-gp function, leading to an accumulation of drugs within the cells and enhancing the efficacy of chemotherapy drugs. We hypothesize that these drugs could improve the effectiveness of antineoplastic drugs, but further research is needed to understand their anticancer mechanisms in different combinations.

6. Conclusion

Drug repurposing approaches, either alone or when combined with Paclitaxel, could help reduce chemoresistance and improve treatment outcomes. Combining antineoplastic agents and repurposed drugs with independent mechanisms of action may be a promising strategy, as it can suppress different chemoresistance mechanisms/pathways. This study shows promising results regarding the potential effect of repurposed drugs as chemosensitizer compounds to enhance Paclitaxel's cytotoxic effects. To the best of our knowledge, this is the first study demonstrating that Pitavastatin and Ivermectin, alone and in combination with Paclitaxel, are viable as a therapeutic approach that can be used for chemoresistant HGSC patients. Since both drugs are clinically available, their use in anti-cancer treatment is feasible. Although pharmacological studies show that the most important results are the effect of combining drugs at lower concentrations, deeper mechanistic studies are recommended to evaluate the anticancer mechanisms underlying these drugs and these combinatory regimens.

In vitro studies using cell line models provide a simple and fast way to screen and identify new candidates for drug repurposing. However, since each patient has specific phenotypic characteristics, genotypic status, and distinctive chemoresistance patterns, further investigations using *ex vivo* models are necessary. For example, using cancer cells obtained from MA drained from HGSC patients.

Our results support further research into using Pitavastatin and Ivermectin as chemosensitizing agents for Paclitaxel resistance. This strategy is especially valuable for

patients who have developed pharmacological resistance to conventional treatment and have been diagnosed with tumors with reduced therapeutical options, such as HGSC.

7. Acknowledgments and Funding

This work was developed at *Instituto de Investigação e Inovação em Saúde (i3S)*, an Associate Laboratory of the *Ministério da Ciência, Tecnologia e Inovação (MCTES),* and it was partially supported by *Fundação para a Ciência e a Tecnologia (FCT).* This research was supported by *Fundo Europeu de Desenvolvimento Regional (FEDER) through the COMPETE 2020–Operational Program for Competitiveness and Internationalization (POCI), Portugal 2020* and *FCT/MCTES*, under the project POCI 01-0145-FEDER-029503 (PTDC/MEC-ONC/29503/2017). M.N. and D.D. acknowledge *FCT/MCTES* and *UE* for financial support through a Ph.D. fellowship (2020.04720.BD and SFRH/BD/140734/2018, respectively) that was co-sponsored by *Fundo Social Europeu (FSE)* through *Programa Operacional Regional Norte (Norte 2020)*. N.V. thankful for the support from *FCT* and *FEDER* award number IF/00092/2014/CP1255/CT0004 and CHAIR in Onco-Innovation from *Faculdade de Medicina da Universidade do Porto (FMUP).*

8. Supplementary Material

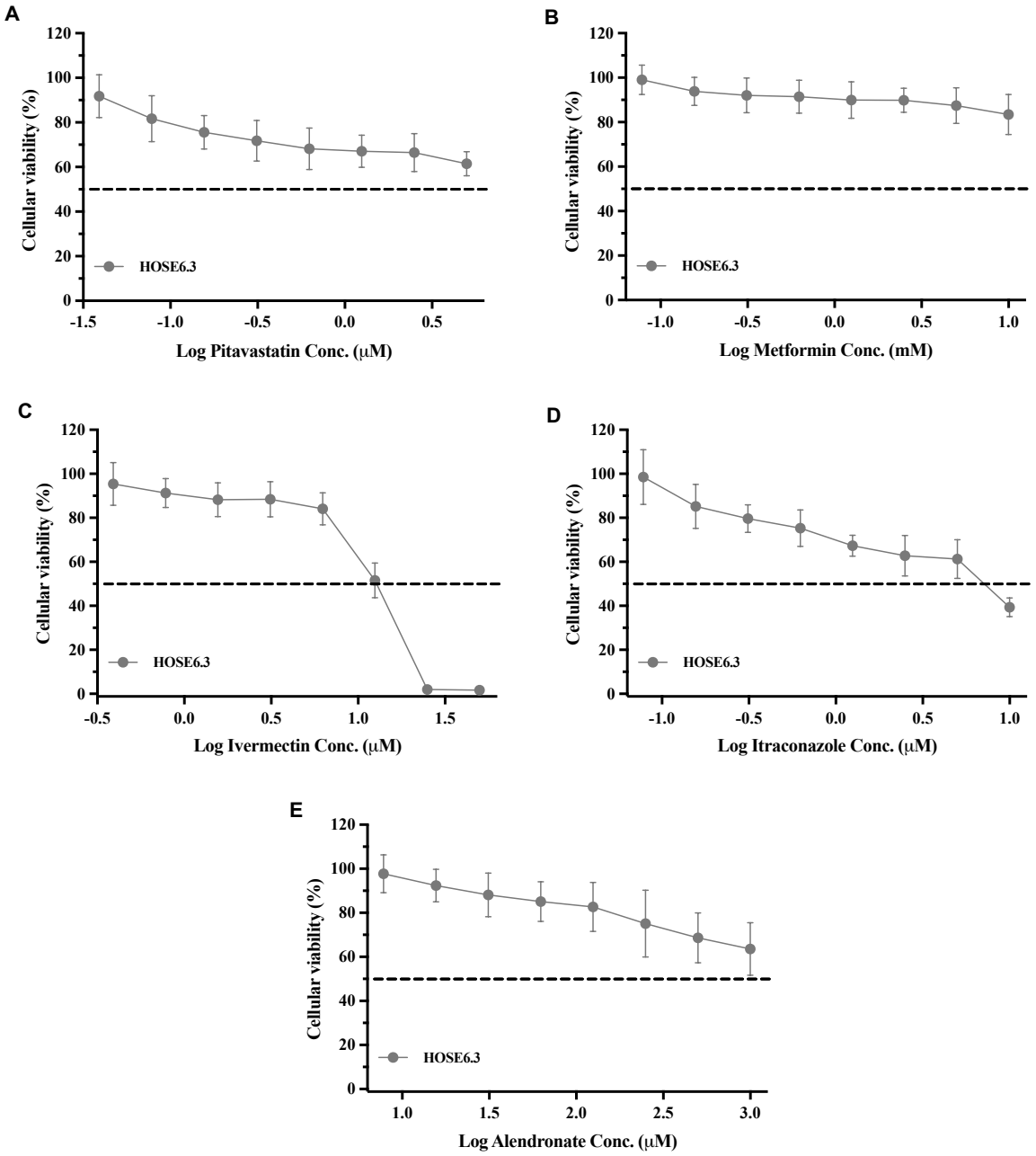


Figure S4. **Repurposed drugs demonstrate low efficacy in reducing the cellular viability of HOSE6.3 cells.** (A – E) Dose-response curves for HOSE6.3 cells, obtained by PB assay after exposure to increasing concentrations of the following drugs for 48 hours: (A) Pitavastatin (0.04 to 5 μM), (B) Metformin (0.08 to 10 mM), (C) Ivermectin (0.39 to 50 μM), (D) Itraconazole (0.39 to 50 μM) and (E) Alendronate (7.81 to 1000 μM). The dotted line in each dose-response curve represents IC_{50} values. All assays were performed in triplicates in at least three independent experiments. The data are expressed as mean ± SD and plotted using GraphPad Prism Software Inc. v8. PB, presto blue; SD, standard deviation.

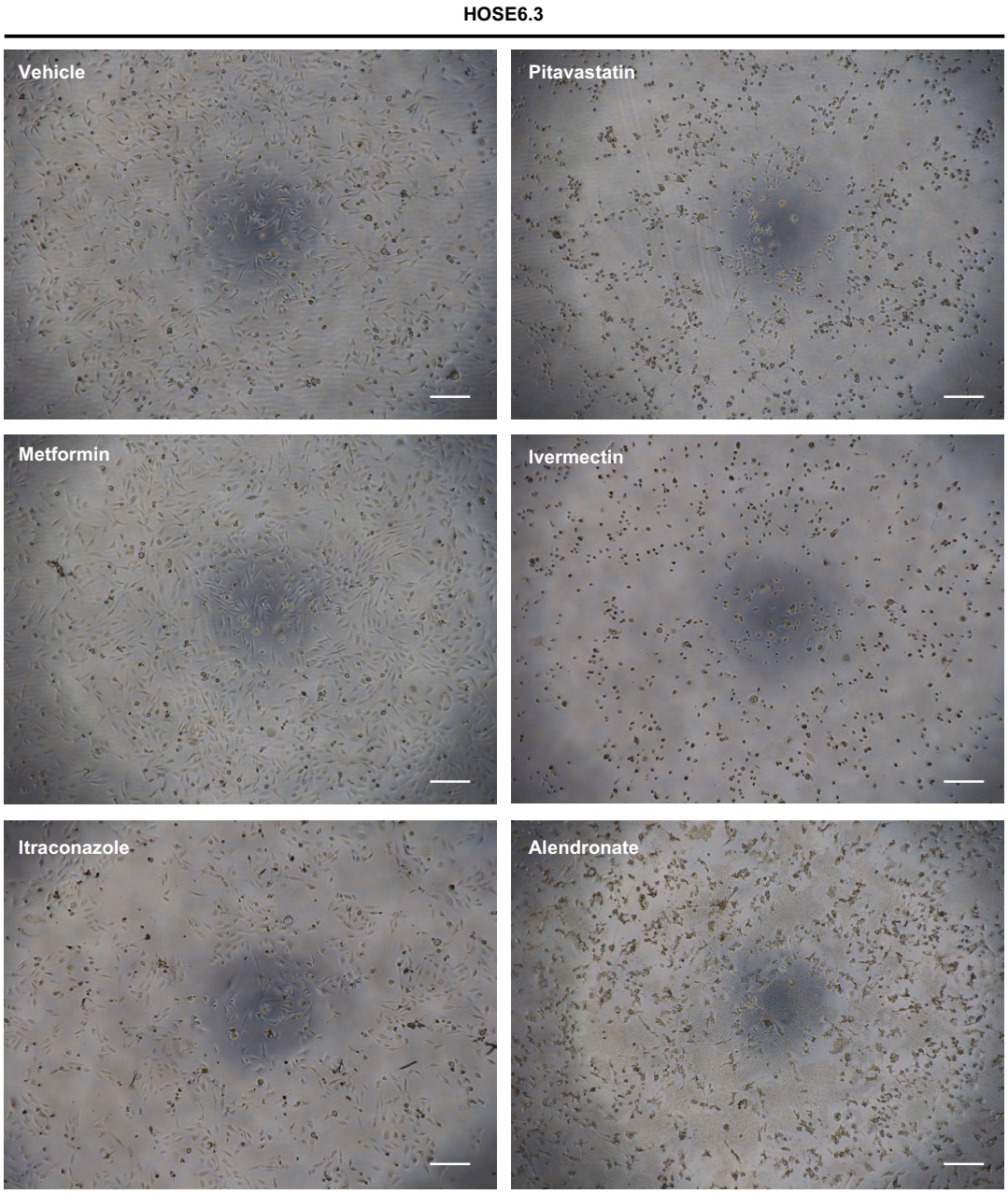


Figure S5. Representative microscopy images of HOSE6.3 cells. Figures were taken after exposure to the vehicle: Pitavastatin, Metformin, Ivermectin, Itraconazole, and Alendronate at the highest concentration used for each drug for 48 hours. All assays were performed in triplicates in at least three independent experiments. Scale bar: 200 μm.

Table S4. The cellular viability (%) of OVCAR8 and OVCAR8 PTX R P cells after treating with Paclitaxel and repurposing drugs. Cellular viability was measured after exposure to a fixed dose-ratio equivalent to 0.25, 0.5, 1, 2, and 4 times the individual IC_{50} values of each drug for 48 hours. The combined treatment was administered simultaneously. All assays were performed in triplicates in at least three independent experiments.

Treatment	Concentration	OVCAR8		OVCAR8 PTX R P	
		Cellular viability (%)		Cellular viability (%)	
		Media	SD	Media	SD
Paclitaxel (nM)	0.25 x IC50	80.757	5.416	90.528	2.353
	0.5 x IC50	78.038	8.142	87.466	4.860
	IC50	53.946	3.312	86.708	4.216
	2 x IC50	29.671	3.816	80.894	7.527
	4 x IC50	12.151	2.665	74.763	1.916
Pitavasvatin (µM)	0.25 x IC50	61.378	8.811	59.998	1.774
	0.5 x IC50	51.912	13.448	50.426	1.186
	IC50	45.624	4.912	45.406	2.741
	2 x IC50	27.970	6.045	28.330	5.862
	4 x IC50	26.234	10.455	26.234	10.455
Paclitaxel (nM) + Pitavastatin (µM)	0.25 x IC50	53.275	7.058	57.336	8.149
	0.5 x IC50	37.656	0.811	36.095	6.457
	IC50	19.100	2.025	24.091	0.683
	2 x IC50	14.958	3.148	15.104	3.044
	4 x IC50	10.729	0.024	11.373	0.620
Metformin (mM)	0.25 x IC50	72.126	1.341	68.105	9.000
	0.5 x IC50	63.520	3.097	59.114	9.045
	IC50	44.207	8.087	44.548	6.851
	2 x IC50	16.568	6.162	14.871	5.490
	4 x IC50	6.948	1.168	12.397	4.071
Paclitaxel (nM) + Metformin (mM)	0.25 x IC50	60.893	14.666	70.029	8.434
	0.5 x IC50	46.734	6.629	57.874	7.065
	IC50	21.111	2.909	26.557	4.411
	2 x IC50	14.153	4.135	14.428	2.235
	4 x IC50	5.543	0.951	9.163	2.125
Ivermectin (µM)	0.25 x IC50	77.004	5.400	81.152	4.877
	0.5 x IC50	69.934	3.792	65.026	10.605
	IC50	46.412	1.176	47.496	1.382
	2 x IC50	0.759	0.072	0.966	0.072
	4 x IC50	0.867	0.140	1.370	0.394
Paclitaxel (nM) + Ivermectin (µM)	0.25 x IC50	69.955	6.855	80.717	3.183
	0.5 x IC50	44.541	3.217	45.360	8.110
	IC50	8.706	2.890	6.195	1.862
	2 x IC50	0.820	0.320	1.048	0.422
	4 x IC50	0.613	0.438	0.865	0.348
Itraconazole (µM)	0.25 x IC50	92.297	10.540	92.844	5.230
	0.5 x IC50	99.490	8.443	97.871	6.224
	IC50	102.809	12.788	95.181	4.623
	2 x IC50	101.169	7.059	87.752	8.305
	4 x IC50	86.903	10.831	73.512	11.071
Paclitaxel (nM) + Itraconazole (µM)	0.25 x IC50	83.754	7.372	95.238	7.076
	0.5 x IC50	68.477	6.173	83.660	4.073
	IC50	45.331	7.790	56.556	3.372
	2 x IC50	31.682	11.529	34.842	5.969
	4 x IC50	22.879	8.467	25.781	5.294
Alendronate (µM)	0.25 x IC50	103.500	14.967	94.205	1.914
	0.5 x IC50	101.117	13.794	84.877	5.677
	IC50	53.983	1.035	43.609	3.973
	2 x IC50	32.912	5.431	32.275	7.048
	4 x IC50	30.497	9.853	30.685	4.090
Paclitaxel (nM) + Alendronate (µM)	0.25 x IC50	86.901	10.541	88.880	11.047
	0.5 x IC50	83.410	8.147	65.998	4.907
	IC50	16.141	4.990	17.529	1.584
	2 x IC50	9.314	7.929	14.731	2.316
	4 x IC50	9.233	7.489	11.088	3.682

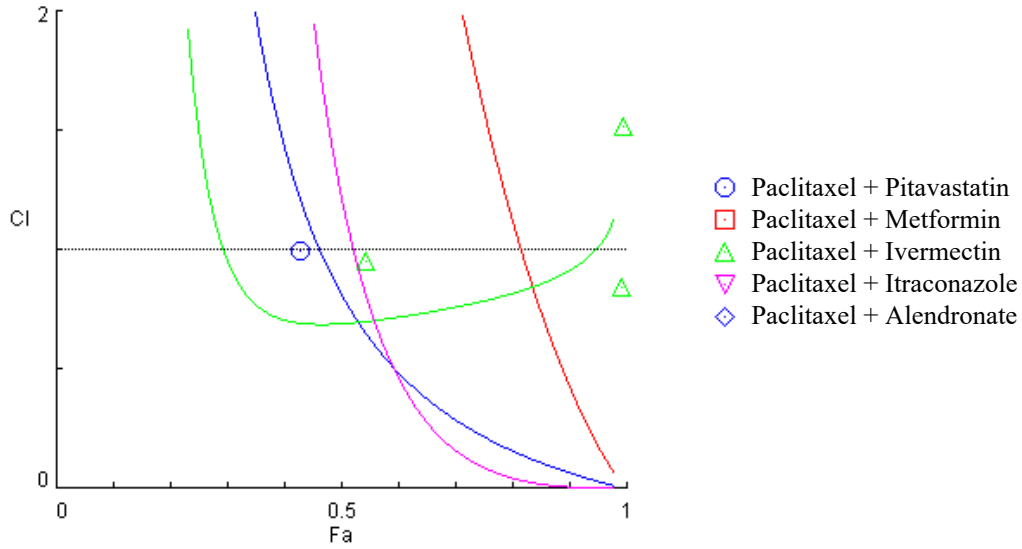


Figure S6. Combining Paclitaxel with repurposed drugs has an antagonistic effect on HOSE6.3 cells. The Chou-Talalay method Fa-CI plot shows the synergism of HOSE6.3 cells after exposure to a fixed dose ratio that corresponds to 0.25, 0.5, 1, 2, and 4 times the individual IC_{50} values for each drug. Paclitaxel was combined simultaneously with Pitavastatin, Metformin, Ivermectin, Itraconazole, or Alendronate for 48 hours. The combined treatment was administered simultaneously. All assays were performed in triplicates in at least three independent experiments. The CI was plotted on the y-axis as a function of Fa on the x-axis to evaluate drug synergism, where CI <1 (synergism), CI =1 (additivity), and CI >1 (antagonism). CI, combinatory index; Fa, effect level.

Table S5. Fa values and the corresponding CI values to determine the synergistic effects of drugs on HOSE6.3 cells. The cells were exposed to a fixed dose ratio equivalent to 0.25, 0.5, 1, 2, and 4 times the individual IC_{50} values of each drug for 48 hours. The combined treatment was administered simultaneously. All assays were performed in triplicates in at least three independent experiments. The CI values indicate the level of drug interaction: CI: >1 (antagonism), CI =1 (additivity), and CI <1 (synergism). CI, combinatory index; Fa, effect level.

				HOSE6.3	
Combination (Drug 1 + Drug 2)	**Total Dose** (Drug 1 + Drug 2)	**Dose** (Drug 1)	**Dose** (Drug 2)	**Fa**	**CI Value**
Paclitaxel (nM) + Pitavastatin (µM)	2.7	2.5	0.2	0.115	26.816
	5.4	5	0.4	0.146	18.988
	10.8	10	0.8	0.234	4.675
	21.6	20	1.6	0.271	4.777
	43.2	40	3.2	0.430	0.994
Paclitaxel (nM) + Metformin (mM)	2.875	2.5	0.375	0.083	101.352
	5.75	5	0.750	0.094	109.733
	11.5	10	1.5	0.132	45.791
	23	20	3	0.156	41.167
	46	40	6	0.181	39.581
Paclitaxel (nM) + Ivermectin (µM)	6.25	2.5	3.75	0.093	57.939
	12.5	5	7.5	0.110	54.256
	25	10	15	0.544	0.956
	50	20	30	0.991	0.842
	100	40	60	0.995	1.515
Paclitaxel (nM) + Itraconazole (µM)	6.25	2.5	3.75	0.041	2364.560
	12.5	5	7.5	0.048	2388.570
	25	10	15	0.102	166.235
	50	20	30	0.137	83.464
	100	40	60	0.155	91.946
Paclitaxel (nM) + Alendronate (µM)	40	2.5	37.5	0.001	1.00E10
	80	5	75	0.030	15657.200
	160	10	150	0.030	31314.4
	320	20	300	0.031	54522.200
	640	40	600	0.084	1457.650

Table S6. The cellular viability (%) of HOSE6.3 cells after treating with Paclitaxel and repurposing drugs. Cellular viability was measured after exposure to a fixed dose ratio that corresponds to 0.25, 0.5, 1, 2, and 4 times the individual IC_{50} values of each drug for 48 hours. The combined treatment was administered simultaneously. All assays were performed in triplicates in at least three independent experiments. SD, standard deviation.

Treatment	Concentration	HOSE6.3	
		Cellular viability (%)	
		Media	SD
Paclitaxel (nM)	0.25 x IC50	78,854	5,925
	0.5 x IC50	75,466	6,905
	IC50	70,822	6,979
	2 x IC50	68,366	5,776
	4 x IC50	65,718	7,079
Pitavasvatin (µM)	0.25 x IC50	81,849	7,681
	0.5 x IC50	76,512	7,815
	IC50	68,462	3,472
	2 x IC50	65,889	5,045
	4 x IC50	61,442	2,761
Paclitaxel (nM) + Pitavastatin (µM)	0.25 x IC50	88,488	5,102
	0.5 x IC50	85,399	5,346
	IC50	76,611	4,971
	2 x IC50	72,886	4,878
	4 x IC50	57,037	6,338
Metformin (mM)	0.25 x IC50	96,286	4,707
	0.5 x IC50	97,224	1,001
	IC50	95,033	1,429
	2 x IC50	96,032	1,778
	4 x IC50	92,366	2,639
Paclitaxel (nM) + Metformin (mM)	0.25 x IC50	91,847	6,149
	0.5 x IC50	90,569	7,830
	IC50	86,845	5,504
	2 x IC50	83,700	2,788
	4 x IC50	81,860	2,706
Ivermectin (µM)	0.25 x IC50	100,990	2,144
	0.5 x IC50	99,694	3,725
	IC50	53,462	2,873
	2 x IC50	0,539	1,365
	4 x IC50	-0,589	0,544
Paclitaxel (nM) + Ivermectin (µM)	0.25 x IC50	90,745	5,112
	0.5 x IC50	89,023	4,590
	IC50	45,582	3,931
	2 x IC50	0,922	1,661
	4 x IC50	0,457	0,938
Itraconazole (µM)	0.25 x IC50	86,353	3,252
	0.5 x IC50	84,356	1,857
	IC50	84,735	3,865
	2 x IC50	79,729	1,179
	4 x IC50	77,370	3,174
Paclitaxel (nM) + Itraconazole (µM)	0.25 x IC50	95,856	1,914
	0.5 x IC50	95,195	1,303
	IC50	89,804	3,721
	2 x IC50	86,268	3,661
	4 x IC50	84,498	3,203
Alendronate (µM)	0.25 x IC50	101,792	6,109
	0.5 x IC50	101,959	6,966
	IC50	92,147	2,125
	2 x IC50	89,188	5,221
	4 x IC50	84,305	5,970
Paclitaxel (nM) + Alendronate (µM)	0.25 x IC50	100,808	2,093
	0.5 x IC50	96,984	1,927
	IC50	96,973	0,865
	2 x IC50	96,946	0,508
	4 x IC50	91,567	1,748

ii. The Antineoplastic Effect of Carboplatin is Potentiated by Combining it with Pitavastatin or Metformin in a Chemoresistant High-Grade Serous Carcinoma Cell Line

1. Abstract

The standard treatment for HGSC is a combination of Carboplatin and Paclitaxel. However, many patients with advanced disease undergo relapse due to becoming resistant to chemotherapy. To address this, researchers are exploring the potential of using a combination of different compounds with independent mechanisms of action, a process called drug repurposing, to increase the success of cancer treatment.

This study aimed to investigate whether combining Carboplatin with repurposed drugs could provide therapeutic benefits. Here, the effects of Carboplatin alone and in combination with several repurposed drugs (Pitavastatin, Metformin, Ivermectin, Itraconazole, and Alendronate) on two types of cancer cell lines, including OVCAR8 (Carboplatin-resistant) and OVCAR8 PTX R P (Carboplatin-Paclitaxel resistant), as well as a non-tumoral cell line (HOSE6.3) was assessed. Here, cellular viability was measured using the PB assay, and the synergistic interactions of the drugs were using the Chou–Talalay, Bliss Independence, and HSA reference models.

Our results showed that combining Carboplatin with Pitavastatin or Metformin had the strongest synergistic and cytotoxic effect on the chemoresistant cancer cells, surpassing the impact of Carboplatin alone. Additionally, combining Carboplatin with most of the repurposed drugs demonstrated a safe pharmacological profile for the non-tumoral cell line.

Overall, it was suggested that Pitavastatin or Metformin could potentially act synergistically in combination with Carboplatin to treat HGSC patients exhibiting resistance to Carboplatin plus Paclitaxel.

Keywords: Carboplatin, Chemoresistance, Drug Repurposing, Pitavastatin, Metformin, High-Grade Serous Carcinoma, Synergy.

1. Introduction

There is a long history of drug combinations in the treatment of OC. The first effective combination was Platinum (Cisplatin or Carboplatin) with Cyclophosphamide (651). In the 1990s, a trial showed that the combination of Cisplatin with Paclitaxel was more effective than the previous regimen (24). As a result, Paclitaxel was included in the first-line therapy

of OC, leading to significant improvement in treatment, especially for advanced disease (24). Another trial in OC at stage IIB–IV demonstrated that Carboplatin-Paclitaxel is a good alternative to the Cisplatin-Paclitaxel combination, with similar effectiveness and lower toxicity (26).

HGSC is commonly treated with a combination of debulking surgery followed by Platinum-Taxane chemotherapy. However, many patients experience recurrences, indicating the presence of cancer cells resistant to the first-line chemotherapy (17, 65, 67, 599). Antineoplastic drugs can be categorized based on their mechanisms of action into alkylating agents, mitotic spindle inhibitors, antimetabolites, and topoisomerase inhibitors, among others (712). Carboplatin, an alkylating agent, is used as a frontline treatment of many neoplasms, including advanced HGSC (649). This chemotherapeutic compound forms reactive platinum complexes that induce inter- and intra-strand cross-linkage of DNA molecules, thereby altering DNA structure and inhibiting DNA synthesis, ultimately leading to cell death (712, 713). The development of platinum resistance remains a significant challenge to the success of chemotherapy, as several molecular mechanisms underlie this process (712-715). Carboplatin resistance is a complex phenomenon involving increased drug detoxification systems, enhanced DNA repair capacity, and improved tolerance to nuclear damage, resulting in reduced accumulation of the drug inside the cell and decreased apoptosis (712, 716, 717). Chemoresistance can occur by intrinsic (the innate resistance of cancer cells to antineoplastic agents before exposure) or acquired resistance (tumors exhibiting a drug-resistant cell population and reduced treatment efficacy after chemotherapy exposure), leading to recurrences that evade the cytotoxic effects of chemotherapy (183, 718, 719). This presents a significant challenge in cancer treatment, as approximately 80 – 90% of cancer-related deaths are directly or indirectly associated with chemoresistance (720, 721).

In therapy-resistant tumors, it is important to find a pharmacological strategy that can improve the effectiveness of the treatment in order to prevent or reverse chemoresistance (718). Drug repurposing is a strategy used to discover new uses for approved compounds beyond their original intended purpose. This approach can reduce the cost and time required to develop new drugs for clinical use (606-608). It is based on the idea that different diseases may share the same therapeutic targets and molecular features (609). Additionally, drug repurposing is a readily available option as these drugs are already on the market, with well-established pharmacological and toxicological profiles. The approval process for a new indication can also be expedited for repurposed drugs compared to the development of

entirely new drugs (610-612). However, integrating repurposed drugs as an alternative in oncology requires the development of appropriate clinical trials to evaluate drug efficacy and determine the maximum tolerated dose to prevent intolerable toxicities (610).

Another way to address chemoresistance is by combining two or more drugs at an optimal synergistic ratio. These drugs should have different mechanisms of action and target different pathways in order to increase sensitivity and treatment efficacy (718). When two or more drugs can interact, they can have a synergic, additive, or antagonistic effect. Synergism is the most desirable drug interaction as it results in a combinatory effect much higher than each drug (620). In antagonism, the combined effect of drugs is less effective than the single activity of each drug (620). Additivity occurs when the combination of both agents corresponds to the sum of the effects of each compound (620). When two or more drugs act synergistically, a better outcome can be achieved as it becomes possible to use lower doses of each drug, thereby reducing systemic toxicity and adverse side effects (615, 621, 622).

In a previous study (722), was confirmed the antitumoral effect of five repurposed drugs in two chemoresistant HGSC cell lines: OVCAR8 (Carboplatin resistant) and OVCAR8 PTX R P (Carboplatin-Paclitaxel resistant) (628). The drugs studied were Pitavastatin (antilipidemic), Metformin (antidiabetic), Ivermectin (antiparasitic), Itraconazole (antifungal), and Alendronate (antiosteoporosis) (722). It was found that the antitumoral activity of Paclitaxel can be effectively improved when combined with Pitavastatin or Ivermectin. These two drugs have an acceptable toxicological profile and can simultaneously increase the activity of Paclitaxel while reducing therapeutical doses (722).

Here, it was hypothesized that Pitavastatin, Metformin, Ivermectin, Itraconazole, or Alendronate could act synergistically with Carboplatin in two chemoresistant HGSC cell line models (OVCAR8 and OVCAR8 PTX R P). Additionally, these combinations were performed in a normal-like cell line (HOSE6.3) to evaluate the safety pharmacological profile.

Our findings demonstrate that combining Carboplatin with Pitavastatin or Metformin has the highest cytotoxic effect and the strongest synergism for the Carboplatin plus Paclitaxel resistant cell line (OVCAR8 PTX R P). This combination has a more potent anti-cancer effect compared to Carboplatin alone. Importantly, combining Carboplatin with these two repurposed drugs has a safe pharmacological profile and does not significantly affect the viability of a non-tumoral cell line (HOSE6.3). In summary, these results support the use of this combination as a viable therapeutic strategy for managing HGSC patients with a Carboplatin plus Paclitaxel-resistant profile.

3. Materials and Methods

3.1. Cell Lines and Culture Conditions

The OVCAR8 (Carboplatin-resistant) (567) and OVCAR8 PTX R P (Carboplatin and Paclitaxel-resistant) (628) cell lines were selected as HGSC models. Additional experiments were carried out using a non-tumoral cell line (HOSE6.3), which is a human ovarian epithelial cell line established from a normal ovary surgically removed from a patient with non-malignant disease (629). More details about cell lines and culture conditions were previously described (722).

3.2. Drugs

Carboplatin, Pitavastatin, Metformin, Ivermectin, Itraconazole, and Alendronate were purchased from Selleckchem (Houston, TX, USA) were dissolved in DMSO (AppliChem, Barcelona, Spain) or distilled water and stored at −80 °C according to the manufacturer's instructions. Immediately before use, an aliquot was diluted to the required concentrations.

3.3. Cell Viability Assays

As previously described, a resazurin-based assay – PB – was performed to determine the effect of single and combination drug treatments on cellular viability (722).

3.4. Drug Treatment and Interaction Analysis

Previous reports provided the IC_{50} values for Carboplatin and each repurposed drug alone (628, 722). These values were used for combination studies, which were performed using increasing concentrations of both drugs in a fixed ratio, as suggested by Chou–Talalay (635) and described in previous methods (623). Briefly, Carboplatin was simultaneously combined with different repurposed drugs in a fixed-dose ratio that corresponds to 0.25, 0.5, 1, 2, and 4 times the individual IC_{50} values for 48 hours.

This study assessed the drug interactions between Carboplatin and repurposed drugs using two different software tools: CompuSyn Software 1.0 (ComboSyn, Inc., New York, NY, USA) and SynergyFinder 2.0 Software (Netphar, Faculty of Medicine, University of Helsinki, Helsinki, Finland). Here, the CI was calculated using the Chou-Talalay method (636) with CompuSyn. A mutually exclusive model, assuming that drugs act through entirely different mechanisms, was used for this analysis (637). The CI is a quantitative representation of pharmacological interactions (CI < 1, synergism; CI = 1, additivity; and CI > 1, antagonism), plotted on the y-axis as a function of Fa on the x-axis to assess drug

synergism between drug combinations. To further analyze the drug combination responses, was used SynergyFinder 2.0 Software to estimate expected drug combination responses based on the Bliss Independence and HSA reference models (638, 644). This software provides interactive analysis and visualization of multidrug combination profiling data, allowing us to observe synergy (in red) and antagonism (in green) on 2D and 3D synergy maps (623). The cNMF algorithm implemented in SynergyFinder 2.0 Software was used for the estimation of outlier measurements (639).

3.5. Microscopic Evaluation

All microscopic figures were captured under a Leica DMi1 inverted phase contrast microscope (Leica Microsystems, Wetzlar, Germany) at 50× magnification.

3.6. Statistical Analysis

All assays were performed in triplicate with at least three independent experiments. The data was expressed as the mean ± SD. Statistical analysis was performed in GraphPad Prism 8 (GraphPad Software Inc., Boston, CA, USA) using ordinary one-way or two-way ANOVA followed by Šıdák's multiple comparison test.

4. Results

4.1. Repurposing Drugs Increase the Efficacy of Carboplatin in Reducing OVCAR8 and OVCAR8 PTX R P Cellular Viability

We recently analyzed the anticancer potential of each repurposed drug when used alone on OVCAR8 and OVCAR8 PTX R P cells. The findings showed that all the drugs effectively reduced cellular viability in both chemoresistant cell lines (722). Additionally, these drugs had minimal to no effect on the viability of HOSE6.3, a normal-like cell line, unlike their impact on tumoral cell lines (722). This suggests that the five repurposed drugs have an acceptable safety profile in normal-like cells while demonstrating significant anticancer efficacy in chemoresistant tumor cells, making them promising candidates for combination therapy with Carboplatin (722). Then was evaluated the combination of Carboplatin with Pitavastatin, Metformin, Ivermectin, Itraconazole, or Alendronate using a predefined combination model (624). The chemoresistant HGSC cells were exposed to the two drugs alone and in a combination at fixed ratios relative to their individual IC_{50} values (**Figure 24 and Table S7).** Furthermore, was performed a morphological evaluation for each treatment condition (**Figure 25**).

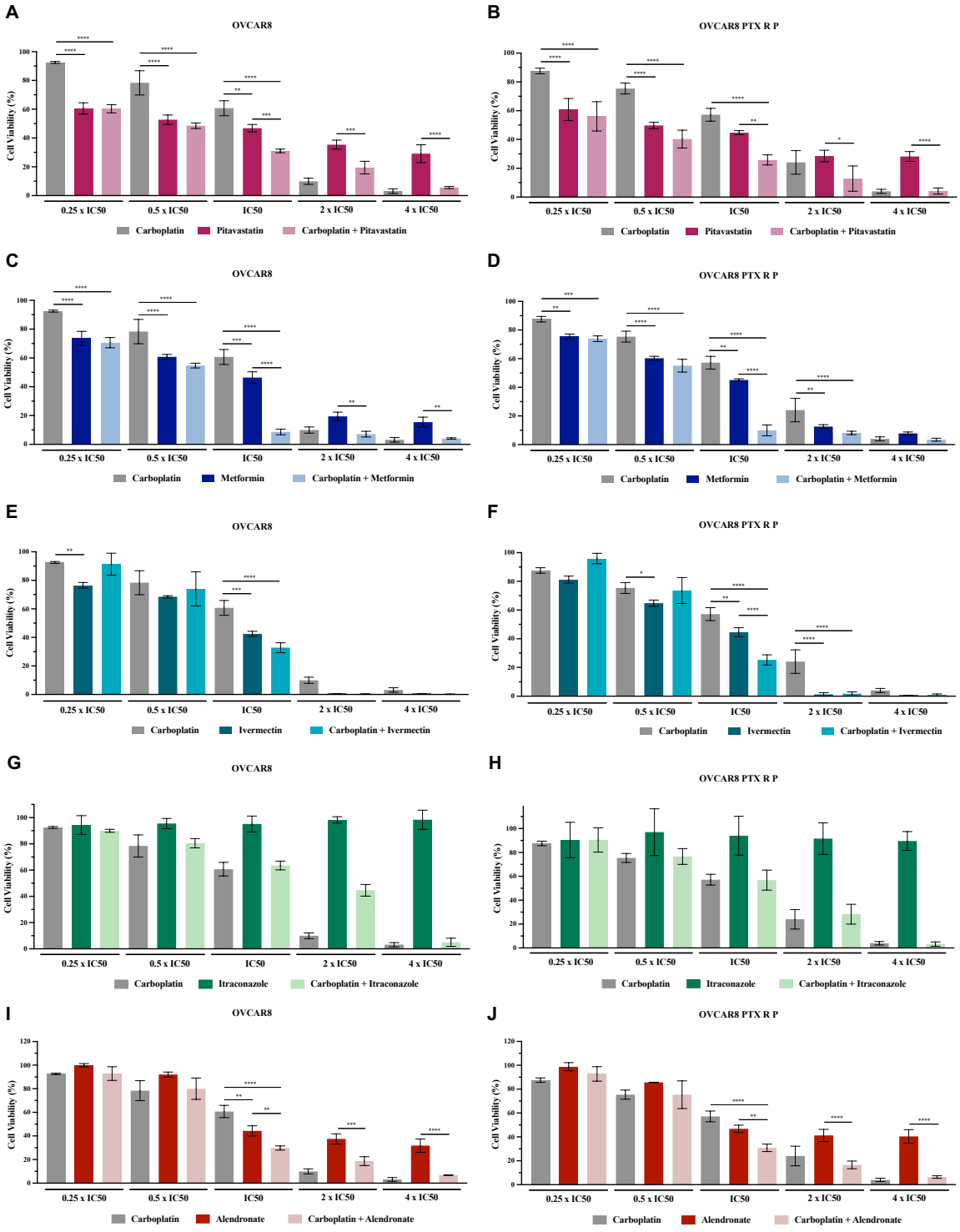


Figure 24. Repurposed drugs increase the efficacy of Carboplatin in reducing the cellular viability of chemoresistant HGSC cells. (**A**–**J**) Bar charts showing cell viability of OVCAR8 (**left**) and OVCAR8 PTX R P (**right**) cells obtained by the PB assay after exposure to fixed-dose ratios corresponding to 0.25, 0.5, 1, 2, and 4 times the individual IC_{50} values of each drug. For 48 hours, Carboplatin was combined with (**A** and **B**) Pitavastatin, (**C** and **D**) Metformin, (**E** and **F**) Ivermectin, (**G** and **H**) Itraconazole and (**I** and **J**) Alendronate. The

combined treatment was administered simultaneously. All assays were performed in triplicate in at least three independent experiments. The data are expressed as the mean ± SD and plotted using GraphPad Prism Software Inc. v6 (GraphPad Software Inc. Boston, CA, USA). Statistical analysis was performed using ordinary one-way ANOVA followed by Šıdák's multiple comparison test (**A**–**J**), with * $p < 0.05$, ** $p < 0.001$, *** $p < 0.005$, and **** $p < 0.0001$ considered statistically significant. HGSC, high-grade serous carcinoma; PB, presto bleu; SD, standard deviation.

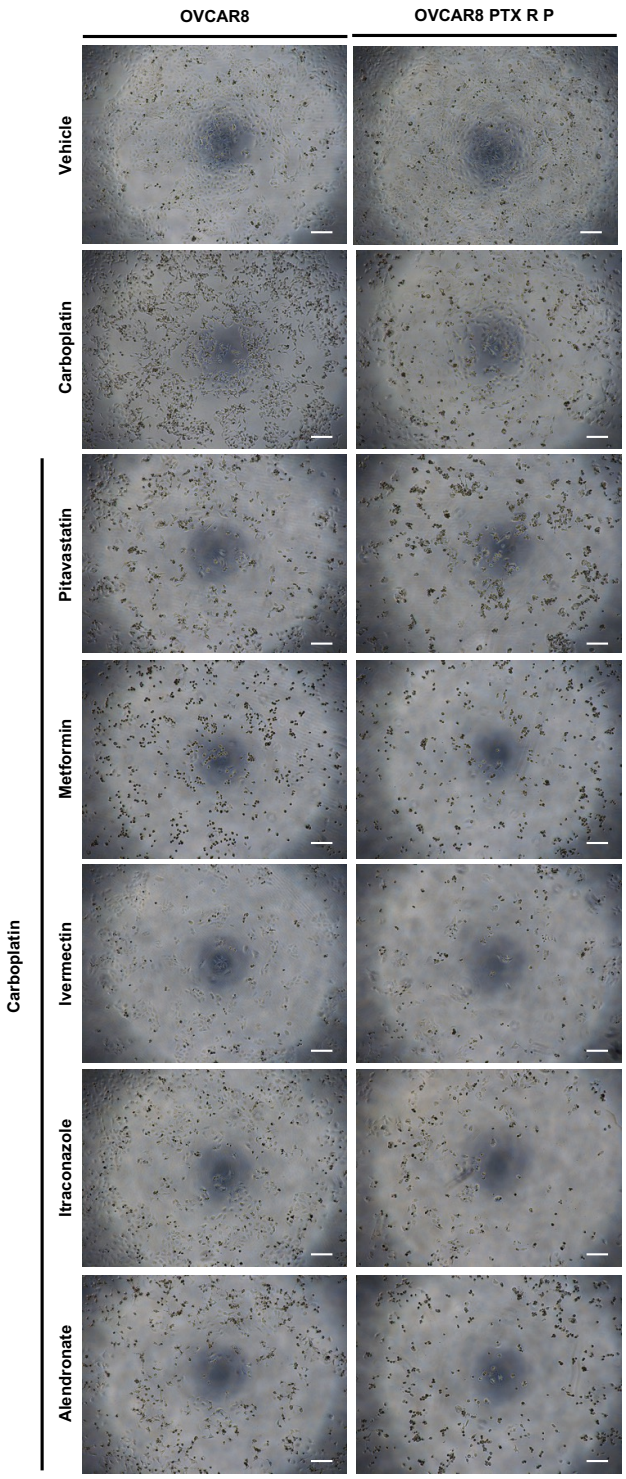


Figure 25. Repurposed drugs improved the cytotoxic effect of Carboplatin on chemoresistant HGSC cells. Representative microscopy images of OVCAR8 and OVCAR8 PTX R P cells after exposure for 48 hours to vehicle, Carboplatin, Carboplatin + Pitavastatin, Carboplatin + Metformin, Carboplatin + Ivermectin, Carboplatin + Itraconazole and Carboplatin + Alendronate at IC_{50} values of each drug. All assays were performed in triplicate in at least three independent experiments. Scale bar, 200 μm. HGSC, high-grade serous carcinoma.

Results showed that combining Carboplatin with Pitavastatin significantly increased the anticancer effect ($p < 0.0001$) for 0.25, 0.5, and 1 times the individual IC_{50} values, compared to Carboplatin as a single agent in OVCAR8 and OVCAR8 PTX R P cells (**Figures 24A and 24B, and Table S7**). The combination of Carboplatin with Metformin resulted in a significant reduction in cellular viability ($p < 0.0001$) for 0.25, 0.5, and 1 times the individual IC_{50} values, compared to Carboplatin alone in OVCAR8 cells (**Figure 24C and Table S7**). For OVCAR8 PTX R P cells, this combination also increased antineoplastic efficacy for 0.25 ($p < 0.005$), 0.5, 1, and 2 ($p < 0.0001$) times the individual IC_{50} values, compared to Carboplatin alone (**Figure 24D and Table S7**). Additionally, combining Carboplatin with Ivermectin led to a significant increase in anticancer effect ($p < 0.0001$) for 1 time the IC_{50} values in OVCAR8, compared to Carboplatin as a single agent (**Figure 24E and Table S7**). For OVCAR8 PTX R P cells, this combination also increased the antineoplastic effect ($p < 0.0001$) for 1 and 2 times the individual IC_{50} values, compared to Carboplatin alone (**Figure 24F and Table S7**). However, combining Carboplatin with Itraconazole did not show a significant reduction in cellular viability for both OVCAR8 and OVCAR8 PTX R P cells, compared to Carboplatin alone (**Figures 24G and 24H, and Table S7**). For both OVCAR8 and OVCAR8 PTX R P cells, a significant increase in antineoplastic effect ($p < 0.0001$) between Carboplatin with Alendronate and Carboplatin alone was obtained at the concentration of 1 time the individual IC_{50} values (**Figures 24I and 24J, and Table S7**).

Interestingly, was also showed a significant decrease in cellular viability for 1 fold the individual IC_{50} values when combining Carboplatin with Pitavastatin ($p < 0.005$ for OVCAR8 and $p < 0.001$ for OVCAR8 PTX R P), Metformin ($p < 0.0001$ for both cell lines), Ivermectin ($p < 0.0001$ for OVCAR8 PTX R P) and Alendronate ($p < 0.001$ for both cell lines), compared to each repurposed drug alone (**Figure 24 and Table S7**).

The results are in line with previous findings, showing morphological differences in OVCAR8 and OVCAR8 PTX R P cells when subjected to combined treatments, as opposed to vehicle and single treatments. The individual therapy for each repurposed drug was previously documented (722). When Carboplatin was combined with Pitavastatin,

Metformin, Ivermectin, and Alendronate at IC_{50} values, it induced a more aggressive phenotype, resulting in decreased cell numbers, reduced aggregate formation, and smaller and rounded cells. This indicates cell death, unlike when Carboplatin was used alone (**Figure 25**). Overall, these four repurposed drugs, when combined with Carboplatin at this specific concentration (IC_{50}), demonstrate a significant increase in cytotoxic effect compared to Carboplatin or even the repurposed drugs used alone.

4.2. Combining Repurposed Drugs with Carboplatin Has a Synergistic Effect on OVCAR8 and OVCAR8 PTX R P Cells

The use of drug combinations is an interesting approach as it allows for a synergistic effect by combining two or more drugs that target different pathways. This approach reduces therapeutic doses, minimizes adverse side effects, and decreases the chances of cells developing MDR. One of the most widely accepted methods for evaluating drug synergism is the Chou–Talalay method due to its quantitative definition, simplicity, flexibility, and efficiency (636, 642). As described by Chou–Talalay, this method for determining synergism is independent of the mechanisms of action of the drugs, making it unnecessary to know the specific mechanisms of action for each drug (636).

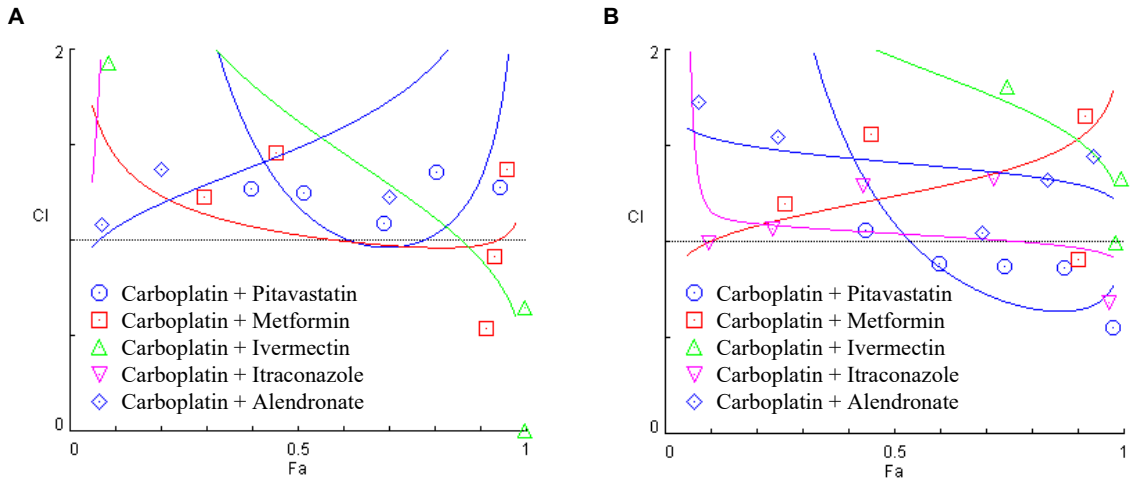
To assess drug synergism, the interaction between Carboplatin and other repurposed drugs was evaluated using the CI obtained through the Chou–Talalay method. The CI is plotted on the y-axis as a function of the Fa on the x-axis (**Figure 26**). The CI value indicates synergism (<1), additivity (=1), or antagonism (>1). At the same time, Fa is a parameter ranging from 0 (indicating that the drug does not affect cellular viability) to 1 (indicating that the drug produces a full effect in decreasing cellular viability) (636, 642).

Our findings for OVCAR8 cells revealed that combining Carboplatin with Pitavastatin, Itraconazole, and Alendronate did not result in any synergistic effect, as indicated by a CI > 1 for all the pairs tested (**Figures 26A and 26C**). When Carboplatin was combined with Metformin, it demonstrated the most promising synergism, with two synergic pairs (CI < 1) for 1 and 2 times the IC_{50} values, yielding Fa values of 0.914 and 0.933, respectively, for OVCAR8 cells (**Figures 26A and 26C**). Additionally, combining Carboplatin with Ivermectin showed the second most promising synergism for OVCAR8 cells, with two synergic pairs (CI < 1) and Fa values of 0.997 and 1 for 2 and 4-fold the IC_{50} values, respectively (**Figures 26A and 26C**).

For OVCAR8 PTX R P cells, combining Carboplatin with Pitavastatin showed the most promising synergism, with four synergic pairs (CI < 1) and Fa values of 0.597, 0.742,

0.872, and 0.978 for 0.5, 1, 2 and 4 times the IC_{50} values, respectively (**Figures 26B and 26C**). Combining Carboplatin with Metformin or Ivermectin resulted in one synergic pair (CI < 1) for 1 and 2 times the IC_{50} values, with Fa values of 0.901 and 0.984, respectively, for OVCAR8 PTX R P cells (**Figures 26B, and 26C**). The combination of Carboplatin with Itraconazole for OVCAR8 PTX R P cells revealed two pairs that were synergic (CI < 1), with Fa values of 0.096 and 0.967 for 0.5 and 4 times the IC_{50} values, respectively (**Figures 26B and 26C**). However, combining Carboplatin with Alendronate did not yield any synergistic effects for OVCAR8 PTX R P cells, with a CI > 1 for all pairs tested (**Figures 26B and 26C**).

In summary, the drug synergism evaluation indicated a consistent pattern in OVCAR8 and OVCAR8 PTX R P cells, which is in line with the previous cellular viability results for all combined treatments.



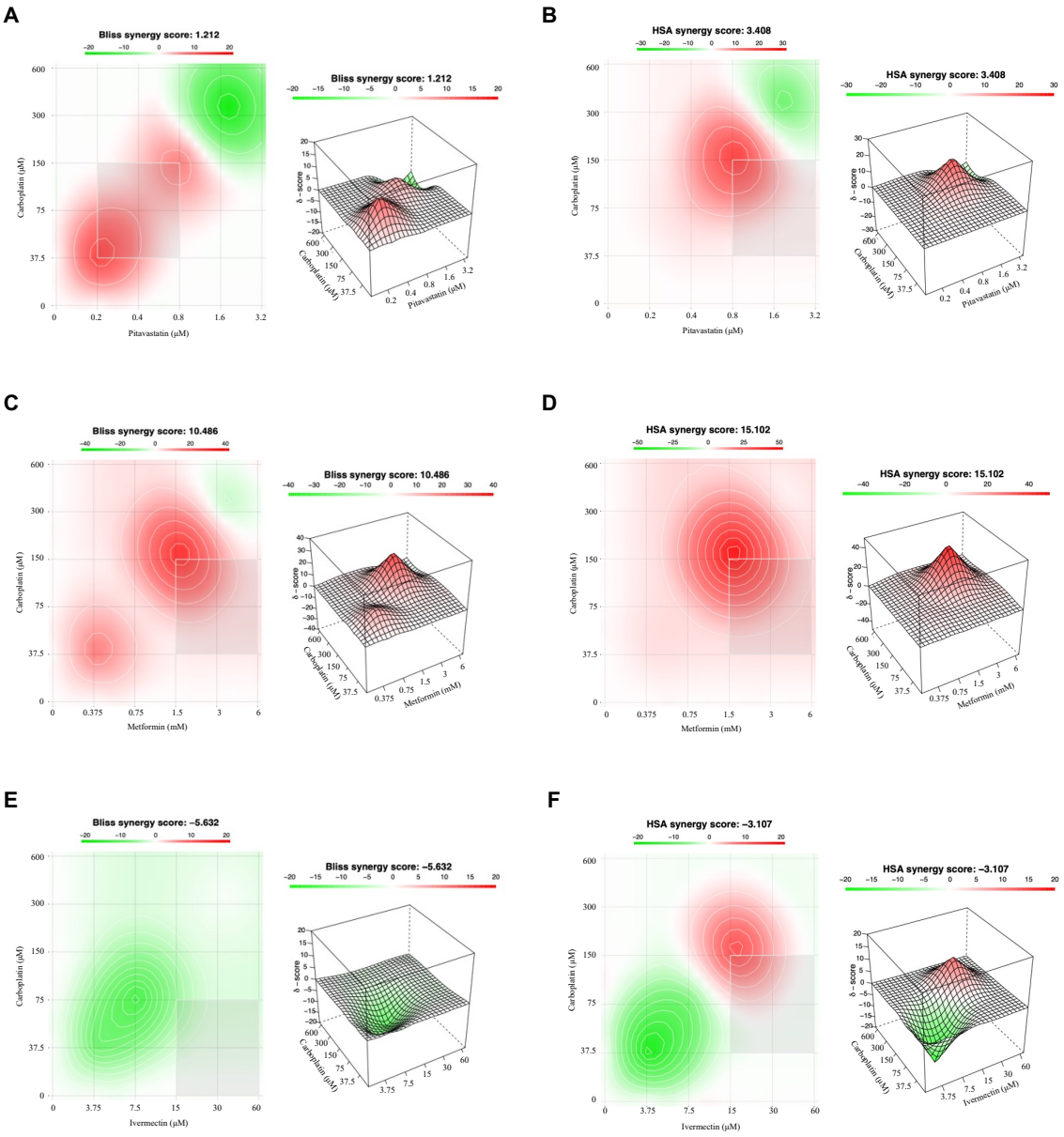
C

Combination (Drug 1 + Drug 2)	Total Dose (Drug 1 + Drug 2)	Dose (Drug 1)	Dose (Drug 2)	OVCAR8 Fa	OVCAR8 CI Value	OVCAR8 PTX R P Fa	OVCAR8 PTX R P CI Value
Carboplatin (μM) + Pitavastatin (μM)	37.7	37.5	0.2	0.397	1.26870	0.439	1.05807
	75.4	75	0.4	0.514	1.24751	**0.597**	**0.88916**
	150.8	150	0.8	0.690	1.08718	**0.742**	**0.87175**
	301.6	300	1.6	0.805	1.35925	**0.872**	**0.86853**
	603.2	600	3.2	0.944	1.28064	**0.978**	**0.55196**
Carboplatin (μM) + Metformin (mM)	37.875	37.5	0.375	0.294	1.22843	0.261	1.19677
	75.75	75	0.750	0.453	1.45753	0.449	1.55811
	151.5	150	1.5	**0.914**	**0.53787**	**0.901**	**0.90633**
	303	300	3	**0.933**	**0.91880**	0.916	1.65285
	606	600	6	0.959	1.37046	0.966	2.02869
Carboplatin (μM) + Ivermectin (μM)	41.25	37.5	3.75	0.087	1.92836	0.042	3.01503
	82.5	75	7.5	0.260	2.30179	0.264	2.30011
	165	150	15	0.672	2.30566	0.747	1.81127
	330	300	30	**0.997**	**0.64952**	**0.984**	**0.99909**
	660	600	60	**1.000**	**0.00225**	0.994	1.32819
Carboplatin (μM) + Itraconazole (μM)	41.25	37.5	3.75	0.100	3.29318	**0.096**	**0.99561**
	82.5	75	7.5	0.195	24.0366	0.234	1.07180
	165	150	15	0.365	247.277	0.432	1.29441
	330	300	30	0.554	2196.75	0.718	1.32748
	660	600	60	0.950	875451	**0.967**	**0.68790**
Carboplatin (μM) + Alendronate (μM)	75	37.5	37.5	0.072	1.08385	0.073	1.73178
	150	75	75	0.200	1.37351	0.246	1.55011
	300	150	150	0.702	1.22940	0.691	1.04475
	600	300	300	0.813	2.01234	0.834	1.32295
	1200	600	600	0.932	2.82271	0.936	1.44773

Figure 26. Combining Carboplatin with repurposed drugs has a synergistic effect on chemoresistant HGSC cells. (**A** and **B**) Chou–Talalay method Fa—CI plot and (**C**) Fa values and respective CI values. The plot illustrates the drug synergism of (**A**) OVCAR8 and (**B**) OVCAR8 PTX R P cells after exposure to fixed-dose ratios that correspond to 0.25, 0.5, 1, 2, and 4-times the individual IC_{50} values for each drug. Carboplatin was combined with Pitavastatin, Metformin, Ivermectin, Itraconazole, and Alendronate for 48 hours. The combined treatment was administered simultaneously. All assays were performed in triplicate in at least three independent experiments. The CI was plotted on the y-axis as a function of Fa on the x-axis to evaluate drug synergism, with CI <1 (synergism, bold), CI =1 (additivity), and CI >1 (antagonism). CI, combinatory index; Fa, effect level; HGSC, high-grade serous carcinoma.

Since the methods used to predict synergism have different mathematical frameworks (643) and can produce slightly different outcomes was also used the Bliss Independence and HSA models (**Figures 27 and 28)** to assess drug interactions and compare the results with the CI values obtained using the Chou-Talalay method. According to the Bliss Independence model, two compounds produce independent effects, and the combination effect can be determined based on the probability of independent events (638, 641, 643). The HSA model, on the other hand, assumes that the expected combination effect

is the highest effect achieved by the most effective drug (623, 638, 643, 682). In both models, the synergy score for a drug combination is averaged over all the dose combination measurements, resulting in positive (synergy, red) and negative (antagonism, green) synergy score values (623).



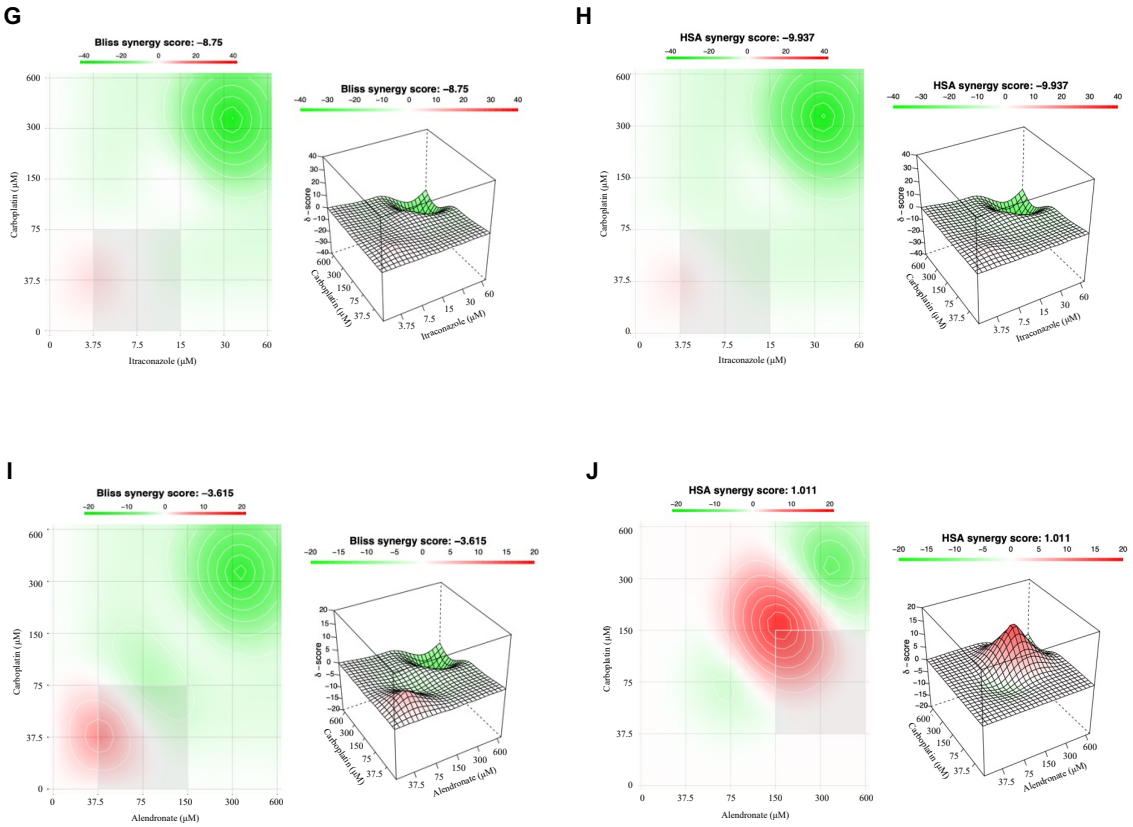


Figure 27. Combining Carboplatin with Metformin has a synergistic effect on OVCAR8 cells. (**A**–**J**) Bliss Independence and HSA synergy 2D and 3D plots, which showed the drug synergism of OVCAR8 cells after exposure to fixed-dose ratios that correspond to 0.25, 0.5, 1, 2, and 4 times the individual IC_{50} values of each drug. Carboplatin was combined with (**A** and **B**) Pitavastatin, (**C** and **D**) Metformin, (**E** and **F**) Ivermectin, (**G** and **H**) Itraconazole, and (**I** and **J**) Alendronate for 48 hours. The combined treatment was administered simultaneously. All assays were performed in triplicate in at least three independent experiments. The synergy scores were categorized as follows: <−10 (antagonism, green), −10 to 10 (additivity, white), and >10 (synergism, red). HSA, high single agent.

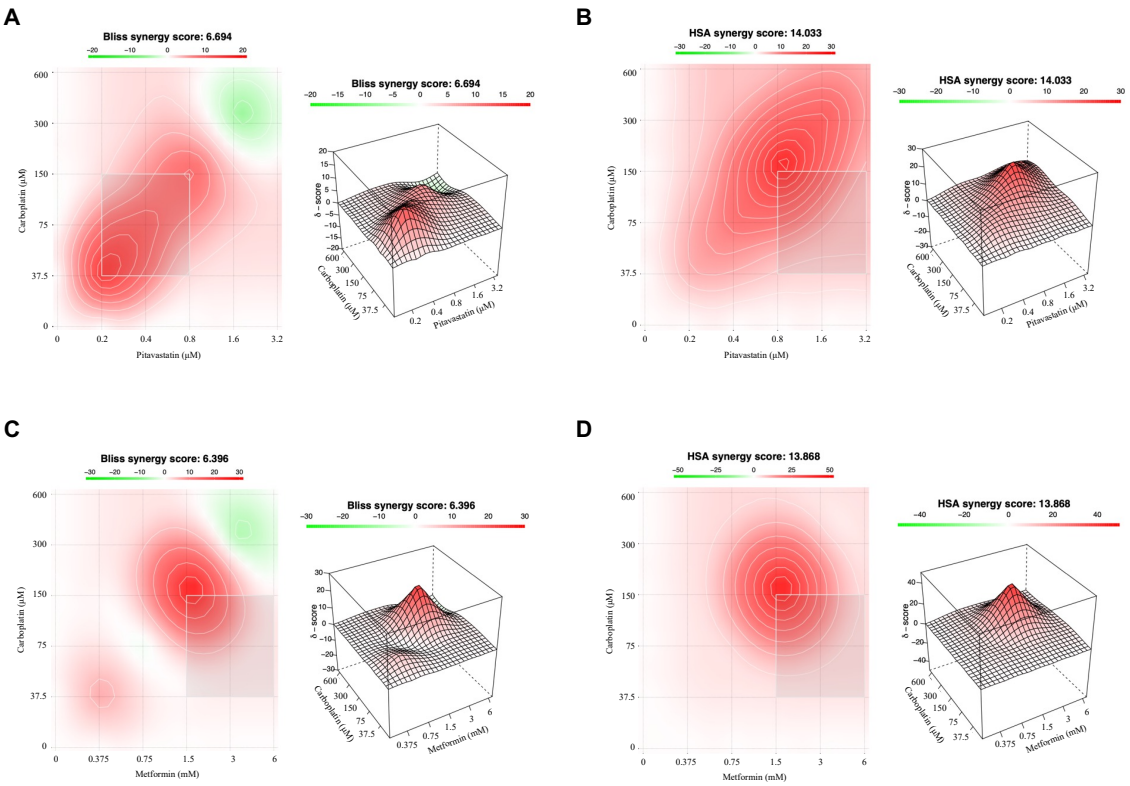
Our findings for OVCAR8 cells using the Bliss Independence and HSA models showed a positive synergy score of 1.212 and 3.408, respectively, when combining Carboplatin with Pitavastatin, indicating additivity (white) (**Figures 27A and 27B**). Additionally, both reference models, along with the Chou–Talalay method, revealed synergic zones (red) for the combinations at lower/intermediate concentrations. For OVCAR8 cells, the combination of Carboplatin with Metformin by the Bliss Independence and HSA models showed a positive synergy score of 10.486 and 15.102, respectively, demonstrating synergism (red), especially for the combinations at lower/intermediate concentrations (**Figures 27C and 27D**). These results are consistent with the Chou–Talalay method and

suggest synergy for the combination of Carboplatin with Metformin. However, when combining Carboplatin with Ivermectin, the Bliss Independence and HSA models showed a negative synergy score of -5.632 and -3.107, suggesting additivity (white) (**Figures 27E and 27F**). However, the HSA model revealed a synergic zone (red) for this combination at intermediate/higher concentrations, which aligns with the Chou–Talalay method. Furthermore, combining Carboplatin with Itraconazole yielded negative synergy scores of -8.750 and -9.937 by the Bliss Independence and HSA models, respectively, indicating additivity (white) (**Figures 27G and 27H**). It's important to note that the simulations for Itraconazole alone have associated errors related to its dose-response curve. Additionally, combining Carboplatin with Alendronate resulted in a synergy score of -3.615 and 1.011, as revealed by the Bliss Independence and HSA models, demonstrating additivity (white) (**Figures 27I and 27J**). However, the HSA model, in alignment with the Chou–Talalay method, presented a synergic zone (red) for the combinations at intermediate concentrations.

Regarding OVCAR8 PTX R P cells, based on the Chou–Talalay, Bliss Independence and HSA models revealed that combining Carboplatin with Pitavastatin resulted in a positive synergy score of 6.694 and 14.033, indicating additivity (white) and synergism (red), respectively. This was mainly observed for the combinations at lower to intermediate concentrations (**Figures 28A and 28B).** Similar findings were observed using Bliss Independence and HSA models, in agreement with the Chou–Talalay method, for OVCAR8 PTX R P combining Carboplatin with Metformin, with synergy scores of 6.396 and 13.868, indicating additivity (white) and synergism (red), especially for combinations at intermediate concentrations (**Figures 28C and 28D**). The combination of Carboplatin and Ivermectin, as projected by Bliss Independence and HSA models, indicated additivity (white) with negative synergy scores of −7.028 and −1.331, respectively, for OVCAR8 PTX R P cells (**Figures 28E and 28F**). Further, according to the Chou–Talalay method, both reference models revealed synergic zones (red) at the intermediate/higher concentrations. For OVCAR8 PTX R P cells, the Bliss Independence and HSA models indicated that combining Carboplatin with Itraconazole resulted in negative synergy scores of -0.433 and -2.141, respectively, suggesting additivity (white) (**Figures 28G and 28H**). It's important to note that Itraconazole alone does not have an ideal dose-response curve. However, the Bliss Independence model showed a synergic zone (red) for the combinations at intermediate concentrations, demonstrating similar results to the Chou–Talalay method. The Bliss Independence and HSA models demonstrated that the combination of Carboplatin and Alendronate resulted in

synergy scores of -3.797 and 4.882, respectively, demonstrating additivity (white) for OVCAR8 PTX R P cells (**Figures 28I and 28J**). Furthermore, the HSA model revealed synergic zones (red) occurring only at higher concentrations. Moreover, the Bliss Independence model aligns with the results obtained by the Chou–Talalay method as it presents more antagonistic (green) zones.

In a previous study (722), the synergic effect results demonstrated that different scores could be obtained on the synergy evaluation models chosen. However, all three methods assessed showed similar results for all the combinations tested. Hence, it has been demonstrated that combining Carboplatin with Pitavastatin or Metformin is the most promising drug combination for the OVCAR8 PTX R P (Carboplatin and Paclitaxel-resistant) cell line.



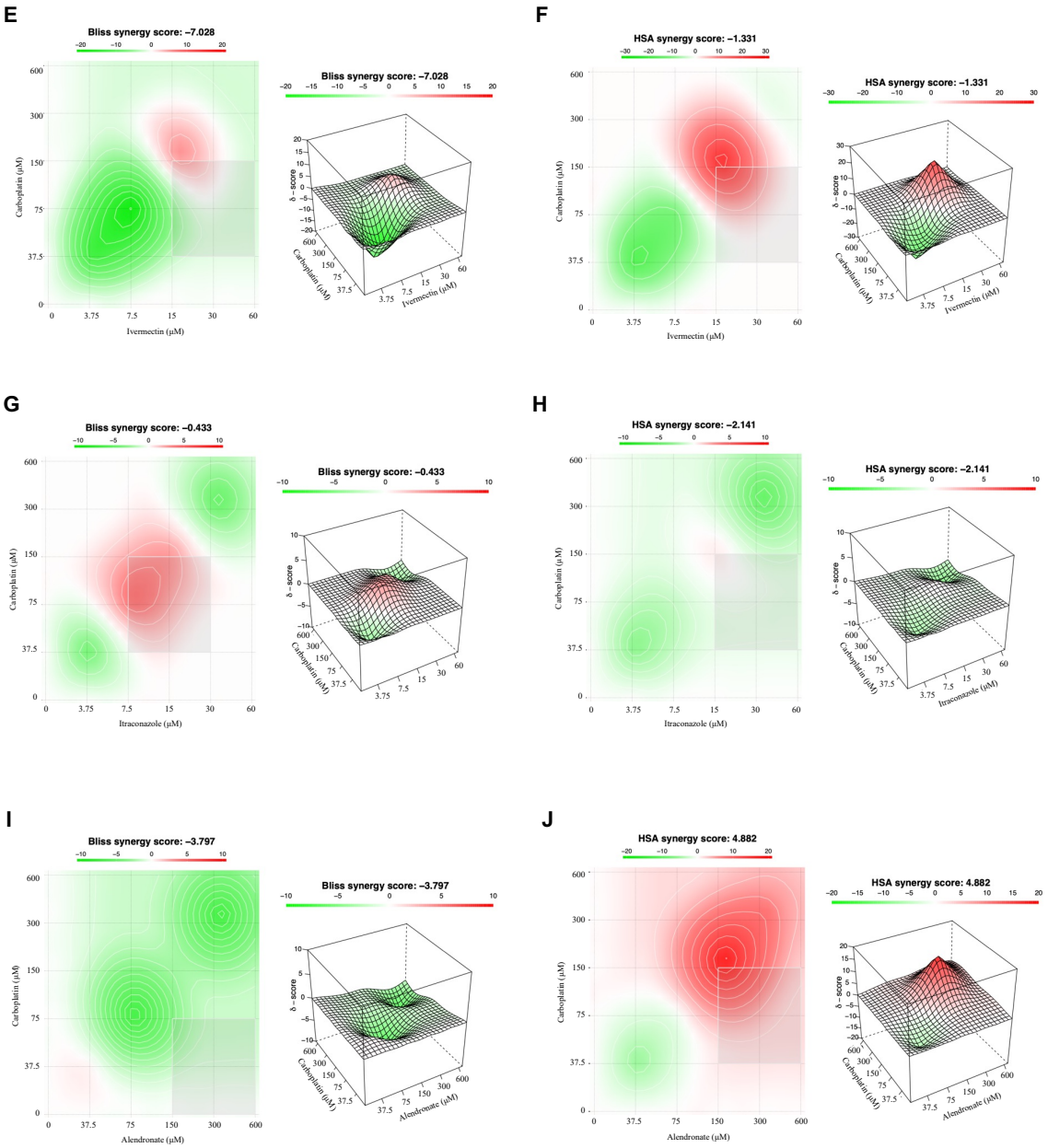


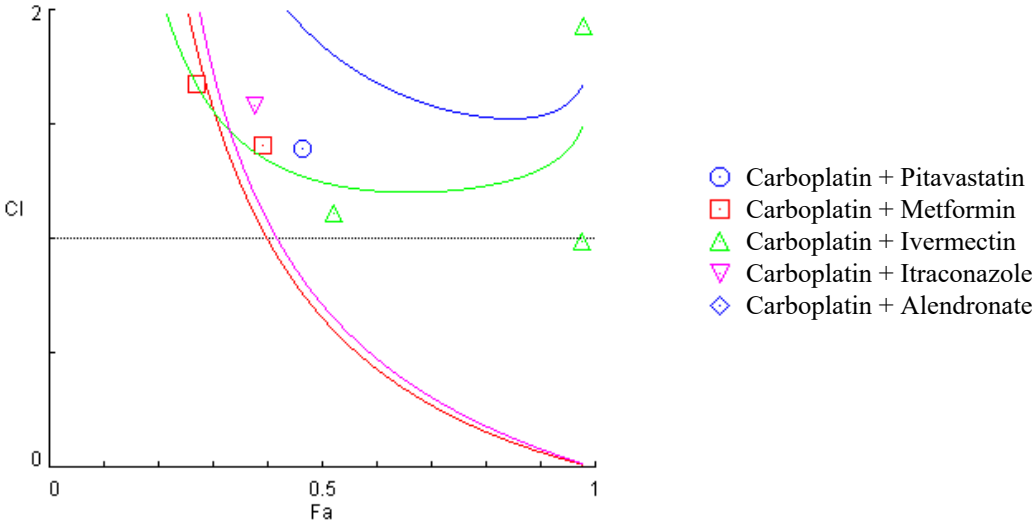
Figure 28. Combining Carboplatin with Pitavastatin and Metformin has a synergistic effect on OVCAR8 PTX R P cells. (A–J) Bliss Independence and HSA synergy 2D and 3D plots, which showed the drug synergism of OVCAR8 cells after exposure to fixed-dose ratios that correspond to 0.25, 0.5, 1, 2, and 4 times the individual IC_{50} values of each drug. Carboplatin was combined with (**A** and **B**) Pitavastatin, (**C** and **D**) Metformin, (**E** and **F**) Ivermectin, (**G** and **H**) Itraconazole, and (**I** and **J**) Alendronate for 48 hours. The combined treatment was administered simultaneously. All assays were performed in triplicate in at least three independent experiments. The synergy scores were categorized as follows: <−10 (antagonism, green), −10 to 10 (additivity, white), and >10 (synergism, red). HSA, high single agent.

The other aim of this study was to assess the safety profile of combining Carboplatin and repurposed drugs in non-tumoral HOSE6.3 cells. In here, was used the same three reference models to evaluate the results. The findings using the Chou-Talalay method showed that combining Carboplatin with all the repurposed drugs resulted in antagonism (green), with all five pairs showing a CI > 1 (**Figure 29 and Table S8**). Furthermore, the Bliss Independence and HSA models indicated that combining Carboplatin with Pitavastatin, Metformin, Ivermectin, Itraconazole, and Alendronate exhibited a stronger and negative synergy score, indicating antagonism (synergy score <-10, green) and additivity (synergy score -10 to 10, white), respectively (**Figure 30**).

The results obtained by the three reference models revealed the same tendency for OVCAR8, OVCAR8 PTX R P, and HOSE6.3 cell lines, demonstrating that all of them generate equivalent outcomes. However, as previously discussed, despite the improvements in the reference models (643), they still present some boundaries (722).

In summary, the results reveal an acceptable safety pharmacological profile of the tested drug combinations in a normal-like cell line and support the proposal to combine Carboplatin with Pitavastatin or Metformin in platinum-taxane-resistant HGSC patients.

A

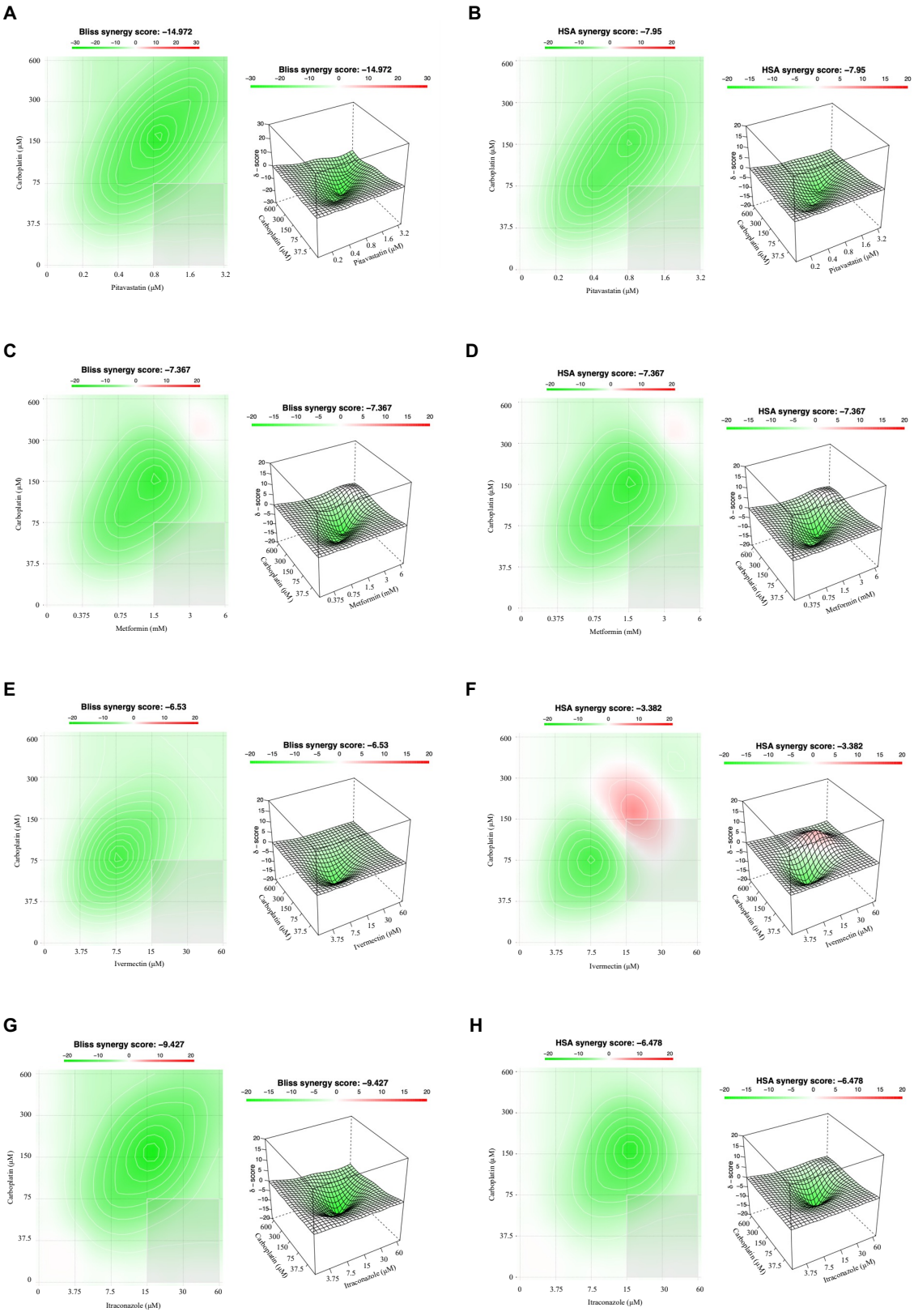


B

HOSE6.3

Combination (Drug 1 + Drug 2)	Total Dose (Drug 1 + Drug 2)	Dose (Drug 1)	Dose (Drug 2)	Fa	CI Value
Carboplatin (µM) + Pitavastatin (µM)	2.7	2.5	0.2	0.145	3.19705
	5.4	5	0.4	0.146	6.27093
	10.8	10	0.8	0.214	4.17256
	21.6	20	1.6	0.296	3.13944
	43.2	40	3.2	0.464	1.39375
Carboplatin (µM) + Metformin (mM)	2.875	2.5	0.375	0.003	5788.95
	5.75	5	0.750	0.06	7.06432
	11.5	10	1.5	0.134	3.40609
	23	20	3	0.272	1.67728
	46	40	6	0.392	1.41100
Carboplatin (µM) + Ivermectin (µM)	6.25	2.5	3.75	0.01	65.0123
	12.5	5	7.5	0.009	153.747
	25	10	15	0.523	1.11281
	50	20	30	0.978	0.99151
	100	40	60	0.981	1.93029
Carboplatin (µM) + Itraconazole (µM)	6.25	2.5	3.75	0.004	1.081E7
	12.5	5	7.5	0.072	45.6098
	25	10	15	0.129	8.19262
	50	20	30	0.252	2.20981
	100	40	60	0.378	1.58340
Carboplatin (µM) + Alendronate (µM)	40	2.5	37.5	0.007	114.442
	80	5	75	0.031	21.0826
	160	10	150	0.055	16.6046
	320	20	300	0.071	21.8303
	640	40	600	0.240	5.46829

Figure 29. Combining Carboplatin with repurposed drugs has an antagonistic effect on HOSE6.3 cells. (**A** and **B**) Chou–Talalay method Fa—CI plot and (**C**) Fa values and respective CI values. The plot illustrates the drug synergism of (**A**) OVCAR8 and (**B**) OVCAR8 PTX R P cells after exposure to fixed-dose ratios that correspond to 0.25, 0.5, 1, 2, and 4-times the individual IC_{50} values for each drug. Carboplatin was combined with Pitavastatin, Metformin, Ivermectin, Itraconazole, and Alendronate for 48 hours. The combined treatment was administered simultaneously. All assays were performed in triplicate in at least three independent experiments. The CI was plotted on the y-axis as a function of Fa on the x-axis to evaluate drug synergism, with CFI <1 (synergism, bold), CI =1 (additivity), and CI >1 (antagonism). CI, combinatory index; Fa, effect level.


A
Bliss synergy score: −14.972
Carboplatin (μM)
Pitavastatin (μM)
δ − score
B
HSA synergy score: −7.95
C
Bliss synergy score: −7.367
Metformin (mM)
D
HSA synergy score: −7.367
E
Bliss synergy score: −6.53
Ivermectin (μM)
F
HSA synergy score: −3.382
G
Bliss synergy score: −9.427
Itraconazole (μM)
H
HSA synergy score: −6.478

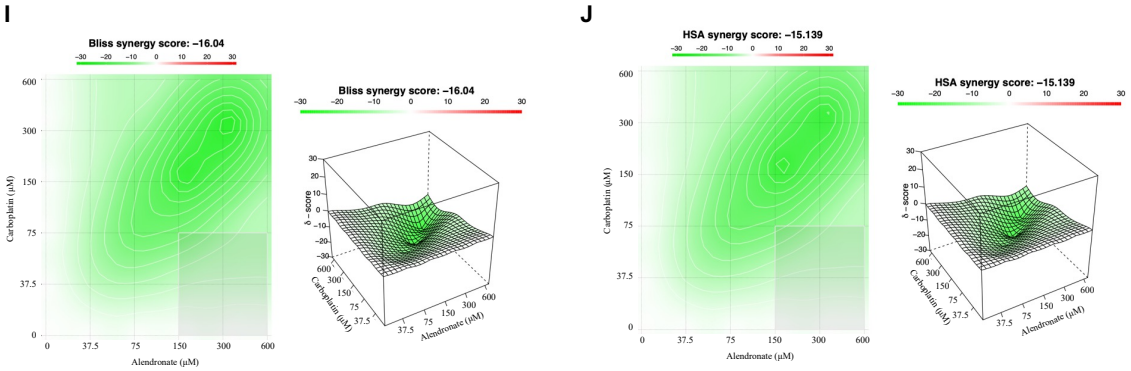


Figure 30. The combination of Carboplatin with repurposed drugs has an antagonistic effect on HOSE6.3 cells. (**A**–**J**) Bliss Independence and HSA synergy 2D and 3D plots, which showed the drug synergism of OVCAR8 cells after exposure to fixed-dose ratios that correspond to 0.25, 0.5, 1, 2, and 4 times the individual IC_{50} values of each drug. Carboplatin was combined with (**A** and **B**) Pitavastatin, (**C** and **D**) Metformin, (**E** and **F**) Ivermectin, (**G** and **H**) Itraconazole, and (**I** and **J**) Alendronate for 48 hours. The combined treatment was administered simultaneously. All assays were performed in triplicate in at least three independent experiments. The synergy scores were categorized as follows: <−10 (antagonism, green), −10 to 10 (additivity, white), and >10 (synergism, red). HSA, high single agent.

5. Discussion

Monotherapy treatments highlight different molecular pathways in tumor cells that can lead to chemoresistance and cancer recurrence. On the other hand, administering two or more drugs together can lead to a more effective therapeutic outcome (614, 645). This enables maximum efficacy to be achieved with lower drug concentrations, thereby reducing toxicity and severe side effects (647). Combining drugs typically involves using a sensitizing drug along with another drug that increases its cytotoxicity by taking advantage of the vulnerable state of the cells caused by the first agent (614, 644).

The combined administration of Carboplatin and Paclitaxel is the standard practice in the management of advanced HGSC (17, 21, 648, 649). However, several studies indicate that even when combined, the cytotoxic effect may still be insufficient, resulting in serious side effects and the emergence of chemoresistant tumor populations, which limits the effectiveness of this combination (653, 654). Therefore, it is imperative to explore alternatives to complement the current platinum-taxane-based regimens in order to reduce the therapeutic dose and exposure time needed to evade or overcome chemoresistance.

There is evidence to suggest that combining chemotherapeutic agents with repurposed drugs can enhance therapeutic efficacy by acting through different mechanisms/pathways in a synergistic or additive manner (567, 631, 640, 641).

Carboplatin, a well-known alkylating agent, interferes with DNA molecules, creating Platinum–DNA adduct and causing DNA cross-linking, which alters the structure and inhibits its synthesis (628, 722), consequently impairing protein synthesis and cell proliferation (651, 652). Some progress has been made in the search for new drugs that could synergize with platinum compounds; however, there is a lack of reports using repurposed drugs with Carboplatin for the treatment of HGSC patients. Nagaraj *et al.* (723) found that combining Indomethacin, a non-steroidal anti-inflammatory agent, with Cisplatin resulted in a more effective decrease in cell viability compared to chemotherapy alone in both Cisplatin-sensitive and resistant OC cells, demonstrating an additive outcome. Chloroquine, an anti-malaria drug, when combined with Cisplatin, increased the cytotoxicity effect by inducing lethal DNA damage and reversing Cisplatin resistance in resistant OC cells (724). Recently, Mariniello *et al.* (725) demonstrated that Tranilast (antiallergic), Telmisartan (antihypertensive), and Amphotericin B (antifungal) enhanced Cisplatin toxicity by stimulating platinum–DNA adduct formation in platinum-resistant OC cells. Another study showed that Mebendazole, an antiparasitic, acts synergistically by sensitizing chemoresistant OC cells to Cisplatin (726). Additionally, several reports indicated that Disulfiram, an antialcoholism drug, enhances sensitivity to Cisplatin in OC cell lines (727) and bladder cancer, presenting a synergistic effect (728). Finally, arsenic compounds, frequently used in traditional Chinese medicine to treat angiogenic diseases, such as cancer, psoriasis, and rheumatoid arthritis, were shown to induce cytotoxicity and have a synergistic effect with Cisplatin in Paclitaxel-resistant OC cells (729).

In several preclinical and retrospective studies, Pitavastatin (661-664), Metformin (631, 665-669), Ivermectin (670-672), Itraconazole (633, 676-678), and Alendronate (679-681) have shown potential as antineoplastic compounds. This study aimed to explore the combined effect of Carboplatin with these five repurposed drugs in Carboplatin-resistant (OVCAR8) and Carboplatin-Paclitaxel-resistant (OVCAR8 PTX R P) cell lines. Previous research has demonstrated the antitumoral activity of these non-oncologic drugs by reducing cellular viability in a concentration-dependent manner in both chemoresistant cell lines (722). Here, tests were conducted using all five agents in combination with Carboplatin using a model previously described (624). Both cell lines were exposed to five concentrations (0.25, 0.5, 1, 2, and 4-fold the IC_{50} values) of each drug alone and combined with the alkylating agent. Then was compared the antineoplastic effect of combining Carboplatin with repurposed agents to Carboplatin or each non-oncologic drug as a single agent. The results indicate that Pitavastatin and Metformin were the most promising

candidates for enhancing the effectiveness of Carboplatin in OVCAR8 PTX R P cells. Additionally, the morphometry of cells showed consistent effects when compared with the results obtained in the cellular viability assays.

The importance of choosing the best reference model to assess drug synergism has been emphasized in various studies. To date, different definitions (640) and methods (641) to determine drug synergism have been described, enhancing the importance of choosing the best reference model according to the data available and study type (643). There are different reference models, such as effect-based (e.g., Combination Subthresholding, HSA, Response Additivity, and Bliss Independence models) or dose-effect-based (e.g., Lower Additivity and Zero Interaction Potency), each explained by different mathematical frameworks based on various definitions of additivity (643). In this study, drug synergism was assessed using three reference models: Chou–Talalay, Bliss Independence, and HSA. The Chou–Talalay model provides a quantitative definition of additive (CI = 1), synergic (CI < 1), and antagonistic (CI > 1) effects based on the median-effect equation derived from the mass-action law principle and encompassing the Michaelis–Menten, Hill, Henderson–Hasselbalch, and Scatchard equations in biochemistry and biophysics (636, 642). The Bliss Independence model assumes that two drugs produce independent effects (638, 644, 682). In contrast, the HSA model suggests that the expected combination effect is the highest effect achieved by the most effective drug (623, 682). Based on these three reference models, the results of synergy analysis demonstrate that Metformin can synergistically decrease cellular viability for HGSC chemoresistant cell lines. Specifically, the Chou–Talalay method shows more synergistic (CI < 1) pairs for OVCAR8 PTX R P (8/25) compared to OVCAR8 (4/25) cells. Interestingly, for OVCAR8 PTX R P, Pitavastatin and Metformin are the most promising drugs at lower concentrations. Consequentially, the combination of Carboplatin with these two repurposed drugs in OVCAR8 PTX R P is encouraging and suitable for additional experiments to test its potential effect in patient-derived cells with chemoresistant disease.

The best pharmacotherapy selectively destroys cancerous cells while minimizing adverse side effects on normal cells. This study tested the combined effect of Carboplatin with five repurposed drugs, and the results showed that this combination therapy has an acceptable safety profile in non-tumoral cell lines.

Statins inhibit HMGCR, leading to the blockage of cholesterol biosynthetic pathways (662, 664, 683). Previous studies demonstrated that combining Statins with Cisplatin resulted in an additive or synergic effect in OC cell lines (730, 731). Another study revealed

that Statin works synergistically with Carboplatin and Paclitaxel (732). However, these results are not consensual, as another study showed an antagonistic effect between Carboplatin and Simvastatin (662). Nevertheless, Martirosyan *et al.* (661) showed that Lovastatin sensitizes chemoresistant cells to Doxorubicin by blocking drug efflux pumps. Previously, it was demonstrated that OVCAR8 PTX R P cells acquired Paclitaxel resistance by significantly increasing P-gp expression (628). In the present study, results with the double-resistant cell line (OVCAR8 PTX R P), using the Chou–Talalay model, showed that Pitavastatin was the most effective repurposed drug considering the lowest IC_{50} values, resulting in four synergic pairs when combined with Carboplatin. On the other hand, no synergic pairs were found for the same combination of OVCAR8 cells. Here, it was hypothesized that the synergic effect of combining Carboplatin with Pitavastatin is related to the chemoresistance background of the OVCAR8 PTX R P cell line since they are also Paclitaxel-resistant and, therefore, share a similar mechanism of resistance. However, more studies are required to clarify these results.

Multiple mechanisms have been proposed for the antineoplastic effects of Metformin, including modulation of immunological and anti-inflammatory responses, inhibition of mTOR, and blocking insulin signals and glucose synthesis via respiratory-chain complex I blockade (683, 685-688). In endometrioid carcinoma, Metformin at clinically relevant concentrations did not show any anticancer activity and, when combined with Carboplatin, did not exhibit synergistic effects (733). However, the results align with other studies showing that Metformin can re-sensitize cells to Cisplatin (666, 734-736), partially reverse platinum resistance (737), or have a benefic synergistic impact when combined with Carboplatin (734, 738, 739). Similarly, in non-small-cell lung cancer, Metformin was found to reverse Carboplatin resistance by inhibiting glucose metabolism partially (740). Cai e*t al.* (741) showed in breast cancer that Metformin is more effective in tumors expressing higher cation transporter levels. Patel *et al.* (742) showed that combining Metformin with Carboplatin or Paclitaxel increases apoptotic activity, suggesting potential as a chemo-adjuvant in OC. However, the results also indicate that the concentration of Metformin needed to achieve a synergic effect is too high (mM) to be translated to the clinical setting. Therefore, further studies are required in order to determine the clinical significance of these *in vitro* results.

Several mechanisms can explain the antineoplastic effect of Ivermectin, a broad-spectrum antiparasitic agent. These mechanisms include the inhibition of MDR, modulation of Akt/mTOR and Wnt/TCF signaling pathways, and inactivation of PAK-1 expression (632, 689-694). Kodama *et al.* (670) showed that combining Paclitaxel with Ivermectin has a

stronger antitumoral effect on OC compared to each drug alone. Moreover, it has been demonstrated that Ivermectin enhances the efficacy of Cisplatin in OC by suppressing the phosphorylation of key molecules in the Akt/mTOR signaling pathway (671). Studies have reported that Ivermectin can reverse chemoresistance in colorectal, breast, and chronic myeloid leukemia cancer cells by inhibiting the EGFR/ERK/Akt/NF-κB pathway (672). Recently, Juarez *et al.* (743) demonstrated that Ivermectin was synergistic with Docetaxel, Cyclophosphamide, and Tamoxifen in breast and prostate cancer cell lines. These studies support the findings that combining Carboplatin with Ivermectin results in a significant increase in the anticancer effect for chemoresistant cell lines, showing a synergistic or at least an additive effect.

Itraconazole, a common antifungal agent, has shown potential as an anticancer treatment when used in clinically recommended doses (673). Numerous studies have indicated that Itraconazole targets different mechanisms, including reversing chemoresistance mediated by P-gp, inhibiting Hedgehog, mTOR, and Wnt/β-catenin signaling pathways, and reducing angiogenesis and lymphangiogenesis (673, 695-699). *In vitro* studies have shown that Itraconazole can reverse P-gp-mediated resistance associated with Docetaxel, Paclitaxel, Vinblastine, Daunorubicin, and Doxorubicin in a concentration-dependent manner (676, 678, 701). Recent preclinical and clinical trials have also indicated that Itraconazole can reverse Paclitaxel resistance (698, 699). Furthermore, a study using patient-derived xenografts models derived from OC chemoresistant patients showed a synergistic effect of combining Itraconazole with Paclitaxel (633). Despite these promising findings, the combination results of this antifungal agent did not lead to an accurate IC_{50} value, making it impossible to infer its therapeutic effect in these cell line models.

Bisphosphonates block farnesyl pyrophosphate synthase, which is located downstream of HMGCR, leading to the impairment of cholesterol biosynthesis (702). Preclinical evidence suggests that Bisphosphonates have antineoplastic activity (744-748). They exhibit an antitumoral property when combined with chemotherapeutic agents, inhibiting tumor proliferation and dissemination of OC (702). Combining Zoledronic Acid with Cisplatin, Doxorubicin, or Paclitaxel showed a synergistic effect by increasing cell death in breast cancer cells (749-751). Göbel *et al.* (752) also demonstrated an antitumor promising impact of Zoledronic Acid in the OC. Another study revealed that Alendronate decreases stromal invasion, tumor burden, and MA, suggesting antineoplastic activity in OC (634). Knight *et al.* (704) demonstrated a direct effect of Bisphosphonates in OC cell lines and tumor-derived cells. However, when combined with Cisplatin or Paclitaxel, the combination

did not result in a significant increase in its chemotherapeutic effect. The results are in agreement with this last study, as was observed an impact of Alendronate in both chemoresistant cell lines (722). Still, when this agent was combined with Carboplatin, was observed an antagonistic or additive effect, suggesting it may not be the best drug partner to integrate with this alkylating agent.

The resistance mechanisms to platinum-based drugs are extremely complex, involving various cellular events such as altered cellular drug accumulation, enhanced detoxification systems, improved DNA repair processes, and reduced apoptosis and autophagy (200, 753). Multiple transporters facilitate the uptake of platinum-based antineoplastic agents; however, changes in their expression level, localization, or activity may reduce the intracellular accumulation of these compounds, thereby diminishing their cytotoxic effect (200). Furthermore, detoxification systems can bind to these compounds and prevent the formation of platinum–DNA adducts (200). Additionally, the activation of the DNA repair process and an increase in apoptosis or autophagy can significantly impact the response to these drugs (200).

One of the most important hallmarks of resistance in platinum-resistant cell lines is the reduced cellular content (754). To ensure the cytotoxic effect, platinum compounds must be accumulated inside tumoral cells. Amplified cellular efflux or diminished cellular influx is associated with chemoresistance, as it prevents cancer cells from being exposed to lethal concentrations of the drugs (200).

Facing this scenario, it is crucial to identify the transporters responsible for platinum uptake and intake and to find effective ways to target them to evade or reverse chemoresistance. An interesting study showed that an increased expression of efflux transporters responsible for copper homeostasis, such as P-type ATPases (ATP7A and ATP7B), predicts shorter survival for OC patients treated with platinum compounds and highlights the significant role of them chemoresistance (755). In platinum resistance cells, the localization of these transports is altered, contributing to drug retention (222, 756). Therefore, downregulating ATP7A/B could be an effective way to overcome chemoresistance (200).

CTR1 is a carrier of Carboplatin, and several studies indicate that low expression reduces the intracellular accumulation of platinum compounds (215). In contrast, high expression makes cancer cells more sensitive to these agents (216, 757).

Further studies are necessary to confirm the results mentioned here. It is crucial to assess whether Pitavastatin and Metformin act as chemosensitizers by functioning as

substrates and modulators of these (or other) important proteins, inhibiting their function and consequently enhancing the cytotoxic effectiveness of the antineoplastic drugs. Platinum resistance is multifactorial, and the molecular mechanisms of resistance and good molecular predictive biomarkers of Carboplatin resistance are yet to be discovered.

6. Conclusion

Combining Carboplatin with Pitavastatin or Metformin could be a promising therapeutic approach for patients with HGSC who are resistant to Carboplatin and Paclitaxel. Both Pitavastatin and Metformin have different mechanisms of action, which can help overcome chemoresistance. To the best of our knowledge, this study was the first that demonstrated that Pitavastatin and Metformin, either alone or in combination with Carboplatin, enhance the effectiveness of this anti-cancer drug in a model of Carboplatin-Paclitaxel chemoresistant HGSC.

In pharmacological studies, it is crucial to observe the effects of combining two or more drugs at lower concentrations. However, conducting more in-depth mechanistic studies is important to understand the anti-cancer effects of combining Carboplatin with Pitavastatin or Metformin in Carboplatin-Paclitaxel chemoresistant HGSC patients. This next step involves evaluating the impact of these combinations in a variety of cell lines with different treatment schemes and expanding the research to *ex vivo* models. This approach is necessary as individual patients have specific phenotypic characteristics, genotypic statuses, and patterns of chemoresistance. Additionally, using patient-derived culture enables the development of drug sensitivity tests to predict clinical responses to therapy and identify more effective treatment regimens.

Overall, these results emphasize Pitavastatin and Metformin as agents that can enhance the sensitivity of platinum-taxane-resistant cancers, supporting further research.

7. Acknowledgments and Funding

This work was developed at *Instituto de Investigação e Inovação em Saúde (i3S)*, an Associate Laboratory of the *Ministério da Ciência, Tecnologia e Inovação (MCTES),* and it was partially supported by *Fundação para a Ciência e a Tecnologia (FCT).* This research was supported by the project “HOPE – Improving Ovarian Cancer Patients Survival,” a donation from an ovarian cancer patient to the Institute of Molecular Pathology and Immunology of the University of Porto (IPATIMUP) and by *Fundo Europeu de Desenvolvimento Regional (FEDER)* through the *COMPETE 2020–Operational Program for*

Competitiveness and Internationalization (POCI), Portugal 2020 and *FCT/MCTES,* under the project POCI 01-0145-FEDER-029503 (PTDC/MEC-ONC/29503/2017). M.N. and D.D. acknowledges *FCT/MCTES* and *UE* for financial support through a PhD. fellowship (2020.04720.BD and SFRH/BD/140734/2018, respectively) that was co-sponsored by *Fundo Social Europeu (FSE)* through *Programa Operacional Regional Norte (Norte 2020).* N.V. thankful for the support from *FCT* and *FEDER* award number IF/00092/2014/CP1255/CT0004 and CHAIR in Onco-Innovation from *Faculdade de Medicina da Universidade do Porto (FMUP).*

8. Supplementary Material

Table S7. The cellular viability (%) of OVCAR8 and OVCAR8 PTX R P cells after treatment with Carboplatin and repurposing drugs. Cellular viability was measured after exposure to a fixed dose ratio corresponding to 0.25, 0.5, 1, 2, and 4 times the individual IC_{50} values of each drug for 48 hours. The combined treatment was administered simultaneously. All assays were done in triplicate in at least three independent experiments. SD, standard deviation.

Treatement	Concentration	OVCAR8		OVCAR8 PTX R P	
		Cellular viability (%)		Cellular viability (%)	
		Media	SD	Media	SD
Carboplatin (μM)	0.25 × IC_{50}	92.531	0.672	87.570	1.918
	0.5 × IC_{50}	78.349	8.436	75.397	3.802
	IC_{50}	60.702	5.190	57.172	4.484
	2 × IC_{50}	9.962	2.159	24.033	8.183
	4 × IC_{50}	3.178	1.576	3.973	1.422
Pitavasvatin (μM)	0.25 × IC_{50}	60.608	3.877	60.785	7.665
	0.5 × IC_{50}	52.738	3.251	49.751	2.207
	IC_{50}	46.854	2.547	44.716	1.406
	2 × IC_{50}	35.398	3.108	28.515	4.045
	4 × IC_{50}	29.124	6.221	28.178	3.446
Carboplatin (μM) + Pitavastatin (μM)	0.25 × IC_{50}	60.349	2.856	56.075	10.193
	0.5 × IC_{50}	48.552	1.908	40.283	6.228
	IC_{50}	31.048	1.237	25.796	3.497
	2 × IC_{50}	19.453	4.417	12.832	8.774
	4 × IC_{50}	5.576	0.735	4.173	2.130
Metformin (mM)	0.25 × IC_{50}	73.629	4.867	75.521	1.641
	0.5 × IC_{50}	60.764	1.710	60.300	1.300
	IC_{50}	46.377	4.049	45.069	0.889
	2 × IC_{50}	19.461	2.920	12.592	1.286
	4 × IC_{50}	15.469	3.467	7.795	1.018
Carboplatin (μM)+ Metformin (mM)	0.25 × IC_{50}	70.624	3.533	73.912	1.977
	0.5 × IC_{50}	54.726	1.645	55.091	4.483
	IC_{50}	8.641	1.962	9.897	3.787
	2 × IC_{50}	7.105	1.963	8.138	1.219
	4 × IC_{50}	4.060	0.503	3.435	1.049
Ivermectin (μM)	0.25 × IC_{50}	76.543	1.978	81.214	2.466
	0.5 × IC_{50}	68.485	0.746	64.803	2.168
	IC_{50}	42.511	1.788	44.580	3.147
	2 × IC_{50}	0.514	0.050	1.210	1.256
	4 × IC_{50}	0.379	0.299	0.494	0.183
Carboplatin (μM)+ Ivermectin (μM)	0.25 × IC_{50}	91.320	7.718	95.832	3.646
	0.5 × IC_{50}	74.018	11.931	73.639	9.023
	IC_{50}	32.828	3.453	25.286	3.508
	2 × IC_{50}	0.290	0.214	1.644	1.348
	4 × IC_{50}	0.020	0.451	0.593	0.905
Itraconazole (μM)	0.25 × IC_{50}	94.332	7.175	90.418	14.825
	0.5 × IC_{50}	95.498	3.874	97.015	19.576
	IC_{50}	95.141	6.063	94.016	16.247
	2 × IC_{50}	98.250	2.400	91.571	13.226
	4 × IC_{50}	98.398	7.288	89.624	7.916
Carboplatin (μM) + Itraconazole (μM)	0.25 × IC_{50}	89.970	1.158	90.445	10.179
	0.5 × IC_{50}	80.492	3.557	76.639	6.622
	IC_{50}	63.513	3.335	56.847	8.386
	2 × IC_{50}	44.603	4.434	28.241	8.300
	4 × IC_{50}	4.998	3.142	3.299	1.794
Alendronate (μM)	0.25 × IC_{50}	99.951	1.327	98.798	3.424
	0.5 × IC_{50}	92.024	2.157	85.644	0.167
	IC_{50}	44.307	4.276	46.798	3.093
	2 × IC_{50}	37.529	4.275	41.214	5.101
	4 × IC_{50}	31.770	5.646	40.422	5.688
Paclitaxel (nM) + Alendronate (μM)	0.25 × IC_{50}	92.829	5.804	92.727	6.105
	0.5 × IC_{50}	80.026	9.039	75.374	11.574
	IC_{50}	29.772	1.781	30.868	3.128
	2 × IC_{50}	18.664	3.727	16.565	3.230
	4 × IC_{50}	6.752	0.061	6.396	1.081

Table S8. **The cellular viability (%) of HOSE6.3 cells after treating with Carboplatin and repurposing drugs**

Cellular viability was measured after exposure to a fixed dose ratio corresponding to 0.25, 0.5, 1, 2, and 4 times the individual IC_{50} values of each drug for 48 hours. The combined treatment was administered simultaneously. All assays were done in triplicate in at least three independent experiments. SD, standard deviation.

Treatment	Concentration	HOSE6.3	
		Cellular viability (%)	
		Media	SD
Carboplatin (μM)	0.25 × IC_{50}	88.270	5.412
	0.5 × IC_{50}	80.640	1.159
	IC_{50}	72.731	4.688
	2 × IC_{50}	73.328	1.388
	4 × IC_{50}	51.060	2.693
Pitavasvatin (μM)	0.25 × IC_{50}	81.849	7.680
	0.5 × IC_{50}	76.512	7.815
	IC_{50}	68.461	3.472
	2 × IC_{50}	65.889	5.045
	4 × IC_{50}	61.442	2.761
Carboplatin (μM) + Pitavastatin (μM)	0.25 × IC_{50}	85.461	3.279
	0.5 × IC_{50}	85.366	2.539
	IC_{50}	78.648	2.658
	2 × IC_{50}	70.445	0.900
	4 × IC_{50}	53.617	2.412
Metformin (mM)	0.25 × IC_{50}	96.286	4.708
	0.5 × IC_{50}	97.225	1.002
	IC_{50}	95.033	1.429
	2 × IC_{50}	96.033	1.778
	4 × IC_{50}	92.366	2.639
Carboplatin (μM) + Metformin (mM)	0.25 × IC_{50}	99.735	1.395
	0.5 × IC_{50}	94.038	1.253
	IC_{50}	86.581	1.751
	2 × IC_{50}	73.321	2.244
	4 × IC_{50}	60.842	0.441
Ivermectin (μM)	0.25 × IC_{50}	100.990	2.144
	0.5 × IC_{50}	99.694	3.725
	IC_{50}	53.462	2.873
	2 × IC_{50}	0.539	1.365
	4 × IC_{50}	0.000	0.544
Carboplatin (μM) + Ivermectin (μM)	0.25 × IC_{50}	99.024	1.122
	0.5 × IC_{50}	99.061	1.886
	IC_{50}	47.689	3.598
	2 × IC_{50}	2.2495	0.514
	4 × IC_{50}	1.942	0.937
Itraconazole (μM)	0.25 × IC_{50}	86.353	3.252
	0.5 × IC_{50}	84.356	1.857
	IC_{50}	84.735	3.865
	2 × IC_{50}	79.729	1.179
	4 × IC_{50}	77.370	3.174
Carboplatin (μM) + Itraconazole (μM)	0.25 × IC_{50}	99.610	1.337
	0.5 × IC_{50}	92.847	1.446
	IC_{50}	87.060	1.599
	2 × IC_{50}	74.815	3.392
	4 × IC_{50}	62.169	0.574
Alendronate (μM)	0.25 × IC_{50}	101.792	6.109
	0.5 × IC_{50}	101.959	6.966
	IC_{50}	92.147	2.125
	2 × IC_{50}	89.188	5.221
	4 × IC_{50}	84.305	5.970
Carboplatin (μM) + Alendronate (μM)	0.25 × IC_{50}	99.274	0.455
	0.5 × IC_{50}	96.901	0.646
	IC_{50}	94.532	3.028
	2 × IC_{50}	92.908	2.486
	4 × IC_{50}	76.021	3.396

iii. Ivermectin Boosts Paclitaxel Effectiveness in High-Grade Serous Carcinoma in 3D Cell Cultures

1. Abstract

Chemoresistance is a major obstacle in HGSC treatment. Although many patients initially respond to chemotherapy, the majority of them relapse due to resistance to Carboplatin and Paclitaxel. In response to these challenges, drug repurposing has surfaced as a potentially effective strategy, capable of working synergically with standard chemotherapy to bypass chemoresistance.

In prior studies, using a 2D cell culture model and two HGSC chemoresistant cell lines, it was demonstrated that combining Carboplatin or Paclitaxel with Pitavastatin or Ivermectin resulted in the highest rates of cytotoxicity and the most notable synergy. This combination offered a greater therapeutic effect than each drug individually.

Acknowledging that 2D cell culture systems are limited in their ability to reflect tumor architecture, 3D cell cultures were generated to provide insights into treatment efficacy tests in more complex cellular models.

We aimed to investigate whether combining Carboplatin or Paclitaxel with Pitavastatin or Ivermectin offers therapeutic benefits in Cultrex RGF Basement Membrane Extract (BME) type 2 based 3D model. Here, the cytotoxic impacts of Carboplatin and Paclitaxel were analyzed, both alone and in combination with Pitavastatin and Ivermectin, on two chemoresistant tumor cell lines, OVCAR8 and OVCAR8 PTX R C in 3D cultures. Cellular viability was assessed using CellTiter-Glo® Luminescent assays. Also, it explored synergistic interactions using Zero Interaction Potency (ZIP), Loewe, Bliss Independence, and HSA reference models, employing SynergyFinder Plus Software.

Our research indicates that combining chemotherapeutic drugs with Pitavastatin or Ivermectin yields significantly more cytotoxic effects than Carboplatin and Paclitaxel monotherapy. Additionally, the combination of Paclitaxel and Ivermectin shows a strong additive effect in 3D chemoresistant cell line models, emphasizing the potential of this two-drug approach for treating HGSC.

Keywords

3D Cultures, Chemoresistance, Drug Repurposing, High-Grade Serous Carcinoma, Drug Synergism.

2. Introduction

The standard treatment for HGSC includes Carboplatin and Paclitaxel; however, these can lead to chemoresistance and adverse side effects, affecting treatment effectiveness (17, 65, 67, 599). Combining repurposed drugs with chemotherapy may enhance efficacy, reduce toxicity, and counter-resistance (606-608). This approach investigates new applications for existing approved drugs, potentially saving time and costs in drug development (606-608). Since these drugs have established pharmacological and toxicological profiles, the approval for new indications is typically faster than for new drugs (610-612). However, to integrate repurposed drugs into oncology, appropriate clinical trials must be established to assess drug efficacy and determine the maximum tolerated dose to avoid intolerable toxicities (610).

Addressing chemoresistance can involve combining drugs at optimal ratios to target different mechanisms, enhancing sensitivity and efficacy (718). Interactions can yield synergistic, additive, or antagonistic effects, with synergy offering the greatest benefit by surpassing individual activities (620). Antagonism reduces effectiveness, while additivity results in a combined impact equal to the sum. Synergistic use often allows for lower dosages, decreasing systemic toxicity and side effects (615, 621, 622).

Pitavastatin, an antilipidemic drug, may benefit cancer therapy through its anti-tumoral effects, reduction of inflammation, and synergistic effects with other drugs (607). Statins inhibit the mevalonate pathway, impacting cell proliferation and survival, potentially slowing tumor growth, and enhancing other treatments (758). Some studies suggest combining statins with chemotherapy improves outcomes by increasing cancer cell sensitivity (722, 759). Statins' anti-inflammatory properties may also reduce the supportive TME (760).

Ivermectin, an antiparasitic agent, may have anti-cancer properties (607). In some cases, it has been found to enhance the effectiveness of chemotherapy drugs and even reverse resistance to them (672, 722). Ivermectin can act as a chemosensitizer by blocking drug efflux, increasing drug accumulation, and improving the efficacy of antineoplastic drugs (607, 761).

Our previous studies indicated that Pitavastatin and Ivermectin significantly decreased the cellular viability of OVCAR8 and OVCAR8 PTX R P cells (722). In contrast, both drugs showed minimal effect on the viability of HOSE6.3, a normal-like cell line, highlighting their differential impact on cancerous versus normal-like cells (722). This suggests that Pitavastatin and Ivermectin maintain a favorable safety profile in normal-like

cells while exhibiting substantial anticancer efficacy in chemoresistant tumor cells, positioning them as promising candidates for combination therapy with Carboplatin and Paclitaxel (722, 759). Moreover, the results showed that combining Carboplatin or Paclitaxel with Pitavastatin had the strongest synergistic and cytotoxic effect on the chemoresistant cancer cells, surpassing the impact of chemotherapeutic drugs alone (722, 759). The same effect was also seen for the combination of Paclitaxel with Ivermectin (722).

It's essential to recognize that 2D cell culture models often fail to accurately mimic the complex architecture *in vivo* environments found in living organisms. These models can oversimplify interactions between cells and their microenvironments, leading to results that may not effectively translate to clinical scenarios (762-764). To address these limitations, researchers have developed 3D cell culture technologies, which provide a more realistic representation of tissue architecture and cellular interactions. Moreover, drugs have more difficulty reaching the cells when they are in a 3D structure, as the increased complexity and density of the 3D microenvironment can impede drug penetration and lead to uneven distribution, in contrast to the more accessible and uniform environment of 2D cell cultures (765-767). Therefore, drug studies can be conducted with greater precision using models, allowing for more reliable insights into how treatments may perform in actual biological systems (762-764).

Here, it was investigated whether combining Carboplatin and Paclitaxel with Pitavastatin and Ivermectin provided therapeutic benefits in a Cultrex RGF BME type 2 - based 3D model using two chemoresistant HGSC cell lines (OVCAR8 and OVCAR8 PTX R C).

Our findings demonstrate that combining Paclitaxel with Pitavastatin or Ivermectin has the highest cytotoxic effect and the strongest synergism for both chemoresistant cell lines compared to Paclitaxel alone. These results, performed in 3D cell line models, support our previous results with 2D cell cultures and reinforce that this combination is a viable therapeutic strategy for managing HGSC patients with a chemoresistant profile.

3. Materials and Methods

3.1. Cell Lines and Culture Conditions

The OVCAR8 (resistant to Carboplatin) (567) and OVCAR8 PTX R C (resistant to both Carboplatin and Paclitaxel) (628) cell lines were chosen as models for HGSC. Further information regarding the cell lines and their culture conditions has been provided previously (722).

3.2. Drugs

Carboplatin, Paclitaxel, Pitavastatin, and Ivermectin were acquired from Selleckchem (Houston, TX, USA). They were dissolved in DMSO (AppliChem, Barcelona, Spain) or distilled water and stored at −80 °C according to the manufacturer's guidelines. Prior to usage, an aliquot was diluted to the necessary concentrations.

3.3. Cell Viability Assay

We employed CellTiter-Glo® luminescent assays to assess cellular viability following the manufacturer's instructions. For creating and sustaining stable 3D dome structures on cell culture plates, was utilized Cultrex RGF BME type 2 (Bio-Techne, Minneapolis, MN, USA). First t, it was started by preparing a cell suspension with 2.5 × 10^3 cells/well in complete media with 60% Cultrex RGF BME type 2 . Next, was carefully added 10 µl of this suspension into each well of a 96-well black/clear bottom plate and incubated at 37 °C with 5% CO_2 for 2 minutes. Afterward, the plate was inverted and left in the incubator for 25 minutes to ensure the full polymerization of the Cultrex RGF BME type 2 . Then, a complete medium was added and incubated under the same conditions. After 96 hours, the cells were treated with escalating concentrations of Carboplatin (37.5 to 600 µM), Paclitaxel (2.5 to 40 nM), Pitavastatin (0.2 to 3.2 µM), and Ivermectin (3.75 to 60 µM), and they remained incubated under identical conditions for an additional 72 hours. Following this was discarded the medium and introduced 50 µl of CellTiter-Glo® 2.0 Reagent (Promega Corporation, Madison, WI, USA), diluted 1:1 in culture medium, allowing it to incubate for 10 minutes at RT, shielded from light to ensure the stability of the luminescent signal. Luminescence was then measured using a Bio Tek Synergy™ 2 multi-mode microplate reader (BioTek, Winooski, VT, USA). The treated cells were compared to control cells, which were considered 100% viable, containing 1% (v/v) of the vehicle (DMSO), with white wells (without cells) as the baseline.

3.4. Drug Treatment and Interaction Analysis

Earlier reports presented the IC_{50} values for each drug (628, 722). These values were utilized in combination studies, which involved varying concentrations of both drugs in a consistent ratio, as outlined in previous methodologies (623). Specifically, Carboplatin or Paclitaxel was used in combination with various repurposed drugs at fixed-dose ratios corresponding to 0.25, 0.5, 1, 2, and 4 times the individual IC_{50} values over 72 hours.

This research further examined the responses to drug combinations using SynergyFinder Plus Software (Netphar, Faculty of Medicine, University of Helsinki, Helsinki, Finland). This software facilitated the estimation of expected drug combination effects based on the ZIP, Loewe, Bliss Independence, and HSA reference models (638, 644). It enables interactive analysis and visualization of multidrug combination profiling, showcasing synergy (in red) and antagonism (in green) on both 2D and 3D synergy maps (623). Additionally, the cNMF algorithm within SynergyFinder Plus Software was employed to identify outlier measurements (639).

3.5. Microscopic Evaluation

All microscopic figures were captured under a Leica DMi1 inverted phase contrast microscope (Leica Microsystems, Wetzlar, Germany) at 50× magnification.

3.6. Statistical Analysis

All assays were performed in triplicate with at least three independent experiments. The data was expressed as the mean ± SD. Statistical analysis was performed in GraphPad Prism 10 (GraphPad Software Inc., Boston, CA, USA) using ordinary one-way or two-way ANOVA followed by Šıdák's multiple comparison test.

4. Results

4.1. Combining Carboplatin with Pitavastatin or Ivermectin Has an Additive Effect on OVCAR8 and OVCAR8 PTX R C Cells

In this study, was utilized a predefined combination model to combine Carboplatin with Pitavastatin and Ivermectin. Chemoresistant HGSC cells were plated in 3D culture and treated with each drug individually and in combination at set ratios based on their IC_{50} values. The findings indicated that for OVCAR8, the combination of Carboplatin and Pitavastatin significantly enhanced the anticancer effect ($p < 0.0001$) at 0.25, 0.5, 1, and 2 times the individual IC_{50} values, compared to Carboplatin alone (**Figure S7A**). For OVCAR8 PTX R C cells, this combination significantly increased the anticancer effect ($p < 0.0001$) for 0.25, 0.5, and 1 times the individual IC_{50} values compared to Carboplatin as a single agent (**Figure S7B**).

For OVCAR8, combining Carboplatin with Ivermectin significantly enhanced the anticancer effect ($p < 0.0001$) at 0.25, 0.5, and 1 times the IC_{50} values, in contrast to Carboplatin alone (**Figure S7C**). For OVCAR8 PTX R C cells, this combination also

heightened the antineoplastic effect at 0.25 ($p < 0.001$) and 0.5 ($p < 0.0001$) times the IC_{50} values, compared to Carboplatin as a single agent (**Figure S7D**).

The synergistic effect is defined as the observed effect exceeding the expected effect derived from reference models (synergy scoring models). Each model operates under different assumptions about the predicted effect due to their unique mathematical frameworks (643). With this in mind, was employed four distinct methods – ZIP, Loewe, Bliss Independence, and HSA models – to evaluate drug interactions and compare the outcomes. The ZIP model calculates the expected effect based on the premise that the two drugs do not enhance each other (768). The Loewe additivity model defines the expected effect $yLOEWE$ as if a drug were combined with itself and incorporates the dose-response curves of each drug (769). The Bliss model operates on the assumption of a stochastic process where two drugs independently exert their effects, allowing for the calculation of the expected combination effect based on the probabilities of independent events (770). HSA asserts that the expected combination effect is equal to the greater effect of the individual drugs (771). In all four models, the synergy score for a drug combination is averaged over all the dose combination measurements, resulting in positive (synergy, red) and negative (antagonism, green) synergy score values (623).

Findings from the analysis of OVCAR8 cells for three of the four models used to assess drug interactions revealed negative synergy scores of -41.19, -45.56, and -43.36 when combining Carboplatin with Pitavastatin, indicating antagonism (green) (**Figures S8A, S8B and S8C**). Yet, the Loewe model shows a positive synergy score of 8.53, suggesting additivity (white) along with some synergistic zones (red) for these combinations at lower and intermediate concentrations (**Figure 31A**). In the case of OVCAR8 PTX R C cells, three of the four models used to assess drug interactions yielded negative synergy scores of -45.77, -48.63, and -47.62, indicating antagonism (green) (**Figures S8D, S8E, and S8F**). Nonetheless, the Loewe model reported a positive synergy score of 6.47, suggesting additivity (white) and some synergistic zones (red) for the combinations at lower to intermediate concentrations (**Figure 31B**).

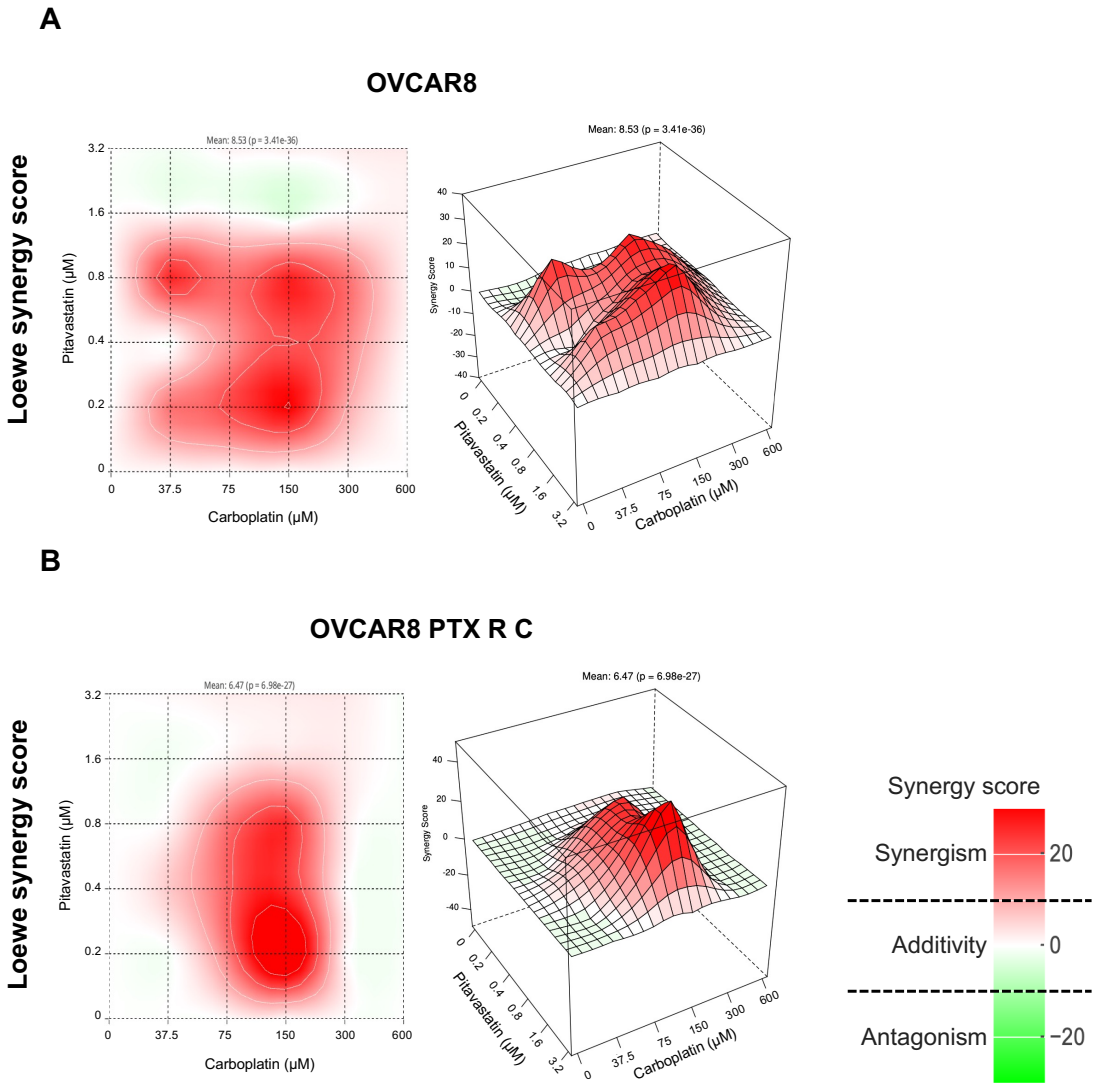


Figure 31. Combining Carboplatin with Pitavastatin has an additive effect on OVCAR8 and OVCAR8 PTX R C cells according to the Loewe synergy model. 2D and 3D synergy plots showed the drug synergism of OVCAR8 (**A**) and OVCAR8 PTX R C (**B**) cells after exposure to fixed-dose ratios that correspond to 0.25, 0.5, 1, 2, and 4 times the individual IC_{50} values of each drug. Carboplatin was combined with Pitavastatin for 72 hours. The combined treatment was administered simultaneously. All assays were performed in triplicate in at least three independent experiments. The synergy scores were categorized as follows: <−10 (antagonism, green), −10 to 10 (additivity, white), and >10 (synergism, red). HSA, high single agent; ZIP, zero interaction potency.

For OVCAR8 cells, the findings for three of the four models used to assess drug interactions indicate negative synergy scores of -37.65, -42.89, and -42.47 when combining Carboplatin with Ivermectin, confirming antagonism (green) (**Figures S9A, S9B, and S9C**). Additionally, the Loewe model indicated a positive synergy score of 11.45, suggesting

synergy (red) (**Figure 32A**). Regarding OVCAR8 PTX R C cells, this combination for three of the four models used to assess drug interactions showed negative synergy scores of -32.70, -38.80, and -27.68, indicating antagonism (green) (**Figures S9D, S9E, and S9F**). Furthermore, the Loewe model reported a positive synergy score of 9.62, suggesting additivity (white) along with some synergistic zones (red) for the combinations at lower and intermediate concentrations (**Figure 32B**).

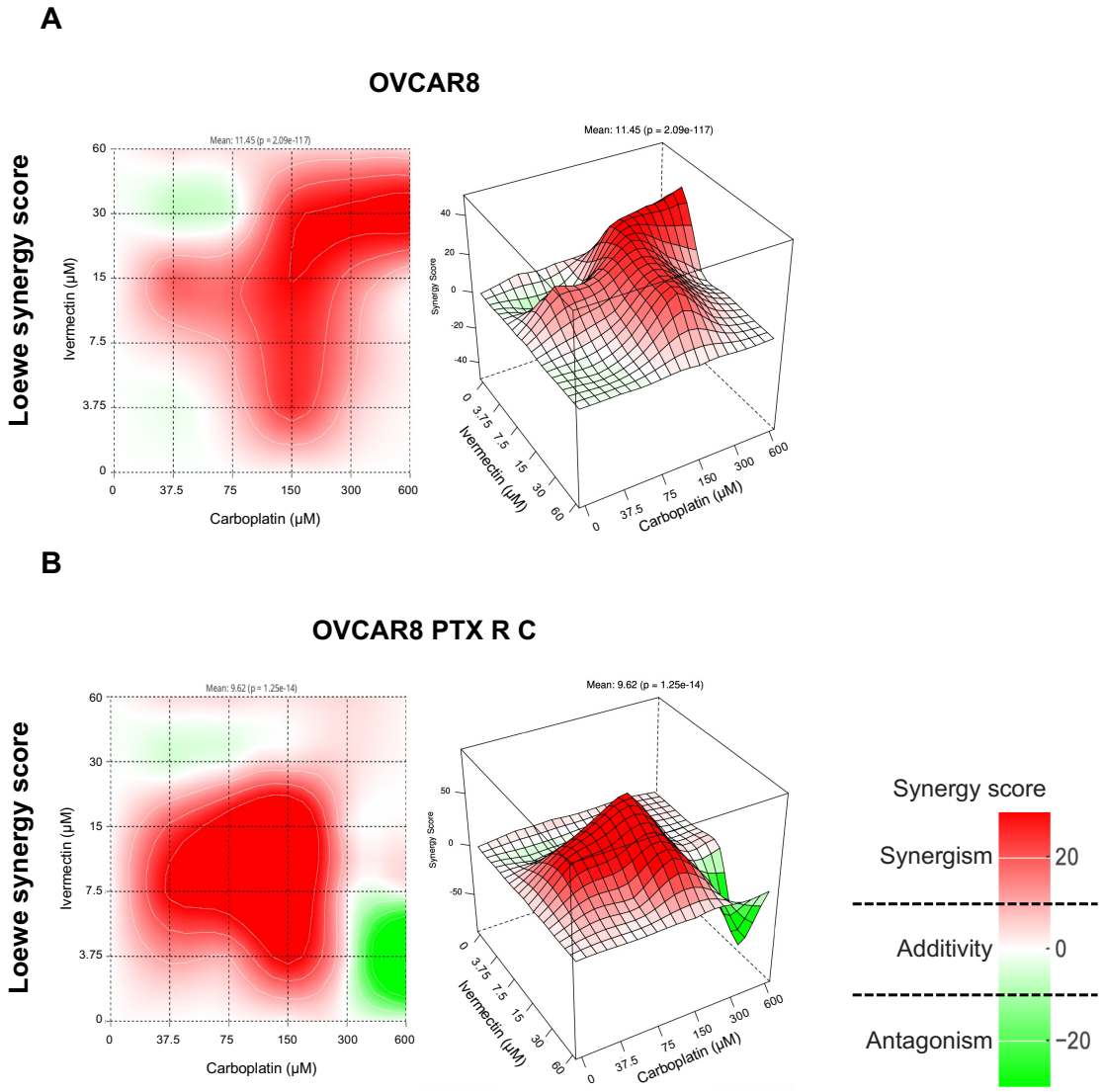


Figure 32. Combining Carboplatin with Ivermectin has an additive effect on OVCAR8 and OVCAR8 PTX R C cells according to the Loewe synergy model. 2D and 3D synergy plots showed the drug synergism of OVCAR8 (**A**) and OVCAR8 PTX R C (**B**) cells after exposure to fixed-dose ratios that correspond to 0.25, 0.5, 1, 2, and 4 times the individual IC_{50} values of each drug. Carboplatin was combined with Ivermectin for 72 hours. The combined treatment was administered simultaneously. All assays were performed in triplicate in at least

three independent experiments. The synergy scores were categorized as follows: <−10 (antagonism, green), −10 to 10 (additivity, white), and >10 (synergism, red). HSA, high single agent; ZIP, zero interaction potency.

4.2. Combining Paclitaxel with Pitavastatin or Ivermectin Has an Additive Effect on OVCAR8 and OVCAR8 PTX R C Cells

We also study the combination of Paclitaxel with Pitavastatin or Ivermectin using the same 3D culture and drug combination model. The findings indicate that in OVCAR8 cells, the combination of Carboplatin and Pitavastatin significantly boosted the anticancer effect at 0.25 ($p < 0.05$) and 0.5, 1, and 2 ($p < 0.0001$) times the individual IC_{50} values in contrast to Paclitaxel alone (**Figure S10A**). In OVCAR8 PTX R C cells, this combination markedly enhanced anticancer efficacy ($p < 0.0001$) at all five IC_{50} values compared to Paclitaxel as a single agent (**Figure S10B**).

For OVCAR8, the combination of Paclitaxel with Ivermectin also resulted in a significant increase in anticancer effects at the tested concentrations ($p < 0.01$ for 0.25 and $p < 0.0001$ for 0.5, 1, and 2 times the IC_{50} values) compared to Paclitaxel alone (**Figure S10C**). In OVCAR8 PTX R C cells, this combination yielded a notable enhancement in anti-tumor effects ($p < 0.0001$) for all five IC_{50} values than Paclitaxel alone (**Figure S10D**).

For OVCAR8 cells across four models used to assess drug interactions, it was found that combining Paclitaxel with Pitavastatin yielded synergy scores of 1.00, -3.04, -6.44, and -5.16, suggesting an additive effect (white). Notably, both reference models also identified synergic zones (red) at intermediate to higher concentrations (**Figures 33A, S11A, S11B, and S11C**). For OVCAR8 PTX R C, the combination of Paclitaxel and Pitavastatin showed HSA and Loewe model synergy scores of -3.13 and -6.19, indicating additivity (white). In contrast, Bliss Independence and ZIP models revealed scores of -11.96 and -11.28, indicating antagonism (green) (**Figures 33B, S11D, S11E and S11F**).

Conversely, the combination of Paclitaxel and Ivermectin indicated additivity (white), with synergy scores of 5.15, -1.12, -1.28, and -0.86 for OVCAR8 cells (**Figures 34A, S12A, S12B and S12C**). All four reference models used to assess drug interactions also indicated synergic zones (red) at low, intermediate, and higher concentrations. For OVCAR8 PTX R C cells, this combination reflected an additive (white) effect as well, with synergy scores of 8.21, 4.03, 0.12, and 0.23 (**Figures 34B, S12D, S12E, and S12F**), but also showing synergic zones (red) at low to intermediate concentrations.

These findings underscore that different synergy evaluation models can yield varying scores; however, all four methods demonstrated consistency in results for the combinations

tested. Thus, it is evident that the combination of Paclitaxel and Ivermectin is the most promising for both HGSC cell lines.

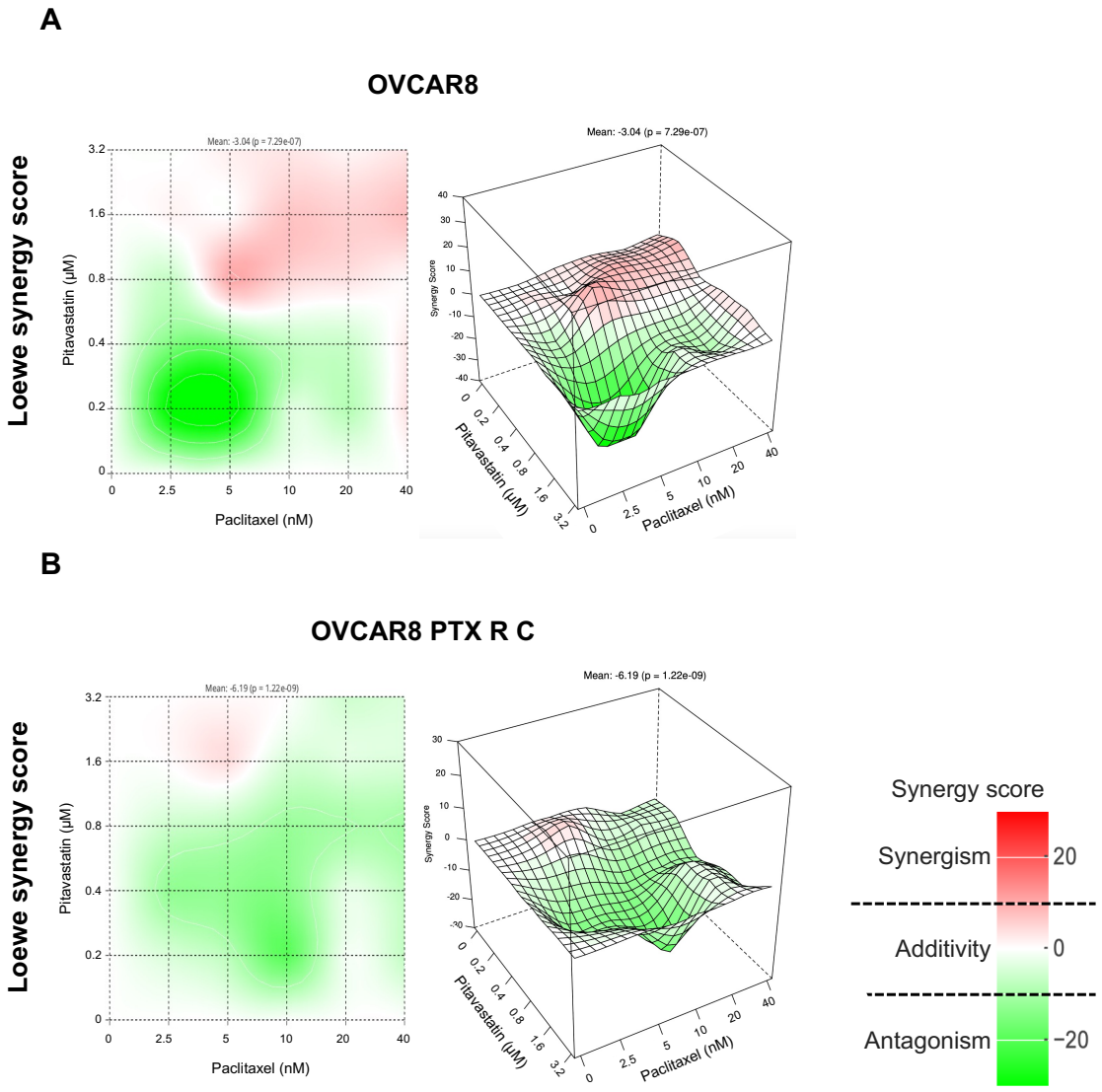


Figure 33. Combining Paclitaxel with Pitavastatin has an additive effect on OVCAR8 and OVCAR8 PTX R C cells according to the Loewe synergy model. 2D and 3D synergy plots showed the drug synergism of OVCAR8 (**A**) and OVCAR8 PTX R C (**B**) cells after exposure to fixed-dose ratios that correspond to 0.25, 0.5, 1, 2, and 4 times the individual IC_{50} values of each drug. Paclitaxel was combined with Pitavastatin for 72 hours. The combined treatment was administered simultaneously. All assays were performed in triplicate in at least three independent experiments. The synergy scores were categorized as follows: <−10 (antagonism, green), −10 to 10 (additivity, white), and >10 (synergism, red). HSA, high single agent; ZIP, zero interaction potency.

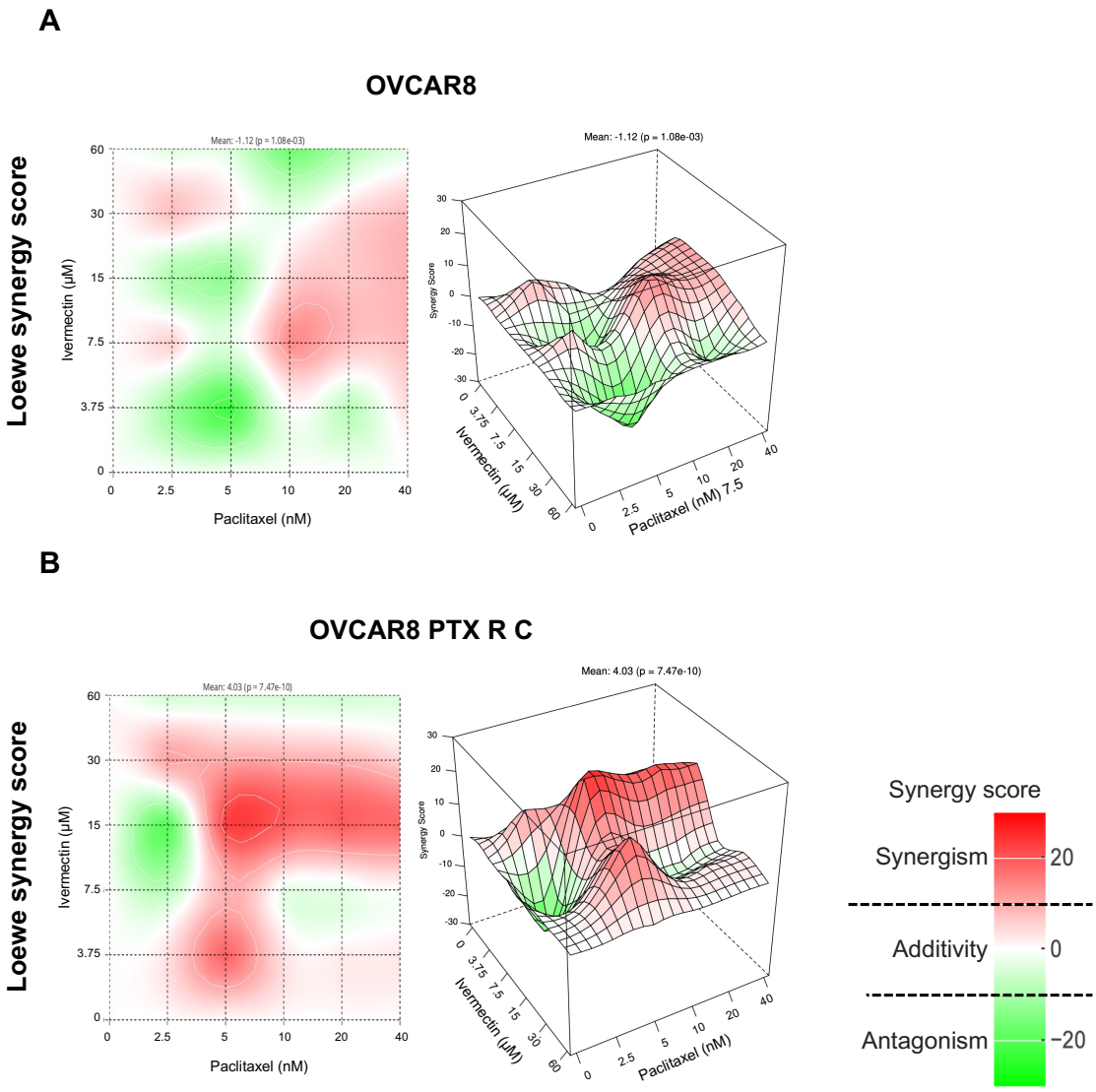


Figure 34. Combining Paclitaxel with Ivermectin has an additive effect on OVCAR8 and OVCAR8 PTX R C cells according to the Loewe synergy model. 2D and 3D synergy plots showed the drug synergism of OVCAR8 (**A**) and OVCAR8 PTX R C (**B**) cells after exposure to fixed-dose ratios that correspond to 0.25, 0.5, 1, 2, and 4 times the individual IC_{50} values of each drug. Paclitaxel was combined with Ivermectin for 72 hours. The combined treatment was administered simultaneously. All assays were performed in triplicate in at least three independent experiments. The synergy scores were categorized as follows: <−10 (antagonism, green), −10 to 10 (additivity, white), and >10 (synergism, red). HSA, high single agent; ZIP, zero interaction potency.

4.3. Morphological Assessment Reveals Drug Efficacy in Combined Treatments

We also performed a morphological assessment for each treatment scenario (see **Figures 35 and 36**) since live and dead cells in 3D cultures exhibit distinct characteristics, including cellular morphology, proliferation, metabolic activity, cell-cell interactions, and

membrane integrity. Recognizing these differences is essential for understanding how cells respond to treatments in 3D cultures, offering valuable insights into drug efficacy.

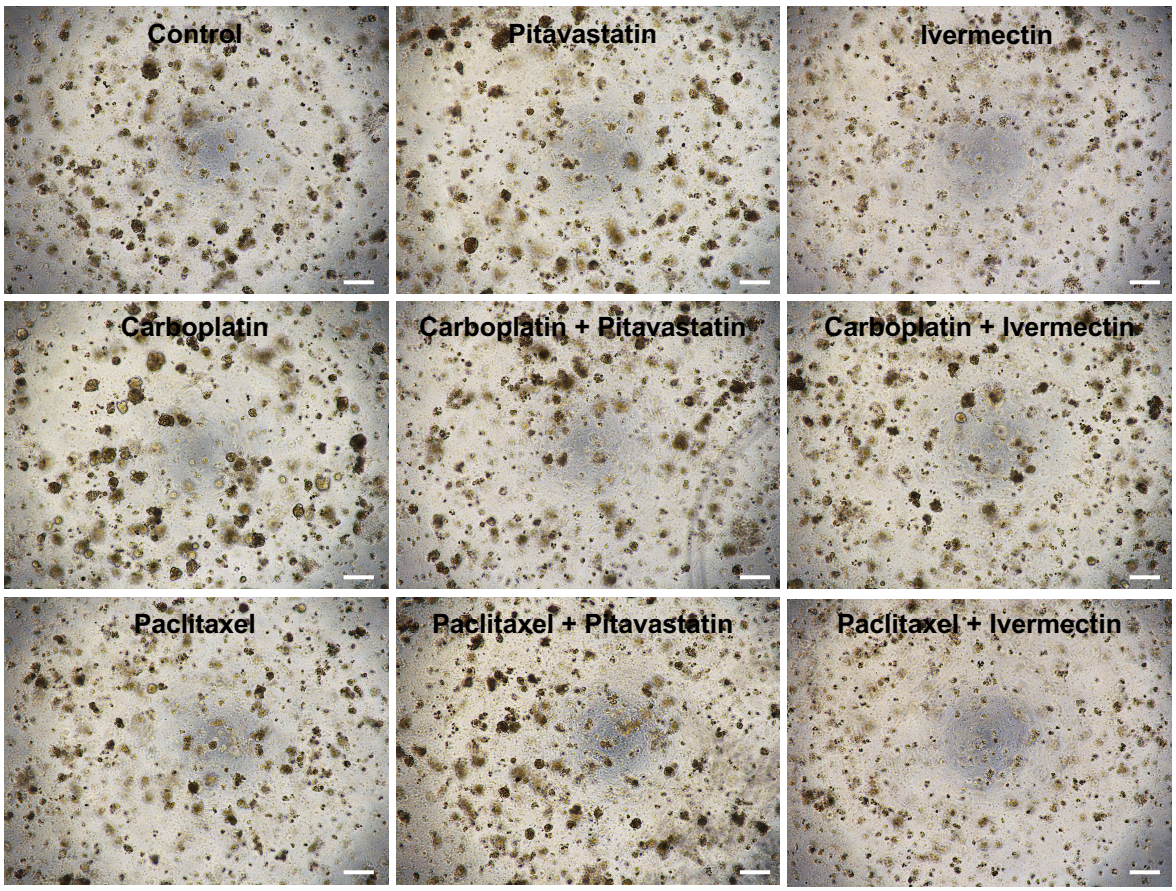


Figure 35. Pitavastatin and Ivermectin improved the cytotoxic effect of Carboplatin and Paclitaxel on OVCAR8 cells. Representative microscopy images of OVCAR8 cells after exposure for 72 hours to control Carboplatin, Paclitaxel, Pitavastatin, Ivermectin, Carboplatin + Pitavastatin, Carboplatin + Ivermectin, Paclitaxel + Pitavastatin and Paclitaxel + Ivermectin at IC_{50} values of each drug (Carboplatin 150 μM, Paclitaxel 10 nM, Pitavastatin 0.8 μM and Ivermectin 15 μM). All assays were performed in triplicate in at least three independent experiments. Scale bar, 200 μm. HGSC, high-grade serous carcinoma.

Our results are in line with previous findings, showing morphological differences in OVCAR8 and OVCAR8 PTX R C cells when subjected to single and combined treatments, as opposed to the control. When Carboplatin or Paclitaxel was combined with Pitavastatin or Ivermectin at IC_{50} values, it induced a more aggressive phenotype, leading to a range of observable characteristics in dead cells within 3D conformation, including decreased cell numbers, reduced aggregate formation, and the presence of smaller and rounded cells

(**Figures 35 and 36**). Additionally, it was observed signs of disrupted cellular structures, such as fragmented nuclei and loss of membrane integrity.

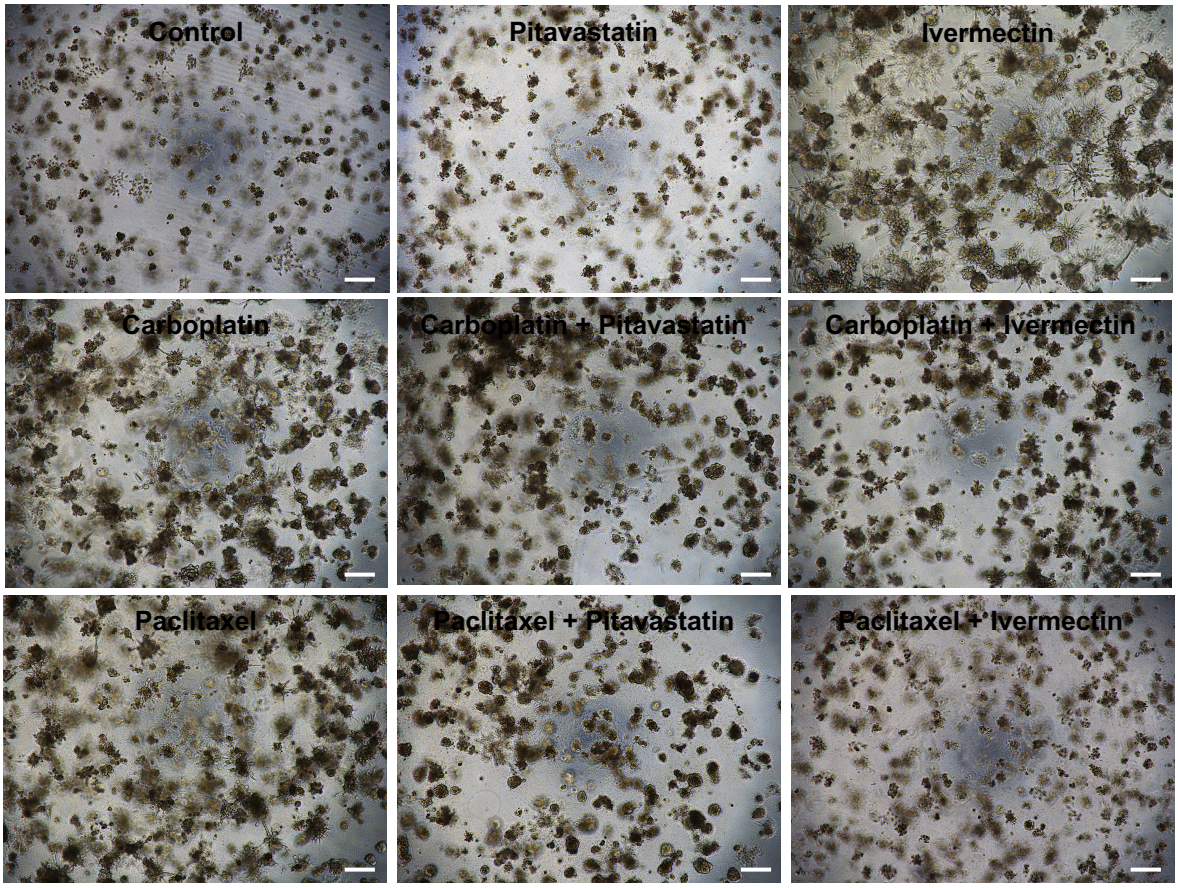


Figure 36. Pitavastatin and Ivermectin improved the cytotoxic effect of Carboplatin and Paclitaxel on OVCAR8 PTX R C cells. Representative microscopy images of OVCAR8 PTX R C cells after exposure for 72 hours to control, Carboplatin, Paclitaxel, Pitavastatin, Ivermectin, Carboplatin + Pitavastatin, Carboplatin + Ivermectin, Paclitaxel + Pitavastatin and Paclitaxel + Ivermectin at IC_{50} values of each drug (Carboplatin 150 μM, Paclitaxel 10 nM, Pitavastatin 0.8 μM and Ivermectin 15 μM. All assays were performed in triplicate in at least three independent experiments. Scale bar, 200 μm. HGSC, high-grade serous carcinoma.

The control for OVCAR8 and OVCAR8 PTX R C cell lines displayed live cells that typically retain a healthy, elongated, or polygonal shape, mirroring their natural tissue architecture. Active mitosis occurs, evidenced by distinct nuclei and clear boundaries between cells. High metabolic activity is indicated by nutrient uptake and the production of metabolic byproducts, as seen in the color saturation of the medium. Robust intercellular connections and signaling foster tissue-like organization and functionality, with cells closely

aggregated and connected and intact cell membranes that prevent cytoplasmic leakage (**Figures 35 and 36**).

In contrast, OVCAR8 and OVCAR8 PTX R C cells subjected to combined treatments show visibly dead cells that are typically smaller and rounded, accompanied by a loss of structural integrity. The notable reduction in cell density resulting from cell death affects aggregate formation as a whole. This includes indications of nuclear fragmentation and chromatin condensation, suggesting apoptosis or necrosis. Additionally, low or absent metabolic activity is reflected in diminished nutrient uptake and a lack of ATP production (**Figures 35 and 36**).

5. Discussion

Evidence suggests that combining chemotherapeutic agents with repurposed drugs can enhance therapeutic efficacy by targeting different mechanisms or pathways in a synergistic or additive way (567, 631, 640, 641). Preclinical and retrospective studies have identified Pitavastatin and Ivermectin as potential antineoplastic compounds (661-664, 670-672). In earlier research using 2D cell cultures, both drugs emerged as promising candidates for enhancing the effectiveness of Carboplatin or Paclitaxel in OVCAR8 and OVCAR8 PTX R P cells (722, 759).

In the current study, we investigated the combined effect of Carboplatin or Paclitaxel with Pitavastatin or Ivermectin on Carboplatin-resistant (OVCAR8) and Carboplatin-Paclitaxel-resistant (OVCAR8 PTX R P) cell lines under 3D culture conditions. Both cell lines were exposed to varying concentrations (0.25, 0.5, 1, 2, and 4-fold the IC_{50} values) of each drug alone and in combination with the chemotherapeutic agents. The results indicated that Ivermectin was the most effective repurposed drug in improving the performance of Paclitaxel in both chemoresistant cell lines under 3D culture conditions. This supports the potential of combining Paclitaxel with repurposed drugs, warranting further investigation to evaluate its impact on patient-derived cells with chemoresistant disease.

Notably, 3D cultures are increasingly recognized for their relevance in drug testing and cancer research. These models provide a more accurate representation of tumor characteristics, such as cellular interactions with stromal cells and ECM components, which are important for understanding metastasis and drug efficacy (763, 772, 773). Additionally, 3D cultures facilitate high-throughput screening that yields more relevant data on drug efficacy and toxicity compared to traditional 2D models (772). They also support

personalized medicine, allowing the evaluation of drug responses in patient-derived cultures to tailor treatment strategies (774).

The efficacy of drugs in 2D cultures may differ significantly from their effects in 3D environments. In 2D models, cells are arranged in a single layer, allowing for more uniform drug diffusion, which can lead to higher effective drug concentrations and more pronounced responses (765-767). Conversely, in 3D cultures, drug penetration can be hindered, especially for cells located deeper within the structure, potentially resulting in a lower effective drug concentration and a slower or less pronounced response (765-767). However, further experimental data are needed to determine whether the reduced efficacy observed in 3D cultures is due to lower drug concentrations or different cellular responses in these two models.

A key challenge in overcoming chemoresistance is the reduced accumulation of chemotherapeutic agents in chemoresistant cell lines. This is often due to altered transporter expression, which reduces intracellular drug levels, thus mitigating cytotoxic effects (200). In particular, P-gp, an efflux transporter, plays a critical role in MDR by actively exporting various chemotherapeutic agents, such as Paclitaxel, from cells, thereby decreasing their intracellular concentrations (775). It has been shown that OVCAR8 PTX R P cells, which are resistant to Paclitaxel, exhibit elevated P-gp expression (628). In this study, the double-resistant OVCAR8 PTX R C cells demonstrated that Ivermectin, when combined with Paclitaxel, significantly increased drug efficacy, particularly in synergistic areas of the response curve.

Ivermectin has been shown to interact with P-gp both as a substrate and a modulator, inhibiting its efflux function and thereby increasing intracellular drug levels (705, 776). This interaction is significant in overcoming chemoresistance, as P-gp is involved in the chemoresistance of tumor cells. By modulating P-gp activity, Ivermectin has the potential to enhance the effectiveness of existing chemotherapy treatments, making it a promising candidate for combination therapies aimed at addressing MDR in cancer.

However, the impact of Ivermectin on P-gp modulation may vary depending on the model system used. In 2D cultures, the lack of cellular interactions and extracellular matrix components may facilitate a more direct impact on P-gp activity, potentially resulting in higher drug concentrations within cells. In contrast, 3D cultures present more complex environments, where cellular interactions, nutrient gradients, and the ECM may limit drug penetration and distribution. Consequently, higher drug concentrations may be needed in 3D models to achieve similar effects on P-gp expression and activity as seen in 2D cultures.

When we compare the results from this study with our earlier work, which used 2D cultures of HGSC chemoresistant cells (722, 759), fewer synergistic pairs were observed in Cultrex RGF BME type 2 based 3D models. This difference may be related to variations in P-gp expression between the two model systems. Studies have shown that P-gp behavior differs significantly between 2D and 3D cultures, influencing both drug effectiveness and resistance (777). Future studies will monitor P-gp activity in 3D cultures using flow cytometry and fluorescent substrates (e.g., RH-123) or confocal microscopy to assess P-gp expression, efflux activity, and localization within these models. These experiments will provide crucial insights into the role of P-gp in resistance and helping to develop more effective therapeutic schemes.

In 3D settings, cells interact in a more physiologically relevant manner, which can alter P-gp expression and function (778-780). These interactions, along with the physical and chemical gradients present in 3D models, can influence drug resistance mechanisms. For example, growth factors, cytokines, and intercellular communication in 3D cultures can promote or reduce P-gp expression and activity (778-780). The cytoskeletal structure, which is critical for the localization and function of P-gp, may also be more complex in 3D models, potentially affecting how P-gp transports drugs to the cell membrane (781). Additionally, the structural characteristics of 3D cultures, such as spheroid formation and scaffold materials, can affect drug penetration and distribution, leading to differential drug exposure and altering P-gp-mediated efflux.

To gain further insight into P-gp behavior and its impact on drug resistance, future research will focus on monitoring P-gp activity in 3D cultures, evaluating the role of P-gp inhibitors, and exploring how these interactions may improve the effectiveness of Paclitaxel and other chemotherapy drugs in resistant HGSC. Investigating P-gp in 3D models will offer valuable information on overcoming resistance in OC and lead to more effective combination therapies.

In conclusion, this study's findings suggest that compounds like Ivermectin may hold significant potential as chemosensitizers in the treatment of chemoresistant HGSC. By modulating P-gp and other transport proteins, Ivermectin could enhance the cytotoxicity of platinum-based therapies, overcoming resistance and improving patient outcomes. Further research is needed to clarify the mechanisms underlying these interactions and explore the clinical applicability of Ivermectin and other repurposed drugs in combination with chemotherapy.

6. Conclusion

3D cell culture models represent more reliable systems in cellular biology and biomedical research. By offering a more precise representation of *in vivo* architecture, these models deepen understanding of intricate biological processes.

Our results showed that the combination of Paclitaxel with Ivermectin presents additivity when used in a Cultrex RGF BME type 2 based 3D cell culture model for HGSC chemoresistant cell lines for the four synergistic interaction reference models tested. Paclitaxel's clinical effectiveness can be reduced due to its active removal from cells through P-gp. Ivermectin acts as both a substrate and modulator of P-gp, attaching to this protein and making it less accessible for other substances. This relationship can increase the effectiveness of chemotherapy drugs. Thus, Ivermectin may function as a supportive addition to Paclitaxel treatment, enhancing therapeutic effectiveness, reducing toxicity associated with Paclitaxel, and helping to overcome chemoresistance.

7. Acknowledgments and Funding

This work was developed at *Instituto de Investigação e Inovação em Saúde (i3S)*, an Associate Laboratory of the *Ministério da Ciência, Tecnologia e Inovação (MCTES),* and it was partially supported by *Fundação para a Ciência e a Tecnologia (FCT).* This research was supported by the project “HOPE – Improving Ovarian Cancer Patients Survival,” a donation from an ovarian cancer patient to the *Institute of Molecular Pathology and Immunology of the University of Porto (IPATIMUP)* and by *Fundo Europeu de Desenvolvimento Regional (FEDER)* through the *COMPETE 2020–Operational Program for Competitiveness and Internationalization (POCI), Portugal 2020* and *FCT/MCTES,* under the project POCI 01-0145-FEDER-029503 (PTDC/MEC-ONC/29503/2017). M.N. acknowledges *FCT/MCTES* and *UE* for financial support through a PhD fellowship (2020.04720.BD and DOI: 10.54499/2020.04720.BD) that was co-sponsored by *Fundo Social Europeu (FSE)* through *Programa Operacional Regional Norte (Norte 2020).*

8. Supplementary Material

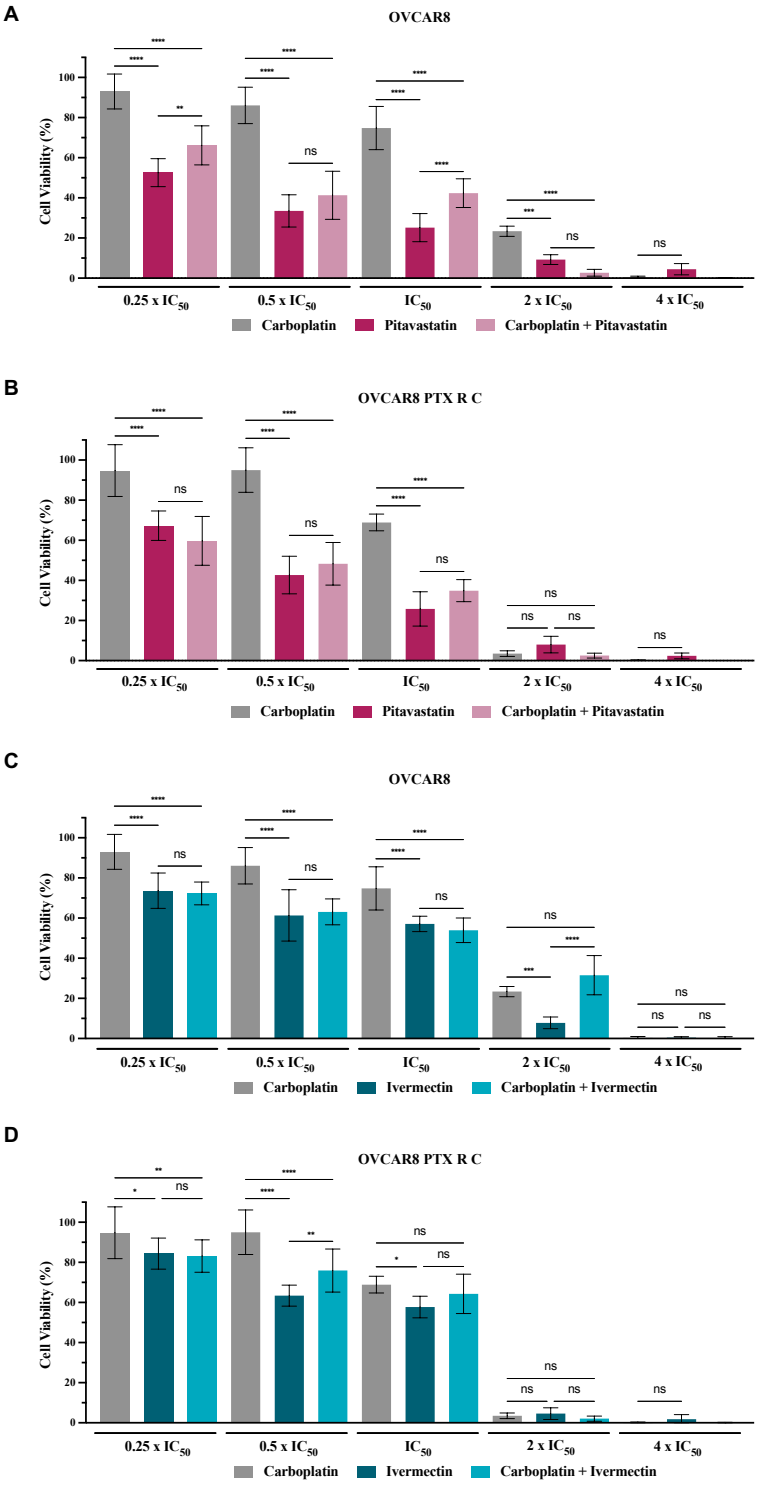


Figure S7. Pitavastatin and Ivermectin increase the efficacy of Carboplatin in reducing the cellular viability of chemoresistant HGSC cells. (**A**–**D**) Bar charts showing cell viability of OVCAR8 and OVCAR8 PTX R C cells obtained by CellTiter-Glo® Luminescent assays after exposure to a fixed-dose ratio that corresponds to 0.25, 0.5, 1, 2, and 4 times the individual IC_{50} values of each drug. For 72 hours, Carboplatin was combined

with (**A** and **B**) Pitavastatin and (**C** and **D**) Ivermectin. The combined treatment was administered simultaneously. All assays were performed in triplicate in at least three independent experiments. The data are expressed as the mean ± standard deviation and plotted using GraphPad Prism Software Inc. v6 (GraphPad Software Inc. Boston, CA, USA). Statistical analysis was performed using ordinary one-way ANOVA followed by Šıd́ák's multiple comparison test (**A**–**D**), with * $p < 0.05$, ** $p < 0.001$, *** $p < 0.005$, and **** $p < 0.0001$ considered statistically significant. HGSC, high-grade serous carcinoma.

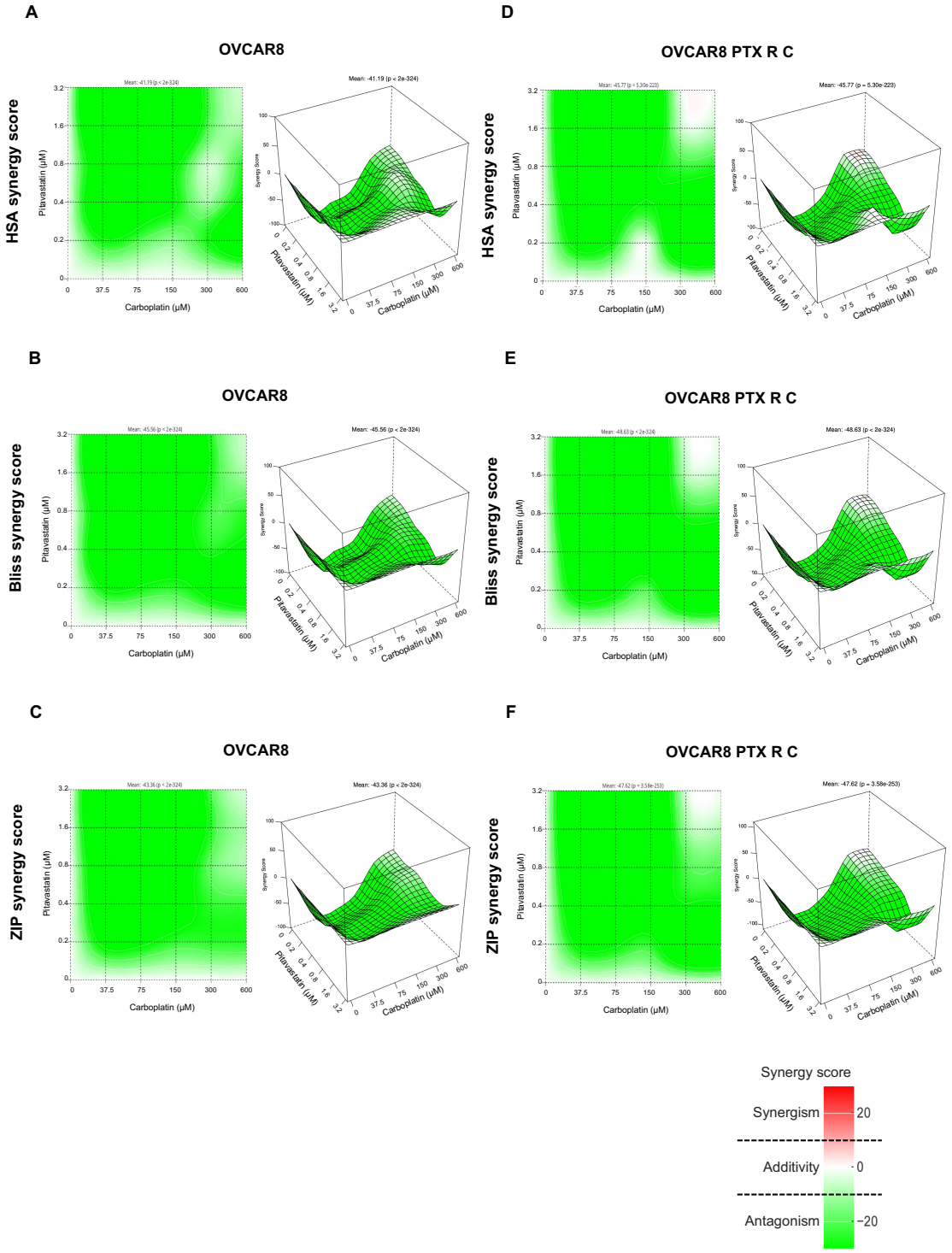


Figure S8. Combining Carboplatin with Pitavastatin has an antagonistic effect on OVCAR8 and OVCAR8 PTX R C cells for HSA, Bliss Independence, and ZIP synergy models. 2D and 3D synergy plots showed the drug synergism of OVCAR8 (**A**–**C**) and OVCAR8 PTX R C (**D**–**F**) cells after exposure to fixed-dose ratios that correspond to 0.25, 0.5, 1, 2, and 4 times the individual IC_{50} values of each drug. Carboplatin was combined with Pitavastatin for 72 hours. The combined treatment was administered simultaneously. All assays were performed in triplicate in at least three independent experiments. The synergy scores were categorized as follows: <−10

(antagonism, green), −10 to 10 (additivity, white), and >10 (synergism, red). HSA, high single agent; ZIP, zero interaction potency.

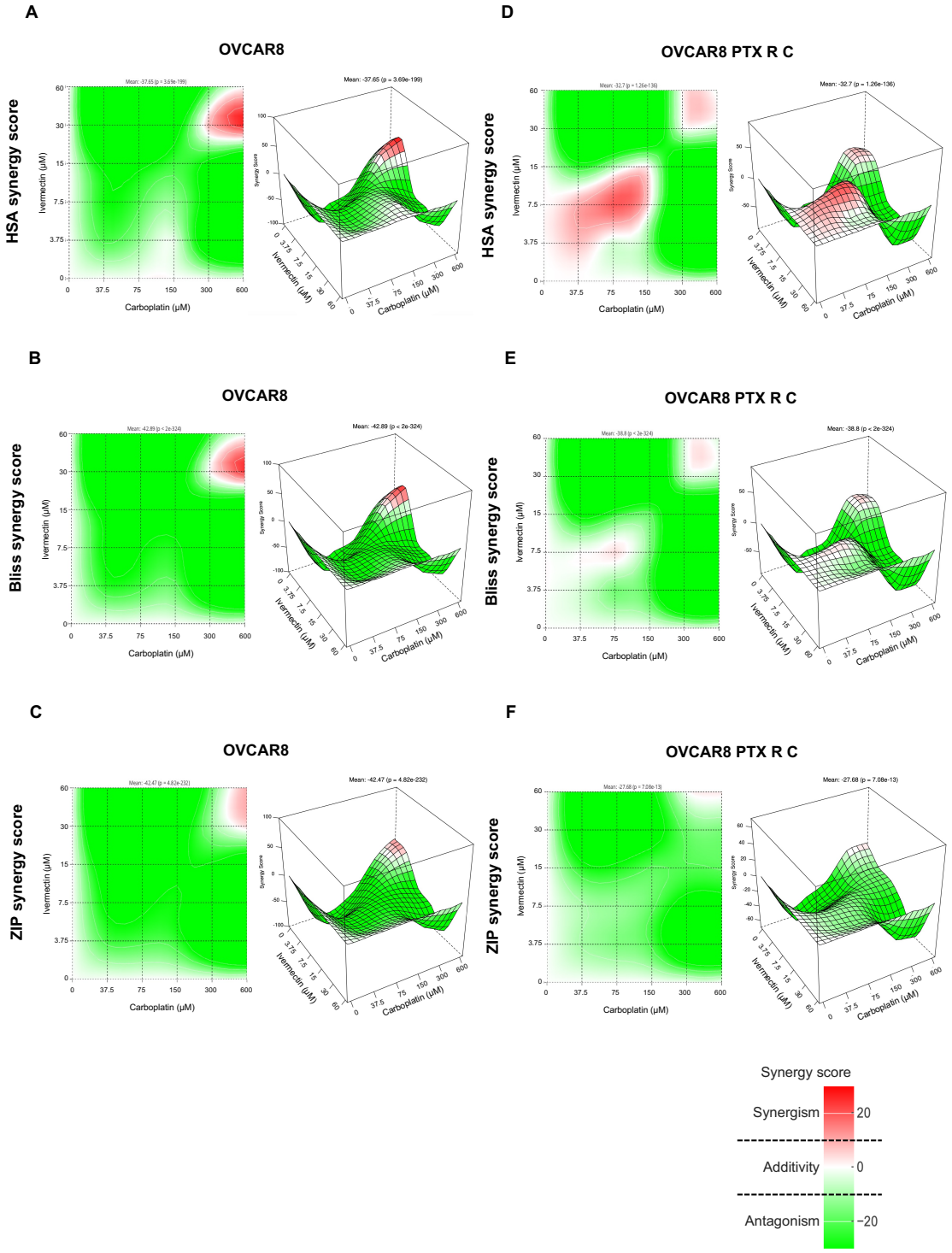


Figure S9. Combining Carboplatin with Ivermectin has an antagonistic effect on OVCAR8 and OVCAR8 PTX R C cells for HSA, Bliss Independence, and ZIP synergy models. 2D and 3D synergy plots showed the drug synergism of OVCAR8 (**A**–**C**) and OVCAR8 PTX R C (**D**–**F**) cells after exposure to fixed-dose ratios that correspond to 0.25, 0.5, 1, 2, and 4 times the individual IC_{50} values of each drug. Carboplatin was combined with Pitavastatin for 72 hours. The combined treatment was administered simultaneously. All assays were performed in triplicate in at least three independent experiments. The synergy scores were categorized as follows: <−10

(antagonism, green), −10 to 10 (additivity, white), and >10 (synergism, red). HSA, high single agent; ZIP, zero interaction potency.

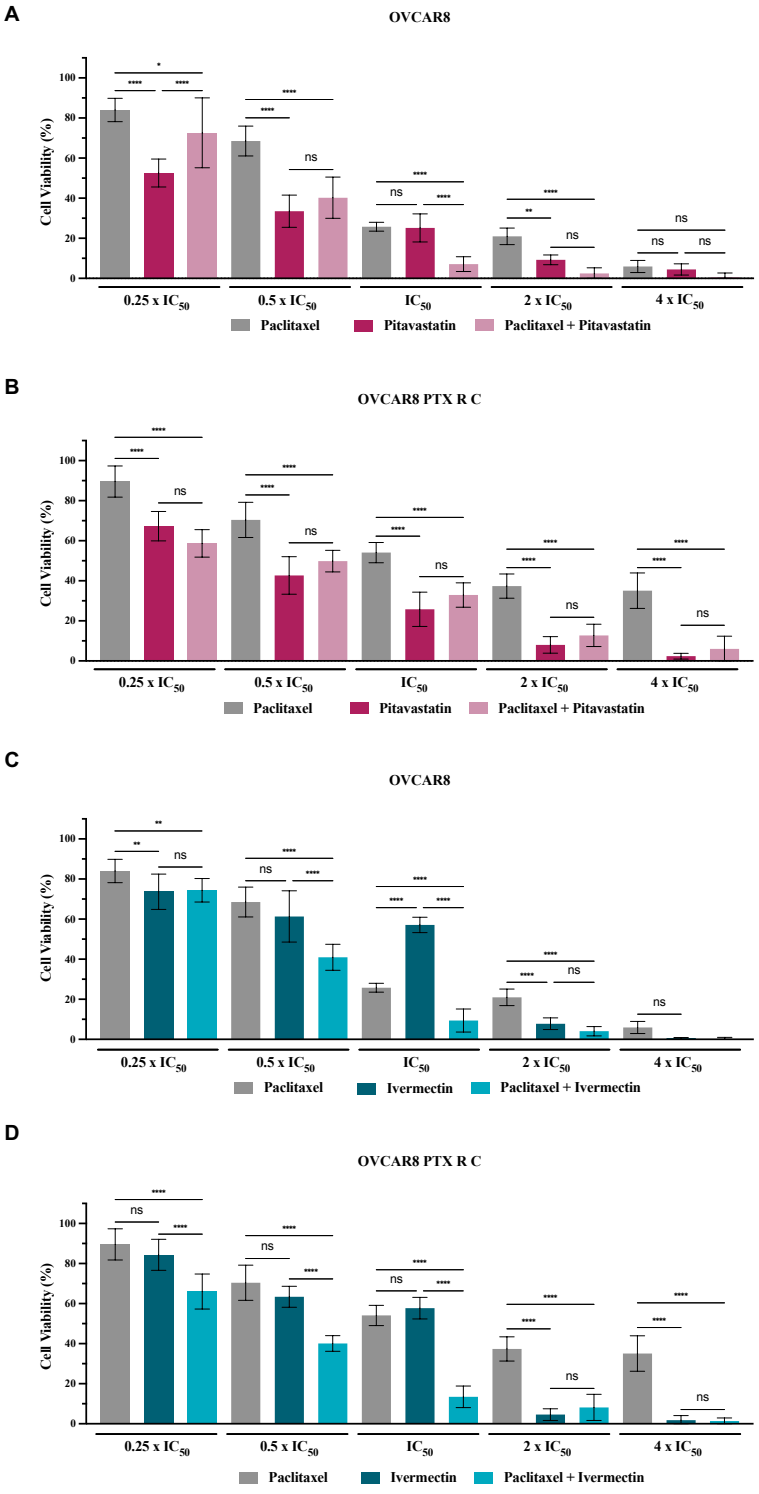


Figure S10. Pitavastatin and Ivermectin increase the efficacy of Paclitaxel in reducing the cellular viability of chemoresistant HGSC cells. (**A**–**D**) Bar charts showing cell viability of OVCAR8 and OVCAR8 PTX R C cells obtained by CellTiter-Glo® Luminescent assays after exposure to a fixed-dose ratio that corresponds to 0.25, 0.5, 1, 2, and 4 times the individual IC_{50} values of each drug. For 72 hours, Carboplatin was combined with (**A** and **B**) Pitavastatin and (**C** and **D**) Ivermectin. The combined treatment was administered simultaneously.

All assays were performed in triplicate in at least three independent experiments. The data are expressed as the mean ± standard deviation and plotted using GraphPad Prism Software Inc. v6 (GraphPad Software Inc. Boston, CA, USA). Statistical analysis was performed using ordinary one-way ANOVA followed by Šıd́ák's multiple comparison test (**A**–**D**), with * $p < 0.05$, ** $p < 0.001$, *** $p < 0.005$, and **** $p < 0.0001$ considered statistically significant. HGSC, high-grade serous carcinoma.

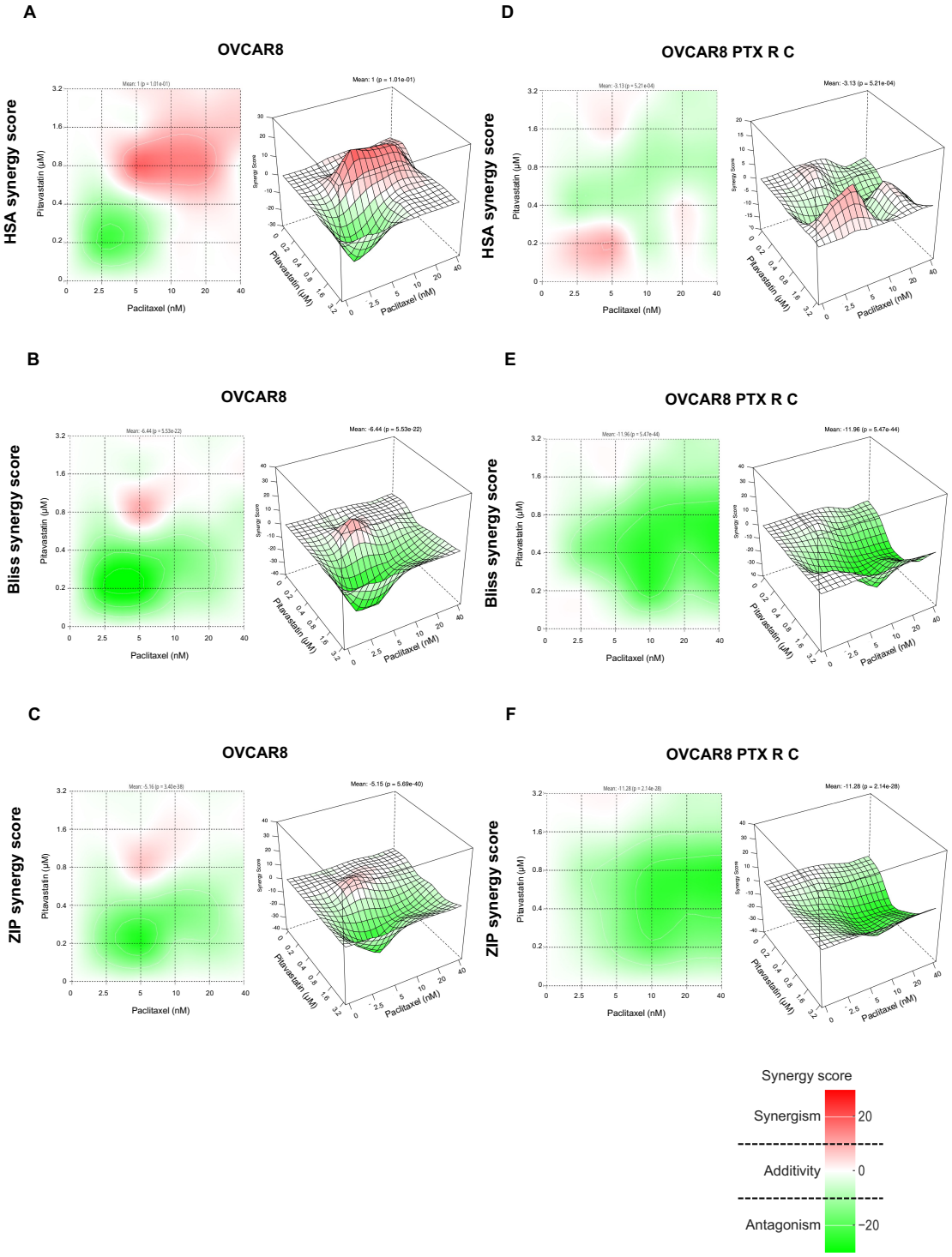


Figure S11. Combining Paclitaxel with Pitavastatin has an antagonistic effect on OVCAR8 and OVCAR8 PTX R C cells for HSA, Bliss Independence, and ZIP synergy models. 2D and 3D synergy plots showed the drug synergism of OVCAR8 (**A**–**C**) and OVCAR8 PTX R C (**D**–**F**) cells after exposure to fixed-dose ratios that correspond to 0.25, 0.5, 1, 2, and 4 times the individual IC_{50} values of each drug. Carboplatin was combined with Pitavastatin for 72 hours. The combined treatment was administered simultaneously. All assays were performed in triplicate in at least three independent experiments. The synergy scores were categorized as follows: <−10

(antagonism, green), −10 to 10 (additivity, white), and >10 (synergism, red). HSA, high single agent; ZIP, zero interaction potency.

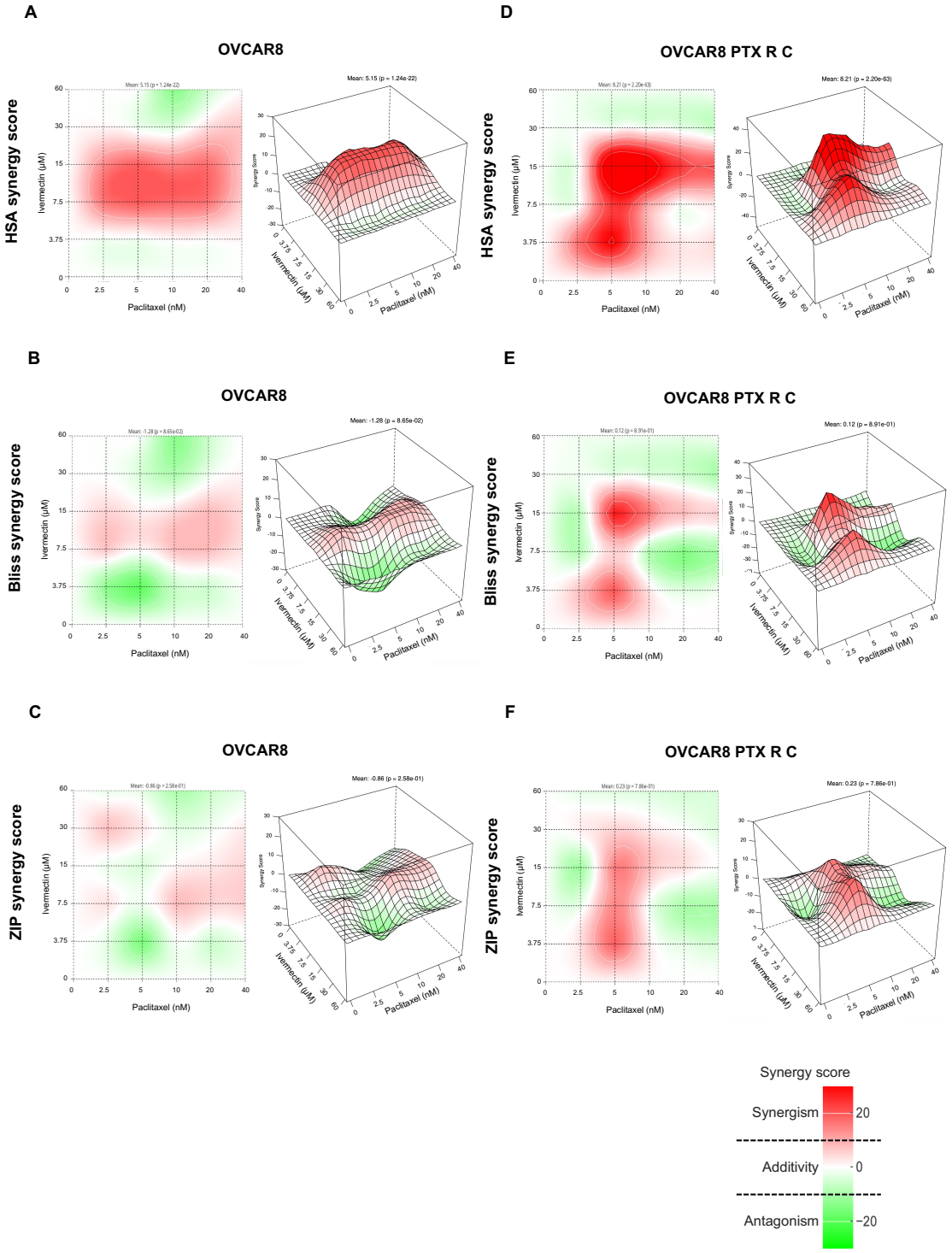


Figure S12. Combining Paclitaxel with Ivermectin has an antagonistic effect on OVCAR8 and OVCAR8 PTX R C cells for HSA, Bliss Independence, and ZIP synergy models. 2D and 3D synergy plots showed the drug synergism of OVCAR8 (**A**–**C**) and OVCAR8 PTX R C (**D**–**F**) cells after exposure to fixed-dose ratios that correspond to 0.25, 0.5, 1, 2, and 4 times the individual IC_{50} values of each drug. Carboplatin was combined with Pitavastatin for 72 hours. The combined treatment was administered simultaneously. All assays were performed in triplicate in at least three independent experiments. The synergy scores were categorized as follows: <−10

(antagonism, green), −10 to 10 (additivity, white), and >10 (synergism, red). HSA, high single agent; ZIP, zero interaction potency.

CHAPTER V

Establishment of Malignant Ascites-Derived Cultures to Perform *Ex Vivo* Drug Efficacy Tests

Development of Patient-Derived Cultures from Ovarian Cancer Malignant Ascites for *Ex Vivo* Drug Testing

1. Abstract

MA is a common feature in advanced OC, particularly in HGSC patients, and represents an underexplored yet highly valuable resource for cancer research. This study explores the potential of MA as a source of biological material for developing patient-derived cultures, hereafter referred to as MA-derived cultures, aiming to deepen our understanding of OC biology and improve personalized therapeutic strategies. By centrifuging, we successfully isolated viable cells from MA samples and established HGSC patient-derived cultures that closely recapitulate the molecular, genetic, and histological characteristics of the original tumors. The findings demonstrate that combining a standard organoid medium (SOM) with the autologous supernatant from MA significantly enhances the growth, viability, and long-term maintenance of these cultures. This combination not only supports the robust expansion of patient-derived models but also enhances their relevance as a platform for personalized drug screening and therapeutic testing. Using MA for culturing patient-specific OC models offers a promising avenue for advancing precision medicine, enabling more targeted and effective treatments tailored to individual patient profiles. Leveraging MA-derived cultures could revolutionize the development of novel therapeutic strategies, improve clinical outcomes, and facilitate the transition from preclinical models to clinical applications in OC.

Keywords

Chemoresistance, Malignant Ascites, Ovarian Cancer, Patient-derived Cultures, Personalized Treatment.

2. Introduction

A key complication in advanced OC, especially in HGSC, is the accumulation of MA – fluid buildup in the peritoneal cavity – which is frequently seen at diagnosis or recurrence (65). MA, a hallmark of metastasis, is strongly associated with shorter PFS and OS in OC patients across most histological subtypes (782, 783), indicating poor prognosis (65). Approximately 90% of patients with advanced (III and IV) OC exhibit this condition (66, 784). This fluid facilitates transcoelomic dissemination, a common route for metastasis in OC,

wherein cancer cells detach from the primary tumor, circulate in suspension, and colonize peritoneal organs, thereby contributing to disease progression (476, 785).

Beyond causing discomfort and significant morbidity, MA serves as a rich and complex biological fluid that contains a wide range of factors contributing to OC progression (66, 73). This fluid is composed not only of exfoliated tumor cells but also of a variety of soluble factors, including cytokines, growth factors, EVs, and metabolites, which can create a pro-tumorigenic TME that facilitates tumor growth, immune evasion, and metastasis (66, 73). Additionally, the cytokines and chemokines present in MA contribute to the creation of a highly inflammatory milieu that supports cancer cell proliferation, angiogenesis, and the spread of tumor cells to distant organs (66, 73).

Despite its strong association with poor progression in OC patients, MA has emerged as a valuable resource for cancer research (66, 73). The fluid collected during cytoreductive surgery or paracentesis provides a continuous and accessible source of tumor material that is crucial for monitoring tumor dynamics and progression. Unlike traditional tumor biopsy samples, MA can be collected repeatedly throughout disease progression, offering a unique advantage for real-time assessment of tumor evolution and treatment responses (67).

When OC patients are hospitalized, MA is often drained for diagnostic purposes. However, if a diagnosis is already established, the fluid is typically discarded. Our research team recognizes the potential value of this fluid at various disease stages. Therefore, since 2019, we have been biobanking MA samples from OC patients at IPOP. To date, we have collected 64 samples from 42 patients across different stages of the disease, ranging from diagnosis to palliative care and covering a variety of platinum response profiles.

Patient-derived cultures have become an essential tool in cancer research, providing a more accurate model of human tumors compared to conventional 2D cell cultures (164, 786, 787). These 3D cultures retain the genetic diversity, architecture, and heterogeneity of the original tumor, enabling more realistic insights into cancer biology (788-790). While 2D cultures often fail to capture the complexity of the TME, MA-derived cultures would allow us to study tumor growth, invasion, and drug responses in a more physiologically relevant context (164, 788, 789, 791). Importantly, MA-derived cultures can be used to explore mechanisms of drug resistance, which is a critical challenge in OC treatment (788, 789).

While MA has great potential as a resource for identifying biomarkers, as addressed in Chapter III, its full potential for testing treatment-specific regimens remains largely unexplored. This study outlines methods for processing, storing, and applying MA, as well as protocols for isolating and preparing the cellular components for further analysis. We

explore the optimization of culture conditions, including media formulations, extracellular matrices, and mechanical factors, to enhance the growth and viability of MA-derived cultures. Additionally, we evaluate the impact of various handling and preservation techniques, as well as the response to chemotherapy, such as Carboplatin, with the goal of establishing a robust model for studying drug resistance and testing new therapeutic approaches for personalized treatment strategies in OC.

3. Materials and Methods

3.1. Patient Samples

All MA samples were obtained from the IPOP Pathology Department Biobank, following the Declaration of Helsinki and ethical guidelines set by the IPOP Ethical Committee (REF CES.092R1/019). Volunteers provided written consent, and access to medical records was granted in compliance with Data Protection Regulations.

3.2. Malignant Ascites Processing and Storage

MA processing and storage were carried out according to the procedure described in Chapter III.

3.3. Establishment and Characterization of Malignant Ascites-derived Cultures

3.3.1. Cultrex Reduced Growth Factor Basement Membrane Extract Cultures

An optimized protocol described by Arias-Diaz *et al.* (792) was employed to establish patient-derived cultures from MA obtained from HGSC patients, hereafter referred to as MA-derived cultures. Briefly, the cell pellet obtained from MA (more details explained in Chapter III) was resuspended in a mixture of 30% SOM (more details described in **Table S9**) and 70% Cultrex RGF BME type 2 (Thermo Fisher Scientific, Waltham, MA, USA), following the method outlined by Arias-Diaz *et al.* Cultrex RGF BME type 2 is an extract that creates a natural ECM hydrogel, which polymerizes at 37 °C, resulting in a reconstituted basement membrane. Notably, Cultrex RGF BME type 2 effectively forms and sustains stable 3D dome structures on cell culture plates. A volume of 40 µl of the mixture (30% SOM + 70% Cultrex RGF BME type 2) containing $2x10^5 – 3x10^6$ cells was plated per droplet in a prewarmed 24-well plate and incubated at 37 °C and 5% CO_2 for 30 minutes to allow the Cultrex RGF BME type 2 to solidify. After polymerization, cells were overlaid with 500 µl of prewarmed SOM with or without 20% autologous supernatants sourced from the MA and incubated at 37 °C and 5% CO_2, with the medium refreshed every 3–4 days.

Passages were conducted when patient-derived cultures achieved ~80% of confluence by adding 500 µl of cold PBS to each well, scraping and collecting the disrupted domes. Next, patient-derived cultures were centrifuged at 500× g for 5 minutes at 4 °C, the supernatant was removed, and 1 mL of TrypLE (Thermo Fisher Scientific, Waltham, MA, USA), a cell dissociation reagent, was added. This was incubated at 37 °C for 5–10 minutes, depending on whether the patient-derived cultures were low-cohesive, cystic, or dense. Then, cold PBS was added to a final volume of 10 mL and centrifuged at 500× g for 5 minutes at 4 °C. Finally, the supernatant was removed, and the pellet was resuspended in the 30% SOM + 70% Cultrex RGF BME type 2 mixture for plating (792). After polymerization, cells were overlaid with 500 µl of prewarmed SOM with or without 20% autologous supernatants sourced from the MA and incubated at 37 °C and 5% CO_2, with the medium refreshed every 3–4 days.

Additionally, two other medium compositions, namely RPMI-1640 medium (Thermo Fisher Scientific, Waltham, MA, USA) and OC Modified Ince (OCMI; Biomol GmbH, Hamburg, Germany), were examined.

3.3.2. PolyHEMA Coating Cultures

To establish patient-derived cultures, polyHEMA (Sigma-Aldrich, St. Louis, MO, USA) coated plates were prepared by dissolving 120 mg/mL of polyHEMA in 95% ethanol. Then, 500 µL of the solution was added to 24 plates, which were dried for 48-72 hours at 55 °C to allow the polyHEMA coating to form a stable surface.

The cell pellet obtained from MA was resuspended in 500 µl of prewarmed SOM medium, with or without 20% autologous supernatants sourced from the MA. This was added to a prewarmed 24-well plate with polyHEMA coating and incubated at 37 °C and 5% CO2, with the medium refreshed every 3–4 days. A second plate was also included in an incubator with agitation at 70 rpm, 37 °C, and 5% CO_2, with the SOM refreshed every 3–4 days.

Passages were conducted when patient-derived cultures achieved ~80% of confluence by collecting all and centrifuging them at 500× g for 5 minutes at 4 °C. Then, the supernatant was removed, and 1 mL of TrypLE (Thermo Fisher Scientific, Waltham, MA, USA), a cell dissociation reagent, was added. This mixture was incubated at 37 °C for 5–10 minutes, depending on whether the patient-derived cultures were low-cohesive, cystic, or dense. Then, cold PBS was added to a final volume of 10 mL and centrifuged at 500× g for 5 minutes at 4 °C. Finally, the supernatant was removed, and the pellet was resuspended in

500 µl of prewarmed SOM medium, with or without 20% autologous supernatants sourced from the MA. This was added to a prewarmed 24-well plate with polyHEMA coating and incubated at 37 °C and 5% CO2, with the medium refreshed every 3–4 days.

Additionally, other medium compositions, including RPMI and OCMI, were examined.

3.4. Histogel™ Cell Processing

Histogel™ cell processing was carried out according to the procedure described in Chapter III and previous publications (628).

3.5. Immunocytochemistry

ICC was carried out according to the procedure described in Chapter III and previous publications (502, 628, 793) with some modifications. Briefly, IHC was conducted using the EnVision FLEX Mini Kit High pH (Agilent Dako, Santa Clara, CA, USA). After deparaffinization and hydration, we performed heat-induced antigen retrieval at 98 °C using EnVision FLEX Target Retrieval Solution high pH (1x) (EnVision FLEX Mini Kit High pH). Then, endogenous peroxidase activity was blocked using the EnVision FLEX Peroxidase blocking reagent (EnVision FLEX Mini Kit High pH). Slides were immunostained using monoclonal antibodies: MUC16 (ready-to-use, M11, Agilent Dako, Santa Clara, CA, USA), Ki67 (1:100; SP6, Thermo Fisher Scientific, Waltham, MA, USA), and cleaved caspase-3 (1:100; D175 5A1E, Cell Signalling Technologies, Danvers MA, USA), and incubated for 1 hour at RT). Detection of primary antibodies was carried out with EnVision FLEX HRP (EnVision FLEX Mini Kit High pH) using a secondary antibody conjugated with HRP-labeled polymer. The visualization of reactions was achieved using EnVision FLEX Substrate buffer and EnVision FLEX DAB (EnVision FLEX Mini Kit High pH), following the manufacturer's instructions.

3.6. CellTiter-Glo® 2.0 Luminescent Cell Viability Assay

To assess the sensitivity of MA-derived cultures to Carboplatin, a CellTiter-Glo® 2.0 Luminescent Cell Viability assay (Promega Corporation, Madison, WI, USA) was performed. The MA-derived cultures were dissociated into single cells. A volume of 10 µl of the mixture (30% SOM + 70% Cultrex RGF BME type 2) containing 5×10^3 cells was plated per droplet in a prewarmed 96-well plate and incubated at 37 °C and 5% CO_2 for 30 minutes to allow the Cultrex RGF BME type 2 to solidify. After polymerization, cells were overlaid with 100 µl of prewarmed SOM, incubated at 37 °C and 5% CO_2, and allowed to proliferate for 96 hours.

Then, cells were treated with increasing concentrations of drugs in technical triplicates. Briefly, Carboplatin was diluted to the required concentrations in SOM without the Y27632 rock inhibitor to avoid its effects on improved survival and reduced apoptosis. The cells were then treated with increasing concentrations of Carboplatin (6.25, 12.50, 25, 50, and 100 µM) for 72 hours and incubated under the same conditions.

After 72 hours of treatment, cell viability/cellular ATP levels were measured using CellTiter-Glo® 2.0 Luminescent Cell Viability assay, and luciferase signals were measured using a Bio Tek Synergy™ 2 multi-mode microplate reader. The data were analyzed with GraphPad Prism software (v.10). Normalization was performed using controls.

3.7. Alamar Blue™ Assay

To assess the sensitivity of patient-derived cultures to Carboplatin, a resazurin-based assay – Alamar Blue™ Cell Viability Reagent (Thermo Fisher Scientific, Waltham, MA, USA) – was performed. The MA-derived cultures were dissociated into single cells. A volume of 10 µl of the mixture (30% SOM + 70% Cultrex RGF BME type 2) containing 5×10^3 cells was plated per droplet in a prewarmed 96-well plate and incubated at 37 °C and 5% CO_2 for 30 minutes to allow the Cultrex RGF BME type 2 to solidify. After polymerization, cells were overlaid with 100 µl of prewarmed SOM, incubated at 37 °C and 5% CO_2, and allowed to proliferate for seven days. When they were fully formed and confluent, they were treated with increasing concentrations of drugs in technical triplicates. Briefly, Carboplatin was diluted to the required concentrations in SOM without the Y27632 rock inhibitor to avoid its effects on improved survival and reduced apoptosis. The cells were then treated with increasing concentrations of Carboplatin (6.25, 12.50, 25, 50, and 100 µM) for three days and incubated under the same conditions. After 72 hours, the SOM with drugs was replaced by fresh SOM without drugs and incubated for another three days under the same conditions.

Therefore, cell viability was assessed six days after the drug was added using the Alamar Blue™ Assay. Briefly, the culture medium was removed, and 100 µL of Alamar Blue™ reagent, diluted in DMEM-F12 (mixture 1:10), was added to the patient-derived cultures. The cells were incubated at 37 °C and 5% CO_2, protected from light for three hours. Fluorescence (560 nm excitation/590 nm emission) was measured using a SpectraMax iD3 multi-mode microplate reader (Molecular Devices, San José, California, USA). The data were analyzed with GraphPad Prism software (v.10). Normalization was performed using controls.

4. Results and Discussion

In this study, we methodically investigated various culture conditions to better understand their influence on MA-derived cultures' growth and viability. Initially, we compared several culture media formulations and dissociation solutions to optimize conditions for long-term culture maintenance (**Figures 37A and 37B**). Next, we compared the best culture medium formulation with and without supplementation of 20% autologous supernatant derived from MA samples (**Figure 37C**). Then, to further explore the impact of extracellular components on the culture systems, different matrices were tested, including PolyHEMA and Cultrex RGF BME type 2 (**Figure 37D**). Both static and agitation culture conditions were explored to understand the influence of mechanical factors, such as shear stress and cell-matrix interactions, on MA-derived culture development and cellular behavior (**Figure 37E**). After that, the effect of placing the samples in culture on the day of collection versus after thawing was evaluated to determine how handling time and preservation conditions influence cell viability and behavior in MA-derived cultures (**Figure 37F**). The effect of Carboplatin treatment was assessed to examine its impact on culture viability and proliferation (**Figure 37G**). Finally, a range of assays were performed to evaluate cellular responses to the treatment quantitatively. These included the CellTiter-Glo® Luminescent Cell Viability and the Alamar Blue™ assays, both of which measure cell viability, proliferation, and metabolic activity (**Figure 37H**).

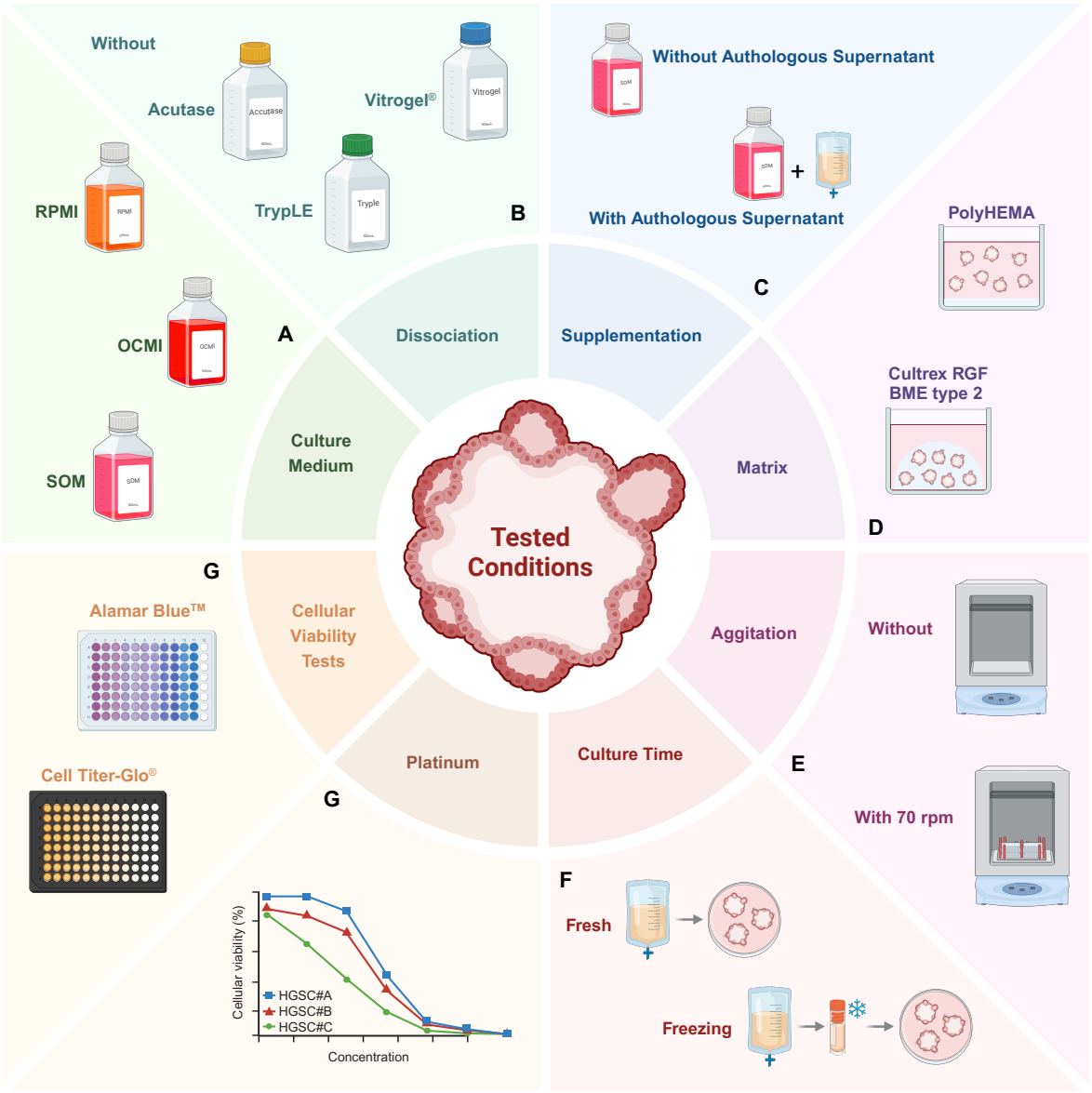


Figure 37. Illustrative figure showing the various methods, techniques, and conditions tested during the development of the patient-derived cultures. Figure created with Biorender.com. OCMI, Ovarian Cancer Modified Ince; RPMI, Roswell Park Memorial Institute; SOM, Standard Organoid Medium.

4.1. SOM is the Best Medium for Malignant Ascites-Derived Cultures

The development of MA-derived cultures is a significant challenge in oncological research, as maintaining the tumor's characteristics *in vitro* requires highly specific culture conditions (794, 795). Different media provide distinct nutritional and environmental conditions that influence cell viability, differentiation, and treatment responses (794, 795). In this context, choosing the appropriate culture medium is crucial for the successful formation, growth, and functionality of patient-derived cultures. Importantly, Senkowski *et al.* showed

that in HGSC, the condition of the media influenced both organoid growth and the response to drugs such as Carboplatin and Paclitaxel (796).

Both commercially available media and self-prepared media have been described for patient-derived cultures from OC samples (164, 167, 168, 179, 790, 797, 798). Here, we tested three potential media, RPMI, OCMI, and SOM, to establish MA-derived cultures within a clinically relevant context timeframe.

RPMI (Thermo Fisher Scientific, Waltham, MA, USA) is a widely used culture medium rich in amino acids, vitamins, and mineral salts. It provides an appropriate environment for most cells in culture, and its balanced formulation promotes cell growth, which is essential for the proliferation and maintenance of cancer cells. RPMI can also be supplemented with growth factors and hormones, tailoring it to the specific needs of patient-derived cultures. However, while RPMI is effective in many contexts, it does not replicate the unique conditions of the OC microenvironment as precisely as other mediums.

OCMI, developed specifically for culturing OC-derived organoids, contains a tailored combination of nutrients, growth factors, and hormones designed to mimic the OC microenvironment (799). This medium supports the formation and maintenance of organoids that closely resemble the original tumors (799). Despite its optimization for OC organoids, our results indicated that OCMI was less effective at maintaining the full spectrum of tumor characteristics observed in MA-derived cultures.

SOM is enriched with factors promoting self-renewal and cell proliferation and proved to be the most successful medium for supporting the growth and viability of MA-derived cultures (165, 792). SOM effectively replicated the diverse and dynamic tumor traits observed in MA samples, preserving the heterogeneity and CSC properties crucial for accurate disease modeling(165, 792). Our experimental results demonstrated that SOM was the only medium capable of maintaining viable MA-derived cultures (**Figures 38 and 39**).

To optimize the environment for MA-derived cultures, we chose to formulate an "in-house" medium (more details in **Table S9**) by purchasing individual components and combining them to match the specific needs of our experiments. This approach allows for more precise control over the concentrations of growth factors, hormones, and essential nutrients, ensuring that the medium closely replicates the physiological conditions of OC. Formulating the medium “in-house” provides flexibility and reduces the variability often seen with batch-to-batch differences in commercially available media. This consistency is crucial for reproducibility and reliable scientific results. Additionally, customizing the medium enables closer replication of the physiological conditions of OC. Purchasing individual

components can also be more economical, particularly given the scale of our research. Furthermore, this strategy allows for easier modification and scaling of the medium for future studies or larger experimental setups, streamlining workflow and resource management

In conclusion, SOM was the only medium tested that supported the growth and viability of MA-derived cultures, making it the optimal choice for establishing these models. This medium not only preserved the TME but also allowed for accurate modeling of CO *in vitro*. As our research progresses, this approach will contribute to more reproducible results.

4.2. Medium Supplementation with Autologous Supernatant is an Advantage to the Growth of Malignant Ascites-Derived Cultures

Due to its potential benefits, autologous MA supernatant is gaining attention as a supplement in patient-derived cultures. A study has applied MA supernatant to organoid cultures, helping to recreate a microenvironment that closely mimics the patient's original tumor (800). This enhances our comprehension of the TME, especially concerning its involvement in chemoresistance and metastasis. Nevertheless, limited research continues to utilize it as a supplement to patient-derived cultures.

Our results showed that MA autologous supernatant enhances the growth and expansion of patient-derived cultures (**Figures 38 and 39**). Specifically, autologous MA supernatant improved the success of patient-derived cultures, as demonstrated in **Figures 38 and 39**, in cases HGSC#55 and HGSC#56. The autologous supernatant contains growth factors, cytokines, amino acids, lipids, and vitamins that promote cell viability, proliferation, and differentiation, creating a better environment for the cells (66). This led to improved cell growth and more consistent, reproducible results. Additionally, MA supernatant supports critical interactions between cancer cells and their matrix, helping maintain the structure and function of the cultures.

Incorporating MA supernatant also offers a better context for evaluating therapeutic responses, providing more meaningful insights into drug efficacy and resistance mechanisms. Using autologous supernatant can modulate the interaction between OC cells and immune/stromal cells, shedding light on why some tumors resist treatment. For example, soluble factors in MA may activate survival pathways, contributing to resistance to drugs like Carboplatin and Paclitaxel.

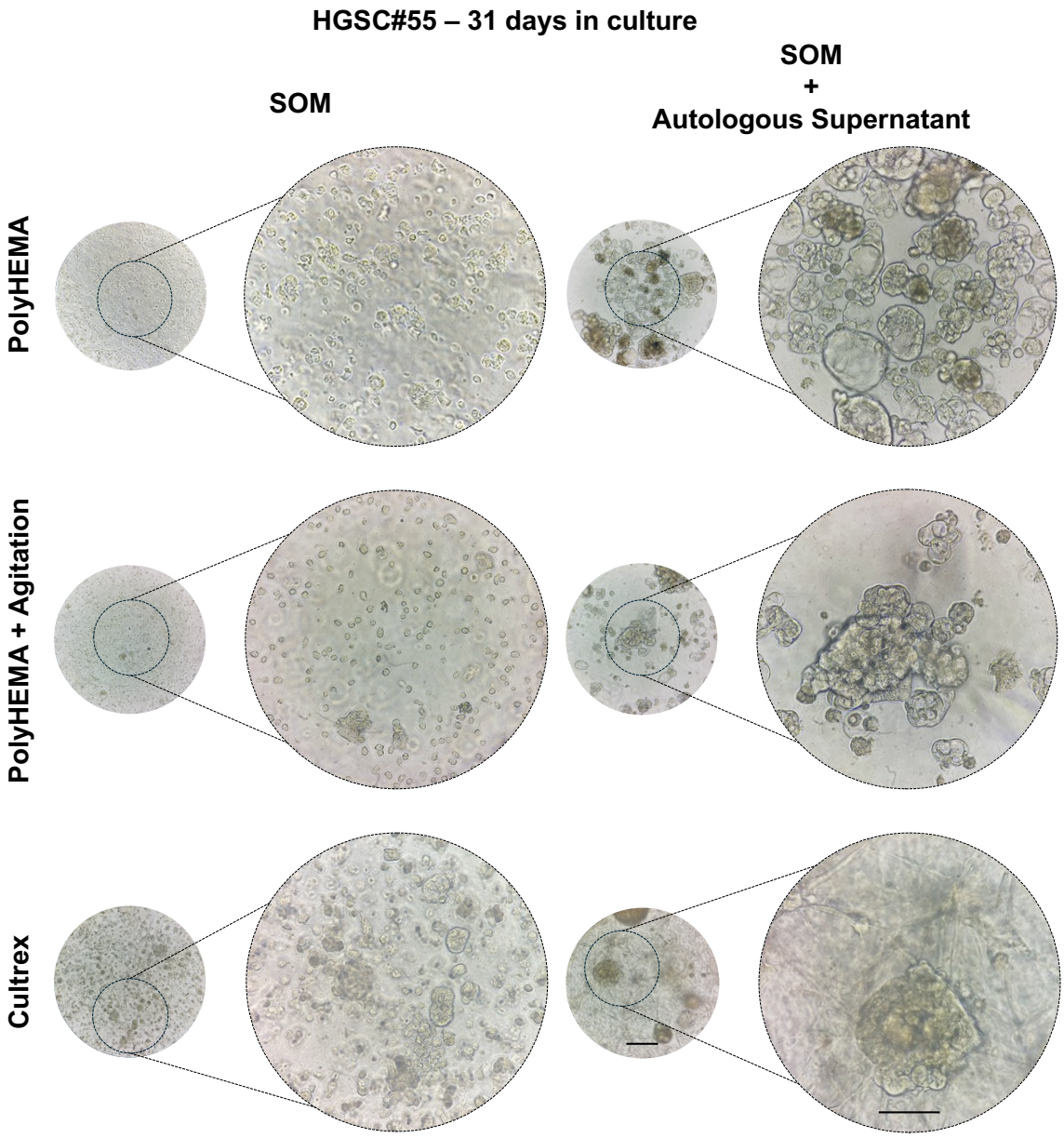


Figure 38. Representative images of MA-derived culture (HGS#55) after 31 days in culture demonstrate the impact of different culture conditions. The conditions compared include SOM versus SOM supplemented with 20% autologous MA supernatant, in PolyHEMA coating, with or without agitation, and Cultrex RGF BME type 2. The image was captured using a VWR® VisiScope® IT415 PH inverted microscope (VWR, Radnor, PA, USA) at magnifications of 200x and 400x. HGSC, high-grade serous carcinoma; SOM, standard organoid medium.

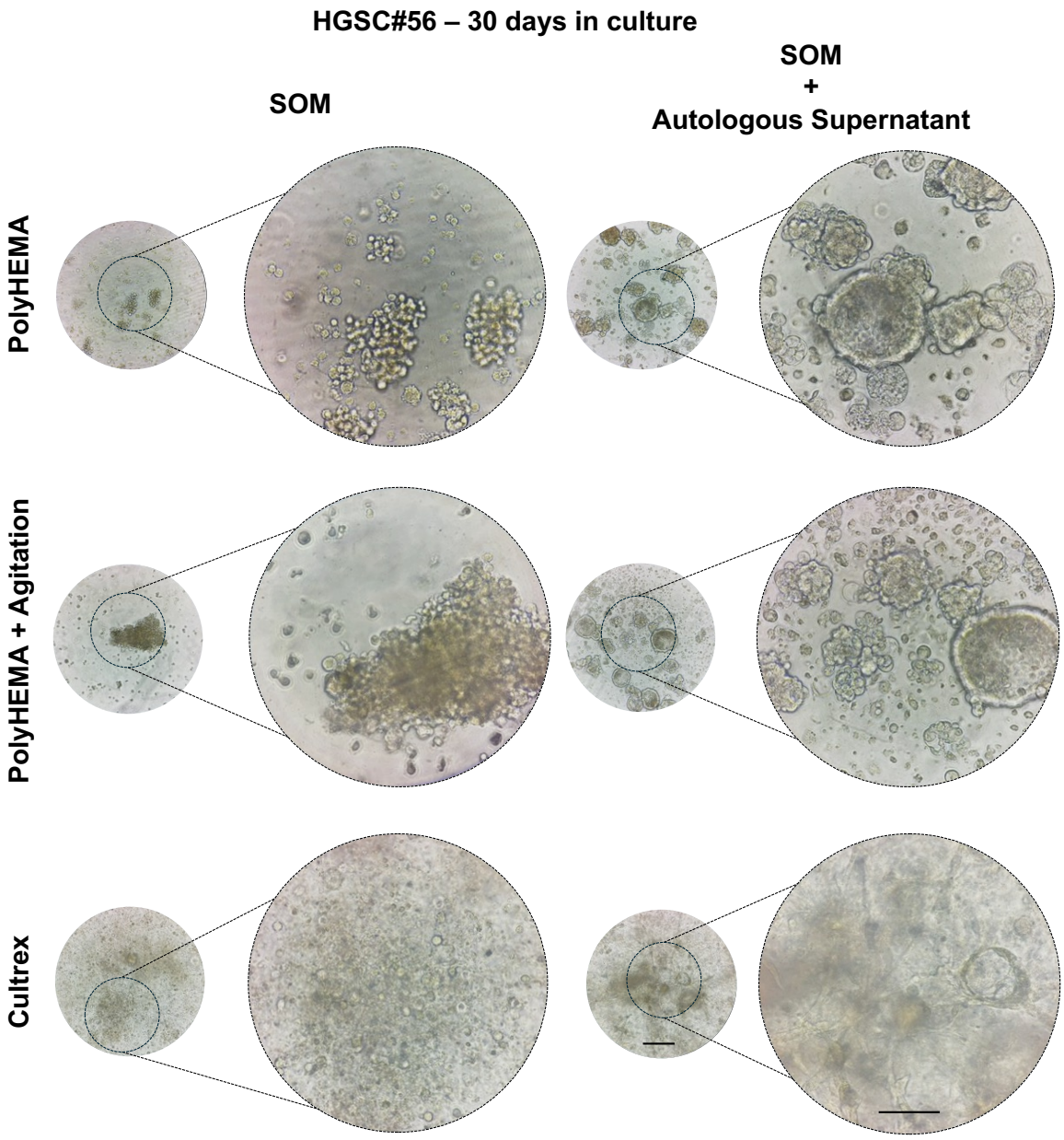


Figure 39. Representative images of MA-derived culture (HGS#56) after 30 days in culture demonstrate the impact of different culture conditions. The conditions compared include SOM versus SOM supplemented with 20% autologous MA supernatant, in PolyHEMA coating, with or without agitation, and Cultrex RGF BME type 2. The image was captured using a VWR® VisiScope® IT415 PH inverted microscope (VWR, Radnor, PA, USA) at magnifications of 200x and 400x. HGSC, high-grade serous carcinoma; SOM, standard organoid medium.

While the presence of MA autologous supernatant can increase fibroblast proliferation – often a challenge in MA-derived cultures – we addressed this issue during passage to new culture flasks (more details in the next section). Fibroblasts, which tend to

adhere even in PolyHEMA-coated flasks, can be selectively removed, allowing for the maintenance of tumor cell cultures (more details in the next section).

MA-derived cultures should be employed to test various chemotherapy agents and drug combinations. An autologous MA supernatant guarantees that these models respond to drugs in a way that closely mirrors the patient's tumor, enabling more accurate testing of potential therapies. High-throughput drug screening should be used on these models to identify novel drug candidates or combinations that may effectively treat chemotherapy-resistant tumors.

In summary, using MA autologous supernatant in MA-derived cultures provided valuable insights into the TME, chemoresistance, and potential treatment strategies. These studies will pave the way for more personalized approaches to treating this challenging disease, as they allow researchers to recreate patient-specific tumor environments and explore new therapeutic options to improve patients' outcomes.

4.3. PolyHEMA Coating is the Most Appropriate Cell Culture Setup to More Rapidly Produce Malignant Ascites-derived Cultures

Selecting an appropriate ECM for culturing patient-derived cultures is crucial for mimicking the TME, supporting cell growth, and enhancing their functionality. ECM plays a key role in maintaining the architecture and behavior of tumor cells (801, 802), directly influencing outcomes in cancer research, particularly in studies focusing on the interaction between cells and their extracellular surroundings. Two commonly used matrix options in this context are Cultrex RGF BME type 2 and polyHEMA coating, each offering unique properties that significantly influence the culture of MA-derived cultures.

Cultrex RGF BME type 2, a commercially available ECM, comprises laminin, collagen type IV, and other natural ECM components that closely resemble the *in vivo* microenvironment (803). This matrix provides an environment conducive to cell adhesion, growth, and differentiation, supporting the formation of tissue-like structures (803). Cultrex RGF BME type 2 composition facilitates the establishment of 3D cultures, closely mimicking the structural and functional characteristics. These properties are essential for maintaining the viability and functionality of patient-derived cultures, enabling more accurate modeling of tumor biology. The presence of laminin and collagen, in particular, plays a significant role in supporting cell adhesion, proliferation, and survival, critical aspects for the long-term maintenance of patient-derived cultures. Cultrex RGF BME type 2 improves the predictive

value of drug testing by fostering a natural ECM environment, allowing for more relevant and translatable assessments of treatment efficacy on MA-derived cultures.

On the other hand, PolyHEMA is a synthetic polymer that creates a non-adhesive surface for cell culture, promoting the formation of floating aggregates rather than adherent cultures. This non-adhesive property prevents excessive cell attachment, allowing for the simulation of the tumor's natural growth patterns, particularly in metastatic niches. Forming 3D floating aggregates on polyHEMA-coated surfaces enhances nutrient availability and reduces waste accumulation, thus improving the growth conditions for MA-derived cultures. Furthermore, polyHEMA is particularly useful for studying cellular behaviors such as migration and invasion, which are critical in cancer progression. The floating aggregates provide an ideal model for investigating these processes, as they resemble how cancer cells interact in a dynamic, non-adherent environment, similar to the conditions encountered *in vivo*, especially during metastasis.

Our results indicate that polyHEMA is the more effective ECM choice for this study. As is evident in **Figures 38 and 39** for cases HGSC#55 and HGSC#56, MA-derived cultures grown on polyHEMA exhibited higher cell viability, greater proliferation, and more consistent growth than those cultured on Cultrex RGF BME type 2. The polyHEMA-coated surfaces facilitated the formation of floating aggregates, better reflecting the growth patterns seen in metastatic OC. These aggregates allowed for improved nutrient diffusion and reduced waste accumulation, leading to healthier and more resilient models (**Figures 38 and 39**).

In contrast, Cultrex RGF BME type 2 did not support the same level of success, with cultures showing slower growth, reduced viability, and less consistent outcomes, as demonstrated in **Figures 38 and 39**. Therefore, the polyHEMA surface appears to provide a more favorable microenvironment for cell attachment, expansion, and the maintenance of structure and function, suggesting it is the superior ECM for maintaining the integrity of these cultures.

Moreover, in PolyHEMA culture is easier to removing fibroblasts than other culture surfaces because they adhere to it while tumor cells remain suspended. This approach allows for the rapid clearance of fibroblasts without significantly affecting the number of tumor cells, as observed in cases HGSC#55 and HGSC#56 (**Figures 40, 41 and 42**). In contrast, with Cultrex RGF BME type 2, the process is more challenging because it forms complex structures that trap fibroblasts within the matrix. Even though some fibroblasts remain attached to the plastic surface during dissociation, many are encapsulated within the

Cultrex RGF BME type 2 matrix and stay in the culture longer, making it harder to eliminate them efficiently (**Figures 40, 41 and 42**).

The choice between Cultrex RGF BME type 2 and polyHEMA should be based on the specific research objectives. For studies focusing on solid tumors and interactions with a natural ECM, Cultrex RGF BME type 2 remains a better choice. However, for studies investigating a liquid metastatic environment, cell migration, and invasion in a floating aggregate model, polyHEMA appears to offer a more suitable platform. In MA, presenting OC cells that survive in aggregates floating in a liquid metastatic niche, polyHEMA culture setup is the more effective approach to mimicking the original TME.

4.4. Maintaining Cell Aggregates is Beneficial in the Early Steps of Malignant Ascites-Derived Cultures Establishment

When working with MA-derived cultures, the decision to dissociate into single cells or maintain them as aggregates significantly impacts growth and functionality. Our results demonstrated that maintaining aggregates is particularly beneficial in the early steps of establishing MA-derived cultures (**Figure 42**). This approach preserves the tumor architecture by keeping the 3D structure and cell organization, closely mimicking the native TME. Aggregates also support key cell-cell interactions and signaling pathways, which are important for the tumor's physiological characteristics, such as differentiation and response to environmental cues. Furthermore, keeping cells in aggregates allows for more accurate studies of tumor behaviors like growth and invasion.

However, once the culture is established, dissociating cells into single cells becomes more advantageous, particularly for promoting cell expansion (**Figure 42**) and certain types of studies, such as gene expression, signaling, and drug response at the single-cell level. Dissociation also enables the exploration of cellular diversity within tumors, such as identifying subpopulations with distinct traits like drug resistance. This method is ideal for high-throughput screening and mechanistic studies, allowing for rapid compound testing and deeper insights into OC drug response pathways. For example, vitrogel is particularly effective in maintaining aggregates, supporting 3D architecture, and mimicking the extracellular matrix, which is vital for preserving tumor physiology. On the other hand, TrypLE is particularly effective for dissociation, providing a good balance between cell separation and maintaining cell viability.

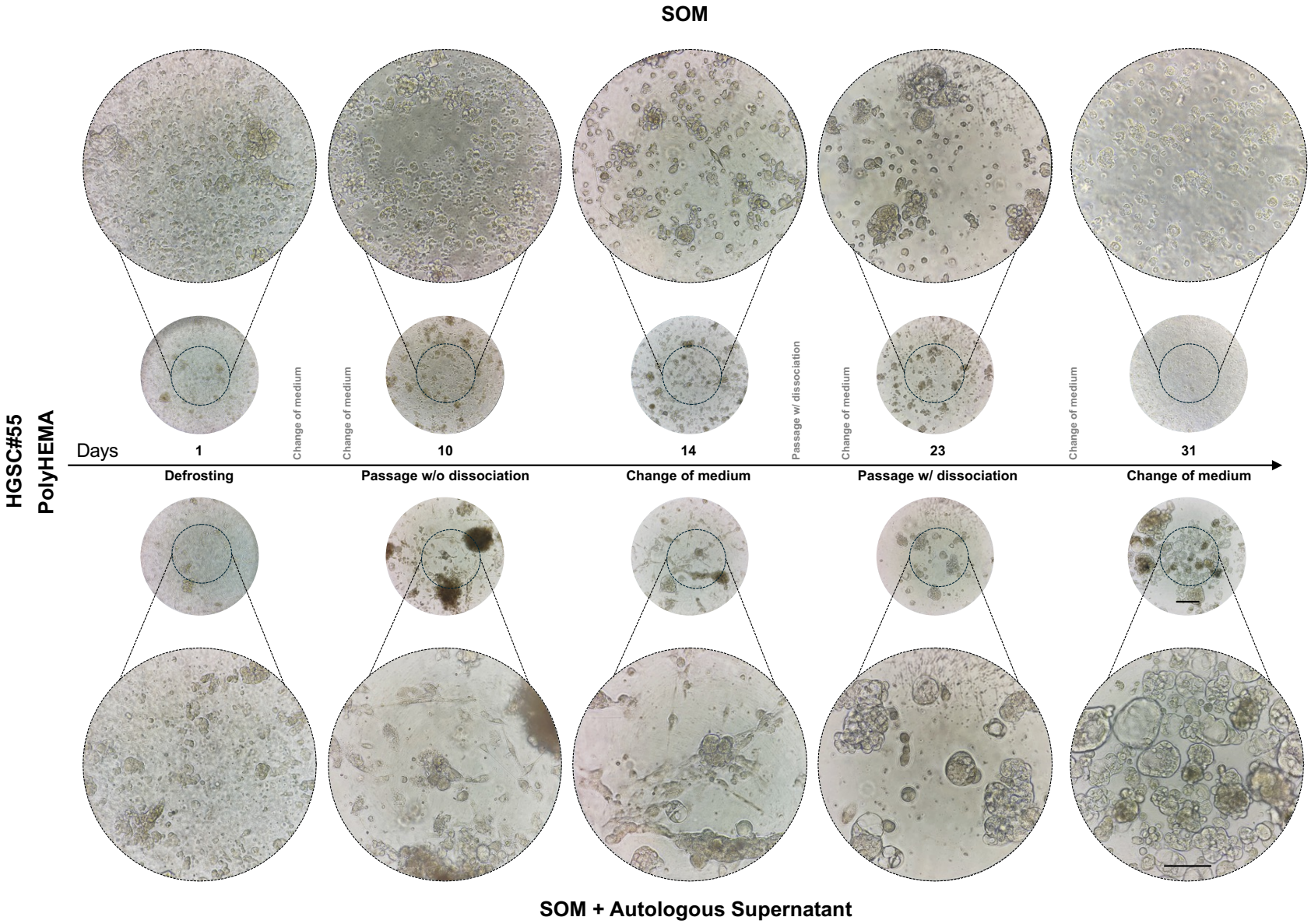

SOM
HGSC#55
PolyHEMA
Days
1
Change of medium
Change of medium
10
14
Passage w/ dissociation
Change of medium
23
Change of medium
31
Defrosting
Passage w/o dissociation
Change of medium
Passage w/ dissociation
Change of medium
SOM + Autologous Supernatant

Figure 40. Representative images of MA-derived culture (HGSC#55) over 31 days in culture illustrate the effects of different culture procedures. The figure shows the development of the MA-derived culture from case HGSC#55, which was thawed after being frozen at -80 ºC for 15 days. The culture was observed over 31 days, with comparisons made between conditions involving cell dissociation (TrypLE, at day 23) and without dissociation (VitroGel® organoid recovery solution, at day 10), as well as media changes (at days 14 and 30). It highlights the differences between cultures with and without supernatant in polyHEMA without agitation. The image was captured using a VWR® VisiScope® IT415 PH inverted microscope (VWR, Radnor, PA, USA) at magnifications of 200x and 400x. HGSC, high-grade serous carcinoma; MA, malignant ascites; SOM, standard organoid medium; w, with; w/o, without.

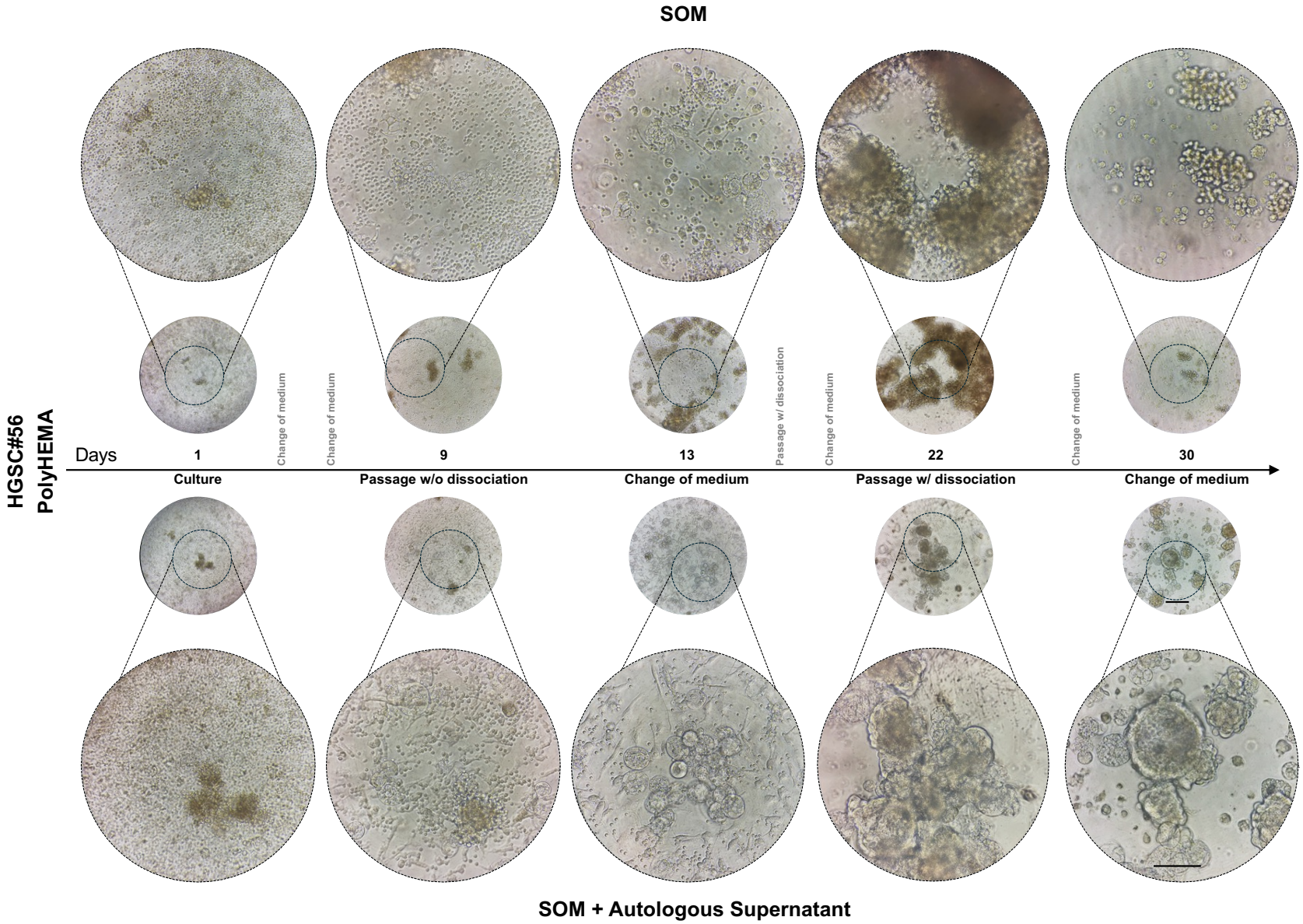

SOM
HGSC#56
PolyHEMA
Days
1
9
13
22
30
Culture
Passage w/o dissociation
Change of medium
Passage w/ dissociation
Change of medium
Change of medium
Change of medium
Passage w/ dissociation
Change of medium
Change of medium
SOM + Autologous Supernatant

Figure 41. Representative images of MA-derived culture (HGSC#56) over 30 days in culture illustrate the effects of different culture procedures. The figure shows the development of the MA-derived culture from case HGSC#56 (platinum-resistant), starting from the day that the MA was collected from the HGSC patient. The culture was observed over 30 days, with comparisons made between conditions involving cell dissociation (TrypLE, at day 22) and without dissociation (VitroGel® organoid recovery solution, at day 9), as well as media changes (at days 13 and 30). It highlights the differences between cultures with and without supernatant in polyHEMA without agitation. The image was captured using a VWR® VisiScope® IT415 PH inverted microscope (VWR, Radnor, PA, USA) at magnifications of 200x and 400x. HGSC, high-grade serous carcinoma; MA, malignant ascites; SOM, standard organoid medium; w, with; w/o, without.

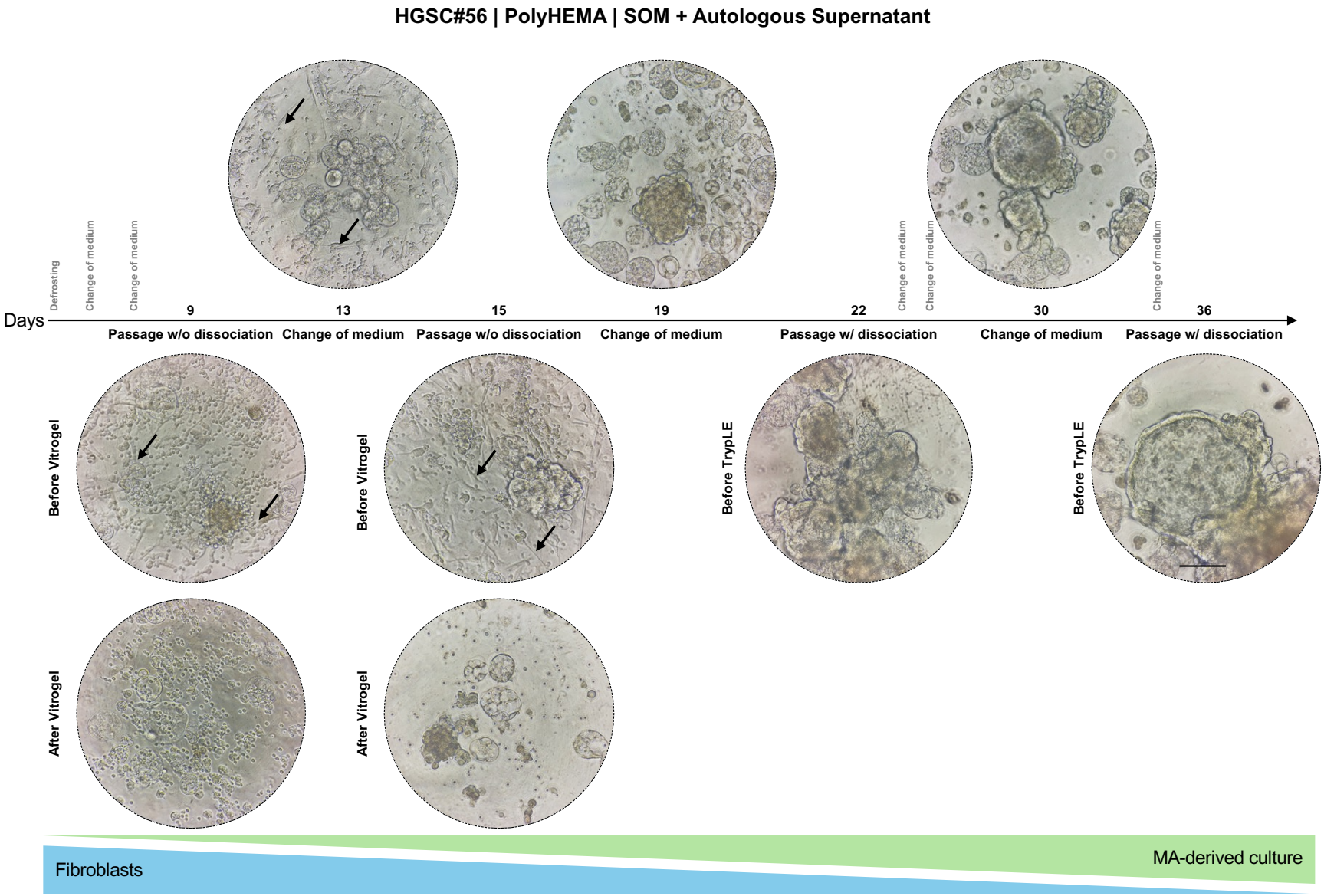

HGSC#56 | PolyHEMA | SOM + Autologous Supernatant
Defrosting
Change of medium
Change of medium
Change of medium
Change of medium
Change of medium
Days
9
13
15
19
22
30
36
Passage w/o dissociation
Change of medium
Passage w/o dissociation
Change of medium
Passage w/ dissociation
Change of medium
Passage w/ dissociation
Before Vitrogel
Before Vitrogel
Before TrypLE
Before TrypLE
After Vitrogel
After Vitrogel
Fibroblasts
MA-derived culture

Figure 42. Representative images of MA-derived culture (HGSC#56) over 36 days in culture highlight the differences after passages and medium changes to reduce the number of fibroblasts and increase Ma-derived culture yield. The figure shows the development of the MA-derived culture from case HGSC#56 (platinum-resistant), starting from the day that the MA was collected from the HGSC patient. The culture was observed over 36 days, with comparisons made between conditions involving cell dissociation (TrypLE, at day 22) and without dissociation (VitroGel® organoid recovery solution, at day 9), as well as media changes (at days 13 and 30). It highlights the differences between culture after passages and medium changes to reduce the number of fibroblasts and increase Ma-derived culture yield. The image was captured using a VWR® VisiScope® IT415 PH inverted microscope (VWR, Radnor, PA, USA) at magnifications of 400x. HGSC, high-grade serous carcinoma; MA, malignant ascites; SOM, standard organoid medium; w, with; w/o, without.

A challenge in MA-derived cultures is the rapid proliferation of fibroblasts, which can complicate the culture process. To address this, efforts were made to eliminate fibroblasts during culture passages. However, the dissociation process can result in the loss of many MA-derived cells, disrupting experiments. In the early stages, maintaining aggregates is essential for efficiently removing fibroblasts, as they tend to grow more quickly than tumor cells and can be more easily eliminated when not embedded in the 3D structure (**Figure 42**). This strategy minimizes tumor cell loss and preserves culture integrity, providing a more stable environment for further manipulation.

Ultimately, choosing between maintaining aggregates or dissociating cells depends on the research goals. Aggregates are crucial in the early stages of culture establishment to preserve tumor structure and enable accurate modeling of growth and microenvironment interactions. Dissociation is better suited for expanding the culture, single-cell analysis, and drug screening. In many cases, a combination of both methods is employed, taking advantage of the strengths of each approach.

4.5. Layered Techniques are More Effective in Maintaining Malignant Ascites-Derived Cultures

Culturing patient-derived cultures from OC MA involves various strategies to enhance growth, mimic tumor behavior, and study disease mechanisms. Aggressive culture techniques, such as spinning or shaking cells, promote their aggregation into spheroids. This method encourages cells to cluster and form 3D structures, closely mimicking the natural growth patterns of OC. Layered techniques, on the other hand, involve depositing cells in a scaffold or matrix stepwise, gradually building up tissue structures. This approach facilitates the construction of complex, layered culture architectures that better mimic native tissue. Our results indicate that layered techniques are more effective in maintaining MA-derived cultures, eliminating the need for shaker-incubators, as shown in **Figures 39 and 40**. This approach supports the growth of more stable, structured tissue architectures while avoiding the complications associated with constant agitation.

4.6. Immunocytochemistry is a Reproducible Technique to Characterize Malignant Ascites-derived Cultures Phenotype

Phenotypic characterization of MA-derived cultures is essential for understanding their biology and evaluating treatment responses. Various techniques, including microscopy,

flow cytometry, and molecular assays, are employed to assess key parameters such as cell viability, proliferation, differentiation, and gene expression in 3D cultures.

ICC is crucial for molecular tumor characterization, particularly in patient-derived cultures. By detecting and localizing specific proteins, ICC provides valuable insights into the expression of molecular markers within the context of tissue architecture. This combination of molecular profiling and preservation of tissue structure enables a more comprehensive understanding of the tumor's biological behavior. In MA-derived models, ICC evaluates key proteins related to differentiation, proliferation, apoptosis, and chemoresistance, which are essential for developing personalized treatment strategies.

Our results from the ICC evaluation of MA-patient cultures suggest that these models effectively retain the morphological and immunophenotypic characteristics of the original MA from which they are derived (**Figure 43**), as described by many other studies (164, 790, 792, 799, 804, 805). The MA-derived cultures exhibit expression patterns of important biomarkers, such as MUC16, with over 75% of cancer cells being positive for membrane expression for this marker, which closely mirrors the expression observed in the original MA sample (data not shown), where more than 75% of the cancer cells were similarly positive (**Figure 43**). This indicates that the culture system preserves key molecular features of the MA original sample, essential for maintaining its relevance in experimental MA-derived culture models.

In addition to preserving tumor-specific markers, our ICC analysis reveals low levels of apoptosis, as demonstrated by cleaved caspase-3 staining, with less than 10% of the cancer cells testing positive (**Figure 43**). This suggests that the MA-derived cultures maintain cell survival and are not undergoing significant cell death, thus reflecting the tumor’s ability to resist apoptotic signals. Conversely, these cultures exhibit notable proliferative activity, as evidenced by Ki67 expression, with over 25% of the cancer cells testing positive (**Figure 43**). This finding suggests that the tumor cells remain proliferative in culture, which is a key characteristic of malignancy and may be important for studying tumor dynamics and response to therapies. For the other two established MA-derived cultures (HGSC#55 and HGSC#56), it was not possible to complete the analysis in time for the submission of this thesis.

By identifying these important biomarker expression patterns, ICC facilitates a detailed characterization of the tumor's molecular profile and enhances the utility of MA-derived cultures as a platform for testing targeted therapies. These models provide valuable insights into how patient-specific tumors might respond to treatment, offering a more

personalized approach to predicting therapeutic efficacy. This makes ICC an indispensable tool in developing novel therapies and assessing individualized treatment strategies.

4.7. Drug Tests in Malignant Ascites-derived Cultures – A Proof of Concept for Future Works

Many studies have used different assays to quantify cellular viability (164, 165, 179, 792). When choosing between CellTiter-Glo® and Alamar Blue™ to access cell viability in patient-derived culture studies, the decision should be based on the specific goals of the experiment: CellTiter-Glo® is ideal for quick, sensitive cell viability measurements, particularly in 3D cultures where direct counting is challenging. Alamar Blue™ is better suited for studies focused on metabolic activity and when cost-effectiveness is a consideration. In many cases, using both assays in complementary ways can help gain a comprehensive understanding of cell health and behavior in patient-derived culture studies.

We have successfully established three platinum-resistant MA-derived cultures (HGSC#32, HGSC#55, and HGSC#56) (**Figures 38, 39 and 44**). Platinum resistance was confirmed *ex vivo* in all cases (**Figure 44**, data not shown for HGSC#55 and HGSC#56). Furthermore, we aim to demonstrate in more cases that all patient-derived cultures replicate clinical responses and display diverse drug responses both between and within patients, in line with findings from other studies (164, 168, 179, 790, 805). Our goal is to develop a living culture derived from MA to accurately reflect OC characteristics, enabling drug screening and personalized therapy. As noted by De Witte *et al.,* patient-derived cultures can be tested for drug response within a maximum timeframe of three weeks, making this approach potentially compatible with clinical practice (179). Moving forward, we plan to test a combination of promising compounds identified through our drug repurposing strategy, particularly those that show potential as partners for Carboplatin and Paclitaxel (further details in Chapter IV). These studies highlight the ability of MA-derived cultures to predict patient responses to therapies, providing a platform for novel therapeutic strategies and personalized treatment models that could guide clinical decisions.

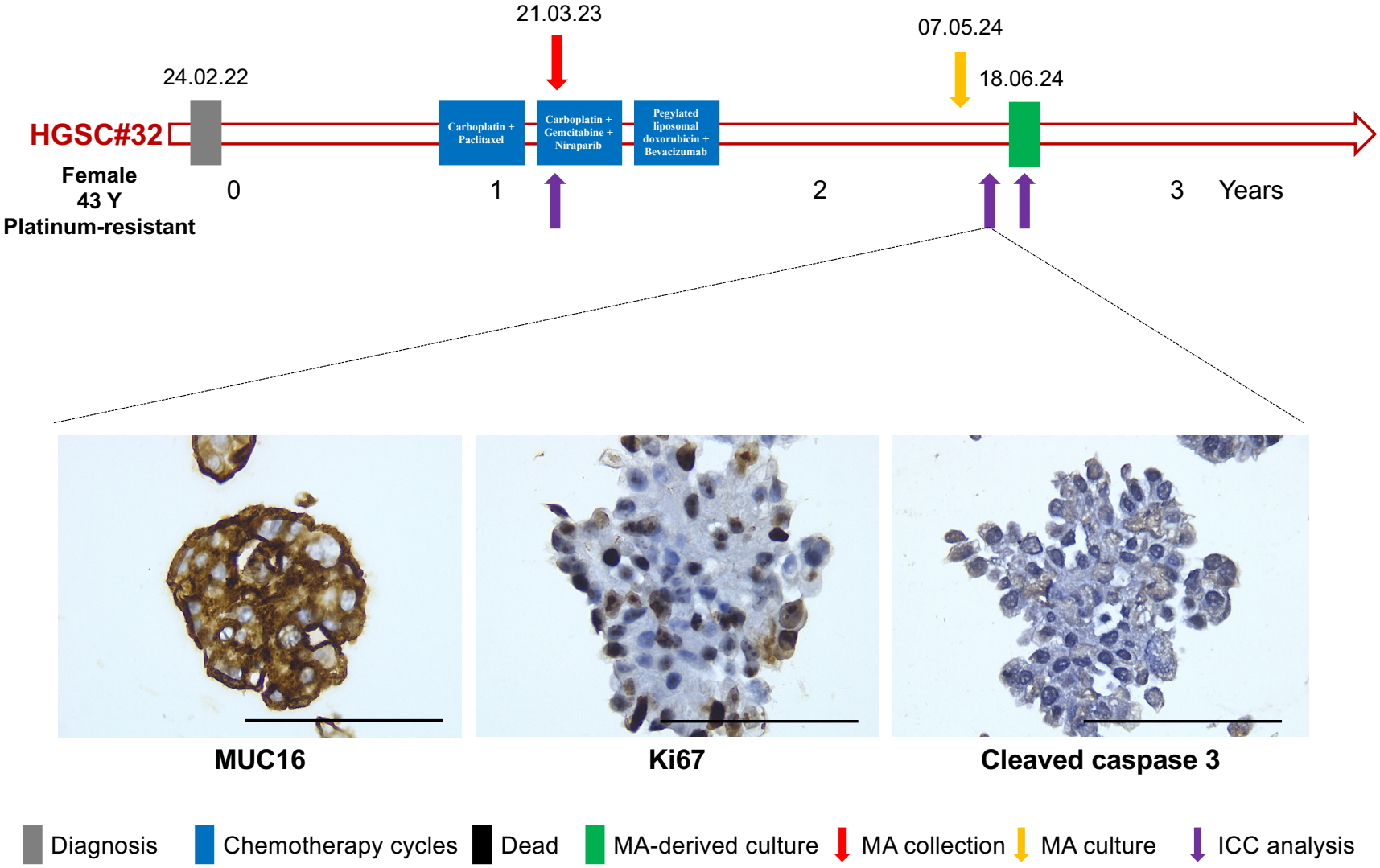

21.03.23
07.05.24
24.02.22
18.06.24
HGSC#32
Carboplatin + Paclitaxel
Carboplatin + Gemcitabine + Niraparib
Pegylated liposomal doxorubicin + Bevacizumab
Female
43 Y
Platinum-resistant
0
1
2
3
Years
MUC16
Ki67
Cleaved caspase 3
Diagnosis
Chemotherapy cycles
Dead
MA-derived culture
MA collection
MA culture
ICC analysis

Figure 43. Representative MA-derived culture model over 30 days in culture, demonstrating the retention of key morphological and immunophenotypic characteristics from the original MA sample. Representative microscopical figures of MUC16, cleaved-caspase 3, and Ki67 protein immunostaining shown by DAB staining (brown) in an MA-derived culture (HGSC#42) over 30 days in culture. All images were taken with a Brightfield Microscope Leica DM2000 LED (Leica Microsystems, Wetzlar, Germany). The figures are taken at 400x magnification, and the scale bar represents 100 µm. DAB, diaminobenzidine; MA, malignant ascites; MUC16, mucin 16.

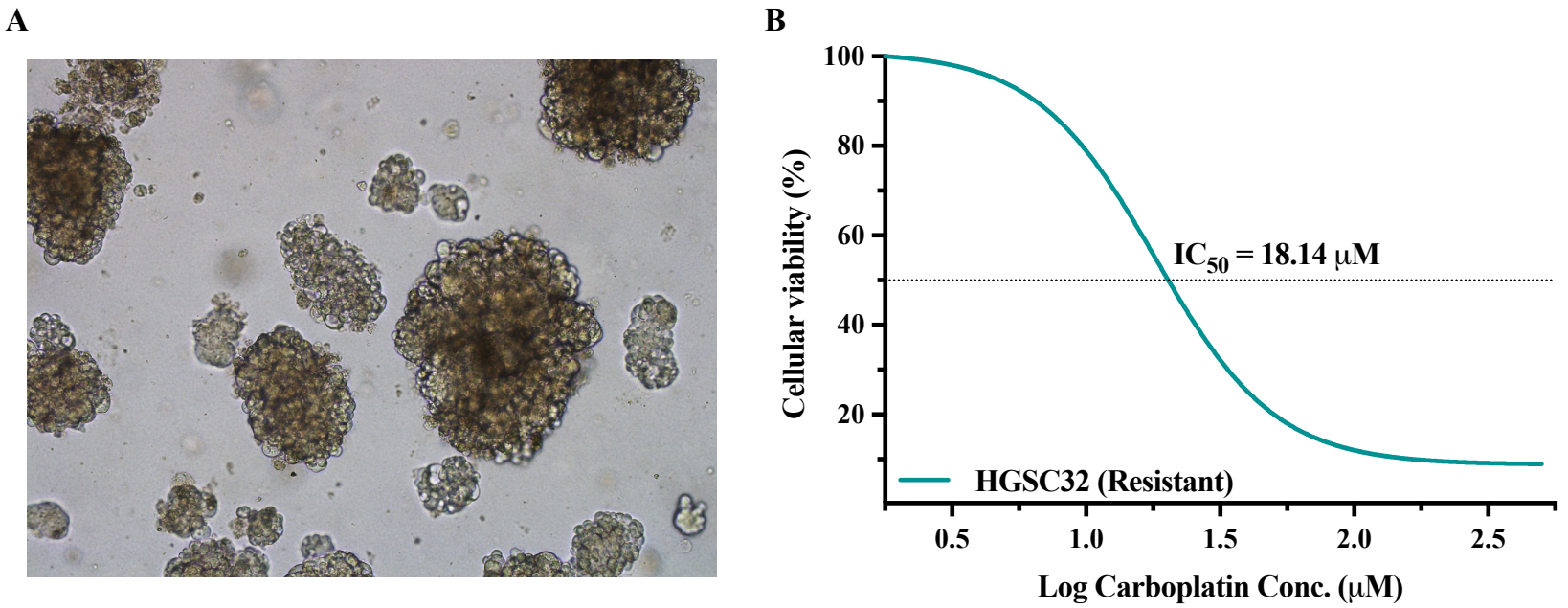


Figure 44. Establishment of patient-derived cultures from the MA of a platinum-resistant HGSC patient (A) Representative figure of MA-derived culture derived from MA (HGSC#32, Passage 2, during 21 days in culture). (B) Dose-response curves of HGSC#32 treated for 72 hours with increasing concentrations of Carboplatin (0 to 500 µM). Cellular viability was measured 4 days after the initiation of Carboplatin treatment using the AlamarBlue™ Assay. Data was plotted, and IC_{50} was calculated using GraphPad Prism Software Inc. v10 (GraphPad Software Inc., San Diego, CA, USA). A dotted line represents the IC_{50} value. HGSC, high-grade serous carcinoma; MA, malignant ascites.

5. Conclusion

MA-derived cultures provide a powerful platform for drug testing and personalized treatment approaches. Given the high recurrence rate of HGSC and the frequent development of chemoresistance, these cultures allow for testing a wide range of drugs or combinations on patient-derived models. This personalized approach can lead to tailored treatments that improve outcomes and minimize ineffective therapies.

Furthermore, MA-derived cultures are dynamic tools for studying the mechanisms of drug resistance. These models can track the evolution of resistance over time, revealing the genetic and molecular changes that drive this process and paving the way for new therapies to overcome resistance.

One of the most promising aspects of patient-derived culture methodology is its potential to transform clinical practice. As the generation of these models becomes faster and more efficient, there is hope that they could be routinely created from a patient's tumor cells at the time of diagnosis or surgery. These models enable real-time testing of different treatment options, assisting oncologists in making better-informed choices about the therapies that are most likely to benefit each patient.

6. Supplementary Material

Table S9. Table displaying the composition of the SOM, outlining the specific components, concentrations, and conditions used to establish MA-derived cultures. MA; malignant ascites; SOM, standard organoid medium (792).

Standard Organoid Medium (SOM)					
Compound	**Supplier**	**Reference**	**Stock concentration**	**Final concentration**	**Volume added** (μl)
DMEM/F12	Biotecnómica	P04-41150	-	-	46030
HEPES	Biotecnómica	P05-01500	1 M	15 mM	7500
Glutamax	Thermo Fisher Scientific	35050061	100X	1X	5000
Anti/anti	Thermo Fisher Scientific	11570486	100X	1X	5000
B27	Thermo Fisher Scientific	17504044	50X	1X	10000
N2	Serana	N2-001-50ML	100X	1X	5000
ITS	Thermo Fisher Scientific	41400045	100X	1X	5000
N-acetylcysteine	Sigma-Aldrich	A7250	6200 nM	1.24 nM	100
Noggin	SinoBiological	10267-H08H	100 mg/mL	0.1 mg/mL	500
Rspo1	Thermo Fisher Scientific	17109861	100 mg/mL	0.2 mg/mL	1000
SB 2021190	Thermo Fisher Scientific	15463629	199.19 mM	9.96 mM	25
Nicotinamide	Sigma-Aldrich	72340	2 M	2 mM	500
b-Estradiol	Sigma-Aldrich	E2257	100 mM	1 nM	5
EGF	Peprotech	AF-100-15	1000 mg/mL	0.05 mg/mL	25
FGF	PeproTech	100-18B	100 mg/mL	2 ng/mL	10
A83	Sigma-Aldrich	SML0788	23.72 mM	474.4 nM	10
Y27632	MedChemExpress	HY-10583	100 mM	5 mM	25

CHAPTER VI

General Discussion, Main Conclusions and Future Perspectives

1. General Discussion

Specific biomarkers associated with cancer differentiation, CSC, and drug resistance can be used to identify chemoresistant OC cell populations in patient-derived samples

The expression levels of biomarkers – MUC16, SOX2, ALDH1A1, CD44v6, and P-gp – can be used in combination (profile) to characterize and differentiate chemoresistant OC cell populations more accurately. A cell population with high levels of ALDH1A1, SOX2, and CD44v6 may represent an aggressive subpopulation of CSCs, while P-gp expression would suggest the presence of Paclitaxel resistance. These biomarkers can be detected in patient-derived samples, including biopsies, primary and metastatic tumors, or even MA, providing a powerful tool to monitor tumor evolution over time and identify chemoresistant populations.

By profiling these biomarkers, clinicians can predict which patients display a chemoresistance profile, develop personalized treatment plans based on the tumor's molecular characterization, and identify novel therapeutic targets, such as inhibitors of drug transporters (e.g., P-gp and MRP2) or DNA repair mechanisms (e.g., RAD51) that could overcome drug resistance. The identification of specific biomarkers related to differentiation, CSCs, and chemoresistance will enhance the ability to diagnose chemoresistant OC cell populations, predict patient outcomes, and potentially guide more effective personalized treatment strategies.

Chemoresistant OC cell line models that exhibit stable resistance profiles are a reliable tool for performing drug discovery studies

The OVCAR8 cell line was a widely used HGSC model that was typically resistant to Carboplatin and sensitive to Paclitaxel. In order to generate chemoresistant variants of this cell line, continuous and pulse exposure to increasing concentrations of Paclitaxel resulted in the selection of subpopulations that could survive despite the drug's presence – OVCAR8 PTX R C and OVCAR8 PTX R P. The establishment of these cell lines was a critical step in modeling chemoresistance in OC and offered a controlled system for studying how chemoresistance developed and persisted over time. The mechanism associated with chemoresistance observed in OVCAR8 PTX R C and OVCAR8 PTX R P cells likely involved an increased expression of P-gp, which actively pumped Paclitaxel out of the cells, reducing its intracellular concentration and effectiveness. Once these chemoresistant cell lines were established, they were able to maintain their resistance profiles over multiple passages and

freeze/thaw cycles. This stability in drug resistance was a key characteristic, making these cell lines useful for long-term studies of chemoresistance. OVCAR8 PTX R C and OVCAR8 PTX R P cells continued to proliferate in the presence of Paclitaxel and demonstrated a stable phenotype, providing a consistent model for evaluating drug resistance mechanisms. Notably, several nationally (3) and internationally (5) recognized research groups, namely in the United Kingdom, Germany, and the United States of America, have requested OVCAR8 PTX R C and OVCAR8 PTX R P cells to conduct further studies on Paclitaxel chemoresistance and associated molecular mechanisms, testing new potential drugs, among others.

Combining drug repurposing with conventional chemotherapy enhances the cytotoxic effects against chemoresistant OC cell populations

The rationale for combining repurposed drugs with standard chemotherapy lies in overcoming mechanisms of resistance, reducing toxicity, and promoting synergistic interactions. The combination of repurposed drugs with Carboplatin and Paclitaxel can help target multiple resistance mechanisms (such as efflux pumps, DNA repair, cell survival pathways, and CSC) that typically allow OC cells to evade chemotherapy. Each repurposed drug has the potential to target one or more of these mechanisms, providing a multifaceted approach to overcoming resistance. Repurposed drugs may allow for lower doses of chemotherapy to be used while maintaining or enhancing their cytotoxic effects, thus reducing the risk of adverse effects and improving the overall therapeutic index. The studied combinations have the potential to act synergistically, meaning that the combined effect of the drugs is greater than the sum of their individual effects. This could result in more effective tumor control, reduced risk of recurrence, and potentially extended survival for patients with chemoresistant OC.

In 2D, we observed that the combination of Paclitaxel with Pitavastatin or Ivermectin demonstrated the highest cytotoxic effect, creating a highly effective synergy compared to using chemotherapy alone. Similarly, combining Carboplatin with Pitavastatin resulted in a robust synergistic and cytotoxic effect greater than expected based on Carboplatin alone. Additionally, combining Paclitaxel or Carboplatin with most of the repurposed drugs demonstrated a safe pharmacological profile for a non-tumoral cell line. In addition to these impressive results, we also extended our analysis to 3D models. The transition from 2D to 3D revealed fewer promising interactions, with some combination pairs exhibiting a decreased pronounced synergistic effect in 3D cultures. Still, the combination of Paclitaxel

and Ivermectin shows a strong additive effect in 3D chemoresistant cell line models, emphasizing the potential of this two-drug approach for treating HGSC patients. Further preclinical and clinical studies are required to validate these combinations and determine their optimal use in OC therapy.

Optimizing culture conditions for MA-derived cultures is essential to rapidly producing these models and performing *ex vivo* drug efficacy tests within a clinically relevant time-frame

Culturing MA-derived cells *ex vivo* has become a valuable tool for studying OC biology, testing new therapeutic drugs, and evaluating their efficacy in a clinically relevant context. However, the viability and functional fidelity of these cells in culture can pose significant challenges, particularly when trying to maintain their heterogeneity and drug responsiveness. In MA-derived cell cultures, the challenge lies in recreating an environment that accurately mimics the TME from which these cells originate. The TME in OC is complex, with various factors, including oxygen levels, nutrient availability, pH, and ECM components, influencing tumor cell behavior. In addition, MA is rich in multiple cytokines, growth factors, and EVs that are important for maintaining tumor cell viability and promoting drug resistance.

Optimizing culture conditions, including the use of specific media, supplements, and culture protocols, significantly enhances the viability, growth, and functionality of MA-derived cultures. Customizing the medium of MA-derived cultures includes factors such as insulin, growth factors (e.g., EGF, FGF), and serum or serum-free formulations that could better support growth and CSC survival. Additionally, adding factors like autologous supernatant could help recreate the TME by mimicking the cytokine profile that influences chemoresistance and immune evasion in OC. The ECM plays a critical role in regulating cell behavior, including proliferation, migration, and drug resistance. In MA-derived cultures, the inclusion of ECM components like collagen, fibronectin, and laminin can provide a more physiologically relevant substrate for cell attachment and growth.

Optimized conditions enable accurate drug response evaluations, improving testing for potential treatments and novel strategies. These models enhance predictions of patient responses to chemotherapy and support personalized medicine in OC.

2. Main Conclusions

Drug repurposing presents significant advantages compared to creating new drugs from scratch, such as shorter development timelines, established safety profiles, and

reduced costs. This strategy is especially beneficial in OC, where therapeutic resistance and recurrence remain significant challenges. Combining drug repurposing with innovative techniques, like new combination therapies and patient-derived cultures, enhances its potential.

Exploring repurposed agents alongside standard therapies, including chemotherapy and targeted treatments such as PARPi, offers new avenues for overcoming resistance mechanisms. These novel combinations are designed to increase tumor sensitivity to chemotherapy, target multiple pathways involved in tumor progression and metastasis, and minimize toxicity by enabling lower doses of each drug.

The presence of MA in OC patients creates a unique TME that enhances chemoresistance by promoting specific signaling pathways. Indeed, many factors within MA contribute to the activation of resistance mechanisms in tumor cells, making them less responsive to standard chemotherapeutic agents.

Patient-derived cultures are emerging as a valuable tool for testing the efficacy of repurposed drugs and new combination therapies. These 3D models, derived from patients' tumor cells, closely replicate the TME, allowing for personalized drug screening and the identification of effective treatments. This capability enables us to tailor therapies to individual patients, predict the most effective combinations of repurposed and conventional treatments, study resistance mechanisms in real-time, and identify alternative therapeutic options for resistant cases. Additionally, patient-derived cultures can reduce reliance on traditional preclinical models, accelerating the development of personalized treatment regimens.

The future of OC treatment hinges on combining drug repurposing with precision medicine. Incorporating repurposed drugs into personalized therapies using patient-derived models could revolutionize OC care. As more repurposed drugs are tested in clinical trials, patients may receive more effective and less toxic treatments. This method not only shows promise for enhancing survival rates but also aims to improve the quality of life for those facing this challenge.

3. Future Perspectives

As research progresses, several exciting future directions are emerging in the field of OC research:

- **Expanding the repurposed drug arsenal:** Ongoing clinical trials are investigating a wide range of repurposed drugs, including antibiotics, antifungals, antiparasitics,

antilipidemics, and antihypertensives. As new combinations are tested, more treatment options for patients with advanced or recurrent OC are likely to emerge.

- **Integration of OMICs and patient-derived cultures to enhance the understanding of tumor biology:** Advances in OMIC technologies, which encompass genomics, transcriptomics, proteomics, and metabolomics, offer comprehensive insights into the molecular profiles of tumors. When combined with patient-derived samples, such as MA, this integration helps identify personalized treatment regimens, reflecting the TME and revealing patient-specific vulnerabilities. The analysis of MA is particularly relevant, as it contains tumor cells and various biomarkers, applying genomic and transcriptomic analyses to these samples for studying treatment resistance and discovering new therapeutic strategies, reflecting the TME and potentially revealing insights into tumor behavior and patient-specific vulnerabilities while guiding targeted therapies. Additionally, proteomic and metabolomic analyses of MA can provide insights into the TME and the metabolic alterations associated with OC, uncovering proteins and metabolites that play critical roles in tumor progression, drug resistance, and patient responses to therapy.
- **Biomarker discovery:** MA-derived OMIC data are crucial for discovering new biomarkers that can improve diagnosis, prognosis, and treatment response. By analyzing the unique molecular profile of a patient's MA, clinicians can tailor therapies to target specific alterations, thereby improving the likelihood of treatment success.
- **Personalized treatment regimens:** By leveraging OMIC data alongside patient-derived cultures, personalized treatment strategies can be developed. This approach aims to identify the most effective therapies while minimizing adverse effects and optimizing patient outcomes.
- **Understanding treatment resistance:** MA is a valuable resource for studying the mechanisms of drug resistance in OC. By analyzing cancer cells within MA and their interactions with the TME, it is possible to identify factors that contribute to treatment failure and explore strategies to overcome resistance.
- **Drug discovery and development:** The combination of OMIC data and patient-derived cultures accelerates the drug discovery process. Multiple drug candidates can be tested that closely mimic patient tumors, facilitating the identification of effective treatments and novel therapeutic targets.
- **Clinical validation and translation**: While patient-derived cultures are powerful research tools, clinical validation is crucial for their application in practice. Clinical trials

guided by screening results from patient-derived cultures aim to demonstrate that these models can improve patient outcomes and reduce the time spent on ineffective treatments.

- **Artificial intelligence (AI) in drug screening:** AI is increasingly used to analyze large datasets generated from patient-derived culture drug screenings. Machine learning algorithms help identify patterns and predict the most effective drug combinations for individual patients, potentially revolutionizing personalized cancer treatment.

In summary, the synergy between drug repurposing, innovative therapeutic strategies, OMIC approaches, and the use of patient-derived samples, including MA, holds significant promise for the future of OC treatment. This integration enables a more comprehensive understanding of tumor biology, facilitates the identification of novel biomarkers, enhances personalized treatment strategies, and provides crucial insights into treatment resistance. Thus, it paves the way for innovative therapeutic strategies and ultimately improves patient outcomes.

REFERENCES

1. Sung H, Ferlay J, Siegel RL, Laversanne M, Soerjomataram I, Jemal A, et al. 2021. Global Cancer Statistics 2020: GLOBOCAN Estimates of Incidence and Mortality Worldwide for 36 Cancers in 185 Countries. CA Cancer J Clin. 71(3):209-249. https://www.ncbi.nlm.nih.gov/pubmed/33538338.
2. Bray F, Moller B. 2006. Predicting the future burden of cancer. Nat Rev Cancer. 6(1):63-74. https://www.ncbi.nlm.nih.gov/pubmed/16372017.
3. Bray F, Laversanne M, Sung H, Ferlay J, Siegel RL, Soerjomataram I, et al. 2024. Global cancer statistics 2022: GLOBOCAN estimates of incidence and mortality worldwide for 36 cancers in 185 countries. CA Cancer J Clin. 74(3):229-263. https://www.ncbi.nlm.nih.gov/pubmed/38572751.
4. Ferlay J LM, Ervik M, Lam F, Colombet M, Mery L, Piñeros M, Znaor A, Soerjomataram I, Bray F Global Cancer Observatory: Cancer Tomorrow (version 1.1). Lyon, France: International Agency for Research on Cancer. Available from: https://gco.iarc.who.int/tomorrow [acessed in 22.10.2024]. [
5. Abreu MH, Lillsunde-Larsson G, Bartosch C, Ricardo S. 2023. Editorial: New molecular approaches to improve gynecological cancer management. Front Oncol. 13:1235035. https://www.ncbi.nlm.nih.gov/pubmed/37416529.
6. Cancer statistics for the year 2020: An overview [Internet]. 2021 [cited Apr 5]. Available from: https://www.ncbi.nlm.nih.gov/pubmed/33818764 [acessed in 22.10.2024].
7. Berek JS, Renz M, Kehoe S, Kumar L, Friedlander M. 2021. Cancer of the ovary, fallopian tube, and peritoneum: 2021 update. Int J Gynaecol Obstet. 155 Suppl 1(Suppl 1):61-85. https://www.ncbi.nlm.nih.gov/pubmed/34669199.
8. Coburn SB, Bray F, Sherman ME, Trabert B. 2017. International patterns and trends in ovarian cancer incidence, overall and by histologic subtype. Int J Cancer. 140(11):2451-2460. https://www.ncbi.nlm.nih.gov/pubmed/28257597.
9. Yoneda A, Lendorf ME, Couchman JR, Multhaupt HA. 2012. Breast and ovarian cancers: a survey and possible roles for the cell surface heparan sulfate proteoglycans. J Histochem Cytochem. 60(1):9-21. https://www.ncbi.nlm.nih.gov/pubmed/22205677.
10. Global Burden of Disease Cancer C, Fitzmaurice C, Abate D, Abbasi N, Abbastabar H, Abd-Allah F, et al. 2019. Global, Regional, and National Cancer Incidence, Mortality, Years of Life Lost, Years Lived With Disability, and Disability-Adjusted Life-Years for 29 Cancer Groups, 1990 to 2017: A Systematic Analysis for the Global Burden of Disease Study. JAMA Oncol. 5(12):1749-1768. https://www.ncbi.nlm.nih.gov/pubmed/31560378.
11. Siegel RL, Miller KD, Fuchs HE, Jemal A. 2021. Cancer Statistics, 2021. CA Cancer J Clin. 71(1):7-33. https://www.ncbi.nlm.nih.gov/pubmed/33433946.
12. Beral V, Million Women Study C, Bull D, Green J, Reeves G. 2007. Ovarian cancer and hormone replacement therapy in the Million Women Study. Lancet. 369(9574):1703-1710. https://www.ncbi.nlm.nih.gov/pubmed/17512855.
13. Wright JD, Chen L, Tergas AI, Patankar S, Burke WM, Hou JY, et al. 2015. Trends in relative survival for ovarian cancer from 1975 to 2011. Obstet Gynecol. 125(6):1345-1352. https://www.ncbi.nlm.nih.gov/pubmed/26000505.
14. De Leo A, Santini D, Ceccarelli C, Santandrea G, Palicelli A, Acquaviva G, et al. 2021. What Is New on Ovarian Carcinoma: Integrated Morphologic and Molecular Analysis Following the New 2020 World Health Organization Classification of Female Genital Tumors. Diagnostics (Basel). 11(4). https://www.ncbi.nlm.nih.gov/pubmed/33919741.
15. Board WCoTE. Female Genital Tumours: WHO Classification of Tumours. 5th ed. Lyon, France: IARC; 2020.
16. Stewart C, Ralyea C, Lockwood S. 2019. Ovarian Cancer: An Integrated Review. Semin Oncol Nurs. 35(2):151-156. https://www.ncbi.nlm.nih.gov/pubmed/30867104.
17. Colombo N, Sessa C, du Bois A, Ledermann J, McCluggage WG, McNeish I, et al. 2019. ESMO-ESGO consensus conference recommendations on ovarian cancer: pathology

and molecular biology, early and advanced stages, borderline tumours and recurrent diseasedagger. Ann Oncol. 30(5):672-705. https://www.ncbi.nlm.nih.gov/pubmed/31046081.
18. Kurta ML, Edwards RP, Moysich KB, McDonough K, Bertolet M, Weissfeld JL, et al. 2014. Prognosis and conditional disease-free survival among patients with ovarian cancer. J Clin Oncol. 32(36):4102-4112. https://www.ncbi.nlm.nih.gov/pubmed/25403208.
19. Ledermann JA, Raja FA, Fotopoulou C, Gonzalez-Martin A, Colombo N, Sessa C, et al. 2013. Newly diagnosed and relapsed epithelial ovarian carcinoma: ESMO Clinical Practice Guidelines for diagnosis, treatment and follow-up. Ann Oncol. 24 Suppl 6:vi24-32. https://www.ncbi.nlm.nih.gov/pubmed/24078660.
20. Schorge JO, Eisenhauer EE, Chi DS. 2012. Current surgical management of ovarian cancer. Hematol Oncol Clin North Am. 26(1):93-109. https://www.ncbi.nlm.nih.gov/pubmed/22244664.
21. Ozols RF, Bundy BN, Greer BE, Fowler JM, Clarke-Pearson D, Burger RA, et al. 2003. Phase III trial of carboplatin and paclitaxel compared with cisplatin and paclitaxel in patients with optimally resected stage III ovarian cancer: a Gynecologic Oncology Group study. J Clin Oncol. 21(17):3194-3200. https://www.ncbi.nlm.nih.gov/pubmed/12860964.
22. Elattar A, Bryant A, Winter-Roach BA, Hatem M, Naik R. 2011. Optimal primary surgical treatment for advanced epithelial ovarian cancer. Cochrane Database Syst Rev. 2011(8):CD007565. https://www.ncbi.nlm.nih.gov/pubmed/21833960.
23. Calvert AH, Boddy A, Bailey NP, Siddiqui N, Humphreys A, Hughes A, et al. 1995. Carboplatin in combination with paclitaxel in advanced ovarian cancer: dose determination and pharmacokinetic and pharmacodynamic interactions. Semin Oncol. 22(5 Suppl 12):91-98; discussion 99-100. https://www.ncbi.nlm.nih.gov/pubmed/7481870.
24. McGuire WP, Hoskins WJ, Brady MF, Kucera PR, Partridge EE, Look KY, et al. 1996. Cyclophosphamide and cisplatin compared with paclitaxel and cisplatin in patients with stage III and stage IV ovarian cancer. N Engl J Med. 334(1):1-6. https://www.ncbi.nlm.nih.gov/pubmed/7494563.
25. Bookman MA, McGuire WP, 3rd, Kilpatrick D, Keenan E, Hogan WM, Johnson SW, et al. 1996. Carboplatin and paclitaxel in ovarian carcinoma: a phase I study of the Gynecologic Oncology Group. J Clin Oncol. 14(6):1895-1902. https://www.ncbi.nlm.nih.gov/pubmed/8656258.
26. du Bois A, Luck HJ, Meier W, Adams HP, Mobus V, Costa S, et al. 2003. A randomized clinical trial of cisplatin/paclitaxel versus carboplatin/paclitaxel as first-line treatment of ovarian cancer. J Natl Cancer Inst. 95(17):1320-1329. https://www.ncbi.nlm.nih.gov/pubmed/12953086.
27. Piccart MJ, Bertelsen K, James K, Cassidy J, Mangioni C, Simonsen E, et al. 2000. Randomized intergroup trial of cisplatin-paclitaxel versus cisplatin-cyclophosphamide in women with advanced epithelial ovarian cancer: three-year results. J Natl Cancer Inst. 92(9):699-708. https://www.ncbi.nlm.nih.gov/pubmed/10793106.
28. Muggia FM, Braly PS, Brady MF, Sutton G, Niemann TH, Lentz SL, et al. 2000. Phase III randomized study of cisplatin versus paclitaxel versus cisplatin and paclitaxel in patients with suboptimal stage III or IV ovarian cancer: a gynecologic oncology group study. J Clin Oncol. 18(1):106-115. https://www.ncbi.nlm.nih.gov/pubmed/10623700.
29. Liu YL, Zhou QC, Iasonos A, Chi DS, Zivanovic O, Sonoda Y, et al. 2020. Pre-operative neoadjuvant chemotherapy cycles and survival in newly diagnosed ovarian cancer: what is the optimal number? A Memorial Sloan Kettering Cancer Center Team Ovary study. Int J Gynecol Cancer. 30(12):1915-1921. https://www.ncbi.nlm.nih.gov/pubmed/33106271.
30. Kehoe S, Hook J, Nankivell M, Jayson GC, Kitchener H, Lopes T, et al. 2015. Primary chemotherapy versus primary surgery for newly diagnosed advanced ovarian cancer

(CHORUS): an open-label, randomised, controlled, non-inferiority trial. Lancet. 386(9990):249-257. https://www.ncbi.nlm.nih.gov/pubmed/26002111.
31. Vergote I, Trope CG, Amant F, Kristensen GB, Ehlen T, Johnson N, et al. 2010. Neoadjuvant chemotherapy or primary surgery in stage IIIC or IV ovarian cancer. N Engl J Med. 363(10):943-953. https://www.ncbi.nlm.nih.gov/pubmed/20818904.
32. Kumar L, Pramanik R, Kumar S, Bhatla N, Malik S. 2015. Neoadjuvant chemotherapy in gynaecological cancers - Implications for staging. Best Pract Res Clin Obstet Gynaecol. 29(6):790-801. https://www.ncbi.nlm.nih.gov/pubmed/25840650.
33. Vergote I, Coens C, Nankivell M, Kristensen GB, Parmar MKB, Ehlen T, et al. 2018. Neoadjuvant chemotherapy versus debulking surgery in advanced tubo-ovarian cancers: pooled analysis of individual patient data from the EORTC 55971 and CHORUS trials. Lancet Oncol. 19(12):1680-1687. https://www.ncbi.nlm.nih.gov/pubmed/30413383.
34. Markman M. 2019. Pharmaceutical Management of Ovarian Cancer: Current Status. Drugs. 79(11):1231-1239. https://www.ncbi.nlm.nih.gov/pubmed/31267481.
35. Agarwal R, Kaye SB. 2003. Ovarian cancer: strategies for overcoming resistance to chemotherapy. Nat Rev Cancer. 3(7):502-516. https://www.ncbi.nlm.nih.gov/pubmed/12835670.
36. Wilson MK, Pujade-Lauraine E, Aoki D, Mirza MR, Lorusso D, Oza AM, et al. 2017. Fifth Ovarian Cancer Consensus Conference of the Gynecologic Cancer InterGroup: recurrent disease. Ann Oncol. 28(4):727-732. https://www.ncbi.nlm.nih.gov/pubmed/27993805.
37. Rossi L, Verrico M, Zaccarelli E, Papa A, Colonna M, Strudel M, et al. 2017. Bevacizumab in ovarian cancer: A critical review of phase III studies. Oncotarget. 8(7):12389-12405. https://www.ncbi.nlm.nih.gov/pubmed/27852039.
38. Burger RA, Brady MF, Bookman MA, Fleming GF, Monk BJ, Huang H, et al. 2011. Incorporation of bevacizumab in the primary treatment of ovarian cancer. N Engl J Med. 365(26):2473-2483. https://www.ncbi.nlm.nih.gov/pubmed/22204724.
39. Perren TJ, Swart AM, Pfisterer J, Ledermann JA, Pujade-Lauraine E, Kristensen G, et al. 2011. A phase 3 trial of bevacizumab in ovarian cancer. N Engl J Med. 365(26):2484-2496. https://www.ncbi.nlm.nih.gov/pubmed/22204725.
40. Pujade-Lauraine E, Hilpert F, Weber B, Reuss A, Poveda A, Kristensen G, et al. 2014. Bevacizumab combined with chemotherapy for platinum-resistant recurrent ovarian cancer: The AURELIA open-label randomized phase III trial. J Clin Oncol. 32(13):1302-1308. https://www.ncbi.nlm.nih.gov/pubmed/24637997.
41. Aghajanian C, Blank SV, Goff BA, Judson PL, Teneriello MG, Husain A, et al. 2012. OCEANS: a randomized, double-blind, placebo-controlled phase III trial of chemotherapy with or without bevacizumab in patients with platinum-sensitive recurrent epithelial ovarian, primary peritoneal, or fallopian tube cancer. J Clin Oncol. 30(17):2039-2045. https://www.ncbi.nlm.nih.gov/pubmed/22529265.
42. Coleman RL, Brady MF, Herzog TJ, Sabbatini P, Armstrong DK, Walker JL, et al. 2017. Bevacizumab and paclitaxel-carboplatin chemotherapy and secondary cytoreduction in recurrent, platinum-sensitive ovarian cancer (NRG Oncology/Gynecologic Oncology Group study GOG-0213): a multicentre, open-label, randomised, phase 3 trial. Lancet Oncol. 18(6):779-791. https://www.ncbi.nlm.nih.gov/pubmed/28438473.
43. Ledermann J, Harter P, Gourley C, Friedlander M, Vergote I, Rustin G, et al. 2014. Olaparib maintenance therapy in patients with platinum-sensitive relapsed serous ovarian cancer: a preplanned retrospective analysis of outcomes by BRCA status in a randomised phase 2 trial. Lancet Oncol. 15(8):852-861. https://www.ncbi.nlm.nih.gov/pubmed/24882434.

44. Mirza MR, Monk BJ, Herrstedt J, Oza AM, Mahner S, Redondo A, et al. 2016. Niraparib Maintenance Therapy in Platinum-Sensitive, Recurrent Ovarian Cancer. N Engl J Med. 375(22):2154-2164. https://www.ncbi.nlm.nih.gov/pubmed/27717299.
45. Coleman RL, Oza AM, Lorusso D, Aghajanian C, Oaknin A, Dean A, et al. 2017. Rucaparib maintenance treatment for recurrent ovarian carcinoma after response to platinum therapy (ARIEL3): a randomised, double-blind, placebo-controlled, phase 3 trial. Lancet. 390(10106):1949-1961. https://www.ncbi.nlm.nih.gov/pubmed/28916367.
46. Taylor KN, Eskander RN. 2018. PARP Inhibitors in Epithelial Ovarian Cancer. Recent Pat Anticancer Drug Discov. 13(2):145-158. https://www.ncbi.nlm.nih.gov/pubmed/29205122.
47. Musacchio L, Cicala CM, Camarda F, Ghizzoni V, Giudice E, Carbone MV, et al. 2022. Combining PARP inhibition and immune checkpoint blockade in ovarian cancer patients: a new perspective on the horizon? ESMO Open. 7(4):100536. https://www.ncbi.nlm.nih.gov/pubmed/35849879.
48. Moore K, Colombo N, Scambia G, Kim BG, Oaknin A, Friedlander M, et al. 2018. Maintenance Olaparib in Patients with Newly Diagnosed Advanced Ovarian Cancer. N Engl J Med. 379(26):2495-2505. https://www.ncbi.nlm.nih.gov/pubmed/30345884.
49. Fong PC, Yap TA, Boss DS, Carden CP, Mergui-Roelvink M, Gourley C, et al. 2010. Poly(ADP)-ribose polymerase inhibition: frequent durable responses in BRCA carrier ovarian cancer correlating with platinum-free interval. J Clin Oncol. 28(15):2512-2519. https://www.ncbi.nlm.nih.gov/pubmed/20406929.
50. Poveda A, Floquet A, Ledermann JA, Asher R, Penson RT, Oza AM, et al. 2021. Olaparib tablets as maintenance therapy in patients with platinum-sensitive relapsed ovarian cancer and a BRCA1/2 mutation (SOLO2/ENGOT-Ov21): a final analysis of a double-blind, randomised, placebo-controlled, phase 3 trial. Lancet Oncol. 22(5):620-631. https://www.ncbi.nlm.nih.gov/pubmed/33743851.
51. Pignata S, Pisano C, Di Napoli M, Cecere SC, Tambaro R, Attademo L. 2019. Treatment of recurrent epithelial ovarian cancer. Cancer. 125 Suppl 24:4609-4615. https://www.ncbi.nlm.nih.gov/pubmed/31967680.
52. Gonzalez-Martin A, Pothuri B, Vergote I, DePont Christensen R, Graybill W, Mirza MR, et al. 2019. Niraparib in Patients with Newly Diagnosed Advanced Ovarian Cancer. N Engl J Med. 381(25):2391-2402. https://www.ncbi.nlm.nih.gov/pubmed/31562799.
53. Ray-Coquard I, Pautier P, Pignata S, Perol D, Gonzalez-Martin A, Berger R, et al. 2019. Olaparib plus Bevacizumab as First-Line Maintenance in Ovarian Cancer. N Engl J Med. 381(25):2416-2428. https://www.ncbi.nlm.nih.gov/pubmed/31851799.
54. Coleman RL, Fleming GF, Brady MF, Swisher EM, Steffensen KD, Friedlander M, et al. 2019. Veliparib with First-Line Chemotherapy and as Maintenance Therapy in Ovarian Cancer. N Engl J Med. 381(25):2403-2415. https://www.ncbi.nlm.nih.gov/pubmed/31562800.
55. Jiang X, Li X, Li W, Bai H, Zhang Z. 2019. PARP inhibitors in ovarian cancer: Sensitivity prediction and resistance mechanisms. J Cell Mol Med. 23(4):2303-2313. https://www.ncbi.nlm.nih.gov/pubmed/30672100.
56. Bever KM, Le DT. 2018. DNA repair defects and implications for immunotherapy. J Clin Invest. 128(10):4236-4242. https://www.ncbi.nlm.nih.gov/pubmed/30272580.
57. Konstantinopoulos PA, Waggoner S, Vidal GA, Mita M, Moroney JW, Holloway R, et al. 2019. Single-Arm Phases 1 and 2 Trial of Niraparib in Combination With Pembrolizumab in Patients With Recurrent Platinum-Resistant Ovarian Carcinoma. JAMA Oncol. 5(8):1141-1149. https://www.ncbi.nlm.nih.gov/pubmed/31194228.
58. Zamarin D, Burger RA, Sill MW, Powell DJ, Jr., Lankes HA, Feldman MD, et al. 2020. Randomized Phase II Trial of Nivolumab Versus Nivolumab and Ipilimumab for Recurrent

or Persistent Ovarian Cancer: An NRG Oncology Study. J Clin Oncol. 38(16):1814-1823. https://www.ncbi.nlm.nih.gov/pubmed/32275468.
59. Khan KA, Kerbel RS. 2018. Improving immunotherapy outcomes with anti-angiogenic treatments and vice versa. Nat Rev Clin Oncol. 15(5):310-324. https://www.ncbi.nlm.nih.gov/pubmed/29434333.
60. Lee JM, Nair J, Zimmer A, Lipkowitz S, Annunziata CM, Merino MJ, et al. 2018. Prexasertib, a cell cycle checkpoint kinase 1 and 2 inhibitor, in BRCA wild-type recurrent high-grade serous ovarian cancer: a first-in-class proof-of-concept phase 2 study. Lancet Oncol. 19(2):207-215. https://www.ncbi.nlm.nih.gov/pubmed/29361470.
61. Sangisetty SL, Miner TJ. 2012. Malignant ascites: A review of prognostic factors, pathophysiology and therapeutic measures. World J Gastrointest Surg. 4(4):87-95. https://www.ncbi.nlm.nih.gov/pubmed/22590662.
62. Chiejina M, Kudaravalli P, Samant H. Ascites. StatPearls. Treasure Island (FL)2022.
63. Cavazzoni E, Bugiantella W, Graziosi L, Franceschini MS, Donini A. 2013. Malignant ascites: pathophysiology and treatment. Int J Clin Oncol. 18(1):1-9. https://www.ncbi.nlm.nih.gov/pubmed/22460778.
64. Kipps E, Tan DS, Kaye SB. 2013. Meeting the challenge of ascites in ovarian cancer: new avenues for therapy and research. Nat Rev Cancer. 13(4):273-282. https://www.ncbi.nlm.nih.gov/pubmed/23426401.
65. Ford CE, Werner B, Hacker NF, Warton K. 2020. The untapped potential of ascites in ovarian cancer research and treatment. Br J Cancer. 123(1):9-16. https://www.ncbi.nlm.nih.gov/pubmed/32382112.
66. Ahmed N, Stenvers KL. 2013. Getting to know ovarian cancer ascites: opportunities for targeted therapy-based translational research. Front Oncol. 3:256. https://www.ncbi.nlm.nih.gov/pubmed/24093089.
67. Rickard BP, Conrad C, Sorrin AJ, Ruhi MK, Reader JC, Huang SA, et al. 2021. Malignant Ascites in Ovarian Cancer: Cellular, Acellular, and Biophysical Determinants of Molecular Characteristics and Therapy Response. Cancers (Basel). 13(17). https://www.ncbi.nlm.nih.gov/pubmed/34503128.
68. Lengyel E. 2010. Ovarian cancer development and metastasis. Am J Pathol. 177(3):1053-1064. https://www.ncbi.nlm.nih.gov/pubmed/20651229.
69. Ayantunde AA, Parsons SL. 2007. Pattern and prognostic factors in patients with malignant ascites: a retrospective study. Ann Oncol. 18(5):945-949. https://www.ncbi.nlm.nih.gov/pubmed/17298959.
70. Krugmann J, Schwarz CL, Melcher B, Sterlacci W, Ozalinskaite A, Lermann J, et al. 2019. Malignant ascites occurs most often in patients with high-grade serous papillary ovarian cancer at initial diagnosis: a retrospective analysis of 191 women treated at Bayreuth Hospital, 2006-2015. Arch Gynecol Obstet. 299(2):515-523. https://www.ncbi.nlm.nih.gov/pubmed/30415435.
71. Szender JB, Emmons T, Belliotti S, Dickson D, Khan A, Morrell K, et al. 2017. Impact of ascites volume on clinical outcomes in ovarian cancer: A cohort study. Gynecol Oncol. 146(3):491-497. https://www.ncbi.nlm.nih.gov/pubmed/28624153.
72. Grabowski JP, Harter P, Heitz F, Pujade-Lauraine E, Reuss A, Kristensen G, et al. 2016. Operability and chemotherapy responsiveness in advanced low-grade serous ovarian cancer. An analysis of the AGO Study Group metadatabase. Gynecol Oncol. 140(3):457-462. https://www.ncbi.nlm.nih.gov/pubmed/26807488.
73. Penet MF, Krishnamachary B, Wildes FB, Mironchik Y, Hung CF, Wu TC, et al. 2018. Ascites Volumes and the Ovarian Cancer Microenvironment. Front Oncol. 8:595. https://www.ncbi.nlm.nih.gov/pubmed/30619738.

74. Coleman RL, Monk BJ, Sood AK, Herzog TJ. 2013. Latest research and treatment of advanced-stage epithelial ovarian cancer. Nat Rev Clin Oncol. 10(4):211-224. https://www.ncbi.nlm.nih.gov/pubmed/23381004.
75. Tan DS, Agarwal R, Kaye SB. 2006. Mechanisms of transcoelomic metastasis in ovarian cancer. Lancet Oncol. 7(11):925-934. https://www.ncbi.nlm.nih.gov/pubmed/17081918.
76. Coelho R, Marcos-Silva L, Ricardo S, Ponte F, Costa A, Lopes JM, et al. 2018. Peritoneal dissemination of ovarian cancer: role of MUC16-mesothelin interaction and implications for treatment. Expert Rev Anticancer Ther. 18(2):177-186. https://www.ncbi.nlm.nih.gov/pubmed/29241375.
77. Coccolini F, Gheza F, Lotti M, Virzi S, Iusco D, Ghermandi C, et al. 2013. Peritoneal carcinomatosis. World J Gastroenterol. 19(41):6979-6994. https://www.ncbi.nlm.nih.gov/pubmed/24222942.
78. Meyers MA. 1973. Distribution of intra-abdominal malignant seeding: dependency on dynamics of flow of ascitic fluid. Am J Roentgenol Radium Ther Nucl Med. 119(1):198-206. https://www.ncbi.nlm.nih.gov/pubmed/4744725.
79. Buy JN, Moss AA, Ghossain MA, Sciot C, Malbec L, Vadrot D, et al. 1988. Peritoneal implants from ovarian tumors: CT findings. Radiology. 169(3):691-694. https://www.ncbi.nlm.nih.gov/pubmed/3186993.
80. Weidle UH, Birzele F, Kollmorgen G, Rueger R. 2016. Mechanisms and Targets Involved in Dissemination of Ovarian Cancer. Cancer Genomics Proteomics. 13(6):407-423. https://www.ncbi.nlm.nih.gov/pubmed/27807064.
81. Al Habyan S, Kalos C, Szymborski J, McCaffrey L. 2018. Multicellular detachment generates metastatic spheroids during intra-abdominal dissemination in epithelial ovarian cancer. Oncogene. 37(37):5127-5135. https://www.ncbi.nlm.nih.gov/pubmed/29789717.
82. Ayhan A, Gultekin M, Taskiran C, Dursun P, Firat P, Bozdag G, et al. 2007. Ascites and epithelial ovarian cancers: a reappraisal with respect to different aspects. Int J Gynecol Cancer. 17(1):68-75. https://www.ncbi.nlm.nih.gov/pubmed/17291234.
83. Kim S, Kim B, Song YS. 2016. Ascites modulates cancer cell behavior, contributing to tumor heterogeneity in ovarian cancer. Cancer Sci. 107(9):1173-1178. https://www.ncbi.nlm.nih.gov/pubmed/27297561.
84. Meads MB, Gatenby RA, Dalton WS. 2009. Environment-mediated drug resistance: a major contributor to minimal residual disease. Nat Rev Cancer. 9(9):665-674. https://www.ncbi.nlm.nih.gov/pubmed/19693095.
85. Shield K, Ackland ML, Ahmed N, Rice GE. 2009. Multicellular spheroids in ovarian cancer metastases: Biology and pathology. Gynecol Oncol. 113(1):143-148. https://www.ncbi.nlm.nih.gov/pubmed/19135710.
86. Latifi A, Luwor RB, Bilandzic M, Nazaretian S, Stenvers K, Pyman J, et al. 2012. Isolation and characterization of tumor cells from the ascites of ovarian cancer patients: molecular phenotype of chemoresistant ovarian tumors. PLoS One. 7(10):e46858. https://www.ncbi.nlm.nih.gov/pubmed/23056490.
87. Shield K, Riley C, Quinn MA, Rice GE, Ackland ML, Ahmed N. 2007. Alpha2beta1 integrin affects metastatic potential of ovarian carcinoma spheroids by supporting disaggregation and proteolysis. J Carcinog. 6:11. https://www.ncbi.nlm.nih.gov/pubmed/17567918.
88. Piche A. 2018. Malignant peritoneal effusion acting as a tumor environment in ovarian cancer progression: Impact and significance. World J Clin Oncol. 9(8):167-171. https://www.ncbi.nlm.nih.gov/pubmed/30622924.
89. Peart T, Ramos Valdes Y, Correa RJ, Fazio E, Bertrand M, McGee J, et al. 2015. Intact LKB1 activity is required for survival of dormant ovarian cancer spheroids. Oncotarget. 6(26):22424-22438. https://www.ncbi.nlm.nih.gov/pubmed/26068970.

90. Dong Y, Stephens C, Walpole C, Swedberg JE, Boyle GM, Parsons PG, et al. 2013. Paclitaxel resistance and multicellular spheroid formation are induced by kallikrein-related peptidase 4 in serous ovarian cancer cells in an ascites mimicking microenvironment. PLoS One. 8(2):e57056. https://www.ncbi.nlm.nih.gov/pubmed/23451143.
91. Jia D, Nagaoka Y, Katsumata M, Orsulic S. 2018. Inflammation is a key contributor to ovarian cancer cell seeding. Sci Rep. 8(1):12394. https://www.ncbi.nlm.nih.gov/pubmed/30120290.
92. Lane D, Matte I, Garde-Granger P, Laplante C, Carignan A, Rancourt C, et al. 2015. Inflammation-regulating factors in ascites as predictive biomarkers of drug resistance and progression-free survival in serous epithelial ovarian cancers. BMC Cancer. 15:492. https://www.ncbi.nlm.nih.gov/pubmed/26122176.
93. Freedman RS, Deavers M, Liu J, Wang E. 2004. Peritoneal inflammation - A microenvironment for Epithelial Ovarian Cancer (EOC). J Transl Med. 2(1):23. https://www.ncbi.nlm.nih.gov/pubmed/15219235.
94. Matte I, Lane D, Laplante C, Rancourt C, Piche A. 2012. Profiling of cytokines in human epithelial ovarian cancer ascites. Am J Cancer Res. 2(5):566-580. https://www.ncbi.nlm.nih.gov/pubmed/22957308.
95. Penson RT, Kronish K, Duan Z, Feller AJ, Stark P, Cook SE, et al. 2000. Cytokines IL-1beta, IL-2, IL-6, IL-8, MCP-1, GM-CSF and TNFalpha in patients with epithelial ovarian cancer and their relationship to treatment with paclitaxel. Int J Gynecol Cancer. 10(1):33-41. https://www.ncbi.nlm.nih.gov/pubmed/11240649.
96. Zhan N, Dong WG, Wang J. 2016. The clinical significance of vascular endothelial growth factor in malignant ascites. Tumour Biol. 37(3):3719-3725. https://www.ncbi.nlm.nih.gov/pubmed/26462841.
97. Ahmed N, Riley C, Oliva K, Rice G, Quinn M. 2005. Ascites induces modulation of alpha6beta1 integrin and urokinase plasminogen activator receptor expression and associated functions in ovarian carcinoma. Br J Cancer. 92(8):1475-1485. https://www.ncbi.nlm.nih.gov/pubmed/15798771.
98. Hamidi H, Ivaska J. 2018. Every step of the way: integrins in cancer progression and metastasis. Nat Rev Cancer. 18(9):533-548. https://www.ncbi.nlm.nih.gov/pubmed/30002479.
99. Giuntoli RL, 2nd, Webb TJ, Zoso A, Rogers O, Diaz-Montes TP, Bristow RE, et al. 2009. Ovarian cancer-associated ascites demonstrates altered immune environment: implications for antitumor immunity. Anticancer Res. 29(8):2875-2884. https://www.ncbi.nlm.nih.gov/pubmed/19661290.
100. Lane D, Matte I, Rancourt C, Piche A. 2011. Prognostic significance of IL-6 and IL-8 ascites levels in ovarian cancer patients. BMC Cancer. 11:210. https://www.ncbi.nlm.nih.gov/pubmed/21619709.
101. Obata NH, Tamakoshi K, Shibata K, Kikkawa F, Tomoda Y. 1997. Effects of interleukin-6 on in vitro cell attachment, migration and invasion of human ovarian carcinoma. Anticancer Res. 17(1A):337-342. https://www.ncbi.nlm.nih.gov/pubmed/9066674.
102. Nilsson MB, Langley RR, Fidler IJ. 2005. Interleukin-6, secreted by human ovarian carcinoma cells, is a potent proangiogenic cytokine. Cancer Res. 65(23):10794-10800. https://www.ncbi.nlm.nih.gov/pubmed/16322225.
103. Tempfer C, Zeisler H, Sliutz G, Haeusler G, Hanzal E, Kainz C. 1997. Serum evaluation of interleukin 6 in ovarian cancer patients. Gynecol Oncol. 66(1):27-30. https://www.ncbi.nlm.nih.gov/pubmed/9234916.
104. Masoumi Moghaddam S, Amini A, Morris DL, Pourgholami MH. 2012. Significance of vascular endothelial growth factor in growth and peritoneal dissemination of ovarian cancer. Cancer Metastasis Rev. 31(1-2):143-162. https://www.ncbi.nlm.nih.gov/pubmed/22101807.

105. Kassim SK, El-Salahy EM, Fayed ST, Helal SA, Helal T, Azzam Eel D, et al. 2004. Vascular endothelial growth factor and interleukin-8 are associated with poor prognosis in epithelial ovarian cancer patients. Clin Biochem. 37(5):363-369. https://www.ncbi.nlm.nih.gov/pubmed/15087251.
106. Zeineldin R, Muller CY, Stack MS, Hudson LG. 2010. Targeting the EGF receptor for ovarian cancer therapy. J Oncol. 2010:414676. https://www.ncbi.nlm.nih.gov/pubmed/20066160.
107. Alper O, Bergmann-Leitner ES, Bennett TA, Hacker NF, Stromberg K, Stetler-Stevenson WG. 2001. Epidermal growth factor receptor signaling and the invasive phenotype of ovarian carcinoma cells. J Natl Cancer Inst. 93(18):1375-1384. https://www.ncbi.nlm.nih.gov/pubmed/11562388.
108. Psyrri A, Kassar M, Yu Z, Bamias A, Weinberger PM, Markakis S, et al. 2005. Effect of epidermal growth factor receptor expression level on survival in patients with epithelial ovarian cancer. Clin Cancer Res. 11(24 Pt 1):8637-8643. https://www.ncbi.nlm.nih.gov/pubmed/16361548.
109. Nakamura K, Sawada K, Kobayashi M, Miyamoto M, Shimizu A, Yamamoto M, et al. 2019. Role of the Exosome in Ovarian Cancer Progression and Its Potential as a Therapeutic Target. Cancers (Basel). 11(8). https://www.ncbi.nlm.nih.gov/pubmed/31405096.
110. Mitra A, Yoshida-Court K, Solley TN, Mikkelson M, Yeung CLA, Nick A, et al. 2021. Extracellular vesicles derived from ascitic fluid enhance growth and migration of ovarian cancer cells. Sci Rep. 11(1):9149. https://www.ncbi.nlm.nih.gov/pubmed/33911091.
111. Alharbi M, Lai A, Sharma S, Kalita-de Croft P, Godbole N, Campos A, et al. 2021. Extracellular Vesicle Transmission of Chemoresistance to Ovarian Cancer Cells Is Associated with Hypoxia-Induced Expression of Glycolytic Pathway Proteins, and Prediction of Epithelial Ovarian Cancer Disease Recurrence. Cancers (Basel). 13(14). https://www.ncbi.nlm.nih.gov/pubmed/34298602.
112. Ahmed N, Greening D, Samardzija C, Escalona RM, Chen M, Findlay JK, et al. 2016. Unique proteome signature of post-chemotherapy ovarian cancer ascites-derived tumor cells. Sci Rep. 6:30061. https://www.ncbi.nlm.nih.gov/pubmed/27470985.
113. Kuk C, Kulasingam V, Gunawardana CG, Smith CR, Batruch I, Diamandis EP. 2009. Mining the ovarian cancer ascites proteome for potential ovarian cancer biomarkers. Mol Cell Proteomics. 8(4):661-669. https://www.ncbi.nlm.nih.gov/pubmed/19047685.
114. Shender VO, Pavlyukov MS, Ziganshin RH, Arapidi GP, Kovalchuk SI, Anikanov NA, et al. 2014. Proteome-metabolome profiling of ovarian cancer ascites reveals novel components involved in intercellular communication. Mol Cell Proteomics. 13(12):3558-3571. https://www.ncbi.nlm.nih.gov/pubmed/25271300.
115. Elschenbroich S, Ignatchenko V, Clarke B, Kalloger SE, Boutros PC, Gramolini AO, et al. 2011. In-depth proteomics of ovarian cancer ascites: combining shotgun proteomics and selected reaction monitoring mass spectrometry. J Proteome Res. 10(5):2286-2299. https://www.ncbi.nlm.nih.gov/pubmed/21491939.
116. Manning-Geist BL, Hicks-Courant K, Gockley AA, Clark RM, Del Carmen MG, Growdon WB, et al. 2018. Moving beyond "complete surgical resection" and "optimal": Is low-volume residual disease another option for primary debulking surgery? Gynecol Oncol. 150(2):233-238. https://www.ncbi.nlm.nih.gov/pubmed/29933927.
117. Cannistra SA. 2004. Cancer of the ovary. N Engl J Med. 351(24):2519-2529. https://www.ncbi.nlm.nih.gov/pubmed/15590954.
118. Becker G, Galandi D, Blum HE. 2006. Malignant ascites: systematic review and guideline for treatment. Eur J Cancer. 42(5):589-597. https://www.ncbi.nlm.nih.gov/pubmed/16434188.

119. Hodge C, Badgwell BD. 2019. Palliation of malignant ascites. J Surg Oncol. 120(1):67-73. https://www.ncbi.nlm.nih.gov/pubmed/30903617.
120. Saiz-Mendiguren R, Gomez-Ayechu M, Noguera JJ, Garcia-Lallana A, Marginet C, Cano D, et al. 2010. [Permanent tunneled drainage for malignant ascites: initial experience with the PleurX(R) catheter]. Radiologia. 52(6):541-545. https://www.ncbi.nlm.nih.gov/pubmed/20863540.
121. Tapping CR, Ling L, Razack A. 2012. PleurX drain use in the management of malignant ascites: safety, complications, long-term patency and factors predictive of success. Br J Radiol. 85(1013):623-628. https://www.ncbi.nlm.nih.gov/pubmed/21427184.
122. Fotopoulou C, Berg T, Hausen A, Hennig R, Jalan R, Malago M, et al. 2019. Continuous low flow ascites drainage through the urinary bladder via the Alfapump system in palliative patients with malignant ascites. BMC Palliat Care. 18(1):109. https://www.ncbi.nlm.nih.gov/pubmed/31805921.
123. Bellot P, Welker MW, Soriano G, von Schaewen M, Appenrodt B, Wiest R, et al. 2013. Automated low flow pump system for the treatment of refractory ascites: a multi-center safety and efficacy study. J Hepatol. 58(5):922-927. https://www.ncbi.nlm.nih.gov/pubmed/23318604.
124. Armstrong DK, Bundy B, Wenzel L, Huang HQ, Baergen R, Lele S, et al. 2006. Intraperitoneal cisplatin and paclitaxel in ovarian cancer. N Engl J Med. 354(1):34-43. https://www.ncbi.nlm.nih.gov/pubmed/16394300.
125. de Bree E, Helm CW. 2012. Hyperthermic intraperitoneal chemotherapy in ovarian cancer: rationale and clinical data. Expert Rev Anticancer Ther. 12(7):895-911. https://www.ncbi.nlm.nih.gov/pubmed/22845405.
126. Abdel Mageed H, Van Der Speeten K, Sugarbaker P. 2021. The many faces of intraperitoneal chemotherapy. Surg Oncol. 40:101676. https://www.ncbi.nlm.nih.gov/pubmed/34875459.
127. Gonzalez-Moreno S, Gonzalez-Bayon LA, Ortega-Perez G. 2010. Hyperthermic intraperitoneal chemotherapy: Rationale and technique. World J Gastrointest Oncol. 2(2):68-75. https://www.ncbi.nlm.nih.gov/pubmed/21160924.
128. Hotouras A, Desai D, Bhan C, Murphy J, Lampe B, Sugarbaker PH. 2016. Heated IntraPEritoneal Chemotherapy (HIPEC) for Patients With Recurrent Ovarian Cancer: A Systematic Literature Review. Int J Gynecol Cancer. 26(4):661-670. https://www.ncbi.nlm.nih.gov/pubmed/26844612.
129. Cianci S, Riemma G, Ronsini C, De Franciscis P, Torella M, Schiattarella A, et al. 2020. Hyperthermic intraperitoneal chemotherapy (HIPEC) for ovarian cancer recurrence: systematic review and meta-analysis. Gland Surg. 9(4):1140-1148. https://www.ncbi.nlm.nih.gov/pubmed/32953629.
130. van Driel WJ, Koole SN, Sikorska K, Schagen van Leeuwen JH, Schreuder HWR, Hermans RHM, et al. 2018. Hyperthermic Intraperitoneal Chemotherapy in Ovarian Cancer. N Engl J Med. 378(3):230-240. https://www.ncbi.nlm.nih.gov/pubmed/29342393.
131. Classe JM, Asselain B, Campion L, Berton D, Frenel JS, Lecuru F, et al. 2021. Survival Outcomes after Hyperthermic Intraperitoneal Chemotherapy for a First Ovarian Cancer Relapse: A Systematic Evidence-Based Review. Cancers (Basel). 14(1). https://www.ncbi.nlm.nih.gov/pubmed/35008336.
132. Aghajanian C, Goff B, Nycum LR, Wang YV, Husain A, Blank SV. 2015. Final overall survival and safety analysis of OCEANS, a phase 3 trial of chemotherapy with or without bevacizumab in patients with platinum-sensitive recurrent ovarian cancer. Gynecol Oncol. 139(1):10-16. https://www.ncbi.nlm.nih.gov/pubmed/26271155.
133. Byrne AT, Ross L, Holash J, Nakanishi M, Hu L, Hofmann JI, et al. 2003. Vascular endothelial growth factor-trap decreases tumor burden, inhibits ascites, and causes

dramatic vascular remodeling in an ovarian cancer model. Clin Cancer Res. 9(15):5721-5728. https://www.ncbi.nlm.nih.gov/pubmed/14654557.
134. Mackey JR, Wood L, Nabholtz J, Jensen J, Venner P. 2000. A phase II trial of triamcinolone hexacetanide for symptomatic recurrent malignant ascites. J Pain Symptom Manage. 19(3):193-199. https://www.ncbi.nlm.nih.gov/pubmed/10760624.
135. Heiss MM, Murawa P, Koralewski P, Kutarska E, Kolesnik OO, Ivanchenko VV, et al. 2010. The trifunctional antibody catumaxomab for the treatment of malignant ascites due to epithelial cancer: Results of a prospective randomized phase II/III trial. Int J Cancer. 127(9):2209-2221. https://www.ncbi.nlm.nih.gov/pubmed/20473913.
136. Numnum TM, Rocconi RP, Whitworth J, Barnes MN. 2006. The use of bevacizumab to palliate symptomatic ascites in patients with refractory ovarian carcinoma. Gynecol Oncol. 102(3):425-428. https://www.ncbi.nlm.nih.gov/pubmed/16797681.
137. Berek JS, Edwards RP, Parker LP, DeMars LR, Herzog TJ, Lentz SS, et al. 2014. Catumaxomab for the treatment of malignant ascites in patients with chemotherapy-refractory ovarian cancer: a phase II study. Int J Gynecol Cancer. 24(9):1583-1589. https://www.ncbi.nlm.nih.gov/pubmed/25254563.
138. Gotlieb WH, Amant F, Advani S, Goswami C, Hirte H, Provencher D, et al. 2012. Intravenous aflibercept for treatment of recurrent symptomatic malignant ascites in patients with advanced ovarian cancer: a phase 2, randomised, double-blind, placebo-controlled study. Lancet Oncol. 13(2):154-162. https://www.ncbi.nlm.nih.gov/pubmed/22192729.
139. Sjoquist KM, Espinoza D, Mileshkin L, Ananda S, Shannon C, Yip S, et al. 2021. REZOLVE (ANZGOG-1101): A phase 2 trial of intraperitoneal bevacizumab to treat symptomatic ascites in patients with chemotherapy-resistant, epithelial ovarian cancer. Gynecol Oncol. 161(2):374-381. https://www.ncbi.nlm.nih.gov/pubmed/33637349.
140. Colombo N, Mangili G, Mammoliti S, Kalling M, Tholander B, Sternas L, et al. 2012. A phase II study of aflibercept in patients with advanced epithelial ovarian cancer and symptomatic malignant ascites. Gynecol Oncol. 125(1):42-47. https://www.ncbi.nlm.nih.gov/pubmed/22112608.
141. Davies B, Brown PD, East N, Crimmin MJ, Balkwill FR. 1993. A synthetic matrix metalloproteinase inhibitor decreases tumor burden and prolongs survival of mice bearing human ovarian carcinoma xenografts. Cancer Res. 53(9):2087-2091. https://www.ncbi.nlm.nih.gov/pubmed/8347186.
142. Watson SA, Morris TM, Parsons SL, Steele RJ, Brown PD. 1996. Therapeutic effect of the matrix metalloproteinase inhibitor, batimastat, in a human colorectal cancer ascites model. Br J Cancer. 74(9):1354-1358. https://www.ncbi.nlm.nih.gov/pubmed/8912529.
143. Parsons SL, Watson SA, Steele RJ. 1997. Phase I/II trial of batimastat, a matrix metalloproteinase inhibitor, in patients with malignant ascites. Eur J Surg Oncol. 23(6):526-531. https://www.ncbi.nlm.nih.gov/pubmed/9484924.
144. Beattie GJ, Smyth JF. 1998. Phase I study of intraperitoneal metalloproteinase inhibitor BB94 in patients with malignant ascites. Clin Cancer Res. 4(8):1899-1902. https://www.ncbi.nlm.nih.gov/pubmed/9717817.
145. Zhao Y, Cao J, Melamed A, Worley M, Gockley A, Jones D, et al. 2019. Losartan treatment enhances chemotherapy efficacy and reduces ascites in ovarian cancer models by normalizing the tumor stroma. Proc Natl Acad Sci U S A. 116(6):2210-2219. https://www.ncbi.nlm.nih.gov/pubmed/30659155.
146. Jatoi A, Nieva JJ, Qin R, Loprinzi CL, Wos EJ, Novotny PJ, et al. 2012. A pilot study of long-acting octreotide for symptomatic malignant ascites. Oncology. 82(6):315-320. https://www.ncbi.nlm.nih.gov/pubmed/22572824.
147. Stuart GC, Nation JG, Snider DD, Thunberg P. 1993. Intraperitoneal interferon in the management of malignant ascites. Cancer. 71(6):2027-2030. https://www.ncbi.nlm.nih.gov/pubmed/7680276.

148. Rath U, Kaufmann M, Schmid H, Hofmann J, Wiedenmann B, Kist A, et al. 1991. Effect of intraperitoneal recombinant human tumour necrosis factor alpha on malignant ascites. Eur J Cancer. 27(2):121-125. https://www.ncbi.nlm.nih.gov/pubmed/1827272.
149. Katano M, Torisu M. 1983. New approach to management of malignant ascites with a streptococcal preparation, OK-432. II. Intraperitoneal inflammatory cell-mediated tumor cell destruction. Surgery. 93(3):365-373. https://www.ncbi.nlm.nih.gov/pubmed/6600854.
150. Torisu M, Katano M, Kimura Y, Itoh H, Takesue M. 1983. New approach to management of malignant ascites with a streptococcal preparation, OK-432. I. Improvement of host immunity and prolongation of survival. Surgery. 93(3):357-364. https://www.ncbi.nlm.nih.gov/pubmed/6187080.
151. Jandu N, Richardson M, Singh G, Hirte H, Hatton MW. 2006. Human ovarian cancer ascites fluid contains a mixture of incompletely degraded soluble products of fibrin that collectively possess an antiangiogenic property. Int J Gynecol Cancer. 16(4):1536-1544. https://www.ncbi.nlm.nih.gov/pubmed/16884362.
152. Rafehi S, Ramos Valdes Y, Bertrand M, McGee J, Prefontaine M, Sugimoto A, et al. 2016. TGFbeta signaling regulates epithelial-mesenchymal plasticity in ovarian cancer ascites-derived spheroids. Endocr Relat Cancer. 23(3):147-159. https://www.ncbi.nlm.nih.gov/pubmed/26647384.
153. Saini U, Naidu S, ElNaggar AC, Bid HK, Wallbillich JJ, Bixel K, et al. 2017. Elevated STAT3 expression in ovarian cancer ascites promotes invasion and metastasis: a potential therapeutic target. Oncogene. 36(2):168-181. https://www.ncbi.nlm.nih.gov/pubmed/27292260.
154. Chen MW, Yang ST, Chien MH, Hua KT, Wu CJ, Hsiao SM, et al. 2017. The STAT3-miRNA-92-Wnt Signaling Pathway Regulates Spheroid Formation and Malignant Progression in Ovarian Cancer. Cancer Res. 77(8):1955-1967. https://www.ncbi.nlm.nih.gov/pubmed/28209618.
155. Newsted D, Banerjee S, Watt K, Nersesian S, Truesdell P, Blazer LL, et al. 2019. Blockade of TGF-beta signaling with novel synthetic antibodies limits immune exclusion and improves chemotherapy response in metastatic ovarian cancer models. Oncoimmunology. 8(2):e1539613. https://www.ncbi.nlm.nih.gov/pubmed/30713798.
156. Lee JM, Kohn EC. 2010. Proteomics as a guiding tool for more effective personalized therapy. Ann Oncol. 21 Suppl 7:vii205-210. https://www.ncbi.nlm.nih.gov/pubmed/20943616.
157. Davidson B, Espina V, Steinberg SM, Florenes VA, Liotta LA, Kristensen GB, et al. 2006. Proteomic analysis of malignant ovarian cancer effusions as a tool for biologic and prognostic profiling. Clin Cancer Res. 12(3 Pt 1):791-799. https://www.ncbi.nlm.nih.gov/pubmed/16467090.
158. Lee JM, Han JJ, Altwerger G, Kohn EC. 2011. Proteomics and biomarkers in clinical trials for drug development. J Proteomics. 74(12):2632-2641. https://www.ncbi.nlm.nih.gov/pubmed/21570499.
159. Bi J, Newtson AM, Zhang Y, Devor EJ, Samuelson MI, Thiel KW, et al. 2021. Successful Patient-Derived Organoid Culture of Gynecologic Cancers for Disease Modeling and Drug Sensitivity Testing. Cancers (Basel). 13(12). https://www.ncbi.nlm.nih.gov/pubmed/34200645.
160. Beshiri ML, Tice CM, Tran C, Nguyen HM, Sowalsky AG, Agarwal S, et al. 2018. A PDX/Organoid Biobank of Advanced Prostate Cancers Captures Genomic and Phenotypic Heterogeneity for Disease Modeling and Therapeutic Screening. Clin Cancer Res. 24(17):4332-4345. https://www.ncbi.nlm.nih.gov/pubmed/29748182.
161. Bartfeld S, Bayram T, van de Wetering M, Huch M, Begthel H, Kujala P, et al. 2015. In vitro expansion of human gastric epithelial stem cells and their responses to bacterial

infection. Gastroenterology. 148(1):126-136 e126. https://www.ncbi.nlm.nih.gov/pubmed/25307862.
162. Huch M, Gehart H, van Boxtel R, Hamer K, Blokzijl F, Verstegen MM, et al. 2015. Long-term culture of genome-stable bipotent stem cells from adult human liver. Cell. 160(1-2):299-312. https://www.ncbi.nlm.nih.gov/pubmed/25533785.
163. Sachs N, de Ligt J, Kopper O, Gogola E, Bounova G, Weeber F, et al. 2018. A Living Biobank of Breast Cancer Organoids Captures Disease Heterogeneity. Cell. 172(1-2):373-386 e310. https://www.ncbi.nlm.nih.gov/pubmed/29224780.
164. Kopper O, de Witte CJ, Lohmussaar K, Valle-Inclan JE, Hami N, Kester L, et al. 2019. An organoid platform for ovarian cancer captures intra- and interpatient heterogeneity. Nat Med. 25(5):838-849. https://www.ncbi.nlm.nih.gov/pubmed/31011202.
165. Boretto M, Maenhoudt N, Luo X, Hennes A, Boeckx B, Bui B, et al. 2019. Patient-derived organoids from endometrial disease capture clinical heterogeneity and are amenable to drug screening. Nat Cell Biol. 21(8):1041-1051. https://www.ncbi.nlm.nih.gov/pubmed/31371824.
166. Drost J, Clevers H. 2018. Organoids in cancer research. Nat Rev Cancer. 18(7):407-418. https://www.ncbi.nlm.nih.gov/pubmed/29692415.
167. Maru Y, Tanaka N, Itami M, Hippo Y. 2019. Efficient use of patient-derived organoids as a preclinical model for gynecologic tumors. Gynecol Oncol. 154(1):189-198. https://www.ncbi.nlm.nih.gov/pubmed/31101504.
168. Hill SJ, Decker B, Roberts EA, Horowitz NS, Muto MG, Worley MJ, Jr., et al. 2018. Prediction of DNA Repair Inhibitor Response in Short-Term Patient-Derived Ovarian Cancer Organoids. Cancer Discov. 8(11):1404-1421. https://www.ncbi.nlm.nih.gov/pubmed/30213835.
169. Kim J, Koo BK, Knoblich JA. 2020. Human organoids: model systems for human biology and medicine. Nat Rev Mol Cell Biol. 21(10):571-584. https://www.ncbi.nlm.nih.gov/pubmed/32636524.
170. Velletri T, Villa CE, Cilli D, Barzaghi B, Lo Riso P, Lupia M, et al. 2021. Single cell-derived spheroids capture the self-renewing subpopulations of metastatic ovarian cancer. Cell Death Differ. https://www.ncbi.nlm.nih.gov/pubmed/34845371.
171. Konecny G, Crohns C, Pegram M, Felber M, Lude S, Kurbacher C, et al. 2000. Correlation of drug response with the ATP tumorchemosensitivity assay in primary FIGO stage III ovarian cancer. Gynecol Oncol. 77(2):258-263. https://www.ncbi.nlm.nih.gov/pubmed/10785475.
172. den Ouden JE, Zaman GJR, Dylus J, van Doornmalen AM, Mulder WR, Grobben Y, et al. 2020. Chemotherapy sensitivity testing on ovarian cancer cells isolated from malignant ascites. Oncotarget. 11(49):4570-4581. https://www.ncbi.nlm.nih.gov/pubmed/33346216.
173. Matte I, Garde-Granger P, Bessette P, Piche A. 2019. Serum CA125 and ascites leptin level ratio predicts baseline clinical resistance to first-line platinum-based treatment and poor prognosis in patients with high grade serous ovarian cancer. Am J Cancer Res. 9(1):160-170. https://www.ncbi.nlm.nih.gov/pubmed/30755819.
174. Kerr EH, Frederick PJ, Egger ME, Stockard CR, Sellers J, DellaManna D, et al. 2013. Lung resistance-related protein (LRP) expression in malignant ascitic cells as a prognostic marker for advanced ovarian serous carcinoma. Ann Surg Oncol. 20(9):3059-3065. https://www.ncbi.nlm.nih.gov/pubmed/23525731.
175. Brooks EA, Gencoglu MF, Corbett DC, Stevens KR, Peyton SR. 2019. An omentum-inspired 3D PEG hydrogel for identifying ECM-drivers of drug resistant ovarian cancer. APL Bioeng. 3(2):026106. https://www.ncbi.nlm.nih.gov/pubmed/31263798.
176. Balasubramanian B, Venkatraman S, Myint KZ, Janvilisri T, Wongprasert K, Kumkate S, et al. 2021. Co-Clinical Trials: An Innovative Drug Development Platform for

Cholangiocarcinoma. Pharmaceuticals (Basel). 14(1). https://www.ncbi.nlm.nih.gov/pubmed/33440754.
177. Phan N, Hong JJ, Tofig B, Mapua M, Elashoff D, Moatamed NA, et al. 2019. A simple high-throughput approach identifies actionable drug sensitivities in patient-derived tumor organoids. Commun Biol. 2:78. https://www.ncbi.nlm.nih.gov/pubmed/30820473.
178. Pasch CA, Favreau PF, Yueh AE, Babiarz CP, Gillette AA, Sharick JT, et al. 2019. Patient-Derived Cancer Organoid Cultures to Predict Sensitivity to Chemotherapy and Radiation. Clin Cancer Res. 25(17):5376-5387. https://www.ncbi.nlm.nih.gov/pubmed/31175091.
179. de Witte CJ, Espejo Valle-Inclan J, Hami N, Lohmussaar K, Kopper O, Vreuls CPH, et al. 2020. Patient-Derived Ovarian Cancer Organoids Mimic Clinical Response and Exhibit Heterogeneous Inter- and Intrapatient Drug Responses. Cell Rep. 31(11):107762. https://www.ncbi.nlm.nih.gov/pubmed/32553164.
180. Chen H, Gotimer K, De Souza C, Tepper CG, Karnezis AN, Leiserowitz GS, et al. 2020. Short-term organoid culture for drug sensitivity testing of high-grade serous carcinoma. Gynecol Oncol. 157(3):783-792. https://www.ncbi.nlm.nih.gov/pubmed/32253045.
181. Takahashi T. 2019. Organoids for Drug Discovery and Personalized Medicine. Annu Rev Pharmacol Toxicol. 59:447-462. https://www.ncbi.nlm.nih.gov/pubmed/30113875.
182. Yang L, Xie HJ, Li YY, Wang X, Liu XX, Mai J. 2022. Molecular mechanisms of platinum-based chemotherapy resistance in ovarian cancer (Review). Oncol Rep. 47(4). https://www.ncbi.nlm.nih.gov/pubmed/35211759.
183. Cornelison R, Llaneza DC, Landen CN. 2017. Emerging Therapeutics to Overcome Chemoresistance in Epithelial Ovarian Cancer: A Mini-Review. Int J Mol Sci. 18(10). https://www.ncbi.nlm.nih.gov/pubmed/29057791.
184. Cancer Genome Atlas Research N. 2011. Integrated genomic analyses of ovarian carcinoma. Nature. 474(7353):609-615. https://www.ncbi.nlm.nih.gov/pubmed/21720365.
185. Yao S, Meric-Bernstam F, Hong D, Janku F, Naing A, Piha-Paul SA, et al. 2022. Clinical characteristics and outcomes of phase I cancer patients with CCNE1 amplification: MD Anderson experiences. Sci Rep. 12(1):8701. https://www.ncbi.nlm.nih.gov/pubmed/35610322.
186. Patch AM, Christie EL, Etemadmoghadam D, Garsed DW, George J, Fereday S, et al. 2015. Whole-genome characterization of chemoresistant ovarian cancer. Nature. 521(7553):489-494. https://www.ncbi.nlm.nih.gov/pubmed/26017449.
187. Rodriguez-Antona C, Ingelman-Sundberg M. 2006. Cytochrome P450 pharmacogenetics and cancer. Oncogene. 25(11):1679-1691. https://www.ncbi.nlm.nih.gov/pubmed/16550168.
188. Gottesman MM, Pastan IH. 2015. The Role of Multidrug Resistance Efflux Pumps in Cancer: Revisiting a JNCI Publication Exploring Expression of the MDR1 (P-glycoprotein) Gene. J Natl Cancer Inst. 107(9). https://www.ncbi.nlm.nih.gov/pubmed/26286731.
189. Minchinton AI, Tannock IF. 2006. Drug penetration in solid tumours. Nat Rev Cancer. 6(8):583-592. https://www.ncbi.nlm.nih.gov/pubmed/16862189.
190. Cummings M, Freer C, Orsi NM. 2021. Targeting the tumour microenvironment in platinum-resistant ovarian cancer. Semin Cancer Biol. 77:3-28. https://www.ncbi.nlm.nih.gov/pubmed/33607246.
191. Nikolaou M, Pavlopoulou A, Georgakilas AG, Kyrodimos E. 2018. The challenge of drug resistance in cancer treatment: a current overview. Clin Exp Metastasis. 35(4):309-318. https://www.ncbi.nlm.nih.gov/pubmed/29799080.
192. Gatti L, Zunino F. 2005. Overview of tumor cell chemoresistance mechanisms. Methods Mol Med. 111:127-148. https://www.ncbi.nlm.nih.gov/pubmed/15911977.

193. Cree IA, Charlton P. 2017. Molecular chess? Hallmarks of anti-cancer drug resistance. BMC Cancer. 17(1):10. https://www.ncbi.nlm.nih.gov/pubmed/28056859.
194. Groenendijk FH, Bernards R. 2014. Drug resistance to targeted therapies: deja vu all over again. Mol Oncol. 8(6):1067-1083. https://www.ncbi.nlm.nih.gov/pubmed/24910388.
195. Braconi L, Dei S, Contino M, Riganti C, Bartolucci G, Manetti D, et al. 2023. Tetrazole and oxadiazole derivatives as bioisosteres of tariquidar and elacridar: New potent P-gp modulators acting as MDR reversers. Eur J Med Chem. 259:115716. https://www.ncbi.nlm.nih.gov/pubmed/37573829.
196. Maloney SM, Hoover CA, Morejon-Lasso LV, Prosperi JR. 2020. Mechanisms of Taxane Resistance. Cancers (Basel). 12(11). https://www.ncbi.nlm.nih.gov/pubmed/33182737.
197. Dei S, Braconi L, Romanelli MN, Teodori E. 2019. Recent advances in the search of BCRP- and dual P-gp/BCRP-based multidrug resistance modulators. Cancer Drug Resist. 2(3):710-743. https://www.ncbi.nlm.nih.gov/pubmed/35582565.
198. Shukla S, Ohnuma S, Ambudkar SV. 2011. Improving cancer chemotherapy with modulators of ABC drug transporters. Curr Drug Targets. 12(5):621-630. https://www.ncbi.nlm.nih.gov/pubmed/21039338.
199. Seiden MV, Swenerton KD, Matulonis U, Campos S, Rose P, Batist G, et al. 2002. A phase II study of the MDR inhibitor biricodar (INCEL, VX-710) and paclitaxel in women with advanced ovarian cancer refractory to paclitaxel therapy. Gynecol Oncol. 86(3):302-310. https://www.ncbi.nlm.nih.gov/pubmed/12217752.
200. Zhou J, Kang Y, Chen L, Wang H, Liu J, Zeng S, et al. 2020. The Drug-Resistance Mechanisms of Five Platinum-Based Antitumor Agents. Front Pharmacol. 11:343. https://www.ncbi.nlm.nih.gov/pubmed/32265714.
201. Damia G, Broggini M. 2019. Platinum Resistance in Ovarian Cancer: Role of DNA Repair. Cancers (Basel). 11(1). https://www.ncbi.nlm.nih.gov/pubmed/30669514.
202. Chen HH, Chen WC, Liang ZD, Tsai WB, Long Y, Aiba I, et al. 2015. Targeting drug transport mechanisms for improving platinum-based cancer chemotherapy. Expert Opin Ther Targets. 19(10):1307-1317. https://www.ncbi.nlm.nih.gov/pubmed/26004625.
203. McMullen M, Madariaga A, Lheureux S. 2021. New approaches for targeting platinum-resistant ovarian cancer. Semin Cancer Biol. 77:167-181. https://www.ncbi.nlm.nih.gov/pubmed/32871277.
204. McGee J, Bookman M, Harter P, Marth C, McNeish I, Moore KN, et al. 2017. Fifth Ovarian Cancer Consensus Conference: individualized therapy and patient factors. Ann Oncol. 28(4):702-710. https://www.ncbi.nlm.nih.gov/pubmed/28119296.
205. Buechel M, Herzog TJ, Westin SN, Coleman RL, Monk BJ, Moore KN. 2019. Treatment of patients with recurrent epithelial ovarian cancer for whom platinum is still an option. Ann Oncol. 30(5):721-732. https://www.ncbi.nlm.nih.gov/pubmed/30887020.
206. Mutch DG, Orlando M, Goss T, Teneriello MG, Gordon AN, McMeekin SD, et al. 2007. Randomized phase III trial of gemcitabine compared with pegylated liposomal doxorubicin in patients with platinum-resistant ovarian cancer. J Clin Oncol. 25(19):2811-2818. https://www.ncbi.nlm.nih.gov/pubmed/17602086.
207. Gynecologic Oncology G, Markman M, Blessing J, Rubin SC, Connor J, Hanjani P, et al. 2006. Phase II trial of weekly paclitaxel (80 mg/m2) in platinum and paclitaxel-resistant ovarian and primary peritoneal cancers: a Gynecologic Oncology Group study. Gynecol Oncol. 101(3):436-440. https://www.ncbi.nlm.nih.gov/pubmed/16325893.
208. Gordon AN, Fleagle JT, Guthrie D, Parkin DE, Gore ME, Lacave AJ. 2001. Recurrent epithelial ovarian carcinoma: a randomized phase III study of pegylated liposomal doxorubicin versus topotecan. J Clin Oncol. 19(14):3312-3322. https://www.ncbi.nlm.nih.gov/pubmed/11454878.

209. Kozlowska E, Vallius T, Hynninen J, Hietanen S, Farkkila A, Hautaniemi S. 2019. Virtual clinical trials identify effective combination therapies in ovarian cancer. Sci Rep. 9(1):18678. https://www.ncbi.nlm.nih.gov/pubmed/31822719.
210. Khan MA, Vikramdeo KS, Sudan SK, Singh S, Wilhite A, Dasgupta S, et al. 2021. Platinum-resistant ovarian cancer: From drug resistance mechanisms to liquid biopsy-based biomarkers for disease management. Semin Cancer Biol. 77:99-109. https://www.ncbi.nlm.nih.gov/pubmed/34418576.
211. Buss I, Hamacher A, Sarin N, Kassack MU, Kalayda GV. 2018. Relevance of copper transporter 1 and organic cation transporters 1-3 for oxaliplatin uptake and drug resistance in colorectal cancer cells. Metallomics. 10(3):414-425. https://www.ncbi.nlm.nih.gov/pubmed/29417972.
212. Nakayama K, Kanzaki A, Ogawa K, Miyazaki K, Neamati N, Takebayashi Y. 2002. Copper-transporting P-type adenosine triphosphatase (ATP7B) as a cisplatin based chemoresistance marker in ovarian carcinoma: comparative analysis with expression of MDR1, MRP1, MRP2, LRP and BCRP. Int J Cancer. 101(5):488-495. https://www.ncbi.nlm.nih.gov/pubmed/12216079.
213. Arts HJ, Katsaros D, de Vries EG, Massobrio M, Genta F, Danese S, et al. 1999. Drug resistance-associated markers P-glycoprotein, multidrug resistance-associated protein 1, multidrug resistance-associated protein 2, and lung resistance protein as prognostic factors in ovarian carcinoma. Clin Cancer Res. 5(10):2798-2805. https://www.ncbi.nlm.nih.gov/pubmed/10537344.
214. Ishida S, McCormick F, Smith-McCune K, Hanahan D. 2010. Enhancing tumor-specific uptake of the anticancer drug cisplatin with a copper chelator. Cancer Cell. 17(6):574-583. https://www.ncbi.nlm.nih.gov/pubmed/20541702.
215. Ishida S, Lee J, Thiele DJ, Herskowitz I. 2002. Uptake of the anticancer drug cisplatin mediated by the copper transporter Ctr1 in yeast and mammals. Proc Natl Acad Sci U S A. 99(22):14298-14302. https://www.ncbi.nlm.nih.gov/pubmed/12370430.
216. Song IS, Savaraj N, Siddik ZH, Liu P, Wei Y, Wu CJ, et al. 2004. Role of human copper transporter Ctr1 in the transport of platinum-based antitumor agents in cisplatin-sensitive and cisplatin-resistant cells. Mol Cancer Ther. 3(12):1543-1549. https://www.ncbi.nlm.nih.gov/pubmed/15634647.
217. Holzer AK, Samimi G, Katano K, Naerdemann W, Lin X, Safaei R, et al. 2004. The copper influx transporter human copper transport protein 1 regulates the uptake of cisplatin in human ovarian carcinoma cells. Mol Pharmacol. 66(4):817-823. https://www.ncbi.nlm.nih.gov/pubmed/15229296.
218. Kalayda GV, Wagner CH, Jaehde U. 2012. Relevance of copper transporter 1 for cisplatin resistance in human ovarian carcinoma cells. J Inorg Biochem. 116:1-10. https://www.ncbi.nlm.nih.gov/pubmed/23010323.
219. Blair BG, Larson CA, Adams PL, Abada PB, Safaei R, Howell SB. 2010. Regulation of copper transporter 2 expression by copper and cisplatin in human ovarian carcinoma cells. Mol Pharmacol. 77(6):912-921. https://www.ncbi.nlm.nih.gov/pubmed/20194531.
220. Owatari S, Akune S, Komatsu M, Ikeda R, Firth SD, Che XF, et al. 2007. Copper-transporting P-type ATPase, ATP7A, confers multidrug resistance and its expression is related to resistance to SN-38 in clinical colon cancer. Cancer Res. 67(10):4860-4868. https://www.ncbi.nlm.nih.gov/pubmed/17510416.
221. Mangala LS, Zuzel V, Schmandt R, Leshane ES, Halder JB, Armaiz-Pena GN, et al. 2009. Therapeutic Targeting of ATP7B in Ovarian Carcinoma. Clin Cancer Res. 15(11):3770-3780. https://www.ncbi.nlm.nih.gov/pubmed/19470734.
222. Chisholm CL, Wang H, Wong AH, Vazquez-Ortiz G, Chen W, Xu X, et al. 2016. Ammonium tetrathiomolybdate treatment targets the copper transporter ATP7A and

enhances sensitivity of breast cancer to cisplatin. Oncotarget. 7(51):84439-84452. https://www.ncbi.nlm.nih.gov/pubmed/27806319.
223. Martinez-Balibrea E, Martinez-Cardus A, Musulen E, Gines A, Manzano JL, Aranda E, et al. 2009. Increased levels of copper efflux transporter ATP7B are associated with poor outcome in colorectal cancer patients receiving oxaliplatin-based chemotherapy. Int J Cancer. 124(12):2905-2910. https://www.ncbi.nlm.nih.gov/pubmed/19296535.
224. Januchowski R, Sterzynska K, Zaorska K, Sosinska P, Klejewski A, Brazert M, et al. 2016. Analysis of MDR genes expression and cross-resistance in eight drug resistant ovarian cancer cell lines. J Ovarian Res. 9(1):65. https://www.ncbi.nlm.nih.gov/pubmed/27756418.
225. Surowiak P, Materna V, Kaplenko I, Spaczynski M, Dolinska-Krajewska B, Gebarowska E, et al. 2006. ABCC2 (MRP2, cMOAT) can be localized in the nuclear membrane of ovarian carcinomas and correlates with resistance to cisplatin and clinical outcome. Clin Cancer Res. 12(23):7149-7158. https://www.ncbi.nlm.nih.gov/pubmed/17145840.
226. Nakamura H, Takada K. 2021. Reactive oxygen species in cancer: Current findings and future directions. Cancer Sci. 112(10):3945-3952. https://www.ncbi.nlm.nih.gov/pubmed/34286881.
227. Redza-Dutordoir M, Averill-Bates DA. 2016. Activation of apoptosis signalling pathways by reactive oxygen species. Biochim Biophys Acta. 1863(12):2977-2992. https://www.ncbi.nlm.nih.gov/pubmed/27646922.
228. Andrews PA, Murphy MP, Howell SB. 1987. Metallothionein-mediated cisplatin resistance in human ovarian carcinoma cells. Cancer Chemother Pharmacol. 19(2):149-154. https://www.ncbi.nlm.nih.gov/pubmed/3568272.
229. Surowiak P, Materna V, Kaplenko I, Spaczynski M, Dietel M, Lage H, et al. 2005. Augmented expression of metallothionein and glutathione S-transferase pi as unfavourable prognostic factors in cisplatin-treated ovarian cancer patients. Virchows Arch. 447(3):626-633. https://www.ncbi.nlm.nih.gov/pubmed/15968547.
230. Gamcsik MP, Kasibhatla MS, Teeter SD, Colvin OM. 2012. Glutathione levels in human tumors. Biomarkers. 17(8):671-691. https://www.ncbi.nlm.nih.gov/pubmed/22900535.
231. Estrela JM, Ortega A, Obrador E. 2006. Glutathione in cancer biology and therapy. Crit Rev Clin Lab Sci. 43(2):143-181. https://www.ncbi.nlm.nih.gov/pubmed/16517421.
232. O'Brien ML, Tew KD. 1996. Glutathione and related enzymes in multidrug resistance. Eur J Cancer. 32A(6):967-978. https://www.ncbi.nlm.nih.gov/pubmed/8763337.
233. Mistry P, Kelland LR, Abel G, Sidhar S, Harrap KR. 1991. The relationships between glutathione, glutathione-S-transferase and cytotoxicity of platinum drugs and melphalan in eight human ovarian carcinoma cell lines. Br J Cancer. 64(2):215-220. https://www.ncbi.nlm.nih.gov/pubmed/1892748.
234. De Luca A, Parker LJ, Ang WH, Rodolfo C, Gabbarini V, Hancock NC, et al. 2019. A structure-based mechanism of cisplatin resistance mediated by glutathione transferase P1-1. Proc Natl Acad Sci U S A. 116(28):13943-13951. https://www.ncbi.nlm.nih.gov/pubmed/31221747.
235. Criscuolo D, Avolio R, Parri M, Romano S, Chiarugi P, Matassa DS, et al. 2022. Decreased Levels of GSH Are Associated with Platinum Resistance in High-Grade Serous Ovarian Cancer. Antioxidants (Basel). 11(8). https://www.ncbi.nlm.nih.gov/pubmed/36009263.
236. Colombo PE, Fabbro M, Theillet C, Bibeau F, Rouanet P, Ray-Coquard I. 2014. Sensitivity and resistance to treatment in the primary management of epithelial ovarian cancer. Crit Rev Oncol Hematol. 89(2):207-216. https://www.ncbi.nlm.nih.gov/pubmed/24071502.

237. Curtin NJ. 2012. DNA repair dysregulation from cancer driver to therapeutic target. Nat Rev Cancer. 12(12):801-817. https://www.ncbi.nlm.nih.gov/pubmed/23175119.
238. Galluzzi L, Senovilla L, Vitale I, Michels J, Martins I, Kepp O, et al. 2012. Molecular mechanisms of cisplatin resistance. Oncogene. 31(15):1869-1883. https://www.ncbi.nlm.nih.gov/pubmed/21892204.
239. Dabholkar M, Vionnet J, Bostick-Bruton F, Yu JJ, Reed E. 1994. Messenger RNA levels of XPAC and ERCC1 in ovarian cancer tissue correlate with response to platinum-based chemotherapy. J Clin Invest. 94(2):703-708. https://www.ncbi.nlm.nih.gov/pubmed/8040325.
240. Helleman J, van Staveren IL, Dinjens WN, van Kuijk PF, Ritstier K, Ewing PC, et al. 2006. Mismatch repair and treatment resistance in ovarian cancer. BMC Cancer. 6:201. https://www.ncbi.nlm.nih.gov/pubmed/16879751.
241. Sakai W, Swisher EM, Karlan BY, Agarwal MK, Higgins J, Friedman C, et al. 2008. Secondary mutations as a mechanism of cisplatin resistance in BRCA2-mutated cancers. Nature. 451(7182):1116-1120. https://www.ncbi.nlm.nih.gov/pubmed/18264087.
242. Sun Y, McCorvie TJ, Yates LA, Zhang X. 2020. Structural basis of homologous recombination. Cell Mol Life Sci. 77(1):3-18. https://www.ncbi.nlm.nih.gov/pubmed/31748913.
243. Brown JS, O'Carrigan B, Jackson SP, Yap TA. 2017. Targeting DNA Repair in Cancer: Beyond PARP Inhibitors. Cancer Discov. 7(1):20-37. https://www.ncbi.nlm.nih.gov/pubmed/28003236.
244. Alsop K, Fereday S, Meldrum C, deFazio A, Emmanuel C, George J, et al. 2012. BRCA mutation frequency and patterns of treatment response in BRCA mutation-positive women with ovarian cancer: a report from the Australian Ovarian Cancer Study Group. J Clin Oncol. 30(21):2654-2663. https://www.ncbi.nlm.nih.gov/pubmed/22711857.
245. Edwards SL, Brough R, Lord CJ, Natrajan R, Vatcheva R, Levine DA, et al. 2008. Resistance to therapy caused by intragenic deletion in BRCA2. Nature. 451(7182):1111-1115. https://www.ncbi.nlm.nih.gov/pubmed/18264088.
246. Weigelt B, Comino-Mendez I, de Bruijn I, Tian L, Meisel JL, Garcia-Murillas I, et al. 2017. Diverse BRCA1 and BRCA2 Reversion Mutations in Circulating Cell-Free DNA of Therapy-Resistant Breast or Ovarian Cancer. Clin Cancer Res. 23(21):6708-6720. https://www.ncbi.nlm.nih.gov/pubmed/28765325.
247. Ray Chaudhuri A, Callen E, Ding X, Gogola E, Duarte AA, Lee JE, et al. 2016. Replication fork stability confers chemoresistance in BRCA-deficient cells. Nature. 535(7612):382-387. https://www.ncbi.nlm.nih.gov/pubmed/27443740.
248. Duan M, Ulibarri J, Liu KJ, Mao P. 2020. Role of Nucleotide Excision Repair in Cisplatin Resistance. Int J Mol Sci. 21(23). https://www.ncbi.nlm.nih.gov/pubmed/33291532.
249. Ferry KV, Hamilton TC, Johnson SW. 2000. Increased nucleotide excision repair in cisplatin-resistant ovarian cancer cells: role of ERCC1-XPF. Biochem Pharmacol. 60(9):1305-1313. https://www.ncbi.nlm.nih.gov/pubmed/11008124.
250. Pajuelo-Lozano N, Bargiela-Iparraguirre J, Dominguez G, Quiroga AG, Perona R, Sanchez-Perez I. 2018. XPA, XPC, and XPD Modulate Sensitivity in Gastric Cisplatin Resistance Cancer Cells. Front Pharmacol. 9:1197. https://www.ncbi.nlm.nih.gov/pubmed/30386247.
251. Zhang Y, Cao J, Meng Y, Qu C, Shen F, Xu L. 2018. Overexpression of xeroderma pigmentosum group C decreases the chemotherapeutic sensitivity of colorectal carcinoma cells to cisplatin. Oncol Lett. 15(5):6336-6344. https://www.ncbi.nlm.nih.gov/pubmed/29616110.
252. Kaufmann SH, Earnshaw WC. 2000. Induction of apoptosis by cancer chemotherapy. Exp Cell Res. 256(1):42-49. https://www.ncbi.nlm.nih.gov/pubmed/10739650.

253. Qian S, Wei Z, Yang W, Huang J, Yang Y, Wang J. 2022. The role of BCL-2 family proteins in regulating apoptosis and cancer therapy. Front Oncol. 12:985363. https://www.ncbi.nlm.nih.gov/pubmed/36313628.
254. Kaloni D, Diepstraten ST, Strasser A, Kelly GL. 2023. BCL-2 protein family: attractive targets for cancer therapy. Apoptosis. 28(1-2):20-38. https://www.ncbi.nlm.nih.gov/pubmed/36342579.
255. Vidot S, Witham J, Agarwal R, Greenhough S, Bamrah HS, Tigyi GJ, et al. 2010. Autotaxin delays apoptosis induced by carboplatin in ovarian cancer cells. Cell Signal. 22(6):926-935. https://www.ncbi.nlm.nih.gov/pubmed/20100569.
256. Gogvadze V, Orrenius S, Zhivotovsky B. 2006. Multiple pathways of cytochrome c release from mitochondria in apoptosis. Biochim Biophys Acta. 1757(5-6):639-647. https://www.ncbi.nlm.nih.gov/pubmed/16678785.
257. Williams J, Lucas PC, Griffith KA, Choi M, Fogoros S, Hu YY, et al. 2005. Expression of Bcl-xL in ovarian carcinoma is associated with chemoresistance and recurrent disease. Gynecol Oncol. 96(2):287-295. https://www.ncbi.nlm.nih.gov/pubmed/15661210.
258. Mano Y, Kikuchi Y, Yamamoto K, Kita T, Hirata J, Tode T, et al. 1999. Bcl-2 as a predictor of chemosensitivity and prognosis in primary epithelial ovarian cancer. Eur J Cancer. 35(8):1214-1219. https://www.ncbi.nlm.nih.gov/pubmed/10615232.
259. Abed MN, Abdullah MI, Richardson A. 2016. Antagonism of Bcl-XL is necessary for synergy between carboplatin and BH3 mimetics in ovarian cancer cells. J Ovarian Res. 9:25. https://www.ncbi.nlm.nih.gov/pubmed/27080533.
260. Witham J, Valenti MR, De-Haven-Brandon AK, Vidot S, Eccles SA, Kaye SB, et al. 2007. The Bcl-2/Bcl-XL family inhibitor ABT-737 sensitizes ovarian cancer cells to carboplatin. Clin Cancer Res. 13(23):7191-7198. https://www.ncbi.nlm.nih.gov/pubmed/18056200.
261. Cheng JQ, Jiang X, Fraser M, Li M, Dan HC, Sun M, et al. 2002. Role of X-linked inhibitor of apoptosis protein in chemoresistance in ovarian cancer: possible involvement of the phosphoinositide-3 kinase/Akt pathway. Drug Resist Updat. 5(3-4):131-146. https://www.ncbi.nlm.nih.gov/pubmed/12237081.
262. Binju M, Amaya-Padilla MA, Wan G, Gunosewoyo H, Suryo Rahmanto Y, Yu Y. 2019. Therapeutic Inducers of Apoptosis in Ovarian Cancer. Cancers (Basel). 11(11). https://www.ncbi.nlm.nih.gov/pubmed/31766284.
263. Mansouri A, Zhang Q, Ridgway LD, Tian L, Claret FX. 2003. Cisplatin resistance in an ovarian carcinoma is associated with a defect in programmed cell death control through XIAP regulation. Oncol Res. 13(6-10):399-404. https://www.ncbi.nlm.nih.gov/pubmed/12725530.
264. Belli C, Trapani D, Viale G, D'Amico P, Duso BA, Della Vigna P, et al. 2018. Targeting the microenvironment in solid tumors. Cancer Treat Rev. 65:22-32. https://www.ncbi.nlm.nih.gov/pubmed/29502037.
265. Ghoneum A, Almousa S, Warren B, Abdulfattah AY, Shu J, Abouelfadl H, et al. 2021. Exploring the clinical value of tumor microenvironment in platinum-resistant ovarian cancer. Semin Cancer Biol. 77:83-98. https://www.ncbi.nlm.nih.gov/pubmed/33476723.
266. Qian J, LeSavage BL, Hubka KM, Ma C, Natarajan S, Eggold JT, et al. 2021. Cancer-associated mesothelial cells promote ovarian cancer chemoresistance through paracrine osteopontin signaling. J Clin Invest. 131(16). https://www.ncbi.nlm.nih.gov/pubmed/34396988.
267. Yoshihara M, Kajiyama H, Yokoi A, Sugiyama M, Koya Y, Yamakita Y, et al. 2020. Ovarian cancer-associated mesothelial cells induce acquired platinum-resistance in peritoneal metastasis via the FN1/Akt signaling pathway. Int J Cancer. 146(8):2268-2280. https://www.ncbi.nlm.nih.gov/pubmed/31904865.

268. Pietila EA, Gonzalez-Molina J, Moyano-Galceran L, Jamalzadeh S, Zhang K, Lehtinen L, et al. 2021. Co-evolution of matrisome and adaptive adhesion dynamics drives ovarian cancer chemoresistance. Nat Commun. 12(1):3904. https://www.ncbi.nlm.nih.gov/pubmed/34162871.
269. Yee C, Dickson KA, Muntasir MN, Ma Y, Marsh DJ. 2022. Three-Dimensional Modelling of Ovarian Cancer: From Cell Lines to Organoids for Discovery and Personalized Medicine. Front Bioeng Biotechnol. 10:836984. https://www.ncbi.nlm.nih.gov/pubmed/35223797.
270. Wang Z, Deng Z, Zhu G. 2019. Emerging platinum(iv) prodrugs to combat cisplatin resistance: from isolated cancer cells to tumor microenvironment. Dalton Trans. 48(8):2536-2544. https://www.ncbi.nlm.nih.gov/pubmed/30633263.
271. Zheng P, Chen L, Yuan X, Luo Q, Liu Y, Xie G, et al. 2017. Exosomal transfer of tumor-associated macrophage-derived miR-21 confers cisplatin resistance in gastric cancer cells. J Exp Clin Cancer Res. 36(1):53. https://www.ncbi.nlm.nih.gov/pubmed/28407783.
272. Zhou B, Sun C, Li N, Shan W, Lu H, Guo L, et al. 2016. Cisplatin-induced CCL5 secretion from CAFs promotes cisplatin-resistance in ovarian cancer via regulation of the STAT3 and PI3K/Akt signaling pathways. Int J Oncol. 48(5):2087-2097. https://www.ncbi.nlm.nih.gov/pubmed/26983899.
273. Tao L, Huang G, Wang R, Pan Y, He Z, Chu X, et al. 2016. Cancer-associated fibroblasts treated with cisplatin facilitates chemoresistance of lung adenocarcinoma through IL-11/IL-11R/STAT3 signaling pathway. Sci Rep. 6:38408. https://www.ncbi.nlm.nih.gov/pubmed/27922075.
274. Ji Z, Tian W, Gao W, Zang R, Wang H, Yang G. 2021. Cancer-Associated Fibroblast-Derived Interleukin-8 Promotes Ovarian Cancer Cell Stemness and Malignancy Through the Notch3-Mediated Signaling. Front Cell Dev Biol. 9:684505. https://www.ncbi.nlm.nih.gov/pubmed/34277625.
275. Wang Y, Qu Y, Niu XL, Sun WJ, Zhang XL, Li LZ. 2011. Autocrine production of interleukin-8 confers cisplatin and paclitaxel resistance in ovarian cancer cells. Cytokine. 56(2):365-375. https://www.ncbi.nlm.nih.gov/pubmed/21742513.
276. Zhang F, Cui JY, Gao HF, Yu H, Gao FF, Chen JL, et al. 2020. Cancer-associated fibroblasts induce epithelial-mesenchymal transition and cisplatin resistance in ovarian cancer via CXCL12/CXCR4 axis. Future Oncol. 16(32):2619-2633. https://www.ncbi.nlm.nih.gov/pubmed/32804554.
277. Wang W, Kryczek I, Dostal L, Lin H, Tan L, Zhao L, et al. 2016. Effector T Cells Abrogate Stroma-Mediated Chemoresistance in Ovarian Cancer. Cell. 165(5):1092-1105. https://www.ncbi.nlm.nih.gov/pubmed/27133165.
278. Akkari L, Joyce JA. 2016. Microenvironmental InterFereNce of metabolism regulates chemosensitivity. Cell Res. 26(8):867-868. https://www.ncbi.nlm.nih.gov/pubmed/27349476.
279. Yang J, Zaman MM, Vlasakov I, Roy R, Huang L, Martin CR, et al. 2019. Adipocytes promote ovarian cancer chemoresistance. Sci Rep. 9(1):13316. https://www.ncbi.nlm.nih.gov/pubmed/31527632.
280. Latifi A, Abubaker K, Castrechini N, Ward AC, Liongue C, Dobill F, et al. 2011. Cisplatin treatment of primary and metastatic epithelial ovarian carcinomas generates residual cells with mesenchymal stem cell-like profile. J Cell Biochem. 112(10):2850-2864. https://www.ncbi.nlm.nih.gov/pubmed/21618587.
281. Ojalvo LS, Thompson ED, Wang TL, Meeker AK, Shih IM, Fader AN, et al. 2018. Tumor-associated macrophages and the tumor immune microenvironment of primary and recurrent epithelial ovarian cancer. Hum Pathol. 74:135-147. https://www.ncbi.nlm.nih.gov/pubmed/29288043.

282. Ferri-Borgogno S, Zhu Y, Sheng J, Burks JK, Gomez JA, Wong KK, et al. 2023. Spatial Transcriptomics Depict Ligand-Receptor Cross-talk Heterogeneity at the Tumor-Stroma Interface in Long-Term Ovarian Cancer Survivors. Cancer Res. 83(9):1503-1516. https://www.ncbi.nlm.nih.gov/pubmed/36787106.
283. Terraneo N, Jacob F, Dubrovska A, Grunberg J. 2020. Novel Therapeutic Strategies for Ovarian Cancer Stem Cells. Front Oncol. 10:319. https://www.ncbi.nlm.nih.gov/pubmed/32257947.
284. Meng E, Long B, Sullivan P, McClellan S, Finan MA, Reed E, et al. 2012. CD44+/CD24- ovarian cancer cells demonstrate cancer stem cell properties and correlate to survival. Clin Exp Metastasis. 29(8):939-948. https://www.ncbi.nlm.nih.gov/pubmed/22610780.
285. Chen X, Zhang J, Zhang Z, Li H, Cheng W, Liu J. 2013. Cancer stem cells, epithelial-mesenchymal transition, and drug resistance in high-grade ovarian serous carcinoma. Hum Pathol. 44(11):2373-2384. https://www.ncbi.nlm.nih.gov/pubmed/23850493.
286. Samardzija C, Quinn M, Findlay JK, Ahmed N. 2012. Attributes of Oct4 in stem cell biology: perspectives on cancer stem cells of the ovary. J Ovarian Res. 5(1):37. https://www.ncbi.nlm.nih.gov/pubmed/23171809.
287. Liu S, Sun J, Cai B, Xi X, Yang L, Zhang Z, et al. 2016. NANOG regulates epithelial-mesenchymal transition and chemoresistance through activation of the STAT3 pathway in epithelial ovarian cancer. Tumour Biol. 37(7):9671-9680. https://www.ncbi.nlm.nih.gov/pubmed/26801672.
288. Lupia M, Angiolini F, Bertalot G, Freddi S, Sachsenmeier KF, Chisci E, et al. 2018. CD73 Regulates Stemness and Epithelial-Mesenchymal Transition in Ovarian Cancer-Initiating Cells. Stem Cell Reports. 10(4):1412-1425. https://www.ncbi.nlm.nih.gov/pubmed/29551673.
289. Cardenas H, Fang F, Jiang G, Perkins SM, Zhang C, Emerson RE, et al. 2021. Methylomic Signatures of High Grade Serous Ovarian Cancer. Epigenetics. 16(11):1201-1216. https://www.ncbi.nlm.nih.gov/pubmed/33289590.
290. Chan DW, Lam WY, Chen F, Yung MMH, Chan YS, Chan WS, et al. 2021. Genome-wide DNA methylome analysis identifies methylation signatures associated with survival and drug resistance of ovarian cancers. Clin Epigenetics. 13(1):142. https://www.ncbi.nlm.nih.gov/pubmed/34294135.
291. Feng LY, Yan BB, Huang YZ, Li L. 2021. Abnormal methylation characteristics predict chemoresistance and poor prognosis in advanced high-grade serous ovarian cancer. Clin Epigenetics. 13(1):141. https://www.ncbi.nlm.nih.gov/pubmed/34289901.
292. Lum E, Vigliotti M, Banerjee N, Cutter N, Wrzeszczynski KO, Khan S, et al. 2013. Loss of DOK2 induces carboplatin resistance in ovarian cancer via suppression of apoptosis. Gynecol Oncol. 130(2):369-376. https://www.ncbi.nlm.nih.gov/pubmed/23684582.
293. Matthews BG, Bowden NA, Wong-Brown MW. 2021. Epigenetic Mechanisms and Therapeutic Targets in Chemoresistant High-Grade Serous Ovarian Cancer. Cancers (Basel). 13(23). https://www.ncbi.nlm.nih.gov/pubmed/34885103.
294. Lund RJ, Huhtinen K, Salmi J, Rantala J, Nguyen EV, Moulder R, et al. 2017. DNA methylation and Transcriptome Changes Associated with Cisplatin Resistance in Ovarian Cancer. Sci Rep. 7(1):1469. https://www.ncbi.nlm.nih.gov/pubmed/28473707.
295. Bonito NA, Borley J, Wilhelm-Benartzi CS, Ghaem-Maghami S, Brown R. 2016. Epigenetic Regulation of the Homeobox Gene MSX1 Associates with Platinum-Resistant Disease in High-Grade Serous Epithelial Ovarian Cancer. Clin Cancer Res. 22(12):3097-3104. https://www.ncbi.nlm.nih.gov/pubmed/26763252.

296. Cacan E, Ali MW, Boyd NH, Hooks SB, Greer SF. 2014. Inhibition of HDAC1 and DNMT1 modulate RGS10 expression and decrease ovarian cancer chemoresistance. PLoS One. 9(1):e87455. https://www.ncbi.nlm.nih.gov/pubmed/24475290.
297. Sun X, Wang S, Gai J, Guan J, Li J, Li Y, et al. 2019. SIRT5 Promotes Cisplatin Resistance in Ovarian Cancer by Suppressing DNA Damage in a ROS-Dependent Manner via Regulation of the Nrf2/HO-1 Pathway. Front Oncol. 9:754. https://www.ncbi.nlm.nih.gov/pubmed/31456942.
298. Islam MM, Banerjee T, Packard CZ, Kotian S, Selvendiran K, Cohn DE, et al. 2017. HDAC10 as a potential therapeutic target in ovarian cancer. Gynecol Oncol. 144(3):613-620. https://www.ncbi.nlm.nih.gov/pubmed/28073598.
299. Liu X, Yu Y, Zhang J, Lu C, Wang L, Liu P, et al. 2018. HDAC1 Silencing in Ovarian Cancer Enhances the Chemotherapy Response. Cell Physiol Biochem. 48(4):1505-1518. https://www.ncbi.nlm.nih.gov/pubmed/30071534.
300. Pink RC, Samuel P, Massa D, Caley DP, Brooks SA, Carter DR. 2015. The passenger strand, miR-21-3p, plays a role in mediating cisplatin resistance in ovarian cancer cells. Gynecol Oncol. 137(1):143-151. https://www.ncbi.nlm.nih.gov/pubmed/25579119.
301. Sun J, Cai X, Yung MM, Zhou W, Li J, Zhang Y, et al. 2019. miR-137 mediates the functional link between c-Myc and EZH2 that regulates cisplatin resistance in ovarian cancer. Oncogene. 38(4):564-580. https://www.ncbi.nlm.nih.gov/pubmed/30166592.
302. Yang H, Kong W, He L, Zhao JJ, O'Donnell JD, Wang J, et al. 2008. MicroRNA expression profiling in human ovarian cancer: miR-214 induces cell survival and cisplatin resistance by targeting PTEN. Cancer Res. 68(2):425-433. https://www.ncbi.nlm.nih.gov/pubmed/18199536.
303. Feng X, Liu N, Deng S, Zhang D, Wang K, Lu M. 2017. miR-199a modulates cisplatin resistance in ovarian cancer by targeting Hif1alpha. Onco Targets Ther. 10:5899-5906. https://www.ncbi.nlm.nih.gov/pubmed/29276393.
304. Wang Y, Bao W, Liu Y, Wang S, Xu S, Li X, et al. 2018. miR-98-5p contributes to cisplatin resistance in epithelial ovarian cancer by suppressing miR-152 biogenesis via targeting Dicer1. Cell Death Dis. 9(5):447. https://www.ncbi.nlm.nih.gov/pubmed/29670086.
305. Xiao F, Li Y, Wan Y, Xue M. 2018. MircroRNA-139 sensitizes ovarian cancer cell to cisplatin-based chemotherapy through regulation of ATP7A/B. Cancer Chemother Pharmacol. 81(5):935-947. https://www.ncbi.nlm.nih.gov/pubmed/29594361.
306. Dwivedi SK, Mustafi SB, Mangala LS, Jiang D, Pradeep S, Rodriguez-Aguayo C, et al. 2016. Therapeutic evaluation of microRNA-15a and microRNA-16 in ovarian cancer. Oncotarget. 7(12):15093-15104. https://www.ncbi.nlm.nih.gov/pubmed/26918603.
307. Chen FD, Chen HH, Ke SC, Zheng LR, Zheng XY. 2018. SLC27A2 regulates miR-411 to affect chemo-resistance in ovarian cancer. Neoplasma. 65(6):915-924. https://www.ncbi.nlm.nih.gov/pubmed/30334452.
308. Tian J, Xu YY, Li L, Hao Q. 2017. MiR-490-3p sensitizes ovarian cancer cells to cisplatin by directly targeting ABCC2. Am J Transl Res. 9(3):1127-1138. https://www.ncbi.nlm.nih.gov/pubmed/28386339.
309. Xiao S, Zhang M, Liu C, Wang D. 2018. MiR-514 attenuates proliferation and increases chemoresistance by targeting ATP binding cassette subfamily in ovarian cancer. Mol Genet Genomics. 293(5):1159-1167. https://www.ncbi.nlm.nih.gov/pubmed/29752546.
310. Wang T, Hao D, Yang S, Ma J, Yang W, Zhu Y, et al. 2019. miR-211 facilitates platinum chemosensitivity by blocking the DNA damage response (DDR) in ovarian cancer. Cell Death Dis. 10(7):495. https://www.ncbi.nlm.nih.gov/pubmed/31235732.
311. Gong TT, Liu XD, Zhan ZP, Wu QJ. 2020. Sulforaphane enhances the cisplatin sensitivity through regulating DNA repair and accumulation of intracellular cisplatin in ovarian cancer cells. Exp Cell Res. 393(2):112061. https://www.ncbi.nlm.nih.gov/pubmed/32437713.

312. Zhao H, Yu X, Ding Y, Zhao J, Wang G, Wu X, et al. 2016. MiR-770-5p inhibits cisplatin chemoresistance in human ovarian cancer by targeting ERCC2. Oncotarget. 7(33):53254-53268. https://www.ncbi.nlm.nih.gov/pubmed/27449101.
313. Rowinsky EK, Donehower RC. 1995. Paclitaxel (taxol). N Engl J Med. 332(15):1004-1014. https://www.ncbi.nlm.nih.gov/pubmed/7885406.
314. Wani MC, Horwitz SB. 2014. Nature as a remarkable chemist: a personal story of the discovery and development of Taxol. Anticancer Drugs. 25(5):482-487. https://www.ncbi.nlm.nih.gov/pubmed/24413390.
315. Wilson L. 1975. Microtubules as drug receptors: pharmacological properties of microtubule protein. Ann N Y Acad Sci. 253:213-231. https://www.ncbi.nlm.nih.gov/pubmed/1096718.
316. Kampan NC, Madondo MT, McNally OM, Quinn M, Plebanski M. 2015. Paclitaxel and Its Evolving Role in the Management of Ovarian Cancer. Biomed Res Int. 2015:413076. https://www.ncbi.nlm.nih.gov/pubmed/26137480.
317. Schiff PB, Fant J, Horwitz SB. 1979. Promotion of microtubule assembly in vitro by taxol. Nature. 277(5698):665-667. https://www.ncbi.nlm.nih.gov/pubmed/423966.
318. Manfredi JJ, Parness J, Horwitz SB. 1982. Taxol binds to cellular microtubules. J Cell Biol. 94(3):688-696. https://www.ncbi.nlm.nih.gov/pubmed/6127342.
319. Orr GA, Verdier-Pinard P, McDaid H, Horwitz SB. 2003. Mechanisms of Taxol resistance related to microtubules. Oncogene. 22(47):7280-7295. https://www.ncbi.nlm.nih.gov/pubmed/14576838.
320. Bhalla KN. 2003. Microtubule-targeted anticancer agents and apoptosis. Oncogene. 22(56):9075-9086. https://www.ncbi.nlm.nih.gov/pubmed/14663486.
321. Komlodi-Pasztor E, Sackett D, Wilkerson J, Fojo T. 2011. Mitosis is not a key target of microtubule agents in patient tumors. Nat Rev Clin Oncol. 8(4):244-250. https://www.ncbi.nlm.nih.gov/pubmed/21283127.
322. Florian S, Mitchison TJ. 2016. Anti-Microtubule Drugs. Methods Mol Biol. 1413:403-421. https://www.ncbi.nlm.nih.gov/pubmed/27193863.
323. Pucci B, Bellincampi L, Tafani M, Masciullo V, Melino G, Giordano A. 1999. Paclitaxel induces apoptosis in Saos-2 cells with CD95L upregulation and Bcl-2 phosphorylation. Exp Cell Res. 252(1):134-143. https://www.ncbi.nlm.nih.gov/pubmed/10502406.
324. Giannakakou P, Nakano M, Nicolaou KC, O'Brate A, Yu J, Blagosklonny MV, et al. 2002. Enhanced microtubule-dependent trafficking and p53 nuclear accumulation by suppression of microtubule dynamics. Proc Natl Acad Sci U S A. 99(16):10855-10860. https://www.ncbi.nlm.nih.gov/pubmed/12145320.
325. Smith ER, Xu XX. 2021. Breaking malignant nuclei as a non-mitotic mechanism of taxol/paclitaxel. J Cancer Biol. 2(4):86-93. https://www.ncbi.nlm.nih.gov/pubmed/35048083.
326. Mitchison TJ, Pineda J, Shi J, Florian S. 2017. Is inflammatory micronucleation the key to a successful anti-mitotic cancer drug? Open Biol. 7(11). https://www.ncbi.nlm.nih.gov/pubmed/29142107.
327. Lee MX, Tan DS. 2018. Weekly versus 3-weekly paclitaxel in combination with carboplatin in advanced ovarian cancer: which is the optimal adjuvant chemotherapy regimen? J Gynecol Oncol. 29(6):e96. https://www.ncbi.nlm.nih.gov/pubmed/30207104.
328. Runowicz CD, Wiernik PH, Einzig AI, Goldberg GL, Horwitz SB. 1993. Taxol in ovarian cancer. Cancer. 71(4 Suppl):1591-1596. https://www.ncbi.nlm.nih.gov/pubmed/8094322.
329. Bookman MA. 2016. Optimal primary therapy of ovarian cancer. Ann Oncol. 27 Suppl 1:i58-i62. https://www.ncbi.nlm.nih.gov/pubmed/27141074.
330. Kavallaris M. 2010. Microtubules and resistance to tubulin-binding agents. Nat Rev Cancer. 10(3):194-204. https://www.ncbi.nlm.nih.gov/pubmed/20147901.

331. Visconti R, Grieco D. 2017. Fighting tubulin-targeting anticancer drug toxicity and resistance. Endocr Relat Cancer. 24(9):T107-T117. https://www.ncbi.nlm.nih.gov/pubmed/28808045.
332. Fojo AT, Menefee M. 2005. Microtubule targeting agents: basic mechanisms of multidrug resistance (MDR). Semin Oncol. 32(6 Suppl 7):S3-8. https://www.ncbi.nlm.nih.gov/pubmed/16360716.
333. Smith ER, Wang JQ, Yang DH, Xu XX. 2022. Paclitaxel resistance related to nuclear envelope structural sturdiness. Drug Resist Updat. 65:100881. https://www.ncbi.nlm.nih.gov/pubmed/36368286.
334. Mosca L, Ilari A, Fazi F, Assaraf YG, Colotti G. 2021. Taxanes in cancer treatment: Activity, chemoresistance and its overcoming. Drug Resist Updat. 54:100742. https://www.ncbi.nlm.nih.gov/pubmed/33429249.
335. Stage TB, Bergmann TK, Kroetz DL. 2018. Clinical Pharmacokinetics of Paclitaxel Monotherapy: An Updated Literature Review. Clin Pharmacokinet. 57(1):7-19. https://www.ncbi.nlm.nih.gov/pubmed/28612269.
336. Barbuti AM, Chen ZS. 2015. Paclitaxel Through the Ages of Anticancer Therapy: Exploring Its Role in Chemoresistance and Radiation Therapy. Cancers (Basel). 7(4):2360-2371. https://www.ncbi.nlm.nih.gov/pubmed/26633515.
337. Callaghan R, Luk F, Bebawy M. 2014. Inhibition of the multidrug resistance P-glycoprotein: time for a change of strategy? Drug Metab Dispos. 42(4):623-631. https://www.ncbi.nlm.nih.gov/pubmed/24492893.
338. Litman T, Druley TE, Stein WD, Bates SE. 2001. From MDR to MXR: new understanding of multidrug resistance systems, their properties and clinical significance. Cell Mol Life Sci. 58(7):931-959. https://www.ncbi.nlm.nih.gov/pubmed/11497241.
339. Januchowski R, Wojtowicz K, Sujka-Kordowska P, Andrzejewska M, Zabel M. 2013. MDR gene expression analysis of six drug-resistant ovarian cancer cell lines. Biomed Res Int. 2013:241763. https://www.ncbi.nlm.nih.gov/pubmed/23484165.
340. Seborova K, Vaclavikova R, Soucek P, Elsnerova K, Bartakova A, Cernaj P, et al. 2019. Association of ABC gene profiles with time to progression and resistance in ovarian cancer revealed by bioinformatics analyses. Cancer Med. 8(2):606-616. https://www.ncbi.nlm.nih.gov/pubmed/30672151.
341. Gottesman MM, Ludwig J, Xia D, Szakacs G. 2006. Defeating drug resistance in cancer. Discov Med. 6(31):18-23. https://www.ncbi.nlm.nih.gov/pubmed/17234123.
342. Waghray D, Zhang Q. 2018. Inhibit or Evade Multidrug Resistance P-Glycoprotein in Cancer Treatment. J Med Chem. 61(12):5108-5121. https://www.ncbi.nlm.nih.gov/pubmed/29251920.
343. Robey RW, Pluchino KM, Hall MD, Fojo AT, Bates SE, Gottesman MM. 2018. Revisiting the role of ABC transporters in multidrug-resistant cancer. Nat Rev Cancer. 18(7):452-464. https://www.ncbi.nlm.nih.gov/pubmed/29643473.
344. Zanger UM, Schwab M. 2013. Cytochrome P450 enzymes in drug metabolism: regulation of gene expression, enzyme activities, and impact of genetic variation. Pharmacol Ther. 138(1):103-141. https://www.ncbi.nlm.nih.gov/pubmed/23333322.
345. van Eijk M, Boosman RJ, Schinkel AH, Huitema ADR, Beijnen JH. 2019. Cytochrome P450 3A4, 3A5, and 2C8 expression in breast, prostate, lung, endometrial, and ovarian tumors: relevance for resistance to taxanes. Cancer Chemother Pharmacol. 84(3):487-499. https://www.ncbi.nlm.nih.gov/pubmed/31309254.
346. McFadyen MC, McLeod HL, Jackson FC, Melvin WT, Doehmer J, Murray GI. 2001. Cytochrome P450 CYP1B1 protein expression: a novel mechanism of anticancer drug resistance. Biochem Pharmacol. 62(2):207-212. https://www.ncbi.nlm.nih.gov/pubmed/11389879.

347. Kamel A, Harriman S. 2013. Inhibition of cytochrome P450 enzymes and biochemical aspects of mechanism-based inactivation (MBI). Drug Discov Today Technol. 10(1):e177-189. https://www.ncbi.nlm.nih.gov/pubmed/24050247.
348. Leskela S, Jara C, Leandro-Garcia LJ, Martinez A, Garcia-Donas J, Hernando S, et al. 2011. Polymorphisms in cytochromes P450 2C8 and 3A5 are associated with paclitaxel neurotoxicity. Pharmacogenomics J. 11(2):121-129. https://www.ncbi.nlm.nih.gov/pubmed/20212519.
349. Leung YK, Lau KM, Mobley J, Jiang Z, Ho SM. 2005. Overexpression of cytochrome P450 1A1 and its novel spliced variant in ovarian cancer cells: alternative subcellular enzyme compartmentation may contribute to carcinogenesis. Cancer Res. 65(9):3726-3734. https://www.ncbi.nlm.nih.gov/pubmed/15867368.
350. Downie D, McFadyen MC, Rooney PH, Cruickshank ME, Parkin DE, Miller ID, et al. 2005. Profiling cytochrome P450 expression in ovarian cancer: identification of prognostic markers. Clin Cancer Res. 11(20):7369-7375. https://www.ncbi.nlm.nih.gov/pubmed/16243809.
351. Zhu Z, Mu Y, Qi C, Wang J, Xi G, Guo J, et al. 2015. CYP1B1 enhances the resistance of epithelial ovarian cancer cells to paclitaxel in vivo and in vitro. Int J Mol Med. 35(2):340-348. https://www.ncbi.nlm.nih.gov/pubmed/25516145.
352. Salehi B, Mishra AP, Nigam M, Sener B, Kilic M, Sharifi-Rad M, et al. 2018. Resveratrol: A Double-Edged Sword in Health Benefits. Biomedicines. 6(3). https://www.ncbi.nlm.nih.gov/pubmed/30205595.
353. Guthrie AR, Chow HS, Martinez JA. 2017. Effects of resveratrol on drug- and carcinogen-metabolizing enzymes, implications for cancer prevention. Pharmacol Res Perspect. 5(1):e00294. https://www.ncbi.nlm.nih.gov/pubmed/28596842.
354. Piotrowska-Kempisty H, Klupczynska A, Trzybulska D, Kulcenty K, Sulej-Suchomska AM, Kucinska M, et al. 2017. Role of CYP1A1 in the biological activity of methylated resveratrol analogue, 3,4,5,4'-tetramethoxystilbene (DMU-212) in ovarian cancer A-2780 and non-cancerous HOSE cells. Toxicol Lett. 267:59-66. https://www.ncbi.nlm.nih.gov/pubmed/28049037.
355. Mozzetti S, Ferlini C, Concolino P, Filippetti F, Raspaglio G, Prislei S, et al. 2005. Class III beta-tubulin overexpression is a prominent mechanism of paclitaxel resistance in ovarian cancer patients. Clin Cancer Res. 11(1):298-305. https://www.ncbi.nlm.nih.gov/pubmed/15671559.
356. Kavallaris M, Kuo DY, Burkhart CA, Regl DL, Norris MD, Haber M, et al. 1997. Taxol-resistant epithelial ovarian tumors are associated with altered expression of specific beta-tubulin isotypes. J Clin Invest. 100(5):1282-1293. https://www.ncbi.nlm.nih.gov/pubmed/9276747.
357. Yang CH, Yap EH, Xiao H, Fiser A, Horwitz SB. 2016. 2-(m-Azidobenzoyl)taxol binds differentially to distinct beta-tubulin isotypes. Proc Natl Acad Sci U S A. 113(40):11294-11299. https://www.ncbi.nlm.nih.gov/pubmed/27651486.
358. Mariani M, Karki R, Spennato M, Pandya D, He S, Andreoli M, et al. 2015. Class III beta-tubulin in normal and cancer tissues. Gene. 563(2):109-114. https://www.ncbi.nlm.nih.gov/pubmed/25839941.
359. Du J, Li B, Fang Y, Liu Y, Wang Y, Li J, et al. 2015. Overexpression of Class III beta-tubulin, Sox2, and nuclear Survivin is predictive of taxane resistance in patients with stage III ovarian epithelial cancer. BMC Cancer. 15:536. https://www.ncbi.nlm.nih.gov/pubmed/26198101.
360. Gan PP, Pasquier E, Kavallaris M. 2007. Class III beta-tubulin mediates sensitivity to chemotherapeutic drugs in non small cell lung cancer. Cancer Res. 67(19):9356-9363. https://www.ncbi.nlm.nih.gov/pubmed/17909044.

361. McCarroll JA, Sharbeen G, Liu J, Youkhana J, Goldstein D, McCarthy N, et al. 2015. betaIII-tubulin: a novel mediator of chemoresistance and metastases in pancreatic cancer. Oncotarget. 6(4):2235-2249. https://www.ncbi.nlm.nih.gov/pubmed/25544769.
362. Wang Y, Cabral F. 2005. Paclitaxel resistance in cells with reduced beta-tubulin. Biochim Biophys Acta. 1744(2):245-255. https://www.ncbi.nlm.nih.gov/pubmed/15950754.
363. Mesquita B, Veiga I, Pereira D, Tavares A, Pinto IM, Pinto C, et al. 2005. No significant role for beta tubulin mutations and mismatch repair defects in ovarian cancer resistance to paclitaxel/cisplatin. BMC Cancer. 5:101. https://www.ncbi.nlm.nih.gov/pubmed/16095531.
364. Smoter M, Bodnar L, Grala B, Stec R, Zieniuk K, Kozlowski W, et al. 2013. Tau protein as a potential predictive marker in epithelial ovarian cancer patients treated with paclitaxel/platinum first-line chemotherapy. J Exp Clin Cancer Res. 32(1):25. https://www.ncbi.nlm.nih.gov/pubmed/23631819.
365. Shigematsu H, Imasaki T, Doki C, Sumi T, Aoki M, Uchikubo-Kamo T, et al. 2018. Structural insight into microtubule stabilization and kinesin inhibition by Tau family MAPs. J Cell Biol. 217(12):4155-4163. https://www.ncbi.nlm.nih.gov/pubmed/30275105.
366. Poruchynsky MS, Giannakakou P, Ward Y, Bulinski JC, Telford WG, Robey RW, et al. 2001. Accompanying protein alterations in malignant cells with a microtubule-polymerizing drug-resistance phenotype and a primary resistance mechanism. Biochem Pharmacol. 62(11):1469-1480. https://www.ncbi.nlm.nih.gov/pubmed/11728383.
367. Yu Y, Gaillard S, Phillip JM, Huang TC, Pinto SM, Tessarollo NG, et al. 2015. Inhibition of Spleen Tyrosine Kinase Potentiates Paclitaxel-Induced Cytotoxicity in Ovarian Cancer Cells by Stabilizing Microtubules. Cancer Cell. 28(1):82-96. https://www.ncbi.nlm.nih.gov/pubmed/26096845.
368. Yang H, Mao W, Rodriguez-Aguayo C, Mangala LS, Bartholomeusz G, Iles LR, et al. 2018. Paclitaxel Sensitivity of Ovarian Cancer Can be Enhanced by Knocking Down Pairs of Kinases that Regulate MAP4 Phosphorylation and Microtubule Stability. Clin Cancer Res. 24(20):5072-5084. https://www.ncbi.nlm.nih.gov/pubmed/30084832.
369. Rana S, Maples PB, Senzer N, Nemunaitis J. 2008. Stathmin 1: a novel therapeutic target for anticancer activity. Expert Rev Anticancer Ther. 8(9):1461-1470. https://www.ncbi.nlm.nih.gov/pubmed/18759697.
370. Su D, Smith SM, Preti M, Schwartz P, Rutherford TJ, Menato G, et al. 2009. Stathmin and tubulin expression and survival of ovarian cancer patients receiving platinum treatment with and without paclitaxel. Cancer. 115(11):2453-2463. https://www.ncbi.nlm.nih.gov/pubmed/19322891.
371. Carneiro BA, El-Deiry WS. 2020. Targeting apoptosis in cancer therapy. Nat Rev Clin Oncol. 17(7):395-417. https://www.ncbi.nlm.nih.gov/pubmed/32203277.
372. Singh R, Letai A, Sarosiek K. 2019. Regulation of apoptosis in health and disease: the balancing act of BCL-2 family proteins. Nat Rev Mol Cell Biol. 20(3):175-193. https://www.ncbi.nlm.nih.gov/pubmed/30655609.
373. Shigemasa K, Katoh O, Shiroyama Y, Mihara S, Mukai K, Nagai N, et al. 2002. Increased MCL-1 expression is associated with poor prognosis in ovarian carcinomas. Jpn J Cancer Res. 93(5):542-550. https://www.ncbi.nlm.nih.gov/pubmed/12036450.
374. Wertz IE, Kusam S, Lam C, Okamoto T, Sandoval W, Anderson DJ, et al. 2011. Sensitivity to antitubulin chemotherapeutics is regulated by MCL1 and FBW7. Nature. 471(7336):110-114. https://www.ncbi.nlm.nih.gov/pubmed/21368834.
375. Habata S, Iwasaki M, Sugio A, Suzuki M, Tamate M, Satohisa S, et al. 2016. BAG3-mediated Mcl-1 stabilization contributes to drug resistance via interaction with USP9X in ovarian cancer. Int J Oncol. 49(1):402-410. https://www.ncbi.nlm.nih.gov/pubmed/27120977.

376. Zaffaroni N, Pennati M, Colella G, Perego P, Supino R, Gatti L, et al. 2002. Expression of the anti-apoptotic gene survivin correlates with taxol resistance in human ovarian cancer. Cell Mol Life Sci. 59(8):1406-1412. https://www.ncbi.nlm.nih.gov/pubmed/12363043.
377. Vivas-Mejia PE, Rodriguez-Aguayo C, Han HD, Shahzad MM, Valiyeva F, Shibayama M, et al. 2011. Silencing survivin splice variant 2B leads to antitumor activity in taxane--resistant ovarian cancer. Clin Cancer Res. 17(11):3716-3726. https://www.ncbi.nlm.nih.gov/pubmed/21512144.
378. Altieri DC. 2010. Survivin and IAP proteins in cell-death mechanisms. Biochem J. 430(2):199-205. https://www.ncbi.nlm.nih.gov/pubmed/20704571.
379. Honda R, Lowe ED, Dubinina E, Skamnaki V, Cook A, Brown NR, et al. 2005. The structure of cyclin E1/CDK2: implications for CDK2 activation and CDK2-independent roles. EMBO J. 24(3):452-463. https://www.ncbi.nlm.nih.gov/pubmed/15660127.
380. Gorski JW, Ueland FR, Kolesar JM. 2020. CCNE1 Amplification as a Predictive Biomarker of Chemotherapy Resistance in Epithelial Ovarian Cancer. Diagnostics (Basel). 10(5). https://www.ncbi.nlm.nih.gov/pubmed/32380689.
381. Arsenic R, Braicu EI, Letsch A, Dietel M, Sehouli J, Keilholz U, et al. 2015. Cancer-testis antigen cyclin A1 is broadly expressed in ovarian cancer and is associated with prolonged time to tumor progression after platinum-based therapy. BMC Cancer. 15:784. https://www.ncbi.nlm.nih.gov/pubmed/26499264.
382. Huang KC, Yang J, Ng MC, Ng SK, Welch WR, Muto MG, et al. 2016. Cyclin A1 expression and paclitaxel resistance in human ovarian cancer cells. Eur J Cancer. 67:152-163. https://www.ncbi.nlm.nih.gov/pubmed/27669502.
383. Au-Yeung G, Lang F, Azar WJ, Mitchell C, Jarman KE, Lackovic K, et al. 2017. Selective Targeting of Cyclin E1-Amplified High-Grade Serous Ovarian Cancer by Cyclin-Dependent Kinase 2 and AKT Inhibition. Clin Cancer Res. 23(7):1862-1874. https://www.ncbi.nlm.nih.gov/pubmed/27663592.
384. Noack S, Raab M, Matthess Y, Sanhaji M, Kramer A, Gyorffy B, et al. 2018. Synthetic lethality in CCNE1-amplified high grade serous ovarian cancer through combined inhibition of Polo-like kinase 1 and microtubule dynamics. Oncotarget. 9(40):25842-25859. https://www.ncbi.nlm.nih.gov/pubmed/29899826.
385. Hayward D, Alfonso-Perez T, Gruneberg U. 2019. Orchestration of the spindle assembly checkpoint by CDK1-cyclin B1. FEBS Lett. 593(20):2889-2907. https://www.ncbi.nlm.nih.gov/pubmed/31469407.
386. Bargiela-Iparraguirre J, Prado-Marchal L, Pajuelo-Lozano N, Jimenez B, Perona R, Sanchez-Perez I. 2014. Mad2 and BubR1 modulates tumourigenesis and paclitaxel response in MKN45 gastric cancer cells. Cell Cycle. 13(22):3590-3601. https://www.ncbi.nlm.nih.gov/pubmed/25483095.
387. Furlong F, Fitzpatrick P, O'Toole S, Phelan S, McGrogan B, Maguire A, et al. 2012. Low MAD2 expression levels associate with reduced progression-free survival in patients with high-grade serous epithelial ovarian cancer. J Pathol. 226(5):746-755. https://www.ncbi.nlm.nih.gov/pubmed/22069160.
388. Sudo T, Nitta M, Saya H, Ueno NT. 2004. Dependence of paclitaxel sensitivity on a functional spindle assembly checkpoint. Cancer Res. 64(7):2502-2508. https://www.ncbi.nlm.nih.gov/pubmed/15059905.
389. Tipton AR, Wang K, Link L, Bellizzi JJ, Huang H, Yen T, et al. 2011. BUBR1 and closed MAD2 (C-MAD2) interact directly to assemble a functional mitotic checkpoint complex. J Biol Chem. 286(24):21173-21179. https://www.ncbi.nlm.nih.gov/pubmed/21525009.
390. Mc Gee MM. 2015. Targeting the Mitotic Catastrophe Signaling Pathway in Cancer. Mediators Inflamm. 2015:146282. https://www.ncbi.nlm.nih.gov/pubmed/26491220.

391. Giovinazzi S, Bellapu D, Morozov VM, Ishov AM. 2013. Targeting mitotic exit with hyperthermia or APC/C inhibition to increase paclitaxel efficacy. Cell Cycle. 12(16):2598-2607. https://www.ncbi.nlm.nih.gov/pubmed/23907120.
392. Raab M, Sanhaji M, Zhou S, Rodel F, El-Balat A, Becker S, et al. 2019. Blocking Mitotic Exit of Ovarian Cancer Cells by Pharmaceutical Inhibition of the Anaphase-Promoting Complex Reduces Chromosomal Instability. Neoplasia. 21(4):363-375. https://www.ncbi.nlm.nih.gov/pubmed/30851646.
393. Ibrahim SL, Abed MN, Mohamed G, Price JC, Abdullah MI, Richardson A. 2023. Inhibition of branched-chain alpha-keto acid dehydrogenase kinase augments the sensitivity of ovarian and breast cancer cells to paclitaxel. Br J Cancer. 128(5):896-906. https://www.ncbi.nlm.nih.gov/pubmed/36526674.
394. Pokhriyal R, Hariprasad R, Kumar L, Hariprasad G. 2019. Chemotherapy Resistance in Advanced Ovarian Cancer Patients. Biomark Cancer. 11:1179299X19860815. https://www.ncbi.nlm.nih.gov/pubmed/31308780.
395. Jeong JY, Kim KS, Moon JS, Song JA, Choi SH, Kim KI, et al. 2013. Targeted inhibition of phosphatidyl inositol-3-kinase p110beta, but not p110alpha, enhances apoptosis and sensitivity to paclitaxel in chemoresistant ovarian cancers. Apoptosis. 18(4):509-520. https://www.ncbi.nlm.nih.gov/pubmed/23371322.
396. Wu YH, Huang YF, Chen CC, Huang CY, Chou CY. 2020. Comparing PI3K/Akt Inhibitors Used in Ovarian Cancer Treatment. Front Pharmacol. 11:206. https://www.ncbi.nlm.nih.gov/pubmed/32194423.
397. Gupta SC, Hevia D, Patchva S, Park B, Koh W, Aggarwal BB. 2012. Upsides and downsides of reactive oxygen species for cancer: the roles of reactive oxygen species in tumorigenesis, prevention, and therapy. Antioxid Redox Signal. 16(11):1295-1322. https://www.ncbi.nlm.nih.gov/pubmed/22117137.
398. Parekh A, Das S, Parida S, Das CK, Dutta D, Mallick SK, et al. 2018. Multi-nucleated cells use ROS to induce breast cancer chemo-resistance in vitro and in vivo. Oncogene. 37(33):4546-4561. https://www.ncbi.nlm.nih.gov/pubmed/29743594.
399. Varghese E, Samuel SM, Liskova A, Samec M, Kubatka P, Busselberg D. 2020. Targeting Glucose Metabolism to Overcome Resistance to Anticancer Chemotherapy in Breast Cancer. Cancers (Basel). 12(8). https://www.ncbi.nlm.nih.gov/pubmed/32806533.
400. Das V, Stepankova J, Hajduch M, Miller JH. 2015. Role of tumor hypoxia in acquisition of resistance to microtubule-stabilizing drugs. Biochim Biophys Acta. 1855(2):172-182. https://www.ncbi.nlm.nih.gov/pubmed/25662312.
401. Karakashev SV, Reginato MJ. 2015. Progress toward overcoming hypoxia-induced resistance to solid tumor therapy. Cancer Manag Res. 7:253-264. https://www.ncbi.nlm.nih.gov/pubmed/26316817.
402. Sermeus A, Genin M, Maincent A, Fransolet M, Notte A, Leclere L, et al. 2012. Hypoxia-induced modulation of apoptosis and BCL-2 family proteins in different cancer cell types. PLoS One. 7(11):e47519. https://www.ncbi.nlm.nih.gov/pubmed/23139748.
403. Chen WT, Yang YJ, Zhang ZD, An Q, Li N, Liu W, et al. 2017. MiR-1307 promotes ovarian cancer cell chemoresistance by targeting the ING5 expression. J Ovarian Res. 10(1):1. https://www.ncbi.nlm.nih.gov/pubmed/28086946.
404. Eoh KJ, Lee SH, Kim HJ, Lee JY, Kim S, Kim SW, et al. 2018. MicroRNA-630 inhibitor sensitizes chemoresistant ovarian cancer to chemotherapy by enhancing apoptosis. Biochem Biophys Res Commun. 497(2):513-520. https://www.ncbi.nlm.nih.gov/pubmed/29452092.
405. Ferreira P, Roela RA, Lopez RVM, Del Pilar Estevez-Diz M. 2020. The prognostic role of microRNA in epithelial ovarian cancer: a systematic review of literature with an overall survival meta-analysis. Oncotarget. 11(12):1085-1095. https://www.ncbi.nlm.nih.gov/pubmed/32256980.

406. Cui Y, She K, Tian D, Zhang P, Xin X. 2016. miR-146a Inhibits Proliferation and Enhances Chemosensitivity in Epithelial Ovarian Cancer via Reduction of SOD2. Oncol Res. 23(6):275-282. https://www.ncbi.nlm.nih.gov/pubmed/27131313.
407. Nakamura K, Sawada K, Miyamoto M, Kinose Y, Yoshimura A, Ishida K, et al. 2019. Downregulation of miR-194-5p induces paclitaxel resistance in ovarian cancer cells by altering MDM2 expression. Oncotarget. 10(6):673-683. https://www.ncbi.nlm.nih.gov/pubmed/30774764.
408. Liu S, Zou B, Tian T, Luo X, Mao B, Zhang X, et al. 2019. Overexpression of the lncRNA FER1L4 inhibits paclitaxel tolerance of ovarian cancer cells via the regulation of the MAPK signaling pathway. J Cell Biochem. 120(5):7581-7589. https://www.ncbi.nlm.nih.gov/pubmed/30444026.
409. Shi C, Wang M. 2018. LINC01118 Modulates Paclitaxel Resistance of Epithelial Ovarian Cancer by Regulating miR-134/ABCC1. Med Sci Monit. 24:8831-8839. https://www.ncbi.nlm.nih.gov/pubmed/30521500.
410. An J, Lv W, Zhang Y. 2017. LncRNA NEAT1 contributes to paclitaxel resistance of ovarian cancer cells by regulating ZEB1 expression via miR-194. Onco Targets Ther. 10:5377-5390. https://www.ncbi.nlm.nih.gov/pubmed/29180871.
411. Klemm F, Joyce JA. 2015. Microenvironmental regulation of therapeutic response in cancer. Trends Cell Biol. 25(4):198-213. https://www.ncbi.nlm.nih.gov/pubmed/25540894.
412. Horowitz M, Esakov E, Rose P, Reizes O. 2020. Signaling within the epithelial ovarian cancer tumor microenvironment: the challenge of tumor heterogeneity. Ann Transl Med. 8(14):905. https://www.ncbi.nlm.nih.gov/pubmed/32793749.
413. Zhang Y, Nowicka A, Solley TN, Wei C, Parikh A, Court L, et al. 2015. Stromal Cells Derived from Visceral and Obese Adipose Tissue Promote Growth of Ovarian Cancers. PLoS One. 10(8):e0136361. https://www.ncbi.nlm.nih.gov/pubmed/26317219.
414. Wang L, Zhang F, Cui JY, Chen L, Chen YT, Liu BW. 2018. CAFs enhance paclitaxel resistance by inducing EMT through the IL-6/JAK2/STAT3 pathway. Oncol Rep. 39(5):2081-2090. https://www.ncbi.nlm.nih.gov/pubmed/29565447.
415. Leung CS, Yeung TL, Yip KP, Wong KK, Ho SY, Mangala LS, et al. 2018. Cancer-associated fibroblasts regulate endothelial adhesion protein LPP to promote ovarian cancer chemoresistance. J Clin Invest. 128(2):589-606. https://www.ncbi.nlm.nih.gov/pubmed/29251630.
416. Pitt JM, Kroemer G, Zitvogel L. 2016. Extracellular vesicles: masters of intercellular communication and potential clinical interventions. J Clin Invest. 126(4):1139-1143. https://www.ncbi.nlm.nih.gov/pubmed/27035805.
417. Vasconcelos MH, Caires HR, Abols A, Xavier CPR, Line A. 2019. Extracellular vesicles as a novel source of biomarkers in liquid biopsies for monitoring cancer progression and drug resistance. Drug Resist Updat. 47:100647. https://www.ncbi.nlm.nih.gov/pubmed/31704541.
418. Rak J. 2013. Extracellular vesicles - biomarkers and effectors of the cellular interactome in cancer. Front Pharmacol. 4:21. https://www.ncbi.nlm.nih.gov/pubmed/23508692.
419. Shen M, Dong C, Ruan X, Yan W, Cao M, Pizzo D, et al. 2019. Chemotherapy-Induced Extracellular Vesicle miRNAs Promote Breast Cancer Stemness by Targeting ONECUT2. Cancer Res. 79(14):3608-3621. https://www.ncbi.nlm.nih.gov/pubmed/31118200.
420. Chen WX, Liu XM, Lv MM, Chen L, Zhao JH, Zhong SL, et al. 2014. Exosomes from drug-resistant breast cancer cells transmit chemoresistance by a horizontal transfer of microRNAs. PLoS One. 9(4):e95240. https://www.ncbi.nlm.nih.gov/pubmed/24740415.
421. Lv MM, Zhu XY, Chen WX, Zhong SL, Hu Q, Ma TF, et al. 2014. Exosomes mediate drug resistance transfer in MCF-7 breast cancer cells and a probable mechanism is delivery

of P-glycoprotein. Tumour Biol. 35(11):10773-10779. https://www.ncbi.nlm.nih.gov/pubmed/25077924.
422. Field JJ, Kanakkanthara A, Miller JH. 2014. Microtubule-targeting agents are clinically successful due to both mitotic and interphase impairment of microtubule function. Bioorg Med Chem. 22(18):5050-5059. https://www.ncbi.nlm.nih.gov/pubmed/24650703.
423. Hatch EM, Hetzer MW. 2015. Linking Micronuclei to Chromosome Fragmentation. Cell. 161(7):1502-1504. https://www.ncbi.nlm.nih.gov/pubmed/26091034.
424. Vargas JD, Hatch EM, Anderson DJ, Hetzer MW. 2012. Transient nuclear envelope rupturing during interphase in human cancer cells. Nucleus. 3(1):88-100. https://www.ncbi.nlm.nih.gov/pubmed/22567193.
425. Lammerding J, Hsiao J, Schulze PC, Kozlov S, Stewart CL, Lee RT. 2005. Abnormal nuclear shape and impaired mechanotransduction in emerin-deficient cells. J Cell Biol. 170(5):781-791. https://www.ncbi.nlm.nih.gov/pubmed/16115958.
426. Smith ER, Capo-Chichi CD, Xu XX. 2018. Defective Nuclear Lamina in Aneuploidy and Carcinogenesis. Front Oncol. 8:529. https://www.ncbi.nlm.nih.gov/pubmed/30524960.
427. Smith ER, Leal J, Amaya C, Li B, Xu XX. 2021. Nuclear Lamin A/C Expression Is a Key Determinant of Paclitaxel Sensitivity. Mol Cell Biol. 41(7):e0064820. https://www.ncbi.nlm.nih.gov/pubmed/33972393.
428. Niu N, Mercado-Uribe I, Liu J. 2017. Dedifferentiation into blastomere-like cancer stem cells via formation of polyploid giant cancer cells. Oncogene. 36(34):4887-4900. https://www.ncbi.nlm.nih.gov/pubmed/28436947.
429. Niu N, Zhang J, Zhang N, Mercado-Uribe I, Tao F, Han Z, et al. 2016. Linking genomic reorganization to tumor initiation via the giant cell cycle. Oncogenesis. 5(12):e281. https://www.ncbi.nlm.nih.gov/pubmed/27991913.
430. Zhang S, Mercado-Uribe I, Liu J. 2014. Tumor stroma and differentiated cancer cells can be originated directly from polyploid giant cancer cells induced by paclitaxel. Int J Cancer. 134(3):508-518. https://www.ncbi.nlm.nih.gov/pubmed/23754740.
431. Chen J, Niu N, Zhang J, Qi L, Shen W, Donkena KV, et al. 2019. Polyploid Giant Cancer Cells (PGCCs): The Evil Roots of Cancer. Curr Cancer Drug Targets. 19(5):360-367. https://www.ncbi.nlm.nih.gov/pubmed/29968537.
432. Niu N, Yao J, Bast RC, Sood AK, Liu J. 2021. IL-6 promotes drug resistance through formation of polyploid giant cancer cells and stromal fibroblast reprogramming. Oncogenesis. 10(9):65. https://www.ncbi.nlm.nih.gov/pubmed/34588424.
433. Patel AG, Sarkaria JN, Kaufmann SH. 2011. Nonhomologous end joining drives poly(ADP-ribose) polymerase (PARP) inhibitor lethality in homologous recombination-deficient cells. Proc Natl Acad Sci U S A. 108(8):3406-3411. https://www.ncbi.nlm.nih.gov/pubmed/21300883.
434. Mateo J, Lord CJ, Serra V, Tutt A, Balmana J, Castroviejo-Bermejo M, et al. 2019. A decade of clinical development of PARP inhibitors in perspective. Ann Oncol. 30(9):1437-1447. https://www.ncbi.nlm.nih.gov/pubmed/31218365.
435. Konstantinopoulos PA, Ceccaldi R, Shapiro GI, D'Andrea AD. 2015. Homologous Recombination Deficiency: Exploiting the Fundamental Vulnerability of Ovarian Cancer. Cancer Discov. 5(11):1137-1154. https://www.ncbi.nlm.nih.gov/pubmed/26463832.
436. Norquist BM, Harrell MI, Brady MF, Walsh T, Lee MK, Gulsuner S, et al. 2016. Inherited Mutations in Women With Ovarian Carcinoma. JAMA Oncol. 2(4):482-490. https://www.ncbi.nlm.nih.gov/pubmed/26720728.
437. Miller RE, Leary A, Scott CL, Serra V, Lord CJ, Bowtell D, et al. 2020. ESMO recommendations on predictive biomarker testing for homologous recombination deficiency and PARP inhibitor benefit in ovarian cancer. Ann Oncol. 31(12):1606-1622. https://www.ncbi.nlm.nih.gov/pubmed/33004253.

438. DiSilvestro P, Banerjee S, Colombo N, Scambia G, Kim BG, Oaknin A, et al. 2023. Overall Survival With Maintenance Olaparib at a 7-Year Follow-Up in Patients With Newly Diagnosed Advanced Ovarian Cancer and a BRCA Mutation: The SOLO1/GOG 3004 Trial. J Clin Oncol. 41(3):609-617. https://www.ncbi.nlm.nih.gov/pubmed/36082969.
439. Hockings H, Miller RE. 2023. The role of PARP inhibitor combination therapy in ovarian cancer. Ther Adv Med Oncol. 15:17588359231173183. https://www.ncbi.nlm.nih.gov/pubmed/37215065.
440. Lord CJ, Ashworth A. 2017. PARP inhibitors: Synthetic lethality in the clinic. Science. 355(6330):1152-1158. https://www.ncbi.nlm.nih.gov/pubmed/28302823.
441. Kaye SB, Lubinski J, Matulonis U, Ang JE, Gourley C, Karlan BY, et al. 2012. Phase II, open-label, randomized, multicenter study comparing the efficacy and safety of olaparib, a poly (ADP-ribose) polymerase inhibitor, and pegylated liposomal doxorubicin in patients with BRCA1 or BRCA2 mutations and recurrent ovarian cancer. J Clin Oncol. 30(4):372-379. https://www.ncbi.nlm.nih.gov/pubmed/22203755.
442. Soberanis Pina P, Lheureux S. 2023. Overcoming PARP inhibitor resistance in ovarian cancer. Int J Gynecol Cancer. 33(3):364-376. https://www.ncbi.nlm.nih.gov/pubmed/36878566.
443. McMullen M, Karakasis K, Madariaga A, Oza AM. 2020. Overcoming Platinum and PARP-Inhibitor Resistance in Ovarian Cancer. Cancers (Basel). 12(6). https://www.ncbi.nlm.nih.gov/pubmed/32560564.
444. Oza AM, Tinker AV, Oaknin A, Shapira-Frommer R, McNeish IA, Swisher EM, et al. 2017. Antitumor activity and safety of the PARP inhibitor rucaparib in patients with high-grade ovarian carcinoma and a germline or somatic BRCA1 or BRCA2 mutation: Integrated analysis of data from Study 10 and ARIEL2. Gynecol Oncol. 147(2):267-275. https://www.ncbi.nlm.nih.gov/pubmed/28882436.
445. Murai J, Huang SY, Das BB, Renaud A, Zhang Y, Doroshow JH, et al. 2012. Trapping of PARP1 and PARP2 by Clinical PARP Inhibitors. Cancer Res. 72(21):5588-5599. https://www.ncbi.nlm.nih.gov/pubmed/23118055.
446. Ashworth A. 2008. Drug resistance caused by reversion mutation. Cancer Res. 68(24):10021-10023. https://www.ncbi.nlm.nih.gov/pubmed/19074863.
447. Swisher EM, Lin KK, Oza AM, Scott CL, Giordano H, Sun J, et al. 2017. Rucaparib in relapsed, platinum-sensitive high-grade ovarian carcinoma (ARIEL2 Part 1): an international, multicentre, open-label, phase 2 trial. Lancet Oncol. 18(1):75-87. https://www.ncbi.nlm.nih.gov/pubmed/27908594.
448. Evans T, Matulonis U. 2017. PARP inhibitors in ovarian cancer: evidence, experience and clinical potential. Ther Adv Med Oncol. 9(4):253-267. https://www.ncbi.nlm.nih.gov/pubmed/28491146.
449. Ortiz M, Wabel E, Mitchell K, Horibata S. 2022. Mechanisms of chemotherapy resistance in ovarian cancer. Cancer Drug Resist. 5(2):304-316. https://www.ncbi.nlm.nih.gov/pubmed/35800369.
450. Pilie PG, Tang C, Mills GB, Yap TA. 2019. State-of-the-art strategies for targeting the DNA damage response in cancer. Nat Rev Clin Oncol. 16(2):81-104. https://www.ncbi.nlm.nih.gov/pubmed/30356138.
451. Burdett NL, Willis MO, Alsop K, Hunt AL, Pandey A, Hamilton PT, et al. 2023. Multiomic analysis of homologous recombination-deficient end-stage high-grade serous ovarian cancer. Nat Genet. 55(3):437-450. https://www.ncbi.nlm.nih.gov/pubmed/36849657.
452. Christie EL, Fereday S, Doig K, Pattnaik S, Dawson SJ, Bowtell DDL. 2017. Reversion of BRCA1/2 Germline Mutations Detected in Circulating Tumor DNA From Patients With High-Grade Serous Ovarian Cancer. J Clin Oncol. 35(12):1274-1280. https://www.ncbi.nlm.nih.gov/pubmed/28414925.

453. Swisher EM, Sakai W, Karlan BY, Wurz K, Urban N, Taniguchi T. 2008. Secondary BRCA1 mutations in BRCA1-mutated ovarian carcinomas with platinum resistance. Cancer Res. 68(8):2581-2586. https://www.ncbi.nlm.nih.gov/pubmed/18413725.
454. Liu L, Cai S, Han C, Banerjee A, Wu D, Cui T, et al. 2020. ALDH1A1 Contributes to PARP Inhibitor Resistance via Enhancing DNA Repair in BRCA2(-/-) Ovarian Cancer Cells. Mol Cancer Ther. 19(1):199-210. https://www.ncbi.nlm.nih.gov/pubmed/31534014.
455. Kondrashova O, Nguyen M, Shield-Artin K, Tinker AV, Teng NNH, Harrell MI, et al. 2017. Secondary Somatic Mutations Restoring RAD51C and RAD51D Associated with Acquired Resistance to the PARP Inhibitor Rucaparib in High-Grade Ovarian Carcinoma. Cancer Discov. 7(9):984-998. https://www.ncbi.nlm.nih.gov/pubmed/28588062.
456. Nesic K, Kondrashova O, Hurley RM, McGehee CD, Vandenberg CJ, Ho GY, et al. 2021. Acquired RAD51C Promoter Methylation Loss Causes PARP Inhibitor Resistance in High-Grade Serous Ovarian Carcinoma. Cancer Res. 81(18):4709-4722. https://www.ncbi.nlm.nih.gov/pubmed/34321239.
457. Pettitt SJ, Krastev DB, Brandsma I, Drean A, Song F, Aleksandrov R, et al. 2018. Genome-wide and high-density CRISPR-Cas9 screens identify point mutations in PARP1 causing PARP inhibitor resistance. Nat Commun. 9(1):1849. https://www.ncbi.nlm.nih.gov/pubmed/29748565.
458. Garg V, Oza AM. 2023. Treatment of Ovarian Cancer Beyond PARP Inhibition: Current and Future Options. Drugs. 83(15):1365-1385. https://www.ncbi.nlm.nih.gov/pubmed/37737434.
459. O'Sullivan J, Tedim Ferreira M, Gagne JP, Sharma AK, Hendzel MJ, Masson JY, et al. 2019. Emerging roles of eraser enzymes in the dynamic control of protein ADP-ribosylation. Nat Commun. 10(1):1182. https://www.ncbi.nlm.nih.gov/pubmed/30862789.
460. Soung YH, Chung J. 2023. Combination Treatment Strategies to Overcome PARP Inhibitor Resistance. Biomolecules. 13(10). https://www.ncbi.nlm.nih.gov/pubmed/37892162.
461. Hashimoto Y, Tanaka H. 2022. Mre11 exonuclease activity promotes irreversible mitotic progression under replication stress. Life Sci Alliance. 5(6). https://www.ncbi.nlm.nih.gov/pubmed/35292537.
462. Dias MP, Moser SC, Ganesan S, Jonkers J. 2021. Understanding and overcoming resistance to PARP inhibitors in cancer therapy. Nat Rev Clin Oncol. 18(12):773-791. https://www.ncbi.nlm.nih.gov/pubmed/34285417.
463. Washington CR, Moore KN. 2022. Resistance to Poly (ADP-Ribose) Polymerase Inhibitors (PARPi): Mechanisms and Potential to Reverse. Curr Oncol Rep. 24(12):1685-1693. https://www.ncbi.nlm.nih.gov/pubmed/36346509.
464. Christie EL, Pattnaik S, Beach J, Copeland A, Rashoo N, Fereday S, et al. 2019. Multiple ABCB1 transcriptional fusions in drug resistant high-grade serous ovarian and breast cancer. Nat Commun. 10(1):1295. https://www.ncbi.nlm.nih.gov/pubmed/30894541.
465. Vaidyanathan A, Sawers L, Gannon AL, Chakravarty P, Scott AL, Bray SE, et al. 2016. ABCB1 (MDR1) induction defines a common resistance mechanism in paclitaxel- and olaparib-resistant ovarian cancer cells. Br J Cancer. 115(4):431-441. https://www.ncbi.nlm.nih.gov/pubmed/27415012.
466. Hustedt N, Durocher D. 2016. The control of DNA repair by the cell cycle. Nat Cell Biol. 19(1):1-9. https://www.ncbi.nlm.nih.gov/pubmed/28008184.
467. Kastan MB, Bartek J. 2004. Cell-cycle checkpoints and cancer. Nature. 432(7015):316-323. https://www.ncbi.nlm.nih.gov/pubmed/15549093.
468. Brill E, Yokoyama T, Nair J, Yu M, Ahn YR, Lee JM. 2017. Prexasertib, a cell cycle checkpoint kinases 1 and 2 inhibitor, increases in vitro toxicity of PARP inhibition by preventing Rad51 foci formation in BRCA wild type high-grade serous ovarian cancer. Oncotarget. 8(67):111026-111040. https://www.ncbi.nlm.nih.gov/pubmed/29340034.

469. MacQueen AJ. 2015. Catching a (Double-Strand) Break: The Rad51 and Dmc1 Strand Exchange Proteins Can Co-occupy Both Ends of a Meiotic DNA Double-Strand Break. PLoS Genet. 11(12):e1005741. https://www.ncbi.nlm.nih.gov/pubmed/26720282.
470. Nair J, Huang TT, Murai J, Haynes B, Steeg PS, Pommier Y, et al. 2020. Resistance to the CHK1 inhibitor prexasertib involves functionally distinct CHK1 activities in BRCA wild-type ovarian cancer. Oncogene. 39(33):5520-5535. https://www.ncbi.nlm.nih.gov/pubmed/32647134.
471. Zhang X, Yao J, Li X, Niu N, Liu Y, Hajek RA, et al. 2023. Targeting polyploid giant cancer cells potentiates a therapeutic response and overcomes resistance to PARP inhibitors in ovarian cancer. Sci Adv. 9(29):eadf7195. https://www.ncbi.nlm.nih.gov/pubmed/37478190.
472. Farkkila A, Rodriguez A, Oikkonen J, Gulhan DC, Nguyen H, Dominguez J, et al. 2021. Heterogeneity and Clonal Evolution of Acquired PARP Inhibitor Resistance in TP53- and BRCA1-Deficient Cells. Cancer Res. 81(10):2774-2787. https://www.ncbi.nlm.nih.gov/pubmed/33514515.
473. Chung AS, Lee J, Ferrara N. 2010. Targeting the tumour vasculature: insights from physiological angiogenesis. Nat Rev Cancer. 10(7):505-514. https://www.ncbi.nlm.nih.gov/pubmed/20574450.
474. Graybill W, Sood AK, Monk BJ, Coleman RL. 2015. State of the science: Emerging therapeutic strategies for targeting angiogenesis in ovarian cancer. Gynecol Oncol. 138(2):223-226. https://www.ncbi.nlm.nih.gov/pubmed/26166806.
475. Mancuso MR, Davis R, Norberg SM, O'Brien S, Sennino B, Nakahara T, et al. 2006. Rapid vascular regrowth in tumors after reversal of VEGF inhibition. J Clin Invest. 116(10):2610-2621. https://www.ncbi.nlm.nih.gov/pubmed/17016557.
476. van Baal J, van Noorden CJF, Nieuwland R, Van de Vijver KK, Sturk A, van Driel WJ, et al. 2018. Development of Peritoneal Carcinomatosis in Epithelial Ovarian Cancer: A Review. J Histochem Cytochem. 66(2):67-83. https://www.ncbi.nlm.nih.gov/pubmed/29164988.
477. Marchetti C, Muzii L, Romito A, Benedetti Panici P. 2019. First-line treatment of women with advanced ovarian cancer: focus on bevacizumab. Onco Targets Ther. 12:1095-1103. https://www.ncbi.nlm.nih.gov/pubmed/30799939.
478. Ellis LM, Hicklin DJ. 2008. Pathways mediating resistance to vascular endothelial growth factor-targeted therapy. Clin Cancer Res. 14(20):6371-6375. https://www.ncbi.nlm.nih.gov/pubmed/18927275.
479. Reinthaller A. 2016. Antiangiogenic therapies in ovarian cancer. Memo. 9(3):139-143. https://www.ncbi.nlm.nih.gov/pubmed/27752291.
480. Itatani Y, Kawada K, Yamamoto T, Sakai Y. 2018. Resistance to Anti-Angiogenic Therapy in Cancer-Alterations to Anti-VEGF Pathway. Int J Mol Sci. 19(4). https://www.ncbi.nlm.nih.gov/pubmed/29670046.
481. Haibe Y, Kreidieh M, El Hajj H, Khalifeh I, Mukherji D, Temraz S, et al. 2020. Resistance Mechanisms to Anti-angiogenic Therapies in Cancer. Front Oncol. 10:221. https://www.ncbi.nlm.nih.gov/pubmed/32175278.
482. Mei C, Gong W, Wang X, Lv Y, Zhang Y, Wu S, et al. 2023. Anti-angiogenic therapy in ovarian cancer: Current understandings and prospects of precision medicine. Front Pharmacol. 14:1147717. https://www.ncbi.nlm.nih.gov/pubmed/36959862.
483. Casanovas O, Hicklin DJ, Bergers G, Hanahan D. 2005. Drug resistance by evasion of antiangiogenic targeting of VEGF signaling in late-stage pancreatic islet tumors. Cancer Cell. 8(4):299-309. https://www.ncbi.nlm.nih.gov/pubmed/16226705.
484. Jin C, Yuan M, Bu H, Jin C. 2022. Antiangiogenic Strategies in Epithelial Ovarian Cancer: Mechanism, Resistance, and Combination Therapy. J Oncol. 2022:4880355. https://www.ncbi.nlm.nih.gov/pubmed/35466318.

485. Bagley RG, Ren Y, Weber W, Yao M, Kurtzberg L, Pinckney J, et al. 2011. Placental growth factor upregulation is a host response to antiangiogenic therapy. Clin Cancer Res. 17(5):976-988. https://www.ncbi.nlm.nih.gov/pubmed/21343374.
486. Zhang G, Liu C, Bai H, Cao G, Cui R, Zhang Z. 2019. Combinatorial therapy of immune checkpoint and cancer pathways provides a novel perspective on ovarian cancer treatment. Oncol Lett. 17(3):2583-2591. https://www.ncbi.nlm.nih.gov/pubmed/30854033.
487. Ellis LM, Hicklin DJ. 2008. VEGF-targeted therapy: mechanisms of anti-tumour activity. Nat Rev Cancer. 8(8):579-591. https://www.ncbi.nlm.nih.gov/pubmed/18596824.
488. Arjaans M, Oude Munnink TH, Oosting SF, Terwisscha van Scheltinga AG, Gietema JA, Garbacik ET, et al. 2013. Bevacizumab-induced normalization of blood vessels in tumors hampers antibody uptake. Cancer Res. 73(11):3347-3355. https://www.ncbi.nlm.nih.gov/pubmed/23580572.
489. Pinto MP, Sotomayor P, Carrasco-Avino G, Corvalan AH, Owen GI. 2016. Escaping Antiangiogenic Therapy: Strategies Employed by Cancer Cells. Int J Mol Sci. 17(9). https://www.ncbi.nlm.nih.gov/pubmed/27608016.
490. Huang M, Lin Y, Wang C, Deng L, Chen M, Assaraf YG, et al. 2022. New insights into antiangiogenic therapy resistance in cancer: Mechanisms and therapeutic aspects. Drug Resist Updat. 64:100849. https://www.ncbi.nlm.nih.gov/pubmed/35842983.
491. Rigamonti N, Kadioglu E, Keklikoglou I, Wyser Rmili C, Leow CC, De Palma M. 2014. Role of angiopoietin-2 in adaptive tumor resistance to VEGF signaling blockade. Cell Rep. 8(3):696-706. https://www.ncbi.nlm.nih.gov/pubmed/25088418.
492. Grepin R, Guyot M, Jacquin M, Durivault J, Chamorey E, Sudaka A, et al. 2012. Acceleration of clear cell renal cell carcinoma growth in mice following bevacizumab/Avastin treatment: the role of CXCL cytokines. Oncogene. 31(13):1683-1694. https://www.ncbi.nlm.nih.gov/pubmed/21909141.
493. Paez-Ribes M, Allen E, Hudock J, Takeda T, Okuyama H, Vinals F, et al. 2009. Antiangiogenic therapy elicits malignant progression of tumors to increased local invasion and distant metastasis. Cancer Cell. 15(3):220-231. https://www.ncbi.nlm.nih.gov/pubmed/19249680.
494. Ferlay J, Colombet M, Soerjomataram I, Dyba T, Randi G, Bettio M, et al. 2018. Cancer incidence and mortality patterns in Europe: Estimates for 40 countries and 25 major cancers in 2018. Eur J Cancer. 103:356-387. https://www.ncbi.nlm.nih.gov/pubmed/30100160.
495. Lisio MA, Fu L, Goyeneche A, Gao ZH, Telleria C. 2019. High-Grade Serous Ovarian Cancer: Basic Sciences, Clinical and Therapeutic Standpoints. Int J Mol Sci. 20(4). https://www.ncbi.nlm.nih.gov/pubmed/30813239.
496. Sehouli J, Stengel D, Elling D, Ortmann O, Blohmer J, Riess H, et al. 2002. First-line chemotherapy with weekly paclitaxel and carboplatin for advanced ovarian cancer: a phase I study. Gynecol Oncol. 85(2):321-326. https://www.ncbi.nlm.nih.gov/pubmed/11972395.
497. Mayerhofer K, Bodner-Adler B, Bodner K, Leodolter S, Kainz C. 2000. Paclitaxel/carboplatin as first-line chemotherapy in advanced ovarian cancer: efficacy and adverse effects with special consideration of peripheral neurotoxicity. Anticancer Res. 20(5C):4047-4050. https://www.ncbi.nlm.nih.gov/pubmed/11268499.
498. Zamagni C, Martoni A, Cacciari N, Gentile A, Pannuti F. 1998. The combination of paclitaxel and carboplatin as first-line chemotherapy in patients with stage III and stage IV ovarian cancer: a phase I-II study. Am J Clin Oncol. 21(5):491-497. https://www.ncbi.nlm.nih.gov/pubmed/9781607.
499. Nunes M, Ricardo S. Chemoresistance in Ovarian Cancer: The Role of Malignant Ascites. In: Lele S, editor. Ovarian Cancer. Brisbane (AU)2022. p. 27-42.
500. Zhang X, Chen L, Liu Y, Xu Y, Zhang X, Shi Y, et al. 2018. Improving the cytological diagnosis of high-grade serous carcinoma in ascites with a panel of complementary

biomarkers in cell blocks. Cytopathology. 29(3):247-253. https://www.ncbi.nlm.nih.gov/pubmed/29280203.
501. Micek HM, Carroll MJ, Barroilhet L, Kreeger PK. 2022. Processing and Analysis of Ascites. Methods Mol Biol. 2424:95-104. https://www.ncbi.nlm.nih.gov/pubmed/34918288.
502. Nunes M, Pacheco F, Coelho R, Leitao D, Ricardo S, David L. 2022. Mesothelin Expression Is Not Associated with the Presence of Cancer Stem Cell Markers SOX2 and ALDH1 in Ovarian Cancer. Int J Mol Sci. 23(3). https://www.ncbi.nlm.nih.gov/pubmed/35162954.
503. Nambirajan A, Jain D. 2018. Cell blocks in cytopathology: An update. Cytopathology. 29(6):505-524. https://www.ncbi.nlm.nih.gov/pubmed/30153355.
504. Pinto D, Chandra A, Crothers BA, Kurtycz DFI, Schmitt F. 2020. The international system for reporting serous fluid cytopathology-diagnostic categories and clinical management. J Am Soc Cytopathol. 9(6):469-477. https://www.ncbi.nlm.nih.gov/pubmed/32620534.
505. Engels M, Michael C, Dobra K, Hjerpe A, Fassina A, Firat P. 2019. Management of cytological material, pre-analytical procedures and bio-banking in effusion cytopathology. Cytopathology. 30(1):31-38. https://www.ncbi.nlm.nih.gov/pubmed/30430668.
506. Uehara T, Yoshida H, Fukuhara M, Yoshida M, Motoi N, Sugawara S, et al. 2020. Efficacy of ascitic fluid cell block for diagnosing primary ovarian, peritoneal, and tubal cancer in patients with peritoneal carcinomatosis with ascites. Gynecol Oncol. 157(2):398-404. https://www.ncbi.nlm.nih.gov/pubmed/32063274.
507. Bansal A, Srinivasan R, Rohilla M, Sundaram A, Rai B, Rajwanshi A, et al. 2020. Morphologic and Immunocytochemical Features of High-Grade Serous Carcinoma of Ovary in Ascitic Fluid Effusion and Fine-Needle Aspiration Cytology. Am J Clin Pathol. 154(1):103-114. https://www.ncbi.nlm.nih.gov/pubmed/32271370.
508. Zurawski VR, Jr., Orjaseter H, Andersen A, Jellum E. 1988. Elevated serum CA 125 levels prior to diagnosis of ovarian neoplasia: relevance for early detection of ovarian cancer. Int J Cancer. 42(5):677-680. https://www.ncbi.nlm.nih.gov/pubmed/3182103.
509. Nowicki A, Kulus M, Wieczorkiewicz M, Pienkowski W, Stefanska K, Skupin-Mrugalska P, et al. 2021. Ovarian Cancer and Cancer Stem Cells-Cellular and Molecular Characteristics, Signaling Pathways, and Usefulness as a Diagnostic Tool in Medicine and Oncology. Cancers (Basel). 13(16). https://www.ncbi.nlm.nih.gov/pubmed/34439332.
510. Abelson S, Shamai Y, Berger L, Shouval R, Skorecki K, Tzukerman M. 2012. Intratumoral heterogeneity in the self-renewal and tumorigenic differentiation of ovarian cancer. Stem Cells. 30(3):415-424. https://www.ncbi.nlm.nih.gov/pubmed/22267284.
511. Garson K, Vanderhyden BC. 2015. Epithelial ovarian cancer stem cells: underlying complexity of a simple paradigm. Reproduction. 149(2):R59-70. https://www.ncbi.nlm.nih.gov/pubmed/25301968.
512. Roy L, Cowden Dahl KD. 2018. Can Stemness and Chemoresistance Be Therapeutically Targeted via Signaling Pathways in Ovarian Cancer? Cancers (Basel). 10(8). https://www.ncbi.nlm.nih.gov/pubmed/30042330.
513. Ottevanger PB. 2017. Ovarian cancer stem cells more questions than answers. Semin Cancer Biol. 44:67-71. https://www.ncbi.nlm.nih.gov/pubmed/28450177.
514. Hu Y, Fu L. 2012. Targeting cancer stem cells: a new therapy to cure cancer patients. Am J Cancer Res. 2(3):340-356. https://www.ncbi.nlm.nih.gov/pubmed/22679565.
515. Fischer AK, Pham DL, Bosmuller H, Lengerke C, Wagner P, Bachmann C, et al. 2019. Comprehensive in situ analysis of ALDH1 and SOX2 reveals increased expression of stem cell markers in high-grade serous carcinomas compared to low-grade serous carcinomas and atypical proliferative serous tumors. Virchows Arch. 475(4):479-488. https://www.ncbi.nlm.nih.gov/pubmed/31451895.

516. Singh S, Brocker C, Koppaka V, Chen Y, Jackson BC, Matsumoto A, et al. 2013. Aldehyde dehydrogenases in cellular responses to oxidative/electrophilic stress. Free Radic Biol Med. 56:89-101. https://www.ncbi.nlm.nih.gov/pubmed/23195683.
517. Kuroda T, Hirohashi Y, Torigoe T, Yasuda K, Takahashi A, Asanuma H, et al. 2013. ALDH1-high ovarian cancer stem-like cells can be isolated from serous and clear cell adenocarcinoma cells, and ALDH1 high expression is associated with poor prognosis. PLoS One. 8(6):e65158. https://www.ncbi.nlm.nih.gov/pubmed/23762304.
518. Bareiss PM, Paczulla A, Wang H, Schairer R, Wiehr S, Kohlhofer U, et al. 2013. SOX2 expression associates with stem cell state in human ovarian carcinoma. Cancer Res. 73(17):5544-5555. https://www.ncbi.nlm.nih.gov/pubmed/23867475.
519. Weina K, Utikal J. 2014. SOX2 and cancer: current research and its implications in the clinic. Clin Transl Med. 3:19. https://www.ncbi.nlm.nih.gov/pubmed/25114775.
520. Bajaj J, Diaz E, Reya T. 2020. Stem cells in cancer initiation and progression. J Cell Biol. 219(1). https://www.ncbi.nlm.nih.gov/pubmed/31874116.
521. Padua D, Barros R, Amaral AL, Mesquita P, Freire AF, Sousa M, et al. 2020. A SOX2 Reporter System Identifies Gastric Cancer Stem-Like Cells Sensitive to Monensin. Cancers (Basel). 12(2). https://www.ncbi.nlm.nih.gov/pubmed/32093282.
522. Ye F, Li Y, Hu Y, Zhou C, Hu Y, Chen H. 2011. Expression of Sox2 in human ovarian epithelial carcinoma. J Cancer Res Clin Oncol. 137(1):131-137. https://www.ncbi.nlm.nih.gov/pubmed/20349085.
523. Zhang J, Chang DY, Mercado-Uribe I, Liu J. 2012. Sex-determining region Y-box 2 expression predicts poor prognosis in human ovarian carcinoma. Hum Pathol. 43(9):1405-1412. https://www.ncbi.nlm.nih.gov/pubmed/22401770.
524. Novak D, Huser L, Elton JJ, Umansky V, Altevogt P, Utikal J. 2020. SOX2 in development and cancer biology. Semin Cancer Biol. 67(Pt 1):74-82. https://www.ncbi.nlm.nih.gov/pubmed/31412296.
525. Moreb JS, Baker HV, Chang LJ, Amaya M, Lopez MC, Ostmark B, et al. 2008. ALDH isozymes downregulation affects cell growth, cell motility and gene expression in lung cancer cells. Mol Cancer. 7:87. https://www.ncbi.nlm.nih.gov/pubmed/19025616.
526. Wen Y, Hou Y, Huang Z, Cai J, Wang Z. 2017. SOX2 is required to maintain cancer stem cells in ovarian cancer. Cancer Sci. 108(4):719-731. https://www.ncbi.nlm.nih.gov/pubmed/28165651.
527. Kaipio K, Chen P, Roering P, Huhtinen K, Mikkonen P, Ostling P, et al. 2020. ALDH1A1-related stemness in high-grade serous ovarian cancer is a negative prognostic indicator but potentially targetable by EGFR/mTOR-PI3K/aurora kinase inhibitors. J Pathol. 250(2):159-169. https://www.ncbi.nlm.nih.gov/pubmed/31595974.
528. Baath M, Westbom-Fremer S, Martin de la Fuente L, Ebbesson A, Davis J, Malander S, et al. 2020. SOX2 is a promising predictor of relapse and death in advanced stage high-grade serous ovarian cancer patients with residual disease after debulking surgery. Mol Cell Oncol. 7(6):1805094. https://www.ncbi.nlm.nih.gov/pubmed/33235906.
529. Tjhay F, Motohara T, Tayama S, Narantuya D, Fujimoto K, Guo J, et al. 2015. CD44 variant 6 is correlated with peritoneal dissemination and poor prognosis in patients with advanced epithelial ovarian cancer. Cancer Sci. 106(10):1421-1428. https://www.ncbi.nlm.nih.gov/pubmed/26250934.
530. Guo C, Song C, Zhang J, Gao Y, Qi Y, Zhao Z, et al. 2022. Revisiting chemoresistance in ovarian cancer: Mechanism, biomarkers, and precision medicine. Genes Dis. 9(3):668-681. https://www.ncbi.nlm.nih.gov/pubmed/35782973.
531. Ozben T. 2006. Mechanisms and strategies to overcome multiple drug resistance in cancer. FEBS Lett. 580(12):2903-2909. https://www.ncbi.nlm.nih.gov/pubmed/16497299.
532. Leonard GD, Fojo T, Bates SE. 2003. The role of ABC transporters in clinical practice. Oncologist. 8(5):411-424. https://www.ncbi.nlm.nih.gov/pubmed/14530494.

533. Goldstein LJ, Galski H, Fojo A, Willingham M, Lai SL, Gazdar A, et al. 1989. Expression of a multidrug resistance gene in human cancers. J Natl Cancer Inst. 81(2):116-124. https://www.ncbi.nlm.nih.gov/pubmed/2562856.
534. Penson RT, Oliva E, Skates SJ, Glyptis T, Fuller AF, Jr., Goodman A, et al. 2004. Expression of multidrug resistance-1 protein inversely correlates with paclitaxel response and survival in ovarian cancer patients: a study in serial samples. Gynecol Oncol. 93(1):98-106. https://www.ncbi.nlm.nih.gov/pubmed/15047220.
535. Dagogo-Jack I, Shaw AT. 2018. Tumour heterogeneity and resistance to cancer therapies. Nat Rev Clin Oncol. 15(2):81-94. https://www.ncbi.nlm.nih.gov/pubmed/29115304.
536. Brodsky AS, Fischer A, Miller DH, Vang S, MacLaughlan S, Wu HT, et al. 2014. Expression profiling of primary and metastatic ovarian tumors reveals differences indicative of aggressive disease. PLoS One. 9(4):e94476. https://www.ncbi.nlm.nih.gov/pubmed/24732363.
537. Paracchini L, Mannarino L, Craparotta I, Romualdi C, Fruscio R, Grassi T, et al. 2021. Regional and temporal heterogeneity of epithelial ovarian cancer tumor biopsies: implications for therapeutic strategies. Oncotarget. 12(24):2404-2417. https://www.ncbi.nlm.nih.gov/pubmed/34853661.
538. Stefanovic S, Wirtz R, Deutsch TM, Hartkopf A, Sinn P, Varga Z, et al. 2017. Tumor biomarker conversion between primary and metastatic breast cancer: mRNA assessment and its concordance with immunohistochemistry. Oncotarget. 8(31):51416-51428. https://www.ncbi.nlm.nih.gov/pubmed/28881657.
539. Cheng WF, Huang CY, Chang MC, Hu YH, Chiang YC, Chen YL, et al. 2009. High mesothelin correlates with chemoresistance and poor survival in epithelial ovarian carcinoma. Br J Cancer. 100(7):1144-1153. https://www.ncbi.nlm.nih.gov/pubmed/19293794.
540. Lyons YA, Reyes HD, McDonald ME, Newtson A, Devor E, Bender DP, et al. 2020. Interval debulking surgery is not worth the wait: a National Cancer Database study comparing primary cytoreductive surgery versus neoadjuvant chemotherapy. Int J Gynecol Cancer. 30(6):845-852. https://www.ncbi.nlm.nih.gov/pubmed/32341114.
541. Gonzalez-Martin A, Sanchez-Lorenzo L, Bratos R, Marquez R, Chiva L. 2014. First-line and maintenance therapy for ovarian cancer: current status and future directions. Drugs. 74(8):879-889. https://www.ncbi.nlm.nih.gov/pubmed/24848752.
542. Kim A, Ueda Y, Naka T, Enomoto T. 2012. Therapeutic strategies in epithelial ovarian cancer. J Exp Clin Cancer Res. 31:14. https://www.ncbi.nlm.nih.gov/pubmed/22330607.
543. Testa U, Petrucci E, Pasquini L, Castelli G, Pelosi E. 2018. Ovarian Cancers: Genetic Abnormalities, Tumor Heterogeneity and Progression, Clonal Evolution and Cancer Stem Cells. Medicines (Basel). 5(1). https://www.ncbi.nlm.nih.gov/pubmed/29389895.
544. Cortez AJ, Tudrej P, Kujawa KA, Lisowska KM. 2018. Advances in ovarian cancer therapy. Cancer Chemother Pharmacol. 81(1):17-38. https://www.ncbi.nlm.nih.gov/pubmed/29249039.
545. Brasseur K, Gevry N, Asselin E. 2017. Chemoresistance and targeted therapies in ovarian and endometrial cancers. Oncotarget. 8(3):4008-4042. https://www.ncbi.nlm.nih.gov/pubmed/28008141.
546. Stordal B, Pavlakis N, Davey R. 2007. A systematic review of platinum and taxane resistance from bench to clinic: an inverse relationship. Cancer Treat Rev. 33(8):688-703. https://www.ncbi.nlm.nih.gov/pubmed/17881133.
547. Naumann RW, Coleman RL. 2011. Management strategies for recurrent platinum-resistant ovarian cancer. Drugs. 71(11):1397-1412. https://www.ncbi.nlm.nih.gov/pubmed/21812505.

548. Mikula-Pietrasik J, Witucka A, Pakula M, Uruski P, Begier-Krasinska B, Niklas A, et al. 2019. Comprehensive review on how platinum- and taxane-based chemotherapy of ovarian cancer affects biology of normal cells. Cell Mol Life Sci. 76(4):681-697. https://www.ncbi.nlm.nih.gov/pubmed/30382284.
549. Bae T, Weon KY, Lee JW, Eum KH, Kim S, Choi JW. 2015. Restoration of paclitaxel resistance by CDK1 intervention in drug-resistant ovarian cancer. Carcinogenesis. 36(12):1561-1571. https://www.ncbi.nlm.nih.gov/pubmed/26442525.
550. Chang MC, Chen CA, Hsieh CY, Lee CN, Su YN, Hu YH, et al. 2009. Mesothelin inhibits paclitaxel-induced apoptosis through the PI3K pathway. Biochem J. 424(3):449-458. https://www.ncbi.nlm.nih.gov/pubmed/19747165.
551. Das T, Anand U, Pandey SK, Ashby CR, Jr., Assaraf YG, Chen ZS, et al. 2021. Therapeutic strategies to overcome taxane resistance in cancer. Drug Resist Updat. 55:100754. https://www.ncbi.nlm.nih.gov/pubmed/33691261.
552. Kelland L. 2007. The resurgence of platinum-based cancer chemotherapy. Nat Rev Cancer. 7(8):573-584. https://www.ncbi.nlm.nih.gov/pubmed/17625587.
553. Sobue S, Mizutani N, Aoyama Y, Kawamoto Y, Suzuki M, Nozawa Y, et al. 2016. Mechanism of paclitaxel resistance in a human prostate cancer cell line, PC3-PR, and its sensitization by cabazitaxel. Biochem Biophys Res Commun. 479(4):808-813. https://www.ncbi.nlm.nih.gov/pubmed/27687545.
554. Song Y, Brady ST. 2015. Post-translational modifications of tubulin: pathways to functional diversity of microtubules. Trends Cell Biol. 25(3):125-136. https://www.ncbi.nlm.nih.gov/pubmed/25468068.
555. Wloga D, Joachimiak E, Fabczak H. 2017. Tubulin Post-Translational Modifications and Microtubule Dynamics. Int J Mol Sci. 18(10). https://www.ncbi.nlm.nih.gov/pubmed/29065455.
556. Amaral MVS, AJ DESP, EL DAS, L DEOS, JH DASM, MEA DEM, et al. 2019. Establishment of Drug-resistant Cell Lines as a Model in Experimental Oncology: A Review. Anticancer Res. 39(12):6443-6455. https://www.ncbi.nlm.nih.gov/pubmed/31810908.
557. Zhang X, Yashiro M, Qiu H, Nishii T, Matsuzaki T, Hirakawa K. 2010. Establishment and characterization of multidrug-resistant gastric cancer cell lines. Anticancer Res. 30(3):915-921. https://www.ncbi.nlm.nih.gov/pubmed/20393015.
558. Chen SY, Hu SS, Dong Q, Cai JX, Zhang WP, Sun JY, et al. 2013. Establishment of paclitaxel-resistant breast cancer cell line and nude mice models, and underlying multidrug resistance mechanisms in vitro and in vivo. Asian Pac J Cancer Prev. 14(10):6135-6140. https://www.ncbi.nlm.nih.gov/pubmed/24289639.
559. Takeda M, Mizokami A, Mamiya K, Li YQ, Zhang J, Keller ET, et al. 2007. The establishment of two paclitaxel-resistant prostate cancer cell lines and the mechanisms of paclitaxel resistance with two cell lines. Prostate. 67(9):955-967. https://www.ncbi.nlm.nih.gov/pubmed/17440963.
560. Tudrej P, Olbryt M, Zembala-Nozynska E, Kujawa KA, Cortez AJ, Fiszer-Kierzkowska A, et al. 2018. Establishment and Characterization of the Novel High-Grade Serous Ovarian Cancer Cell Line OVPA8. Int J Mol Sci. 19(7). https://www.ncbi.nlm.nih.gov/pubmed/30018258.
561. Teng PN, Bateman NW, Wang G, Litzi T, Blanton BE, Hood BL, et al. 2017. Establishment and characterization of a platinum- and paclitaxel-resistant high grade serous ovarian carcinoma cell line. Hum Cell. 30(3):226-236. https://www.ncbi.nlm.nih.gov/pubmed/28251557.
562. Chen FQ, Zhang JM, Fang XF, Yu H, Liu YL, Li H, et al. 2017. Reversal of paclitaxel resistance in human ovarian cancer cells with redox-responsive micelles consisting of alpha-tocopheryl succinate-based polyphosphoester copolymers. Acta Pharmacol Sin. 38(6):859-873. https://www.ncbi.nlm.nih.gov/pubmed/28260803.

563. Chu SW, Badar S, Morris DL, Pourgholami MH. 2009. Potent inhibition of tubulin polymerisation and proliferation of paclitaxel-resistant 1A9PTX22 human ovarian cancer cells by albendazole. Anticancer Res. 29(10):3791-3796. https://www.ncbi.nlm.nih.gov/pubmed/19846910.
564. Feng J, Peng Z, Gao L, Yang X, Sun Z, Hou X, et al. 2021. ClC-3 promotes paclitaxel resistance via modulating tubulins polymerization in ovarian cancer cells. Biomed Pharmacother. 138:111407. https://www.ncbi.nlm.nih.gov/pubmed/33765585.
565. Szenajch J, Szabelska-Beresewicz A, Swiercz A, Zyprych-Walczak J, Siatkowski I, Goralski M, et al. 2020. Transcriptome Remodeling in Gradual Development of Inverse Resistance between Paclitaxel and Cisplatin in Ovarian Cancer Cells. Int J Mol Sci. 21(23). https://www.ncbi.nlm.nih.gov/pubmed/33287223.
566. Wang L, Jia E. 2016. Ovarian cancer targeted hyaluronic acid-based nanoparticle system for paclitaxel delivery to overcome drug resistance. Drug Deliv. 23(5):1810-1817. https://www.ncbi.nlm.nih.gov/pubmed/26530693.
567. Schilder RJ, Hall L, Monks A, Handel LM, Fornace AJ, Jr., Ozols RF, et al. 1990. Metallothionein gene expression and resistance to cisplatin in human ovarian cancer. Int J Cancer. 45(3):416-422. https://www.ncbi.nlm.nih.gov/pubmed/2307530.
568. Jensen NF, Stenvang J, Beck MK, Hanakova B, Belling KC, Do KN, et al. 2015. Establishment and characterization of models of chemotherapy resistance in colorectal cancer: Towards a predictive signature of chemoresistance. Mol Oncol. 9(6):1169-1185. https://www.ncbi.nlm.nih.gov/pubmed/25759163.
569. McDermott M, Eustace AJ, Busschots S, Breen L, Crown J, Clynes M, et al. 2014. In vitro Development of Chemotherapy and Targeted Therapy Drug-Resistant Cancer Cell Lines: A Practical Guide with Case Studies. Front Oncol. 4:40. https://www.ncbi.nlm.nih.gov/pubmed/24639951.
570. Coelho R, Ricardo S, Amaral AL, Huang YL, Nunes M, Neves JP, et al. 2020. Regulation of invasion and peritoneal dissemination of ovarian cancer by mesothelin manipulation. Oncogenesis. 9(6):61. https://www.ncbi.nlm.nih.gov/pubmed/32612258.
571. Avninder S, Ylaya K, Hewitt SM. 2008. Tissue microarray: a simple technology that has revolutionized research in pathology. J Postgrad Med. 54(2):158-162. https://www.ncbi.nlm.nih.gov/pubmed/18480540.
572. Simon R, Mirlacher M, Sauter G. 2004. Tissue microarrays. Methods Mol Med. 97:377-389. https://www.ncbi.nlm.nih.gov/pubmed/15064506.
573. Coelho R, Marcos-Silva L, Mendes N, Pereira D, Brito C, Jacob F, et al. 2018. Mucins and Truncated O-Glycans Unveil Phenotypic Discrepancies between Serous Ovarian Cancer Cell Lines and Primary Tumours. Int J Mol Sci. 19(7). https://www.ncbi.nlm.nih.gov/pubmed/30011875.
574. Henriques AC, Silva PMA, Sarmento B, Bousbaa H. 2021. Antagonizing the spindle assembly checkpoint silencing enhances paclitaxel and Navitoclax-mediated apoptosis with distinct mechanistic. Sci Rep. 11(1):4139. https://www.ncbi.nlm.nih.gov/pubmed/33603057.
575. Silva PM, Ribeiro N, Lima RT, Andrade C, Diogo V, Teixeira J, et al. 2017. Suppression of spindly delays mitotic exit and exacerbates cell death response of cancer cells treated with low doses of paclitaxel. Cancer Lett. 394:33-42. https://www.ncbi.nlm.nih.gov/pubmed/28249757.
576. Silva PM, Tavares AA, Bousbaa H. 2015. Co-silencing of human Bub3 and dynein highlights an antagonistic relationship in regulating kinetochore-microtubule attachments. FEBS Lett. 589(23):3588-3594. https://www.ncbi.nlm.nih.gov/pubmed/26526612.
577. Choi CH. 2005. ABC transporters as multidrug resistance mechanisms and the development of chemosensitizers for their reversal. Cancer Cell Int. 5:30. https://www.ncbi.nlm.nih.gov/pubmed/16202168.

578. Choi YH, Yu AM. 2014. ABC transporters in multidrug resistance and pharmacokinetics, and strategies for drug development. Curr Pharm Des. 20(5):793-807. https://www.ncbi.nlm.nih.gov/pubmed/23688078.
579. Cunnea P, Stronach EA. 2014. Modeling platinum sensitive and resistant high-grade serous ovarian cancer: development and applications of experimental systems. Front Oncol. 4:81. https://www.ncbi.nlm.nih.gov/pubmed/24860781.
580. Hubaux R, Thu KL, Vucic EA, Pikor LA, Kung SH, Martinez VD, et al. 2015. Microtubule affinity-regulating kinase 2 is associated with DNA damage response and cisplatin resistance in non-small cell lung cancer. Int J Cancer. 137(9):2072-2082. https://www.ncbi.nlm.nih.gov/pubmed/25907283.
581. Li L, Huang X, Huang R, Gou S, Wang Z, Wang H. 2018. Pt(IV) prodrugs containing microtubule inhibitors displayed potent antitumor activity and ability to overcome cisplatin resistance. Eur J Med Chem. 156:666-679. https://www.ncbi.nlm.nih.gov/pubmed/30031977.
582. Stordal B, Hamon M, McEneaney V, Roche S, Gillet JP, O'Leary JJ, et al. 2012. Resistance to paclitaxel in a cisplatin-resistant ovarian cancer cell line is mediated by P-glycoprotein. PLoS One. 7(7):e40717. https://www.ncbi.nlm.nih.gov/pubmed/22792399.
583. Patel RP, Kuhn S, Yin D, Hotz JM, Maher FA, Robey RW, et al. 2021. Cross-resistance of cisplatin selected cells to anti-microtubule agents: Role of general survival mechanisms. Transl Oncol. 14(1):100917. https://www.ncbi.nlm.nih.gov/pubmed/33129114.
584. Huang HK, Lin YH, Chang HA, Lai YS, Chen YC, Huang SC, et al. 2020. Chemoresistant ovarian cancer enhances its migration abilities by increasing store-operated Ca(2+) entry-mediated turnover of focal adhesions. J Biomed Sci. 27(1):36. https://www.ncbi.nlm.nih.gov/pubmed/32079527.
585. Kim HS, Oh JM, Jin DH, Yang KH, Moon EY. 2008. Paclitaxel induces vascular endothelial growth factor expression through reactive oxygen species production. Pharmacology. 81(4):317-324. https://www.ncbi.nlm.nih.gov/pubmed/18322419.
586. Ganesh T, Yang C, Norris A, Glass T, Bane S, Ravindra R, et al. 2007. Evaluation of the tubulin-bound paclitaxel conformation: synthesis, biology, and SAR studies of C-4 to C-3' bridged paclitaxel analogues. J Med Chem. 50(4):713-725. https://www.ncbi.nlm.nih.gov/pubmed/17263521.
587. White D, Honore S, Hubert F. 2017. Exploring the effect of end-binding proteins and microtubule targeting chemotherapy drugs on microtubule dynamic instability. J Theor Biol. 429:18-34. https://www.ncbi.nlm.nih.gov/pubmed/28645857.
588. Woods CM, Zhu J, McQueney PA, Bollag D, Lazarides E. 1995. Taxol-induced mitotic block triggers rapid onset of a p53-independent apoptotic pathway. Mol Med. 1(5):506-526. https://www.ncbi.nlm.nih.gov/pubmed/8529117.
589. Wang TH, Wang HS, Soong YK. 2000. Paclitaxel-induced cell death: where the cell cycle and apoptosis come together. Cancer. 88(11):2619-2628. https://www.ncbi.nlm.nih.gov/pubmed/10861441.
590. Nanayakkara AK, Follit CA, Chen G, Williams NS, Vogel PD, Wise JG. 2018. Targeted inhibitors of P-glycoprotein increase chemotherapeutic-induced mortality of multidrug resistant tumor cells. Sci Rep. 8(1):967. https://www.ncbi.nlm.nih.gov/pubmed/29343829.
591. Cascorbi I. 2011. P-glycoprotein: tissue distribution, substrates, and functional consequences of genetic variations. Handb Exp Pharmacol. (201):261-283. https://www.ncbi.nlm.nih.gov/pubmed/21103972.
592. Bourhis J, Goldstein LJ, Riou G, Pastan I, Gottesman MM, Benard J. 1989. Expression of a human multidrug resistance gene in ovarian carcinomas. Cancer Res. 49(18):5062-5065. https://www.ncbi.nlm.nih.gov/pubmed/2766278.

593. Fojo AT, Shen DW, Mickley LA, Pastan I, Gottesman MM. 1987. Intrinsic drug resistance in human kidney cancer is associated with expression of a human multidrug-resistance gene. J Clin Oncol. 5(12):1922-1927. https://www.ncbi.nlm.nih.gov/pubmed/3681376.
594. Pirker R, Goldstein LJ, Ludwig H, Linkesch W, Lechner C, Gottesman MM, et al. 1989. Expression of a multidrug resistance gene in blast crisis of chronic myelogenous leukemia. Cancer Commun. 1(2):141-144. https://www.ncbi.nlm.nih.gov/pubmed/2639725.
595. Mechetner E, Kyshtoobayeva A, Zonis S, Kim H, Stroup R, Garcia R, et al. 1998. Levels of multidrug resistance (MDR1) P-glycoprotein expression by human breast cancer correlate with in vitro resistance to taxol and doxorubicin. Clin Cancer Res. 4(2):389-398. https://www.ncbi.nlm.nih.gov/pubmed/9516927.
596. Burns BS, Edin ML, Lester GE, Tuttle HG, Wall ME, Wani MC, et al. 2001. Selective drug resistant human osteosarcoma cell lines. Clin Orthop Relat Res. (383):259-267. https://www.ncbi.nlm.nih.gov/pubmed/11210963.
597. Reinecke P, Schmitz M, Schneider EM, Gabbert HE, Gerharz CD. 2000. Multidrug resistance phenotype and paclitaxel (Taxol) sensitivity in human renal carcinoma cell lines of different histologic types. Cancer Invest. 18(7):614-625. https://www.ncbi.nlm.nih.gov/pubmed/11036469.
598. Zhang H, Xu H, Ashby CR, Jr., Assaraf YG, Chen ZS, Liu HM. 2021. Chemical molecular-based approach to overcome multidrug resistance in cancer by targeting P-glycoprotein (P-gp). Med Res Rev. 41(1):525-555. https://www.ncbi.nlm.nih.gov/pubmed/33047304.
599. Matulonis UA, Sood AK, Fallowfield L, Howitt BE, Sehouli J, Karlan BY. 2016. Ovarian cancer. Nat Rev Dis Primers. 2:16061. https://www.ncbi.nlm.nih.gov/pubmed/27558151.
600. Jordan MA, Wilson L. 2004. Microtubules as a target for anticancer drugs. Nat Rev Cancer. 4(4):253-265. https://www.ncbi.nlm.nih.gov/pubmed/15057285.
601. Scripture CD, Figg WD, Sparreboom A. 2006. Peripheral neuropathy induced by paclitaxel: recent insights and future perspectives. Curr Neuropharmacol. 4(2):165-172. https://www.ncbi.nlm.nih.gov/pubmed/18615126.
602. Yamamoto S, Egashira N. 2020. Drug Repositioning for the Prevention and Treatment of Chemotherapy-Induced Peripheral Neuropathy: A Mechanism- and Screening-Based Strategy. Front Pharmacol. 11:607780. https://www.ncbi.nlm.nih.gov/pubmed/33519471.
603. Di Nicolantonio F, Mercer SJ, Knight LA, Gabriel FG, Whitehouse PA, Sharma S, et al. 2005. Cancer cell adaptation to chemotherapy. BMC Cancer. 5:78. https://www.ncbi.nlm.nih.gov/pubmed/16026610.
604. Wang X, Zhang H, Chen X. 2019. Drug resistance and combating drug resistance in cancer. Cancer Drug Resist. 2:141-160. https://www.ncbi.nlm.nih.gov/pubmed/34322663.
605. Bertolini F, Sukhatme VP, Bouche G. 2015. Drug repurposing in oncology--patient and health systems opportunities. Nat Rev Clin Oncol. 12(12):732-742. https://www.ncbi.nlm.nih.gov/pubmed/26483297.
606. Zheng W, Sun W, Simeonov A. 2018. Drug repurposing screens and synergistic drug-combinations for infectious diseases. Br J Pharmacol. 175(2):181-191. https://www.ncbi.nlm.nih.gov/pubmed/28685814.
607. Nunes M, Henriques Abreu M, Bartosch C, Ricardo S. 2020. Recycling the Purpose of Old Drugs to Treat Ovarian Cancer. Int J Mol Sci. 21(20). https://www.ncbi.nlm.nih.gov/pubmed/33092251.
608. Armando RG, Mengual Gomez DL, Gomez DE. 2020. New drugs are not enoughdrug repositioning in oncology: An update. Int J Oncol. 56(3):651-684. https://www.ncbi.nlm.nih.gov/pubmed/32124955.

609. Jourdan JP, Bureau R, Rochais C, Dallemagne P. 2020. Drug repositioning: a brief overview. J Pharm Pharmacol. 72(9):1145-1151. https://www.ncbi.nlm.nih.gov/pubmed/32301512.
610. Pantziarka P, Bouche G, Meheus L, Sukhatme V, Sukhatme VP, Vikas P. 2014. The Repurposing Drugs in Oncology (ReDO) Project. Ecancermedicalscience. 8:442. https://www.ncbi.nlm.nih.gov/pubmed/25075216.
611. Ishida J, Konishi M, Ebner N, Springer J. 2016. Repurposing of approved cardiovascular drugs. J Transl Med. 14:269. https://www.ncbi.nlm.nih.gov/pubmed/27646033.
612. Iwata H, Sawada R, Mizutani S, Yamanishi Y. 2015. Systematic drug repositioning for a wide range of diseases with integrative analyses of phenotypic and molecular data. J Chem Inf Model. 55(2):446-459. https://www.ncbi.nlm.nih.gov/pubmed/25602292.
613. Correia A, Silva D, Correia A, Vilanova M, Gartner F, Vale N. 2018. Study of New Therapeutic Strategies to Combat Breast Cancer Using Drug Combinations. Biomolecules. 8(4). https://www.ncbi.nlm.nih.gov/pubmed/30558247.
614. Bayat Mokhtari R, Homayouni TS, Baluch N, Morgatskaya E, Kumar S, Das B, et al. 2017. Combination therapy in combating cancer. Oncotarget. 8(23):38022-38043. https://www.ncbi.nlm.nih.gov/pubmed/28410237.
615. Smalley KS, Haass NK, Brafford PA, Lioni M, Flaherty KT, Herlyn M. 2006. Multiple signaling pathways must be targeted to overcome drug resistance in cell lines derived from melanoma metastases. Mol Cancer Ther. 5(5):1136-1144. https://www.ncbi.nlm.nih.gov/pubmed/16731745.
616. Mei L, Chen Y, Wang Z, Wang J, Wan J, Yu C, et al. 2015. Synergistic anti-tumour effects of tetrandrine and chloroquine combination therapy in human cancer: a potential antagonistic role for p21. Br J Pharmacol. 172(9):2232-2245. https://www.ncbi.nlm.nih.gov/pubmed/25521075.
617. Gao Y, Xiao X, Zhang C, Yu W, Guo W, Zhang Z, et al. 2017. Melatonin synergizes the chemotherapeutic effect of 5-fluorouracil in colon cancer by suppressing PI3K/AKT and NF-kappaB/iNOS signaling pathways. J Pineal Res. 62(2). https://www.ncbi.nlm.nih.gov/pubmed/27865009.
618. Greco F, Vicent MJ. 2009. Combination therapy: opportunities and challenges for polymer-drug conjugates as anticancer nanomedicines. Adv Drug Deliv Rev. 61(13):1203-1213. https://www.ncbi.nlm.nih.gov/pubmed/19699247.
619. Palmer AC, Sorger PK. 2017. Combination Cancer Therapy Can Confer Benefit via Patient-to-Patient Variability without Drug Additivity or Synergy. Cell. 171(7):1678-1691 e1613. https://www.ncbi.nlm.nih.gov/pubmed/29245013.
620. Tallarida RJ. 2007. Interactions between drugs and occupied receptors. Pharmacol Ther. 113(1):197-209. https://www.ncbi.nlm.nih.gov/pubmed/17079019.
621. Parhi P, Mohanty C, Sahoo SK. 2012. Nanotechnology-based combinational drug delivery: an emerging approach for cancer therapy. Drug Discov Today. 17(17-18):1044-1052. https://www.ncbi.nlm.nih.gov/pubmed/22652342.
622. Shi J, Votruba AR, Farokhzad OC, Langer R. 2010. Nanotechnology in drug delivery and tissue engineering: from discovery to applications. Nano Lett. 10(9):3223-3230. https://www.ncbi.nlm.nih.gov/pubmed/20726522.
623. Duarte D, Cardoso A, Vale N. 2021. Synergistic Growth Inhibition of HT-29 Colon and MCF-7 Breast Cancer Cells with Simultaneous and Sequential Combinations of Antineoplastics and CNS Drugs. Int J Mol Sci. 22(14). https://www.ncbi.nlm.nih.gov/pubmed/34299028.

624. Duarte D, Vale N. 2020. New Trends for Antimalarial Drugs: Synergism between Antineoplastics and Antimalarials on Breast Cancer Cells. Biomolecules. 10(12). https://www.ncbi.nlm.nih.gov/pubmed/33271968.
625. Rushworth LK, Hewit K, Munnings-Tomes S, Somani S, James D, Shanks E, et al. 2020. Repurposing screen identifies mebendazole as a clinical candidate to synergise with docetaxel for prostate cancer treatment. Br J Cancer. 122(4):517-527. https://www.ncbi.nlm.nih.gov/pubmed/31844184.
626. Buranrat B, Suwannaloet W, Naowaboot J. 2017. Simvastatin potentiates doxorubicin activity against MCF-7 breast cancer cells. Oncol Lett. 14(5):6243-6250. https://www.ncbi.nlm.nih.gov/pubmed/29113274.
627. Lee JO, Kang MJ, Byun WS, Kim SA, Seo IH, Han JA, et al. 2019. Metformin overcomes resistance to cisplatin in triple-negative breast cancer (TNBC) cells by targeting RAD51. Breast Cancer Res. 21(1):115. https://www.ncbi.nlm.nih.gov/pubmed/31640742.
628. Nunes M, Silva PMA, Coelho R, Pinto C, Resende A, Bousbaa H, et al. 2021. Generation of Two Paclitaxel-Resistant High-Grade Serous Carcinoma Cell Lines With Increased Expression of P-Glycoprotein. Front Oncol. 11:752127. https://www.ncbi.nlm.nih.gov/pubmed/34745981.
629. Tsao SW, Mok SC, Fey EG, Fletcher JA, Wan TS, Chew EC, et al. 1995. Characterization of human ovarian surface epithelial cells immortalized by human papilloma viral oncogenes (HPV-E6E7 ORFs). Exp Cell Res. 218(2):499-507. https://www.ncbi.nlm.nih.gov/pubmed/7796885.
630. de Wolf E, Abdullah MI, Jones SM, Menezes K, Moss DM, Drijfhout FP, et al. 2017. Dietary geranylgeraniol can limit the activity of pitavastatin as a potential treatment for drug-resistant ovarian cancer. Sci Rep. 7(1):5410. https://www.ncbi.nlm.nih.gov/pubmed/28710496.
631. Dang JH, Jin ZJ, Liu XJ, Hu D, Wang J, Luo Y, et al. 2017. Metformin in combination with cisplatin inhibits cell viability and induces apoptosis of human ovarian cancer cells by inactivating ERK 1/2. Oncol Lett. 14(6):7557-7564. https://www.ncbi.nlm.nih.gov/pubmed/29344202.
632. Hashimoto H, Messerli SM, Sudo T, Maruta H. 2009. Ivermectin inactivates the kinase PAK1 and blocks the PAK1-dependent growth of human ovarian cancer and NF2 tumor cell lines. Drug Discov Ther. 3(6):243-246. https://www.ncbi.nlm.nih.gov/pubmed/22495656.
633. Choi CH, Ryu JY, Cho YJ, Jeon HK, Choi JJ, Ylaya K, et al. 2017. The anti-cancer effects of itraconazole in epithelial ovarian cancer. Sci Rep. 7(1):6552. https://www.ncbi.nlm.nih.gov/pubmed/28747628.
634. Hashimoto K, Morishige K, Sawada K, Tahara M, Kawagishi R, Ikebuchi Y, et al. 2005. Alendronate inhibits intraperitoneal dissemination in in vivo ovarian cancer model. Cancer Res. 65(2):540-545. https://www.ncbi.nlm.nih.gov/pubmed/15695397.
635. Zhang N, Fu JN, Chou TC. 2016. Synergistic combination of microtubule targeting anticancer fludelone with cytoprotective panaxytriol derived from panax ginseng against MX-1 cells in vitro: experimental design and data analysis using the combination index method. Am J Cancer Res. 6(1):97-104. https://www.ncbi.nlm.nih.gov/pubmed/27073727.
636. Chou TC. 2010. Drug combination studies and their synergy quantification using the Chou-Talalay method. Cancer Res. 70(2):440-446. https://www.ncbi.nlm.nih.gov/pubmed/20068163.
637. Roell KR, Reif DM, Motsinger-Reif AA. 2017. An Introduction to Terminology and Methodology of Chemical Synergy-Perspectives from Across Disciplines. Front Pharmacol. 8:158. https://www.ncbi.nlm.nih.gov/pubmed/28473769.

638. Ianevski A, Giri AK, Aittokallio T. 2020. SynergyFinder 2.0: visual analytics of multi-drug combination synergies. Nucleic Acids Res. 48(W1):W488-W493. https://www.ncbi.nlm.nih.gov/pubmed/32246720.
639. Ianevski A, Giri AK, Gautam P, Kononov A, Potdar S, Saarela J, et al. 2019. Prediction of drug combination effects with a minimal set of experiments. Nat Mach Intell. 1(12):568-577. https://www.ncbi.nlm.nih.gov/pubmed/32368721.
640. Goldin A, Mantel N. 1957. The employment of combinations of drugs in the chemotherapy of neoplasia: a review. Cancer Res. 17(7):635-654. https://www.ncbi.nlm.nih.gov/pubmed/13460966.
641. Greco WR, Bravo G, Parsons JC. 1995. The search for synergy: a critical review from a response surface perspective. Pharmacol Rev. 47(2):331-385. https://www.ncbi.nlm.nih.gov/pubmed/7568331.
642. Chou TC. 2006. Theoretical basis, experimental design, and computerized simulation of synergism and antagonism in drug combination studies. Pharmacol Rev. 58(3):621-681. https://www.ncbi.nlm.nih.gov/pubmed/16968952.
643. Duarte D, Vale N. 2022. Evaluation of synergism in drug combinations and reference models for future orientations in oncology. Curr Res Pharmacol Drug Discov. 3:100110. https://www.ncbi.nlm.nih.gov/pubmed/35620200.
644. Duarte D, Vale N. 2021. Combining repurposed drugs to treat colorectal cancer. Drug Discov Today. https://www.ncbi.nlm.nih.gov/pubmed/34592446.
645. Piccolo MT, Menale C, Crispi S. 2015. Combined anticancer therapies: an overview of the latest applications. Anticancer Agents Med Chem. 15(4):408-422. https://www.ncbi.nlm.nih.gov/pubmed/25584691.
646. Ayoub NM. 2021. Editorial: Novel Combination Therapies for the Treatment of Solid Cancers. Front Oncol. 11:708943. https://www.ncbi.nlm.nih.gov/pubmed/34222030.
647. Costa B, Amorim I, Gartner F, Vale N. 2020. Understanding Breast cancer: from conventional therapies to repurposed drugs. Eur J Pharm Sci. 151:105401. https://www.ncbi.nlm.nih.gov/pubmed/32504806.
648. Bookman MA, Greer BE, Ozols RF. 2003. Optimal therapy of advanced ovarian cancer: carboplatin and paclitaxel versus cisplatin and paclitaxel (GOG158) and an update on GOG0182-ICON5. Int J Gynecol Cancer. 13 Suppl 2:149-155. https://www.ncbi.nlm.nih.gov/pubmed/14656272.
649. du Bois A, Neijt JP, Thigpen JT. 1999. First line chemotherapy with carboplatin plus paclitaxel in advanced ovarian cancer--a new standard of care? Ann Oncol. 10 Suppl 1:35-41. https://www.ncbi.nlm.nih.gov/pubmed/10219451.
650. Bukowska B, Gajek A, Marczak A. 2015. Two drugs are better than one. A short history of combined therapy of ovarian cancer. Contemp Oncol (Pozn). 19(5):350-353. https://www.ncbi.nlm.nih.gov/pubmed/26793017.
651. McGuire WP, 3rd. 2003. Current status of taxane and platinum-based chemotherapy in ovarian cancer. J Clin Oncol. 21(10 Suppl):133s-135s. https://www.ncbi.nlm.nih.gov/pubmed/12743128.
652. Rabik CA, Dolan ME. 2007. Molecular mechanisms of resistance and toxicity associated with platinating agents. Cancer Treat Rev. 33(1):9-23. https://www.ncbi.nlm.nih.gov/pubmed/17084534.
653. Dermitzakis EV, Kimiskidis VK, Lazaridis G, Alexopoulou Z, Timotheadou E, Papanikolaou A, et al. 2016. The impact of paclitaxel and carboplatin chemotherapy on the autonomous nervous system of patients with ovarian cancer. BMC Neurol. 16(1):190. https://www.ncbi.nlm.nih.gov/pubmed/27716097.
654. Fotopoulou C. 2014. Limitations to the use of carboplatin-based therapy in advanced ovarian cancer. EJC Suppl. 12(2):13-16. https://www.ncbi.nlm.nih.gov/pubmed/26759527.

655. Yan X, Yu Q, Guo L, Guo W, Guan S, Tang H, et al. 2017. Positively Charged Combinatory Drug Delivery Systems against Multi-Drug-Resistant Breast Cancer: Beyond the Drug Combination. ACS Appl Mater Interfaces. 9(8):6804-6815. https://www.ncbi.nlm.nih.gov/pubmed/28185449.
656. Zimmermann GR, Lehar J, Keith CT. 2007. Multi-target therapeutics: when the whole is greater than the sum of the parts. Drug Discov Today. 12(1-2):34-42. https://www.ncbi.nlm.nih.gov/pubmed/17198971.
657. Hirst J, Pathak HB, Hyter S, Pessetto ZY, Ly T, Graw S, et al. 2018. Licofelone Enhances the Efficacy of Paclitaxel in Ovarian Cancer by Reversing Drug Resistance and Tumor Stem-like Properties. Cancer Res. 78(15):4370-4385. https://www.ncbi.nlm.nih.gov/pubmed/29891506.
658. Togashi K, Okada M, Yamamoto M, Suzuki S, Sanomachi T, Seino S, et al. 2018. A Small-molecule Kinase Inhibitor, CEP-1347, Inhibits Survivin Expression and Sensitizes Ovarian Cancer Stem Cells to Paclitaxel. Anticancer Res. 38(8):4535-4542. https://www.ncbi.nlm.nih.gov/pubmed/30061219.
659. Yamamoto M, Suzuki S, Togashi K, Sanomachi T, Seino S, Kitanaka C, et al. 2018. AS602801, an Anticancer Stem Cell Candidate Drug, Reduces Survivin Expression and Sensitizes A2780 Ovarian Cancer Stem Cells to Carboplatin and Paclitaxel. Anticancer Res. 38(12):6699-6706. https://www.ncbi.nlm.nih.gov/pubmed/30504379.
660. Branco H, Oliveira J, Antunes C, Santos LL, Vasconcelos MH, Xavier CPR. 2022. Pirfenidone Sensitizes NCI-H460 Non-Small Cell Lung Cancer Cells to Paclitaxel and to a Combination of Paclitaxel with Carboplatin. Int J Mol Sci. 23(7). https://www.ncbi.nlm.nih.gov/pubmed/35408988.
661. Martirosyan A, Clendening JW, Goard CA, Penn LZ. 2010. Lovastatin induces apoptosis of ovarian cancer cells and synergizes with doxorubicin: potential therapeutic relevance. BMC Cancer. 10:103. https://www.ncbi.nlm.nih.gov/pubmed/20298590.
662. Robinson E, Nandi M, Wilkinson LL, Arrowsmith DM, Curtis AD, Richardson A. 2013. Preclinical evaluation of statins as a treatment for ovarian cancer. Gynecol Oncol. 129(2):417-424. https://www.ncbi.nlm.nih.gov/pubmed/23402903.
663. Jones HM, Fang Z, Sun W, Clark LH, Stine JE, Tran AQ, et al. 2018. Erratum: Atorvastatin exhibits anti-tumorigenic and anti-metastatic effects in ovarian cancer in vitro. Am J Cancer Res. 8(5):915. https://www.ncbi.nlm.nih.gov/pubmed/29888764.
664. Stine JE, Guo H, Sheng X, Han X, Schointuch MN, Gilliam TP, et al. 2016. The HMG-CoA reductase inhibitor, simvastatin, exhibits anti-metastatic and anti-tumorigenic effects in ovarian cancer. Oncotarget. 7(1):946-960. https://www.ncbi.nlm.nih.gov/pubmed/26503475.
665. Lengyel E, Litchfield LM, Mitra AK, Nieman KM, Mukherjee A, Zhang Y, et al. 2015. Metformin inhibits ovarian cancer growth and increases sensitivity to paclitaxel in mouse models. Am J Obstet Gynecol. 212(4):479 e471-479 e410. https://www.ncbi.nlm.nih.gov/pubmed/25446664.
666. Yang C, Zhao N, Li D, Zou G, Chen Y. 2019. Metformin improves the sensitivity of ovarian cancer cells to chemotherapeutic agents. Oncol Lett. 18(3):2404-2411. https://www.ncbi.nlm.nih.gov/pubmed/31402943.
667. Du J, Shi HR, Ren F, Wang JL, Wu QH, Li X, et al. 2017. Inhibition of the IGF signaling pathway reverses cisplatin resistance in ovarian cancer cells. BMC Cancer. 17(1):851. https://www.ncbi.nlm.nih.gov/pubmed/29241458.
668. Rattan R, Graham RP, Maguire JL, Giri S, Shridhar V. 2011. Metformin suppresses ovarian cancer growth and metastasis with enhancement of cisplatin cytotoxicity in vivo. Neoplasia. 13(5):483-491. https://www.ncbi.nlm.nih.gov/pubmed/21532889.

669. Xie Y, Peng Z, Shi M, Ji M, Guo H, Shi H. 2014. Metformin combined with p38 MAPK inhibitor improves cisplatin sensitivity in cisplatinresistant ovarian cancer. Mol Med Rep. 10(5):2346-2350. https://www.ncbi.nlm.nih.gov/pubmed/25118792.
670. Kodama M, Kodama T, Newberg JY, Katayama H, Kobayashi M, Hanash SM, et al. 2017. In vivo loss-of-function screens identify KPNB1 as a new druggable oncogene in epithelial ovarian cancer. Proc Natl Acad Sci U S A. 114(35):E7301-E7310. https://www.ncbi.nlm.nih.gov/pubmed/28811376.
671. Zhang X, Qin T, Zhu Z, Hong F, Xu Y, Zhang X, et al. 2020. Ivermectin Augments the In Vitro and In Vivo Efficacy of Cisplatin in Epithelial Ovarian Cancer by Suppressing Akt/mTOR Signaling. Am J Med Sci. 359(2):123-129. https://www.ncbi.nlm.nih.gov/pubmed/32039764.
672. Jiang L, Wang P, Sun YJ, Wu YJ. 2019. Ivermectin reverses the drug resistance in cancer cells through EGFR/ERK/Akt/NF-kappaB pathway. J Exp Clin Cancer Res. 38(1):265. https://www.ncbi.nlm.nih.gov/pubmed/31215501.
673. Pantziarka P, Sukhatme V, Bouche G, Meheus L, Sukhatme VP. 2015. Repurposing Drugs in Oncology (ReDO)-itraconazole as an anti-cancer agent. Ecancermedicalscience. 9:521. https://www.ncbi.nlm.nih.gov/pubmed/25932045.
674. Tsubamoto H, Sonoda T, Yamasaki M, Inoue K. 2014. Impact of combination chemotherapy with itraconazole on survival of patients with refractory ovarian cancer. Anticancer Res. 34(5):2481-2487. https://www.ncbi.nlm.nih.gov/pubmed/24778064.
675. Tsubamoto H, Sonoda T, Ikuta S, Tani S, Inoue K, Yamanaka N. 2015. Combination Chemotherapy with Itraconazole for Treating Metastatic Pancreatic Cancer in the Second-line or Additional Setting. Anticancer Res. 35(7):4191-4196. https://www.ncbi.nlm.nih.gov/pubmed/26124377.
676. Takara K, Tanigawara Y, Komada F, Nishiguchi K, Sakaeda T, Okumura K. 1999. Cellular pharmacokinetic aspects of reversal effect of itraconazole on P-glycoprotein-mediated resistance of anticancer drugs. Biol Pharm Bull. 22(12):1355-1359. https://www.ncbi.nlm.nih.gov/pubmed/10746169.
677. Ghadi M, Hosseinimehr SJ, Amiri FT, Mardanshahi A, Noaparast Z. 2021. Itraconazole synergistically increases therapeutic effect of paclitaxel and (99m)Tc-MIBI accumulation, as a probe of P-gp activity, in HT-29 tumor-bearing nude mice. Eur J Pharmacol. 895:173892. https://www.ncbi.nlm.nih.gov/pubmed/33497608.
678. Iida N, Takara K, Ohmoto N, Nakamura T, Kimura T, Wada A, et al. 2001. Reversal effects of antifungal drugs on multidrug resistance in MDR1-overexpressing HeLa cells. Biol Pharm Bull. 24(9):1032-1036. https://www.ncbi.nlm.nih.gov/pubmed/11558564.
679. Muinelo-Romay L, Garcia D, Alonso-Alconada L, Vieito M, Carmona M, Martinez N, et al. 2013. Zoledronic acid as an antimetastatic agent for different human tumor cell lines. Anticancer Res. 33(12):5295-5300. https://www.ncbi.nlm.nih.gov/pubmed/24324062.
680. Coleman RE, Winter MC, Cameron D, Bell R, Dodwell D, Keane MM, et al. 2010. The effects of adding zoledronic acid to neoadjuvant chemotherapy on tumour response: exploratory evidence for direct anti-tumour activity in breast cancer. Br J Cancer. 102(7):1099-1105. https://www.ncbi.nlm.nih.gov/pubmed/20234364.
681. Bosch-Barrera J, Merajver SD, Menendez JA, Van Poznak C. 2011. Direct antitumour activity of zoledronic acid: preclinical and clinical data. Clin Transl Oncol. 13(3):148-155. https://www.ncbi.nlm.nih.gov/pubmed/21421459.
682. Cokol M. 2013. Drugs and their interactions. Curr Drug Discov Technol. 10(2):106-113. https://www.ncbi.nlm.nih.gov/pubmed/23237673.
683. Laezza C, Malfitano AM, Proto MC, Esposito I, Gazzerro P, Formisano P, et al. 2010. Inhibition of 3-hydroxy-3-methylglutaryl-coenzyme A reductase activity and of Ras farnesylation mediate antitumor effects of anandamide in human breast cancer cells. Endocr Relat Cancer. 17(2):495-503. https://www.ncbi.nlm.nih.gov/pubmed/20304978.

684. Balasubramanian R, Maideen NMP. 2021. HMG-CoA Reductase Inhibitors (Statins) and their Drug Interactions Involving CYP Enzymes, P-glycoprotein and OATP Transporters-An Overview. Curr Drug Metab. 22(5):328-341. https://www.ncbi.nlm.nih.gov/pubmed/33459228.
685. Pearce EL, Walsh MC, Cejas PJ, Harms GM, Shen H, Wang LS, et al. 2009. Enhancing CD8 T-cell memory by modulating fatty acid metabolism. Nature. 460(7251):103-107. https://www.ncbi.nlm.nih.gov/pubmed/19494812.
686. Moiseeva O, Deschenes-Simard X, Pollak M, Ferbeyre G. 2013. Metformin, aging and cancer. Aging (Albany NY). 5(5):330-331. https://www.ncbi.nlm.nih.gov/pubmed/23660016.
687. Zakikhani M, Dowling RJ, Sonenberg N, Pollak MN. 2008. The effects of adiponectin and metformin on prostate and colon neoplasia involve activation of AMP-activated protein kinase. Cancer Prev Res (Phila). 1(5):369-375. https://www.ncbi.nlm.nih.gov/pubmed/19138981.
688. Kurelac I, Umesh Ganesh N, Iorio M, Porcelli AM, Gasparre G. 2020. The multifaceted effects of metformin on tumor microenvironment. Semin Cell Dev Biol. 98:90-97. https://www.ncbi.nlm.nih.gov/pubmed/31091466.
689. Didier A, Loor F. 1996. The abamectin derivative ivermectin is a potent P-glycoprotein inhibitor. Anticancer Drugs. 7(7):745-751. https://www.ncbi.nlm.nih.gov/pubmed/8949985.
690. Juarez M, Schcolnik-Cabrera A, Duenas-Gonzalez A. 2018. The multitargeted drug ivermectin: from an antiparasitic agent to a repositioned cancer drug. Am J Cancer Res. 8(2):317-331. https://www.ncbi.nlm.nih.gov/pubmed/29511601.
691. Melotti A, Mas C, Kuciak M, Lorente-Trigos A, Borges I, Ruiz i Altaba A. 2014. The river blindness drug Ivermectin and related macrocyclic lactones inhibit WNT-TCF pathway responses in human cancer. EMBO Mol Med. 6(10):1263-1278. https://www.ncbi.nlm.nih.gov/pubmed/25143352.
692. Dominguez-Gomez G, Chavez-Blanco A, Medina-Franco JL, Saldivar-Gonzalez F, Flores-Torrontegui Y, Juarez M, et al. 2018. Ivermectin as an inhibitor of cancer stemlike cells. Mol Med Rep. 17(2):3397-3403. https://www.ncbi.nlm.nih.gov/pubmed/29257278.
693. Liu J, Liang H, Chen C, Wang X, Qu F, Wang H, et al. 2019. Ivermectin induces autophagy-mediated cell death through the AKT/mTOR signaling pathway in glioma cells. Biosci Rep. 39(12). https://www.ncbi.nlm.nih.gov/pubmed/31755894.
694. Seth C, Mas C, Conod A, Mueller J, Siems K, Kuciak M, et al. 2016. Long-Lasting WNT-TCF Response Blocking and Epigenetic Modifying Activities of Withanolide F in Human Cancer Cells. PLoS One. 11(12):e0168170. https://www.ncbi.nlm.nih.gov/pubmed/27973612.
695. Kim J, Tang JY, Gong R, Kim J, Lee JJ, Clemons KV, et al. 2010. Itraconazole, a commonly used antifungal that inhibits Hedgehog pathway activity and cancer growth. Cancer Cell. 17(4):388-399. https://www.ncbi.nlm.nih.gov/pubmed/20385363.
696. Liu R, Li J, Zhang T, Zou L, Chen Y, Wang K, et al. 2014. Itraconazole suppresses the growth of glioblastoma through induction of autophagy: involvement of abnormal cholesterol trafficking. Autophagy. 10(7):1241-1255. https://www.ncbi.nlm.nih.gov/pubmed/24905460.
697. Liang G, Liu M, Wang Q, Shen Y, Mei H, Li D, et al. 2017. Itraconazole exerts its anti-melanoma effect by suppressing Hedgehog, Wnt, and PI3K/mTOR signaling pathways. Oncotarget. 8(17):28510-28525. https://www.ncbi.nlm.nih.gov/pubmed/28212537.
698. Tsubamoto H, Inoue K, Sakata K, Ueda T, Takeyama R, Shibahara H, et al. 2017. Itraconazole Inhibits AKT/mTOR Signaling and Proliferation in Endometrial Cancer Cells. Anticancer Res. 37(2):515-519. https://www.ncbi.nlm.nih.gov/pubmed/28179296.

699. Ueda T, Tsubamoto H, Inoue K, Sakata K, Shibahara H, Sonoda T. 2017. Itraconazole Modulates Hedgehog, WNT/beta-catenin, as well as Akt Signalling, and Inhibits Proliferation of Cervical Cancer Cells. Anticancer Res. 37(7):3521-3526. https://www.ncbi.nlm.nih.gov/pubmed/28668841.
700. Vreugdenhil G, Raemaekers JM, van Dijke BJ, de Pauw BE. 1993. Itraconazole and multidrug resistance: possible effects on remission rate and disease-free survival in acute leukemia. Ann Hematol. 67(3):107-109. https://www.ncbi.nlm.nih.gov/pubmed/8396989.
701. Shirakawa K, Takara K, Tanigawara Y, Aoyama N, Kasuga M, Komada F, et al. 1999. Interaction of docetaxel ("Taxotere") with human P-glycoprotein. Jpn J Cancer Res. 90(12):1380-1386. https://www.ncbi.nlm.nih.gov/pubmed/10665657.
702. Gronich N, Rennert G. 2013. Beyond aspirin-cancer prevention with statins, metformin and bisphosphonates. Nat Rev Clin Oncol. 10(11):625-642. https://www.ncbi.nlm.nih.gov/pubmed/24080598.
703. Yuasa T, Kimura S, Ashihara E, Habuchi T, Maekawa T. 2007. Zoledronic acid - a multiplicity of anti-cancer action. Curr Med Chem. 14(20):2126-2135. https://www.ncbi.nlm.nih.gov/pubmed/17691952.
704. Knight LA, Conroy M, Fernando A, Polak M, Kurbacher CM, Cree IA. 2005. Pilot studies of the effect of zoledronic acid (Zometa) on tumor-derived cells ex vivo in the ATP-based tumor chemosensitivity assay. Anticancer Drugs. 16(9):969-976. https://www.ncbi.nlm.nih.gov/pubmed/16162973.
705. Seelig A. 2020. P-Glycoprotein: One Mechanism, Many Tasks and the Consequences for Pharmacotherapy of Cancers. Front Oncol. 10:576559. https://www.ncbi.nlm.nih.gov/pubmed/33194688.
706. Abbasi MM, Valizadeh H, Hamishehkar H, Zakeri-Milani P. 2016. Inhibition of P-glycoprotein expression and function by anti-diabetic drugs gliclazide, metformin, and pioglitazone in vitro and in situ. Res Pharm Sci. 11(3):177-186. https://www.ncbi.nlm.nih.gov/pubmed/27499787.
707. Li Y, Wang M, Zhi P, You J, Gao JQ. 2018. Metformin synergistically suppress tumor growth with doxorubicin and reverse drug resistance by inhibiting the expression and function of P-glycoprotein in MCF7/ADR cells and xenograft models. Oncotarget. 9(2):2158-2174. https://www.ncbi.nlm.nih.gov/pubmed/29416762.
708. Lespine A, Dupuy J, Orlowski S, Nagy T, Glavinas H, Krajcsi P, et al. 2006. Interaction of ivermectin with multidrug resistance proteins (MRP1, 2 and 3). Chem Biol Interact. 159(3):169-179. https://www.ncbi.nlm.nih.gov/pubmed/16384552.
709. Tapaninen T, Backman JT, Kurkinen KJ, Neuvonen PJ, Niemi M. 2011. Itraconazole, a P-glycoprotein and CYP3A4 inhibitor, markedly raises the plasma concentrations and enhances the renin-inhibiting effect of aliskiren. J Clin Pharmacol. 51(3):359-367. https://www.ncbi.nlm.nih.gov/pubmed/20400651.
710. Miyama T, Takanaga H, Matsuo H, Yamano K, Yamamoto K, Iga T, et al. 1998. P-glycoprotein-mediated transport of itraconazole across the blood-brain barrier. Antimicrob Agents Chemother. 42(7):1738-1744. https://www.ncbi.nlm.nih.gov/pubmed/9661014.
711. Prueksaritanont T, Chu X, Evers R, Klopfer SO, Caro L, Kothare PA, et al. 2014. Pitavastatin is a more sensitive and selective organic anion-transporting polypeptide 1B clinical probe than rosuvastatin. Br J Clin Pharmacol. 78(3):587-598. https://www.ncbi.nlm.nih.gov/pubmed/24617605.
712. Bukowski K, Kciuk M, Kontek R. 2020. Mechanisms of Multidrug Resistance in Cancer Chemotherapy. Int J Mol Sci. 21(9). https://www.ncbi.nlm.nih.gov/pubmed/32370233.
713. Nussbaumer S, Bonnabry P, Veuthey JL, Fleury-Souverain S. 2011. Analysis of anticancer drugs: a review. Talanta. 85(5):2265-2289. https://www.ncbi.nlm.nih.gov/pubmed/21962644.

714. Luqmani YA. 2005. Mechanisms of drug resistance in cancer chemotherapy. Med Princ Pract. 14 Suppl 1:35-48. https://www.ncbi.nlm.nih.gov/pubmed/16103712.
715. Vadlapatla RK, Vadlapudi AD, Pal D, Mitra AK. 2013. Mechanisms of drug resistance in cancer chemotherapy: coordinated role and regulation of efflux transporters and metabolizing enzymes. Curr Pharm Des. 19(40):7126-7140. https://www.ncbi.nlm.nih.gov/pubmed/23829373.
716. Wang D, Lippard SJ. 2005. Cellular processing of platinum anticancer drugs. Nat Rev Drug Discov. 4(4):307-320. https://www.ncbi.nlm.nih.gov/pubmed/15789122.
717. Stewart DJ. 2007. Mechanisms of resistance to cisplatin and carboplatin. Crit Rev Oncol Hematol. 63(1):12-31. https://www.ncbi.nlm.nih.gov/pubmed/17336087.
718. Ramos A, Sadeghi S, Tabatabaeian H. 2021. Battling Chemoresistance in Cancer: Root Causes and Strategies to Uproot Them. Int J Mol Sci. 22(17). https://www.ncbi.nlm.nih.gov/pubmed/34502361.
719. Vaidya FU, Sufiyan Chhipa A, Mishra V, Gupta VK, Rawat SG, Kumar A, et al. 2020. Molecular and cellular paradigms of multidrug resistance in cancer. Cancer Rep (Hoboken).e1291. https://www.ncbi.nlm.nih.gov/pubmed/33052041.
720. Mansoori B, Mohammadi A, Davudian S, Shirjang S, Baradaran B. 2017. The Different Mechanisms of Cancer Drug Resistance: A Brief Review. Adv Pharm Bull. 7(3):339-348. https://www.ncbi.nlm.nih.gov/pubmed/29071215.
721. Krzystyniak J, Ceppi L, Dizon DS, Birrer MJ. 2016. Epithelial ovarian cancer: the molecular genetics of epithelial ovarian cancer. Ann Oncol. 27 Suppl 1:i4-i10. https://www.ncbi.nlm.nih.gov/pubmed/27141069.
722. Nunes M, Duarte D, Vale N, Ricardo S. 2022. Pitavastatin and Ivermectin Enhance the Efficacy of Paclitaxel in Chemoresistant High-Grade Serous Carcinoma. Cancers. 14(18):4357. https://www.mdpi.com/2072-6694/14/18/4357.
723. Nagaraj AB, Wang QQ, Joseph P, Zheng C, Chen Y, Kovalenko O, et al. 2018. Using a novel computational drug-repositioning approach (DrugPredict) to rapidly identify potent drug candidates for cancer treatment. Oncogene. 37(3):403-414. https://www.ncbi.nlm.nih.gov/pubmed/28967908.
724. Hwang JR, Kim WY, Cho YJ, Ryu JY, Choi JJ, Jeong SY, et al. 2020. Chloroquine reverses chemoresistance via upregulation of p21(WAF1/CIP1) and autophagy inhibition in ovarian cancer. Cell Death Dis. 11(12):1034. https://www.ncbi.nlm.nih.gov/pubmed/33277461.
725. Mariniello M, Petruzzelli R, Wanderlingh LG, La Montagna R, Carissimo A, Pane F, et al. 2020. Synthetic Lethality Screening Identifies FDA-Approved Drugs that Overcome ATP7B-Mediated Tolerance of Tumor Cells to Cisplatin. Cancers (Basel). 12(3). https://www.ncbi.nlm.nih.gov/pubmed/32155756.
726. Huang L, Zhao L, Zhang J, He F, Wang H, Liu Q, et al. 2021. Antiparasitic mebendazole (MBZ) effectively overcomes cisplatin resistance in human ovarian cancer cells by inhibiting multiple cancer-associated signaling pathways. Aging (Albany NY). 13(13):17407-17427. https://www.ncbi.nlm.nih.gov/pubmed/34232919.
727. Guo F, Yang Z, Kulbe H, Albers AE, Sehouli J, Kaufmann AM. 2019. Inhibitory effect on ovarian cancer ALDH+ stem-like cells by Disulfiram and Copper treatment through ALDH and ROS modulation. Biomed Pharmacother. 118:109371. https://www.ncbi.nlm.nih.gov/pubmed/31545281.
728. Kita Y, Hamada A, Saito R, Teramoto Y, Tanaka R, Takano K, et al. 2019. Systematic chemical screening identifies disulfiram as a repurposed drug that enhances sensitivity to cisplatin in bladder cancer: a summary of preclinical studies. Br J Cancer. 121(12):1027-1038. https://www.ncbi.nlm.nih.gov/pubmed/31673101.
729. Byun JM, Lee DS, Landen CN, Kim DH, Kim YN, Lee KB, et al. 2019. Arsenic trioxide and tetraarsenic oxide induce cytotoxicity and have a synergistic effect with cisplatin in

paclitaxel-resistant ovarian cancer cells. Acta Oncol. 58(11):1594-1602. https://www.ncbi.nlm.nih.gov/pubmed/31257975.
730. Kato S, Smalley S, Sadarangani A, Chen-Lin K, Oliva B, Branes J, et al. 2010. Lipophilic but not hydrophilic statins selectively induce cell death in gynaecological cancers expressing high levels of HMGCoA reductase. J Cell Mol Med. 14(5):1180-1193. https://www.ncbi.nlm.nih.gov/pubmed/19432822.
731. Taylor-Harding B, Orsulic S, Karlan BY, Li AJ. 2010. Fluvastatin and cisplatin demonstrate synergistic cytotoxicity in epithelial ovarian cancer cells. Gynecol Oncol. 119(3):549-556. https://www.ncbi.nlm.nih.gov/pubmed/20837358.
732. Kobayashi Y, Kashima H, Rahmanto YS, Banno K, Yu Y, Matoba Y, et al. 2017. Drug repositioning of mevalonate pathway inhibitors as antitumor agents for ovarian cancer. Oncotarget. 8(42):72147-72156. https://www.ncbi.nlm.nih.gov/pubmed/29069775.
733. Schrauwen S, Coenegrachts L, Cattaneo A, Hermans E, Lambrechts D, Amant F. 2015. The antitumor effect of metformin with and without carboplatin on primary endometrioid endometrial carcinoma in vivo. Gynecol Oncol. 138(2):378-382. https://www.ncbi.nlm.nih.gov/pubmed/26050920.
734. Zheng Y, Zhu J, Zhang H, Liu Y, Sun H. 2018. Metformin inhibits ovarian cancer growth and migration in vitro and in vivo by enhancing cisplatin cytotoxicity. Am J Transl Res. 10(10):3086-3098. https://www.ncbi.nlm.nih.gov/pubmed/30416652.
735. Gotlieb WH, Saumet J, Beauchamp MC, Gu J, Lau S, Pollak MN, et al. 2008. In vitro metformin anti-neoplastic activity in epithelial ovarian cancer. Gynecol Oncol. 110(2):246-250. https://www.ncbi.nlm.nih.gov/pubmed/18495226.
736. Dos Santos Guimaraes I, Ladislau-Magescky T, Tessarollo NG, Dos Santos DZ, Gimba ERP, Sternberg C, et al. 2018. Chemosensitizing effects of metformin on cisplatin- and paclitaxel-resistant ovarian cancer cell lines. Pharmacol Rep. 70(3):409-417. https://www.ncbi.nlm.nih.gov/pubmed/29627688.
737. Ricci F, Brunelli L, Affatato R, Chila R, Verza M, Indraccolo S, et al. 2019. Overcoming platinum-acquired resistance in ovarian cancer patient-derived xenografts. Ther Adv Med Oncol. 11:1758835919839543. https://www.ncbi.nlm.nih.gov/pubmed/31258626.
738. Erices R, Bravo ML, Gonzalez P, Oliva B, Racordon D, Garrido M, et al. 2013. Metformin, at concentrations corresponding to the treatment of diabetes, potentiates the cytotoxic effects of carboplatin in cultures of ovarian cancer cells. Reprod Sci. 20(12):1433-1446. https://www.ncbi.nlm.nih.gov/pubmed/23653391.
739. Wen KC, Sung PL, Wu ATH, Chou PC, Lin JH, Huang CF, et al. 2020. Neoadjuvant metformin added to conventional chemotherapy synergizes anti-proliferative effects in ovarian cancer. J Ovarian Res. 13(1):95. https://www.ncbi.nlm.nih.gov/pubmed/32825834.
740. Liu Y, He C, Huang X. 2017. Metformin partially reverses the carboplatin-resistance in NSCLC by inhibiting glucose metabolism. Oncotarget. 8(43):75206-75216. https://www.ncbi.nlm.nih.gov/pubmed/29088858.
741. Cai H, Everett RS, Thakker DR. 2019. Efficacious dose of metformin for breast cancer therapy is determined by cation transporter expression in tumours. Br J Pharmacol. 176(15):2724-2735. https://www.ncbi.nlm.nih.gov/pubmed/31032880.
742. Patel S, Kumar L, Singh N. 2015. Metformin and epithelial ovarian cancer therapeutics. Cell Oncol (Dordr). 38(5):365-375. https://www.ncbi.nlm.nih.gov/pubmed/26266765.
743. Juarez M, Schcolnik-Cabrera A, Dominguez-Gomez G, Chavez-Blanco A, Diaz-Chavez J, Duenas-Gonzalez A. 2020. Antitumor effects of ivermectin at clinically feasible concentrations support its clinical development as a repositioned cancer drug. Cancer Chemother Pharmacol. 85(6):1153-1163. https://www.ncbi.nlm.nih.gov/pubmed/32474842.

744. Jagdev SP, Coleman RE, Shipman CM, Rostami HA, Croucher PI. 2001. The bisphosphonate, zoledronic acid, induces apoptosis of breast cancer cells: evidence for synergy with paclitaxel. Br J Cancer. 84(8):1126-1134. https://www.ncbi.nlm.nih.gov/pubmed/11308265.
745. Lee MV, Fong EM, Singer FR, Guenette RS. 2001. Bisphosphonate treatment inhibits the growth of prostate cancer cells. Cancer Res. 61(6):2602-2608. https://www.ncbi.nlm.nih.gov/pubmed/11289137.
746. Shipman CM, Rogers MJ, Apperley JF, Russell RG, Croucher PI. 1997. Bisphosphonates induce apoptosis in human myeloma cell lines: a novel anti-tumour activity. Br J Haematol. 98(3):665-672. https://www.ncbi.nlm.nih.gov/pubmed/9332325.
747. Wood J, Bonjean K, Ruetz S, Bellahcene A, Devy L, Foidart JM, et al. 2002. Novel antiangiogenic effects of the bisphosphonate compound zoledronic acid. J Pharmacol Exp Ther. 302(3):1055-1061. https://www.ncbi.nlm.nih.gov/pubmed/12183663.
748. Gnant M, Clezardin P. 2012. Direct and indirect anticancer activity of bisphosphonates: a brief review of published literature. Cancer Treat Rev. 38(5):407-415. https://www.ncbi.nlm.nih.gov/pubmed/21983264.
749. Ibrahim T, Liverani C, Mercatali L, Sacanna E, Zanoni M, Fabbri F, et al. 2013. Cisplatin in combination with zoledronic acid: a synergistic effect in triple-negative breast cancer cell lines. Int J Oncol. 42(4):1263-1270. https://www.ncbi.nlm.nih.gov/pubmed/23403907.
750. Neville-Webbe HL, Evans CA, Coleman RE, Holen I. 2006. Mechanisms of the synergistic interaction between the bisphosphonate zoledronic acid and the chemotherapy agent paclitaxel in breast cancer cells in vitro. Tumour Biol. 27(2):92-103. https://www.ncbi.nlm.nih.gov/pubmed/16582586.
751. Neville-Webbe HL, Rostami-Hodjegan A, Evans CA, Coleman RE, Holen I. 2005. Sequence- and schedule-dependent enhancement of zoledronic acid induced apoptosis by doxorubicin in breast and prostate cancer cells. Int J Cancer. 113(3):364-371. https://www.ncbi.nlm.nih.gov/pubmed/15455384.
752. Gobel A, Zinna VM, Dell'Endice S, Jaschke N, Kuhlmann JD, Wimberger P, et al. 2020. Anti-tumor effects of mevalonate pathway inhibition in ovarian cancer. BMC Cancer. 20(1):703. https://www.ncbi.nlm.nih.gov/pubmed/32727400.
753. Tendulkar S, Dodamani S. 2021. Chemoresistance in Ovarian Cancer: Prospects for New Drugs. Anticancer Agents Med Chem. 21(6):668-678. https://www.ncbi.nlm.nih.gov/pubmed/32900355.
754. Lai YH, Kuo C, Kuo MT, Chen HHW. 2018. Modulating Chemosensitivity of Tumors to Platinum-Based Antitumor Drugs by Transcriptional Regulation of Copper Homeostasis. Int J Mol Sci. 19(5). https://www.ncbi.nlm.nih.gov/pubmed/29772714.
755. Cerovska E, Elsnerova K, Vaclavikova R, Soucek P. 2017. The role of membrane transporters in ovarian cancer chemoresistance and prognosis. Expert Opin Drug Metab Toxicol. 13(7):741-753. https://www.ncbi.nlm.nih.gov/pubmed/28511565.
756. Kalayda GV, Wagner CH, Buss I, Reedijk J, Jaehde U. 2008. Altered localisation of the copper efflux transporters ATP7A and ATP7B associated with cisplatin resistance in human ovarian carcinoma cells. BMC Cancer. 8:175. https://www.ncbi.nlm.nih.gov/pubmed/18565219.
757. Holzer AK, Howell SB. 2006. The internalization and degradation of human copper transporter 1 following cisplatin exposure. Cancer Res. 66(22):10944-10952. https://www.ncbi.nlm.nih.gov/pubmed/17108132.
758. Zeybek B, Costantine M, Kilic GS, Borahay MA. 2018. Therapeutic Roles of Statins in Gynecology and Obstetrics: The Current Evidence. Reprod Sci. 25(6):802-817. https://www.ncbi.nlm.nih.gov/pubmed/29320955.

759. Nunes M, Duarte D, Vale N, Ricardo S. 2022. The Antineoplastic Effect of Carboplatin Is Potentiated by Combination with Pitavastatin or Metformin in a Chemoresistant High-Grade Serous Carcinoma Cell Line. Int J Mol Sci. 24(1). https://www.ncbi.nlm.nih.gov/pubmed/36613537.
760. Liu C, Chen H, Hu B, Shi J, Chen Y, Huang K. 2023. New insights into the therapeutic potentials of statins in cancer. Front Pharmacol. 14:1188926. https://www.ncbi.nlm.nih.gov/pubmed/37484027.
761. Tang M, Hu X, Wang Y, Yao X, Zhang W, Yu C, et al. 2021. Ivermectin, a potential anticancer drug derived from an antiparasitic drug. Pharmacol Res. 163:105207. https://www.ncbi.nlm.nih.gov/pubmed/32971268.
762. Jensen C, Teng Y. 2020. Is It Time to Start Transitioning From 2D to 3D Cell Culture? Front Mol Biosci. 7:33. https://www.ncbi.nlm.nih.gov/pubmed/32211418.
763. Abuwatfa WH, Pitt WG, Husseini GA. 2024. Scaffold-based 3D cell culture models in cancer research. J Biomed Sci. 31(1):7. https://www.ncbi.nlm.nih.gov/pubmed/38221607.
764. Law AMK, Rodriguez de la Fuente L, Grundy TJ, Fang G, Valdes-Mora F, Gallego-Ortega D. 2021. Advancements in 3D Cell Culture Systems for Personalizing Anti-Cancer Therapies. Front Oncol. 11:782766. https://www.ncbi.nlm.nih.gov/pubmed/34917509.
765. Hoffmann OI, Ilmberger C, Magosch S, Joka M, Jauch KW, Mayer B. 2015. Impact of the spheroid model complexity on drug response. J Biotechnol. 205:14-23. https://www.ncbi.nlm.nih.gov/pubmed/25746901.
766. Lee JM, Mhawech-Fauceglia P, Lee N, Parsanian LC, Lin YG, Gayther SA, et al. 2013. A three-dimensional microenvironment alters protein expression and chemosensitivity of epithelial ovarian cancer cells in vitro. Lab Invest. 93(5):528-542. https://www.ncbi.nlm.nih.gov/pubmed/23459371.
767. Sheta R, Bachvarova M, Plante M, Renaud MC, Sebastianelli A, Gregoire J, et al. 2020. Development of a 3D functional assay and identification of biomarkers, predictive for response of high-grade serous ovarian cancer (HGSOC) patients to poly-ADP ribose polymerase inhibitors (PARPis): targeted therapy. J Transl Med. 18(1):439. https://www.ncbi.nlm.nih.gov/pubmed/33213473.
768. Yadav B, Wennerberg K, Aittokallio T, Tang J. 2015. Searching for Drug Synergy in Complex Dose-Response Landscapes Using an Interaction Potency Model. Comput Struct Biotechnol J. 13:504-513. https://www.ncbi.nlm.nih.gov/pubmed/26949479.
769. Loewe S. 1953. The problem of synergism and antagonism of combined drugs. Arzneimittelforschung. 3(6):285-290. https://www.ncbi.nlm.nih.gov/pubmed/13081480.
770. BLISS CI. 1939. THE TOXICITY OF POISONS APPLIED JOINTLY. Annals of Applied Biology. 26(3):585-615. https://onlinelibrary.wiley.com/doi/abs/10.1111/j.1744-7348.1939.tb06990.x.
771. Berenbaum MC. 1989. What is synergy? Pharmacol Rev. 41(2):93-141. https://www.ncbi.nlm.nih.gov/pubmed/2692037.
772. Urzi O, Gasparro R, Costanzo E, De Luca A, Giavaresi G, Fontana S, et al. 2023. Three-Dimensional Cell Cultures: The Bridge between In Vitro and In Vivo Models. Int J Mol Sci. 24(15). https://www.ncbi.nlm.nih.gov/pubmed/37569426.
773. Manduca N, Maccafeo E, De Maria R, Sistigu A, Musella M. 2023. 3D cancer models: One step closer to in vitro human studies. Front Immunol. 14:1175503. https://www.ncbi.nlm.nih.gov/pubmed/37114038.
774. Li Y, Tang P, Cai S, Peng J, Hua G. 2020. Organoid based personalized medicine: from bench to bedside. Cell Regen. 9(1):21. https://www.ncbi.nlm.nih.gov/pubmed/33135109.
775. Nunes M, Bartosch C, Abreu MH, Richardson A, Almeida R, Ricardo S. 2024. Deciphering the Molecular Mechanisms behind Drug Resistance in Ovarian Cancer to

Unlock Efficient Treatment Options. Cells. 13(9). https://www.ncbi.nlm.nih.gov/pubmed/38727322.
776. Lespine A, Menez C, Bourguinat C, Prichard RK. 2012. P-glycoproteins and other multidrug resistance transporters in the pharmacology of anthelmintics: Prospects for reversing transport-dependent anthelmintic resistance. Int J Parasitol Drugs Drug Resist. 2:58-75. https://www.ncbi.nlm.nih.gov/pubmed/24533264.
777. Veiga-Matos J, Morales AI, Prieto M, Remiao F, Silva R. 2023. Study Models of Drug-Drug Interactions Involving P-Glycoprotein: The Potential Benefit of P-Glycoprotein Modulation at the Kidney and Intestinal Levels. Molecules. 28(22). https://www.ncbi.nlm.nih.gov/pubmed/38005253.
778. Nikdouz A, Orso F. 2023. Emerging roles of 3D-culture systems in tackling tumor drug resistance. Cancer Drug Resist. 6(4):788-804. https://www.ncbi.nlm.nih.gov/pubmed/38263982.
779. Filipiak-Duliban A, Brodaczewska K, Kajdasz A, Kieda C. 2022. Spheroid Culture Differentially Affects Cancer Cell Sensitivity to Drugs in Melanoma and RCC Models. Int J Mol Sci. 23(3). https://www.ncbi.nlm.nih.gov/pubmed/35163092.
780. Langhans SA. 2018. Three-Dimensional in Vitro Cell Culture Models in Drug Discovery and Drug Repositioning. Front Pharmacol. 9:6. https://www.ncbi.nlm.nih.gov/pubmed/29410625.
781. Fu D, Arias IM. 2012. Intracellular trafficking of P-glycoprotein. Int J Biochem Cell Biol. 44(3):461-464. https://www.ncbi.nlm.nih.gov/pubmed/22212176.
782. du Bois A, Reuss A, Pujade-Lauraine E, Harter P, Ray-Coquard I, Pfisterer J. 2009. Role of surgical outcome as prognostic factor in advanced epithelial ovarian cancer: a combined exploratory analysis of 3 prospectively randomized phase 3 multicenter trials: by the Arbeitsgemeinschaft Gynaekologische Onkologie Studiengruppe Ovarialkarzinom (AGO-OVAR) and the Groupe d'Investigateurs Nationaux Pour les Etudes des Cancers de l'Ovaire (GINECO). Cancer. 115(6):1234-1244. https://www.ncbi.nlm.nih.gov/pubmed/19189349.
783. Anuradha S, Webb PM, Blomfield P, Brand AH, Friedlander M, Leung Y, et al. 2014. Survival of Australian women with invasive epithelial ovarian cancer: a population-based study. Med J Aust. 201(5):283-288. https://www.ncbi.nlm.nih.gov/pubmed/25163381.
784. Huang H, Li YJ, Lan CY, Huang QD, Feng YL, Huang YW, et al. 2013. Clinical significance of ascites in epithelial ovarian cancer. Neoplasma. 60(5):546-552. https://www.ncbi.nlm.nih.gov/pubmed/23790174.
785. Cho A, Howell VM, Colvin EK. 2015. The Extracellular Matrix in Epithelial Ovarian Cancer - A Piece of a Puzzle. Front Oncol. 5:245. https://www.ncbi.nlm.nih.gov/pubmed/26579497.
786. Avci CB, Bagca BG, Shademan B, Takanlou LS, Takanlou MS, Nourazarian A. 2024. The future of cancer therapy: exploring the potential of patient-derived organoids in drug development. Front Cell Dev Biol. 12:1401504. https://www.ncbi.nlm.nih.gov/pubmed/38835507.
787. Tong L, Cui W, Zhang B, Fonseca P, Zhao Q, Zhang P, et al. 2024. Patient-derived organoids in precision cancer medicine. Med. 5(11):1351-1377. https://www.ncbi.nlm.nih.gov/pubmed/39341206.
788. Barbosa MAG, Xavier CPR, Pereira RF, Petrikaite V, Vasconcelos MH. 2021. 3D Cell Culture Models as Recapitulators of the Tumor Microenvironment for the Screening of Anti-Cancer Drugs. Cancers (Basel). 14(1). https://www.ncbi.nlm.nih.gov/pubmed/35008353.
789. Porter RJ, Murray GI, McLean MH. 2020. Current concepts in tumour-derived organoids. Br J Cancer. 123(8):1209-1218. https://www.ncbi.nlm.nih.gov/pubmed/32728094.

790. Nanki Y, Chiyoda T, Hirasawa A, Ookubo A, Itoh M, Ueno M, et al. 2020. Patient-derived ovarian cancer organoids capture the genomic profiles of primary tumours applicable for drug sensitivity and resistance testing. Sci Rep. 10(1):12581. https://www.ncbi.nlm.nih.gov/pubmed/32724113.
791. Battistini C, Cavallaro U. 2023. Patient-Derived In Vitro Models of Ovarian Cancer: Powerful Tools to Explore the Biology of the Disease and Develop Personalized Treatments. Cancers (Basel). 15(2). https://www.ncbi.nlm.nih.gov/pubmed/36672318.
792. Arias-Diaz AE, Ferreiro-Pantin M, Barbazan J, Perez-Beliz E, Ruiz-Banobre J, Casas-Arozamena C, et al. 2023. Ascites-Derived Organoids to Depict Platinum Resistance in Gynaecological Serous Carcinomas. Int J Mol Sci. 24(17). https://www.ncbi.nlm.nih.gov/pubmed/37686015.
793. Nunes M, Nunes D, Ricardo S. Cell Microarray: An Approach to Evaluate Drug-Induced Alterations in Protein Expression. In: Sergi CM, editor. Advancements in Cancer Research. Brisbane (AU)2023.
794. Thorel L, Perreard M, Florent R, Divoux J, Coffy S, Vincent A, et al. 2024. Patient-derived tumor organoids: a new avenue for preclinical research and precision medicine in oncology. Exp Mol Med. 56(7):1531-1551. https://www.ncbi.nlm.nih.gov/pubmed/38945959.
795. Jubelin C, Munoz-Garcia J, Griscom L, Cochonneau D, Ollivier E, Heymann MF, et al. 2022. Three-dimensional in vitro culture models in oncology research. Cell Biosci. 12(1):155. https://www.ncbi.nlm.nih.gov/pubmed/36089610.
796. Senkowski W, Gall-Mas L, Falco MM, Li Y, Lavikka K, Kriegbaum MC, et al. 2023. A platform for efficient establishment and drug-response profiling of high-grade serous ovarian cancer organoids. Dev Cell. 58(12):1106-1121 e1107. https://www.ncbi.nlm.nih.gov/pubmed/37148882.
797. Maenhoudt N, Vankelecom H. 2021. Protocol for establishing organoids from human ovarian cancer biopsies. STAR Protoc. 2(2):100429. https://www.ncbi.nlm.nih.gov/pubmed/33870230.
798. Hoffmann K, Berger H, Kulbe H, Thillainadarasan S, Mollenkopf HJ, Zemojtel T, et al. 2020. Stable expansion of high-grade serous ovarian cancer organoids requires a low-Wnt environment. EMBO J. 39(6):e104013. https://www.ncbi.nlm.nih.gov/pubmed/32009247.
799. Ince TA, Sousa AD, Jones MA, Harrell JC, Agoston ES, Krohn M, et al. 2015. Characterization of twenty-five ovarian tumour cell lines that phenocopy primary tumours. Nat Commun. 6:7419. https://www.ncbi.nlm.nih.gov/pubmed/26080861.
800. Velletri T, Villa CE, Cilli D, Barzaghi B, Lo Riso P, Lupia M, et al. 2022. Single cell-derived spheroids capture the self-renewing subpopulations of metastatic ovarian cancer. Cell Death Differ. 29(3):614-626. https://www.ncbi.nlm.nih.gov/pubmed/34845371.
801. Winkler J, Abisoye-Ogunniyan A, Metcalf KJ, Werb Z. 2020. Concepts of extracellular matrix remodelling in tumour progression and metastasis. Nat Commun. 11(1):5120. https://www.ncbi.nlm.nih.gov/pubmed/33037194.
802. Popova NV, Jucker M. 2022. The Functional Role of Extracellular Matrix Proteins in Cancer. Cancers (Basel). 14(1). https://www.ncbi.nlm.nih.gov/pubmed/35008401.
803. Benton G, Arnaoutova I, George J, Kleinman HK, Koblinski J. 2014. Matrigel: from discovery and ECM mimicry to assays and models for cancer research. Adv Drug Deliv Rev. 79-80:3-18. https://www.ncbi.nlm.nih.gov/pubmed/24997339.
804. Labrosse KB, Lombardo FC, Rimmer N, Nunez Lopez M, Fedier A, Heinzelmann-Schwarz V, et al. 2024. Protocol for quantifying drug sensitivity in 3D patient-derived ovarian cancer models. STAR Protoc. 5(3):103274. https://www.ncbi.nlm.nih.gov/pubmed/39172645.

805. Maenhoudt N, Defraye C, Boretto M, Jan Z, Heremans R, Boeckx B, et al. 2020. Developing Organoids from Ovarian Cancer as Experimental and Preclinical Models. Stem Cell Reports. 14(4):717-729. https://www.ncbi.nlm.nih.gov/pubmed/32243841.

SEDE ADMINISTRATIVA

INSTITUTO DE **CIÊNCIAS BIOMÉDICAS ABEL SALAZAR**

FACULDADE DE **MEDICINA**